ELUCIDATION OF ANTI-PROLIFERATIVE AND PRO-APOPTOTIC SIGNALING INDUCED BY THE IMMUNOMODULATORY BENZODIAZEPINE BZ-423

by

Thomas B. Sundberg

A dissertation submitted in partial fulfillment
of the requirements for the degree of
Doctor of Philosophy
(Chemistry)
in the University of Michigan
2009

Doctoral Committee:

Professor Gary D. Glick, Chair
Professor David P. Ballou
Professor Carol A. Fierke
Professor E. Neil G. Marsh
Associate Professor Anna K. Mapp

This dissertation is dedicated to the three most important people in my life -
Drs. Kenneth, Alice and Melissa Sundberg.

ACKNOWLEDGMENTS

This thesis could not have been completed without the help and support from everyone I have worked with over the past six years. First, I would like to thank my advisor Gary Glick for his guidance, intellect, expertise and boundless energy as well as for fostering a world-class scientific training environment. But most of all, I would like to thank Gary for always demanding excellence out of me (and everyone else in lab) - being held to your high standards has made a tremendous difference in my professional development.

In addition, I would like to thank the members of my dissertation committee: David Ballou, Carol Fierke, Neil Marsh, and Anna Mapp. Thank you for taking time out of your busy schedules to serve on my committee as well as provide helpful insights into my research and write reference letters.

A very special thank you goes out to all current and former Glick lab members – Joanne Cleary, Neal Blatt, Tony Boitano, Tony Opipari, Lara Swenson, Katie Groendyke, Gina Ney, Shawn Stevens, Richard Frazee, Xueni Chen, Li Wang, Tasha Francis, Dan Wahl, Melissa Bobeck, Ben Farrar, Jenny Rush and Costas Lyssiotis - whom I have had the pleasure of working alongside. Your intelligence, humor, energy and enthusiasm made lab a pleasant place to come everyday. I wish you all the best! In particular, I would like to thank Tony Opipari for his expertise and enthusiasm as well as

Tony Boitano and Katie Groendyke for peer mentorship provided early in my graduate school career. In addition, I thank Gary, Dan, Lara, Tony Opipari as well as Peter Toogood and Jim Mobley for taking time out of their busy schedules to read and critique my thesis.

I am also grateful for members of other laboratories whose collaborative efforts made this research possible. Chitra Subramanian prepared reagents essential for investigation of Bz-423-induced growth arrest, Rao Bhagavathula harvested skin cells, and Lijun Tan provided expert advice on the intricacies of cell biology. In addition, I would like to thank Prof. Jeffrey Rathmell from Duke University Medical School for helpful advice and the generous gift of a constitutively active Akt construct.

Finally, I would be remiss in failing to thank my friends and family. Thank you Dan and Suzanne Wahl for letting me live in your house this summer and Tim and Laura Bauler for numerous dinners and more numerous answers to my immunology questions. I must also thank my parents Ken and Alice and sister Elizabeth for their love, encouragement and advice. But most of all, it would have been impossible to complete this thesis without the steadfast love and support of my wife Melissa. Thank you, my dear, for being there for me throughout this process.

TABLE OF CONTENTS

CHAPTER 2

LIST OF TABLES

Table

LIST OF FIGURES

Figure

LIST OF ABBREVIATIONS

AA	Antimycin A
Act D	Actinomycin D
ADP	Adenosine-5′-diphosphate
AICD	Activation induced cell death
AIF	Apoptosis inducing factor
AMPK	AMP-activated protein kinase
ANT	Adenine nucleotide translocator
Apaf-1	Apoptosis protease activating factor-1
APC	Antigen-presenting cell
As_2O_3	Arsenic trioxide
ASO	Anti-sense oligonucleotide
ASK1	Apoptosis signal-regulated kinase-1
ATP	Adenosine-5′-triphosphate
BA	Bongkrekic acid
Bad	Bcl-2 agonist of cell death
Bak	Bcl-2 antagonist killer1
Bax	Bcl-2-associated X protein
Bcl-2	B cell CLL/lymphoma 2

bHLHzip	basic Helix/Loop/Helix-Leucine Zipper
BH	Bcl-2 homology
t-BHP	*tert*-Butyl hydroperoxide
Bid	BH3-interacting death domain agonist
Bik	Bcl-2-interacting killer
Bim	Bcl-2-interacting protein
BL	Burkitt's Lymphoma
Bmf	Bcl-2 modifying factor
BSA	Bovine serum albumin
BSO	L-buthionine sulfoximine
CBR	Central benzodiazepine receptor
CD	Cluster of differentiation
CDK	Cyclin-dependent kinase
CDDP	Cis-diamineplatinum(II)dichloride
CHX	Cycloheximide
CICD	Caspase-independent cell death
CK	Creatine kinase
CLAMI	Cell lysis and mitochondrial isolation
4-Cl-Dz	4′-Chlorodiazepam
CRAC	Ca^{2+}-release activated Ca^{2+} channel
CsA	Cyclosporine A
CTLA-4	Cytotoxic T lymphocyte antigen-4
CTLA-4Ig	Cytotoxic T lymphocyte antigen-4•Immunoglobin fusion protein

CuZnSOD	Copper and zinc superoxide dismutases
CypD	Cyclophillin D
Cyt. *c*	Cytochrome *c*
Cz	Clonazepam
DISC	Death-inducing signaling complex
DCFH-DA	Dichlorofluorescin diacetate
DFMO	Difluoromethylornithine
DHE	Dihydroethidium
DKO	Double knockout
DLC	Dynein light chain
DMSO	Dimethylsulfoxide
Drp-1	dynamin-related protein-1
Dz	Diazepam
EC_{50}	Effective concentration that produces a response in 50% of the cells
EndoG	Endonuclease G
ER	Endoplasmic reticulum
ERK	Extracellular signal-regulated kinase
ETC	Electron transport chain
FBS	Fetal bovine serum
FADD	Fas-associated death domain
FCCP	Carbonyl cyanide-4 (trfluoromethoxy) phenylhydrazone
Fe-S	Iron-sulfur cluster

FOXO3a	Forkhead box O3a
GABA	γ-aminobutyric acid
GC	Germinal center
GF	Growth factor
GFP	Green fluorescent protein
GI_{50}	Effective concentration that inhibits 50% growth
GPX	Glutathione peroxidase
GSIS	Glucose-stimulated insulin secretion
GSH	Glutathione
GSK-3β	Glycogen synthase kinase-3β
GSSG	Glutathione disulfide
GST	Glutathione *S*-transferase
H_2O_2	Hydrogen peroxide
HDAC	Histone deacetylase
HEK 293	Human embryonic kidney 293
HIF-1α	Hypoxia inducible factor-1α
HK	Hexokinase
HPLC	High pressure liquid chromatography
Hrk	Harakiri
HSP	Heat shock proteins
HSV	Herpes simplex virus
HUVAC	Human umbilical vein endothelial cell
IAP	Inhibitor of apoptosis

IFN-γ	Interferon-γ
InsP3	Inositol-1,4,5-trisphosphate
IL-2	Interleukin-2
JNK	c-Jun N-teminal kinase
K_d	Equilibrium dissociation constant
K_i	Equilibrium dissociation constant for binding of an inhibitor to an enzyme
LC_{50}	Lethal concentration that kills 50% of the cells
LUV	Large unilamellar vesicle
lpr	lymphoproliferative
MAPK	Mitogen-activated protein kinases
MAPKK	Mitogen-activated protein kinase kinase
MAPKKK	Mitogen-activated protein kinase kinase kinase
MB1	Myc box I
Mcl-1	Myeloid cell leukemia 1
2-ME	2-methoxyesteradiol
MEF	Mouse embryonic fibroblasts
mGSH	Mitochondrial glutathione
MHC	Major histocompatability complex
Mfn2	Mitofusion 2
MIS	Mitochondrial intermembrane space
MnSOD	Manganese superoxide dismutase
MnTBAP	Manganese(III)*meso*-tetrakis(4-benzoic acid)porphyrin
MOMP	Mitochondrial outer membrane permeabilization

mRNA	messenger RNA
mPT	Mitochondrial permeability transition
mTOR	Mammalin target of rapamycin
MX	Myxothiazole A
MRC	Mitochondrial respiratory chain
mtDNA	Mitochondrial DNA
NFAT	Nuclear factor of activated T cells
NPA	3-nitropropionic acid
NZB/W	F_1 offspring of NZB x NZW mice
$O_2^{\bullet-}$	Superoxide
OAZ1	Ornithine decarboxylase antizyme-1
ODC	Ornithine decarboxylase
OMM	Outer mitochondrial membrane
OPA1	Optic atrophy type 1 protein
OSCP	Oligomycin sensitive conferring protein
$p56^{Lck}$	Lymphocyte-specific kinase
PARP-1	Poly (ADP-ribose) polymerase-1
PCD	Programmed cell death
PBR	Peripheral benzodiazepine receptor
PBS	Phosphate buffered saline
PCC	Pigeon cytochrome *c*
PD-1	Programmed death-1
PD-1L	Programmed death-1 ligand

PI	Propidium iodide
P_i	Inorganic phosphate
PI3K	Phosphatidylinositol 3-kinase
PKA	Protein kinase A
PK 11195	1-(2-chlorophenyl)-N-methyl-N-(1-methylpropyl)-3-Isoquinoline carboxamide
PLA2	Phospholipase A2
PMA	Phorphol 12-myristate 13-acetate
pRb	Retinoblastoma protein
PT	Permeability transition
PTEN	Phosphatase and tensin homolog
PTP	Protein tyrsonine phosphatase
PUMA	p53-upregulated modulator of apoptosis
Q	Ubiquinone
$QH^{\bullet-}$	Ubisemiquinone anion
QH_2	Ubiquinol
RNAi	RNA interference
ROS	Reactive oxygen species
RSK	p90 ribosoml S6 kinase
SAHA	Suberoylanilide hydroxamic acid
SAPK	Stress-activated protein kinase
SAR	Structure activity relationship
SfA	Sangliferin A
Skp2	S-phase kinase-associated protein 2

siRNA	Small inhibitory RNA
SLE	Systemic lupus erythematosus
SMPs	Submitochondrial particles
Smac/DIABLO	Second mitochondrial-derived activator of caspase/direct IAP-associated binding protein with low PI
SRB	Sulforhodamine B
STS	Staurosporine
TCA	Trichloroacetic acid
TCR	T cell antigen receptor
TEM	Transmission electron microscopy
TNF	Tumor necrosis factor
TLR	Toll-like receptor
TRAIL	TNF-related apoptosis inducing ligand
TRAF2	TNF receptor–associated factor 2
Trx	Thioredoxin
β-TRCP	β-Transducin repeating containing protein
TTFA	Thenoyltrifluoroacetone
UV	Ultraviolet
VDAC	Voltage-dependant anion channel
zVAD	Benzyloxycarbonyl-valine-alanine-aspartic acid fluoromethyl ketone
$\Delta\varphi_m$	Mitochondrial transmembrane potential

ABSTRACT

Bz-423 is a non-anxiolytic 1,4-benzodiazepine that ameliorates disease in animal models of lupus, arthritis and psoriasis. Concomitant with these therapeutic effects, Bz-423 induces lineage-specific apoptosis of pathogenic lymphocytes or selectively blocks proliferation of psoriatic skin cells. Mechanistic studies in B cells demonstrated that Bz-423 promotes mitochondrial superoxide ($O_2^{\bullet-}$) production, and the magnitude of this response distinguishes between growth arrest and apoptosis. The Bz-423-induced $O_2^{\bullet-}$ response results from modulation of the F_oF_1-ATPase. Bz-423 binds to the oligomycin sensitivity-conferring protein (OSCP) component of the F_oF_1-ATPase, which causes the rate of ATP synthesis to slow and forces the mitochondrial respiratory chain into a reduced state that favors overproduction of $O_2^{\bullet-}$.

The overarching goal of the experiments described in this dissertation is, therefore, to identify factors underlying the selective effects of Bz-423 on pathogenic cells *in vivo* by elucidating signaling pathways that link elevated mitochondrial $O_2^{\bullet-}$ production to growth arrest or apoptosis. Towards this goal, proteasomal degradation of c-Myc, an oncogenic transcription factor that regulates cell-cycle progression, was identified as an essential component of the mechanism leading to Bz-423-induced growth arrest. While this mechanism was identified in B cells, it likely contributes to the anti-psoriatic activity because c-Myc levels are reduced in psoriatic skin treated with Bz-423.

Although Bz-423 specifically depletes pathogenic $CD4^+$ T cells in the MRL/MpJ-Fas^{lpr} murine model of lupus, the apoptotic response to Bz-423 has been characterized primarily in B cells. To address this point, Bz-423-induced apoptosis was investigated in $CD4^+$ T cell leukemia lines. Unlike some pro-oxidants, Bz-423-induced $O_2^{\bullet-}$ does not cause opening of the mitochondrial permeability transition pore, but instead triggers a specific, extra-mitochondrial cascade marked by increased levels of the pro-apoptototic Bcl-2 family proteins Noxa and Bak. The resulting activation of Bak, commits a cell to die in response to Bz-423 by inducing release of apoptogenic proteins (e.g., cytochrome *c*) sequestered inside mitochondria. Intersection of this apoptotic mechanism with vulnerabilities in autoreactive T cells, including mitochondrial bioenergetic abnormalities favoring overproduction $O_2^{\bullet-}$ and upregulation of Noxa in response to antigenic stimulation, likely underlies the selective depletion of pathogenic lymphocytes *in vivo*.

CHAPTER 1

INTRODUCTION

Mitochondria are central regulators of cell fate: A principle cellular function of mitochondria is to perform oxidative phosphorylation, a process that generates ATP using energy derived from the controlled oxidation of glucose [1]. Because a cell must maintain ATP levels to remain viable, inhibition of oxidative phosphorylation can lead to death [2, 3]. However, mitochondria can influence cell fate by a variety of other mechanisms including release of pro-apoptotic proteins into the cytosol [4], production of reactive oxygen species [5], and regulation of cellular Ca^{2+} levels [6]. Through these effects, mitochondria contribute to a wide variety of cellular process including apoptosis [4], autophagy [7], T cell activation [8], and insulin secretion by pancreatic β-cells [9]. It is not surprising, therefore, that mitochondrial abnormalities are associated with a wide variety of pathological conditions including cancer [10], autoimmune disease (e.g., systemic lupus erythematosus (SLE)) [11], Parkinson's disease [12], Alzheimer's disease [13], as well as the natural process of aging [14]. In addition, a number of small molecules have been identified whose therapeutic effects arise from manipulation of mitochondrial activity [15]. This chapter will introduce key aspects in mitochondrial structure, function and regulation with particular attention paid to mechanisms by which mitochondrial activity can be modulated therapeutically.

Mitochondrial numbers, sub-cellular distribution, and structure: Mitochondria are dynamic organelles – mitochondrial morphology and sub-cellular distribution vary both between cell types and within a particular cell in response to changes in physiological conditions [16]. For example, mitochondria exist as an extended tubular network in endothelial cells such as fibroblasts or hepatocytes [16]. In contrast, mitochondria form discrete "sausage-shaped" units (~3-4 nm in length and ~1 nm in diameter) in lymphocytes (Figure 1.1A and [16-18]). The extended mitochondrial network in endothelial cells is fragmented by the mitochondrial fission machinery (e.g., the dynamin-related GTPase Drp1, the large transmembrane GTPase Mfn2 and the lipid transferase endophillin B1) during mitosis to allow equal distribution of mitochondria between daughter cells [19]. Mitochondrial fragmentation is also observed during apoptosis, although this response is not necessary for cell death (see Chapter 3 Introduction; [20]).

Comparisons of transmission electron microscopy images indicate that mitochondrial numbers vary widely between cell-types [16]. For instance, endothelial cells have ~50 mitochondria per cell, while cardiac muscle cells contain $>10^3$ mitochondria, presumably due to their elevated ATP demands [16]. In contrast, mitochondria are present in lower numbers in lymphocytes [16, 18]. For example, human peripheral blood T cells only contain only three mitochondria on average [21], which presumably contributes to the low level of mitochondrial respiration (i.e., O_2 consumption) in this cell-type [22]. However, mitochondrial mass is increased more than five-fold in T cells 24 h after antigenic stimulation, which corresponds to the elevated energy demands associated with increased proliferation and secretion of immune effector

molecules [23]. In addition, peripheral blood T cells from SLE patients, which are subject to persistent stimulation by self-antigens, have more than eight mitochondria per cell [21]. Hence, mitochondrial numbers are variable between cell-types and appear to be increased when energetic demands are elevated.

Distribution of mitochondria within the cytosol is cell-type dependent [18, 24]. Mitochondria are organized into filaments that surround axons in neurons and contractile fibers in skeletal-muscle cells [25]. In contrast, sperm contain a sheath of mitochondria that surrounds flagella and allows for efficient production of ATP needed to power motility [24]. In many cell-types, mitochondria are found close to the endoplasmic reticulum (ER), which enables rapid equilibration of Ca^{2+} between these two organelles [26]. In addition, mitochondrial sub-cellular distribution can be altered in response to changes in physiological conditions. For example, mitochondria redistribute to the plasma membrane in lymphocytes following antigenic stimulation, where they uptake Ca^{2+} entering the cell through Ca^{2+}-release activated Ca^{2+} (CRAC) channels [27]. Mitochondria then slowly release stored Ca^{2+}, which prevents the initial Ca^{2+} flux from reaching dangerous levels, but also maintains an elevated intracellular concentration of Ca^{2+} ($[Ca^{2+}]_i$) over time [27]. Buffering of the Ca^{2+} flux-induced antigen-receptor stimulation is an example of how mitochondria regulate cell fate independent of ATP synthesis.

Despite the heterogeneity in mitochondrial number and sub-cellular distribution, this organelle displays a conserved structural organization characterized by a double membrane, which defines two internal compartments (Figure 1.1B; [28]). The mitochondrial outer membrane separates bulk cytosol from the mitochondrial inter-

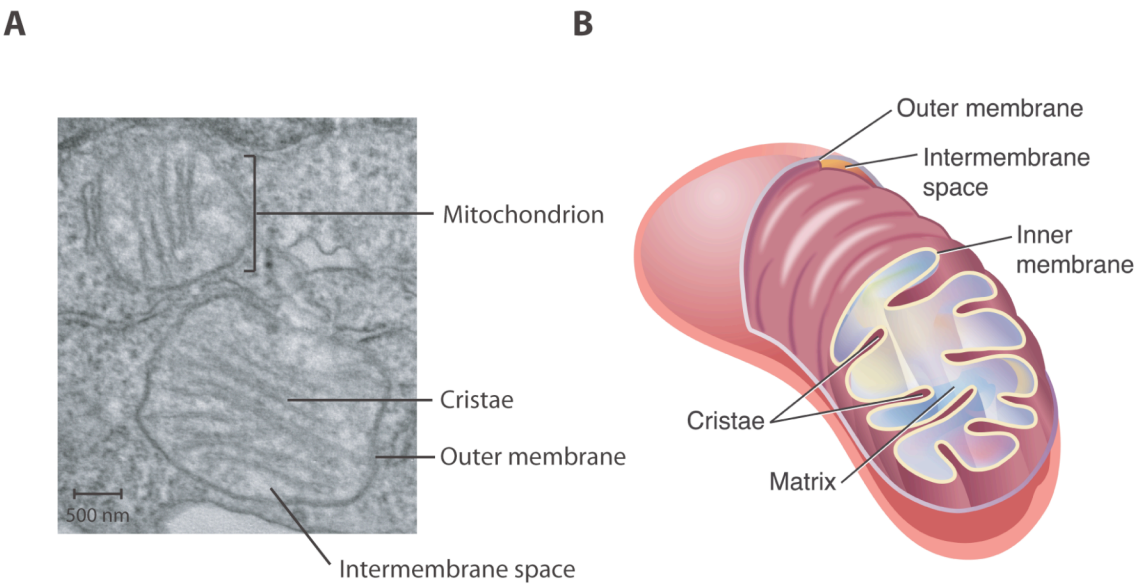

Figure 1.1 - Mitochondrial structural features. (A) Mitochondrial structural features apparent in a transmission electron microscopy image of a CCRF-CEM T cell leukemia cell (13,500x). (B) Mitochondrial structural diagram illustrating key features [29]. Figure adapted from [30]. See text for details.

membrane space (MIS). Due to the presence of non-specific channels (porins) such as the voltage-dependent anion channel (VDAC), the translocase of the outer membrane (TOM), and the peptide-sensitive channel (PSC), the mitochondrial outer membrane is permeable to molecules (e.g., ions, metabolic intermediates and small proteins) with molecular weight <5 kDa [31]. Proteins that trigger apoptosis upon release into the cytosol (e.g., cytochrome *c*,) are sequestered in the MIS [4]. Hence, loss of mitochondrial outer membrane integrity is often the point at which cells are committed to the death in response to apoptotic stimuli (see Chapter 3 Introduction) [32].

The mitochondrial inner membrane lacks porins and is therefore impermeable to charged species, except those with specific transporters such as phosphate (HPO_4^{2-}/OH^-

antiporter) [33], ATP and ADP (adenine nucleotide transporter (ANT)) [34], and Ca^{2+} (mitochondrial Ca^{2+}-uniporter) [35]. Along with these transporters, the mitochondria inner membrane also houses mitochondrial respiratory chain (MRC) complexes, which are described in detail in the following section. The total surface area of the mitochondrial inner membrane is increased due to the presence of multiple folds that form invaginations known as cristae (Figure 1.1; [36]). The compartment within the mitochondrial inner membrane is known as the matrix and houses tricarboxylic-acid (TCA)-cycle enzymes, which provide reducing equivalents to the MRC by oxidizing the glycolysis endproduct, pyruvate [37].

Mitochondrial respiratory chain: The MRC is composed of five complexes, the properties of which are summarized in Table 1.1 [38]. Complexes I-IV are collectively referred to as the electron transport chain (ETC) because they shuttle electrons from NADH (or $FADH_2$) to molecular oxygen [39]. ETC complexes I, III and IV span the mitochondrial inner membrane, while complex II is associated with the matrix face of the mitochondrial inner membrane via two anchor proteins (Figure 1.2; [40]).

Electrons enter the ETC at complex I (NADH dehydrogenase) and II (succinate dehydrogenase) [41-43]. NADH dehydrogenase is composed of 42 subunits and has a total molecular weight >900 kDa, making it the largest of the ETC complexes [44]. Complex I transfers electrons from NADH through a series of flavin-mononucleotides and iron-sulfur (Fe-S) clusters before reducing ubiquinone (Q) to ubiquinol (QH_2) [44]. Transfer of electrons from QH_2 to cytochrome *c* occurs at complex III (ubiquinone-cytochrome *c* oxidoreductase) via a series of redox intermediates including hemes, Fe-S clusters and ubisemiquinone ($QH^{\bullet -}$) [45].

Complex	Name	Reaction Catalyzed
I	NADH-ubiquinone oxidoreductase	$NADH + Q + 5H_i^+ \rightarrow NAD + QH_2 + 4H_o^+$
II	Succinate-ubiquinone oxidoreductase	$succinate + Q \rightarrow fumarate + QH_2$
III	Ubiquinone-cytochrome *c* oxidoreductase	$QH_2 + 2cyt\ c^{3+} + 2H_i^+ \rightarrow Q + 2cyt\ c^{2+} + 2H_o^+$
IV	Cytochrome *c* oxidase	$4cyt\ c^{2+} + 8H_i^+ + O_2 \rightarrow 4cyt\ c^{3+} + 4H_o^+ + H_2O$
V	F_oF_1-ATPase	$ADP + P_i \rightarrow ATP + H_2O$

Table 1.1 – Properties of mammalian mitochondrial respiratory chain complexes. Q and QH_2: oxidized and reduced forms of ubiquinone, respectively. H_i^+ and H_o^+: proton that is on the matrix or MIS side of the mitochondrial inner membrane, respectively. Data for this table is from [46].

Finally, complex IV (cytochrome *c* oxidase) transfers electrons from cytochrome *c* to molecular oxygen, which becomes fully reduced to water [47]. The net pathway within the ETC from NADH to O_2 is depicted below (Equation 1.1).

(1.1)

NADH → **NADH dehydrogenase** → ubiquinone →
cytochrome c oxidoreductase → cytochrome c → **cytochrome c oxidase** → O_2

Complex II is the smallest component of the MRC (molecular weight ~100 kDa) and transfers electrons from the TCA-cycle intermediate succinate to Q via a prosthetic

$FADH_2$ group [48]. Flow of electrons from NADH or $FADH_2$ to O_2 is assured because each intermediate in the ETC has a higher affinity for electrons than its precursors (i.e., redox potentials increase) [49].

Transfer of electrons from NADH or $FADH_2$ to O_2 by ETC complexes I, III and IV is accompanied by transport of protons across the mitochondrial inner membrane from the matrix to the MIS (Figure 1.2; [50]). Proton pumping by complexes I, III and IV converts free energy liberated during the electron transfer reactions to establish an electrochemical gradient of 100-200 mV across the mitochondrial inner membrane [51]. This electrochemical gradient has two components, the difference in the concentration of protons on each side (ΔpH_m), and the electrical potential ($\Delta\psi_m$) [52]. However, $\Delta\psi_m$ is the dominant component because the pH difference between the matrix and MIS is small (~0.5 units), which ensures a nearly neutral pH environment for enzymes in both compartments [53]. Transfer of protons out of the matrix causes this compartment to become negatively charged relative to the MIS. Hence, accumulation of positively-charged dyes (e.g., tetramethyl rhodium methyl ester (TMRM)) in the matrix can be used to monitor changes in $\Delta\psi_m$ [54].

The final component of the MRC is the F_oF_1-ATPase (complex V), which utilizes energy stored in the mitochondrial electrochemical gradient to synthesize ATP from ADP and P_i (see Figure 1.2; [55]). The mammalian F_oF_1-ATPase contains 16 subunits and has a total molecular weight >600 kDa (Figure 1.3). These subunits are classified into three domains (Figure 1.3). The α_3, β_3, γ, δ, and ε subunits are grouped into the F_1 domain, which protrudes into the matrix and contains the catalytic sites for ATP synthesis. The

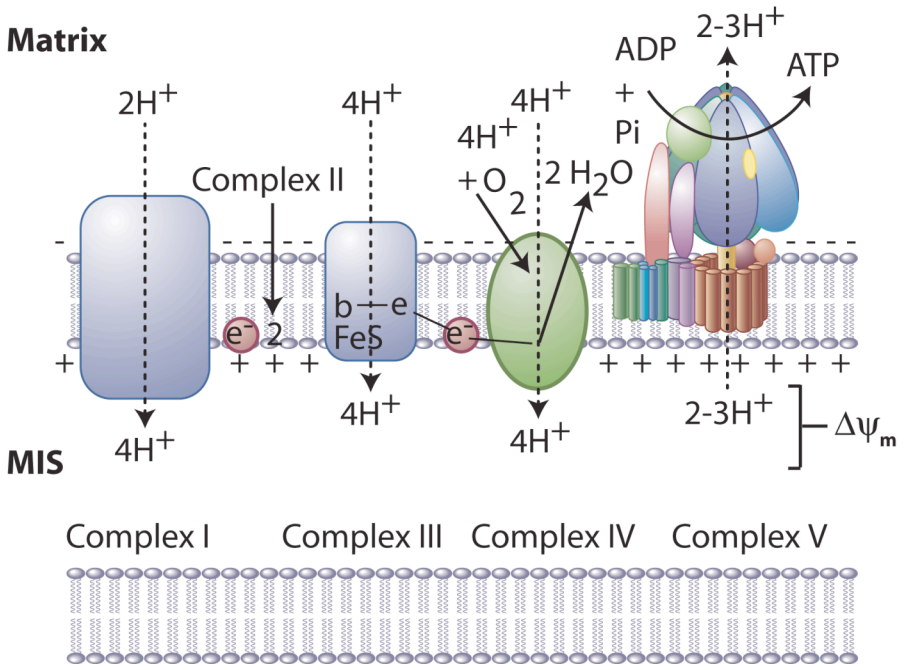

Figure 1.2 – Organization of the mitochondrial respiratory chain. The mitochondrial respiratory chain (MRC) is composed of five complexes. Complexes I, II, III and IV are collectively referred to as the electron transport chain (ETC) because they shuttle reducing equivalents from NADH or $FADH_2$ to O_2. Electron transport within complexes I, III and IV is coupled to pumping of protons from the matrix to the mitochondrial intermembrane space (MIS), which results in formation of an electrochemical gradient ($\Delta\psi_m$) across the mitochondrial inner membrane. Once in the MIS, protons return to the matrix through complex V, the F_oF_1-ATPase. This passage of protons supplies the energy necessary for synthesis of ATP by the F_oF_1-ATPase. See text for further detail. Figure adapted from [56].

membrane imbedded F_o domain is composed of the $c_{10\text{-}12}$ ring along with a number of accessory subunits. The F_1 and F_o domains are linked by a peripheral stalk, which contains subunits b, d and the oligomycin sensitivity-conferring protein (OSCP) (Figure 1.3).

Energy required for synthesis of ATP by the F_oF_1-ATPase is derived from passage of protons from the matrix to the MIS via a channel adjacent to the $c_{10\text{-}12}$ ring in F_o

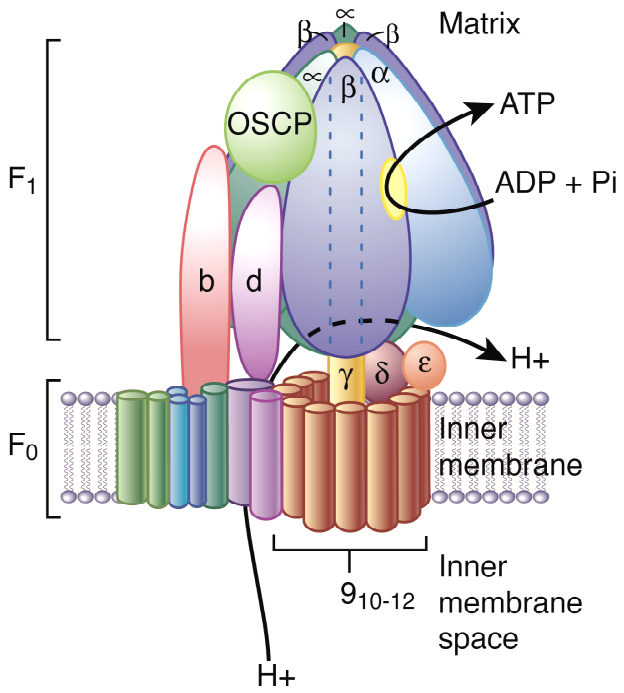

Figure 1.3 – Proposed structure of the mammalian F_oF_1-ATPase. The F_oF_1-ATPase is composed of three of three domains – a soluble F_1 domain that contains the catalytic sites for ATP synthesis, an insoluble F_o domain containing the proton channel, and the peripheral stalk (subunits b, d and the oligomycin sensitivity-conferring protein (OSCP)) which links F_1 and F_o. See text for additional detail. Figure adapted from [57].

(Figure 1.3; [57]). Passage of protons through F_o channel causes the central portion of the F_oF_1-ATPase ($c_{10\text{-}12}$, γ, δ, and ε) to rotate relative to the surrounding subunits [55]. Resulting changes in the orientation of γ relative to the $\alpha_3\beta_3$ hexamer induces conformational changes in the β subunits that drive ATP synthesis [55]. The peripheral stalk acts as a stator that maintains orientation of the $\alpha_3\beta_3$ hexamer in one orientation while γ rotates [57]. Hence, synthesis of ATP by the F_oF_1-ATPase is coupled to the $\Delta\psi_m$ generated by the ETC via by passage of protons through F_o.

Mitochondrial respiration: As described above, synthesis of ATP by the F_oF_1-ATPase depends on the electrochemical gradient established by the ETC. However, changes in F_oF_1-ATPase activity can also affect electron transport by the ETC. Protons are unable to pass through the F_o channel when the F_oF_1-ATPase is inactive, which results in their accumulation in the MIS and hyperpolarization of $\Delta\psi_m$ (>150 mV) [58, 59]. The increase in proton motive force under these conditions makes pumping of protons from the matrix to the MIS energetically disfavored [43]. As a result, electron transport within the ETC slows when F_oF_1-ATPase activity is suppressed. This decrease in ETC activity is often measured in terms of mitochondrial respiration (i.e., O_2 consumption) because molecular oxygen is the terminal electron acceptor within the chain [60].

This relationship between F_oF_1-ATPase and ETC activity was first characterized in experiments examining O_2 consumption by isolated mitochondria [61]. This approach identified four respiratory states based on the order reagents are added to an O_2 electrode (Table 1.2). In state 1, isolated mitochondria were incubated in buffer containing P_i, but lacking ADP or substrates for the ETC. As a result, the rate of O_2 consumption is low during State 1. State 2 results from addition of ETC substrates, which is marked by generation of $\Delta\psi_m$ due to proton pumping by complexes I, III and IV. However, the rate of O_2 consumption remains low during state 2 because the F_oF_1-ATPase is inactive. Addition of ADP then stimulates F_oF_1-ATPase activity, which decreases $\Delta\psi_m$ and increases O_2 consumption. This respiration state marked by high rates of O_2 consumption and ATP synthesis is termed state 3. F_oF_1-ATPase activity is again reduced when all of the ADP is converted to ATP. As a result, $\Delta\psi_m$ increases and O_2 consumption decreases

Respiratory State	Characteristics
1	Mitochondria in buffer containing only P_i (low respiratory rate)
2	ETC substrates added (low respiratory rate due to lack of ADP)
3	Addition of ADP (high respiratory rate)
4	All ADP converted to ATP (respiratory rate slows)

Table 1.2 - Mitochondrial respiratory states. See text for details. Table based on data from [61].

as mitochondria enter state 4. Thus, suppression of F_oF_1-ATPase activity can lead to slowing of electron transport by the ETC due to accumulation of protons in the MIS.

Production of superoxide $O_2^{\bullet-}$ by the electron transport chain: $O_2^{\bullet-}$ is produced via the single-electron reduction of molecular oxygen [62]. This reactive oxygen species (ROS) is a constituitive byproduct of oxidative phosphorylation owing to the presence of reactive intermediates (e.g., Fe-S clusters, flavoproteins and ubisemiquinones ($QH^{\bullet-}$)) competent for the one-electron reduction of O_2 [43]. These reactive intermediates are sequestered within ETC complexes in the mitochondrial inner membrane to minimize release of electrons to O_2 [42]. Nevertheless, between 0.5-3% of O_2 consumed during state 3 respiration is converted to $O_2^{\bullet-}$ [63-65].

Production of $O_2^{\bullet-}$ is enhanced under conditions where F_oF_1-ATPase activity is suppressed, but the ETC remains active (e.g., state 4 respiration). As described above, decreased F_oF_1-ATPase activity prevents passage of protons through the F_o channel, which results in their accumulation of the MIS and hyperpolarization of $\Delta\psi_m$ (>150 mV). The increase in proton motive force under these conditions makes pumping of protons from the matrix to the MIS energetically disfavored. As a result, electron transport

slows, which causes reactive intermediates throughout the ETC to be more reduced on average [43]. The extended half-life of reactive intermediates (e.g., Fe-S clusters, flavoproteins and ubisemiquinones) capable of donating an electron to molecular oxygen then leads to increased production of O_2^- [43].

Although single-electron reduction of molecular oxygen can in principle occur throughout the ETC, studies with isolated mitochondria suggest that complexes I and III are the primary sources of $O_2^{\bullet-}$ [66-68]. Production of $O_2^{\bullet-}$ by complex I has been studied primarily using the rodenticide rotenone, which inhibits the passage of electrons from the terminal Fe-S cluster to ubiquinone (Figure 1.4; [69]). This block leaves proximal complex I intermediates in a reduced state and Fe-S centers [70, 71], flavin mononucleotide co-factors [72] as well as an enzyme-bound NADH [73] have all been implicated as the source of $O_2^{\bullet-}$ production. Regardless of the reactive intermediate(s) involved, these studies have demonstrated that production of $O_2^{\bullet-}$ by complex I occurs solely into the mitochondrial matrix (Figure 1.4; [68, 69, 72, 74-78]).

Complex III, by contrast, can release $O_2^{\bullet-}$ into both the matrix and MIS (Figure 1.4). During active respiration ubisemiquinones ($UQ^{\bullet-}$) are generated transiently at reaction centers on the matrix and MIS faces of complex III [79]. Autooxidation of $UQ^{\bullet-}$ can lead to production of $O_2^{\bullet-}$ (Reaction 1.2). Thus, release of O_2^- by complex III increases in response to conditions that extend the half-life of the $UQ^{\bullet-}$ intermediates [79].

(1.2) $$UQ^{\bullet-} + O_2 \rightarrow Q + H^+ + O_2^{\bullet-}$$

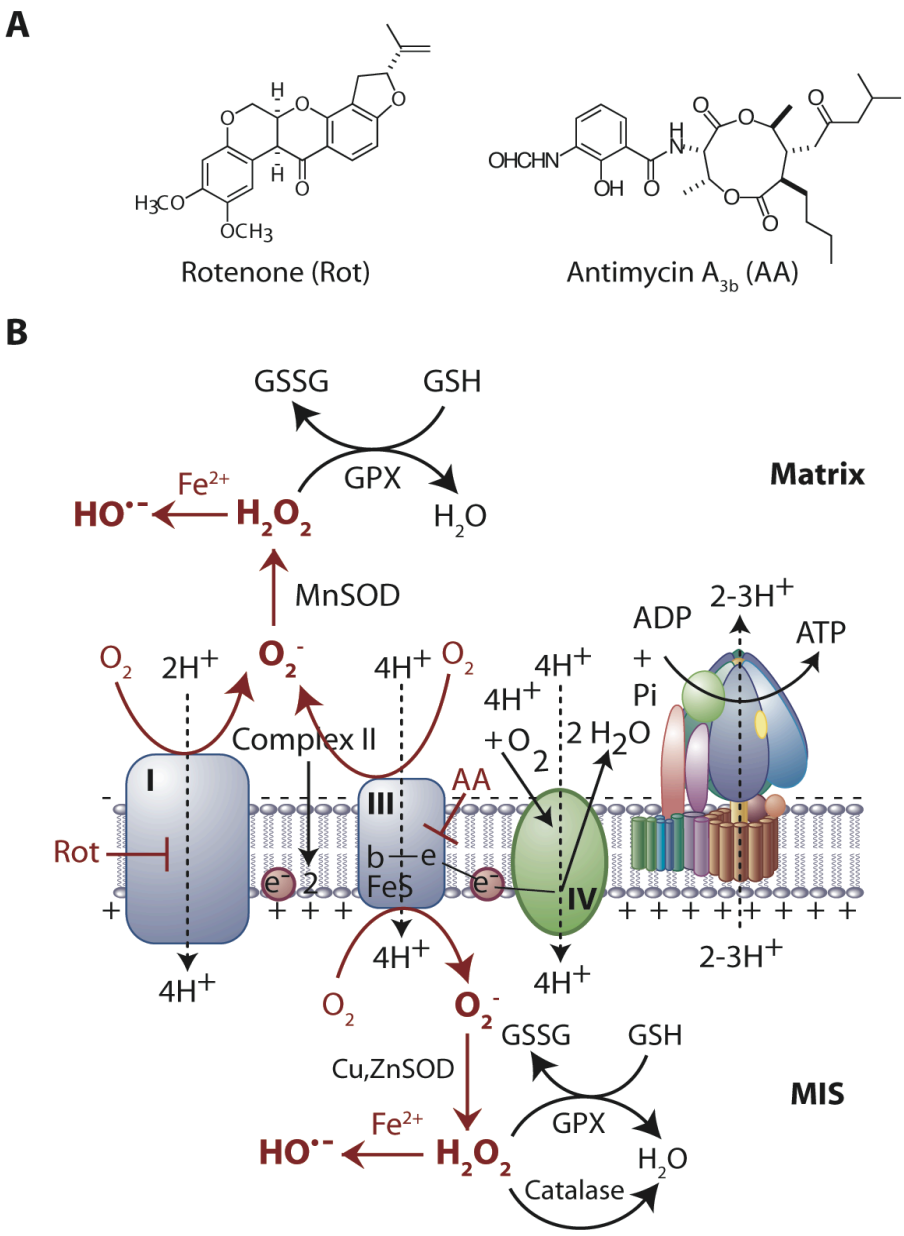

Figure 1.4 – Production of $O_2^{\bullet-}$ by the electron transport chain. (A) Chemical structure of the complex I inhibitor rotenone and the complex III inhibitor antimycin A. (B) Complexes I and III are the primary centers of $O_2^{\bullet-}$ production in the ETC. Rotenone blocks ubiquinol (QH_2) reduction by complex I, which leads to release of $O_2^{\bullet-}$ into the mitochondrial matrix. Complex III shuttles electrons from QH_2 to cytochrome c via a cyclic series of reactions. Antimycin A blocks regeneration of QH_2, which leads to accumulation of ubisemiquinone intermediates on the matrix and MIS face of complex III, and release of $O_2^{\bullet-}$ into both compartments. Once formed, $O_2^{\bullet-}$ is converted to H_2O_2 via MnSOD in the matrix and Cu,ZnSOD in the MIS. H_2O_2 is further reduced to water by catalase and/or glutathione peroxidase (GPX) or to hydroxyl radical ($HO^{\bullet}$) by Fenton-like chemistry. See text for further detail. Figure adapted from [26].

For instance, the antibiotic antimycin A inhibits oxidation of $QH^{\bullet-}$ to Q at the reactive site on the matrix face of complex III [80]. Because distal electron transfer reactions are not impaired in the presence of antimycin A, $QH^{\bullet-}$ intermediates accumulate at reaction centers adjacent to both the matrix and MIS reaction centers, and release of $O_2^{\bullet-}$ into both compartments (Figure 1.4; [42, 67, 81]). Production of $O_2^{\bullet-}$ by the ETC is considered in more detail in the discussion for Chapter 3.

Characteristics of reactive oxygen species: Due to the presence of an unpaired electron, $O_2^{\bullet-}$ is more reactive than molecular oxygen. For example, $O_2^{\bullet-}$ oxidizes Fe-S clusters at rates that are often diffusion limited [82]. In this reaction, reduction of $O_2^{\bullet-}$ to H_2O_2 is tied to conversion of Fe^{2+} to Fe^{3+}, which can then be released from the Fe-S cluster [83]. The TCA-cycle enzyme aconitase is inactivated by $O_2^{\bullet-}$ due to oxidation of the solvent exposed Fe-α within the catalytic site $[4Fe\text{-}4S]^{2+}$ cluster (k ~5 x 10^6 $M^{-1}s^{-1}$) [84]. Thus, aconitase inactivation represents a sensitive assay for increased levels of $O_2^{\bullet-}$ in the mitochondrial matrix [77, 84, 85].

In addition to oxidation of Fe-S clusters, $O_2^{\bullet-}$ is rapidly converted into hydrogen peroxide (H_2O_2) either by spontaneous dismutation (k ~4.5 x 10^5 $M^{-1}s^{-1}$) at physiological pH or through a reaction catalyzed by superoxide dismutases (SODs) [83]. In the mitochondrial matrix, this reaction is accomplished by an SOD containing a manganese co-factor (MnSOD; k ~1.2 x 10^9 $M^{-1}s^{-1}$), while another isoform (Cu,Zn-SOD; k ~0.6 x 10^9 $M^{-1}s^{-1}$) is present in the cytosol and MIS (Figure 1.4; [83]). $O_2^{\bullet-}$ also reacts with thiols, however, this process is disfavored *in vivo* because it is slow (1 - 10^3 $M^{-1}s^{-1}$) relative to Fe-S cluster oxidation or dismutation into H_2O_2 [86]. Due to rapid oxidation of Fe-S

clusters or conversion to H_2O_2 via dismutation reactions, cellular $O_2^{\bullet-}$ concentrations are estimated at $<10^{-11}$ M [87].

H_2O_2 can also oxidize Fe-S clusters, but this process is slow (k ~1-10^2 $M^{-1}s^{-1}$) relative to the oxidation of cysteine thiols (Cys-SH) to sulfenic acids (Cys-SOH), which occurs at rates up to 10^6 $M^{-1}s^{-1}$ [88]. Once formed, Cys-SOH groups can condense with vicinal Cys-SH to form disulfide linkages [88]. In addition, H_2O_2 can further oxidize Cys-OH groups to sulfinic (Cys-SO_2H) or sulphonic (Cys-SO_3H) acids [88]. Because sulfenic acid formation is mediated by nucleophilic attack on the peroxide bond, thiolate anions (Cys-S^-) are more reactive than their protonated counterparts [89]. Consequently, reaction rates of cysteines with H_2O_2 vary widely (k ~10-10^6 $M^{-1}s^{-1}$), depending on the local protein environment [88, 89]. Neighboring positively charged residues, which lower the thiol pK_a by stabilizing the resulting Cys-S^-, enhance reactivity [89]. Differences in the reactivity of cysteine thiols with H_2O_2 appear to confer selectivity *in vivo*. For instance, because a specific set of proteins were found to contain oxidized Cys-SH residues in a proteome-wide study of peripheral blood T cells pulsed with H_2O_2 (1 mM) for 5 minutes [90].

While $O_2^{\bullet-}$ and H_2O_2 display specificity in terms of their biological targets, hydroxyl radical ($HO^{\bullet}$) indiscriminately reacts with carbohydrates, lipids, proteins, and DNA at rates that are diffusion-limited (k ~10^9) [91, 92]. $HO^{\bullet}$ is generated by reduction of H_2O_2 via metal-based Fenton chemistry (Reaction 1.3; [93]).

(1.3) $$H_2O_2 + Fe^{2+} \rightarrow HO^{\bullet} + HO^- + Fe^{3+}$$

$HO^{\bullet}$ can oxidize cysteine thiols, add to alkenes, and extract hydrogen atoms from saturated carbons [93]. The resulting carbon-centered radicals can then form cross-links with other biological macromolecules [93]. In addition, $HO^{\bullet}$ can damage DNA by degrading nucleotides and cleaving phosphodiester linkages [91]. Because of these properties, the toxicity effects of $[H_2O_2]$ >1 mM (e.g., lipid peroxidation) are thought to primarily result from $HO^{\bullet}$ formation [91, 93].

To limit the deleterious production of $HO^{\bullet}$ by Fenton chemistry, H_2O_2 is reduced to water by two cellular antioxidant systems. These are the enzyme catalase, which is present in the cytosol and MIS, and catalyzes dismutation of H_2O_2 to H_2O and O_2 (Figure 1.4; [94]). In addition, glutathione peroxidase (GPX) can reduce H_2O_2 using electrons generated from oxidation of the tripeptide γ-glutamyl-cysteinyl-glycine (glutathione; (GSH)) to the corresponding disulfide (GSSG) [95]. GSH is synthesized by the sequential actions of γ-glutamyl-cysteine synthetase and glutathione synthetase and is present in millimolar concentrations (0.5-10 mM) in both the mitochondria and the cytosol [96]. Regeneration of GSH is mediated by glutathione reductase (GPR), which reduces GSSG using electrons derived from NADH (Figure 1.4; [96]). Glutathione peroxidase/reductase couples are present in the matrix, cytosol and MIS [95]. Together, catalase and GPX maintain steady-state H_2O_2 levels at $<10^{-7}$ M [82].

In addition to differences in their chemical reactivity, $O_2^{\bullet-}$ and H_2O_2 vary in terms of their lipid solubility. Because $O_2^{\bullet-}$ is charged it cannot diffuse through lipid bilayers, while H_2O_2 is neutral and therefore lipid soluble [62]. As described above, the mitochondrial inner membrane is highly impermeable to charged species in the absence of specific transporters [34] As a result, $O_2^{\bullet-}$ released into the mitochondrial matrix is

unable to escape from this compartment [97]. The inability of $O_2^{\bullet-}$ to escape from the matrix explains the lack of $O_2^{\bullet-}$ release from isolated mitochondria following inhibition of complex I with rotenone [82, 98]. In contrast, the $O_2^{\bullet-}$ dismutation product H_2O_2 can diffuse through the mitochondrial inner membrane [91]. Thus, the increase in matrix $O_2^{\bullet-}$ levels induced by inhibition of complex I with rotenone is detected results in enhanced release of H_2O_2 from mitochondria [74, 77].

While $O_2^{\bullet-}$ is usually trapped in the matrix, it can escape from the MIS [99, 100]. Experiments using the electron-paramagnetic resonance (EPR) spin trap 5,5'-dimethyl-1-pyrroline-*N*-oxide (DMPO) to detect $O_2^{\bullet-}$ released from isolated mitochondria indicate that this ROS escapes the MIS at rate of ~0.04 nmol/min/mg protein during state 3 respiration [101]. Consistent with data indicating that complex III releases $O_2^{\bullet-}$ into both the matrix and MIS, the rate of $O_2^{\bullet-}$ production by from isolated mitochondria is increased more than eight-fold in the presence of antimycin A [101]. Transport of $O_2^{\bullet-}$ out of the MIS is likely mediated by porins in the mitochondrial outer membrane [31]. In particular, the VDAC appears to play a role in $O_2^{\bullet-}$ transport, because inhibition of this porin with 4,4'-diisothiocyanon-2,2-disulfonic acid stilbene (DIDS) reduced release of $O_2^{\bullet-}$ from isolated mitochondria treated by >50% [101]. Hence, both $O_2^{\bullet-}$ released from the ETC and its dismutation product H_2O_2 can escape from the mitochondria and modulate biological processes external to this organelle.

Redox-regulated signaling cascades: As described above, $O_2^{\bullet-}$ released from the ETC, along with its dismutation product H_2O_2, can escape from mitochondria into the surrounding cellular environment [91, 100, 101]. O_2^{-} can also be produced by plasma membrane NADPH oxidases [102, 103]. This enzyme complex is composed of six

proteins that house an enzyme-bound FAD and two heme groups that shuttle reducing equivalents from NADPH to O_2 [102, 103]. NADPH oxidases were first characterized in phagocytic cells (e.g., macrophages, neutrophils, and dendritic cells) that release $O_2^{\bullet-}$ in response to pathogen ingestion [104, 105]. Plasma membrane NADPH complexes have been characterized on a variety of non-phagocytic cells, including lymphocytes [106], fibroblasts [107], endothelial cells [108], vascular smooth muscle cells [109], and cardiac myocytes [110]. These non-phagocytic NADPH oxidase isoforms produce $O_2^{\bullet-}$ in lymphocytes subject to antigenic stimulation or endothelial cells stimulated with growth factors [106, 111, 112]. Spontaneous or Cu,Zn-SOD-mediated dismutation of $O_2^{\bullet-}$ then leads to elevation of intracellular H_2O_2 levels [83]. Although cells contain other redox active enzymes, including xanthine oxidase, monoamine oxidase, cyclooxygenase and cytochrome P450s, the mitochondrial ETC and plasma membrane NADPH oxidases are thought to be the primary sources of intracellular ROS [112].

Once present in the cytosol $O_2^{\bullet-}$, H_2O_2 and other forms of oxidative stress (e.g., GSH-derivatizing agents) can have effects on cells ranging from promoting survival and proliferation to induction of growth arrest and cell death [82, 112-115]. Many of the effects are mediated activation of mitogen-activated protein kinase (MAPK) cascades [113]. MAPK signaling involves sequential activation of mitogen-activated protein kinase kinase kinase (MAPKKK), mitogen-activated protein kinase kinase (MAPKK), and MAPK [116, 117]. Eukaryotic cells have three primary MAPK pathways, which are defined by the kinase activated at the end of the cascade – extracellular signal-regulated kinase (ERK), c-Jun amino-terminal kinase (JNK) and p38 MAPK (Figure 1.5; [116, 117]). Activation of ERK is generally associated with increased proliferation and

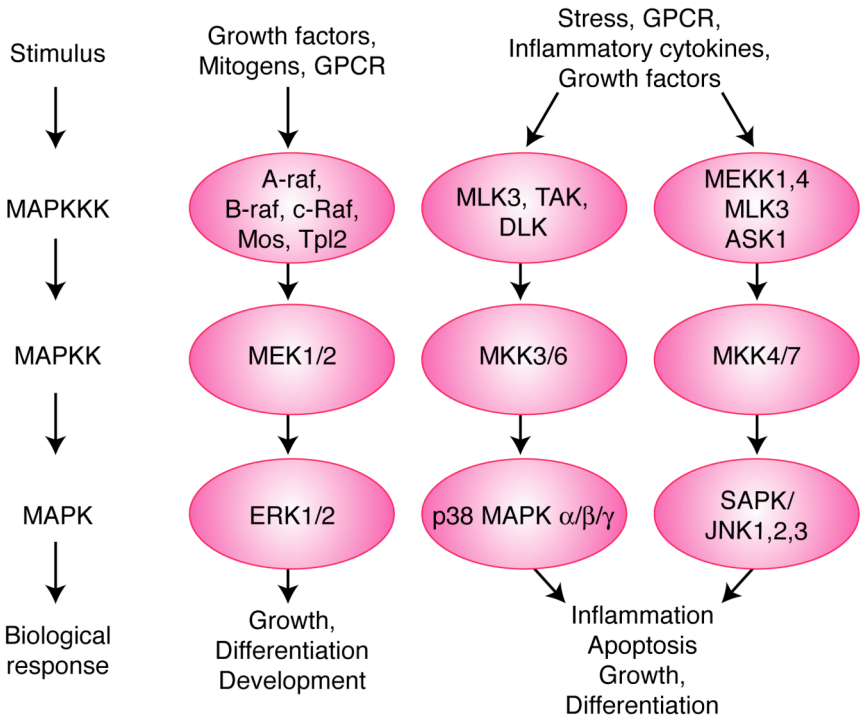

Figure 1.5 – Mitogen-activated protein (MAP) kinase signaling pathways. MLK, mixed lineage kinase; MEKK, MAP/ERK kinase kinase, TGF-β activated kinase; MKK, MAP kinase kinase; MEK, MAP kinase/ERK kinase; DLK, dual leucine-zipper bearing kinase. Figure adopted from [116].

enhanced survival, whereas activation of the JNK and p38 MAPK pathways can lead to growth arrest and apoptosis [118]. Therefore, JNK and p38 MAPK are often collectively referred to stress-activated protein kinases (SAPK) [118]. The balance between ERK and JNK/p38 signaling often dictates whether a cell will proliferate or die [118].

Redox-regulation of the ERK1/2 pathway has been primarily studied in the context of growth factor (GF) signaling in endothelial cell-types [119-121]. Epidermal growth factor (EGF), insulin-like growth factor (IGF), platelet-derived growth factor (PDGF) and vascular endothelial growth factor (VEGF) transmit their effects through binding to their cognate receptor tyrosine kinases (RTK) [122]. Engagement of GF receptors triggers autophosphorylation of intracellular domain tyrosine residues, which

leads to recruitment of adaptor molecules (e.g., the small GTPase Ras) and activation of the MAPKKK Raf-1 [123]. Activated Raf-1 then phosphorylates MAP/ERK kinase kinase-1/2 (MEK1/2), which in turns, phosphorylates and activates ERK1/2 (Figure 1.5; [116, 117]). Activation of ERK1/2 is countered by protein tyrosine phosphatases (PTPs), which limit recruitment of Ras and Raf-1 by dephosphorylation GF receptor tyrosine residues [121].

GF stimulation also leads to an increase in intracellular $O_2^{\bullet-}$ and H_2O_2 levels [124-126]. This ROS response is thought to result from activation of non-phagocytic plasma membrane NADPH oxidases and is essential for GF signaling [126]. If the H_2O_2 burst that results from stimulating of human umbical vein endothelial cells (HUVECs) is scavenged with anti-oxidants (e.g., vitamin E or the GPX mimic Ebelsen) ERK1/2 phosphorylation is blocked [124, 125]. Conversely, incubation of HUVECs or the mouse kidney cell line TKPTS with concentrations of H_2O_2 between 0.01 - 0.2 mM induces ERK1/2 phosphorylation in the absence of GFs [111, 127]. Induction of ERK1/2 phosphorylation appears to be a selective property of H_2O_2. This has been demonstrated in human umbilical cord endothelial cells (HUVECs) using either the Cu-chelator ATN-224 or reduction Cu,ZnSOD expression by siRNA knockdown [111]. Either mechanism of suppressing Cu,ZnSOD activity elevated intracellular $O_2^{\bullet-}$ levels at the expense of H_2O_2 levels [111]. These changes in basal ROS levels were accompanied by a decrease in basal levels of phospho-ERK1/2 [111]. In addition, suppressing Cu,Zn-SOD activity with ATN-224 blocked the increases in ERK1/2 phosphorylation observed in HUVECs or A431 human epithelial carcinoma cells following stimulation EGF [111].

Activation of ERK1/2 by H_2O_2 added exogenously or produced in response to GF stimulation is thought to result from inactivation of protein tyrosine phosphatases (PTPs) [112], which dephosphorylate tyrosine residues on the intracellular domains of GF receptors [121]. PTPs contain a conversed catalytic site Cys-SH residue, which has a pKa lower than that of GSH ((<5.4 versus 8.8 pKa units, respectively; [119]) due to the presence of neighboring residues with positively-charged side chains [119-121]. The pKa of this Cys-SH increases its reactivity with H_2O_2 by stabilizing the Cys-S^- anion (see above). As a result, the PTPs Cdc25B and PTP1B are oxidized in HUVECs treated with H_2O_2 (0.1 mM) or stimulated with VEGF [111]. Together, these studies suggest a mechanism where GF stimulation leads to an increase in intracellular $O_2^{\bullet-}$ levels, which after conversion to H_2O_2 potentiates GF signaling (e.g., ERK1/2 activation) by inactivating PTPs. In support of this hypothesis, inhibition of Cu,Zn-SOD with ATN-224 reduces phosphorylation of an intracellular tyrosine residue on the EGF receptor in HUVECs stimulated with EGF [111].

The SAPK JNK and p38 can also be activated in response to oxidative stress. Increased phosphorylation of JNK and p38 MAPK in response to H_2O_2 has been demonstrated in a variety of cell types, including fibroblasts [128], intestinal epithelial cells [129], mouse kidney cells [127], and Jurkat T cells [120]. Activation of JNK and/or p38 MAPK often occurs at higher concentrations of H_2O_2 than those required to stimulate activation of ERK1/2 [113]. For example, treatment of the mouse kidney TKPTS cells to concentrations of H_2O_2 between 0.01 - 0.2 mM for 1 h increases phospho-ERK1/2 levels and stimulates proliferation [127]. In contrast, exposure to >0.2 mM H_2O_2 for 1 h or 0.01 - 0.2 mM H_2O_2 for 12 h causes activation of JNK and apoptotic cell death [127]. A

functional contribution of JNK to this response was demonstrated by transfection of TKPTS cells with a kinase-dead JNK (i.e., dominant-negative) construct, which blocked apoptosis induced by concentrations H_2O_2 between 0.2 - 1 mM [127]. At concentrations >1 mM H_2O_2 induced necrosis due to non-specific oxidation of phospholipids [127]. These studies have led to development of a model wherein transient, low levels of H_2O_2 stimulate growth by activating ERK1/2, while sustained and/or high levels of H_2O_2 trigger apoptosis by activating the JNK and p38 MAPK [113].

Apoptosis signal-regulated kinase-1 (ASK1) is a MAPKKK upstream of JNK and p38 MAPK that is increasingly recognized as a cytosolic redox sensor [130, 131]. In unstressed cells, ASK1 is sequestered in an inactive complex with thioredoxin-1 (Thx-1), a small (12 kDa) protein that contains two redox-sensitive Cys-SH residues [132]. Various forms of oxidative stress disrupt the ASK1•Thx complex, which is the rate-limiting step in a series of modifications including homo-oligomerization and *trans*-autophosphorylation that eventually results in activation of ASK1 [133, 134]. Once activated, ASK1 promotes apoptosis by phosphorylating MAPKK 3/6 and 4/7, which then results in activation of JNK and p38 (Figure 1.5; [116, 117]). Disruption of the ASK1•Thx complex is observed in mouse embryonic fibroblasts (MEFs) following treatment with H_2O_2, the thiol-crosslinking reagent diamide, or *tert*-butyl hydroperoxide [131, 135]. Indicative of a functional role for ASK1 as an upstream redox-sensor, MEFs lacking this MAPKKK are resistant to apoptosis induced these forms of oxidative stress [131, 135].

Along with peroxides and thiol-crosslinking reagents, $O_2^{\bullet-}$ itself appears capable of activating ASK1 [113, 131, 134, 136]. Binding of the inflammatory cytokine tumor

necrosis factor-α (TNF-α) to its cognate receptor stimulates plasma membrane NADH oxidases and leads to a burst of $O_2^{\bullet-}$ production [137]. Dissociation of ASK1•Thx complexes and downstream activation of JNK is observed in MEFs, HT1080 human fibroscarcoma cells, and Jurkat T cell leukemia cells in response to TNF-α [131, 134, 136]. A specific role for $O_2^{\bullet-}$ in TNF-α-induced activation of ASK1 has been demonstrated by scavenging this ROS with the MnSOD mimetic Mn(III) *tetrakis* (4-benzoic acid) porphyrin (MnTBAP) in HT1080 cells [136]. In addition to TNF-α, $O_2^{\bullet-}$ dependent activation of ASK1 and apoptosis has been described in Jurkat T cells treated methyl glyoxal, a toxic glycolytic byproduct that inhibits SODs and GPX [138]. Thus, ASK1 is a cytosolic redox sensor capable of signaling apoptosis via activation of JNK/p38 MAPK signaling in response to both $O_2^{\bullet-}$ and H_2O_2.

Other cell signaling pathways besides the MAPK cascades are also redox-sensitive [112, 113]. One prominent example is the serine/threonine kinase Akt, which promotes survival and proliferation (see Chapter 3 Introduction; [139, 140]). Activation of Akt requires phosphorylation of Thr308 and Ser473 to stabilize the catalytic domain [139]. These phosphorylation events require recruitment of Akt to the plasma membrane via interactions between its amino-terminal Pleckstin homology (PH) domain and the lipid second messenger phosphatidylinositol-3,4,5-triphosphate (PtdIns(3,4,5)P_3) [139]. Plasma-membrane PtdIns(3,4,5)P_3 levels are determined by the balance of activity of phosphatidylinositol-3-kinase (PI3K) lipid kinases and lipid phosphatases such as PTEN, the phosphatase and tensin homolog deleted on chromosome 10 (Figure 1.6; [139]).

Similar to PTPs, PTEN contains a conserved catalytic site Cys-SH residue that is essential for activity [141]. Treatment of recombinant PTEN with H_2O_2 (0.2 mM) leads

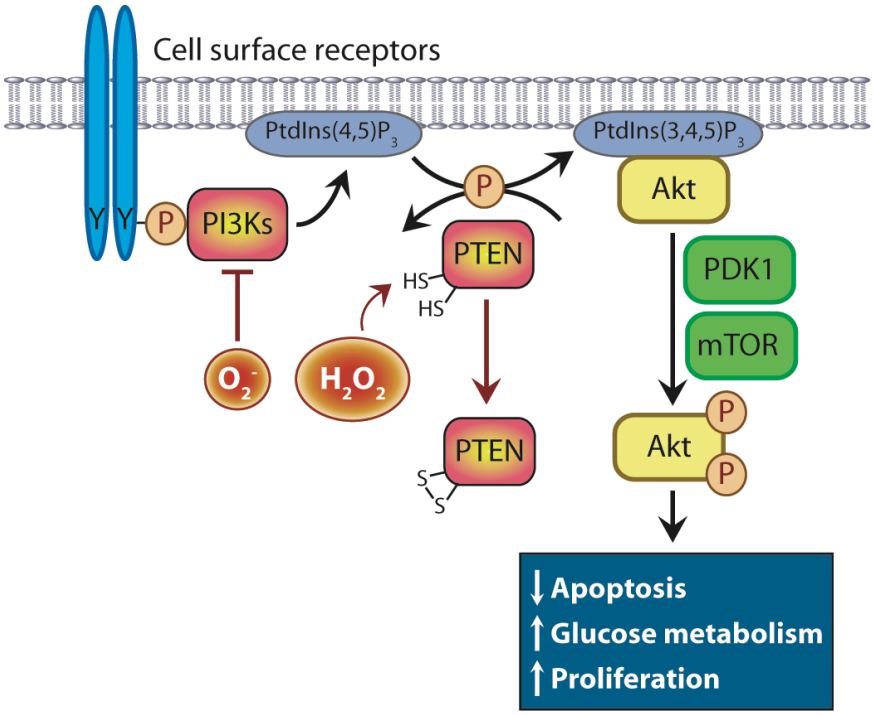

Figure 1.6 – $O_2^{\bullet-}$ and H_2O_2 differentially regulate activation of Akt. Engagement of cell-surface receptors leads to autophosphorylation of tyrosine residues (Y) on their intracellular domains and recruitment of the lipid kinase, phosphatidylinositol-3-kinase (PI3K). PI3K generates membrane-bound PtdIns(3,4,5)P_3) by direct phosphorylation of Ptd(4,5)P_3. The lipid second messenger PtdIns(3,4,5)P_3 acts as a docking platform for the pleckstin-homolog-domain containing kinase Akt. Phosphorylation of membrane-associated Akt by pleckstrin-domain kinase1 (PDK1) and mammalian target or rapamycin (mTOR) promotes activity by stabilizing the kinase domain. Once activated, Akt suppresses apoptosis, upregulates glucose metabolism and stimulates proliferation. Activation of Akt is opposed by the lipid phosphatase PTEN, which converts PtdIns(3,4,5)P_3 to PtdIns(4,5)P_3. H_2O_2 promotes Akt phosphorylation (activation) by oxidation cysteine residues in the catalytic site of PTEN, which permits accumulation of PtdIns(3,4,5)P_3 and the resulting activation of Akt. In contrast, $O_2^{\bullet-}$ leads to decrease in phospho-Akt levels. Constitutively-membrane targeted Akt constructs are insensitive to $O_2^{\bullet-}$ induced dephosphorylation, which suggests that $O_2^{\bullet-}$ interferes with PI3K recruitment and/or activity. See text for additional detail.

to oxidation of this residue to the corresponding Cys-SOH, which can then condense with a vicinal Cys-SH (Figure 1.6; [142]). The resulting disulfide bond inactivates PTEN and is associated with a change in electrophoretic mobility [142]. Inactivation of PTEN is

also observed *in vivo* following exposure of HEK 293 or the Raji Burkitt's lymphoma B cell line to H_2O_2 (0.5 mM) [143, 144]. Inactivation of PTEN leaves PI3K activity unopposed and the resulting increase in PtdIns(3,4,5)P_3 levels leads to activation of Akt (Figure 1.6; [139]). Oxidative activation of Akt is also observed in Raji B cells treated with the complex I inhibitor rotenone or renal proximal tubular cells exposed to the pro-oxidant toxin 2-dichlorovinyl cysteine [144, 145]. In both cases, Akt activation is thought to act a compensatory survival stimulus, in part due to inhibitory phosphorylation of ASK1 [146].

In contrast to the stimulatory effects of H_2O_2 on Akt activity, elevated intracellular $O_2^{\bullet-}$ levels decrease phosphorylation of PtdIns(4,5)P_3, and thereby, activation of Akt (Figure 1.6). For example, the estrogen metabolite 2-methoxyestradiol (2ME) causes accumulation of $O_2^{\bullet-}$ by a mechanism thought to involve inhibition of SODs [147, 148]. 2ME induced $O_2^{\bullet-}$ leads to a decrease in Akt phosphorylation in Jurkat T cells, which have elevated basal phospho-Akt levels due to deficient expression of PTEN [147, 149]. Similarly, the mitochondrial pro-oxidant arsenic trioxide (As_2O_3, Trisenox) has been shown to induce $O_2^{\bullet-}$-dependent dephosphorylation of Akt in the CCRF-CEM T cell leukemia line, which also lacks PTEN [150]. In either case, inactivation of Akt by $O_2^{\bullet-}$ appears to result from suppression of PI3K activity because expression of a myristolated Akt construct that is targeted to the plasma independent of PtdIns(3,4,5)P_3 levels preserves phospho-Akt levels in the presence of 2ME or Trisenox [147, 150]. In addition, expression of the membrane-targeted Akt construct blocks 2ME or Trisenox induced apoptosis, which argues for a functional role for $O_2^{\bullet-}$-dependent Akt

dephosphorylation in this response [147, 150]. Thus, Akt is a redox-sensitive, pro-survival kinase that is regulated differentially by $O_2^{\bullet-}$ and H_2O_2 (Figure 1.6).

Mitochondria and cell death: The contribution of mitochondria to various forms of cell death illustrates the ability of this organelle to regulate cell fate. Cell death is divided into three functional categories (necrosis, apoptosis, and autophagy) based on changes in cellular morphology and DNA fragmentation [151]. In 1972, Kerr, Wyllie, and Currie differentiated between necrosis, an unregulated form of cell death resulting from rapid disruption of cellular homeostasis, and apoptosis, a regimented form of cell death characterized by stepwise destruction of a cell [152].

Necrosis is a passive form of cell death that results from depletion of ATP below levels required to sustain viability, and is often associated with non-specific injury such as blunt trauma, exposure to toxins or loss of blood supply [153]. This form of cell death is characterized morphologically by vacuolization of the cytoplasm and disintegration of the plasma membrane (Figure 1.7C; [151]). The resulting disorderly release of cellular contents can trigger an inflammatory response leading to damage of surrounding tissue [154]. Although necrotic cells frequently exhibit changes in nuclear morphology, the chromosomal condensation and DNA fragmentation characteristic of apoptosis is not observed [151]. Because necrosis often results from depletion of ATP, this form of cell death can be caused by inhibition of oxidative phosphorylation [155]. For instance, the complex III inhibitor antimycin A (0.25 μM) depletes ATP levels by >70% in mouse proximal tubular cells, and induces to necrosis [156].

The term apoptosis is an adaptation of Greek word referring to dropping of petals or leaves from a healthy plant and refers to a stepwise, ATP-dependent form of cell death

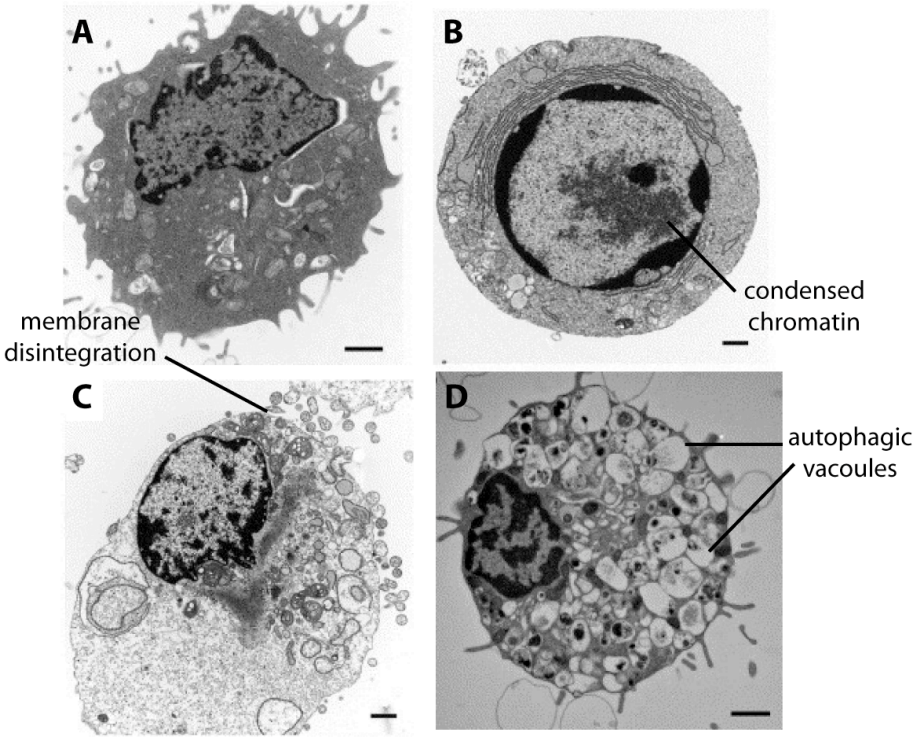

Figure 1.7 – Morphological features of autophagic, apoptotic and necrotic cells. (A) Unstressed cells. (B) Apoptotic cells display characteristic features including membrane blebbing, cytosolic condensation and chromosomal condensation. (C and D) The distinction between necrotic and autophagic death is less clear. Depletion of ATP can trigger necrosis, but may also stimulates autophagy as the cell tries to correct this decline in energy reserves by catabolizing its constituent molecules. Thus, vacuolation of the cytoplasm is observed in both autophagic cells (D) and in cells stimulated to undergo programmed necrosis (C). However, plasma membrane disintegration in necrotic cells (C) is not observed during autophagy. The scale bar represents 1 μm. Figure adapted from [151].

[151]. Characteristics of apoptotic cells include nuclear fragmentation, cleavage of chromosomal DNA into 200-bp long fragments, as well as reduction in cytoplasmic volume (Figure 1.7B; [151, 157]). Unlike rupture of the plasma membrane during necrosis, apoptotic cells are packaged into membrane-enclosed vesicles known as apoptotic bodies, which are engulfed by marcrophages and other phagocytic cells [158].

Because the plasma membrane remains intact during this process, apoptosis does not trigger inflammatory responses [159]. These morphological and nuclear changes associated with apoptosis result from activation of caspases, a family of cysteine aspartyl proteases that cleave key structural proteins and activate DNAses [160].

Caspase activation can result either from stimulation of cell surface death receptors or release of pro-apoptotic proteins (e.g., cytochrome *c*) from the MIS (see Chapter 3 Introduction). Hence, loss of mitochondrial outer membrane is a pivotal signaling event during apoptosis induced by a variety of stimuli [157]. Mitochondria can also participate in the initiation of apoptosis by production of ROS. For instance, the estrogen metabolite 2ME causes an accumulation of $O_2^{\bullet-}$ that signals apoptosis [147, 148]. This ROS response is thought to result from inhibition of SODs, which prevents scavenging of $O_2^{\bullet-}$ released from the MRC [148].

Autophagy, which literally means to eat oneself, is a catabolic program characterized by the formation of autophagic vacuoles, swelling of the Golgi, as well as dilation of the mitochondria and the endoplasmic reticulum (Figure 1.7D; [161]). Autophagic vacuoles are vesicles with double membranes that form in the cytosol and encapsulate organelles and the bulk cytoplasm [162]. These vacuoles are then acidified by fusion with lysosomes, which then leads to degradation of encapsulated components [162]. Autophagy, like apoptosis, can be induced in response to increased mitochondrial ROS production [163]. For example, treatment of human embryonic kidney (HEK) 293 cells with the ETC complex I inhibitor rotenone leads to induction of autophagy or apoptosis, with the magnitude of H_2O_2 production discriminating between these responses [164]. The role of autophagy in cell death is controversial because this process

can promote survival by eliminating damaged organelles (e.g., mitochondria overproducing ROS) and providing an internal source of ATP and biosynthetic intermediates when external nutrients are limiting [151, 165, 166]. However, autophagy can also be triggered by cytotoxic stimuli under conditions where apoptosis is blocked, suggesting that this response can serve as a mechanism of cell death [167, 168].

Mitochondrial respiratory signaling: As described above, activity of the F_oF_1-ATPase and the ETC are linked by $\Delta\psi_m$, which reaches a steady-state of ~150 mV due to balancing pumping of protons into the MIS by the ETC with their return to the matrix by passage through the F_oF_1-ATPase during ATP synthesis [43, 59]. When activity of the ETC exceeds that of the F_oF_1-ATPase, protons accumulate in the MIS leading to hyperpolarization ($\Delta\psi_m$ >150 mV). Due to the increase in proton-motive force under these conditions, electron transport slows, which forces the ETC into a reduced state that favors production of $O_2^{\bullet-}$ [43]. As such, increased ETC activity or inhibition of F_oF_1-ATPase activity may affect cell fate by stimulating production of ATP and/or ROS.

An obvious means of suppressing F_oF_1-ATPase activity is removal of ADP. For instance, addition of ETC substrates to isolated mitochondria in the absence of ADP leads to establishment of $\Delta\psi_m$ [58]. However, because the F_oF_1-ATPase is not active, $\Delta\psi_m$ cannot be dissipated and ETC activity slows [61]. The reduced rate of electron transport within the ETC leads to accumulation of reactive ETC intermediates component for single-electron reduction of O_2, leading to 4-fold increase in production of $O_2^{\bullet-}$ [100]. A six-fold increase in H_2O_2 production has also been reported in isolated mitochondria undergoing state 2 respiration due to addition of malate and glutamate, which stimulate

production of NADH by the TCA-cycle [58]. This increase in H_2O_2 production is attribute to dismutation of $O_2^{\bullet-}$ released from the ETC [97].

Xenobiotic inhibitors can also be used to reduce F_oF_1-ATPase activity (Figure 1.8; [15]). For example, the polyketide F_oF_1-ATPase inhibitor oligomycin reduces the rate of state 3 respiration in rat liver mitochondria by >90% [169]. In addition, oligomycin and increases production of $O_2^{\bullet-}$ and H_2O_2 by isolated rat liver mitochondrial four and six-fold, respectively [58, 100]. Other inhibitors of the F_oF_1-ATPase, including the 1,4-benzodiazepine Bz-423 and diindolylmethane (DIM), have likewise been shown to promote production of $O_2^{\bullet-}$ and H_2O_2 by isolated mitochondria [170, 171]. Along with these effects in isolated mitochondria, F_oF_1-ATPase inhibitors also promote changes in whole cells consistent with induction of a mitochondrial respiratory transition. For example, oligomycin reduces O_2 consumption in the Jurkat T cell leukemia lines by >80% [172]. Also consistent with transition from state 3-to-4 respiration, oligomycin and Bz-423 have been shown to hyperpolarize $\Delta\psi_m$ in a Burkitt's lymphoma B cell line (Ramos) [173], whereas DIM increased $\Delta\psi_m$ in MCF-7 human mammary carcinoma cells [171]. Finally, intracellular ROS levels ($O_2^{\bullet-}$ and H_2O_2) are elevated in Ramos B cells or MCF-7 cells treated with Bz-423 or DIM, respectively [170, 171, 174]. Together, these data demonstrate that F_oF_1-ATPase inhibitors can be used to promote mitochondrial $O_2^{\bullet-}$ production by inducing a transition from state-3-to-4 respiration.

Oligomycin is a high-affinity inhibitor of the F_oF_1-ATPase (K_i ~10 nM; [173]) that severely reduces ATP levels in cells that depend primarily oxidative phosphorylation to generate ATP [2], and is unsuitably toxic for clinical use (e.g., the LD_{33} of oligomycin is <0.5 mg/kg in rats; [175]). In contrast, Bz-423 and DIM are moderate-affinity

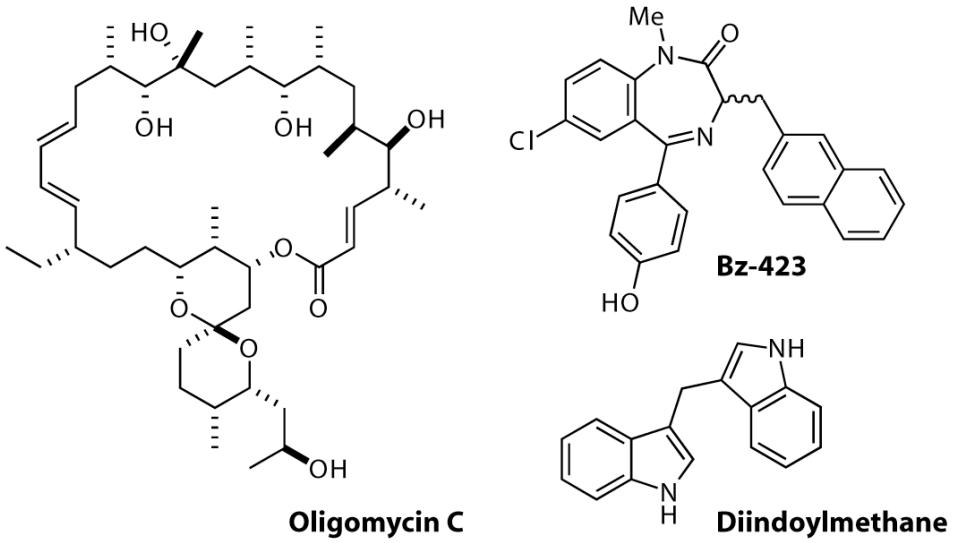

Figure 1.8 – Chemical structures of the F_oF_1-ATPase inhibitors oligomycin, diindolylmethane and Bz-423.

inhibitors of the F_oF_1-ATPase (K_i ~10 and ~25 μM, respectively; [173, 176]), and thus have less severe effects on cellular ATP levels ([171] and this work). In addition, the growth-inhibitory and pro-apoptotic effects of Bz-423 and DIM depend on increased mitochondrial ROS production rather than depletion of ATP [170, 171, 174]. DIM has been used successfully in animal models of cancer [177, 178], while Bz-423 has displayed efficacy in murine models of lupus, arthritis and psoriasis (see Chapter 2 Introduction; [170, 179, 180]). These findings suggest that the F_oF_1-ATPase can be targeted therapeutically by xenobiotic inhibitors that promote mitochondrial ROS production without severely depleting ATP (Figure 1.9). Modulation of the F_oF_1-ATPase by Bz-423 will be considered in detail in Chapter 3.

While suppression of F_oF_1-ATPase activity leads to hyperpolarization of $\Delta\psi_m$, this effect can also result from increased in ETC activity. An important distinction between

these mechanisms is that the F_oF_1-ATPase remains active in the latter. In fact, increased ETC activity is expected to stimulate ATP synthesis by the F_oF_1-ATPase by increasing the concentration of protons in the MIS. Elevation of cellular ATP levels as a result of increased ETC activity is an essential component of the signaling cascade that leads to secretion of insulin by pancreatic β-cells in response to an increase in blood glucose levels [9]. This process, termed glucose-stimulated insulin secretion (GSIS) is unique to pancreatic β-cells, and represents the primary mechanism by which mammals regulate blood glucose levels [181].

GSIS does not result from binding of glucose to a specific receptor in pancreatic β-cells [9]. Instead, β-cells take up glucose via by facilitated diffusion by the glucose transporter Glut1 and then metabolized it to give downstream signals that stimulate insulin secretion. Mitochondrial metabolism is tightly coupled to glucose levels (e.g., >90% of glucose molecules are fully oxidized to CO_2 via the TCA-cycle) in β-cells due to low levels of lactate dehydrogenase, an enzyme that prevents the glycolytic endproduct pyruvate from entering the TCA-cycle by converting it to lactate [182]. This high rate of flux through the TCA-cycle makes β-cell mitochondria highly responsive to increases in blood glucose levels [9]. For example, switching isolated β-cells from low to high glucose (5 mM to 25 mM, respectively) leads to a three-fold increase in NADH levels within five minutes [183]. Increased NADH levels stimulate the ETC, which results in hyperpolarization of $\Delta\psi_m$ as transport of protons into the MIS overtakes their return to the matrix via the F_oF_1-ATPase (Figure 1.9; [8, 184]). Increased $\Delta\psi_m$, in turn, promotes ATP synthesis by the F_oF_1-ATPase leading to a 40% increase in ATP levels in isolated β-cells within 10 minutes of conversion to high glucose media [185].

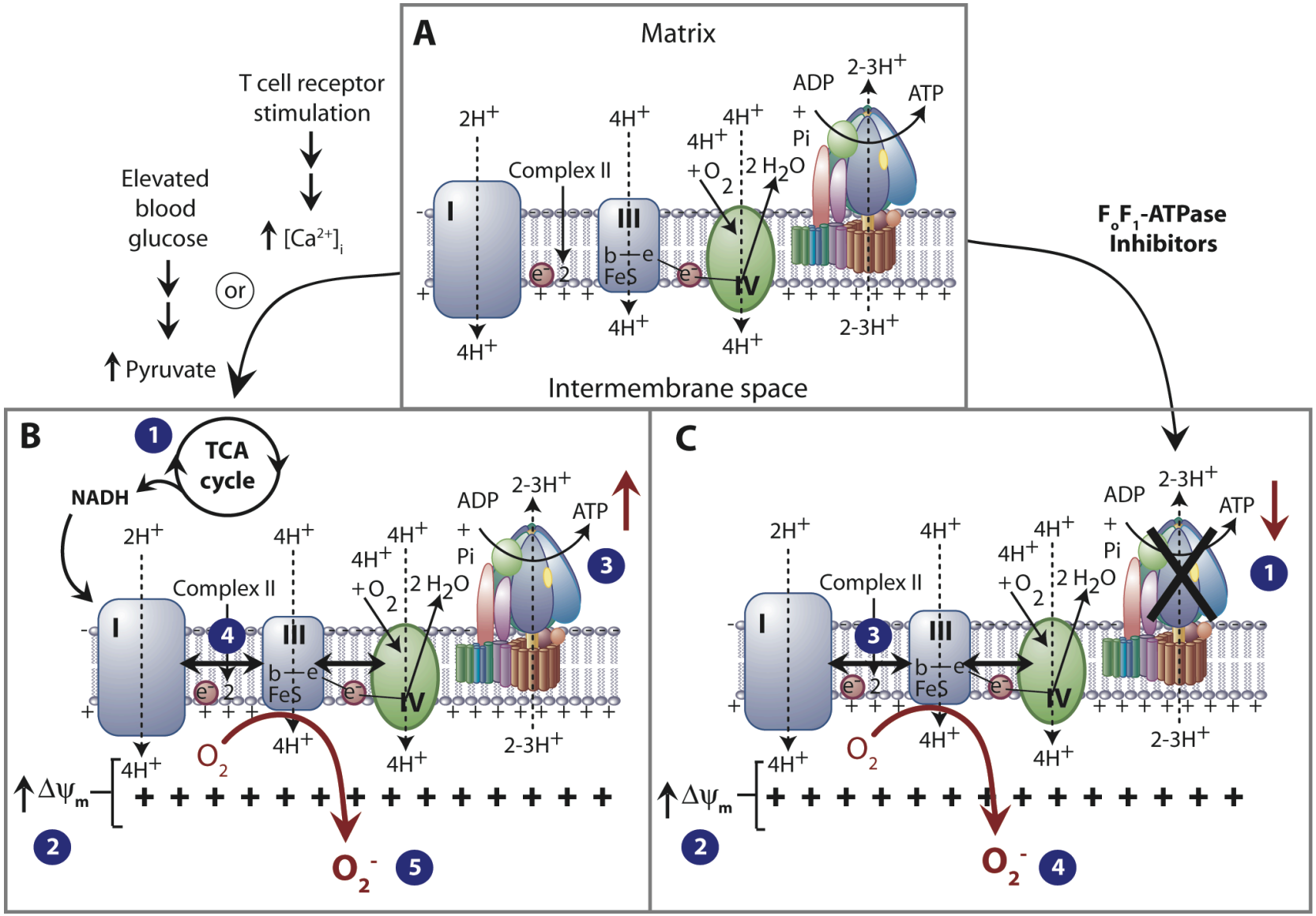
A
Matrix
Intermembrane space
T cell receptor stimulation
Elevated blood glucose
or
↑ [Ca2+]i
↑ Pyruvate
F0F1-ATPase Inhibitors
Complex II
b—e
FeS
ADP + Pi
ATP
2-3H+
2H+
4H+
+O2
2 H2O
B
C
TCA cycle
NADH
ΔΨm
O2
O2-

Figure 1.9 – Changes in electron transport chain and F_oF_1-ATPase activity can promote ATP and/or $O_2^{\bullet-}$ production. (A) Balancing of the pumping of protons into the MIS by the ETC with their return to the matrix by passage through the F_oF_1-ATPase during ATP synthesis results in a steady-state $\Delta\psi_m$ ~150 mV [43, 59]. (B) ETC activity is increased in response to conditions (e.g., glucose stimulation of pancreatic β-cells or antigen receptor stimulation of T lymphocytes) that stimulate the TCA-cycle (**1**). The resulting increase in ETC activity leads accumulation of protons (**+**) in the MIS **(2)** beyond the capacity to be dissipated by the F_oF_1-ATPase. Stimulation of the ETC saturates the F_oF_1-ATPase leading to an increase in ATP synthesis (**3**), but also causing electron carriers within the chain to become more reduced (**4**; indicated by bidirectional arrows). This extends the half-life of ETC intermediates competent for single electron reduction of O_2, leading to increase production of $O_2^{\bullet-}$ (**5**). (C) Inhibitors of the F_oF_1-ATPase trigger a similar process by suppressing ATP synthesis and proton translocation (**1**). Continued proton pumping by the ETC leads to hyperpolarization of $\Delta\psi_m$ (**2**). Again, the increase in proton motive force under these conditions slows electron transport by the ETC (**3**) eventually leading to increased $O_2^{\bullet-}$ production (**4**). While $O_2^{\bullet-}$ production is elevated in both B and C, the F_oF_1-ATPase remains fully in B. See text for additional detail. Figure adopted from [8, 9, 43].

The increase in mitochondrial ATP production in glucose-stimulated β-cells shifts the cytosolic ATP:ADP ratio, which causes ATP-sensitive K^+ (K_{ATP}) channels in the plasma membrane to adopt a low-conductance conformation [186]. Closure of K_{ATP} channels depolarizes the plasma membrane, which leads to opening of voltage-dependent Ca^{2+} channels [186]. As in other exocytosis events, influx of extracellular Ca^{2+} then triggers secretion of insulin granules [186].

The essential contribution of mitochondria ATP synthesis to GSIS has been demonstrated in studies using the β-cell-derived line, βHC9, in which the ETC is non-functional due to depletion of mitochondrial DNA (mtDNA) [187]. GSIS is quantitatively abolished in mtDNA-deficient βHC9 cells [187]. However, a blunted response (~40% of that observed βHC9 cells containing mtDNA) is observed following addition of agents that trigger influx of extracellular Ca^{2+} independent of the

mitochondria, which indicates that depletion of mtDNA does not abolish the capacity of βHC9 to synthesize insulin [187]. The essential role increases ETC and F_oF_1-ATPase activities play in GSIS by pancreatic β-cells illustrates the capacity of mitochondria to both respond to and potentiate cellular signal transduction.

Stimulation of TCA-cycle activity also plays an essential role in the response of T lymphocytes to antigenic stimulation [8]. While details of proximal T cell antigen receptor (TCR) signaling are beyond the scope of this chapter, stimulation of the TCR by either endogenous ligands or agonist antibodies precipitates a signal transduction cascade that leads to a two-fold (~75 to ~150 nM) increase in $[Ca^{2+}]_i$) within seconds [188]. This rapid rise in $[Ca^{2+}]_i$ is followed by a decline to basal levels over the period of hours [188]. As mentioned above, mitochondria buffer TCR-stimulation induced Ca^{2+} flux by acting as a low-affinity, high capacity Ca^{2+} store [26]. Uptake of excess $[Ca^{2+}]_i$ into the matrix is driven by the negative electrochemical potential of this compartment and is mediated by Ca^{2+}-uniporters in the mitochondrial inner membrane [27].

Elevated mitochondrial Ca^{2+} ($[Ca^{2+}]_m$) levels stimulates the Ca^{2+}-dependent TCA-cycle enzymes, pyruvate dehydrogenase (PDH), isocitrate dehydrogenase, and oxoglutarate dehydrogenase [189]. These effects combine to elevate NADH levels two-fold [188]. As in GSIS, levels of NADH increase ETC activity, causing proton transport to outpace dissipation of $\Delta\psi_m$ by the passage of protons through F_o during ATP synthesis. While this effect promotes synthesis of ATP by the F_oF_1-ATPase, it also forces the ETC into a reduced state favoring production of $O_2^{\bullet-}$ (Figure 1.9B; [8, 184, 188]). Enhanced production of $O_2^{\bullet-}$ by the mitochondria is expected to be responsible for increased levels of H_2O_2 and $O_2^{\bullet-}$ observed within 10 minutes of TCR stimulation [106, 190]. In support

of this hypothesis, suppression of complex I activity with chemical inhibitors or knockdown of chaperone proteins required for assembly of this complex blocked the increase in H_2O_2 levels induced by TCR stimulation of murine $CD4^+$ T cells [106, 191].

Increased mitochondrial ROS production appears to play an essential role in the response of T cells to antigenic stimulation [106, 188, 190]. This possibility was first demonstrated by the ability of antioxidants to limit proliferation and production of immune effector molecules (e.g., cytokines) induced TCR stimulation. For example, reducing H_2O_2 levels after TCR stimulation by treatment with the glutathione peroxidase mimetic, Ebselen, or ectopic expression of catalase, decreased proliferation of murine $CD4^+$ T cells by >80% [188]. In addition, the flavin-modifying compound diphenylene iodonium (DPI), which inhibits complex I of the MRC, caused a concentration-dependent reduction (maximum inhibition >80%) in proliferation following TCR stimulation of murine $CD4^+$ T cells [106]. The essential contribution of mitochondrial ROS production during T cell activation has led to the hypothesis that this response signals the presence of energetic conditions (e.g., high levels of ETC substrates) capable of supporting increased proliferation [8].

The contribution of mitochondria to GSIS by pancreactic β-cells and T cell activation highlights the capacity of this organelle to regulate cell fate. These responses share a common mechanism in which stimulation of the TCA-cycle leads to an increase in mitochondrial NADH levels, and as a result, enhanced ETC activity [8, 27]. This increase in ETC activity causes an imbalance in the transport of protons into the MIS and their return to matrix via the F_oF_1-ATPase [43]. While this imbalance stimulates F_oF_1-ATPase activity, it also forces the ETC into a reduced state favoring production of $O_2^{\bullet-}$

[43]. The resulting increase in ATP levels and production of $O_2^{\bullet-}$ (and its dismutation product H_2O_2), then signal GSIS or T cell activation. By these mechanisms, mitochondria act as a signaling locus that senses increases in glucose levels or $[Ca^{2+}]_i$ and communicate these changes to the cell via by production of ATP or ROS (Figure 1.9). Therefore, inhibitors of the F_oF_1-ATPase that promote production of $O_2^{\bullet-}$ by the ETC without severely depleting ATP represent a potential means to exploit these signaling mechanism therapeutically.

Summary: Agents that induce apoptosis in autoreactive lymphocytes without suppressing normal immune function have therapeutic potential for treatment of autoimmune diseases such as SLE. Work in our laboratory has led to the identification of the 1,4-benzodiazepine Bz-423, which has anti-proliferative and pro-apoptotic activity against transformed B cells *in vitro*. Administration of Bz-423 in murine models of lupus and psoriasis ameliorated disease, and these therapeutic effects were accompanied by selective depletion of pathogenic lymphocytes or reduced proliferation of psoriatic skin cells (i.e., keratinocytes) without disruption of the underlying dermis. Both the pro-apoptotic and growth-inhibitory activities of Bz-423 result from binding to the OSCP component of the F_oF_1-ATPase. Modulation of this enzyme by Bz-423 stimulates production of $O_2^{\bullet-}$ by the mitochondrial respiratory chain, and the magnitude of this response dictates whether a cell will cease proliferating or die.

The goal of my research is, therefore, to elucidate the signal transduction pathways linking Bz-423-induced $O_2^{\bullet-}$ production to growth arrest or apoptosis, with the goal of identifying factors that underlie the selective effects on pathogenic cells *in vivo*. In Chapter 2, the anti-proliferative activity of Bz-423 in Burkitt's lymphoma B cells is

shown to result from proteasomal degradation of the oncogenic transcription factor c-Myc. While this mechanism was identified in B cells, similar effects are observed in keratinocytes and are expected to contribute to the anti-psoriatic activity of Bz-423. In Chapter 3, Bz-423-induced apoptosis was investigated in T cell leukemia lines. Unlike some pro-oxidant small molecules, Bz-423 does not trigger opening of the mitochondrial permeability transition (mPT) pore. Rather, Bz-423-induced $O_2^{\bullet-}$ initiates a specific, extra-mitochondrial apoptotic cascade that culminates in preferential activation of Bak. Activation of this multi-BH-domain pro-apoptotic Bcl-2 protein results in release of cytochrome *c* and other apoptogenic proteins from the MIS, which commits a cell to die in response to Bz-423. Insight into the selective effects of Bz-423 in vivo is then afforded by integrating knowledge of this apoptotic mechanism with the characteristics of autoimmune lymphocytes.

BIBLIOGRAPHY

1. Scheffler, I.E. (1999) Structure and morphology. In Mitochondria. (New York: Wiley-Liss, Inc.), p. 16.

2. Leist, M., Single, B., Castoldi, A.F., Kuhnle, S., and Nicotera, P. (1997). Intracellular adenosine triphosphate (ATP) concentration: a switch in the decision between apoptosis and necrosis. J Exp Med *185*, 1481-1486.

3. Eguchi, Y., Shimizu, S., and Tsujimoto, Y. (1997). Intracellular ATP levels determine cell death fate by apoptosis or necrosis. Cancer Res *57*, 1835-1840.

4. Chipuk, J.E., Bouchier-Hayes, L., and Green, D.R. (2006). Mitochondrial outer membrane permeabilization during apoptosis: the innocent bystander scenario. Cell Death Differ *13*, 1396-1402.

5. Brand, M.D., Affourtit, C., Esteves, T.C., Green, K., Lambert, A.J., Miwa, S., Pakay, J.L., and Parker, N. (2004). Mitochondrial superoxide: production, biological effects, and activation of uncoupling proteins. Free Radic Biol Med *37*, 755-767.

6. Brookes, P.S., Yoon, Y., Robotham, J.L., Anders, M.W., and Sheu, S.S. (2004). Calcium, ATP, and ROS: a mitochondrial love-hate triangle. Am J Physiol Cell Physiol *287*, C817-833.

7. Chen, Y., and Gibson, S.B. (2008). Is mitochondrial generation of reactive oxygen species a trigger for autophagy? Autophagy *4*, 246-248.

8. Jones, R.G., and Thompson, C.B. (2007). Revving the engine: signal transduction fuels T cell activation. Immunity *27*, 173-178.

9. Wiederkehr, A., and Wollheim, C.B. (2006). Minireview: implication of mitochondria in insulin secretion and action. Endocrinology *147*, 2643-2649.

10. Pelicano, H., Carney, D., and Huang, P. (2004). ROS stress in cancer cells and therapeutic implications. Drug Resist Updat *7*, 97-110.

11. Nagy, G., Koncz, A., and Perl, A. (2005). T- and B-cell abnormalities in systemic lupus erythematosus. Crit Rev Immunol *25*, 123-140.

12. Chinta, S.J., and Andersen, J.K. (2008). Redox imbalance in Parkinson's disease. Biochim Biophys Acta *1780*, 1362-1367.

13. Fukui, H., and Moraes, C.T. (2008). The mitochondrial impairment, oxidative stress and neurodegeneration connection: reality or just an attractive hypothesis? Trends Neurosci *31*, 251-256.

14. Wei, Y.H., Lu, C.Y., Lee, H.C., Pang, C.Y., and Ma, Y.S. (1998). Oxidative damage and mutation to mitochondrial DNA and age-dependent decline of mitochondrial respiratory function. Ann N Y Acad Sci *854*, 155-170.

15. Toogood, P.L. (2008). Mitochondrial drugs. Curr Opin Chem Biol *12*, 457-463.

16. Song, W., Bossy, B., Martin, O.J., Hicks, A., Lubitz, S., Knott, A.B., and Bossy-Wetzel, E. (2008). Assessing mitochondrial morphology and dynamics using fluorescence wide-field microscopy and 3D image processing. Methods.

17. Mayhew, T.M., Burgess, A.J., Gregory, C.D., and Atkinson, M.E. (1979). On the problem of counting and sizing mitochondria: a general reappraisal based on ultrastructural studies of mammalian lymphocytes. Cell Tissue Res *204*, 297-303.

18. Acehan, D., Xu, Y., Stokes, D.L., and Schlame, M. (2007). Comparison of lymphoblast mitochondria from normal subjects and patients with Barth syndrome using electron microscopic tomography. Lab Invest *87*, 40-48.

19. Chen, H., and Chan, D.C. (2005). Emerging functions of mammalian mitochondrial fusion and fission. Hum Mol Genet *14 Spec No. 2*, R283-289.

20. Sheridan, C., Delivani, P., Cullen, S.P., and Martin, S.J. (2008). Bax- or Bak-induced mitochondrial fission can be uncoupled from cytochrome C release. Mol Cell *31*, 570-585.

21. Nagy, G., Barcza, M., Gonchoroff, N., Phillips, P.E., and Perl, A. (2004). Nitric oxide-dependent mitochondrial biogenesis generates Ca2+ signaling profile of lupus T cells. J Immunol *173*, 3676-3683.

22. Fox, C.J., Hammerman, P.S., and Thompson, C.B. (2005). Fuel feeds function: energy metabolism and the T-cell response. Nat Rev Immunol *5*, 844-852.

23. D'Souza, A.D., Parikh, N., Kaech, S.M., and Shadel, G.S. (2007). Convergence of multiple signaling pathways is required to coordinately up-regulate mtDNA and mitochondrial biogenesis during T cell activation. Mitochondrion *7*, 374-385.

24. Turner, R.M. (2003). Tales from the tail: what do we really know about sperm motility? J Androl *24*, 790-803.

25. Scheffler, I.E. (1999) Structure and morphology. In Mitochondria. (New York: Wiley-Liss, Inc.), p. 16.

26. Camello-Almaraz, C., Gomez-Pinilla, P.J., Pozo, M.J., and Camello, P.J. (2006). Mitochondrial reactive oxygen species and Ca2+ signaling. Am J Physiol Cell Physiol *291*, C1082-1088.

27. Parekh, A.B. (2008). Mitochondrial regulation of store-operated CRAC channels. Cell Calcium *44*, 6-13.

28. Scheffler, I.E. (1999) Structure and morphology. In Mitochondria. (New York: Wiley-Liss, Inc.), p. 16.

29. Scheffler, I.E. (1999) Structure and morphology. In Mitochondria. (New York: Wiley-Liss, Inc.), p. 16.

30. Scheffler, I.E. (1999) Structure and morphology. In Mitochondria. (New York: Wiley-Liss, Inc.), p. 16.

31. Sorgato, M.C., and Moran, O. (1993). Channels in mitochondrial membranes: knowns, unknowns, and prospects for the future. Crit Rev Biochem Mol Biol *28*, 127-171.

32. Colell, A., Ricci, J.E., Tait, S., Milasta, S., Maurer, U., Bouchier-Hayes, L., Fitzgerald, P., Guio-Carrion, A., Waterhouse, N.J., Li, C.W., Mari, B., Barbry, P., Newmeyer, D.D., Beere, H.M., and Green, D.R. (2007). GAPDH and autophagy preserve survival after apoptotic cytochrome c release in the absence of caspase activation. Cell *129*, 983-997.

33. Walker, J.E., and Runswick, M.J. (1993). The mitochondrial transport protein superfamily. J Bioenerg Biomembr *25*, 435-446.

34. Sharer, J.D. (2005). The adenine nucleotide translocase type 1 (ANT1): a new factor in mitochondrial disease. IUBMB Life *57*, 607-614.

35. Kirichok, Y., Krapivinsky, G., and Clapham, D.E. (2004). The mitochondrial calcium uniporter is a highly selective ion channel. Nature *427*, 360-364.

36. Scheffler, I.E. (1999) Structure and morphology. In Mitochondria. (New York: Wiley-Liss, Inc.), p. 16.

37. Scheffler, I.E. (1999) Metabolic Pathways Inside Mitochondria. In Mitochondria. (New York: Wiley-Liss, Inc.), pp. 246-270.

38. Lehninger, AL., Nelson, DL., Cox, MM. (1993). Oxidative Phosphorylation and Photophosphorylation. In Principles of Biochemistry, 2nd Ed. (New York`; Worth Publishers), pp. 542-561.

39. Lehninger, AL., Nelson, DL., Cox, MM. (1993). Oxidative Phosphorylation and Photophosphorylation. In Principles of Biochemistry, 2nd Ed. (New York`; Worth Publishers), pp. 542-561.

40. Lehninger, AL., Nelson, DL., Cox, MM. (1993). Oxidative Phosphorylation and Photophosphorylation. In Principles of Biochemistry, 2nd Ed. (New York`; Worth Publishers), pp. 542-561.

41. Lenaz, G. (2001). The mitochondrial production of reactive oxygen species: mechanisms and implications in human pathology. IUBMB Life *52*, 159-164.

42. Turrens, J.F. (2003). Mitochondrial formation of reactive oxygen species. J Physiol *552*, 335-344.

43. Adam-Vizi, V., and Chinopoulos, C. (2006). Bioenergetics and the formation of mitochondrial reactive oxygen species. Trends Pharmacol Sci *27*, 639-645.

44. Hirst, J. (2005). Energy transduction by respiratory complex I--an evaluation of current knowledge. Biochem Soc Trans *33*, 525-529.

45. Crofts, A.R. (2004). The cytochrome bc1 complex: function in the context of structure. Annu Rev Physiol *66*, 689-733.

46. Lehninger, AL., Nelson, DL., Cox, MM. (1993). Oxidative Phosphorylation and Photophosphorylation. In Principles of Biochemistry, 2nd Ed. (New York`; Worth Publishers), pp. 542-561.

47. Khalimonchuk, O., and Rodel, G. (2005). Biogenesis of cytochrome c oxidase. Mitochondrion *5*, 363-388.

48. Lehninger, AL., Nelson, DL., Cox, MM. (1993). Oxidative Phosphorylation and Photophosphorylation. In Principles of Biochemistry, 2nd Ed. (New York`; Worth Publishers), pp. 542-561.

49. Lehninger, AL., Nelson, DL., Cox, MM. (1993). Oxidative Phosphorylation and Photophosphorylation. In Principles of Biochemistry, 2nd Ed. (New York`; Worth Publishers), pp. 542-561.

50. Lehninger, AL., Nelson, DL., Cox, MM. (1993). Oxidative Phosphorylation and Photophosphorylation. In Principles of Biochemistry, 2nd Ed. (New York`; Worth Publishers), pp. 542-561.

51. Scheffler, I.E. (1999). Mitochondrial Electron Transport and Oxidative Phosphorylation. In Mitochondria. (New York: Wiley-Liss, Inc.), pp. 141-252.

52. Scheffler, I.E. (1999). Mitochondrial Electron Transport and Oxidative Phosphorylation. In Mitochondria. (New York: Wiley-Liss, Inc.), pp. 141-252.

53. Scheffler, I.E. (1999). Mitochondrial Electron Transport and Oxidative Phosphorylation. In Mitochondria. (New York: Wiley-Liss, Inc.), pp. 141-252.

54. Rasola, A., and Geuna, M. (2001). A flow cytometry assay simultaneously detects independent apoptotic parameters. Cytometry *45*, 151-157.

55. Boyer, P.D. (1997). The ATP synthase--a splendid molecular machine. Annu Rev Biochem *66*, 717-749.

56. Lehninger, AL., Nelson, DL., Cox, MM. (1993). Oxidative Phosphorylation and Photophosphorylation. In Principles of Biochemistry, 2nd Ed. (New York`; Worth Publishers), pp. 542-561.

57. Devenish, R.J., Prescott, M., Boyle, G.M., and Nagley, P. (2000). The Oligomycin Axis of Mitochondrial ATP Synthase: OSCP and the Proton Channel. J Bioenerg Biomembr *32*, 507-515.

58. Korshunov, S.S., Skulachev, V.P., and Starkov, A.A. (1997). High protonic potential actuates a mechanism of production of reactive oxygen species in mitochondria. FEBS Lett *416*, 15-18.

59. Perl, A., Gergely, P., Jr., Nagy, G., Koncz, A., and Banki, K. (2004). Mitochondrial hyperpolarization: a checkpoint of T-cell life, death and autoimmunity. Trends Immunol *25*, 360-367.

60. Scheffler, I.E. (1999). Mitochondrial Electron Transport and Oxidative Phosphorylation. In Mitochondria. (New York: Wiley-Liss, Inc.), pp. 141-252.

61. Chance, B., and Williams, G.R. (1955). Respiratory enzymes in oxidative phosphorylation. III. The steady state. J Biol Chem *217*, 409-427.

62. Fridovich, I. (1978). The biology of oxygen radicals. Science *201*, 875-880.

63. Boveris, A. (1977). Mitochondrial production of superoxide radical and hydrogen peroxide. Adv Exp Med Biol *78*, 67-82.

64. Cino, M., and Del Maestro, R.F. (1989). Generation of hydrogen peroxide by brain mitochondria: the effect of reoxygenation following postdecapitative ischemia. Arch Biochem Biophys *269*, 623-638.

65. Kwong, L.K., and Sohal, R.S. (1998). Substrate and site specificity of hydrogen peroxide generation in mouse mitochondria. Arch Biochem Biophys *350*, 118-126.

66. Boveris, A., Cadenas, E., and Stoppani, A.O. (1976). Role of ubiquinone in the mitochondrial generation of hydrogen peroxide. Biochem J *156*, 435-444.

67. Turrens, J.F., Alexandre, A., and Lehninger, A.L. (1985). Ubisemiquinone is the electron donor for superoxide formation by complex III of heart mitochondria. Arch Biochem Biophys *237*, 408-414.

68. Turrens, J.F., and Boveris, A. (1980). Generation of superoxide anion by the NADH dehydrogenase of bovine heart mitochondria. Biochem J *191*, 421-427.

69. Okun, J.G., Lummen, P., and Brandt, U. (1999). Three classes of inhibitors share a common binding domain in mitochondrial complex I (NADH:ubiquinone oxidoreductase). J Biol Chem *274*, 2625-2630.

70. Genova, M.L., Ventura, B., Giuliano, G., Bovina, C., Formiggini, G., Parenti Castelli, G., and Lenaz, G. (2001). The site of production of superoxide radical in mitochondrial Complex I is not a bound ubisemiquinone but presumably iron-sulfur cluster N2. FEBS Lett *505*, 364-368.

71. Kushnareva, Y., Murphy, A.N., and Andreyev, A. (2002). Complex I-mediated reactive oxygen species generation: modulation by cytochrome c and NAD(P)+ oxidation-reduction state. Biochem J *368*, 545-553.

72. Kudin, A.P., Bimpong-Buta, N.Y., Vielhaber, S., Elger, C.E., and Kunz, W.S. (2004). Characterization of superoxide-producing sites in isolated brain mitochondria. J Biol Chem *279*, 4127-4135.

73. Krishnamoorthy, G., and Hinkle, P.C. (1988). Studies on the electron transfer pathway, topography of iron-sulfur centers, and site of coupling in NADH-Q oxidoreductase. J Biol Chem *263*, 17566-17575.

74. St-Pierre, J., Buckingham, J.A., Roebuck, S.J., and Brand, M.D. (2002). Topology of superoxide production from different sites in the mitochondrial electron transport chain. J Biol Chem *277*, 44784-44790.

75. Lambert, A.J., and Brand, M.D. (2004). Inhibitors of the quinone-binding site allow rapid superoxide production from mitochondrial NADH:ubiquinone oxidoreductase (complex I). J Biol Chem *279*, 39414-39420.

76. Pelicano, H., Feng, L., Zhou, Y., Carew, J.S., Hileman, E.O., Plunkett, W., Keating, M.J., and Huang, P. (2003). Inhibition of mitochondrial respiration: a novel strategy to enhance drug-induced apoptosis in human leukemia cells by a reactive oxygen species-mediated mechanism. J Biol Chem *278*, 37832-37839.

77. Muller, F.L., Liu, Y., and Van Remmen, H. (2004). Complex III releases superoxide to both sides of the inner mitochondrial membrane. J Biol Chem *279*, 49064-49073.

78. Bove, J., Prou, D., Perier, C., and Przedborski, S. (2005). Toxin-induced models of Parkinson's disease. NeuroRx *2*, 484-494.

79. Cape, J.L., Bowman, M.K., and Kramer, D.M. (2006). Understanding the cytochrome bc complexes by what they don't do. The Q-cycle at 30. Trends Plant Sci *11*, 46-55.

80. Crofts, A.R., Barquera, B., Gennis, R.B., Kuras, R., Guergova-Kuras, M., and Berry, E.A. (1999). Mechanism of ubiquinol oxidation by the bc(1) complex: different domains of the quinol binding pocket and their role in the mechanism and binding of inhibitors. Biochemistry *38*, 15807-15826.

81. Cape, J.L., Bowman, M.K., and Kramer, D.M. (2007). A semiquinone intermediate generated at the Qo site of the cytochrome bc1 complex: importance for the Q-cycle and superoxide production. Proc Natl Acad Sci U S A *104*, 7887-7892.

82. D'Autreaux, B., and Toledano, M.B. (2007). ROS as signalling molecules: mechanisms that generate specificity in ROS homeostasis. Nat Rev Mol Cell Biol *8*, 813-824.

83. Fridovich, I. (1995). Superoxide radical and superoxide dismutases. Annu Rev Biochem *64*, 97-112.

84. Beinert, H., Kennedy, M.C., and Stout, C.D. (1996). Aconitase as Ironminus signSulfur Protein, Enzyme, and Iron-Regulatory Protein. Chem Rev *96*, 2335-2374.

85. Bulteau, A.L., Ikeda-Saito, M., and Szweda, L.I. (2003). Redox-dependent modulation of aconitase activity in intact mitochondria. Biochemistry *42*, 14846-14855.

86. Winterbourn, C.C., and Metodiewa, D. (1999). Reactivity of biologically important thiol compounds with superoxide and hydrogen peroxide. Free Radic Biol Med *27*, 322-328.

87. Halliwell, B.`; Gutteridge, J.M.C. (1999). Free Radicals in Biology and Medicine (Oxford`; Oxford University Press). p144.

88. Poole, L.B., Karplus, P.A., and Claiborne, A. (2004). Protein sulfenic acids in redox signaling. Annu Rev Pharmacol Toxicol *44*, 325-347.

89. Gilbert, H.F. (1990). Molecular and cellular aspects of thiol-disulfide exchange. Adv Enzymol Relat Areas Mol Biol *63*, 69-172.

90. Fratelli, M., Demol, H., Puype, M., Casagrande, S., Eberini, I., Salmona, M., Bonetto, V., Mengozzi, M., Duffieux, F., Miclet, E., Bachi, A., Vandekerckhove, J., Gianazza, E., and Ghezzi, P. (2002). Identification by redox proteomics of glutathionylated proteins in oxidatively stressed human T lymphocytes. Proc Natl Acad Sci U S A *99*, 3505-3510.

91. Fridovich, I. (1999). Fundamental aspects of reactive oxygen species, or what's the matter with oxygen? Ann N Y Acad Sci *893*, 13-18.

92. Kedziora-Kornatowska, K.Z., Luciak, M., Blaszczyk, J., and Pawlak, W. (1998). Lipid peroxidation and activities of antioxidant enzymes in erythrocytes of patients with non-insulin dependent diabetes with or without diabetic nephropathy. Nephrol Dial Transplant *13*, 2829-2832.

93. Imlay, J.A. (2003). Pathways of oxidative damage. Annu Rev Microbiol *57*, 395-418.

94. Zamocky, M., Furtmuller, P.G., and Obinger, C. (2008). Evolution of catalases from bacteria to humans. Antioxid Redox Signal *10*, 1527-1548.

95. Sies, H. (1999). Glutathione and its role in cellular functions. Free Radic Biol Med *27*, 916-921.

96. Griffith, O.W., and Meister, A. (1985). Origin and turnover of mitochondrial glutathione. Proc Natl Acad Sci U S A *82*, 4668-4672.

97. Adam-Vizi, V. (2005). Production of reactive oxygen species in brain mitochondria: contribution by electron transport chain and non-electron transport chain sources. Antioxid Redox Signal *7*, 1140-1149.

98. Melov, S., Coskun, P., Patel, M., Tuinstra, R., Cottrell, B., Jun, A.S., Zastawny, T.H., Dizdaroglu, M., Goodman, S.I., Huang, T.T., Miziorko, H., Epstein, C.J., and Wallace, D.C. (1999). Mitochondrial disease in superoxide dismutase 2 mutant mice. Proc Natl Acad Sci U S A *96*, 846-851.

99. Finkel, T. (1999). Signal transduction by reactive oxygen species in non-phagocytic cells. J Leukoc Biol *65*, 337-340.

100. Fink, B.D., Reszka, K.J., Herlein, J.A., Mathahs, M.M., and Sivitz, W.I. (2005). Respiratory uncoupling by UCP1 and UCP2 and superoxide generation in endothelial cell mitochondria. Am J Physiol Endocrinol Metab *288*, E71-79.

101. Han, D., Antunes, F., Canali, R., Rettori, D., and Cadenas, E. (2003). Voltage-dependent anion channels control the release of the superoxide anion from mitochondria to cytosol. J Biol Chem *278*, 5557-5563.

102. Takeya, R., and Sumimoto, H. (2006). Regulation of novel superoxide-producing NAD(P)H oxidases. Antioxid Redox Signal *8*, 1523-1532.

103. Sumimoto, H. (2008). Structure, regulation and evolution of Nox-family NADPH oxidases that produce reactive oxygen species. Febs J *275*, 3249-3277.

104. Gaut, J.P., Yeh, G.C., Tran, H.D., Byun, J., Henderson, J.P., Richter, G.M., Brennan, M.L., Lusis, A.J., Belaaouaj, A., Hotchkiss, R.S., and Heinecke, J.W. (2001). Neutrophils employ the myeloperoxidase system to generate antimicrobial brominating and chlorinating oxidants during sepsis. Proc Natl Acad Sci U S A *98*, 11961-11966.

105. Gaut, J.P., Byun, J., Tran, H.D., Lauber, W.M., Carroll, J.A., Hotchkiss, R.S., Belaaouaj, A., and Heinecke, J.W. (2002). Myeloperoxidase produces nitrating oxidants in vivo. J Clin Invest *109*, 1311-1319.

106. Jackson, S.H., Devadas, S., Kwon, J., Pinto, L.A., and Williams, M.S. (2004). T cells express a phagocyte-type NADPH oxidase that is activated after T cell receptor stimulation. Nat Immunol *5*, 818-827.

107. Thannickal, V.J., Aldweib, K.D., and Fanburg, B.L. (1998). Tyrosine phosphorylation regulates H2O2 production in lung fibroblasts stimulated by transforming growth factor beta1. J Biol Chem *273*, 23611-23615.

108. Bae, Y.S., Kang, S.W., Seo, M.S., Baines, I.C., Tekle, E., Chock, P.B., and Rhee, S.G. (1997). Epidermal growth factor (EGF)-induced generation of hydrogen peroxide. Role in EGF receptor-mediated tyrosine phosphorylation. J Biol Chem *272*, 217-221.

109. Suh, Y.A., Arnold, R.S., Lassegue, B., Shi, J., Xu, X., Sorescu, D., Chung, A.B., Griendling, K.K., and Lambeth, J.D. (1999). Cell transformation by the superoxide-generating oxidase Mox1. Nature *401*, 79-82.

110. Zweier, J.L., Broderick, R., Kuppusamy, P., Thompson-Gorman, S., and Lutty, G.A. (1994). Determination of the mechanism of free radical generation in human aortic endothelial cells exposed to anoxia and reoxygenation. J Biol Chem *269*, 24156-24162.

111. Juarez, J.C., Manuia, M., Burnett, M.E., Betancourt, O., Boivin, B., Shaw, D.E., Tonks, N.K., Mazar, A.P., and Donate, F. (2008). Superoxide dismutase 1 (SOD1) is essential for H2O2-mediated oxidation and inactivation of phosphatases in growth factor signaling. Proc Natl Acad Sci U S A *105*, 7147-7152.

112. Genestra, M. (2007). Oxyl radicals, redox-sensitive signalling cascades and antioxidants. Cell Signal *19*, 1807-1819.

113. Matsuzawa, A., and Ichijo, H. (2005). Stress-responsive protein kinases in redox-regulated apoptosis signaling. Antioxid Redox Signal *7*, 472-481.

114. Nathan, C. (2003). Specificity of a third kind: reactive oxygen and nitrogen intermediates in cell signaling. J Clin Invest *111*, 769-778.

115. Cakir, Y., and Ballinger, S.W. (2005). Reactive species-mediated regulation of cell signaling and the cell cycle: the role of MAPK. Antioxid Redox Signal *7*, 726-740.

116. Johnson, G.L., and Lapadat, R. (2002). Mitogen-activated protein kinase pathways mediated by ERK, JNK, and p38 protein kinases. Science *298*, 1911-1912.

117. Chang, L., and Karin, M. (2001). Mammalian MAP kinase signalling cascades. Nature *410*, 37-40.

118. Kyriakis, J.M., and Avruch, J. (2001). Mammalian mitogen-activated protein kinase signal transduction pathways activated by stress and inflammation. Physiol Rev *81*, 807-869.

119. Winterbourn, C.C., and Hampton, M.B. (2008). Thiol chemistry and specificity in redox signaling. Free Radic Biol Med *45*, 549-561.

120. Lee, K., and Esselman, W.J. (2002). Inhibition of PTPs by H(2)O(2) regulates the activation of distinct MAPK pathways. Free Radic Biol Med *33*, 1121-1132.

121. Chiarugi, P. (2005). PTPs versus PTKs: the redox side of the coin. Free Radic Res *39*, 353-364.

122. Lodish, H.`; Berk, A.`; Matsudaira, P.`; Kaiser, C.`; Krieger, M.`; Scott, M.`; Zipursky, S.`; Darnell, J. (2004). Receptor Tyrosine Kinases and Activation of Ras. In Molecular Cell Biology. Vol 5. (New York`; W.H. Freeman and Company). pp. 587-592.

123. Lodish, H.`; Berk, A.`; Matsudaira, P.`; Kaiser, C.`; Krieger, M.`; Scott, M.`; Zipursky, S.`; Darnell, J. (2004). Receptor Tyrosine Kinases and Activation of Ras. In Molecular Cell Biology. Vol 5. (New York`; W.H. Freeman and Company). pp. 587-592.

124. Tonks, N.K. (2005). Redox redux: revisiting PTPs and the control of cell signaling. Cell *121*, 667-670.

125. Rhee, S.G. (2006). Cell signaling. H2O2, a necessary evil for cell signaling. Science *312*, 1882-1883.

126. Ushio-Fukai, M. (2006). Redox signaling in angiogenesis: role of NADPH oxidase. Cardiovasc Res *71*, 226-235.

127. Arany, I., Megyesi, J.K., Kaneto, H., Tanaka, S., and Safirstein, R.L. (2004). Activation of ERK or inhibition of JNK ameliorates H(2)O(2) cytotoxicity in mouse renal proximal tubule cells. Kidney Int *65*, 1231-1239.

128. Shin, M.H., Rhie, G.E., Kim, Y.K., Park, C.H., Cho, K.H., Kim, K.H., Eun, H.C., and Chung, J.H. (2005). H2O2 accumulation by catalase reduction changes MAP kinase signaling in aged human skin in vivo. J Invest Dermatol *125*, 221-229.

129. Zhou, Y., Wang, Q., Evers, B.M., and Chung, D.H. (2005). Signal transduction pathways involved in oxidative stress-induced intestinal epithelial cell apoptosis. Pediatr Res *58*, 1192-1197.

130. Ichijo, H., Nishida, E., Irie, K., ten Dijke, P., Saitoh, M., Moriguchi, T., Takagi, M., Matsumoto, K., Miyazono, K., and Gotoh, Y. (1997). Induction of apoptosis by ASK1, a mammalian MAPKKK that activates SAPK/JNK and p38 signaling pathways. Science *275*, 90-94.

131. Matsuzawa, A., Nishitoh, H., Tobiume, K., Takeda, K., and Ichijo, H. (2002). Physiological roles of ASK1-mediated signal transduction in oxidative stress- and endoplasmic reticulum stress-induced apoptosis: advanced findings from ASK1 knockout mice. Antioxid Redox Signal *4*, 415-425.

132. Powis, G., and Montfort, W.R. (2001). Properties and biological activities of thioredoxins. Annu Rev Pharmacol Toxicol *41*, 261-295.

133. Saitoh, M., Nishitoh, H., Fujii, M., Takeda, K., Tobiume, K., Sawada, Y., Kawabata, M., Miyazono, K., and Ichijo, H. (1998). Mammalian thioredoxin is a direct inhibitor of apoptosis signal-regulating kinase (ASK) 1. Embo J *17*, 2596-2606.

134. Gotoh, Y., and Cooper, J.A. (1998). Reactive oxygen species- and dimerization-induced activation of apoptosis signal-regulating kinase 1 in tumor necrosis factor-alpha signal transduction. J Biol Chem *273*, 17477-17482.

135. Tobiume, K., Matsuzawa, A., Takahashi, T., Nishitoh, H., Morita, K., Takeda, K., Minowa, O., Miyazono, K., Noda, T., and Ichijo, H. (2001). ASK1 is required for sustained activations of JNK/p38 MAP kinases and apoptosis. EMBO Rep *2*, 222-228.

136. Dasgupta, J., Subbaram, S., Connor, K.M., Rodriguez, A.M., Tirosh, O., Beckman, J.S., Jourd'Heuil, D., and Melendez, J.A. (2006). Manganese superoxide dismutase protects from TNF-alpha-induced apoptosis by increasing the steady-state production of H2O2. Antioxid Redox Signal *8*, 1295-1305.

137. De Keulenaer, G.W., Alexander, R.W., Ushio-Fukai, M., Ishizaka, N., and Griendling, K.K. (1998). Tumour necrosis factor alpha activates a p22phox-based NADH oxidase in vascular smooth muscle. Biochem J *329 (Pt 3)*, 653-657.

138. Du, J., Suzuki, H., Nagase, F., Akhand, A.A., Ma, X.Y., Yokoyama, T., Miyata, T., and Nakashima, I. (2001). Superoxide-mediated early oxidation and activation of ASK1 are important for initiating methylglyoxal-induced apoptosis process. Free Radic Biol Med *31*, 469-478.

139. Sale, E.M., and Sale, G.J. (2008). Protein kinase B: signalling roles and therapeutic targeting. Cell Mol Life Sci *65*, 113-127.

140. Hennessy, B.T., Smith, D.L., Ram, P.T., Lu, Y., and Mills, G.B. (2005). Exploiting the PI3K/AKT pathway for cancer drug discovery. Nat Rev Drug Discov *4*, 988-1004.

141. Ross, S.H., Lindsay, Y., Safrany, S.T., Lorenzo, O., Villa, F., Toth, R., Clague, M.J., Downes, C.P., and Leslie, N.R. (2007). Differential redox regulation within the PTP superfamily. Cell Signal *19*, 1521-1530.

142. Lee, S.R., Yang, K.S., Kwon, J., Lee, C., Jeong, W., and Rhee, S.G. (2002). Reversible inactivation of the tumor suppressor PTEN by H2O2. J Biol Chem *277*, 20336-20342.

143. Cheung, S.M., Kornelson, J.C., Al-Alwan, M., and Marshall, A.J. (2007). Regulation of phosphoinositide 3-kinase signaling by oxidants: hydrogen peroxide selectively enhances immunoreceptor-induced recruitment of phosphatidylinositol (3,4) bisphosphate-binding PH domain proteins. Cell Signal *19*, 902-912.

144. Pelicano, H., Xu, R.H., Du, M., Feng, L., Sasaki, R., Carew, J.S., Hu, Y., Ramdas, L., Hu, L., Keating, M.J., Zhang, W., Plunkett, W., and Huang, P. (2006). Mitochondrial respiration defects in cancer cells cause activation of Akt survival pathway through a redox-mediated mechanism. J Cell Biol *175*, 913-923.

145. Shaik, Z.P., Fifer, E.K., and Nowak, G. (2008). Akt activation improves oxidative phosphorylation in renal proximal tubular cells following nephrotoxicant injury. Am J Physiol Renal Physiol *294*, F423-432.

146. Kim, A.H., Khursigara, G., Sun, X., Franke, T.F., and Chao, M.V. (2001). Akt phosphorylates and negatively regulates apoptosis signal-regulating kinase 1. Mol Cell Biol *21*, 893-901.

147. Gao, N., Rahmani, M., Dent, P., and Grant, S. (2005). 2-Methoxyestradiol-induced apoptosis in human leukemia cells proceeds through a reactive oxygen species and Akt-dependent process. Oncogene *24*, 3797-3809.

148. Huang, P., Feng, L., Oldham, E.A., Keating, M.J., and Plunkett, W. (2000). Superoxide dismutase as a target for the selective killing of cancer cells. Nature *407*, 390-395.

149. Astoul, E., Edmunds, C., Cantrell, D.A., and Ward, S.G. (2001). PI 3-K and T-cell activation: limitations of T-leukemic cell lines as signaling models. Trends Immunol *22*, 490-496.

150. Bornhauser, B.C., Bonapace, L., Lindholm, D., Martinez, R., Cario, G., Schrappe, M., Niggli, F.K., Schafer, B.W., and Bourquin, J.P. (2007). Low-dose arsenic trioxide sensitizes glucocorticoid-resistant acute lymphoblastic leukemia cells to dexamethasone via an Akt-dependent pathway. Blood *110*, 2084-2091.

151. Edinger, A.L., and Thompson, C.B. (2004). Death by design: apoptosis, necrosis and autophagy. Curr Opin Cell Biol *16*, 663-669.

152. Kerr, J.F., Wyllie, A.H., and Currie, A.R. (1972). Apoptosis: a basic biological phenomenon with wide-ranging implications in tissue kinetics. Br J Cancer *26*, 239-257.

153. Schweichel, J.U., and Merker, H.J. (1973). The morphology of various types of cell death in prenatal tissues. Teratology *7*, 253-266.

154. Kazama, H., Ricci, J.E., Herndon, J.M., Hoppe, G., Green, D.R., and Ferguson, T.A. (2008). Induction of immunological tolerance by apoptotic cells requires caspase-dependent oxidation of high-mobility group box-1 protein. Immunity *29*, 21-32.

155. Skulachev, V.P. (2006). Bioenergetic aspects of apoptosis, necrosis and mitoptosis. Apoptosis *11*, 473-485.

156. Lieberthal, W., Menza, S.A., and Levine, J.S. (1998). Graded ATP depletion can cause necrosis or apoptosis of cultured mouse proximal tubular cells. Am J Physiol *274*, F315-327.

157. Danial, N.N., and Korsmeyer, S.J. (2004). Cell death: critical control points. Cell *116*, 205-219.

158. Fadok, V.A., Bratton, D.L., Frasch, S.C., Warner, M.L., and Henson, P.M. (1998). The role of phosphatidylserine in recognition of apoptotic cells by phagocytes. Cell Death Differ *5*, 551-562.

159. Levine, J.S., and Koh, J.S. (1999). The role of apoptosis in autoimmunity: immunogen, antigen, and accelerant. Semin Nephrol *19*, 34-47.

160. Thornberry, N.A., and Lazebnik, Y. (1998). Caspases: enemies within. Science *281*, 1312-1316.

161. Levine, B., and Klionsky, D.J. (2004). Development by self-digestion: molecular mechanisms and biological functions of autophagy. Dev Cell *6*, 463-477.

162. Klionsky, D.J., and Emr, S.D. (2000). Autophagy as a regulated pathway of cellular degradation. Science *290*, 1717-1721.

163. Scherz-Shouval, R., and Elazar, Z. (2007). ROS, mitochondria and the regulation of autophagy. Trends Cell Biol *17*, 422-427.

164. Chen, Y., McMillan-Ward, E., Kong, J., Israels, S.J., and Gibson, S.B. (2007). Mitochondrial electron-transport-chain inhibitors of complexes I and II induce autophagic cell death mediated by reactive oxygen species. J Cell Sci *120*, 4155-4166.

165. Lindsten, T., Golden, J.A., Zong, W.X., Minarcik, J., Harris, M.H., and Thompson, C.B. (2003). The proapoptotic activities of Bax and Bak limit the size of the neural stem cell pool. J Neurosci *23*, 11112-11119.

166. Deckwerth, T.L., Easton, R.M., Knudson, C.M., Korsmeyer, S.J., and Johnson, E.M., Jr. (1998). Placement of the BCL2 family member BAX in the death pathway of sympathetic neurons activated by trophic factor deprivation. Exp Neurol *152*, 150-162.

167. Yu, L., Alva, A., Su, H., Dutt, P., Freundt, E., Welsh, S., Baehrecke, E.H., and Lenardo, M.J. (2004). Regulation of an ATG7-beclin 1 program of autophagic cell death by caspase-8. Science *304*, 1500-1502.

168. Mills, K.R., Reginato, M., Debnath, J., Queenan, B., and Brugge, J.S. (2004). Tumor necrosis factor-related apoptosis-inducing ligand (TRAIL) is required for induction of autophagy during lumen formation in vitro. Proc Natl Acad Sci U S A *101*, 3438-3443.

169. Kim, S.B., and Berdanier, C.D. (1999). Oligomycin sensitivity of mitochondrial F(1)F(0)-ATPase in diabetes-prone BHE/Cdb rats. Am J Physiol *277*, E702-707.

170. Blatt, N.B., Bednarski, J.J., Warner, R.E., Leonetti, F., Johnson, K.M., Boitano, A., Yung, R., Richardson, B.C., Johnson, K.J., Ellman, J.A., Opipari, A.W., Jr., and Glick, G.D. (2002). Benzodiazepine-induced superoxide signals B cell apoptosis: mechanistic insight and potential therapeutic utility. J Clin Invest *110*, 1123-1132.

171. Gong, Y., Sohn, H., Xue, L., Firestone, G.L., and Bjeldanes, L.F. (2006). 3,3'-Diindolylmethane is a novel mitochondrial H(+)-ATP synthase inhibitor that can induce p21(Cip1/Waf1) expression by induction of oxidative stress in human breast cancer cells. Cancer Res *66*, 4880-4887.

172. Schieke, S.M., Phillips, D., McCoy, J.P., Jr., Aponte, A.M., Shen, R.F., Balaban, R.S., and Finkel, T. (2006). The mammalian target of rapamycin (mTOR) pathway regulates mitochondrial oxygen consumption and oxidative capacity. J Biol Chem *281*, 27643-27652.

173. Johnson, K.M.C., J.; Fierke, C.A.; Opipari A.W.; Glick, G.D. (2006). Mechanistic Basis for Therapeutic Targeting of the Mitochondrial F1Fo-ATPase. ACS Chemical Biology *1*, 304-308.

174. Boitano, A., Emal, C.D., Leonetti, F., Blatt, N.B., Dineen, T.A., Ellman, J.A., Roush, W.R., Opipari, A.W., and Glick, G.D. (2003). Structure activity studies of a novel cytotoxic benzodiazepine. Bioorg Med Chem Lett *13*, 3327-3330.

175. Kramar, R., Hohenegger, M., Srour, A.N., and Khanakah, G. (1984). Oligomycin toxicity in intact rats. Agents Actions *15*, 660-663.

176. Riby, J.E., Firestone, G.L., and Bjeldanes, L.F. (2008). 3,3'-diindolylmethane reduces levels of HIF-1alpha and HIF-1 activity in hypoxic cultured human cancer cells. Biochem Pharmacol *75*, 1858-1867.

177. Chen, I., McDougal, A., Wang, F., and Safe, S. (1998). Aryl hydrocarbon receptor-mediated antiestrogenic and antitumorigenic activity of diindolylmethane. Carcinogenesis *19*, 1631-1639.

178. Wattenberg, L.W., and Loub, W.D. (1978). Inhibition of polycyclic aromatic hydrocarbon-induced neoplasia by naturally occurring indoles. Cancer Res *38*, 1410-1413.

179. Bhagavathula, N., Nerusu, K.C., Hanosh, A., Aslam, M.N., Sundberg, T.B., Opipari, A.W., Jr., Johnson, K., Kang, S., Glick, G.D., and Varani, J. (2008). 7-Chloro-5-(4-hydroxyphenyl)-1-methyl-3-(naphthalen-2-ylmethyl)-4,5-dihydr o-1H-benzo[b][1,4]diazepin-2(3H)-one (Bz-423), a benzodiazepine, suppresses keratinocyte proliferation and has antipsoriatic activity in the human skin-severe, combined immunodeficient mouse transplant model. J Pharmacol Exp Ther *324*, 938-947.

180. Bednarski, J.J., Lyssiotis, C.A., Roush, R., Boitano, A.E., Glick, G.D., and Opipari, A.W., Jr. (2004). A novel benzodiazepine increases the sensitivity of B cells to receptor stimulation with synergistic effects on calcium signaling and apoptosis. J Biol Chem *279*, 29615-29621.

181. Lowell, B.B., and Shulman, G.I. (2005). Mitochondrial dysfunction and type 2 diabetes. Science *307*, 384-387.

182. Sekine, N., Cirulli, V., Regazzi, R., Brown, L.J., Gine, E., Tamarit-Rodriguez, J., Girotti, M., Marie, S., MacDonald, M.J., Wollheim, C.B., and et al. (1994). Low lactate dehydrogenase and high mitochondrial glycerol phosphate dehydrogenase in pancreatic beta-cells. Potential role in nutrient sensing. J Biol Chem *269*, 4895-4902.

183. Antinozzi, P.A., Ishihara, H., Newgard, C.B., and Wollheim, C.B. (2002). Mitochondrial metabolism sets the maximal limit of fuel-stimulated insulin secretion in a model pancreatic beta cell: a survey of four fuel secretagogues. J Biol Chem *277*, 11746-11755.

184. McCormack, J.G., Halestrap, A.P., and Denton, R.M. (1990). Role of calcium ions in regulation of mammalian intramitochondrial metabolism. Physiol Rev *70*, 391-425.

185. Ishihara, H., Maechler, P., Gjinovci, A., Herrera, P.L., and Wollheim, C.B. (2003). Islet beta-cell secretion determines glucagon release from neighbouring alpha-cells. Nat Cell Biol *5*, 330-335.

186. Henquin, J.C. (2004). Pathways in beta-cell stimulus-secretion coupling as targets for therapeutic insulin secretagogues. Diabetes *53 Suppl 3*, S48-58.

187. Noda, M., Yamashita, S., Takahashi, N., Eto, K., Shen, L.M., Izumi, K., Daniel, S., Tsubamoto, Y., Nemoto, T., Iino, M., Kasai, H., Sharp, G.W., and Kadowaki, T. (2002). Switch to anaerobic glucose metabolism with NADH accumulation in the beta-cell model of mitochondrial diabetes. Characteristics of betaHC9 cells deficient in mitochondrial DNA transcription. J Biol Chem *277*, 41817-41826.

188. Jones, R.G., Bui, T., White, C., Madesh, M., Krawczyk, C.M., Lindsten, T., Hawkins, B.J., Kubek, S., Frauwirth, K.A., Wang, Y.L., Conway, S.J., Roderick, H.L., Bootman, M.D., Shen, H., Foskett, J.K., and Thompson, C.B. (2007). The proapoptotic factors Bax and Bak regulate T Cell proliferation through control of endoplasmic reticulum Ca(2+) homeostasis. Immunity *27*, 268-280.

189. Denton, R.M., and McCormack, J.G. (1990). Ca2+ as a second messenger within mitochondria of the heart and other tissues. Annu Rev Physiol *52*, 451-466.

190. Devadas, S., Zaritskaya, L., Rhee, S.G., Oberley, L., and Williams, M.S. (2002). Discrete generation of superoxide and hydrogen peroxide by T cell receptor stimulation: selective regulation of mitogen-activated protein kinase activation and fas ligand expression. J Exp Med *195*, 59-70.

191. Kaminski, M., Kiessling, M., Suss, D., Krammer, P.H., and Gulow, K. (2007). Novel role for mitochondria: protein kinase Ctheta-dependent oxidative signaling organelles in activation-induced T-cell death. Mol Cell Biol *27*, 3625-3639.

CHAPTER 2

BZ-423 INHIBITS B CELL PROLIFERATION BY TARGETING C-MYC PROTEIN FOR RAPID AND SPECIFIC DEGRADATION

Introduction

Comparison of Bz-423 to other 1,4-benzodiazepines: The immunomodulatory agent Bz-423 was identified by screening a library of 1,4-benzodiazepines for lymphotoxic activity in the Ramos Burkitt's lymphoma B cell line (Figure 2.1A; [1]). In this screen, Bz-423 caused a concentration-dependent reduction in the viability of Ramos B cells with an EC_{50} ~6 μM after 24 h [1]. 1,4-Benzodiazepines were evaluated because this chemotype has been demonstrated not to damage DNA or interfere with nucleotide metabolism [2]. As a result, lymphotoxic 1,4-benzodiazepines were expected to display novel mechanism(s) of action with the potential for greater selectivity than that observed with conventional cytotoxic agents.

The 1,4-benzodiazepine scaffold, composed of a benzene ring fused to seven-membered diazepine ring containing an aryl substituent at C5 (Figure 2.1B), is the consensus structure for a well-studied class of anxiolytics, anti-convulsants, and hypnotics [3]. These activities arise from binding to the central benzodiazepine receptor (CBR), which is a component of γ-aminobutyric acid (GABA)-gated chloride channel ($GABA_A$) found exclusively on the plasma membrane of post-synaptic neurons [2]. 1,4-Benzodiazepines are allosteric regulators of the CBR•$GABA_A$ complex that potentiates

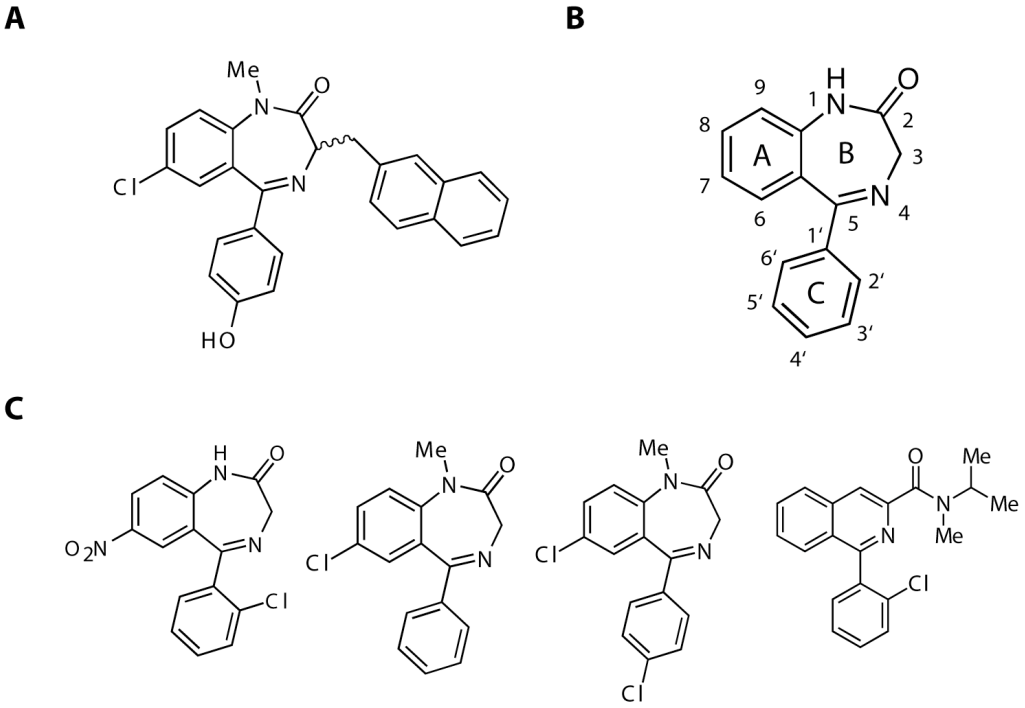

	Clonazepam	Diazepam	4′-Chlorodiazepam	PK 11195
CBR	3	17	73,000	4,000
IC_{50} (nM)				
PBR	5,100	29	4	2

Figure 2.1 – Comparison of Bz-423 to high affinity ligands of the central and peripheral benzodiazepine receptors. (A) Chemical structure of Bz-423. (B) General structure and numbering of the "classical" benzodiazepine ring system. (C) Chemical structures of high-affinity ligands of the central and peripheral benzodiazepine receptors. IC_{50} data is the concentration of each compound required to inhibit 50% binding of either [^{3}H]-flunitrazepam to the CBR or [^{3}H]-4'-chlorodiazepam to the PBR [4]. CBR, central benzodiazepine receptor; PBR, peripheral benzodiazepine receptor.

the response to GABA [2]. The resulting increase in chloride current is then responsible for the sedative and anti-anxiety effects of CBR ligands [2].

Since their initial development in the 1950's thousands of 1,4-benzodiazepine ligands of the CBR have been prepared, which enables detailed analysis of the structure-

activity relationships (SAR) for CBR binding and anxiolytic activity *in vivo* (all data is from [5]). Binding to the CBR requires an aromatic or hetero-aromatic ring (ring A), which is believed to participate in π/π stacking with aromatic residues in the receptor. Substitution of the 7-position with an electronegative group (e.g., halogen or nitro) increases *in vitro* affinity and anxiolytic activity. In contrast, substituents at positions 6, 8 or 9 are not permitted. A proton-accepting group (e.g., carbonyl) is required at the 2-position of ring B, putatively to interact with a receptor histidine residue. *N*-alkyl substitution on the amide nitrogen is permitted, although sterically bulky substituents (e.g., *tert*-butyl) are unfavored. Binding is also disrupted by incorporation of sterically bulky substituents at the methylene 3-position. The 5-phenyl ring C is not required for binding *in vitro*, but increases anxiolytic activity *in vivo*. Substitution at the 4'-*para*-position on ring C is disfavored. However, 2'-*ortho*-substituents are permitted, which suggests that limitations at the 4'-position are steric, rather than electronic, in nature.

The consensus SAR described above is apparent in the structures of the high affinity CBR ligands clonazepam (Cz) and diazepam (Dz), which bind with an IC_{50} of 3 and 17 nM, respectively [6]. Both compounds contain electron-withdrawing groups at the 7-position and lack substituents at the methylene 3-position and 4'-position on the phenyl ring [7]. In contrast, Bz-423 contains a napthylalanine substituent at the 3-position and a 4'-phenolic hydroxyl, which are expected to disfavor binding to the CBR (Figure 2.1A; [1]). Indeed, concentration of Bz-423 above the EC_{50} for cell death (≤10 μM) failed to displace the CBR ligand flunitrazepam in competitive binding experiments. Also consistent with lacking of binding to the CBR, grooming habits are not altered in mice treated with Bz-423 [1, 8].

In 1977 Braestrup and Squires identified a 1,4-benzodiazepine receptor distinct from the CBR by analyzing binding of [^{3}H]-Dz in sub-cellular fractions from rat brain, lung, liver and kidney [9]. [^{3}H]-Dz bound a single high affinity site (IC_{50} ~3 μM) on rat brain membrane fractions, but also bound mitochondrial fractions from the lung, liver and kidneys with slightly lower affinity (IC_{50} ~30 μM) [9]. Surprisingly, this binding appeared to result from interaction with a receptor distinct from the CBR, because 4'-chlorodiazepam (4'-Cl-Dz; Figure 2.1C), which does not bind the CBR, displaced [^{3}H]Dz [9]. This "peripheral binding" activity is now recognized to result from interaction of Dz with the peripheral benzodiazepine receptor (PBR), an 18 kDa protein primarily localized to the mitochondrial outer membrane [10]. The PBR displays a nearly ubiquitous tissue distribution, having been identified in heart, brain, adrenal, muscle, lymphoid, and reproductive tissues, but unlike the CBR, is not highly expressed in the central nervous system [11].

The PBR is localized to the mitochondrial outer membrane where it binds to the voltage-dependent anion channel (VDAC) [12]. The PBR•VDAC complex, along with the adenine nucleotide transporter (ANT), form the minimal consensus components of the mitochondrial permeability transition (mPT) pore [10]. The mPT pore is an important regulator of cellular Ca^{2+} homeostasis and apoptosis (see Chapter 3 Introduction). The PBR also mediates import of cytosolic cholesterol into the mitochondria, which is the rate-limiting step in steroid biosynthesis [13]. In addition, the PBR has been implicated in mitochondrial Ca^{2+} channel activity, porphyrin transport, heme biosynthesis, and regulation of anion transport by VDAC [12]. Despite these varied activities, the precise physiological function of the PBR remains enigmatic [12, 14].

Moreover, a clear pharmacological role for binding of the PBR with either high affinity 1,4-benzodiazepine ligands (e.g., 4'-Cl-Dz; IC_{50} ~4 nM) or isoquinoline carboxamides (e.g., PK 11195, IC_{50} ~2 nM) has yet to be established (Figure 2.3; [15]). Although both PK 11195 and 4-Cl-Dz are pro-apoptotic and growth inhibitory, these effects are only observed at concentrations greatly exceeding those needed to bind the PBR [16, 17]. For example, the EC_{50} for cell death induced by PK 11195 and 4'-Cl-Dz in Ramos B cells (90 and 130 μM, respectively [18]) is $>10^5$ K_d for PBR binding. In addition, concentrations of PK 11195 or 4-Cl-Dz that inhibit proliferation or induce apoptosis are not altered by reducing expression of the PBR with siRNA [19, 20]. These observations suggest that pharmacology associated with 4-Cl-Dz and PK 11195 does not result from binding to the PBR.

Bz-423 differs structurally from 1,4-benzodiazepine ligands (e.g., 4'-Cl-Dz) of the PBR by the 3-position naphthylalanine and 4'-phenolic hydroxyl substituents, both of which are required for cytotoxic activity [1]. These structural variations suggest that Bz-423 is not a high-affinity ligand of the PBR. This hypothesis has been evaluated in a competitive radioligand-binding assay, in which Bz-423 displaced radiolabeled PK 11195 with K_i ~0.3 μM, which is >100-fold lower affinity than 4'-Cl-Dz or PK 11195 [21]. While Bz-423 binds to the PBR with sub-micromolar affinity, this interaction is not expected to be responsible for the lymphotoxic activity. For instance, the EC_{50} for Bz-423-induced killing in Ramos B cells is at least 15-fold lower than that of either 4-Cl-Dz or PK 11195 (~6 versus >90 μM, respectively [18]), despite binding the PBR with >100-fold lower affinity [22]. In addition, preincubation of Ramos B cells with excess PK11195 (>20 μM) does not block killing by Bz-423 [1]. Collectively, these data

indicate that the unique structural features of Bz-423 preclude binding to the CBR and convey lymphotoxic activity that is independent of the PBR.

Bz-423 ameliorates disease in lupus-prone mice: The cytotoxic activity of Bz-423 was first identified in Ramos B cells [1]; a Burkitt's lymphoma line that originates from the pathogenic conversion of germinal center (GC) B cells [23]. GCs are observed in secondary lymphoid organs (e.g., lymph nodes, tonsils, and the spleen) where B-lymphocytes undergo affinity maturation, a process that selects for those cells expressing high-affinity antigen-receptors [24]. B cells that survive affinity maturation are, therefore, capable of generating high affinity antibodies [25]. Deregulation of affinity maturation is associated with production of high-affinity antibodies against self-antigens and autoimmune diseases [25, 26]. For instance, lupus-like renal disease in (NZB x NZW)F_1 (NZB/W) mice results from aberrant survival of GC B cells, enabling accumulation self-reactive clones that become activated and produce pathogenic autoantibodies [27, 28].

Because Ramos B cells model some aspects of GC physiology [23], it was reasoned that Bz-423 might improve disease in NZB/W mice by killing GC B cells. Indeed, Bz-423 reduced immune complex deposition and related renal disease (i.e., glomerulonephritis) in NZB/W mice [1]. Disease improvement was accompanied by a ~15% decrease in total splenic B cells, while T cell numbers were unchanged [1]. The reduction in the total B cell splenocytes population is a consequence of a >40% reduction in GC number and size [1]. These changes appear to result from increased apoptosis of GC B cells because spleens from Bz-423-treated NZB/W mice had more apoptotic cells than vehicle-treated spleens, as assessed by terminal deoxynucleotidyl transferase biotin-

dUTP nick end labeling (TUNEL) staining [1]. Also consistent with the decrease in GC numbers and size resulting from increased apoptosis of GC B cells, TUNEL-positive cells were detected exclusively within the remaining GCs [1]. These findings demonstrate that the apoptogenic activity of Bz-423 extends to the GC B cells *in vivo*, but more significantly, that this activity can be harnessed to treat diseases associated with aberrant survival of pathogenic lymphocytes.

Molecular target and mechanism of action: A rise in intracellular superoxide ($O_2^{\bullet-}$) levels within 1 h is the first change detected in Ramos B cells treated with Bz-423. Production of this reactive oxygen species (ROS) is followed at 4 h by release cytochrome *c* from the mitochondria, caspase activation, and DNA fragmentation, which are characteristic *late* apoptotic changes (see Chapter 3 Introduction; [1]). Scavenging $O_2^{\bullet-}$ with antioxidants inhibits all subsequent components of the death cascade and maintains viability, which indicates that elevated $O_2^{\bullet-}$ production signals apoptosis [1, 29]. Cell fractionation experiments revealed that the $O_2^{\bullet-}$ response results from interaction between Bz-423 and a target within the mitochondria [1]. Affinity-based screening of a phage-display human cDNA library identified the oligomycin sensitivity-conferring protein (OSCP), a subunit of the mitochondrial F_oF_1-ATPase, as a binding partner for Bz-423 [30]. Bz-423 inhibits the F_oF_1-ATPase in mitochondrial preparations and this inhibition depends on presence of the OSCP [30]. Reducing expression of the OSCP by RNA interference (RNAi) desensitizes cells to Bz-423-induced $O_2^{\bullet-}$ production and apoptosis, which links these responses to the effects of Bz-423 on the F_oF_1-ATPase.

Prior work in Ramos B cells and other Burkitt's lymphoma lines has demonstrated that sub-toxic concentrations of Bz-423 block growth by preventing

passage through the G_1-S cell cycle checkpoint [22]. The anti-proliferative activity of Bz-423 could also result from modulation of the F_oF_1-ATPase or from binding to another target. The PBR ligands PK11195 and 4-Cl-Dz have growth-inhibitory properties in a variety of cell-types including B lymphocytes [16, 17, 22]. Hence, Bz-423-induced growth arrest could result from binding to the PBR. However, anti-proliferative concentrations of Bz-423 generate $O_2^{\bullet-}$, and scavenging this ROS restores normal growth [22]. In contrast, anti-proliferative concentrations of PK11195 and 4-Cl-Dz do not elevate intracellular $O_2^{\bullet-}$ levels [16, 17, 22]. In addition, the GI_{50} for Bz-423-induced growth arrest is elevated by >50% in cells where OSCP levels have been reduced by RNAi [31]. Together, these data suggest that Bz-423-induced apoptosis and growth arrest both arise from OSCP-dependent modulation of the F_oF_1-ATPase depending on the magnitude of $O_2^{\bullet-}$ production.

Bz-423 has anti-psoriatic activity: The top layer of human skin, or epidermis, is primarily composed of keratinocytes [32]. Over a period of ~30 days, keratinocytes are pushed to the skin surface by continual division of underlying keratinocyte stem cells [32]. In healthy skin, this progression is accompanied by differentiation, which is characterized by morphological changes as well as secretion of large volumes of lipids and the extracellular matrix protein, keratin [33]. Once at the skin surface, terminally differentiated keratinocytes undergo programmed cell death and are sloughed off [32, 33]. The underlying dermis, in contrast, is not shed and is primarily populated by dermal fibroblasts along with keratinocyte stem cells [34].

Psoriasis is a chronic inflammatory skin disease characterized by thickened, scaly lesions known as plaques [35]. This disease is associated with increased proliferation and

altered differentiation of keratinocytes resulting in epidermal hyperplasia [33]. Current treatments for mild to moderate psoriasis rely on topically applied corticosteroids (e.g., Clobesterol propionate) to reduce epidermal hyperplasia [36]. Over time, however, steroid treatment results in atrophy of the underlying dermis, causing a disruption of normal skin architecture [36]. These effects on underlying and adjacent skin, combined with systemic side effects related to suppression of adrenal function, limit the use of topical corticosteroids [36]. Consequently, there is a need for therapies that reduce psoriatic epidermal hyperplasia by selectively blocking keratinocyte proliferation.

A contributing factor to the hypoproliferative phenotype in psoriatic skin is deregulated expression of c-Myc, an oncogenic transcription factor that stimulates cell cycle progression [37]. Structure, function, and regulation of c-Myc is described in detail below. c-Myc plays a physiological role in promoting keratinocyte proliferation after these cells emerge from the underlying stem cell compartment [33, 38]. As a result, c-Myc is detected in the basal (i.e., bottom most) layer of keratinocytes in both healthy and psoriatic skin. In healthy skin, c-Myc is not present in suprabasal keratinocytes, such that these cells lose their proliferative capacity and undergo terminal differentiation [38, 39]. However, c-Myc can be readily detected in the expanded subrabasal layer of keratinocytes in psoriatic lesions [38, 39]. In addition, specific overexpression of c-Myc in subrabasal keratinocytes results in changes (e.g., epidermal hyperplasia) characteristic of psoriatic skin [40].

Recent evidence suggests that ROS may play a role in keratinocyte differentiation [41]. In particular, $O_2^{\bullet -}$ levels are four-fold higher in kerationcytes than dermal fibroblasts [41]. This high level of in intracellular $O_2^{\bullet -}$ is thought to result from nearly

undetectable levels of MnSOD [41]. Along with (and perhaps due to) increased levels of $O_2^{\bullet-}$, the ratio of oxidized to reduced glutathione is more than two-fold greater in keratinocytes than fibroblasts [41]. These differences suggest that epidermal keratinocytes may be susceptible to growth arrest induced by agents that, like Bz-423, stimulate $O_2^{\bullet-}$ production. This hypothesis suggests that concentrations of Bz-423 that block lymphocyte proliferation might have anti-psoriatic activity resulting from preferential suppression of keratinocyte proliferation.

As an initial test of this hypothesis, the effects of Bz-423 on keratinocyte and fibroblast proliferation were examined in monolayer culture. Bz-423-induced $O_2^{\bullet-}$ production is detected by oxidation of the $O_2^{\bullet-}$-selective dye dihydroxyethidium (DHE). Cellular ROS levels can also be assessed with 2,7-dichlorodihydrofluorescein (DCFH), which is oxidized to its fluorescent derivative dichlorofluorescein (DCF) by H_2O_2 as well as by hydroxyl radical, lipid peroxides and peroxynitrite (see Chapter 1 [42]). H_2O_2 can be produced by either spontaneous or SOD-catalyzed dismutation of $O_2^{\bullet-}$ (see Chapter 1), which suggests that Bz-423 might also increase intracellular H_2O_2 levels. In support of this hypothesis, increased levels of H_2O_2 are detected in Ramos B cells and keratinocytes treated with Bz-423 [22, 43]. Perhaps due to the lower levels of reduced glutathione in keratinocytes relative to dermal fibroblast, the EC_{50} for Bz-423-induced H_2O_2 production was decreased three-fold in keratinocytes relative to dermal fibroblasts (<2 versus >6 μM, respectively) [43]. In addition, Bz-423 suppressed keratinocyte proliferation at concentrations >10-fold lower (0.9 versus >10 μM, respectively) that those required to block growth of dermal fibroblasts [43].

Based on these results in monolayer cultures, the anti-psoriatic activity of Bz-423 was evaluated in human skin organ cultures treated with retinoic acid (RA) [43]. This model was examined because psoriatic and RA-induced epidermal hyperplasia both result from kerationcyte hyperproliferation [44, 45]. Bz-423 reduced the epidermal thickness of RA treated skin [43]. This effect was accompanied by a decrease in the number of epidermal cells (i.e., keratinocytes) positive for Ki-67, a nuclear protein exclusively expressed in proliferating cells [43]. This observation suggests that Bz-423 reduces RA induced epidermal hyperplasia by blocking keratinocyte hyperproliferation. Significantly, these effects were not accompanied by changes in the size or structure of the underlying dermis [43].

To determine whether Bz-423 also suppresses proliferation of psoriatic keratinocytes, a topical formation of Bz-423 was applied to human psoriatic skin grafted onto severe, combined immunodeficient (SCID) mice [46]. In this model, topical application of Bz-423 (2.5%) for two weeks decreased epidermal thickness and the number of Ki-67-positive cells [46]. Unlike grafts treated with topical preparations of the corticosteroid Clobesterol propionate (0.05%), the therapeutic effects of Bz-423 were not accompanied by disruption of normal skin architecture. These studies demonstrate that Bz-423 has preferential growth inhibitory effects on keratinocytes relative to dermal fibroblasts, which results in reduction of RA and psoriatic epidermal hyperplasia without causing atrophy of the underlying skin.

Regulation of G_1-S cell cycle progression: Bz-423-induced growth arrest is associated with accumulation of cells at the G_1-S cell cycle checkpoint [22]. Cells commit to mitosis once DNA replication begins during S phase. Consequently, G_1-S

phase progression is tightly regulated by mechanisms collectively referred to as a checkpoint. S-phase induction is signaled by activation of the E2F family of transcription factors, which induce expression of genes required for DNA replication and an increase in cell size [47]. In quiescent cells, retinoblastoma (pRb) family proteins inhibit expression of S-phase genes by sequestering E2F transcription factors. In response to mitogenic stimuli (e.g., ligation growth factor receptors), pRb is multiply phosphorylated by cyclin-dependent kinases (CDKs) [48], which results in derepression of E2F-dependent gene transcription and progression through the G_1-S checkpoint (Figure 2.2; [49]).

Impaired G_1-S progression in the presence of Bz-423 suggests that CDK activity may be reduced. CDK activity depends on the relative levels of cyclins and CDK inhibitors. CDK4 and CDK6 are active when bound by D-type cyclins, whereas binding of E-type cyclins activates CDK2. CDK inhibitors are small proteins that interfere with CDK activity by either preventing association with cyclins or binding to the ATP-binding groove in CDK catalytic domains. Two families of CDK inhibitors oppose G_1-S phase progression. The Ink4 family of CDK inhibitors ($p15^{Ink4b}$, $p16^{Ink4a}$, $p18^{Ink4c}$ and $p19^{Ink4d}$) bind to CDK4 and CDK6 and prevent their association with D-type cyclins [50]. In contrast, the Cip/Kip family of CDK inhibitors ($p21^{Cip1}$, $p27^{Kip1}$ and $p57^{Kip2}$) prevent binding of CDK2 with E-type cyclins (Figure 2.2; [51, 52]). Overexpression of cyclins stimulates growth and reduces growth factor dependence, while high levels of CDK inhibitors block growth [53-55]. Like endogenous CDK inhibitors, small molecule inhibitors of these kinases reduce pRb phosphorylation and block growth [52]. As such, several small-molcule CDK inhibitors are being developed as chemotherapeutics [56].

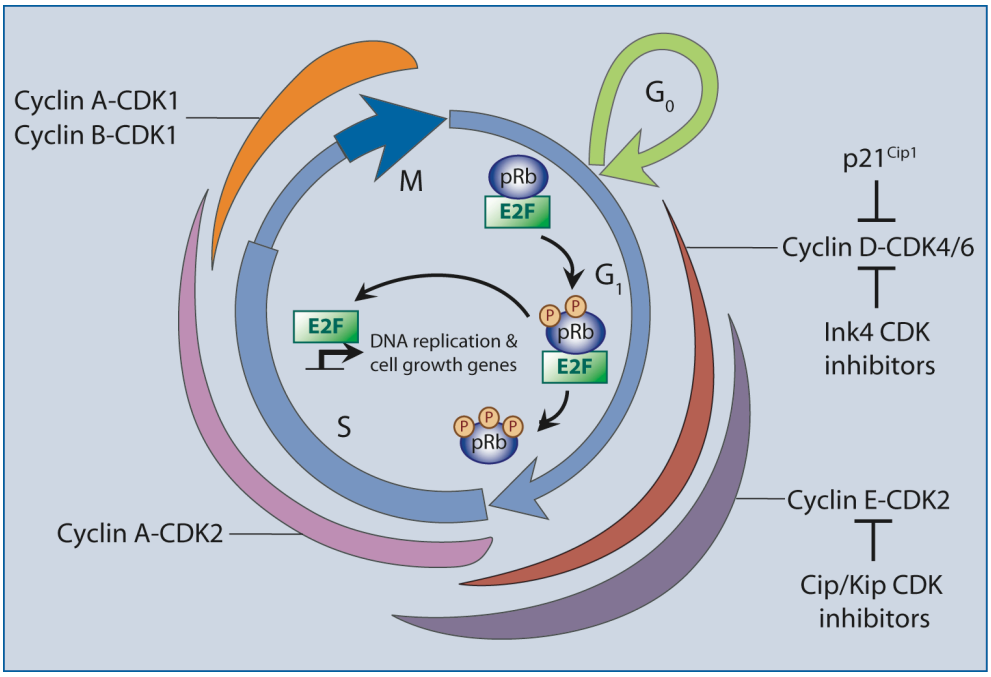

Figure 2.2 - Regulation of G_1-S phase progression. Passage from G_1 to S phase results from activation of E2F transcription factors, which induce genes necessary for DNA replication and cell growth. During G_1, E2F transcription factors are bound to retinoblastoma protein (pRb) or other pocket proteins (e.g., p107 or 130; not shown). Phosphorylation of pRb by cyclin-dependent kinases (CDKs) disrupts the pRb-E2F complex. CDKs are only active when complexed with cyclins. Complexes of CDK4 or CDK6 with D-type cyclins phosphorylated pRb early in G_1, while cyclin E-CDK2 complexes active immediately prior to S-phase. The size of the crescent indicates the magnitude of cyclin-CDK complex activity at particular points within the cell cycle. Cyclin D-CDK4/6 activity is opposed by Ink4 ($p15^{Ink4b}$, $p16^{Ink4a}$, $p18^{Ink4c}$ and $p19^{Ink4d}$) family of CDK inhibitors and $p21^{Cip1}$, a member of the Cip/Kip family of CDK inhibitors. Cip/Kip ($p21^{Cip1}$, $p27^{Kip1}$ and $p57^{Kip2}$) CDK inhibitors also inhibit cyclin E-CDK2 complexes. See text for additional detail. Figure adopted from [57].

The oncogenic transcription factor c-Myc: The cytostatic activity of Bz-423 is unlikely to result from direct inhibition of CDKs. An affinity-based screen failed to identify CDKs as binding partners for Bz-423 [30]. In addition, as is observed for Bz-423-induced apoptosis, antioxidants that scavenge $O_2^{\bullet-}$ restore normal growth [22]. The shared dependence of Bz-423-induced apoptosis and growth arrest on $O_2^{\bullet-}$ suggests that

both responses result from effects of Bz-423 on the F_oF_1-ATPase. Besides direct inhibition of CDK activity, G_1 arrest can also result from modulation of transcription factors that control expression of cyclins, CDKs and CDK inhibitors. For instance, the CDK inhibitor $p21^{Cip1}$ is upregulated in a p53-dependent manner in response to DNA damage [58]. However, induction of $p21^{Cip1}$ is unlikely to contribute to Bz-423-induced growth arrest because one copy of *p53* is deleted in Ramos B cells while the remainin allele encodes a transcriptionally inactive mutant [59].

G_1 arrest can also result from reductions in the levels and/or activity of transcription factors that promote proliferation. For example, stimulation with the growth-inhibitory cytokine transforming growth factor-β (TGF-β) prevents S-phase induction by suppressing expression of the oncogenic transcription factor c-Myc [60]. The *myc* gene was identified 30 years ago from a cellular DNA sequence captured by several chicken retroviruses [61]. Since then, genetic alterations involving Myc proteins, including N-Myc and L-Myc, such as translocation, gene amplification and stabilizing point mutations have been identified in many human malignancies [62-64]. Burkitt's lymphoma, a cancer of B cells, is specifically associated with c-Myc levels that are elevated due to translocation of *cmyc* to the immunoglobulin gene locus, which places it under the transcriptional control of powerful immunoglobulin enhancers [65].

c-Myc promotes passage through the G_1-S checkpoint by coordinately regulating genes essential for cell cycle progression (Table 2.1). In particular, c-Myc activates transcription of CDK2, CDK4 and CDK6 as well as D- and E-type cyclins, and it represses transcription of $p15^{Ink4b}$, $p21^{Cip1}$ and $p27^{Kip1}$. Expression of cyclins and CDKs can be induced by transcription factors including nuclear factor of activated T cells

(NFAT) [66], nuclear factor-κB (NF-κB) [67, 68], and signal transducers and activators of transcription (STAT) [69]. Unlike these transcription factors, however, forced expression of c-Myc is sufficient to stimulate DNA synthesis in quiescent fibroblasts [70-72]. Conversely, cell cycle progression is impaired in *cmyc*-null fibroblasts due to a block at the G_1-S checkpoint [73, 74]. Because of these properties, c-Myc is described as a 'master regulator' of G_1-S phase progression [75].

c-Myc plays an essential role in lymphocyte maturation and proliferation [76-78]. For example, c-Myc mRNA and protein levels are elevated during T cell development in the thymus [78]. Likewise, *cmyc* induction is observed in B cell development during the burst of proliferation that accompanies productive assembly of the B-cell receptor (BCR) [78]. In quiescent, mature T cells, c-Myc expression is suppressed due to a block in transcriptional elongation, as well as by rapid degradation of *cmyc* mRNA [77]. These inhibitory mechanisms are relieved following stimulation of the T cell antigen receptor (TCR), which results in a >10-fold increase in c-Myc expression in activated T cells [77]. A similar increase in c-Myc expression is observed following BCR stimulation of mature B cells [78]. These changes appear to be functionally consequential because antigen-receptor stimulation-induced proliferation is reduced in c-Myc deficient B and T cells. Hence, c-Myc appears to play an essential role in normal lymphocyte development as well proliferation of activated B and T cells during an immune response. However, deregulated expression of c-Myc in hematopoetic cells can result in pathologies (e.g., Burkitt's lymphoma) resulting from unrestrained lymphocyte proliferation [75].

Gene Target	Description	Regulation
AIM1	AIM1 Absent in melanoma 1	Activated
CCNA2	cyclin A2	Activated
CCNB1	cyclin B1	Activated
CCND1	cyclin D1	Repressed
CCND2	cyclin D2	Activated
CCND3	cyclin D3	Activated
CCNE1	cyclin E1	Activated
CCNG2	U2AF1 U2(RNU2) small nuclear RNA auxiliary factor 1	Repressed
CDC2	cyclin dependent kinase 1; cell division cycle 2	Activated
CDC25A	CDC25A Cell division cycle 25A	Activated
CDC25C	CDC25C Cell division cycle 25C	Activated
CDC2L1	CDC2L1 Cell division cycle 2-like 1 (PITSLRE proteins)	Activated
CDK4	CDK4 Cyclin-dependent kinase 4	Activated
CDK4	Cyclin-dependent kinase 4	Activated
CDK6	cyclin-dependent kinase 6	Activated
CDKN1A	cyclin-dependent kinase inhibitor 1A (p21, Cip1)	Repressed
CDKN1B	cyclin-dependent kinase inhibitor 1B (p27, Kip1)	Repressed
CDKN2B	cyclin-dependent kinase inhibitor 2B (p15, Ink4b)	Repressed
CEB1	LOC51191 Cyclin-E binding protein 1	Activated
CHES1	checkpoint regulator	Repressed
CKS2	CDC28 protein kinase regulatory subunit 2	Activated
E2F1	E2F1: E2F transcription factor 1	Activated
E2F2	E2F2: E2F transcription factor 2	Activated
E2F3	E2F transcription factor 3	Activated
E2IG3	nucleotide b.prot., estradiol-induced	Activated
PCNA	Proliferating cell nuclear antigen	Activated
RB1	retinoblastoma 1	Repressed
ATR	ataxia telangiectasia/Rad3 related	Activated
PELP1	proline-, glutamic acid-, leucine-rich protein 1	Activated

Table 2.1 – c-Myc target genes associated with cell cycle progression. For a complete list of c-Myc target genes curated by the National Library of Medicine, see http://www.myc-cancer-gene.org.

c-Myc is a basic helix-loop-helix leucine zipper (bHLHZip) transcription factor that forms a heterodimer with Max, a smaller bHLHZip protein (Figure 2.3; [75]). c-Myc-Max heterodimers activate transcription of target genes by binding consensus DNA recognition sequences (CACA/GTG) known as E-boxes [79]. In addition, Myc is recruited to non-consensus sequences though interactions with protein inhibitor of activated Stat X (PIASX also known as Miz1) and specificity protein-1 (Sp1) (Figure 2.3; [80, 81]). c-Myc binding represses activity of these transcription factors, which results in reduced expression of growth inhibitory proteins such as $p15^{Ink4b}$, $p21^{Cip1}$ and $p27^{Kip1}$ [80]. Given that it is unlikely that Bz-423 directly inhibits CDKs, G_1 arrest could result from modulation of transcription factors such as c-Myc that control levels of cyclins, CDKs and CDK inhibitors.

Statement of problem: Elevated mitochondrial $O_2^{\bullet-}$ production is the proximal signal for Bz-423-induced growth arrest and apoptosis. However, the signal transduction pathway linking this response to effects on the cell cycle were not known. The studies described in this chapter were undertaken to gain insight into the mechanism linking increased mitochondrial $O_2^{\bullet-}$ production to impaired cell cycle progression. These experiments were primarily conducted using Ramos B cells because this cell line models aspects of GC physiology, and Bz-423 has specific effects on GCs *in vivo*. Despite being carried out in transformed B cells, results of these studies are also expected to provide insight into the growth-inhibitory activity of Bz-423 in psoriatic keratinocytes.

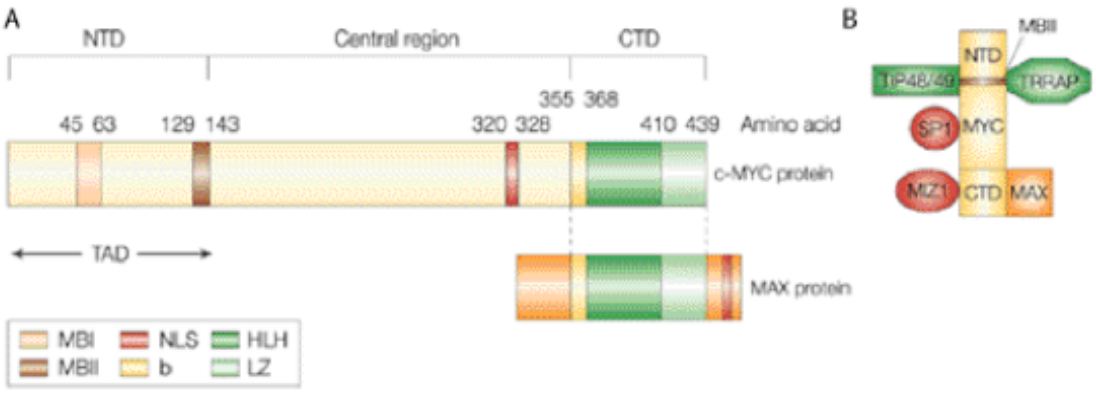

Figure 2.3 – c-Myc protein functional domains. (A) The carboxy-terminal domain (CTD) of human Myc protein harbors the basic Helix/Loop/Helix-Leucine Zipper (bHLHZip) motif required for dimerization with Max and subsequent DNA binding. The amino-terminal domain (NTD) contains the conserved Myc Boxes' I and II (MBI and MBII), which are essential for the transactivation of Myc target genes. (B) Myc-interacting proteins include co-activator TRRAP (transformation/transcription domain-associated protein), which possesses histone acetyltransferase (HAT) activity, TIP48 and TIP49 proteins interact with the NTD of c-Myc and are implicated in chromatin remodeling due to their ATP-hydrolyzing and helicase activities. c-Myc also binds proteins involved in transcriptional repression, such as the transcription factors Miz1 and Sp1. Figure adapted from [75].

Results

Bz-423 modulates cellular polyamine metabolism: A complex network of signals, many of which are controlled at the transcriptional level, regulate G_1-S phase progression [75, 78, 82, 83]. Consequently, initial experiments using genome-wide cDNA microarray analysis were employed to identify potential responses that couple Bz-423-induced $O_2^{\bullet-}$ production to growth arrest. For this experiment, RNA was isolated from Ramos B cells treated with Bz-423 (10 μM, 4 h), and changes in gene expression were examined relative to transcript levels in vehicle treated cells. This time-point was analyzed to identify changes in mRNA levels related to the induction of growth arrest rather than

non-specific consequences of impaired cell cycle progression. All experiments investigating the mechanism of Bz-423-induced growth arrest were carried out in media containing 10% (v/v) fetal bovine serum (FBS). High serum media was used to provide levels of growth factors that suppress background killing in Ramos B cells to be cultured for periods >24 h [22]. Extended time points were used to study the anti-proliferative activity of Bz-423, because the difference in cell numbers between normally proliferating and growth-inhibited Ramos B cells is greater [22].

It is well established, however, that non-specific serum binding regulates the bioavailability of 1,4-benzodiazepines by altering concentrations of the free drug [84]. For example, at 10 μM Bz-423 nearly 99% of the drug is serum-bound in media containing 10% FBS [22]. Therefore, initial studies of the lymphotoxic activity of Bz-423 were carried out in reduced FBS (2% v/v) media, which revealed an EC_{50} for cell death ~6 μM, whereas the drug concentration reducing growth by 50% (GI_{50}) is ~2 μM [22]. The lymphotoxic activity of Bz-423 against Ramos B cells is observed in media contain 10% FBS, but with an EC_{50} ~25 μM at 24 h [22]. Similarly, in Ramos B cells, the GI_{50} for Bz-423-induced growth arrest is ~11 μM after 72 h [22].

Exposure to Bz-423 was accompanied by increases in the mRNA levels of genes involved in glycolysis, oxidative phosphorylation, and stress responses (Table 2.2). The most pronounced change in terms of the number of genes induced is an increase in glycolytic enzymes (Table 2.2). This observation suggests that cells treated with Bz-423 may increase glycolytic ATP production to partially offset impaired oxidative phosphorylation due to the effects of Bz-423 on the F_oF_1-ATPase. Consistent with this hypothesis, increased glucose uptake and lactate production is observed in cells treated

Gene	Function	Fold Induction
Glyceraldehyde-3-phosphate dehydrogenase	Glycolysis	23
Transketolase	Glycolysis	14
Phosphoglycerate kinase	Glycolysis	13
Enolase I	Glycolysis	11
Glucose phosphate isomerase	Glycolysis	9
Pyruvate kinase	Glycolysis	9
Mitochondrial F_o complex, subunit g	OXPHOS	12
NADH Dehydrogenase	OXPHOS	12
Adenine nucleotide translocator	Mitochondrial ATP/ADP Transport	20
Heat shock 60 kD protein 1	Stress Response	12
Heat shock 90 KD protein 1, β	Stress Response	21
Ornithine decarboxylase antizyme1	Polyamine Regulation	16

Table 2.2 - Genes upregulated by Bz-423. RNA was isolated from Ramos B cells treated with Bz-423 (10 μM) for 4 h in complete media containing 10% FBS and hybridized to a HGU133A Affymetrix Gene Chip. Fold mRNA increase is relative to vehicle. Fold changes represent the mean of two separate experiments. OXPHOS, oxidative phosphorylation.

with the macrolide F_oF_1-ATPase inhibitor, oligomycin [85-87]. When oxidative phosphorylation is impaired, pyruvate is reduced to lactate to regenerate NAD^+ instead of serving as carbon source for the TCA-cycle [88]. While these effects are consistent with modulation of the F_oF_1-ATPase, it is unlikely that Bz-423-induced growth arrest is signaled by increased glycolytic ATP production.

This analysis also demonstrated that ornithine decarboxylase antizyme 1 (OAZ1) was induced (Table 2.2). OAZ1 depletes cellular polyamines by acting as negative regulator of ornithine decarboxylase (ODC), an enzyme that mediates the conversion of the non-coded amino acid ornithine to putrescine in a rate-controlling step in polyamine biosynthesis [89]. Specifically, OAZ1 binding disrupts active ODC homodimers and further targets ODC for proteasomal degradation (Figure 2.4). Polyamines are low-

molecular weight organic cations that form complexes with nucleic acids and are required for normal proliferation [90]. Depletion of cellular polyamines blocks growth and, if sustained, results in cell death [91-93]. The increase in OAZ1 transcript levels suggests that the cytostatic activity of Bz-423 may result from changes in cellular polyamine metabolism. Specifically, elevated OAZ1 expression would be expected to increase proteasomal degradation of ODC, thereby limiting polyamine biosynthesis and blocking growth.

To test this hypothesis, production of [^{3}H]-putrescine from [^{3}H]-ornithine was measured in the vehicle and in Bz-423-treated Ramos B cells. Consistent with increased *oaz1* transcript levels, exposure to Bz-423 for 4 h reduced ODC activity (Figure 2.5A). To determine if the reduction in ODC activity translates into decreased cellular polyamine levels, Bz-423-treated Ramos B cells were lysed with trichloroacetic acid (TCA), and acid-soluble polyamines were converted to their benzoyl chloride derivatives and quantified by reversed-phase HPLC [92]. A reduction in cellular polyamine levels was observed after treatment with Bz-423 (Figure 2.5B). At concentrations of Bz-423 above the GI_{50} (11.5 ± 0.8 μM; [22]), the reduction was equivalent to that induced by the specific ODC inhibitor D,L-α-difluoromethylornithine (DFMO; [90]). Analyzing the effect of Bz-423 on cellular polyamines as a function of time revealed that this decrease was complete by 6 h, which corresponds to the increase in *oaz1* mRNA detected in the gene expression profile at 4 h (Figure 2.5C). These findings demonstrate that growth-inhibitory concentrations of Bz-423 reduce ODC activity and deplete cellular polyamine pools.

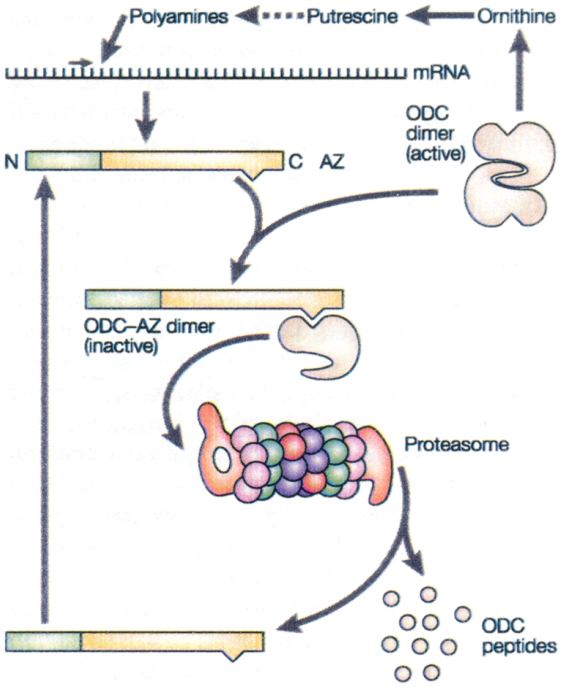

Figure 2.4 - OAZ1-depedent regulatory feedback mechanism stabilizing cellular polyamine pools. Polyamines promote OAZ1 expression by inducing a translational frameshift in *oaz1* mRNA. The carboxy-terminal half of AZ1 interacts with ODC, generating OAZ1-ODC heterodimers at the expense of enzymatically active ODC homodimers. The OAZ1 amino-terminal half then targets OAZ1-ODC to the proteasome, which results in degradation of ODC. OAZ1-mediated inhibition and destruction of ODC reduces polyamine biosynthesis, which completes the regulatory circuit by decreasing levels of polyamines available to promote OAZ1 translation. Figure adapted from [89].

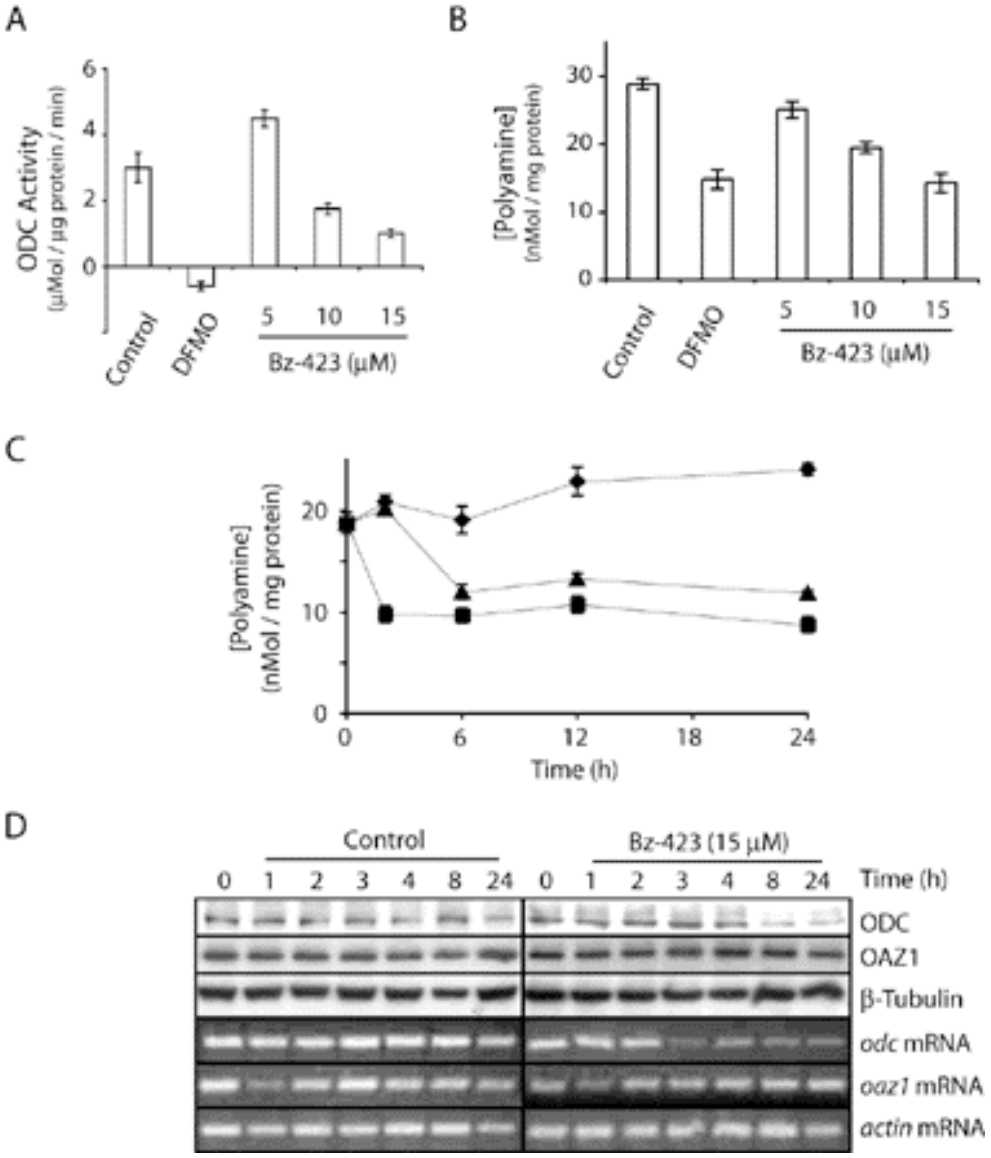

Figure 2.5 - Bz-423 modulates cellular polyamine metabolism. Ramos B cells were treated with either DFMO (1 mM) or the indicated concentrations of Bz-423, and (A) ODC activity was evaluated at 4 h as the amount of [^{3}H]putrescine produced from [^{3}H]ornithine and (B) cellular polyamine levels were quantified at 24 h by reversed-phase HPLC. (C) Total cellular polyamine levels were evaluated by reversed-phase HPLC in Ramos B cells treated with vehicle (◆), DFMO (1 mM; ■) or Bz-423 (15 µM; ▲) for the indicated times. DFMO is a selective, cell-permeable, non-reversible inhibitor of ODC (IC_{50} = 7.5 µM; [94]). (D) Whole cell lysates or cellular RNA were harvested from Ramos B cells treated with Bz-423 (15 µM) for indicated times. Immunoblotting or RT-PCR was performed to detect ODC and OAZ1 protein or mRNA levels, respectively. For C and D, 15 µM Bz-423 was employed because this concentration reduces growth by >80% without causing cell death [22]. All panels are representative of at least two separate experiments.

To determine whether the decrease in ODC activity corresponds with changes in the levels of ODC or OAZ1, amounts of both proteins were analyzed in lysates from Bz-423-treated Ramos B cells. Growth-inhibitory concentrations of Bz-423 substantially reduced ODC protein by 4 h (Figure 2.5D). Unexpectedly, however, OAZ1 protein levels were unchanged over the same time period. In addition, no change in *oaz1* mRNA levels, as detected by RT-PCR, was observed at time points up to 24 h. In contrast, a decrease in *odc* transcript levels was detected at 3 h (Figure 2.3D), which precedes the reduction in ODC protein at 4 h and cellular polyamine levels at 6 h. In sum, although the reduction in ODC protein levels is consistent with the effect of Bz-423 on cellular polyamines, the absence of an increase in OAZ1 protein argues that this decrease is not mediated by an OAZ1-dependent post-translational mechanism. Instead, the decrease in *odc* mRNA levels suggests that Bz-423 may reduce transcriptional activity of the *odc* gene

Bz-423 decreases c-Myc protein levels: The *odc* promoter region contains sequences that allow for responses to hormones, growth factors, and oncogenes, including a cAMP-response element, CAAT and LSF motifs, AP1 consensus sequences, and a GC-rich Sp1 binding site, as well as two E-box sequences bound by c-Myc/Max heterodimers [95, 96]. Despite the presence of binding sites for other transcription factors, inactivating mutations of both E-boxes reduce *odc* transcript levels by >80% in WI-38 human fibroblasts which suggests that Myc primarily drives transcription of *odc* [96]. Hence, the decrease in *odc* mRNA observed in Bz-423-treated Ramos B cells could result from a decrease in c-Myc levels and/or activity. To evaluate this hypothesis,

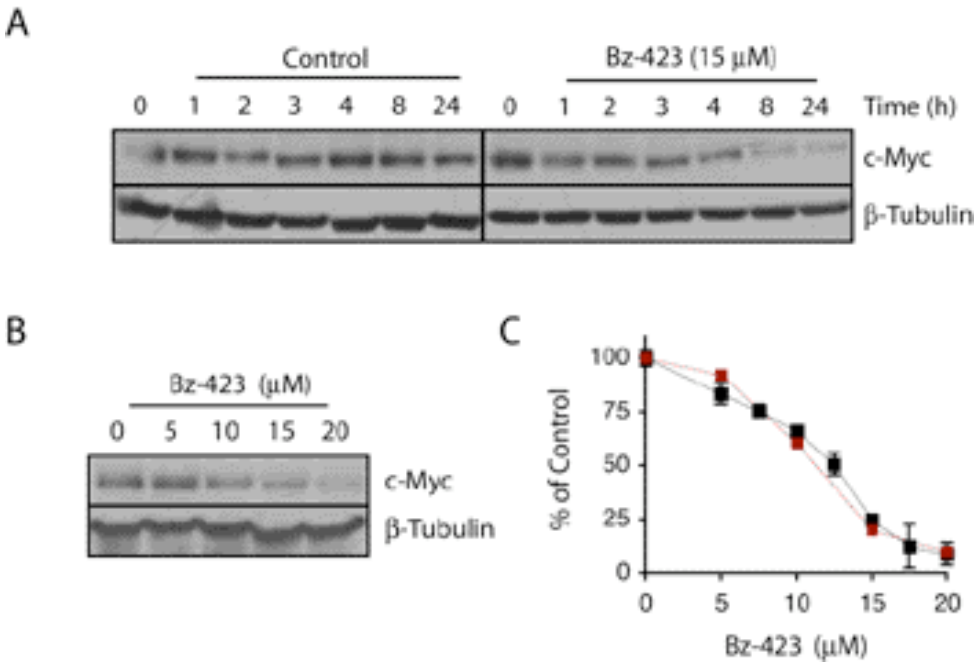

Figure 2.6 - Bz-423 induces a rapid decrease in c-Myc levels. (A) Whole cell lysates were isolated from Ramos B cells treated with Bz-423 (15 µM) for the indicated times and immunoblots were performed with specific antibodies as indicated. (B) Ramos B cells were treated with indicated concentrations of Bz-423 for 8 h and whole cell lysates were immunoblotted with specific antibodies as indicated. (C) The reduction in Myc levels at 8 h (■) was quantified by densitometry and compared to percent growth arrest (■) for Ramos B cells at 48 h. Panel A is representative of at least five separate experiments and panel B and C are representative of at least two separate experiments.

c-Myc protein levels were examined in lysates from Ramos B cells. This analysis revealed a 30% decrease in Myc protein by 1 h, which continued to fall to <10% of control by 8 h (Figure 2.6A). The Bz-423-induced decrease in Myc levels at 8 h is concentration-dependent (Figure 2.6B), and the magnitude of this decrease parallels percent growth arrest at 48 h (Figure 2.6C). These data suggest that the effects of Bz-423 on *odc* expression, as well as proliferation, might arise due to a decrease in c-Myc protein.

$O_2^{\bullet-}$ mediates the effect of Bz-423 on c-Myc and polyamine metabolism: Binding of Bz-423 to the OSCP component of the F_oF_1-ATPase slows the rate of ATP synthesis and triggers a mitochondrial respiratory transition, placing the MRC in a reduced state that favors the production of $O_2^{\bullet-}$ [1, 30]. The magnitude of Bz-423-induced $O_2^{\bullet-}$ response is concentration-dependent, such that sub-toxic concentrations of Bz-423 produce proportionally less $O_2^{\bullet-}$ and arrest growth of Burkitt's lymphoma cells at the G_1 checkpoint [22]. Bz-423-induced growth arrest also depends on the $O_2^{\bullet-}$ produced by modulation of the F_oF_1-ATPase. Thus, scavenging Bz-423-induced $O_2^{\bullet-}$ with the manganese superoxide dismutase (MnSOD) mimetic MnTBAP blocks the antiproliferative effects of Bz-423 in Ramos B cells [22]. Similarly, non-lymphoid cells (i.e., MCF-7 breast cancer cells) stably expressing high levels of MnSOD were less sensitive to Bz-423-induced growth arrest [22]. Finally, human embryonic kidney (HEK) 293 cells, in which OSCP levels had been stably diminished by RNA interference, produced less $O_2^{\bullet-}$ in response to Bz-423, and correspondingly, required higher concentrations of Bz-423 to induce growth arrest relative to control cells. Collectively, these findings demonstrate that growth arrest is linked to binding of Bz-423 to the OSCP by the $O_2^{\bullet-}$ signal [97].

Reduction in c-Myc protein and downstream effects on *odc* expression and on cellular polyamines are predicted to be components of the mechanism leading to Bz-423-induced growth arrest. Thus, these responses are also expected to be $O_2^{\bullet-}$-dependent. In support of this hypothesis, pretreatment with MnTBAP prevented the decrease in Myc levels and stabilized *odc* expression (Figure 2.7A). In addition, scavenging $O_2^{\bullet-}$ blocked the decrease in cellular polyamine levels (Figure 2.7B). Collectively, these results couple

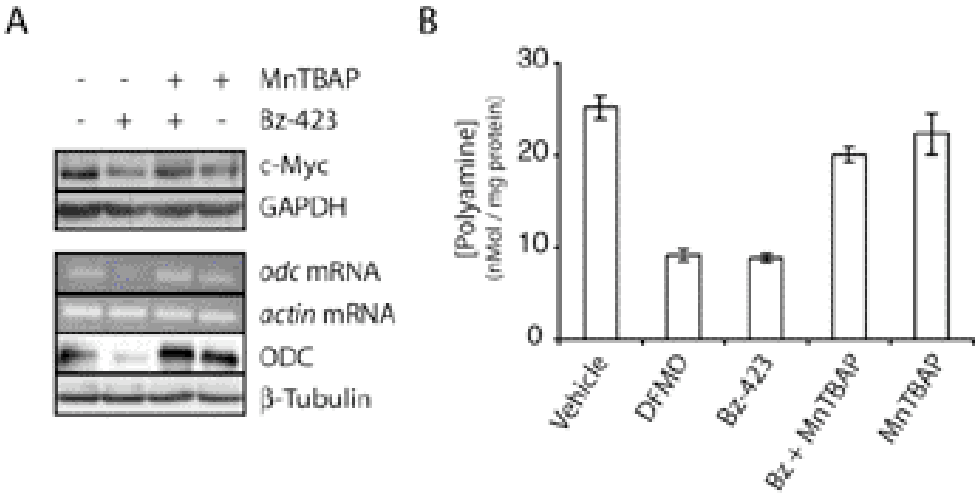

Figure 2.7 - Scavenging Bz-423-induced $O_2^{\bullet-}$ blocks the decrease in c-Myc levels, ODC expression, and polyamine levels. (A) Whole cell lysates or RNA were prepared from Ramos B cells pretreated with MnTBAP (100 μM) and then treated with Bz-423 (15 μM) for 8 h. Immunoblotting or RT-PCR was performed to evaluate Myc and ODC protein and mRNA levels, respectively. (B) Ramos B cells were treated with DFMO (1 mM) for 24 h or pretreated with MnTBAP (100 μM) and then treated with Bz-423 (15 μM) for 24 h and concentrations of cellular polyamines determined by reverse-phase HPLC. Both panels are representative of two separate experiments.

the Bz-423-induced $O_2^{\bullet-}$ response to the decrease in Myc protein and the subsequent effects on *odc* expression and cellular polyamine levels.

Bz-423 modulates proteins that control G_1-S phase progression: Besides transcriptional activation of *odc*, c-Myc promotes passage through the G_1 checkpoint by both transcriptional activation and repression of cell cycle regulatory genes [75]. Cell cycle progression is directed by cyclin-dependent kinases (CDKs), whose activity is dictated by the relative levels of cyclins and CDK inhibitors (CDKI) [48]. In particular, active complexes of CDK2, CDK4, or CDK6 with D-type cyclins as well as complexes of E-type cyclins and CDK2 promote the G_1-S transition. Cyclin-CDK complexes are inhibited by CDKIs including $p21^{Cip1}$ and $p27^{Kip1}$ [51]. Myc promotes the G_1-S transition by activating transcription of CDK2, 4 and 6 as well as D- and E-type cyclins, and

moreover, represses transcription $p21^{Cip1}$ and $p27^{Kip1}$ [75, 98, 99]. Because Bz-423 rapidly decreased c-Myc protein levels, we also expected to observe increased expression of CDKIs and decreased levels of CDK2, 4 and 6 as well as D- and E-type cyclins.

In accordance with the effect of Bz-423 on c-Myc protein levels, CDK4 was decreased to <10% of basal levels within 3 h of treatment. Levels of CDK2 and CDK6 were reduced to similar extent, but not until 24 h. Cyclin D3 was reduced to 20% of control by 2 h, whereas levels of cyclin D1 and D2 were maintained in the presence of Bz-423 for up to 24 h. Cyclin E1 levels were reduced by >50% following exposure to Bz-423 for 1 h and continued to decline till reduced by >90% after 24 h. The CDK inhibitor $p21^{Cip1}$ was nearly undetectable in untreated Ramos B cells, and did not rise in response to Bz-423. In contrast, $p27^{Kip1}$ levels increased two-fold after treatment with Bz-423 for 8 h (Figure 2.8). The decreases in cyclin D3, cyclin E1, and CDK4 occur earlier and to a greater extent than induction of $p21^{Cip1}$ or $p27^{Kip1}$. Although the basis for this difference is not known, it may be due to the dependence of $p21^{Cip1}$ or $p27^{Kip1}$ induction on processes in addition to reduction of c-Myc levels. For example, the growth-suppressive cytokine TGF-β induces *$p21^{Cip1}$* via a process that depends both on transcriptional repression of c-Myc as well as transcriptional activation by the Sp1/KLF (Krupple-like factors) family of transcription factors [100-102]. In contrast, genes that depend on c-Myc for expression, such as ODC [95] or cyclin D3 [103] should be more sensitive to decreased levels of this transcription factor. Overall, the observed changes in the levels of cyclins, CDKs and CDK inhibitors are consistent with the G_1 arrest induced by a decrease in c-Myc protein levels.

The primary substrates of the CDKs are the retinoblastoma (pRb) protein family, which includes pRb, p107 and p130 [49]. In their hypophosphorylated state, pRb proteins bind to members of the E2F family of transcription factors, and block transcription of E2F-regulated genes that drive S-phase entry. Phosphorylation pRb serine and threonine residues by CDKs results in derepression of E2F-dependent gene transcription and progression through the G_1 checkpoint [49]. Because Bz-423 reduces expression of D- and E-type cyclins as well as CDK2, CDK4 and CDK6, we expected to observe decreased phosphorylation of pRb. Consistent with this prediction, the overall phosphorylation state of pRb decreased following treatment with Bz-423, as indicated by an increase in electrophoretic mobility on SDS-PAGE (Figure 2.8).

Cyclin-CDK complexes phosphorylate a specific subset of pRb residues. For example, complexes of D-type cyclins with either CDK4 or CDK6 phosphorylate pRb at serine residues S780, S807 and S811, while cyclin E-CDK2 complexes specifically phosphorylate S795 [104, 105]. Based on these specificities, antibodies specific for phosphorylation of Ser780, Ser795, and Ser807/811 were used to assess whether reduced CDK2, CDK4 and/or CDK6 activities contributed to the overall decrease in pRb phosphorylation (Figure 2.6). Although CDK2 levels do not decrease until 8 h of exposure to Bz-423, CDK2 activity (evaluated in terms of pRb phosphorylation at S795) is undetectable by 3 h. Diminished CDK4/6 activity (i.e., phosphorylation of pRb at S780 and S807/S811) was also observed by 3 h, but both bands are present at >50% of control levels until 8 h (Figure 2.8). This difference may be due to the greater redundancy among the D-type cyclin-CDK4/6 complexes. Specifically, although cyclin

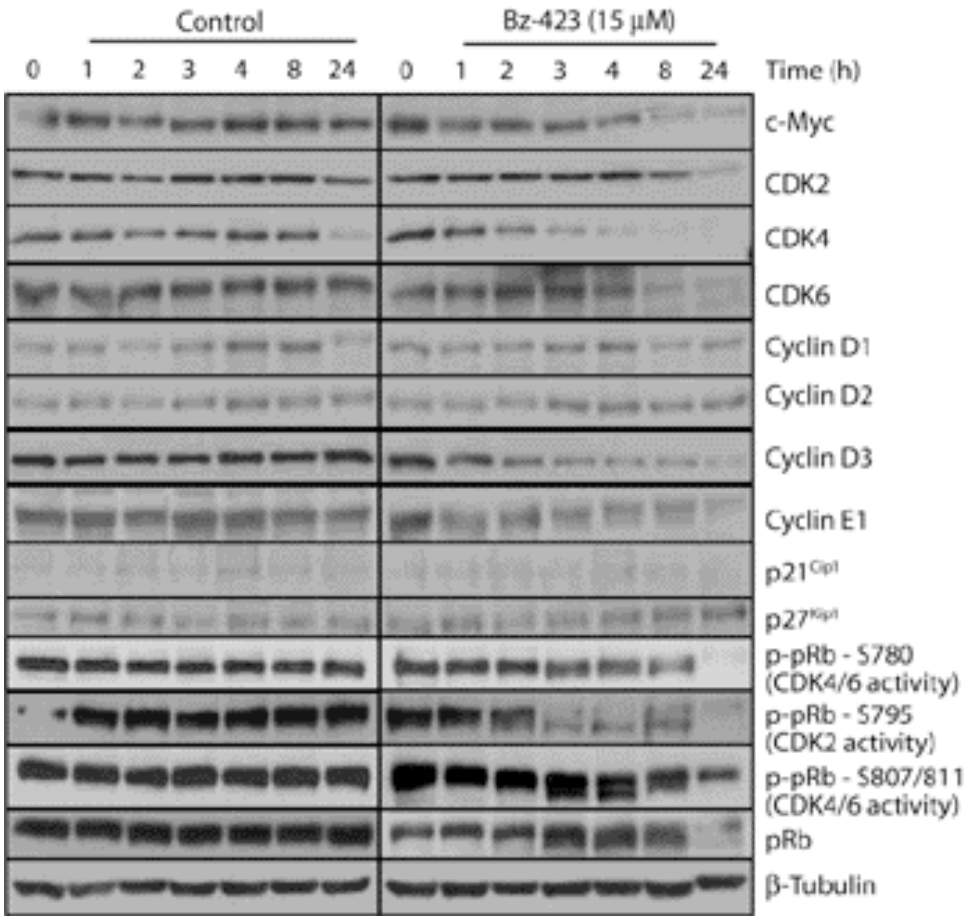

Figure 2.8 - Bz-423 modulates levels of G_1-S checkpoint proteins. Whole cell lysates were isolated from Ramos B cells that had been treated with Bz-423 (15 μM) for the indicated times, and immunoblots were performed with specific antibodies. Immunoblots are from a single experiment.

D3 and CDK4 are rapidly depleted, complexes of CDK6 with cyclin D1 or D2 may be able to maintain phosphorylation of pRb at S780 and S807/811 [106]. In contrast, levels of cyclin E1 are reduced after treatment of Ramos B cells with Bz-423 for 1 h, whereas expression of cyclin E2 was below the limits of detection by immunoblot. Consequently, the reduction in cyclin E1 is expected to translate into a rapid decrease in pRb phosphorylation at S795, despite the presence of normal CDK2 levels. Overall, the

decreases in phosphorylation of specific pRb residues are consistent with both the changes in the levels cyclins and CDKs induced by Bz-423 as well as G_1 arrest.

Bz-423 reduces c-Myc levels in keratinocytes: Bz-423-induced destabilization of c-Myc in Ramos B cells raised questions of whether a similar process is engaged in non-lymphoid cell-types. Keratinocytes were examined because Bz-423 inhibits growth of this cell-type *in vitro* (GI_{50} ~1 μM; [43]) and reduces epidermal hyperplasia in human psoriatic skin grafts [46]). In addition, as described in the introduction to this chapter, deregulated c-Myc expression appears to contribute to epidermal hyperplasia in psoriasis [33, 37, 38], which suggests that growth-inhibitory activity of Bz-423 in keratinocytes might result from destabilization of this transcription factor.

As an initial test of this hypothesis, levels of c-Myc, cyclin D3, pRb and phospho-pRb were evaluated in lysates from keratinocytes treated with Bz-423. Growth-inhibitory concentrations of Bz-423 (0.5 - 4 μM; [43]) did not reduce c-Myc or cyclin D3 levels or pRb phosphorylation after 8 h. However, treatment with Bz-423 for 24 h resulted in a concentration-dependent reduction in levels of Myc as well as cyclin D3 (Figure 2.7). These changes were accompanied by decreases in pRb phosphorylation as evidenced by increased mobility on SDS-PAGE and decreased immunoreactivity with an antibody specific for phosphorylation of pRb at Ser795 (Figure 2.9). These observations demonstrate that anti-proliferative concentrations of Bz-423 induce intracellular signaling events in keratinocytes that are consistent with those changes induced in Ramos B cells as well as a block in proliferation.

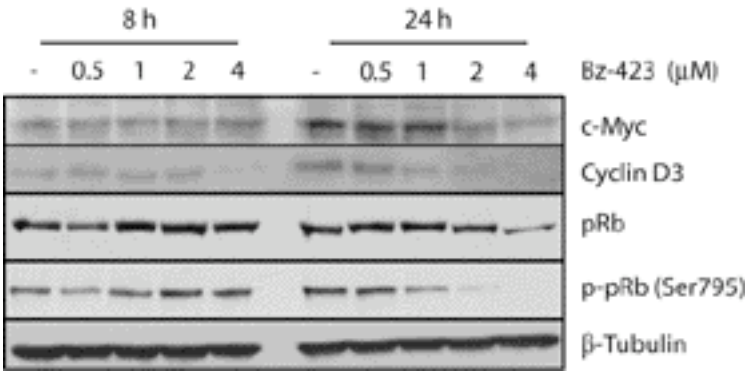

Figure 2.9 - Bz-423 reduces c-Myc levels in keratinocytes. Whole cell lysates were prepared from kerationcytes treated with the indicated concentrations for 8 h or 24 h, after which, immunoblots were prepared with specific antibodies as indicated. This figure is representative of two separate experiments.

Levels of c-Myc were evaluated by immunohistochemical staining of human psoriatic skin grafts treated with a topical formation of Bz-423 (2.5%; applied twice daily for two weeks) to determine whether c-Myc was reduced by Bz-423 *in vivo* [46]. At the conclusion of treatment, c-Myc-positive cells were detected in the subrabasal layer of vehicle-treated grafts, while none were present in psoriatic skin exposed to Bz-423 [46]. This change was accompanied by a reduced number of cells staining positive for the proliferative marker Ki-67 in the subrabasal layer [46]. In addition, Bz-423 caused a 43% decrease in epidermal thickness relative to vehicle-treated grafts [46]. Importantly, disruptions of normal skin architecture (e.g., flattening of the dermal-epidermal interface) did not accompany these beneficial effects [46]. This selectivity suggests that the hyperproliferative phenotype of keratinocytes in the subrabasal layer of psoriatic skin predisoposes these cells to Bz-423-induced c-Myc destabilization and growth arrest. In support of this hypothesis, c-Myc and Ki-67 staining in the basal layer of epidermal cells was equivalent in Bz-423 and vehicle-treated grafts [46].

Bz-423 depletes c-Myc by a mechanism that involves the proteasome: c-Myc levels are tightly regulated by processes governing both mRNA and protein stability [62, 75, 107]. For example, despite constitutive utilization of the *cmyc* promoter, quiescent lymphocytes have low *cmyc* transcript levels as a result of a block in transcriptional elongation, as well as rapid degradation of *cmyc* mRNA [108, 109]. Proliferation accompanying lymphocyte activation depends, in part, upon mechanisms that elevate c*myc* expression by overcoming these blocks [77]. To determine if Bz-423 decreases c-Myc protein by a mechanism involving either reduced transcription or mRNA stability, RNA was isolated from Bz-423-treated Ramos B cells, and steady-state c*myc* mRNA levels were assessed by semi-quantitative RT-PCR. As seen in Figure 2.6A, c*myc* mRNA levels remained unchanged for up to 8 h with only a 50% decrease observed at 24 h. In contrast, Myc protein levels are reduced by 30% within 1 h of treatment and steadily decline to <10% of control by 8 h (Figure 2.10A). Thus, *myc* transcript levels remain stable during the period in which Myc protein declines, arguing that Bz-423 lowers Myc levels by a process that stimulates degradation of this protein.

Levels of Myc protein are regulated by mechanisms that target this protein for degradation by the 26S proteasome [110-115]. In particular, ubiquitin-dependent proteasomal degradation of Myc is signaled by post-translational modification of residues within a highly conserved region spanning amino acids 45-63, known as Myc box 1 (MB1) (Figure 2.10B). Within MB1, S62 and T58 are phosphorylated by mitogen-activated kinases and glycogen-synthase kinase-3β (GSK-3β), respectively [111]. Phosphorylation of S62 is initially stabilizing, but also primes Myc for subsequent phosphorylation of T58 by GSK-3β [110, 111]. Recognition of phosphorylated T58 by

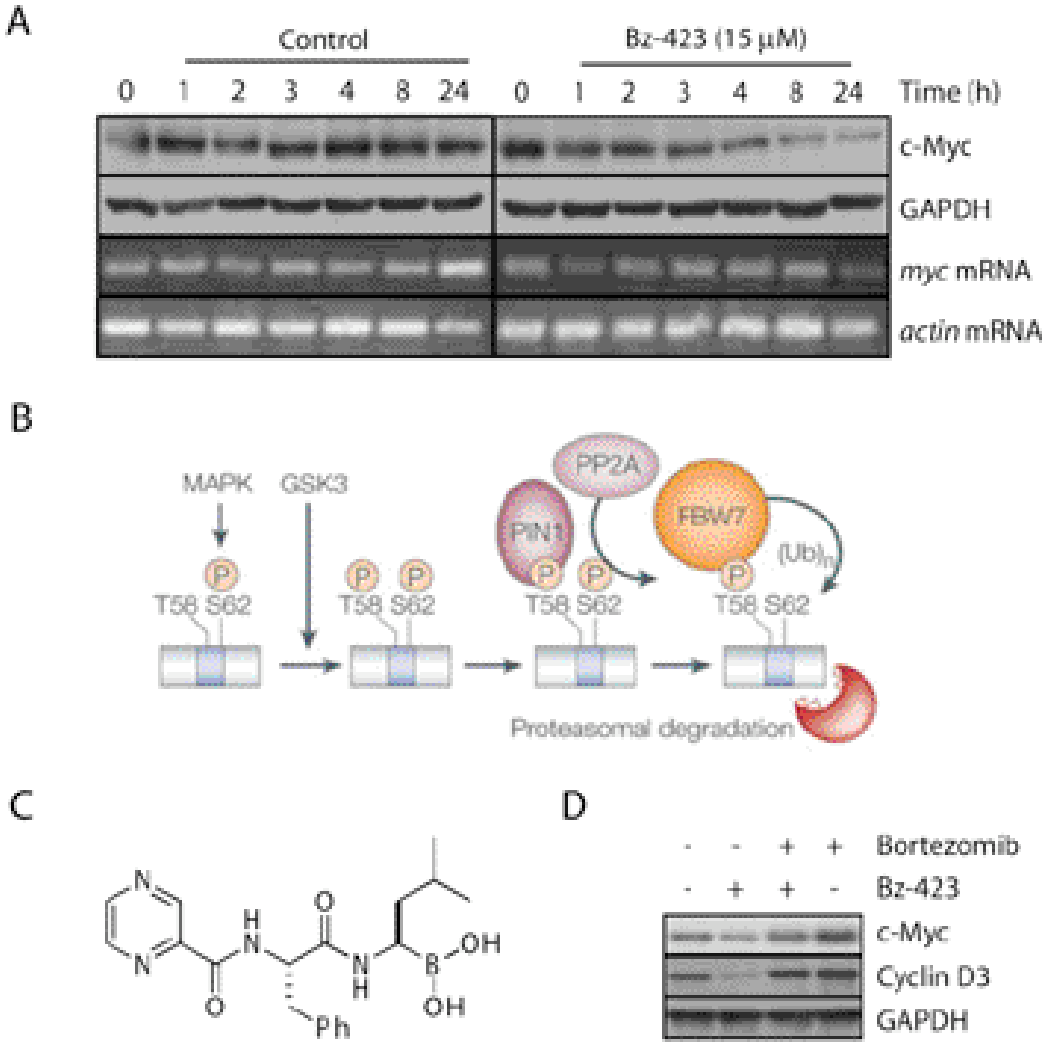

Figure 2.10 - Bz-423 decrease c-Myc by a mechanism involving the proteasome. (A) Whole cell lysates or RNA were isolated from Ramos B cells treated with Bz-423 (15 μM) for the indicated times, after which, immunoblotting or RT-PCR was performed for Myc protein or mRNA levels, respectively. (B) Model for regulation of Myc stability by phosphorylation of Myc Box I (MBI) residues Ser62 and Thr58. Adapted from Adhikary and Eilers [62]. (C) Chemical structure of Bortezomib, a potent, cell-permeable, reversible inhibitor of the 26S proteasome (IC_{50} = 10 nM; [116]). (D) Whole cell lysates were prepared from Ramos B cells that had been pretreated with Bortezomib (2.5 μM) and then incubated with Bz-423 (15 μM) for 6 h. Bortezomib was employed at a concentration shown to inhibit in other systems [117]. Immunoblots were performed with specific antibodies as indicated and are representative of at least two separate experiments.

the prolyl isomerase (PIN1) leads to isomerization of P59, which enables protein phosphatase-2A (PP2A) to cleave the phosphate residue from S62 [115]. The ubiquitin ligase SCF^{Fbw7} (Fbw7) recognizes the phospho-T58 species and then ubiquinylates c-Myc, targeting it for proteasomal degradation (Figure 2.10B; [112-115]).

The essential role of the ubiquitin-proteasome pathway in regulating c-Myc protein stability suggests that Bz-423 might reduce Myc levels by targeting it for proteasomal degradation. To test this hypothesis, Ramos B cells were treated with Bz-423 along with bortezomib, a dipeptidyl bononic acid inhibitor of the 26S proteasome [116]. Blocking proteasome activity in Ramos B cells prevented the Bz-423-induced decrease in Myc and cyclin D3, a Myc-dependent gene product (Figure 2.10C). This observation indicates that Bz-423 induces proteasomal degradation of Myc, perhaps due to increased phosphorylation of MBI residues that trigger ubiquitination.

Myc Box I (MBI) phospho-residues are required for the effects of Bz-423 on c-Myc and proliferation: The dependence of the Bz-423-induced decrease in Myc on proteasome function suggests that this process may involve *cis*-acting MB1 residues commonly involved in ubiquitin-mediated proteolysis. To evaluate this hypothesis, Ramos B cells were stably transfected with Flag epitope-tagged wild-type Myc or mutants in which T58, S62 or both residues were substituted with alanine (Figure 2.10A). When clones stably expressing these proteins were exposed to Bz-423, the levels of Flag epitope-tagged wild-type Myc and the Myc^{S62A} mutant decreased in a time course similar to the reduction of endogenous Myc in cells transfected with an empty vector (Figure2.11B). As predicted by the essential role of T58 in ubiquitin-mediated degradation of Myc, the Myc^{T58A} mutant and the double mutant $Myc^{T58A/S62A}$ proteins were

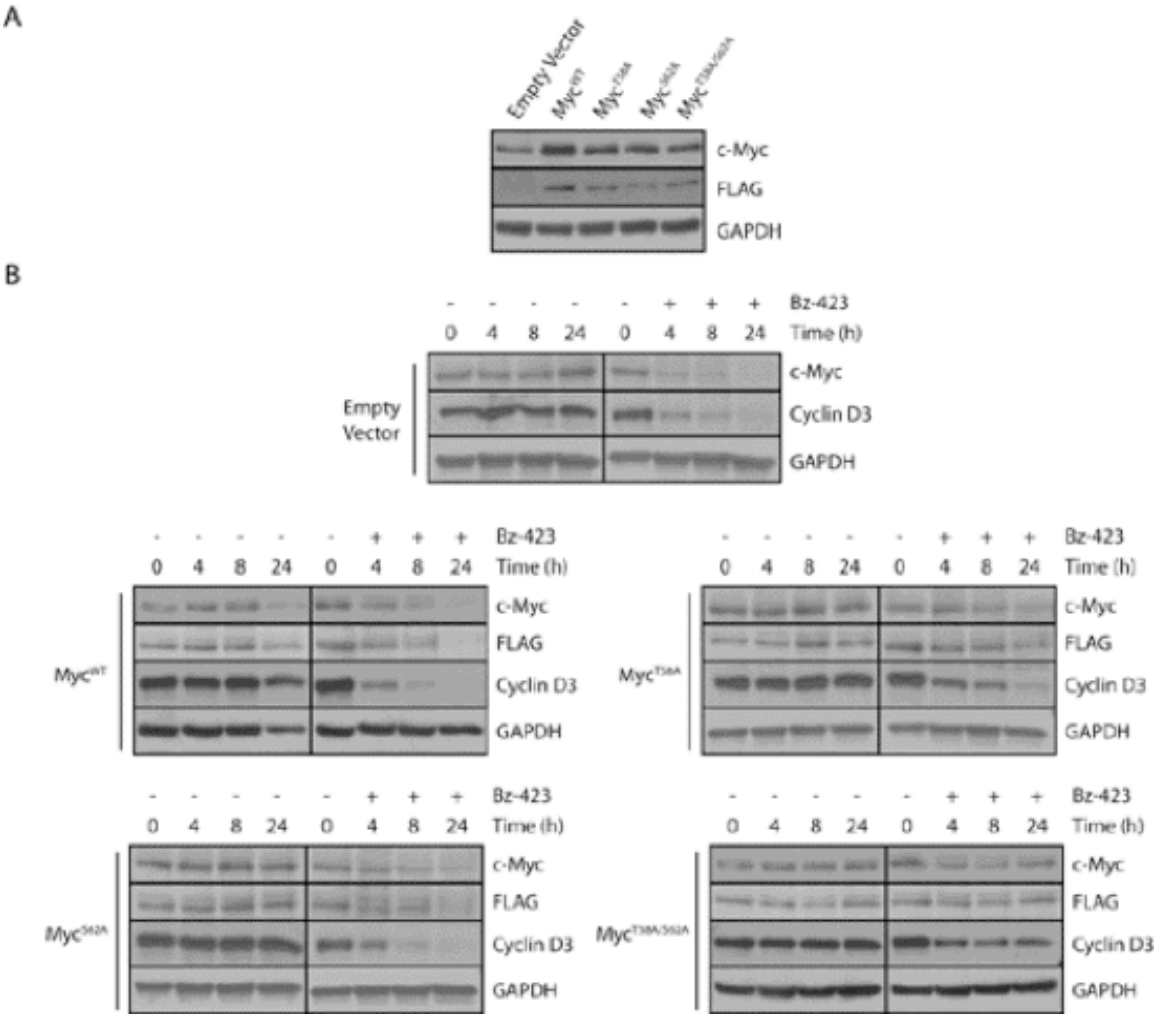

Figure 2.11 - Phospho-sensitive c-Myc residue T58 is critical for Bz-423-induced degradation of c-Myc. (A) Expression of Flag-epitope tagged wild-type Myc or mutants with alanine substitutions at T58, S62 or both residues was confirmed by immunoblotting whole cell lysates from Ramos B cell clones with specific antibodies as indicated. (B) The Ramos B cells clones in (A) were treated with Bz-423 (15 μM) for the indicated times and levels of Myc, Flag and cyclin D3 were evaluated by immunoblotting whole cell lysates with specific antibodies. Both panels are representative of two separate experiments.

Ramos B Cell Clone	Growth Arrest; GI_{50} (μM)	Cell Death; EC_{50} (μM)
Wild type	10 ± 1.1	5.93 ± 0.3
Vector	10.5 ± 0.8	5.87 ± 0.5
Myc^{WT}	11.0 ± 0.9	5.60 ± 0.4
Myc^{T58A}	15.6 ± 1.4	6.34 ± 0.4
Myc^{S62A}	12.9 ± 1.4	5.38 ± 0.4
$Myc^{T58A/S62A}$	15.8 ± 0.6	6.09 ± 0.1

Table 2.3 – c-Myc phospho-residue T58 is critical for Bz-423-induced growth arrest, but dispensable for cell death. Growth arrest was evaluated using by the SRB assay after 48 h in media containing 10% FBS. Cell death was quantified in terms of PI positivity after 24 h in media containing 2% FBS. Each GI_{50} and EC_{50} value was determined in triplicate via non-linear regression of the corresponding concentration-response curves.

substantially resistant to Bz-423-induced degradation relative to transfected wild-type Myc and endogenous Myc in vector control cells (Figure 2.9B). In addition, the Bz-423-induced decrease in the Myc-dependent gene product cyclin D3 was attenuated by expression of Myc^{T58A} or $Myc^{T58A/S62A}$ relative to cells transfected with Myc^{S62A}, wild-type Myc or an empty vector (Figure 2.7B). These results indicate that T58 is critical for Bz-423-induced degradation of Myc and the subsequent decrease in cyclin D3.

Wild type c-Myc and MB1 phospho-residue mutants were tested for sensitivity to Bz-423-induced growth inhibition and G_1 cell cycle arrest to determine if the decrease in Myc protein levels is necessary for these processes. After treatment with Bz-423 for 48 h, the GI_{50} was significantly increased in Ramos B cells expressing c-Myc^{T58A} and c-$Myc^{T58A/S62A}$ (P <0.04 and P <0.02, respectively) compared with clones transfected with wild-type c-Myc, whereas the increase in GI_{50} in Ramos B cells expressing Myc^{S62A} did not reach statistical significance (P >0.1; Table 2.3).

In addition, cells transfected with an empty vector, wild type c-Myc, or c-Myc^{S62A} accumulated at the G_1 checkpoint, as observed previously in Bz-423-treated Ramos B cells (Figure 2.12; [22]). In contrast, Ramos B cells expressing c-Myc^{T58A} and c-Myc$^{T58A/S62A}$ showed no significant difference in cell cycle distribution compared to vehicle-treated cells (Figure 2.12). Finally, although c-Myc levels are also decreased by cytotoxic concentrations of Bz-423 [118], the EC_{50} for cell death was not increased in Ramos B cells expressing c-Myc phospho-residue mutants (Table 2.3). Collectively, these findings indicate that the reduction in levels c-Myc protein is necessary for Bz-423-induced growth arrest in Ramos B cells.

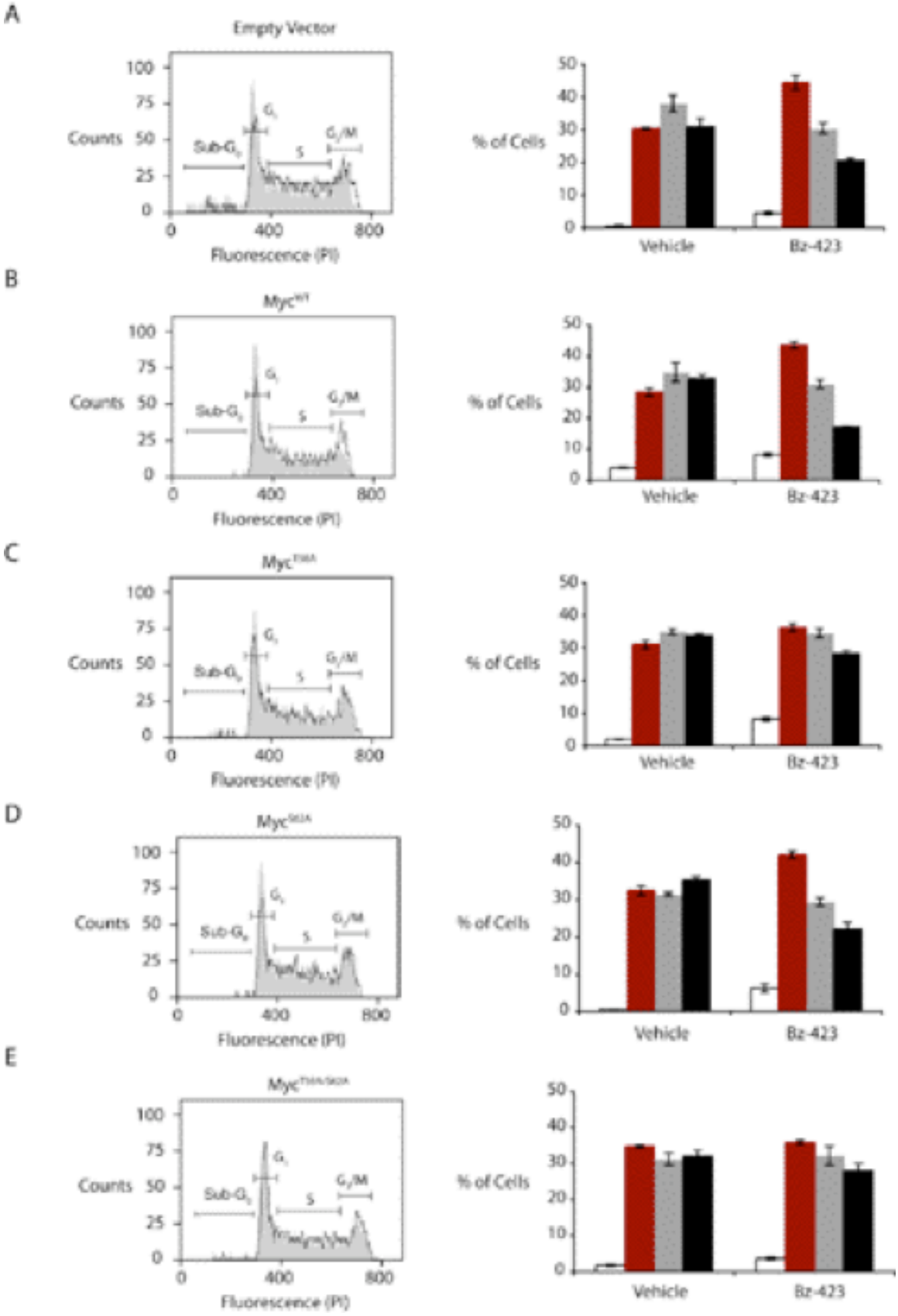
A
Empty Vector
Counts
Sub-G1
G1
S
G2/M
Fluorescence (PI)
% of Cells
Vehicle
Bz-423
B
Myc^WT
C
Myc^T58A
D
Myc^S62A
E
Myc^T58A/S62A

Figure 2.12 - Phospho-sensitive c-Myc residue T58 is critical for Bz-423-induced G_1 arrest. Ramos B cell clones stably transfected with empty vector (A) or Flag epitope-tagged wild-type Myc (B) or Myc with alanine substitution at T58 (C), S62 (D) or both residues (E) were treated with vehicle (*black histogram*) or Bz-423 (15 μM; *gray histogram*) for 24 h and cell cycle distribution was determined in triplicate by PI staining and flow cytometry. *Graphs*, percentage of cells in the Sub-G_0 (*white bars*), G_1 (*red bars*), S (*grey bars*) and G_2 (*black bars*) phases of the cell cycle for each experimental condition. All panels are representative of two separate experiments.

Bz-423-induced c-Myc degradation is independent of T58 phosphorylation by GSK-3β: Alanine substitution of the MB1 phospho-residue T58 stabilizes Myc in the presence of Bz-423. This observation suggests that Bz-423 may trigger ubiquitin-mediated proteolysis of c-Myc by inducing phosphorylation of T58. To explore this possibility, lysates from Bz-423-treated Ramos B cells were immunoblotted with an antibody that recognizes c-Myc either singly phosphorylated at T58 or doubly phosphorylated T58 and S62, but does not recognize species that are either not phosphorylated or singly phosphorylated at S62 [110, 111]. Surprisingly, an increase in phospho-Myc species was not detected prior to the reduction in total Myc levels. Instead, levels of T58 phosphorylated Myc decreased with equivalent kinetics to total Myc protein (Figure 2.13A). As a control, lysates were prepared from Ramos B cells following stimulation of the B cell antigen receptor (BCR), which has been shown to induce phosphorylation of c-Myc at Thr58 [104, 119]. In these BCR-stimulated cells, an initial accumulation of total and phospho-(T58/S62) c-Myc was observed, with a maximum reached at 4 h, followed by a decrease in both species to sub-basal levels by 24 h (Figure 2.13B). The absence of an early rise in T58 phosphorylation in response to Bz-423 suggests that the decrease in Myc is not signaled by phosphorylation of this residue.

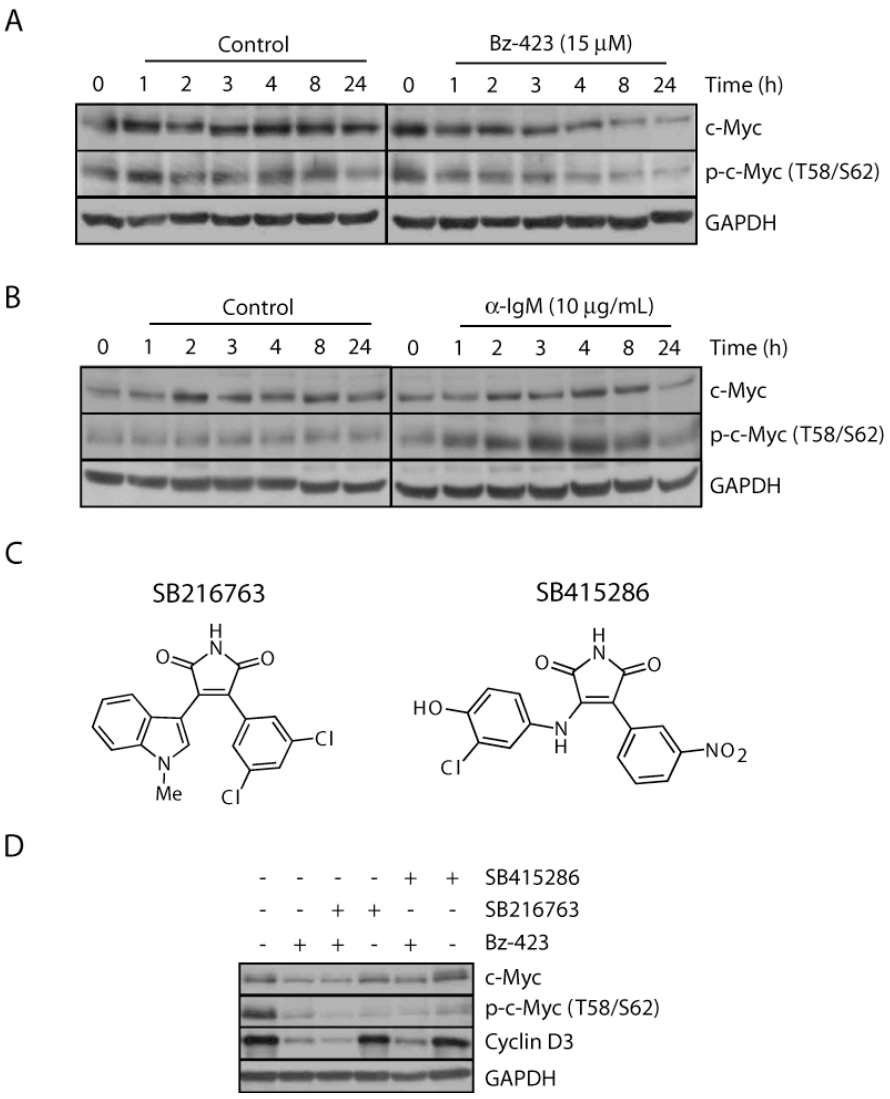

Figure 2.13 - Bz-423 does not induce T58 phosphorylation. Ramos B cells were treated with (A) Bz-423 (15 μM) or (B) α-IgM (10 μg/mL), after which, whole cell lysates were immunoblotted with specific antibodies as indicated. (C) Structures of the cell-permeable, selective, reversible GSK-3β inhibitors SB-216763 and SB-415286 (IC_{50}s = 34 nM and 78 nM, respectively; [120]) (D) Whole cell lysates were prepared from Ramos B cells that had been pretreated with the GSK-3β inhibitors SB-216763 (30 μM) or SB-415286 (30 μM) and then treated with Bz-423 for (15 μM) for 6 h and immunoblots performed with specific antibodies as indicated. SB-216763 and SB-415286 were used at concentrations shown to inhibit GSK-3β in other systems [120]. Panel A is representative of three separate experiments, while Panels B and D are from a single experiment.

Proteasomal degradation of Myc following serum withdrawal and B cell-receptor ligation is mediated by phosphorylation of T58 by GSK-3β [104, 110, 111, 119]. However, the absence of increased T58 phosphorylation in response to Bz-423 suggests that GSK-3β is not involved. To further exclude this possibility, Ramos B cells were treated with two structurally distinct GSK-3β inhibitors (SB-216763 and SB-415286; [120]) prior to incubation with Bz-423 (Figure 2.13C). Neither inhibitor prevented the Bz-423-induced decrease in Myc or the associated reduction in cyclin D3 (Figure 2.13D), which is consistent with the absence of increased phospho-T58 levels. Inhibition of GSK-3β by SB-216763 or SB-415286 was demonstrated by reduced levels of the c-Myc species recognized by the phospho-Myc (T58/S62) specific antibody (Figure 2.13D). Thus, although Bz-423 induces proteasomal degradation of Myc, this process appears to be independent of T58 phosphorylation by GSK-3β. This is similar to proteasomal degradation of c-Myc induced by the small-molecule, Degrasyn, which likewise is independent of GSK-3β (see Chapter 2 Discussion; [121]).

Bz-423 induces rapid, proteasome-dependent degradation of β-catenin: The inability of GSK-3β inhibitors to prevent Bz-423-induced Myc degradation indicates that this process does not involve phosphorylation of T58. Nevertheless, alanine substitution of T58 stabilizes Myc levels and restores normal growth, which suggests that processes involving this residue contribute to cytostatic effect of Bz-423. A plausible explanation for this apparent contradiction is that Bz-423 may act downstream of T58 phosphorylation to increase the efficiency of Myc processing by the 26S proteasome. Rate-limiting steps in proteasomal degradation include both protein-specific modifications (e.g., phosphorylation), as well as the enzymatic attachment of ubiquitin to

target proteins [122, 123]. Therefore, Bz-423-induced $O_2^{\bullet-}$ may enhance proteosomal processing of Myc by increasing the expression and/or activity of ubiquitin ligases. In support of this hypothesis, cellular ubiqutin-ligase activity is elevated in response to oxidative stress (see Chapter 2 Discussion; [124-126]).

The hypothesis that Bz-423 increases cellular ubiquitin-ligase activity suggests that levels of other labile proteins may also be diminished. One such protein is the transcription factor β-catenin, which in the absence of Wnt signaling, is rapidly targeted to ubiquitin-proteasome pathway as result of phosphorylation by GSK-3β [127]. Signals triggered by binding of Wnt ligands to their cognate Frizzled (Fzd) receptors inhibit GSK-3β, which leads to accumulation of β-catenin and transcriptional activation of target genes [128]. Because the ubiquitin ligase complexes targeting Myc and β-catenin share several molecular components (see Discussion; [129]), we hypothesized that Bz-423 might also destabilize β-catenin. Indeed, Bz-423 treatment promotes rapid, proteasomal-dependent degradation of β-catenin in Ramos B cells (Figure 2.14A and B). Interestingly, although the GSK-3β inhibitors, SB-216763 and SB-415286, caused accumulation of β-catenin, they failed to protect against Bz-423-induced degradation of this transcription factor (Figure 2.14C). These results with β-catenin support a model whereby Bz-423 destabilizes labile proteins such as Myc by stimulating the ubiquitin-proteasome pathway downstream of GSK-3β. However, Bz-423 does not promote indiscriminate degradation of short-lived proteins, because levels of CDK2 as well as cyclin D1 and D2, are maintained in Ramos B cells treated with Bz-423 for up to 8 h (Figure 2.8).

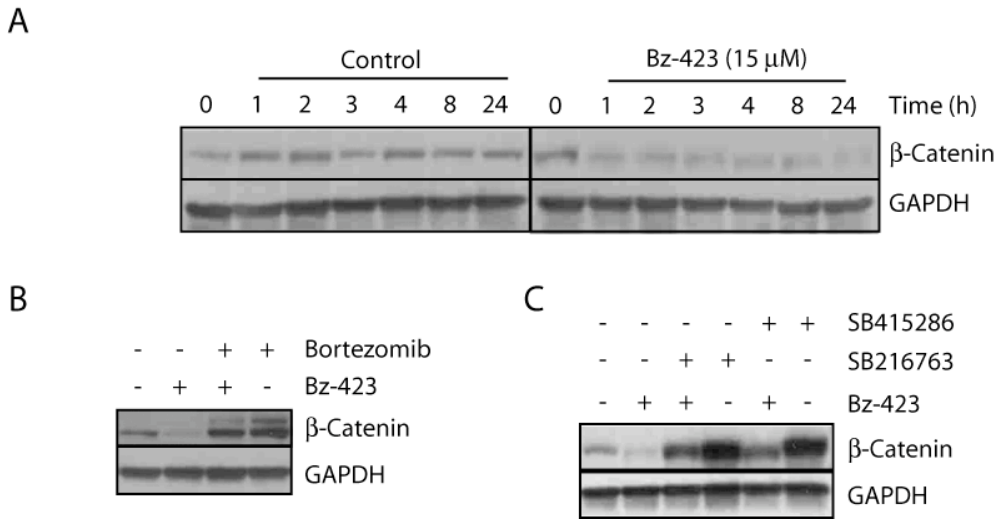

Figure 2.14 - Bz-423 induces rapid, proteasome-dependent degradation of β-catenin. (A) Ramos B cells were treated with vehicle or Bz-423 (15 μM) for the indicated times, after which, whole cell lysates were immunoblotted with specific antibodies as indicated. (B) Whole cell lysates were prepared from Ramos B cells that had been pretreated with Bortezomib (2.5 μM) and then incubated with Bz-423 (15 μM) for 2 h. Immunoblots were then performed with specific antibodies as indicated. All panels are from a single experiment. (C) Whole cell lysates were prepared from Ramos B cells that had been pretreated with the GSK-3β inhibitors, SB-216763 (30 μM) or SB-415286 (30 μM), and then treated with Bz-423 for (15 μM) for 2 h. Immunoblots were performed with specific antibodies as indicated. All panels are representative of two independent experiments.

Effect of other oxidizing agents on c-Myc levels: The decrease in Myc levels triggered by Bz-423 suggests that elevated levels of intracellular $O_2^{\bullet-}$ trigger a specific regulatory mechanism that leads to degradation of c-Myc by the proteasome. To explore this possibility, Ramos B cells were treated with the oxidants hydrogen peroxide (H_2O_2) and *tert*-butyl hydroperoxide (*t*-BHP), as well as with arsenic trioxide (ATO), an agent that promotes $O_2^{\bullet-}$ production from mitochondrial respiratory chain [130, 131]. Neither H_2O_2 nor *t*-BHP altered levels of Myc or cyclin D3 (Figure 2.15A and B). In contrast, both

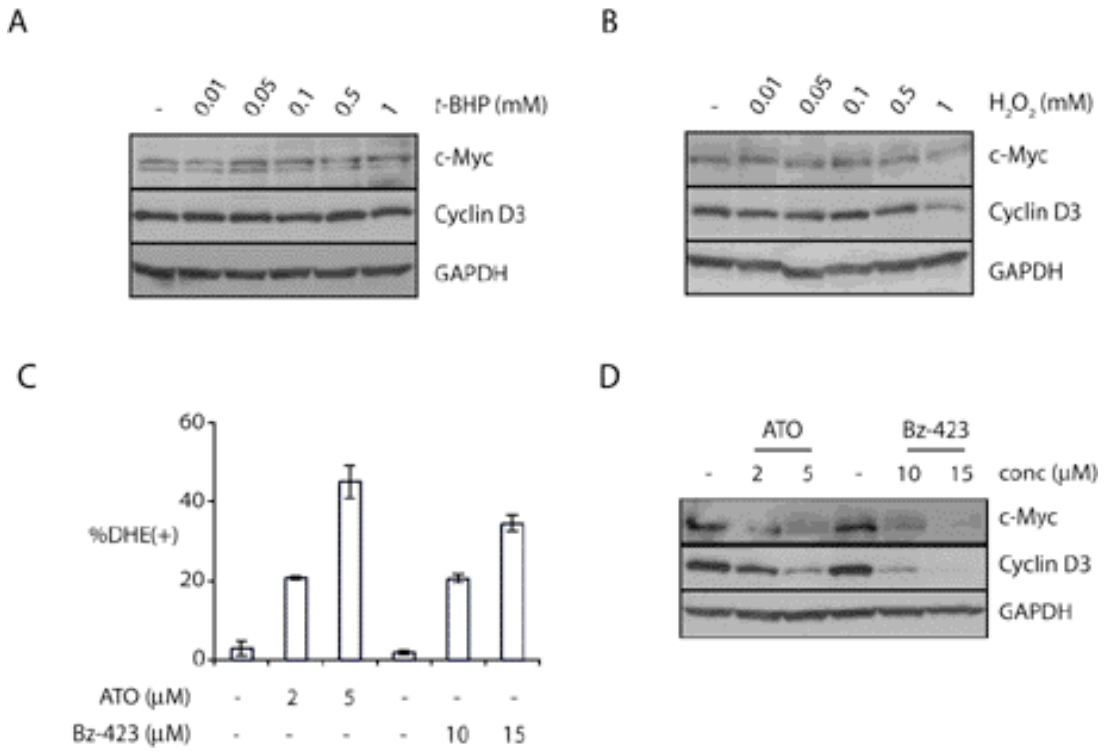

Figure 2.15 – c-Myc is depleted by agents that produce $O_2^{\bullet-}$, but not by exogenous peroxides. (A and B) Whole cell lysates were prepared from Ramos B cells treated with the indicated concentrations of H_2O_2 or *t*-BHP for 6 h, after which immunoblots were performed with specific antibodies as indicated. (C) $O_2^{\bullet-}$ production was detected in Ramos B cells treated with the indicated concentrations of ATO or Bz-423 for 1 h by staining with DHE. (D) Whole cell lysates were prepared from Ramos B cells with the indicated concentrations of ATO or Bz-423 for 6 h, after which immunoblots were performed with specific antibodies as indicated. All panels are the results from a single experiment.

c-Myc and cyclin D3 were reduced in Ramos B cells exposed to ATO (Figure 2.15C and D). These data indicate that c-Myc protein levels are stable in Ramos B cells treated with exogenous peroxides, which suggests that the signaling mechanism that leads to c-Myc degradation in response specifically engaged by agents that, like Bz-423 or ATO, increase intracellular $O_2^{\bullet-}$ levels.

Discussion

Bz-423 stimulates mitochondrial $O_2^{\bullet-}$ production by modulating the F_oF_1-ATPase [30]. While high levels of this ROS signal apoptosis, the proportionally lower $O_2^{\bullet-}$ response induced by sub-toxic concentrations of Bz-423 arrests growth [22]. The studies described in this chapter identify degradation of the oncogenic transcription factor c-Myc as a key element in Bz-423-induced growth arrest (Figure 2.16). This decrease the in levels of c-Myc protein, in turn, results in predictable effects on the expression of c-Myc target genes necessary for cell cycle progression and polyamine biosynthesis. Because inhibitors of the cell cycle machinery and agents that deplete cellular polyamines each block growth [94, 132], the cytostatic activity of Bz-423 is expected to arise from inhibitory effects on both processes. The SOD mimetic MnTBAP blocks the reduction in c-Myc levels demonstrating that this response is connected to the effects of Bz-423 on the F_oF_1-ATPase by the $O_2^{\bullet-}$ signal.

The reduction in c-Myc protein induced by Bz-423 appears to be mediated by the ubiquitin-proteasome pathway, because inhibition of the proteasome or alanine substitution of phospho-residues critical for ubiquitinylation stabilizes c-Myc levels. Exogenous peroxides fail to recapitulate the effects of Bz-423 on c-Myc stability. However, decreased c-Myc levels are observed following exposure to agents (e.g., ATO) that stimulate $O_2^{\bullet-}$ production; this suggests that the ubiqutin-proteasome pathway specifically responds to this ROS. In addition to its effects on B cells, Bz-423 blocks proliferation of psoriatic keratinocytes *in vitro* and reduces epidermal hyperplasia in psoriatic human skin grafted onto SCID mice. Bz-423-induced growth arrest in psoriatic keratinocytes is accompanied by reductions in levels of c-Myc, cyclin D3 and pRb

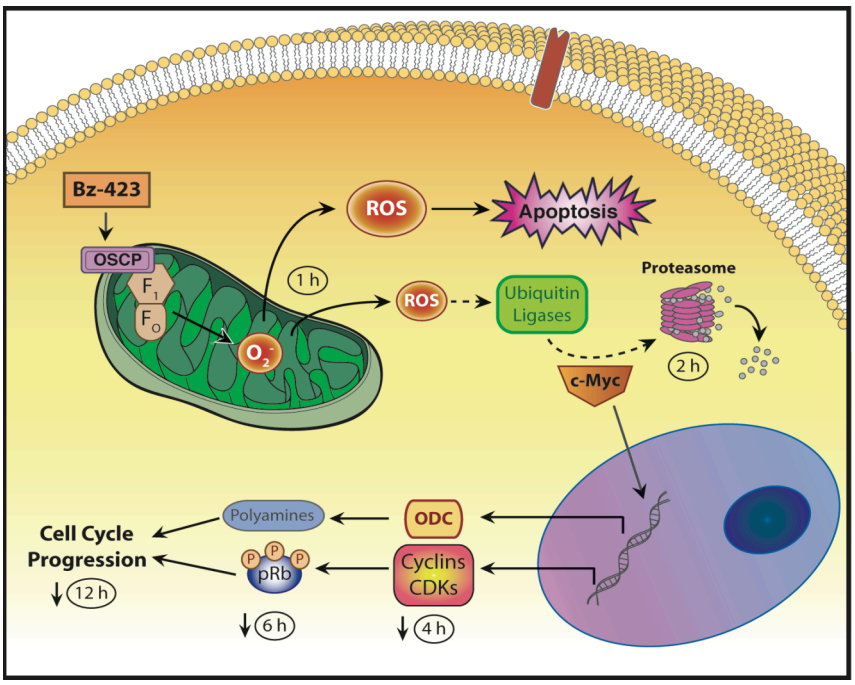

Figure 2.16 - Bz-423-induced growth inhibitory signaling in Ramos B cells.

phosphorylation. These observations suggest that Bz-423-induced c-Myc destabilization is not limited to Ramos B cells, but also contributes to the anti-proliferative activity of this compound in other cell-types. In sum, these findings identify a mitochondrial $O_2^{\bullet-}$-dependent mechanism that regulates c-Myc protein stability and suggest that Bz-423 may have therapeutic activity against malignant diseases associated with deregulation of Myc proteins.

Regulation of c-Myc protein stability by the ubiquitin-proteasome system: The ubiquitin-proteasome system is responsible for degradation of the vast majority of cellular proteins. Proteins are targeted for degradation by "tagging" them with ubiquitin, a 76-amino acid polypeptide that is conserved in all eukaryotes [133, 134]. After attachment, the ubiquitin tag serves as a substrate for sequential rounds of ubiquitination,

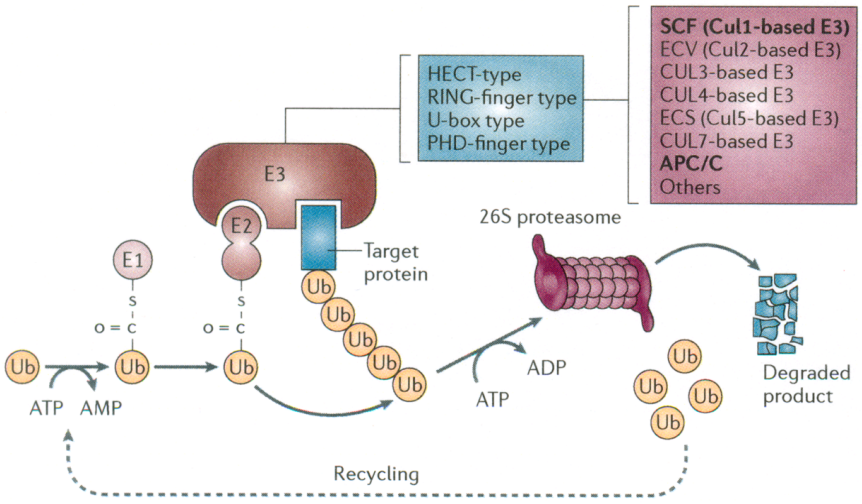

Figure 2.17 - Overview of the ubiquitin-proteasome pathway. See text for details. Figure taken from [129].

and once polyubiquinated, proteins are then recognized and degraded by the 26S proteasome (Figure 2.17). Ubiquitination begins with ATP-dependent activation of the ubiquitin carboxyl terminus by ubiquitin-activating enzymes (E1). Activated ubiquitin is transferred to a cysteine on ubiquitin-conjugating enzymes (E2), and then further shuttled to substrate proteins in cooperation with ubiquitin ligases (E3). Substrate specificity is determined by the E3 ubiquitin ligases, which act as a reaction platform that brings E2 enzymes and target proteins into proximity (Figure 2.15; [129]).

While there are a small number of ubiquitin-activating and ubiquitin-conjugating enzymes, the E3 family is estimated to contain >500 members and serve as critical regulators of biological processes including cell division, proliferation, differentiation, lymphocyte activation and carcinogenesis [129, 135, 136]. This vast array of proteins is divided into four major classes on the basis of specific structural motifs: HECT-type, RING-finger-type, U-box-type, or PHD-finger-type [129]. RING-finger-type ligases are

the largest E3 class, and are further divided into several subclasses, among which, cullin-based ligases are one of the largest individual sub-classes of E3. Cullin-based E3 ligases, known as SCF complexes, consist of three invariable components *S*kp1, *C*ullin1, and RBX1, as well as a variable *F*-box protein that is responsible for substrate recognition (Figure 2.18; [129]). While the physiological role of most of the >70 F-box proteins is still unknown, three of these ubiquitin ligases – S-phase kinases-associated protein 2 (Skp2), F-box and WD-40 domain protein 7 (Fbw7), and β-transduction repeat-containing protein (β-TRCP) - play key roles in regulating cell cycle progression (Figure 2.18; [129]). In particular, SCF^{Skp2} (Skp2) and SCF^{Fbw7} (Fbw7) regulate Myc protein stability [137]. SCF^{Skp2} (Skp2) was the first ubiquitin ligase identified for Myc [138]. Studies with Myc deletion mutants have demonstrated that Skp2 associates with amino acids 379-418 as well as 129-147. The later region encompasses the conserved degron Myc Box II (MBII) and contains one lysine (K144), which is efficiently ubiquitinylated by Skp2 [139]. Correspondingly, forced expression of Skp2 increases proteolysis of c-Myc and retards growth in Rat1 cells [139].

Despite the destabilizing effect of Skp2 on c-Myc in overexpression studies, several lines of evidence suggest that this ubiquitin ligase does not mediate the effects of Bz-423 on Myc. First, endogenous levels of Skp2 promote growth by stimulating the G_1-S phase transition [129]. The growth promoting activity of Skp2 is due, in part, to targeting of the CDKIs $p21^{Cip1}$ and $p27^{Kip1}$ to the ubiquitin-proteasome pathway [140, 141]. Skp2-mediated ubiquitinylation and the resultant proteasomal degradation of $p21^{Cip1}$ is stimulated by H_2O_2 in a variety of cell types [126]. However, unlike the effects of Bz-

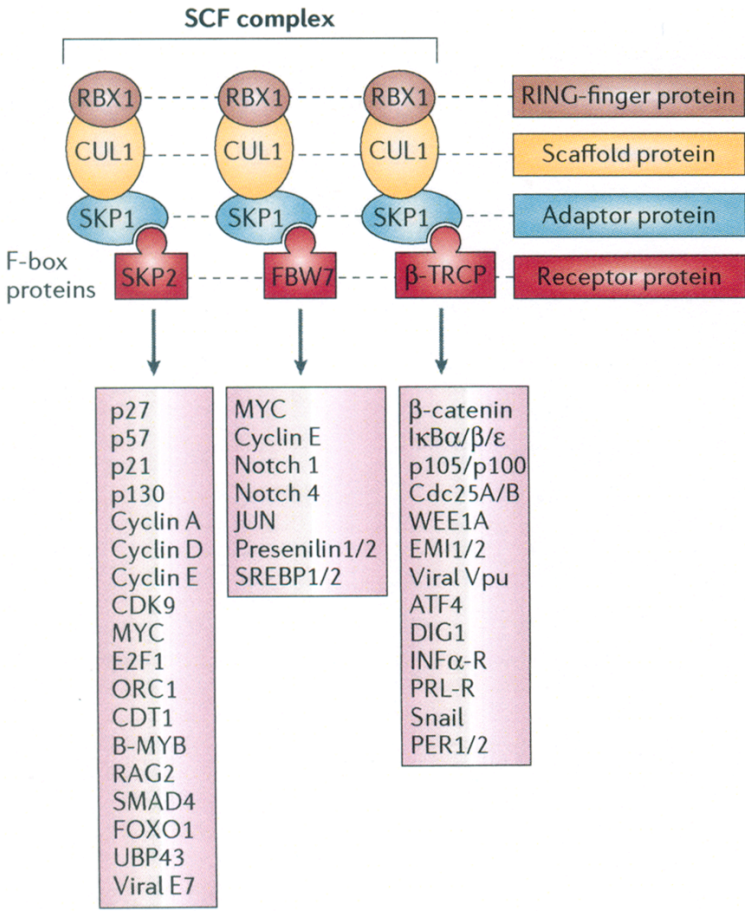

Figure 2.18 - The E3 ubiquitin ligases Skp2, Fbw7 and β–TRCP dictate substrate specificity of SCF complexes. See text for details. Figure taken from [129].

423 on c-Myc, this reduction in $p21^{Cip1}$ levels stimulates proliferation [126]. Second, Skp2-dependent ubiquitylation stimulates expression of c-Myc-target genes [142]. Co-expression of Skp2 and c-Myc has a synergistic effect in a luciferase reporter assay using the promoter of the c-Myc target gene α-prothymosin [139]. In addition, c-Myc and Skp2, along with several subunits of the proteasome, appear to associate with the cyclin D2 promoter in chromatin immunoprecipitation studies [138]. These findings suggest Skp2-mediated ubiquitylation of c-Myc acts as a "licensing mechanism" by limiting the half-life of a highly transcriptionaly-active, ubiquitinated c-Myc species

[143]. The role of Skp2 as a Myc transcriptional co-activator suggests that this ubiquitin ligase does not mediate Bz-423-induced Myc degradation. More significantly, relative to Bz-423-induced Myc degradation, however, is that Myc T58A mutants remain sensitive to ubiquitinylation by Skp2 [138, 139].

A second SCF-type ubiquitin ligase, SCF^{Fbw7} (Fbw7), recognizes c-Myc phosphorylated at Ser62 and Thr58 within the Myc Box I (MBI) degradation domain (degron) [112-114]. Ser62 is a substrate for several kinases, including extracellular signal-regulate kinase (ERK), c-Jun N-terminal kinase (JNK), and the cyclin B-CDK1 complex (Figure 2.18; [111, 144-146]). Although initially stabilized, phosphorylation pf Ser62 primes Myc for phosphorylation by glycogen synthase kinase-3β (GSK-3β), a downstream effector of both the Wnt and phosphatidylinositol 3-kinase (PI3K)-Akt pathways [110]. A unique feature of GSK-3β is that this kinase recognizes substrates only after a 'priming' phosphorylation at the +4 position. In addition to Myc, Fbw7-dependent ubiquitylation of c-Jun, cyclin E1, and sterol regulating element binding protein (SREBP) is stimulated by GSK-3β phosphorylation (Figure 2.19; [135]). In an analogous mechanism, β-catenin is recognized by the SCF-family ubiquitin ligase $SCF^{\beta\text{-}TRCP}$ (β-TRCP) as result of sequential phosphorylation by Casein Kinase I and GSK-3β [128]. In an atypical signaling mechanism, the Fbw7 substrate-priming activity of GSK-3β is negatively regulated by the Wnt and PI3K-Akt pathways, which prevents degradation of proteins essential for cell growth and proliferation. Conversely then, interfering with these pathways or otherwise stimulating GSK-3β activity represents a potentially valuable strategy to regulate oncogenes such as Myc, cyclin E1, and β-catenin [147, 148].

The inhibitory effect of alanine substitution at Thr58 on Bz-423-induced Myc degradation suggested that this process might be signaled by GSK-3β phosphorylation and the resultant Fbw7-mediated ubiquitinylation. However, increased Thr58 phosphorylation is not observed in response to Bz-423, and moreover, GSK-3β inhibitors fail to stabilize Myc levels. Consequently, Bz-423 does not appear to signal Myc degradation by inducing phosphorylation of Thr58. However, Fbw7 activity might be enhanced downstream of Thr58 phosphorylation, perhaps due to increased expression of Fbw7 or another component of the SCF^{Fbw7} ubiquitin-ligase complex. Interestingly, elevated levels of high-molecular-weight ubiquitin conjugates are observed in bovine lens epithelial cells exposed to H_2O_2 [124]. This increase is accompanied by a >5 fold elevation in ubiquitin thiol ester formation. An analogous increase in ubiquitin-conjugation activity was observed in H_2O_2-treated C_2C_{12} muscle myotubes, along with elevated expression of proteasome subunits and the ubiquitin conjugating enzyme $E2_{14K}$ [125]. Although decreased Myc and cyclin D3 levels were not observed in H_2O_2-treated Ramos B cells, these studies demonstrate that the ubiquitin-proteasome pathway activity can be stimulated by oxidative stress.

In addition to c-Myc, Bz-423 also promotes rapid degradation of the Wnt signaling transcription factor β-catenin via a mechanism that depends on the proteasome, but is independent of GSK-3β. Because β-catenin is a substrate for another SCF-type ubiquitin ligase, $SCF^{\beta\text{-}TRCP}$ [149], these observations support the hypothesis that Bz-423-induced c-Myc degradation may result from a general increase in activity of the ubiquitin-proteasomal pathway. In agreement with this model, Myc is subject to rapid, proteasomal degradation following UV irradiation of Ls174T human colon carcinoma

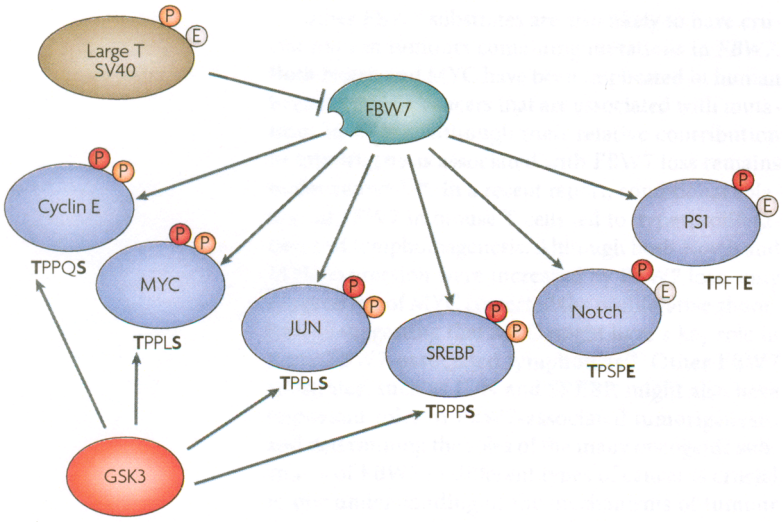

Figure 2.19 - GSK-3β phosphorylation primes multiple substrates for recognition by Fbw7. Fbw7 substrates share a consensus phospho-degron motif. In most cases, the central phospho-threonine is followed by a phospho-serine in the +4 position that serves as a primer for GSK-3β. In Notch and presenilin (PS1) the +4 negative charge is replaced by glutamate. SREBP, sterol regulatory element binding protein. Figure taken from [135].

cells or MRC5-SV fibroblasts by a mechanism that is partially blocked by alanine substitution of Thr58, but does not require GSK-3β activity or Skp2 [150, 151]. This response is speculated to function in a manner analogous to p53 induction, by limiting proliferation of cells in which UV-induced genomic instability could lead to neoplastic growth [150, 151].

Recently, the HECT (homology to E6-AP C-terminus) family protein HectH9 has been identified as a non-SCF-type ubiquitin ligase that targets c-Myc [152]. Like Skp2, HectH9 appears to stimulate c-Myc transcriptional activity. In particular, ubiquitinylation of c-Myc by HectH9 promotes association with the histone acetyltransferase CBP/p300, an essential co-factor for c-Myc-directed transcriptional activation [152, 153]. Correspondingly, arginine substitutions of six carboxy-terminal

lysine residues, known to be ubiquitylated by HectH9 blocked activation of a subset of c-Myc target genes, but failed alter c-Myc protein stability [152]. These findings suggest that regulation of HectH9 by c-Myc is independent of MBI phospho-residues, although this hypothesis has not been formally evaluated [154]. Consequently, a role for HectH9 in Bz-423-induced c-Myc degradation appears unlikely, although the potential exists that this ubiquitin ligase may be differentially regulated in response to elevated mitochondrial $O_2^{\bullet -}$ production.

Comparison to other c-Myc-directed therapeutic strategies: c-Myc proteins are rational therapeutic targets because these proteins are deregulated in a variety of hematological malignancies as well as solid tumors [64]. For instance, Burkitt's lymphoma, a cancer of B cells, arises due to translocations of *myc* to immunoglobulin gene loci, placing it under the transcriptional control of powerful immunoglobulin enhancers [63]. Similarly, *nmyc* gene amplification and its resultant overexpression is observed in greater than 50% of glioblastomas [155], and Myc deregulation is frequently observed in cancers of the prostate, ovary, and breast [156-159]. As many as 70,000 cancer deaths per year in the United States are estimated to result from deregulation of Myc proteins [98]. The potential of anti-c-Myc therapies is demonstrated by studies of tumor development, where *myc* expression can be toggled by placing it under control of Tamoxifen-sensitive promoter. For example, induction of *myc* expression in pancreatic β-cells triggers rapid development of vascularized, invasive tumors [160]. However, even in established malignancies, removing Tamoxifen results in rapid, complete tumor regression [160]. Surprisingly, transient c-Myc inactivation is sufficient to impair tumor growth and induce devascularization [160]. Similarly, a study using c-Myc transgene-

dependent osteosarcomas demonstrated that re-addition of Tamoxifen, following a brief removal, induced re-expression of c-Myc not only failed to restore the malignant phenotype [161]. Moreover, re-expression of c-Myc triggered apoptosis in established tumors [161]. Spurred by the promising results from these studies, several strategies have been developed that target c-Myc expression, transcriptional activity, or post-translational stability (Figure 2.20; [162, 163]).

The therapeutic potential of targeting c-Myc was initially demonstrated by use of antisense oligonucleotides (ASOs) or peptide-nucleic acids (PNAs) to reduce *myc* expression. As single agents, ASOs targeting *myc* or *nmyc* have proven efficacious in xenograft tumor transplant models, including Burkitt's lymphoma [164], large B cell lymphoma [165], breast carcinoma [166], malignant melanoma [167], and neuroblastoma [168]. In addition to reducing tumor mass, sensitivity to the DNA-damaging agent cis-platin was enhanced by prior exposure to c-Myc-directed ASOs in some studies [167, 169]. PNAs have improved stability relative to ASOs due to substitution of the sugar-phosphate DNA backbone with polyamide-(-2-aminoethyl) glycine linkages [170]. A Myc-directed PNA covalently linked to a nuclear localization sequence successfully reduced *Myc* expression and blocked growth in several Burkitt's lymphoma lines [171]. More significantly, a PNA targeting the immunoglobulin enhancer successful reduced Myc levels and blocked tumor growth in a Burkitt's lymphoma xenograft transplant model [172]. Although the efficacy of ASO- or PNA-based anti-Myc therapies has yet to be demonstrated in a clinical trial, these preclinical studies further demonstrated that Myc is viable cancer drug target.

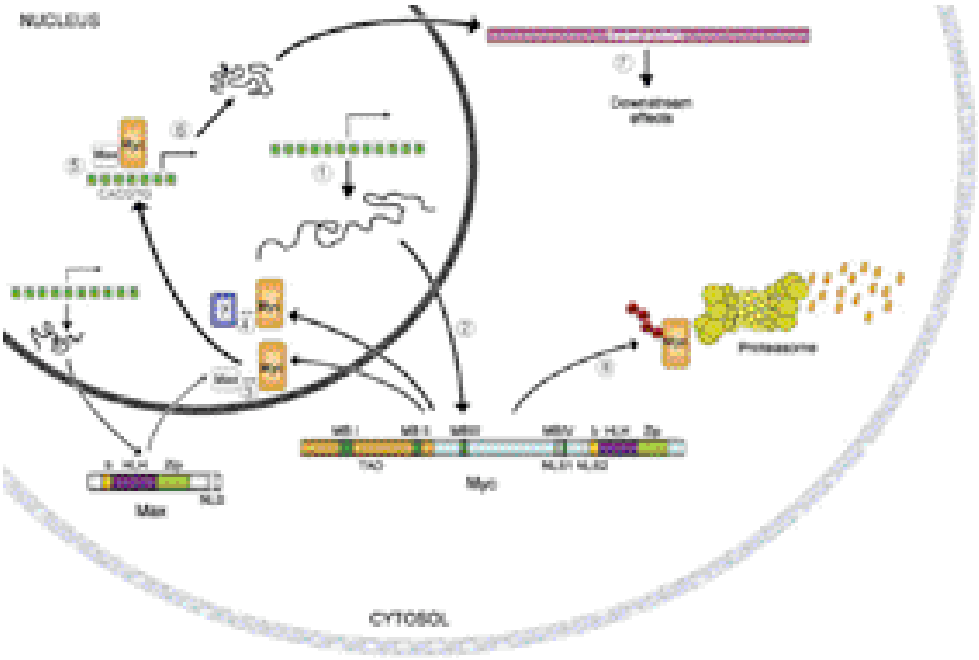

Figure 2.20 - Therapeutic strategies that target c-Myc. Experimental strategies that been used to modulate c-Myc expression and activity include: (1) inhibition of myc expression at the DNA and mRNA level by interfering with transcription (anti-sense oligonucleotides and siRNAs); (2) blockade of c-Myc expression at the protein level (small molecules); (3) disruption of c-Myc/Max dimerization (small molecules); (4) blockage of c-Myc interaction with other transcriptional co-activators (small molecules); (5) interference with c-Myc/Max binding to DNA (decoy oligonucleotides); (6) inhibition of expression of c-Myc target genes (anti-sense oligonucleotides and siRNAs); (7) modulation of the function of key c-Myc target genes (small molecules); and (8) promotion of c-Myc protein degradation (small molecules). See text for details. Figure adapted from [163].

Small interfering RNAs (siRNAs) directed against *myc* have been employed extensively for the validation of new c-Myc target genes [172-176]. As expected, reductions in *myc* expression in these studies were accompanied by reduced proliferation. Similarly, siRNA-mediated reduction in c-Myc levels in MCF-7 breast cancer cells inhibited colony formation and reduced growth of tumor xenografts [177]. Phosphorodiamidate morpholino oligomers (PMOs) are structurally modified ASOs in which the deoxyribose sugar is replaced with a morpholine ring and the phosphodiester

backbone is substituted with phosphorodiamidate linkages [178]. The c*myc*-directed PMO, AVI-4126, inhibited tumor growth in murine cancer xenografts [179]. Moreover, administration of this PMO restored sensitivity to cisplatin and pacilitaxel in resistant tumors in the Lewis lung carcinoma model [178]. These studies further demonstrate the potential of anti-c-Myc therapies and demonstrate that c-Myc-directed PMOs are safe, although their clinical efficacy remains untested.

Heterodimerization with the small bHLHZip domain protein Max is a prerequisite for Myc-directed transcriptional activation [62]. Based on this requirement, several groups have sought to identify compounds that disrupt c-Myc/Max association. In seminal work, Berg, *et. al*. identified inhibitors of c-Myc/Max dimerization using an *in vitro* fluorescence resonance energy transfer (FRET)-based assay (Figure 2.21; [180]). Two compounds from this screen prevented colony formation of c-Myc-transformed chicken embryo fibroblasts at micromolar concentrations. The Prochownik group identified inhibitors of c-Myc/Max dimerization (**3-6**) using a yeast two-hybrid system in which association of the bHLHzip domains of c-Myc and Max reconstitutes an active transcription factor capable of inducing β-galactosidase expression (Figure 2.21; [181]). This approach successfully identified several compounds that inhibit Myc-dependent transcriptional activation and block proliferation of c-Myc transformed fibroblasts. Finally, inhibitors of transcriptional activation by N-Myc were identified using a luciferase reporter under the control of the *odc* promoter [182]. Several candidate molecules (IC_{50} < 10 μM) from this screen blocked growth of N-Myc overexpressing cells.

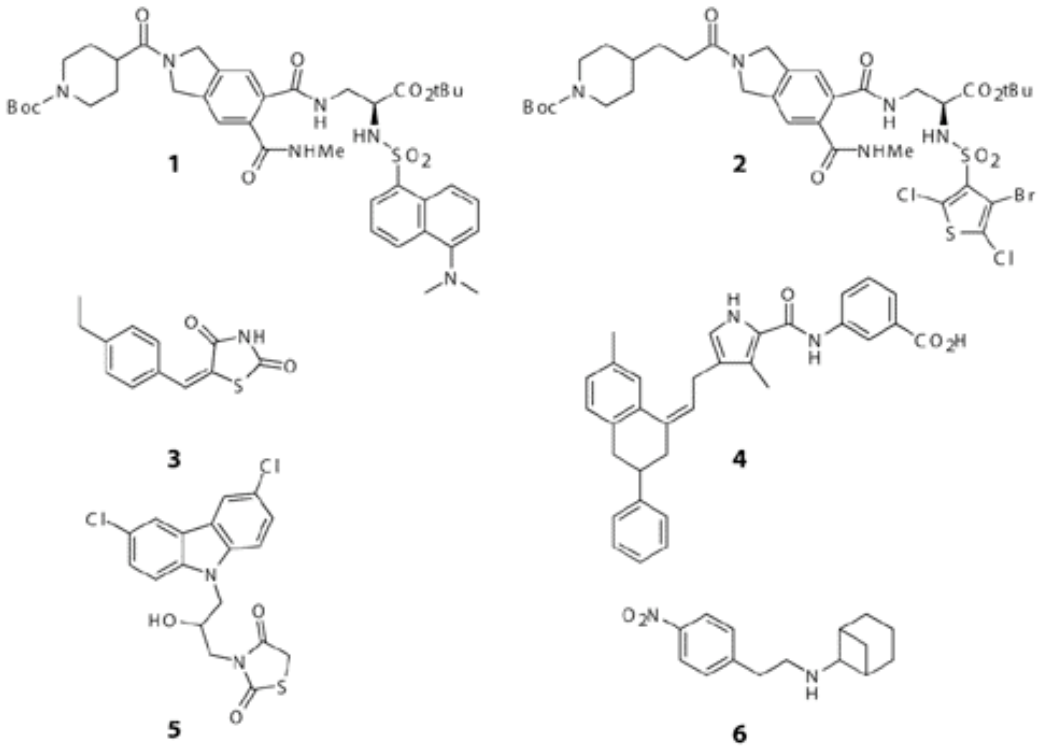

Figure 2.21 – Small-molecule inhibitors of c-Myc-Max dimerization. Compounds **1** and **2** were identified by Berg, *et al*. by their ability to disrupt Myc-Max dimers in FRET-based assay [180]. Compounds **3-6** were identified by Prochownk, *et al.* using a similar approach [181].

Collectively, these studies demonstrate that small, drug-like molecules can be used to modulate c-Myc function. Of concern, however, is that inhibitors of c-Myc/Max heterodimerization typically display little selectively between cells expressing high and low c-Myc levels [181], suggesting the potential for mechanism-based toxicities. On a more fundamental level, the effectiveness of small molecule inhibitors of c-Myc/Max dimerization may be inherently limited because, independent of Max, c-Myc can still repress transcription of many genes that block proliferation (e.g., $p15^{Ink4b}$ and $p21^{Cip1}$) by interacting with transcription factors such as Sp1 and Miz-1 [62, 80].

Ideally, anti-Myc therapies will intervene in cells where Myc expression/activity is deregulated, while sparing normal cells. Based on this principle, Mo and Henriksson screened the National Cancer Institute Diversity Library for members that selectively inhibit proliferation of tumor cells with elevated Myc levels [183]. This approach identified two compounds that preferentially block proliferation of mouse embryonic fibroblasts in which high Myc levels are achieved by expression of Tet-inducible *myc* transgene (Figure 2.22). Although these compounds inhibit Myc-dependent transcriptional activation, Myc levels and association with Max were unaffected, which suggests that these small molecules trigger an unidentified regulatory mechanism. The presence of elevated levels of c-Myc in tumor cells also underlies the selective killing of melanomas by the proteasome inhibitor Bortezomib relative to normal melanocytes [184]. Mechanistically, proteasome inhibition further increases endogenously high Myc levels in the melanoma cells, which results in transcriptional activation of the pro-apoptotic Bcl-2 protein Noxa [184]. Together, these studies highlight the potential of exploiting "surplus" levels of oncogenic transcription factors (e.g., c-Myc) that are often observed in malignant cells.

Once expressed, the activity of a given protein can be modulated by a multitude of post-translational modifications. Most decisive among these mechanisms, however, is proteasomal degradation. As described in the previous section, the ubiquitin-proteasome system tightly controls c-Myc protein levels. Consequently, agents that stimulate this pathway represent potentially useful candidates to control dangerous c-Myc levels. This approach was validated by studies with a fusion protein, designated Max-U, comprised

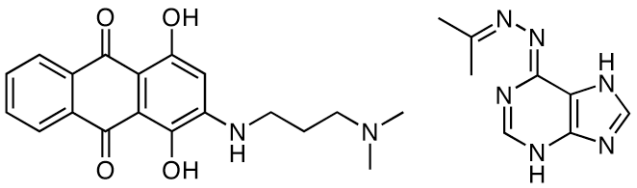

Figure 2.22 – Small molecules that selectively block proliferation in cells expressing high levels of c-Myc.

of Max and the U box-type E3 ubiquitin ligase CHIP [185]. Max-U promotes Myc ubiquitylation *in vitro*, and reduces Myc levels and arrests growth when expressed in the Namalwa Burkitt's lymphoma B cell line [185]. The results presented in this chapter demonstrate that Bz-423 blocks proliferation of Ramos B cells by triggering rapid, proteasomal degradation of Myc. This finding, coupled with the accompanying reduction in β-catenin levels (Figure 2.10), suggests that activity of the ubiquitin-proteasome pathway is upregulated in response to Bz-423-induced mitochondrial $O_2^{\bullet-}$ production.

Like Bz-423, the synthetic small molecule Degrasyn has recently been shown to promote proteasomal degradation of c-Myc (Figure 2.23; [121]). Degrasyn-induced c-Myc degradation appears to occur by a process distinct from that engaged by Bz-423 because a construct lacking MBI region remains sensitive [121]. In contrast, a c-Myc mutant lacking amino acids 316-378 was stabilized in the presence of Degrasyn [121]. This carboxy-terminal region had not previously been shown to be associated with proteasomal degradation. Significantly, Degrasyn reduced Myc levels and inhibited tumor growth in A375 melanoma xenografts [121]. Degrasyn was originally identified as

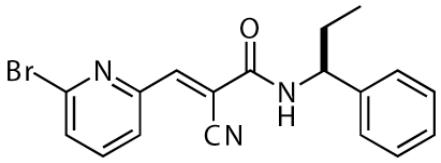

Figure 2.23 - Degrasyn, a small molecule that targets c-Myc to the ubiquitin-proteasome pathway.

an inhibitor of cytokine-stimulated signal transduction and activator of transcription 3 (STAT3) activation [186]. The molecular target and signaling transduction pathway(s) underlying the effects on STAT3 activation and Myc stability have not been identified [121, 186]. Collectively, these studies demonstrate that the ubiquitin-proteasomal pathway can be manipulated to regulate Myc protein stability, and in particular, the results with Bz-423 and Degrasyn demonstrate that this can be accomplished using small, drug-like molecules.

Role of cell cycle progression in lymphocyte activation: Normal immune responses are initiated by a small number of reactive T lymphocytes that once activated, expand into a large population of antigen-specific cells [106, 187]. This expansion coincides with the acquisition of effector functions such as capacity to produce inflammatory cytokines such as interleukin-2 (IL-2) [188]. T cell activation depends on two signals: stimulation of T cell antigen receptor (TCR) and ligation of co-stimulatory receptors (e.g., CD28) by pathogen-associated inflammatory signals. TCR stimulation triggers a rise in intracellular Ca^{2+} that results in activation of the transcription factor NFAT, while mitogen-activated protein (MAP) kinase cascades downstream of CD28 potentiate this response by an alternative set of transcription factors including AP1,

CREB and NFκB (Figure 2.24A; [189]). Stimulation of the TCR in the absence of CD28 results in defective assembly of transcription factor complexes, and renders T cells hypo-responsive to subsequent activation [190-193]. Induction of this unresponsive state, known as anergy, is an important mechanism in the maintenance of tolerance to self-antigens, which are not accompanied by non-specific pathogen-associated inflammatory triggers such as lipolysaccharides or viral DNA (Figure 2.24B; [190, 191, 194-196]).

Although T cell activation is initiated by stimulation of cell-surface receptors, cell cycle progression is increasingly recognized as playing a regulatory role in this process [106, 197]. For example, T cells that progress through multiple divisions (>5) after TCR/CD28 stimulation proliferate rapidly and produce high levels of IL-2 when restimulated [198]. In contrast, cells that fail to divide following the initial stimulus are also unresponsive to subsequent stimulation [198, 199]. Correspondingly, arrest of T cell proliferation at the G_1 checkpoint by rapamycin or butyrate induces anergy [200, 201]. Growth arrest alone, however, is not sufficient to induce anergy because TCR/CD28 stimulated T cells can produce IL-2 in the presence of the ribonucleotide reductase inhibitor hydroxyurea, which arrests growth during S phase [201]. Together, these studies demonstrate that cell cycle progression, and particularly biochemical events associated with the G_1-S transition, are critical for avoidance of anergy and robust T cell activation.

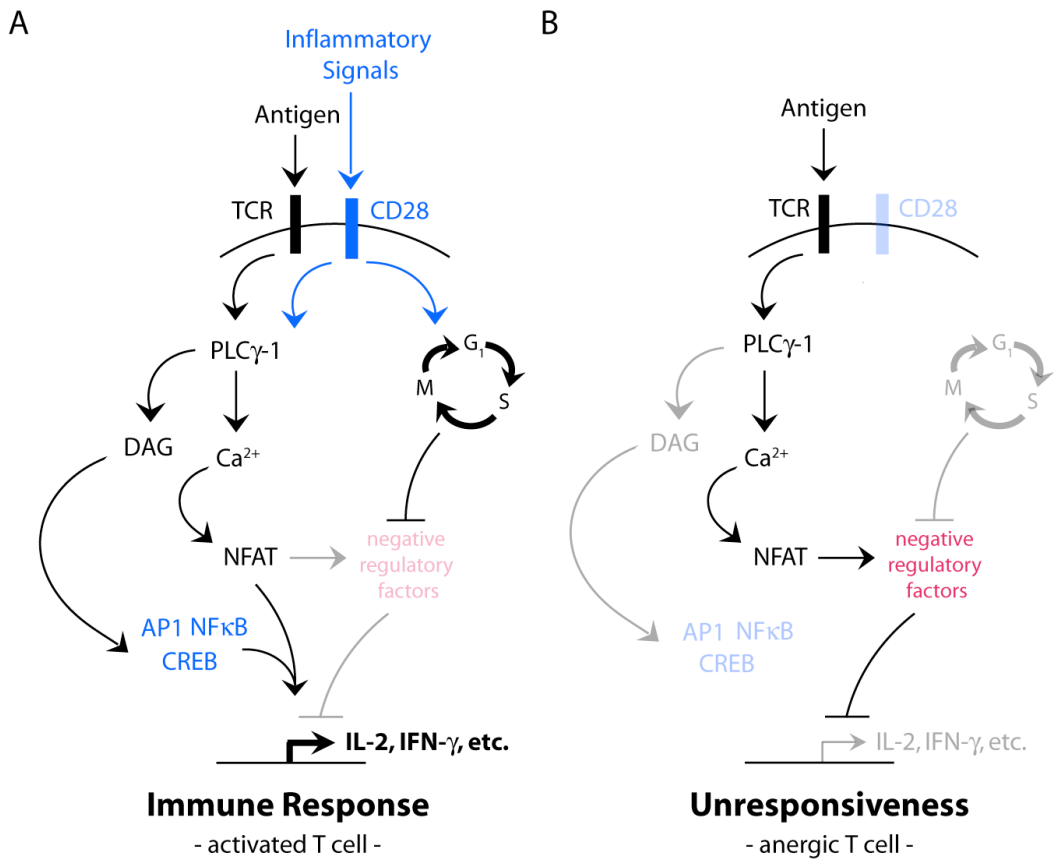

Figure 2.24 – Signaling pathways leading to T cell activation and anergy. (A) Under optimal conditions (i.e., stimulation of T cells through both the TCR and co-receptors such as CD28), NFAT binds promoter regions of cytokines and other proteins expressed during T cell activation in conjunction with other transcription factors including AP1, NFκB and CREB and induce expression of these genes. Cell cycle progression promotes T cell activation by inhibiting negative regulatory factors (e.g., Smad transcription factors). (B) Anergic conditions (e.g., TCR stimulation in the absence of CD28 signals) leads to activation of NFAT alone, which is not sufficient to induce cytokine expression. In addition, NFAT activation in the absence of AP1, NFκB and CREB promotes transcription of genes mediating anergy (e.g., $p27^{Kip1}$). Figure adopted from [197].

Anergic T cells exhibit normal levels of CDK4/6 activity, but have reduced CDK2 activity [106, 202, 203]. Correspondingly, elevated levels of $p27^{Kip1}$, which preferentially targets cyclin E-CDK2 complexes, are a nearly universal feature of anergic T cells [199, 202-207]. Furthermore, increased levels of this CDKI appear to be

functionally consequential because forced $p27^{Kip1}$ expression is sufficient to induce anergy in T lymphocytes, even when subject to combined TCR and CD28 stimulation [202]. Conversely, $p27^{Kip1}$-deficient T cells are resistant to anergy induced that is *in vitro* by TCR stimulation in the presence of CTLA-4Ig, a reagent that blocks CD28 signaling [208]. Correspondingly, blocking co-stimulatory receptor signaling with CTLA-4Ig promotes long-term survival of cardiac allografts by inducing anergy in recipient T lymphocytes [209], but fails to prevent graft rejection by $p27^{Kip1}$-null recipients [210]. T cell activation, therefore, depends on active cyclin E-CDK2 complexes, and conversely low levels of $p27^{Kip1}$.

The essential contribution of $p27^{Kip1}$ to induction of anergy suggests that this process results from reduced phosphorylation of CDK2 substrates. To identify relevant CDK2 substrates, Rao, *et al*. prepared a 'knock-in' mouse expressing a $p27^{Kip1}$ variant (p27Δ) lacking the CDK binding domain [203]. This functional inactivation of $p27^{Kip1}$ conveys constituitive CDK2 activity, and as result, T cells from these mice are resistant to CTLA-4Ig-induced anergy *in vitro* and *in vivo* [203]. Surprisingly, equivalent levels of overall pRb phosphorylation are observed in T cells from p27Δ and wild-type $p27^{Kip1}$ mice in response to anergizing stimuli [203]. This finding suggests that (1) T cells possess sufficient CDK4/6 activity to maintain pRb phosphorylation, even in the presence of high levels of $p27^{Kip1}$, such that (2) anergy results from decreased phosphorylation of other CDK2 substrates. In contrast to pRb, expression of p27Δ maintains phosphorylation of Smad3, a CDK2 substrate and transcriptional repressor of the *il2* gene, in T cells exposed to anergic stimuli. In contrast, reduced Smad3 phosphorylation and, IL-2 production are observed in anergized wild-type T cells [203]. A functional role

for CDK2 phosphorylation of Smad3 was demonstreated by expression of a Smad3 variant with mutated CDK2 phosphorylation sites. Expression of this Smad3 mutant overcame the constitutive CDK2 activity, and re-sensitized p27Δ T cells to anergic stimuli [203]. Consequently, cyclin E-CDK2 activity appears necessary for avoidance of anergy, although this effect is mediated by phosphorylation of substrates other than pRb.

The requirement for CDK2 activity for T cell activation suggests that CDK inhibitors may be able to promote transplant survival and treat autoimmune diseases by blunting pathological T cell responses [197]. This has been demonstrated experimentally by using a peptide derived from amino acids 140 - 160 of the CDKI $p21^{Cip1}$. Administration of this $p21^{Cip1}$-derived peptide to NZB/w mice reduces activated splenic B and T cell subsets and ameliorates renal disease (Figure 2.25; [211]). Similarly, the small-molecule CDK2 inhibitor Seliciclib improves disease in NZB/W mice (Figure 2.25; [212]). Splenic T and B cells from Seliciclib-treated mice displayed reduced proliferation and inflammatory cytokine production following *ex vivo* stimulation [212]. Unresponsiveness to *ex vivo* stimulation is characteristic of anergic lymphocytes. Like these agents, Bz-423 improves renal disease in the NZB/W murine model of lupus. Although specific apoptosis of pathogenic GC B cells is observed in Bz-423-treated NZB/W mice [1], immunomodulatory mechanisms such as induction of anergy, which can result from impaired cell cycle progression, may also contribute to the *in vivo* efficacy.

Summary: Bz-423 blocks proliferation in Ramos B cells by inducing a rapid reduction in Myc protein levels. Because c-Myc is a transcriptional activator of both cyclins and CDKs, this effect results in decreased CDK2 and CDK4/6 activity, which

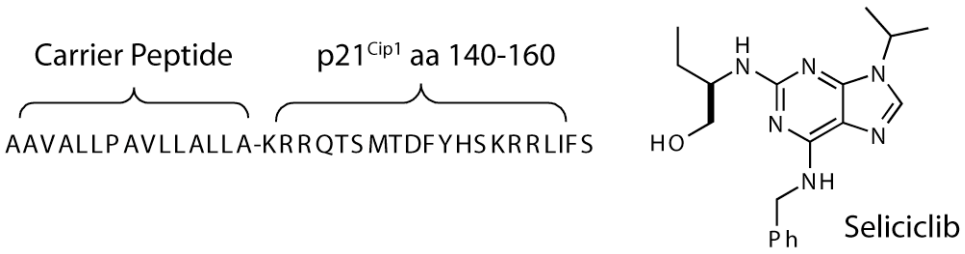

Figure 2.25 - p21^{Cip1}-derived peptide and the small-molecule CDK2 inhibitor Seliciclib ameliorate autoimmune nephritis in NZB/W mice.

leads to a block in proliferation at the G_1 checkpoint. Given that c-Myc proteins are deregulated in a wide variety of human cancers, considerable attention has been paid to development of strategies to regulate their levels and/or activity. Although small molecule inhibitors of c-Myc transcriptional activation have been developed, reduction in c-Myc levels has primarily been accomplished by genetic silencing with siRNAs or nucleic acid-derived anti-genes. Consequently, the ability of a small, drug-like molecule like Bz-423 to rapidly deplete c-Myc levels is unique. Finally, the requirement for cell cycle progression for lymphocyte activation suggests that low levels of $O_2^{\bullet-}$ produced by sub-apoptotic concentrations of Bz-423 may have other immunomodulatory consequences such as induction of anergy in T cells.

Statement of collaboration: Gina Ney identified the induction of OAZ1 in the mRNA expression profile and performed the ODC activity assays. Chitra Subramanian (University of Michigan, Department of Pediatrics) prepared the mammalian expression plasmids containing either wild type Myc or alanine mutants of Thr58, Ser62 or both residues. Narasimharao Bhagavathula (University of Michigan Department of Pathology) harvested keratinocytes.

Materials and Methods

Reagents: Bz-423 was first dissolve in DMSO (16 mM), and then diluted as 10x stocks with culture media. The 10x Bz-423 stocks were applied to cell cultures such that DMSO was present at a final concentration of 0.5% (v/v) in all experiments. DFMO was diluted in PBS (100 mM). Arsenic trioxide (ATO) was diluted in 0.1 N NaOH (100 mM). α-IgM F(ab')$_2$ fragment and α-IgG were obtained from Jackson Laboratories. Manganese(III) *meso*-tetrakis(4-benzoid acid)porphyrin (MnTBAP) was purchased from Alexis Biochemicals and diluted in 1:1 EtOH:dH_2O (v/v) (100 mM). Bortezomib was a gift from V. Castle (University of Michigan) and dissolved in DMSO (100 mM). SB216763 and SB415286 were purchased from Calbiochem and dissolved in DMSO (both 100 mM). DHE was purchased from Invitrogen. All other reagents were purchased from Sigma-Aldrich.

Cell lines and culture: Ramos B cells were purchased from ATCC and maintained in RPMI 1640 containing 10% heat-inactivated fetal bovine serum (FBS: Mediatech), penicillin (100 U/mL), streptomycin (100 μg/mL) and L-glutamine (290 μg/mL) (Gibco). Cells were propagated in a humidified incubator (37 °C, 5% CO_2). Experiments were performed in media (0.5 x 10^6 cells/mL) containing 2% or 10% FBS as indicated. Cells were incubated with inhibitors at 37 °C for 30 min prior to addition of the compounds being tested.

Transfection and selection of c-Myc clones: Expression plasmids for Myc^{WT}, Myc^{T58A}, Myc^{S62A} and $Myc^{T58A/S62A}$ were prepared by Chitra Subramanian [213]. Ramos B cells (7 x 10^6) were washed once with ice-cold PBS, suspended in electroporation buffer T (Amaxa), combined with desired plasmid (2 μg), and electroporated using program G-

16 in a Amaxa Nucleofection apparatus. Samples were then diluted in fresh complete media, and after 24 h stably transfected cells were selected by continuous culture in complete media supplemented with geneticin (1.6 mg/mL; Life Technologies).

Detection of intracellular $O_2^{\bullet-}$: Intracellular $O_2^{\bullet-}$ was measured using DHE. Stocks of DHE (10 mM) were prepared in DMSO prior to each use. To measure intracellular $O_2^{\bullet-}$ levels, cell cultures (5 x 10^5 cells/mL) were incubated with DHE (7.5 μM) for 30 min at 37 °C. The DHE-treated cells were immediately evaluated by flow cytometry. Ethidium fluorescence from the conversion of DHE was detected in the FL2 channel of a FACSCalibur flow cytometer (Becton Dickinson). Data was analyzed using the CellQuest software (Becton Dickinson).

Detection of cell death and cellular DNA content: Cell viability was assessed by staining with propidium iodide (PI, 1 μg/mL) at room temperature (~25 °C) for 5 min. PI fluorescence was measured in the FL3 channel using a FACSCalibur. Measurement of hypodiploid DNA content was conducted after incubating cells in labeling solution (50 μg/mL of PI in PBS containing 0.2% Triton and 10 μg/mL RNAse A) at 4 ˚C for 12 h. PI fluorescence was measured in the FL2 channel on a linear scale. Data were analyzed excluding aggregates using the CellQuest software.

Preparation of whole cell extracts: Cells (20 x 10^6) were pelleted and supernatants were aspirated. Cell pellets were washed once with 1 ml PBS before lysis with 500 μL of WCE lysis buffer (25 mM Hepes pH 7.7, 150 mM NaCl, 2.5 mM $MgCl_2$, 0.2 mM EDTA, 0.1% Triton X-100, 20 mM β-glycerophophate, 0.5 mM DTT) with protease inhibitors (1 mM PMSF and complete protease inhibitor cocktail pellet (Roche)) and phosphatase inhibitors (3.3 mM NaF and 0.1 mM sodium orthovanadate). Following

incubation on ice for 30 min, the lysed cells were centrifuged (12,000*g,* 30 min at 4 °C). Total protein content in the supernatant was quantified by the Bradford protein assay [214].

Immunoblot Analysis: Cell lysates were denatured by boiling with one-fifth volume of 5X SDS sample buffer (250 mM Tris Cl pH 6.8, glycerol (40% v/v), SDS (8% w/v), 2-mercaptoethanol (8% v/v), Bromophenol Blue (0.2% w/v)). Proteins were subjected to electrophoresis by SDS-PAGE and transferred on to a PVDF membrane (Bio-Rad), and incubated with primary antibodies from the proteins of interest in phosphate buffered saline containing 5% nonfat dry milk, 0.1% Tween 20. The antibodies for ODC (catalog # O1136) or FLAG (catalog # F3165) or β-tubulin (catalog #T4026) were purchased from Sigma-Aldrich. The ODC antizyme 1 (OAZ1) antibody (catalog #PW8885) was purchased from Biomol International. Antibodies for p-Myc (T58/S62) (catalog #9401), CDK6 (catalog 3136), retinoblastoma protein (pRb; catalog #9309), phospho-pRb (S780; catalog #9307), phospho-pRb (S795; catalog #9301) and phospho-pRb (S807/S811; catalog #9308) were purchased from Cell Signaling Technology. Antibodies for Myc (catalog #551101), β-Catenin (catalog #610514), $p27^{Kip1}$ (catalog #610241), cyclin D1 (catalog #556470), cyclin D2 (catalog #554201), cyclin D3 (catalog #554195), cyclin E1 (catalog #554182), CDK2 (catalog #610145) and CDK4 (catalog #559693) were purchased from Becton Dickenson. Membranes were then incubated with horseradish-peroxidase conjugated secondary antibodies and immune complexes were visualized with Enhanced Chemiluminescence Reagent (GE Healthcare).

RNA Isolation and Reverse Transcriptase-PCR: RNA was isolated using a RNeasy mini kit (Qiagen). Semi-quantitative reverse transcription-PCR (RT-PCR) was

performed using a SuperScript III One-Step RT-PCR Kit (Invitrogen). For reactions, 50 ng of sample RNA was combined with 2X Reaction Mix, forward Primer (10 μM), reverse primer (10 μM), SuperScript III RT/ Platinum *Taq* High Fidelity Enzyme Mix and sufficient autoclaved dH_2O for a total volume of 50 μL. The following primer pairs were used: *odc* (forward GAGCACATCCCAAAGCAAGT and reverse TCCAGAGTCGACGGAAAGTA), *oaz1* (forward AGCAGTGAGAGTTCCAGGGTC and reverse ACTGCAAAGCTGTCCTTGCTC), *myc* (forward TTCGGGTAGTGGAAAACCAG and reverse CAGCAGCTCGAATTTCTTCC) and β-actin (forward TGGCATGTTACCAACTGGGACG and reverse GCTTCTCTTTTGATGTCACGCAGCG). Reactions were heated at 50 °C for 20 min in a PTC100 Thermocycler (MJ Research Inc.) to synthesis cDNA and these products were amplified by 35 of following cycles: 94 °C for 15 s, 60 °C for 30 s and 68 °C for 30 s. PCR products were then cooled to 68 °C for 10 min, separated from template RNA by electrophoresis in agarose (1%) gel with 50 μM ethidium bromide, and visualized with a UV lamp.

Sulforhodamine B (SRB) assay: Growth inhibition was determined using the SRB assay for total protein content developed by the NCI/NIH Developmental Therapeutics Program [215]. Cells were introduced into a 96 well microtiter plate in the appropriate media (100 μL) at a plating density of 2,500 cells/well and incubated for 24 h prior to treatment. At the time of treatment the plating media was removed and replaced with appropriate media (180 μL). At indicated time points the cells were fixed *in situ* by addition of 50 μL of ice cold trichloroacetic acid (TCA) (50% w/v) (final concentration, 10% TCA) and incubated 60 min at 4 ˚C. The supernatant was discarded and plates were

washed with dH_2O (5 x 100 µL) and air-dried. SRB solution (100 µL at 0.4% (w/v)) in acetic acid (1%) was added to each well and plates were incubated for 10 min at room temperature. After staining, unbound dye was removed by washing with acetic acid (1%, 5 x 100 µL), and plates were air-dried. Bound stain was solubilized with trizma base (10 mM, 150 µL), and the absorbance was read on an automated plate reader at a wavelength of 515 nm. Using the absorbance measurements [time zero, (Tz), control growth, (C), and test growth in the presence of drug (Ti)], the percentage growth inhibition is calculated by the following equations:

$$[(Ti-Tz)/(C-Tz)] \times 100 \text{ for concentrations for which } Ti \geq Tz$$

$$[(Ti-Tz)/Tz] \times 100 \text{ for concentrations for which } Ti < Tz.$$

Synthesis of benzoyl chloride polyamine derivatives: Standard samples of the polyamines putrescine (PUT), spermidine (SPD), spermine (SPM), and the internal standard, diaminonane (DAN), were prepared according to the method of Schenkel, et al [216]. In a representative procedure, SPM (0.1 g, 0.287 mmol) was dissolved in an aqueous solution of 2M NaOH (15 mL) to which benzoyl chloride (1.0 mL, 8.75 mmol) was added dropwise at 0 °C. The solution was allowed to warm to rt over 2h, extracted with $CHCl_3$ (3 x 10 mL), and concentrated under reduced pressure to yield a white solid. The white solid was dissolved in (1:1) MeOH/ddH_2O (10 mL), stirred at rt overnight, extracted with $CHCl_3$ (3 x 10 mL) and concentrated under reduced pressure yielding a white solid. Benzoylation of all primary and/or secondary amines was confirmed by ES LRMS (Table 2.#). Standard solutions of benzoylated polyamines were prepared in (3:2) MeOH:dH_2O (v/v) at concentration of 250 mM.

Polyamine	Benzoylated Derivative	Predicted MW	ES LRMS $[M+Na]^+$
Putrescine	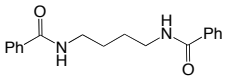	296.36	319.2
Spermidine	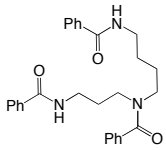	457.56	480.1
Spermine	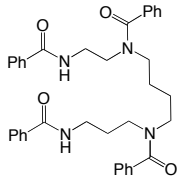	618.76	641.3
Diaminonane (Internal Standard)	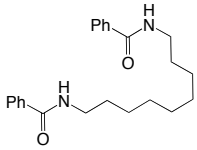	366.50	389.2

Table 2.4 - Mass Spectroscopy Data for Benzoylated Polyamine Derivatives

Isolation and derivatization of polyamines: Cells were washed once in ice-cold PBS and lysed in a 1.0 mL solution of PBS along with trichloroacetic acid (10%) and the internal standard DAN (45 μM). Acid-soluble polyamines were separated from precipitated protein by centrifugation (12,000 rpm, 3 min). The supernatant was diluted with 2M NaOH (1.0 mL) and neutral polyamines were derivatized by addition of neat benzoyl chloride (5.0 μL). The solution was vortex-mixed for 1 min and then stirred on a low-speed shaker at rt for 2h. The reaction mixture was extracted with $CHCl_3$ (2 x 2 mL) and concentrated under reduced pressure to yield a white powder. The white powder was dissolved in (1:1) MeOH/ddH_2O (1.5 mL) and allowed to stand at rt overnight. The

aqueous layer was made basic by addition of 1 M NaOH (2 mL), extracted with $CHCl_3$ (2 x 2 mL), and concentrated under reduced pressure to yield a white powder.

HPLC Analysis: Benzoylated polyamines were separated and quantified using an HPLC system consisting of two Waters 600 pumps, a Waters 600E system controller, a Waters USK injector with a 200 μL injector loop and a Waters 484 UV variable wavelength adsorbance detector. Data aquistion and processing was performed using Waters Empower Pro software. Polyamines were separated using a Waters Spherisorb C_{18} S3 ODS2 column (15 x 0.46 cm I.D.; 3 μm particle size) protected by a guard column (3 x 0.46 cm I.D.; 5 μm particle size). Samples were dissolved in (3:2) MeOH/dH_2O (0.2 mL) and filtered through a Whatmann 0.45 μm polypropylene membrane, and aliquots (20 μL) were injected onto the column described above. The mobile phase was a mixture of solvent A (water) and B (methanol). Samples were eluted from 61% of B (0 to 3 min) to 67% B (4.5 to 14 min) and then immediately returned to 61% solvent B (14 to 15 min), and the initial conditions were restored for 15 min. The flow rate was 0.8 mL/min, and the detection was performed at 229 nm (detector sensitivity 0.1 aufs). Calibration of chromatogram peak area to nmol polyamine was performed by co-injection of known volumes of standard polyamine solutions. Polyamine content of biological samples was determined by comparision of the area of a given polyamine peak to the peak area of the internal standard DAN. Polyamine content was reported relative to total sample protein as determined by the Bradford protein assay [214].

BIBLIOGRAPHY

1. Blatt, N.B., Bednarski, J.J., Warner, R.E., Leonetti, F., Johnson, K.M., Boitano, A., Yung, R., Richardson, B.C., Johnson, K.J., Ellman, J.A., Opipari, A.W., Jr., and Glick, G.D. (2002). Benzodiazepine-induced superoxide signals B cell apoptosis: mechanistic insight and potential therapeutic utility. J Clin Invest *110*, 1123-1132.

2. Haefely, W. (1990). The GABA-benzodiazepine interaction fifteen years later. Neurochem Res *15*, 169-174.

3. Nickell, P.V.`; Ward, H.E.`; Booth, R.G. (1996). Antianxiety Agents. In Burger's Medicinal Chemistry and Drug Discovery. Ed. Wolf, M.E. (New York`; Wiley-Interscience), Vol 5., pp. 153-185.

4. Groh, B., and Muller, W.E. (1985). A comparison of the relative in vitro and in vivo binding affinities of various benzodiazepines and related compounds for the benzodiazepine receptor and for the peripheral benzodiazepine binding site. Res Commun Chem Pathol Pharmacol *49*, 463-466.

5. Nickell, P.V.`; Ward, H.E.`; Booth, R.G. (1996). Antianxiety Agents. In Burger's Medicinal Chemistry and Drug Discovery. Ed. Wolf, M.E. (New York```; Wiley-Interscience), Vol 5., pp. 171-173.

6. Nickell, P.V.`; Ward, H.E.`; Booth, R.G. (1996). Antianxiety Agents. In Burger's Medicinal Chemistry and Drug Discovery. Ed. Wolf, M.E. (New York`; Wiley-Interscience), Vol 5., pp. 153-185.

7. Nickell, P.V.`; Ward, H.E.`; Booth, R.G. (1996). Antianxiety Agents. In Burger's Medicinal Chemistry and Drug Discovery. Ed. Wolf, M.E. (New York```; Wiley-Interscience), Vol 5., pp. 171-173.

8. Bednarski, J.J., Warner, R.E., Rao, T., Leonetti, F., Yung, R., Richardson, B.C., Johnson, K.J., Ellman, J.A., Opipari, A.W., Jr., and Glick, G.D. (2003). Attenuation of autoimmune disease in Fas-deficient mice by treatment with a cytotoxic benzodiazepine. Arthritis Rheum *48*, 757-766.

9. Braestrup, C., and Squires, R.F. (1977). Specific benzodiazepine receptors in rat brain characterized by high-affinity (3H)diazepam binding. Proc Natl Acad Sci U S A *74*, 3805-3809.

10. Joseph-Liauzun, E., Farges, R., Delmas, P., Ferrara, P., and Loison, G. (1997). The Mr 18,000 subunit of the peripheral-type benzodiazepine receptor exhibits both benzodiazepine and isoquinoline carboxamide binding sites in the absence of the voltage-dependent anion channel or of the adenine nucleotide carrier. J Biol Chem *272*, 28102-28106.

11. Woods, M.J., and Williams, D.C. (1996). Multiple forms and locations for the peripheral-type benzodiazepine receptor. Biochem Pharmacol *52*, 1805-1814.

12. Casellas, P., Galiegue, S., and Basile, A.S. (2002). Peripheral benzodiazepine receptors and mitochondrial function. Neurochem Int *40*, 475-486.

13. Zisterer, D.M., and Williams, D.C. (1997). Peripheral-type benzodiazepine receptors. Gen Pharmacol *29*, 305-314.

14. Gavish, M., Bachman, I., Shoukrun, R., Katz, Y., Veenman, L., Weisinger, G., and Weizman, A. (1999). Enigma of the peripheral benzodiazepine receptor. Pharmacol Rev *51*, 629-650.

15. Selleri, S., Bruni, F., Costagli, C., Costanzo, A., Guerrini, G., Ciciani, G., Costa, B., and Martini, C. (2001). 2-Arylpyrazolo[1,5-a]pyrimidin-3-yl acetamides. New potent and selective peripheral benzodiazepine receptor ligands. Bioorg Med Chem *9*, 2661-2671.

16. Camins, A., Diez-Fernandez, C., Pujadas, E., Camarasa, J., and Escubedo, E. (1995). A new aspect of the antiproliferative action of peripheral-type benzodiazepine receptor ligands. Eur J Pharmacol *272*, 289-292.

17. Gorman, A.M., O'Beirne, G.B., Regan, C.M., and Williams, D.C. (1989). Antiproliferative action of benzodiazepines in cultured brain cells is not mediated through the peripheral-type benzodiazepine acceptor. J Neurochem *53*, 849-855.

18. Cleary, J., Johnson, K.M., Opipari, A.W., Jr., and Glick, G.D. (2007). Inhibition of the mitochondrial F1F0-ATPase by ligands of the peripheral benzodiazepine receptor. Bioorg Med Chem Lett *17*, 1667-1670.

19. Gonzalez-Polo, R.A., Carvalho, G., Braun, T., Decaudin, D., Fabre, C., Larochette, N., Perfettini, J.L., Djavaheri-Mergny, M., Youlyouz-Marfak, I., Codogno, P., Raphael, M., Feuillard, J., and Kroemer, G. (2005). PK11195 potently sensitizes to apoptosis induction independently from the peripheral benzodiazepin receptor. Oncogene *24*, 7503-7513.

20. Kletsas, D., Li, W., Han, Z., and Papadopoulos, V. (2004). Peripheral-type benzodiazepine receptor (PBR) and PBR drug ligands in fibroblast and fibrosarcoma cell proliferation: role of ERK, c-Jun and ligand-activated PBR-independent pathways. Biochem Pharmacol *67*, 1927-1932.

21. Boitano, A., Emal, C.D., Leonetti, F., Blatt, N.B., Dineen, T.A., Ellman, J.A., Roush, W.R., Opipari, A.W., and Glick, G.D. (2003). Structure activity studies of a novel cytotoxic benzodiazepine. Bioorg Med Chem Lett *13*, 3327-3330.

22. Boitano, A., Ellman, J.A., Glick, G.D., and Opipari, A.W., Jr. (2003). The proapoptotic benzodiazepine Bz-423 affects the growth and survival of malignant B cells. Cancer Res *63*, 6870-6876.

23. Gregory, C.D., Tursz, T., Edwards, C.F., Tetaud, C., Talbot, M., Caillou, B., Rickinson, A.B., and Lipinski, M. (1987). Identification of a subset of normal B cells with a Burkitt's lymphoma (BL)-like phenotype. J Immunol *139*, 313-318.

24. Thorbecke, G.J., Amin, A.R., and Tsiagbe, V.K. (1994). Biology of germinal centers in lymphoid tissue. Faseb J *8*, 832-840.

25. Neuberger, G., Schneider, G., and Eisenhaber, F. (2007). pkaPS: prediction of protein kinase A phosphorylation sites with the simplified kinase-substrate binding model. Biol Direct *2*, 1.

26. Suzuki, N., Mihara, S., and Sakane, T. (1997). Development of pathogenic anti-DNA antibodies in patients with systemic lupus erythematosus. Faseb J *11*, 1033-1038.

27. Portanova, J.P., Creadon, G., Zhang, X., Smith, D.S., Kotzin, B.L., and Wysocki, L.J. (1995). An early post-mutational selection event directs expansion of autoreactive B cells in murine lupus. Mol Immunol *32*, 117-135.

28. Shlomchik, M.J., Craft, J.E., and Mamula, M.J. (2001). From T to B and back again: positive feedback in systemic autoimmune disease. Nat Rev Immunol *1*, 147-153.

29. Bednarski, J.J., Lyssiotis, C.A., Roush, R., Boitano, A.E., Glick, G.D., and Opipari, A.W., Jr. (2004). A novel benzodiazepine increases the sensitivity of B cells to receptor stimulation with synergistic effects on calcium signaling and apoptosis. J Biol Chem *279*, 29615-29621.

30. Johnson, K.M., Chen, X., Boitano, A., Swenson, L., Opipari, A.W., Jr., and Glick, G.D. (2005). Identification and validation of the mitochondrial F1F0-ATPase as the molecular target of the immunomodulatory benzodiazepine Bz-423. Chem Biol *12*, 485-496.

31. Boitano, AE. Mechanisms of a Pro-apoptotic Benzodiazepine. University of Michigan. 2005.

32. Tschachler, E. (2007). Psoriasis: the epidermal component. Clin Dermatol *25*, 589-595.

33. Bowcock, A.M., and Krueger, J.G. (2005). Getting under the skin: the immunogenetics of psoriasis. Nat Rev Immunol *5*, 699-711.

34. Sorrell, J.M., and Caplan, A.I. (2004). Fibroblast heterogeneity: more than skin deep. J Cell Sci *117*, 667-675.

35. Lebwohl, M. (2003). Psoriasis. Lancet *361*, 1197-1204.

36. Reid, D.C., and Kimball, A.B. (2005). Clobetasol propionate foam in the treatment of psoriasis. Expert Opin Pharmacother *6*, 1735-1740.

37. Watt, F.M., Frye, M., and Benitah, S.A. (2008). MYC in mammalian epidermis: how can an oncogene stimulate differentiation? Nat Rev Cancer *8*, 234-242.

38. Gandarillas, A., and Watt, F.M. (1995). Changes in expression of members of the fos and jun families and myc network during terminal differentiation of human keratinocytes. Oncogene *11*, 1403-1407.

39. Bull, J.J., Muller-Rover, S., Patel, S.V., Chronnell, C.M., McKay, I.A., and Philpott, M.P. (2001). Contrasting localization of c-Myc with other Myc superfamily transcription factors in the human hair follicle and during the hair growth cycle. J Invest Dermatol *116*, 617-622.

40. Waikel, R.L., Wang, X.J., and Roop, D.R. (1999). Targeted expression of c-Myc in the epidermis alters normal proliferation, differentiation and UV-B induced apoptosis. Oncogene *18*, 4870-4878.

41. Hornig-Do, H.T., von Kleist-Retzow, J.C., Lanz, K., Wickenhauser, C., Kudin, A.P., Kunz, W.S., Wiesner, R.J., and Schauen, M. (2007). Human epidermal keratinocytes accumulate superoxide due to low activity of Mn-SOD, leading to mitochondrial functional impairment. J Invest Dermatol *127*, 1084-1093.

42. Gomes, A., Fernandes, E., and Lima, J.L. (2005). Fluorescence probes used for detection of reactive oxygen species. J Biochem Biophys Methods *65*, 45-80.

43. Varani, J., Bhagavathula, N., Nerusu, K.C., Sherzer, H., Fay, K., Boitano, A.E., Glick, G.D., Johnson, K., Kang, S., and Opipari, A.W., Jr. (2005). A novel benzodiazepine selectively inhibits keratinocyte proliferation and reduces retinoid-induced epidermal hyperplasia in organ-cultured human skin. J Pharmacol Exp Ther *313*, 56-63.

44. Elder, J.T., Fisher, G.J., Lindquist, P.B., Bennett, G.L., Pittelkow, M.R., Coffey, R.J., Jr., Ellingsworth, L., Derynck, R., and Voorhees, J.J. (1989). Overexpression of transforming growth factor alpha in psoriatic epidermis. Science *243*, 811-814.

45. Gottlieb, A.B., Chang, C.K., Posnett, D.N., Fanelli, B., and Tam, J.P. (1988). Detection of transforming growth factor alpha in normal, malignant, and hyperproliferative human keratinocytes. J Exp Med *167*, 670-675.

46. Bhagavathula, N., Nerusu, K.C., Hanosh, A., Aslam, M.N., Sundberg, T.B., Opipari, A.W., Jr., Johnson, K., Kang, S., Glick, G.D., and Varani, J. (2008). 7-Chloro-5-(4-hydroxyphenyl)-1-methyl-3-(naphthalen-2-ylmethyl)-4,5-dihydr o-1H-benzo[b][1,4]diazepin-2(3H)-one (Bz-423), a benzodiazepine, suppresses keratinocyte proliferation and has antipsoriatic activity in the human skin-severe, combined immunodeficient mouse transplant model. J Pharmacol Exp Ther *324*, 938-947.

47. van den Heuvel, S., and Dyson, N.J. (2008). Conserved functions of the pRB and E2F families. Nat Rev Mol Cell Biol *9*, 713-724.

48. Murray, A.W. (2004). Recycling the cell cycle: cyclins revisited. Cell *116*, 221-234.

49. Cobrinik, D. (2005). Pocket proteins and cell cycle control. Oncogene *24*, 2796-2809.

50. Vidal, A., and Koff, A. (2000). Cell-cycle inhibitors: three families united by a common cause. Gene *247*, 1-15.

51. Sherr, C.J., and Roberts, J.M. (1999). CDK inhibitors: positive and negative regulators of G1-phase progression. Genes Dev *13*, 1501-1512.

52. Dai, Y., and Grant, S. (2003). Cyclin-dependent kinase inhibitors. Curr Opin Pharmacol *3*, 362-370.

53. Komata, T., Kanzawa, T., Takeuchi, H., Germano, I.M., Schreiber, M., Kondo, Y., and Kondo, S. (2003). Antitumour effect of cyclin-dependent kinase inhibitors (p16(INK4A), p18(INK4C), p19(INK4D), p21(WAF1/CIP1) and p27(KIP1)) on malignant glioma cells. Br J Cancer *88*, 1277-1280.

54. Tashiro, E., Tsuchiya, A., and Imoto, M. (2007). Functions of cyclin D1 as an oncogene and regulation of cyclin D1 expression. Cancer Sci *98*, 629-635.

55. Tashiro, E., Maruki, H., Minato, Y., Doki, Y., Weinstein, I.B., and Imoto, M. (2003). Overexpression of cyclin D1 contributes to malignancy by up-regulation of fibroblast growth factor receptor 1 via the pRB/E2F pathway. Cancer Res *63*, 424-431.

56. McInnes, C. (2008). Progress in the evaluation of CDK inhibitors as anti-tumor agents. Drug Discov Today.

57. Nigg, E.A. (1995). Cyclin-dependent protein kinases: key regulators of the eukaryotic cell cycle. Bioessays *17*, 471-480.

58. Garner, E., and Raj, K. (2008). Protective mechanisms of p53-p21-pRb proteins against DNA damage-induced cell death. Cell Cycle *7*, 277-282.

59. Allday, M.J., Inman, G.J., Crawford, D.H., and Farrell, P.J. (1995). DNA damage in human B cells can induce apoptosis, proceeding from G1/S when p53 is transactivation competent and G2/M when it is transactivation defective. Embo J *14*, 4994-5005.

60. Orian, A., and Eisenman, R.N. (2001). TGF-beta flips the Myc switch. Sci STKE *2001*, PE1.

61. Bister, K., and Jansen, H.W. (1986). Oncogenes in retroviruses and cells: biochemistry and molecular genetics. Adv Cancer Res *47*, 99-188.

62. Adhikary, S., and Eilers, M. (2005). Transcriptional regulation and transformation by Myc proteins. Nat Rev Mol Cell Biol *6*, 635-645.

63. Boxer, L.M., and Dang, C.V. (2001). Translocations involving c-myc and c-myc function. Oncogene *20*, 5595-5610.

64. Nesbit, C.E., Tersak, J.M., and Prochownik, E.V. (1999). MYC oncogenes and human neoplastic disease. Oncogene *18*, 3004-3016.

65. Battey, J., Moulding, C., Taub, R., Murphy, W., Stewart, T., Potter, H., Lenoir, G., and Leder, P. (1983). The human c-myc oncogene: structural consequences of translocation into the IgH locus in Burkitt lymphoma. Cell *34*, 779-787.

66. Ding, J., Zhang, R., Li, J., Xue, C., and Huang, C. (2006). Involvement of nuclear factor of activated T cells 3 (NFAT3) in cyclin D1 induction by B[a]PDE or B[a]PDE and ionizing radiation in mouse epidermal Cl 41 cells. Mol Cell Biochem *287*, 117-125.

67. Feng, B., Cheng, S., Hsia, C.Y., King, L.B., Monroe, J.G., and Liou, H.C. (2004). NF-kappaB inducible genes BCL-X and cyclin E promote immature B-cell proliferation and survival. Cell Immunol *232*, 9-20.

68. Grumont, R.J., Rourke, I.J., O'Reilly, L.A., Strasser, A., Miyake, K., Sha, W., and Gerondakis, S. (1998). B lymphocytes differentially use the Rel and nuclear factor kappaB1 (NF-kappaB1) transcription factors to regulate cell cycle progression and apoptosis in quiescent and mitogen-activated cells. J Exp Med *187*, 663-674.

69. Martino, A., Holmes, J.H.t., Lord, J.D., Moon, J.J., and Nelson, B.H. (2001). Stat5 and Sp1 regulate transcription of the cyclin D2 gene in response to IL-2. J Immunol *166*, 1723-1729.

70. Kohl, N.E., and Ruley, H.E. (1987). Role of c-myc in the transformation of REF52 cells by viral and cellular oncogenes. Oncogene *2*, 41-48.

71. Land, H., Chen, A.C., Morgenstern, J.P., Parada, L.F., and Weinberg, R.A. (1986). Behavior of myc and ras oncogenes in transformation of rat embryo fibroblasts. Mol Cell Biol *6*, 1917-1925.

72. Mougneau, E., Lemieux, L., Rassoulzadegan, M., and Cuzin, F. (1984). Biological activities of v-myc and rearranged c-myc oncogenes in rat fibroblast cells in culture. Proc Natl Acad Sci U S A *81*, 5758-5762.

73. Mateyak, M.K., Obaya, A.J., Adachi, S., and Sedivy, J.M. (1997). Phenotypes of c-Myc-deficient rat fibroblasts isolated by targeted homologous recombination. Cell Growth Differ *8*, 1039-1048.

74. Schorl, C., and Sedivy, J.M. (2003). Loss of protooncogene c-Myc function impedes G1 phase progression both before and after the restriction point. Mol Biol Cell *14*, 823-835.

75. Pelengaris, S., Khan, M., and Evan, G. (2002). c-MYC: more than just a matter of life and death. Nat Rev Cancer *2*, 764-776.

76. Pelengaris, S., and Khan, M. (2003). The many faces of c-MYC. Arch Biochem Biophys *416*, 129-136.

77. Lindsten, T., June, C.H., and Thompson, C.B. (1988). Multiple mechanisms regulate c-myc gene expression during normal T cell activation. Embo J *7*, 2787-2794.

78. Huang, C.Y., Bredemeyer, A.L., Walker, L.M., Bassing, C.H., and Sleckman, B.P. (2008). Dynamic regulation of c-Myc proto-oncogene expression during lymphocyte development revealed by a GFP-c-Myc knock-in mouse. Eur J Immunol *38*, 342-349.

79. Haggerty, T.J., Zeller, K.I., Osthus, R.C., Wonsey, D.R., and Dang, C.V. (2003). A strategy for identifying transcription factor binding sites reveals two classes of genomic c-Myc target sites. Proc Natl Acad Sci U S A *100*, 5313-5318.

80. Gartel, A.L., Ye, X., Goufman, E., Shianov, P., Hay, N., Najmabadi, F., and Tyner, A.L. (2001). Myc represses the p21(WAF1/CIP1) promoter and interacts with Sp1/Sp3. Proc Natl Acad Sci U S A *98*, 4510-4515.

81. Wanzel, M., Herold, S., and Eilers, M. (2003). Transcriptional repression by Myc. Trends Cell Biol *13*, 146-150.

82. Letterio, J.J. (2005). TGF-beta signaling in T cells: roles in lymphoid and epithelial neoplasia. Oncogene *24*, 5701-5712.

83. Schwartz, D., and Rotter, V. (1998). p53-dependent cell cycle control: response to genotoxic stress. Semin Cancer Biol *8*, 325-336.

84. Fehske, K.J., Muller, W.E., and Wollert, U. (1981). The location of drug binding sites in human serum albumin. Biochem Pharmacol *30*, 687-692.

85. Becker, M., Newman, S., and Ismail-Beigi, F. (1996). Stimulation of GLUT1 glucose transporter expression in response to inhibition of oxidative phosphorylation: role of reduced sulfhydryl groups. Mol Cell Endocrinol *121*, 165-170.

86. Hamrahian, A.H., Zhang, J.Z., Elkhairi, F.S., Prasad, R., and Ismail-Beigi, F. (1999). Activation of Glut1 glucose transporter in response to inhibition of oxidative phosphorylation. Arch Biochem Biophys *368*, 375-379.

87. Matheson, B.K., Adams, J.L., Zou, J., Patel, R., and Franklin, R.B. (2007). Effect of metabolic inhibitors on ATP and citrate content in PC3 prostate cancer cells. Prostate *67*, 1211-1218.

88. Fox, C.J., Hammerman, P.S., and Thompson, C.B. (2005). Fuel feeds function: energy metabolism and the T-cell response. Nat Rev Immunol *5*, 844-852.

89. Coffino, P. (2001). Regulation of cellular polyamines by antizyme. Nat Rev Mol Cell Biol *2*, 188-194.

90. Thomas, T., and Thomas, T.J. (2001). Polyamines in cell growth and cell death: molecular mechanisms and therapeutic applications. Cell Mol Life Sci *58*, 244-258.

91. Jun, J.Y., Griffith, J.W., Bruggeman, R., Washington, S., Demers, L.M., Verderame, M.F., and Manni, A. (2007). Effects of polyamine depletion by alpha-difluoromethylornithine on in vitro and in vivo biological properties of 4T1 murine mammary cancer cells. Breast Cancer Res Treat *105*, 29-36.

92. Nitta, T., Igarashi, K., and Yamamoto, N. (2002). Polyamine depletion induces apoptosis through mitochondria-mediated pathway. Exp Cell Res *276*, 120-128.

93. Wallace, H.M. (2007). Targeting polyamine metabolism: a viable therapeutic/preventative solution for cancer? Expert Opin Pharmacother *8*, 2109-2116.

94. Qu, N., Ignatenko, N.A., Yamauchi, P., Stringer, D.E., Levenson, C., Shannon, P., Perrin, S., and Gerner, E.W. (2003). Inhibition of human ornithine decarboxylase activity by enantiomers of difluoromethylornithine. Biochem J *375*, 465-470.

95. Bello-Fernandez, C., Packham, G., and Cleveland, J.L. (1993). The ornithine decarboxylase gene is a transcriptional target of c-Myc. Proc Natl Acad Sci U S A *90*, 7804-7808.

96. Pegg, A.E. (2006). Regulation of ornithine decarboxylase. J Biol Chem *281*, 14529-14532.

97. Boitano, A.E. (2005). Mechanisms of a pro-apoptotic benzodiazepine, University of Michigan, Ann Arbor.

98. Dang, C.V. (1999). c-Myc target genes involved in cell growth, apoptosis, and metabolism. Mol Cell Biol *19*, 1-11.

99. Fernandez, P.C., Frank, S.R., Wang, L., Schroeder, M., Liu, S., Greene, J., Cocito, A., and Amati, B. (2003). Genomic targets of the human c-Myc protein. Genes Dev *17*, 1115-1129.

100. Ellenrieder, V. (2008). TGFbetaregulated gene expression by Smads and Sp1/KLF-like transcription factors in cancer. Anticancer Res *28*, 1531-1539.

101. Narla, G., Kremer-Tal, S., Matsumoto, N., Zhao, X., Yao, S., Kelley, K., Tarocchi, M., and Friedman, S.L. (2007). In vivo regulation of p21 by the Kruppel-like factor 6 tumor-suppressor gene in mouse liver and human hepatocellular carcinoma. Oncogene *26*, 4428-4434.

102. Wu, J., and Lingrel, J.B. (2004). KLF2 inhibits Jurkat T leukemia cell growth via upregulation of cyclin-dependent kinase inhibitor p21WAF1/CIP1. Oncogene *23*, 8088-8096.

103. Yu, Q., Ciemerych, M.A., and Sicinski, P. (2005). Ras and Myc can drive oncogenic cell proliferation through individual D-cyclins. Oncogene *24*, 7114-7119.

104. Banerji, L., Glassford, J., Lea, N.C., Thomas, N.S., Klaus, G.G., and Lam, E.W. (2001). BCR signals target p27(Kip1) and cyclin D2 via the PI3-K signalling pathway to mediate cell cycle arrest and apoptosis of WEHI 231 B cells. Oncogene *20*, 7352-7367.

105. Zarkowska, T., and Mittnacht, S. (1997). Differential phosphorylation of the retinoblastoma protein by G1/S cyclin-dependent kinases. J Biol Chem *272*, 12738-12746.

106. Rowell, E.A., and Wells, A.D. (2006). The role of cyclin-dependent kinases in T-cell development, proliferation, and function. Crit Rev Immunol *26*, 189-212.

107. Luscher, B. (2001). Function and regulation of the transcription factors of the Myc/Max/Mad network. Gene *277*, 1-14.

108. Reed, J.C., Nowell, P.C., and Hoover, R.G. (1985). Regulation of c-myc mRNA levels in normal human lymphocytes by modulators of cell proliferation. Proc Natl Acad Sci U S A *82*, 4221-4224.

109. Schneider, E.E., Albert, T., Wolf, D.A., and Eick, D. (1999). Regulation of c-myc and immunoglobulin kappa gene transcription by promoter-proximal pausing of RNA polymerase II. Curr Top Microbiol Immunol *246*, 225-231.

110. Gregory, M.A., Qi, Y., and Hann, S.R. (2003). Phosphorylation by glycogen synthase kinase-3 controls c-myc proteolysis and subnuclear localization. J Biol Chem *278*, 51606-51612.

111. Sears, R., Nuckolls, F., Haura, E., Taya, Y., Tamai, K., and Nevins, J.R. (2000). Multiple Ras-dependent phosphorylation pathways regulate Myc protein stability. Genes Dev *14*, 2501-2514.

112. Welcker, M., Orian, A., Grim, J.E., Eisenman, R.N., and Clurman, B.E. (2004). A nucleolar isoform of the Fbw7 ubiquitin ligase regulates c-Myc and cell size. Curr Biol *14*, 1852-1857.

113. Welcker, M., Orian, A., Jin, J., Grim, J.E., Harper, J.W., Eisenman, R.N., and Clurman, B.E. (2004). The Fbw7 tumor suppressor regulates glycogen synthase kinase 3 phosphorylation-dependent c-Myc protein degradation. Proc Natl Acad Sci U S A *101*, 9085-9090.

114. Yada, M., Hatakeyama, S., Kamura, T., Nishiyama, M., Tsunematsu, R., Imaki, H., Ishida, N., Okumura, F., Nakayama, K., and Nakayama, K.I. (2004). Phosphorylation-dependent degradation of c-Myc is mediated by the F-box protein Fbw7. Embo J *23*, 2116-2125.

115. Yeh, E., Cunningham, M., Arnold, H., Chasse, D., Monteith, T., Ivaldi, G., Hahn, W.C., Stukenberg, P.T., Shenolikar, S., Uchida, T., Counter, C.M., Nevins, J.R., Means, A.R., and Sears, R. (2004). A signalling pathway controlling c-Myc degradation that impacts oncogenic transformation of human cells. Nat Cell Biol *6*, 308-318.

116. Rajkumar, S.V., Richardson, P.G., Hideshima, T., and Anderson, K.C. (2005). Proteasome inhibition as a novel therapeutic target in human cancer. J Clin Oncol *23*, 630-639.

117. Fernandez, Y., Miller, T.P., Denoyelle, C., Esteban, J.A., Tang, W.H., Bengston, A.L., and Soengas, M.S. (2006). Chemical blockage of the proteasome inhibitory function of bortezomib: impact on tumor cell death. J Biol Chem *281*, 1107-1118.

118. Boitano, A.E. (2005). Mechanisms of a Pro-apoptotic Benzodiazepine. University of Michigan, Ann Arbor.

119. Chandramohan, V., Jeay, S., Pianetti, S., and Sonenshein, G.E. (2004). Reciprocal control of Forkhead box O 3a and c-Myc via the phosphatidylinositol 3-kinase pathway coordinately regulates p27Kip1 levels. J Immunol *172*, 5522-5527.

120. Coghlan, M.P., Culbert, A.A., Cross, D.A., Corcoran, S.L., Yates, J.W., Pearce, N.J., Rausch, O.L., Murphy, G.J., Carter, P.S., Roxbee Cox, L., Mills, D., Brown, M.J., Haigh, D., Ward, R.W., Smith, D.G., Murray, K.J., Reith, A.D., and Holder, J.C. (2000). Selective small molecule inhibitors of glycogen synthase kinase-3 modulate glycogen metabolism and gene transcription. Chem Biol *7*, 793-803.

121. Bartholomeusz, G., Talpaz, M., Bornmann, W., Kong, L.Y., and Donato, N.J. (2007). Degrasyn activates proteasomal-dependent degradation of c-Myc. Cancer Res *67*, 3912-3918.

122. Ang, X.L., and Wade Harper, J. (2005). SCF-mediated protein degradation and cell cycle control. Oncogene *24*, 2860-2870.

123. Cardozo, T., and Pagano, M. (2004). The SCF ubiquitin ligase: insights into a molecular machine. Nat Rev Mol Cell Biol *5*, 739-751.

124. Jahngen-Hodge, J., Obin, M.S., Gong, X., Shang, F., Nowell, T.R., Jr., Gong, J., Abasi, H., Blumberg, J., and Taylor, A. (1997). Regulation of ubiquitin-conjugating enzymes by glutathione following oxidative stress. J Biol Chem *272*, 28218-28226.

125. Li, Y.P., Chen, Y., Li, A.S., and Reid, M.B. (2003). Hydrogen peroxide stimulates ubiquitin-conjugating activity and expression of genes for specific E2 and E3 proteins in skeletal muscle myotubes. Am J Physiol Cell Physiol *285*, C806-812.

126. Hwang, C.Y., Kim, I.Y., and Kwon, K.S. (2007). Cytoplasmic localization and ubiquitination of p21(Cip1) by reactive oxygen species. Biochem Biophys Res Commun *358*, 219-225.

127. Luu, H.H., Zhang, R., Haydon, R.C., Rayburn, E., Kang, Q., Si, W., Park, J.K., Wang, H., Peng, Y., Jiang, W., and He, T.C. (2004). Wnt/beta-catenin signaling pathway as a novel cancer drug target. Curr Cancer Drug Targets *4*, 653-671.

128. Prestwich, T.C., and Macdougald, O.A. (2007). Wnt/beta-catenin signaling in adipogenesis and metabolism. Curr Opin Cell Biol *19*, 612-617.

129. Nakayama, K.I., and Nakayama, K. (2006). Ubiquitin ligases: cell-cycle control and cancer. Nat Rev Cancer *6*, 369-381.

130. Pelicano, H., Feng, L., Zhou, Y., Carew, J.S., Hileman, E.O., Plunkett, W., Keating, M.J., and Huang, P. (2003). Inhibition of mitochondrial respiration: a novel strategy to enhance drug-induced apoptosis in human leukemia cells by a reactive oxygen species-mediated mechanism. J Biol Chem *278*, 37832-37839.

131. Zheng, Y., Shi, Y., Tian, C., Jiang, C., Jin, H., Chen, J., Almasan, A., Tang, H., and Chen, Q. (2004). Essential role of the voltage-dependent anion channel (VDAC) in mitochondrial permeability transition pore opening and cytochrome c release induced by arsenic trioxide. Oncogene *23*, 1239-1247.

132. Alessi, F., Quarta, S., Savio, M., Riva, F., Rossi, L., Stivala, L.A., Scovassi, A.I., Meijer, L., and Prosperi, E. (1998). The cyclin-dependent kinase inhibitors olomoucine and roscovitine arrest human fibroblasts in G1 phase by specific inhibition of CDK2 kinase activity. Exp Cell Res *245*, 8-18.

133. Hershko, A., Ciechanover, A., and Varshavsky, A. (2000). Basic Medical Research Award. The ubiquitin system. Nat Med *6*, 1073-1081.

134. Pickart, C.M. (2004). Back to the future with ubiquitin. Cell *116*, 181-190.

135. Welcker, M., and Clurman, B.E. (2008). FBW7 ubiquitin ligase: a tumour suppressor at the crossroads of cell division, growth and differentiation. Nat Rev Cancer *8*, 83-93.

136. Zheng, Y., Zha, Y., and Gajewski, T.F. (2008). Molecular regulation of T-cell anergy. EMBO Rep *9*, 50-55.

137. Amati, B. (2004). Myc degradation: dancing with ubiquitin ligases. Proc Natl Acad Sci U S A *101*, 8843-8844.

138. Kim, S.Y., Herbst, A., Tworkowski, K.A., Salghetti, S.E., and Tansey, W.P. (2003). Skp2 regulates Myc protein stability and activity. Mol Cell *11*, 1177-1188.

139. von der Lehr, N., Johansson, S., Wu, S., Bahram, F., Castell, A., Cetinkaya, C., Hydbring, P., Weidung, I., Nakayama, K., Nakayama, K.I., Soderberg, O., Kerppola, T.K., and Larsson, L.G. (2003). The F-box protein Skp2 participates in c-Myc proteosomal degradation and acts as a cofactor for c-Myc-regulated transcription. Mol Cell *11*, 1189-1200.

140. Carrano, A.C., Eytan, E., Hershko, A., and Pagano, M. (1999). SKP2 is required for ubiquitin-mediated degradation of the CDK inhibitor p27. Nat Cell Biol *1*, 193-199.

141. Yu, Z.K., Gervais, J.L., and Zhang, H. (1998). Human CUL-1 associates with the SKP1/SKP2 complex and regulates p21(CIP1/WAF1) and cyclin D proteins. Proc Natl Acad Sci U S A *95*, 11324-11329.

142. Vervoorts, J., Luscher-Firzlaff, J., and Luscher, B. (2006). The ins and outs of MYC regulation by posttranslational mechanisms. J Biol Chem *281*, 34725-34729.

143. Muratani, M., and Tansey, W.P. (2003). How the ubiquitin-proteasome system controls transcription. Nat Rev Mol Cell Biol *4*, 192-201.

144. Luscher, B., and Eisenman, R.N. (1992). Mitosis-specific phosphorylation of the nuclear oncoproteins Myc and Myb. J Cell Biol *118*, 775-784.

145. Lutterbach, B., and Hann, S.R. (1994). Hierarchical phosphorylation at N-terminal transformation-sensitive sites in c-Myc protein is regulated by mitogens and in mitosis. Mol Cell Biol *14*, 5510-5522.

146. Noguchi, K., Kitanaka, C., Yamana, H., Kokubu, A., Mochizuki, T., and Kuchino, Y. (1999). Regulation of c-Myc through phosphorylation at Ser-62 and Ser-71 by c-Jun N-terminal kinase. J Biol Chem *274*, 32580-32587.

147. Hennessy, B.T., Smith, D.L., Ram, P.T., Lu, Y., and Mills, G.B. (2005). Exploiting the PI3K/AKT pathway for cancer drug discovery. Nat Rev Drug Discov *4*, 988-1004.

148. Herbst, A., and Kolligs, F.T. (2007). Wnt signaling as a therapeutic target for cancer. Methods Mol Biol *361*, 63-91.

149. Nakayama, K., Hatakeyama, S., Maruyama, S., Kikuchi, A., Onoe, K., Good, R.A., and Nakayama, K.I. (2003). Impaired degradation of inhibitory subunit of NF-kappa B (I kappa B) and beta-catenin as a result of targeted disruption of the beta-TrCP1 gene. Proc Natl Acad Sci U S A *100*, 8752-8757.

150. Britton, S., Salles, B., and Calsou, P. (2008). c-MYC protein is degraded in response to UV irradiation. Cell Cycle *7*, 63-70.

151. Popov, N., Herold, S., Llamazares, M., Schulein, C., and Eilers, M. (2007). Fbw7 and Usp28 regulate myc protein stability in response to DNA damage. Cell Cycle *6*, 2327-2331.

152. Adhikary, S., Marinoni, F., Hock, A., Hulleman, E., Popov, N., Beier, R., Bernard, S., Quarto, M., Capra, M., Goettig, S., Kogel, U., Scheffner, M., Helin, K., and Eilers, M. (2005). The ubiquitin ligase HectH9 regulates transcriptional activation by Myc and is essential for tumor cell proliferation. Cell *123*, 409-421.

153. Vervoorts, J., Luscher-Firzlaff, J.M., Rottmann, S., Lilischkis, R., Walsemann, G., Dohmann, K., Austen, M., and Luscher, B. (2003). Stimulation of c-MYC transcriptional activity and acetylation by recruitment of the cofactor CBP. EMBO Rep *4*, 484-490.

154. Hann, S.R. (2006). Role of post-translational modifications in regulating c-Myc proteolysis, transcriptional activity and biological function. Semin Cancer Biol *16*, 288-302.

155. Hui, A.B., Lo, K.W., Yin, X.L., Poon, W.S., and Ng, H.K. (2001). Detection of multiple gene amplifications in glioblastoma multiforme using array-based comparative genomic hybridization. Lab Invest *81*, 717-723.

156. Baker, V.V., Borst, M.P., Dixon, D., Hatch, K.D., Shingleton, H.M., and Miller, D. (1990). c-myc amplification in ovarian cancer. Gynecol Oncol *38*, 340-342.

157. Bubendorf, L., Kononen, J., Koivisto, P., Schraml, P., Moch, H., Gasser, T.C., Willi, N., Mihatsch, M.J., Sauter, G., and Kallioniemi, O.P. (1999). Survey of gene amplifications during prostate cancer progression by high-throughout fluorescence in situ hybridization on tissue microarrays. Cancer Res *59*, 803-806.

158. Escot, C., Theillet, C., Lidereau, R., Spyratos, F., Champeme, M.H., Gest, J., and Callahan, R. (1986). Genetic alteration of the c-myc protooncogene (MYC) in human primary breast carcinomas. Proc Natl Acad Sci U S A *83*, 4834-4838.

159. Park, K., Kwak, K., Kim, J., Lim, S., and Han, S. (2005). c-myc amplification is associated with HER2 amplification and closely linked with cell proliferation in tissue microarray of nonselected breast cancers. Hum Pathol *36*, 634-639.

160. Pelengaris, S., Khan, M., and Evan, G.I. (2002). Suppression of Myc-induced apoptosis in beta cells exposes multiple oncogenic properties of Myc and triggers carcinogenic progression. Cell *109*, 321-334.

161. Jain, M., Arvanitis, C., Chu, K., Dewey, W., Leonhardt, E., Trinh, M., Sundberg, C.D., Bishop, J.M., and Felsher, D.W. (2002). Sustained loss of a neoplastic phenotype by brief inactivation of MYC. Science *297*, 102-104.

162. Prochownik, E.V. (2004). c-Myc as a therapeutic target in cancer. Expert Rev Anticancer Ther *4*, 289-302.

163. Vita, M., and Henriksson, M. (2006). The Myc oncoprotein as a therapeutic target for human cancer. Semin Cancer Biol *16*, 318-330.

164. Huang, Y., Snyder, R., Kligshteyn, M., and Wickstrom, E. (1995). Prevention of tumor formation in a mouse model of Burkitt's lymphoma by 6 weeks of treatment with anti-c-myc DNA phosphorothioate. Mol Med *1*, 647-658.

165. Smith, J.B., and Wickstrom, E. (1998). Antisense c-myc and immunostimulatory oligonucleotide inhibition of tumorigenesis in a murine B-cell lymphoma transplant model. J Natl Cancer Inst *90*, 1146-1154.

166. Carroll, J.S., Swarbrick, A., Musgrove, E.A., and Sutherland, R.L. (2002). Mechanisms of growth arrest by c-myc antisense oligonucleotides in MCF-7 breast cancer cells: implications for the antiproliferative effects of antiestrogens. Cancer Res *62*, 3126-3131.

167. Leonetti, C., Biroccio, A., Candiloro, A., Citro, G., Fornari, C., Mottolese, M., Del Bufalo, D., and Zupi, G. (1999). Increase of cisplatin sensitivity by c-myc antisense oligodeoxynucleotides in a human metastatic melanoma inherently resistant to cisplatin. Clin Cancer Res *5*, 2588-2595.

168. Weiss, W.A., Aldape, K., Mohapatra, G., Feuerstein, B.G., and Bishop, J.M. (1997). Targeted expression of MYCN causes neuroblastoma in transgenic mice. Embo J *16*, 2985-2995.

169. Citro, G., D'Agnano, I., Leonetti, C., Perini, R., Bucci, B., Zon, G., Calabretta, B., and Zupi, G. (1998). c-myc antisense oligodeoxynucleotides enhance the efficacy of cisplatin in melanoma chemotherapy in vitro and in nude mice. Cancer Res *58*, 283-289.

170. Pooga, M., Land, T., Bartfai, T., and Langel, U. (2001). PNA oligomers as tools for specific modulation of gene expression. Biomol Eng *17*, 183-192.

171. Cutrona, G., Carpaneto, E.M., Ulivi, M., Roncella, S., Landt, O., Ferrarini, M., and Boffa, L.C. (2000). Effects in live cells of a c-myc anti-gene PNA linked to a nuclear localization signal. Nat Biotechnol *18*, 300-303.

172. Boffa, L.C., Cutrona, G., Cilli, M., Mariani, M.R., Matis, S., Pastorino, M., Damonte, G., Millo, E., Roncella, S., and Ferrarini, M. (2005). Therapeutically promising PNA complementary to a regulatory sequence for c-myc: pharmacokinetics in an animal model of human Burkitt's lymphoma. Oligonucleotides *15*, 85-93.

173. Li, C.M., Margolin, A.A., Salas, M., Memeo, L., Mansukhani, M., Hibshoosh, H., Szabolcs, M., Klinakis, A., and Tycko, B. (2006). PEG10 is a c-MYC target gene in cancer cells. Cancer Res *66*, 665-672.

174. Guney, I., Wu, S., and Sedivy, J.M. (2006). Reduced c-Myc signaling triggers telomere-independent senescence by regulating Bmi-1 and p16(INK4a). Proc Natl Acad Sci U S A *103*, 3645-3650.

175. Mukherjee, S., and Conrad, S.E. (2005). c-Myc suppresses p21WAF1/CIP1 expression during estrogen signaling and antiestrogen resistance in human breast cancer cells. J Biol Chem *280*, 17617-17625.

176. Arabi, A., Wu, S., Ridderstrale, K., Bierhoff, H., Shiue, C., Fatyol, K., Fahlen, S., Hydbring, P., Soderberg, O., Grummt, I., Larsson, L.G., and Wright, A.P. (2005). c-Myc associates with ribosomal DNA and activates RNA polymerase I transcription. Nat Cell Biol *7*, 303-310.

177. Wang, Y.H., Liu, S., Zhang, G., Zhou, C.Q., Zhu, H.X., Zhou, X.B., Quan, L.P., Bai, J.F., and Xu, N.Z. (2005). Knockdown of c-Myc expression by RNAi inhibits MCF-7 breast tumor cells growth in vitro and in vivo. Breast Cancer Res *7*, R220-228.

178. Opalinska, J.B., Kalota, A., Chattopadhyaya, J., Damha, M., and Gewirtz, A.M. (2006). Nucleic acid therapeutics for hematologic malignancies--theoretical considerations. Ann N Y Acad Sci *1082*, 124-136.

179. Iversen, P.L., Arora, V., Acker, A.J., Mason, D.H., and Devi, G.R. (2003). Efficacy of antisense morpholino oligomer targeted to c-myc in prostate cancer xenograft murine model and a Phase I safety study in humans. Clin Cancer Res *9*, 2510-2519.

180. Berg, T., Cohen, S.B., Desharnais, J., Sonderegger, C., Maslyar, D.J., Goldberg, J., Boger, D.L., and Vogt, P.K. (2002). Small-molecule antagonists of Myc/Max dimerization inhibit Myc-induced transformation of chicken embryo fibroblasts. Proc Natl Acad Sci U S A *99*, 3830-3835.

181. Yin, X., Giap, C., Lazo, J.S., and Prochownik, E.V. (2003). Low molecular weight inhibitors of Myc-Max interaction and function. Oncogene *22*, 6151-6159.

182. Lu, X., Pearson, A., and Lunec, J. (2003). The MYCN oncoprotein as a drug development target. Cancer Lett *197*, 125-130.

183. Mo, H., and Henriksson, M. (2006). Identification of small molecules that induce apoptosis in a Myc-dependent manner and inhibit Myc-driven transformation. Proc Natl Acad Sci U S A *103*, 6344-6349.

184. Nikiforov, M.A., Riblett, M., Tang, W.H., Gratchouck, V., Zhuang, D., Fernandez, Y., Verhaegen, M., Varambally, S., Chinnaiyan, A.M., Jakubowiak, A.J., and Soengas, M.S. (2007). Tumor cell-selective regulation of NOXA by c-MYC in response to proteasome inhibition. Proc Natl Acad Sci U S A *104*, 19488-19493.

185. Hatakeyama, S., Watanabe, M., Fujii, Y., and Nakayama, K.I. (2005). Targeted destruction of c-Myc by an engineered ubiquitin ligase suppresses cell transformation and tumor formation. Cancer Res *65*, 7874-7879.

186. Bartholomeusz, G.A., Talpaz, M., Kapuria, V., Kong, L.Y., Wang, S., Estrov, Z., Priebe, W., Wu, J., and Donato, N.J. (2007). Activation of a novel Bcr/Abl destruction pathway by WP1130 induces apoptosis of chronic myelogenous leukemia cells. Blood *109*, 3470-3478.

187. Krammer, P.H., Arnold, R., and Lavrik, I.N. (2007). Life and death in peripheral T cells. Nat Rev Immunol *7*, 532-542.

188. Murphy, K.M., and Reiner, S.L. (2002). The lineage decisions of helper T cells. Nat Rev Immunol *2*, 933-944.

189. Serfling, E., Klein-Hessling, S., Palmetshofer, A., Bopp, T., Stassen, M., and Schmitt, E. (2006). NFAT transcription factors in control of peripheral T cell tolerance. Eur J Immunol *36*, 2837-2843.

190. Choi, S., and Schwartz, R.H. (2007). Molecular mechanisms for adaptive tolerance and other T cell anergy models. Semin Immunol *19*, 140-152.

191. Powell, J.D. (2006). The induction and maintenance of T cell anergy. Clin Immunol *120*, 239-246.

192. Gimmi, C.D., Freeman, G.J., Gribben, J.G., Gray, G., and Nadler, L.M. (1993). Human T-cell clonal anergy is induced by antigen presentation in the absence of B7 costimulation. Proc Natl Acad Sci U S A *90*, 6586-6590.

193. Linsley, P.S., Brady, W., Grosmaire, L., Aruffo, A., Damle, N.K., and Ledbetter, J.A. (1991). Binding of the B cell activation antigen B7 to CD28 costimulates T

cell proliferation and interleukin 2 mRNA accumulation. J Exp Med *173*, 721-730.

194. Matzinger, P. (2002). The danger model: a renewed sense of self. Science *296*, 301-305.

195. Anderson, C.C., and Chan, W.F. (2004). Mechanisms and models of peripheral CD4 T cell self-tolerance. Front Biosci *9*, 2947-2963.

196. Parish, I.A., and Heath, W.R. (2008). Too dangerous to ignore: self-tolerance and the control of ignorant autoreactive T cells. Immunol Cell Biol *86*, 146-152.

197. Wells, A.D. (2007). Cyclin-dependent kinases: molecular switches controlling anergy and potential therapeutic targets for tolerance. Semin Immunol *19*, 173-179.

198. Wells, A.D., Gudmundsdottir, H., and Turka, L.A. (1997). Following the fate of individual T cells throughout activation and clonal expansion. Signals from T cell receptor and CD28 differentially regulate the induction and duration of a proliferative response. J Clin Invest *100*, 3173-3183.

199. Wells, A.D., Walsh, M.C., Sankaran, D., and Turka, L.A. (2000). T cell effector function and anergy avoidance are quantitatively linked to cell division. J Immunol *165*, 2432-2443.

200. Jackson, S.K., DeLoose, A., and Gilbert, K.M. (2002). The ability of antigen, but not interleukin-2, to promote n-butyrate-induced T helper 1 cell anergy is associated with increased expression and altered association patterns of cyclin-dependent kinase inhibitors. Immunology *106*, 486-495.

201. Powell, J.D., Lerner, C.G., and Schwartz, R.H. (1999). Inhibition of cell cycle progression by rapamycin induces T cell clonal anergy even in the presence of costimulation. J Immunol *162*, 2775-2784.

202. Boussiotis, V.A., Freeman, G.J., Taylor, P.A., Berezovskaya, A., Grass, I., Blazar, B.R., and Nadler, L.M. (2000). p27kip1 functions as an anergy factor inhibiting interleukin 2 transcription and clonal expansion of alloreactive human and mouse helper T lymphocytes. Nat Med *6*, 290-297.

203. Li, L., Iwamoto, Y., Berezovskaya, A., and Boussiotis, V.A. (2006). A pathway regulated by cell cycle inhibitor p27Kip1 and checkpoint inhibitor Smad3 is involved in the induction of T cell tolerance. Nat Immunol *7*, 1157-1165.

204. Asai, K., Hachimura, S., Kimura, M., Toraya, T., Yamashita, M., Nakayama, T., and Kaminogawa, S. (2002). T cell hyporesponsiveness induced by oral administration of ovalbumin is associated with impaired NFAT nuclear translocation and p27kip1 degradation. J Immunol *169*, 4723-4731.

205. Jackson, S.K., DeLoose, A., and Gilbert, K.M. (2001). Induction of anergy in Th1 cells associated with increased levels of cyclin-dependent kinase inhibitors p21Cip1 and p27Kip1. J Immunol *166*, 952-958.

206. Kudo, H., Matsuoka, T., Mitsuya, H., Nishimura, Y., and Matsushita, S. (2002). Cross-linking HLA-DR molecules on Th1 cells induces anergy in association with increased level of cyclin-dependent kinase inhibitor p27(Kip1). Immunol Lett *81*, 149-155.

207. Nourse, J., Firpo, E., Flanagan, W.M., Coats, S., Polyak, K., Lee, M.H., Massague, J., Crabtree, G.R., and Roberts, J.M. (1994). Interleukin-2-mediated elimination of the p27Kip1 cyclin-dependent kinase inhibitor prevented by rapamycin. Nature *372*, 570-573.

208. Rowell, E.A., Walsh, M.C., and Wells, A.D. (2005). Opposing roles for the cyclin-dependent kinase inhibitor p27kip1 in the control of CD4+ T cell proliferation and effector function. J Immunol *174*, 3359-3368.

209. Larsen, C.P., Elwood, E.T., Alexander, D.Z., Ritchie, S.C., Hendrix, R., Tucker-Burden, C., Cho, H.R., Aruffo, A., Hollenbaugh, D., Linsley, P.S., Winn, K.J., and Pearson, T.C. (1996). Long-term acceptance of skin and cardiac allografts after blocking CD40 and CD28 pathways. Nature *381*, 434-438.

210. Rowell, E.A., Wang, L., Hancock, W.W., and Wells, A.D. (2006). The cyclin-dependent kinase inhibitor p27kip1 is required for transplantation tolerance induced by costimulatory blockade. J Immunol *177*, 5169-5176.

211. Goulvestre, C., Chereau, C., Nicco, C., Mouthon, L., Weill, B., and Batteux, F. (2005). A mimic of p21WAF1/CIP1 ameliorates murine lupus. J Immunol *175*, 6959-6967.

212. Zoja, C., Casiraghi, F., Conti, S., Corna, D., Rottoli, D., Cavinato, R.A., Remuzzi, G., and Benigni, A. (2007). Cyclin-dependent kinase inhibition limits glomerulonephritis and extends lifespan of mice with systemic lupus. Arthritis Rheum *56*, 1629-1637.

213. Sundberg, T.B., Ney, G.M., Subramanian, C., Opipari, A.W., Jr., and Glick, G.D. (2006). The immunomodulatory benzodiazepine Bz-423 inhibits B-cell proliferation by targeting c-myc protein for rapid and specific degradation. Cancer Res *66*, 1775-1782.

214. Bradford, M.M. (1976). A rapid and sensitive method for the quantitation of microgram quantities of protein utilizing the principle of protein-dye binding. Anal Biochem *72*, 248-254.

215. Voigt, W. (2005). Sulforhodamine B assay and chemosensitivity. Methods Mol Med *110*, 39-48.

216. Schenkel, E., Berlaimont, V., Dubois, J., Helson-Cambier, M., and Hanocq, M. (1995). Improved high-performance liquid chromatographic method for the determination of polyamines as their benzoylated derivatives: application to P388 cancer cells. J Chromatogr B Biomed Appl *668*, 189-197.

CHAPTER 3

MECHANISM OF T CELL APOPTOSIS INDUCED BY BZ-423

Introduction

Apoptotic signaling pathways: Apoptosis in vertebrates is mediated by the executioner caspases-3 and -7, which are activated by a complex series of steps initated either by ligation of cell-surface death receptors (extrinsic pathway) or release of apoptotic mediators from the mitochondria (intrinsic pathway) (Figure 3.1; [1]). Stimulation of cell-surface death receptors (e.g., Fas) by their cognate ligands leads to assembly of a death-inducing signaling complex (DISC) comprising the receptor, adaptor proteins (e.g., Fas-associated death-domain protein (FADD)), and the initiator pro-caspases-8 or -10 (Figure 3.1; [1]). DISC assembly promotes auto-activation of caspase-8 or -10, which then proteolytically process the executioner caspases-3 and -7 to their active forms [1]. In addition to Fas, the extrinsic pathway can be triggered by engagement of cell-surface death receptors for tumor necrosis factor (TNF) and TNF-related apoptosis-inducing ligand (TRAIL) [2, 3].

Caspase activation by the intrinsic pathway results from release of apoptogenic proteins from the mitochondrial inter-membrane space (MIS) (Figure 3.1; [4]). These

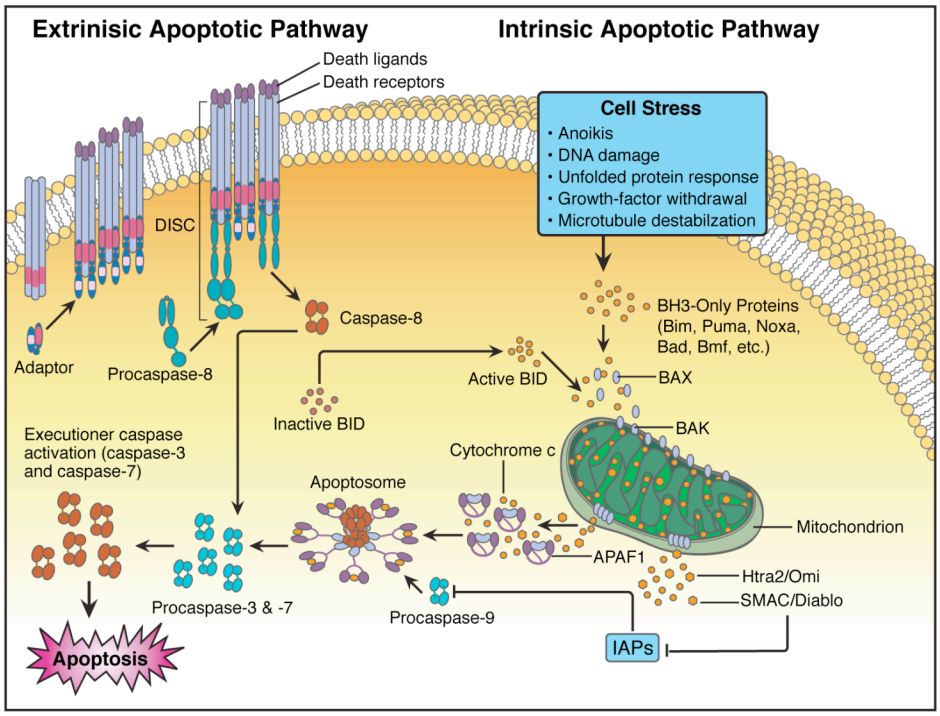

Figure 3.1 - Intrinsic and extrinsic apoptotic pathways. See text for details. Figure adapted from [5].

factors include several proteins that initiate or regulate caspase activation, including cytochrome *c*, Smac/DIABLO (second mitochondria-derived activator of caspase/direct inhibitor of apoptosis (IAP)-associated binding protein with low PI) and HtrA2/Omi [5]. After release from the MIS, cytochrome *c* engages the apoptosis protease activating factor-1 (Apaf-1), which in the presence of dATP, results in assembly of the apoptosome [1]. This complex provides a platform for binding of multiple copies of caspase-9, the initiator caspase of the intrinsic pathway, enabling their auto-activation [1]. Once activated, caspase-9 activates the executioner caspases-3 and -7. Inhibitor of apoptosis proteins (IAPs) suppress the intrinsic pathway by blocking the proteolytic activity of caspase-9 [6]. Smac/Diablo and HtrA2/Omi relieve this inhibition by binding to IAPs with higher affinity than active caspase-9 (Figure 3.1; [7]).

Along with proteins that activate caspases, apoptosis-inducing factor (AIF) and endonuclease G (EndoG), two proteins that induce chromosomal condensation and DNA fragmentation independent of caspase activation are released from the MIS [8, 9]. Once in the cytosol, both proteins translocate to the nucleus where they induce DNA double-strand breaks in 50 kbp increments [8, 9]. In addition, EndoG promotes breakdown of smaller DNA fragments by stimulating the exonuclease DNAse I [10]. These properties have led to speculation that AIF and EndoG may be capable of triggering caspase-independent cell death (CICD). However, studies in mouse embryonic fibroblasts (MEFs) or HeLa cervical carcinoma cells treated with the cytotoxic drugs, actinomycin D and staurosporine, demonstrated that release of AIF and EndoG depends on caspase activation [11, 12]. Thus, EndoG and AIF appear to be components of a DNA degradation pathway initiated as a result of caspase activation.

Release of pro-apoptotic MIS proteins via sustained opening of the mPT pore: Release of pro-apoptotic proteins from the MIS is a critical step in committing a cell to die. One mechanism by which this process can occur is sustained opening of the mitochondrial permeability transition (mPT) pore. The mPT pore is a multi-protein complex that spans the inner and outer mitochondrial membranes [13]. Proposed components of this complex include voltage-dependent anion channels (VDACs), adenine nucleotide translocator (ANT), Cyclophillin D (CypD), hexokinase (HK), creatine kinase (CK) and the peripheral benzodiazepine receptor (PBR) (Figure 3.2; [13]). The mPT pore can adopt several distinct states ranging from a closed conformation with limited permeability to an open conformation that allows passage of

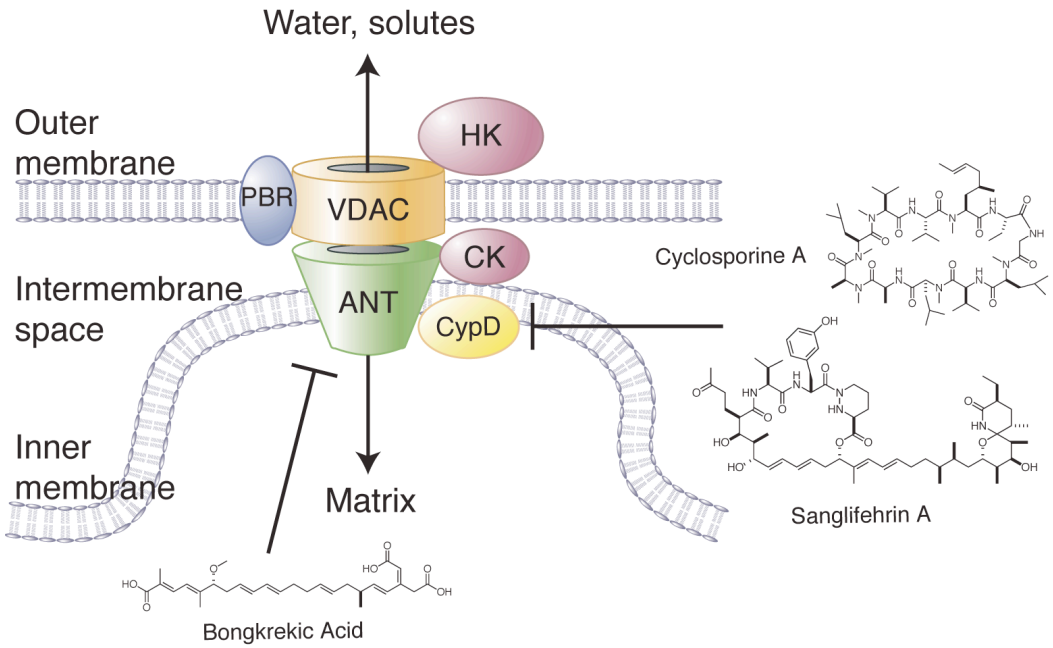

Figure 3.2 - Proposed components of the mitochondrial permeability transition (mPT) pore. Voltage-dependent anion channel (VDAC), adenine nucleotide translocator (ANT), cyclophillin D (CypD), hexokinase (HK) and creatine kinase (CK) are shown. Inhibitors of mPT pore opening include Bongkrekic acid, which locks the mPT pore in a closed conformation, as well as the CypD inhibitors cyclosporine A and sanglifehrin A. Figure adopted from [14].

solutes <1.5 kDa. Adoption of an open conformation by the mPT enables uptake of ions and biosynthetic intermediates into the mitochondrial matrix [15].

Opening of the mPT pore can occur transiently in response to an increase in intracellular Ca^{2+} [15]. Uptake of Ca^{2+} by mitochondria plays an essential role in T cell activation by buffering the intracellular Ca^{2+} flux induced by T cell receptor (TCR) ligation [16-18]. Sustained opening of the mPT pore, in contrast, results in osmotic swelling of the matrix, impaired oxidative phosphorylation due to collapse of $\Delta\psi_m$, and rupture of the mitochondrial outer membrane [13]. Responses consistent with sustained mPT pore opening (e.g., large-amplitude swelling and release of pro-apoptotic MIS

proteins) are observed in isolated mitochondria exposed to concentrations of Ca^{2+} >150 μM [19].

Ca^{2+}-dependent mPT pore opening appears to result from stimulation of the peptidylprolyl isomerase (PPIase) activity of CypD [20]. Evidence for this mechanism comes from the ability of the CypD inhibitors, cyclosporine A (CsA) and sanglifehrin A (SfA), to block Ca^{2+} induced opening of the mPT pore (Figure 3.2; [21, 22]). While both molecules block the PPIase activity of CypD [21, 22], CsA also disrupts binding of CypD to ANT [23]. Regulation of the mPT pore has also been investigated by targeted deletion of CypD (gene name *Ppif*, peptidylprolyl *cis-trans* isomerase). Consistent with inhibitory effects of CsA and SfA, a three-fold excess of Ca^{2+} is required to trigger mPT pore opening in liver mitochondria isolated from *Ppif*$^{-/-}$ mice relative to liver mitochondria from wild-type mice [24, 25]. In addition, hepatocytes from *Ppif*$^{-/-}$ mice are resistant to apoptosis induced by depletion of endoplasmic reticulum (ER) Ca^{2+} stores with thapsigargin [24]. Thus, sustained opening of the mPT pore is an apoptotic response that can result from stimulation of CypD by deregulated Ca^{2+} flux [19].

Oxidative stress can also trigger sustained opening of the mPT pore. Large-amplitude swelling is observed in isolated rat liver mitochondria treated with H_2O_2 or *tert*-butyl hydroperoxide (*t*-BHP), or with menadione [26, 27], which generates $O_2^{\bullet-}$ via redox cycling reactions with ETC flavoproteins [28]. Evidence of mPT pore opening (i.e., large-amplitude swelling and cytochrome *c* release) is also observed in isolated rat liver mitochondria treated with rotenone [29]. This compound elevates levels of $O_2^{\bullet-}$ in the mitochondrial matrix by inhibiting complex I of the ETC [30, 31]. Rotenone-induced mPT pore opening is blocked by CsA or the ANT ligand Bongkrekic acid (BA) [29, 32],

which locks this channel in a low-permeability conformation (Figure 3.2; [33]). Sustained opening of the mPT pore is defined in terms of effects (e.g., release of cytochrome *c* or large-amplitude swelling) on isolated mitochondria. There is evidence, however, that this mechanism occurs in intact cells. For instance, CsA inhibits rotenone induced apoptosis in WB-F344 rat liver cells [32]. Similarly, cell death triggered by the burst of mitochondrial $O_2^{\bullet-}$ production that accompanies re-oxygenation of hypoxic cells is prevented by pre-treatment CsA or BA [34].

The capacity of oxidizing agents to trigger mPT pore opening suggests that component(s) of this complex are redox-regulated. One possible redox-sensitive target is the ATP/ADP antiporter ANT, which contains three matrix-exposed cysteines [35, 36]. Several studies indicate that the conformation of the ANT depends oxidation state of these residues. For example, agents (e.g., diazenzedicarboxylic acid bis 5*N*,*N*-dimethylamide (diamide)) that oxidize vicinal dithiols to the corresponding disulfides can permeabilize liposomes reconstituted with purified ANT [37]. Diamide also oxidizes ANT thiols and triggers mPT pore opening in rat liver mitochondria and intact 2B4.11 murine T cells [37]. Large amplitude swelling of isolated rat liver mitochondria induced by diamide of by the pro-oxidants *t*-BHP or menadione, is inhibited by pre-treatment exogenous glutathione [26]. In addition, mPT pore opening induced by these oxidizing agents is prevented by *N*-ethyl maleimide, which prevents formation of disulfide bonds by derivatizing single cysteine thiols [26]. These findings demonstrate that oxidative stress triggers opening of the mPT pore, and are consistent with a model whereby this process may be mediated oxidation of matrix-exposed ANT thiols.

The Bcl-2 protein family regulates mitochondrial outer membrane integrity: Pro-apoptotic proteins can also be released from the MIS by mitochondrial outer membrane permeabilization (MOMP). This process is regulated by the B cell lymphoma 2 (Bcl-2) protein family [38]. *Bcl-2*, was identified as a gene overexpressed due to a t(14;18) chromosome translocation in B cell follicular lymphomas [39]. Overexpression results because this translocation places *bcl-2* under control of powerful immunoglobulin enhancers [40, 41]. Because a similar chromosomal translocation is observed with the gene encoding the oncogenic transcription factor c-Myc in Burkitt's lymphoma [42], Bcl-2 was likewise hypothesized to be an oncogene. To evaluate this hypothesis, Adams and Cory introduced a *bcl-2* transgene into hematopoetic stem cells of both wild type and Eμ-myc transgenic mice, which constitutively express high levels of c-Myc in B cell lineages [43]. While Bcl-2 is not itself tumorigenic, it cooperates with c-Myc to promote tumor development in B cell precursors [43]. Korsmeyer, *et al* separately demonstrated that *bcl-2* overexpression blocks death induced by withdrawal of the pro-survival cytokine interleukin-3 (IL-3) from hematopoetic cells without stimulating proliferation [44, 45]. Together these observations indicated that unlike previously identified oncogenes (e.g., c-Myc or Ras) which all enhance proliferation, Bcl-2 contributed to neoplasia by inhibiting cell death [46]. Soon thereafter, the Green laboratory demonstrated that Bcl-2 blocks mitochondrial-dependent caspase activation in *Xenopus* oocyte extracts [47].

Since these seminal studies, a number of proteins with sequence homology to Bcl-2 have been identified. While several of these "Bcl-2 family proteins" function analogously to Bcl-2, others promote apoptosis. The Bcl-2 protein family is therefore

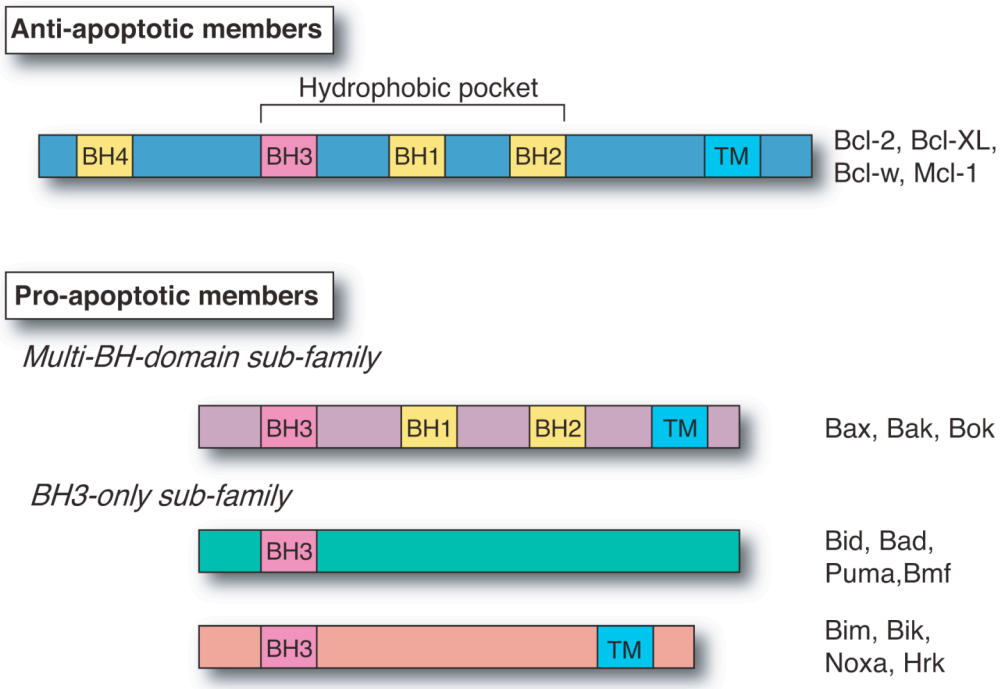

Figure 3.3 - Bcl-2 family proteins. Figure adopted from [38].

sub-divided into three groups based on the presence of up to four Bcl-2 homology (BH) domains (Figure 3.3; [38]). Anti-apoptotic Bcl-2 proteins (e.g., Bcl-2, Bcl-w, Bcl-2 related gene, long isoform (Bcl-x_L), A1, and Myeloid cell leukemia-1 (Mcl-1) exhibit homology in all four BH domains and are generally localized to the mitochondrial outer membrane (Figure 3.3; [48]). Bcl-2 and Bcl-x_L also associate with the endoplasmic reticulum (ER), and there is accumulating evidence that these proteins contribute to ER-Ca^{2+} homeostasis [49]. For instance, Bcl-2 and Bcl-x_L stimulate leakage of ER Ca^{2+} into the cytosol by binding to inositol triphosphate ($InsP_3$) receptors [50, 51]. As a result, Ca^{2+} flux is decreased in Jurkat T cells overexpressing Bcl-2 following treatment with thapsigargin, which causes emptying of ER Ca^{2+} stores [52]. This activity of Bcl-2 and

Bcl-x_L is speculated to promote survival by reducing ER-Ca^{2+} flux, which can lead to apoptosis by triggering sustained opening of the mPT pore [13, 49].

Pro-apoptotic Bcl-2 proteins lack the BH4 domain and are divided into two classes - multi-BH-domain pro-apoptotic and BH3-only proteins. The multi-BH-domain pro-apoptotic class contains three proteins (Bcl-2 associated x protein (Bax), Bcl-2 antagonist killer 1 (Bak) and Bcl-2 related ovarian killer (Bok)) that exhibit sequence conservation in BH1-3 domains (Figure 3.3; [38]). Bak is constitutively localized to the mitochondrial outer membrane where it is bound by anti-apoptotic Bcl-2 proteins (e.g., Mcl-1 and Bcl-x_L) as well as the voltage-dependent anion channel (VDAC) [53, 54]. Bax resides primarily as a monomer in the cytosol and redistributes to the mitochondrial outer membrane in response to apoptotic stimuli [55, 56]. Bok expression is limited to reproductive tissues, and despite exhibiting sequence homology to Bax and Bak, its role in apoptosis has received little attention [57].

BH3-only proteins (Bcl-2 antagonist of cell death (Bad), Bcl-2 interacting domain death agonist (Bid), Bcl-2 interacting killer (Bik), Bcl-2 interacting mediator of cell death (Bim), Bcl-2 modifying factor (Bmf), Harakiri (Hrk), Noxa and p53-upregulated modulator of apoptosis (Puma)) display sequence conservation only in the BH3 domain (Figure 3.3; [38]). BH3-only proteins are upregulated by transcriptional induction or post-translational activation in response to stress stimuli, and promote apoptosis by neutralizing anti-apoptotic Bcl-2 proteins and/or activating Bax and Bak [58, 59]. Proposed mechanisms by which BH3-only proteins activate Bax and Bak will be described in detail in the following section.

The multi-BH-domain proapoptotic Bcl-2 proteins Bax and Bak are effector proteins that respond to signals from anti-apoptotic Bcl-2 proteins and BH3-only proteins. When pro-apoptotic signaling from BH3-only proteins predominates, Bak undergoes a conformational change (termed activation) resulting in exposure of a cryptic amino-terminal epitope [60]. Bax undergoes an analogous conformational change in response to apoptotic stimuli, but must also translocate from the cytosol to the mitochondrial outer membrane in order to promote release of apoptogenic MIS proteins. Redistribution of Bax in response to apoptotic stimuli appears to be independent of Bcl-2 proteins, which only interact with Bax once localized to the mitochondrial outer membrane [55].

Bax translocation appears, instead, to be regulated by phosphorylation. For example, Bax is phosphorylated at Thr167 by the SAP kinase, c-Jun N-terminal kinase (JNK), in human hepatoma Hep2G cells following exposure to UV light, H_2O_2, or the topoisomerase II inhibitor, etoposide [61]. Thr167 phosphorylation appears to be a critical apoptotic signal, because substitution of alanine for this phospho-residue blocks Bax translocation induced by UV light, H_2O_2, or etoposide. Conversely, redistribution of Bax to the mitochondria is opposed by the pro-survival kinase Akt. This was first demonstrated by Rathmell, *et al* who found that Bax activation following growth-factor withdrawal can be prevented by expression of a constitutively active Akt transgene [62]. Constitutive activation of Akt has also been shown to impede Bax translocation in neutrophils and murine T cell lymphomas [63, 64]. In neutrophils this results from phosphorylation of Bax by Akt at Ser184 [64]. In T cells, however, Akt-dependent

sequestration of Bax in the cytosol requires an amino-terminal region spanning amino acids 13-29 [63].

The hypothesis that activated Bax and Bak release pro-apoptotic MIS proteins by forming pores in the mitochondrial outer membrane was suggested by sequence homologies between Bcl-2 proteins and bacterial toxins that form channels in lipid membranes [65]. Experimental support for this mechanism was provided by direct imaging of activated Bax in lipid bilayers by atomic force microscopy, which demonstrated the presence of toroidal-shaped pores [66]. These channels appear sufficiently large to promote release of pro-apoptotic MIS proteins because activated Bax or Bak have been shown to induce release of cytochrome *c* from liposomes composed of lipids present in the mitochondrial outer membrane [67]. This finding is significant because it demonstrates that permeabilization of the mitochondrial outer membrane by Bax or Bak can occur independently of other proteins (e.g., VDAC) that reside in this lipid bilayer.

There is accumulating evidence, however, that interactions between activated Bax and Bak and proteins that control mitochondrial fission and fusion may contribute to loss of mitochondrial outer membrane integrity. In unstressed cells, mitochondria exist as an extended tubular network [68]. Mitochondrial fission machinery (e.g., the dynamin-related GTPase DRP1, the large transmembrane GTPase Mfn2 and lipid transferase endophillin B1) fragment this network during mitosis to enable equal distribution of mitochondria between daughter cells [68]. Mitochondrial fragmentation is also observed during apoptosis, where it is thought to promote release of MIS proteins by destabilizing the outer mitochondrial membrane [69]. Additional evidence for a role of mitochondrial

fission in MOMP is provided by the ability of a dominant-negative DRP1 mutant to delay cytochrome *c* release and apoptosis induced by the pan-kinase inhibitor, staurosporine, in HeLa cervical carcinoma cells [70]. A role for the Bcl-2 family proteins in this process is suggested by studies demonstrating that activated Bax and Bak coalesce at foci of mitochondrial fission and interact with DRP-1 and Mfn2 prior to MOMP [70, 71]. However, staurosporine-induced Bax and Bak activation is still observed in HeLa cells expressing the dominant negative DRP-1 mutant [70]. These findings indicate that mitochondrial fission accelerates the loss of mitochondrial outer membrane integrity, but that this process is only engaged after activation of Bax and Bak.

Crystal structures of the Bcl-2 proteins, Bcl-x_L, Bcl-2, Bcl-w, Mcl-1, Bax, and Bak, reveal a conserved helical bundle tertiary structure containing a prominent hydrophobic cleft formed by the α-helical BH1, -2 and -3 domains (Figure 3.3; [72-76]). Among the BH3-only proteins, only Bid displays a tertiary structure [77]. The remaining BH3-only proteins are either intrinsically unstructured or do not share the same tertiary fold as to multi-BH-domain Bcl-2 proteins, which suggests that their BH3-only domain was acquired by convergent evolution [78]. Crystal structures of Bcl-x_L have been solved in which the hydrophobic groove is occupied by the BH3-domain sequences from Bak, Bad or Bim [79-81]. These co-structures suggest that binding BH3-only proteins as well as Bax Bak to anti-apoptotic Bcl-2 proteins is mediated by interactions between the BH3 domain helix of BH3-only proteins, Bax and Bak and this hydrophobic cleft on anti-apoptotic Bcl-2 proteins. Despite this conserved protein-protein interaction motif, Bax and Bak specifically associate with different subsets of anti-apoptotic Bcl-2 proteins.

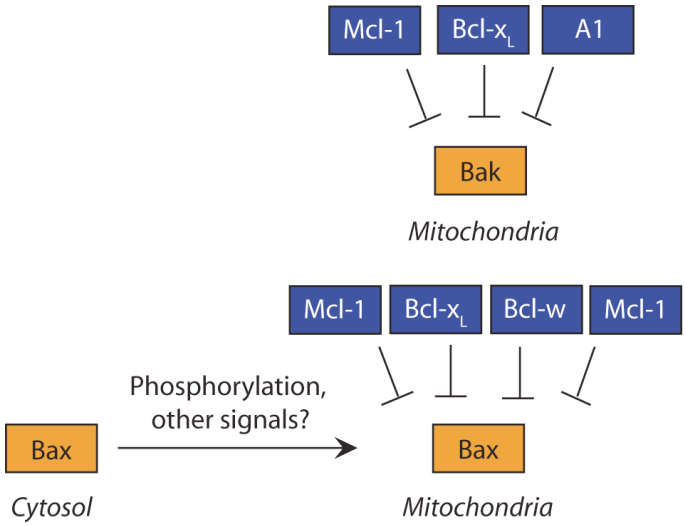

Figure 3.4 - Constraint of Bax and Bak by anti-apoptotic Bcl-2 proteins. Bak is constitutively localized to the mitochondrial outer membrane where it is subject to inhibitory binding by Mcl-1, Bcl-x_L and A1. In contrast, Bax is present in the cytosol and redistributes to the mitochondria prior to apoptosis. Although phosphorylation appears to play a role, the signals regulating Bax translocation are not fully clear (see text for details). Once localized to the mitochondrial outer membrane, Bax homo-oligomerization is prevented by binding of Mcl-1, Bcl-x_L, Bcl-2 and Bcl-w. Figure adopted from [82].

Bak activation is opposed by direct inhibitory binding of Mcl-1, A1, and Bcl-x_L (Figure 3.4; [54, 83]). By contrast, after redistribution to the mitochondrial outer membrane, Bax is bound by Mcl-1, Bcl-2, Bcl-x_L and Bcl-w (Figure 3.4; [84]). Specificity is also observed with respect to binding of BH3-only proteins to Bax and Bak as well as the anti-apoptotic Bcl-2 proteins. These associations and their implications for Bax and Bak activation are described below.

Activation of Bax and Bak by BH3-only proteins: Bax and Bak (and perhaps Bok) are the only pro-apoptotic Bcl-2 proteins capable of causing loss of mitochondrial outer membrane integrity. Given this position as gatekeepers of the mitochondrial apoptotic pathway, *bax* and/or *bak* deficient mice were predicted to display significant

abnormalities due to blocked apoptosis. Targeted gene deletion of *bak* or *bax* produced either no phenotype or mild lymphoid hyperplasia in aged mice, respectively [85, 86]. In contrast, mice lacking both proteins, which were generated collaboratively by the Thompson and Korsmeyer laboratories, display an array of defects [86]. Due to the presence of excess cells in the central nervous system, most $bax^{-/-}$, $bak^{-/-}$ mice die at or just before birth [86]. Those animals reaching adulthood display persistence of interdigital webbing, fetal ocular vasculature, and imperforate vaginas in females [86-88]. In addition, T cells from $bax^{-/-}$, $bak^{-/-}$, mice are resistant to cytokine-withdrawal induced apoptosis resulting in abnormal accumulation of activated T cells in the spleen and lymph nodes [89]. These observations demonstrate that Bax and Bak function redundantly during embryonic development and immune system homeostasis in adult animals, but that their combined absence causes defects in processes (e.g., deletion of interdigital tissue and activated T cells) mediated by the mitochondrial apoptotic pathway.

Reliably obtaining cells from $bax^{-/-}$, $bak^{-/-}$ mice is challenging because they are born well below Mendellian frequency. To circumvent this issue, embryonic fibroblasts were isolated from $bax^{-/-}$, $bak^{-/-}$ or double-knockout mice and immortalized by transfection with cDNA that encodes the SV40 tumor virus [87]. These murine embryonic fibroblasts (MEFs) have been widely used to study the role of Bax and/or Bak in the response to apoptotic stimuli [90]. Equivalent, partial protection (i.e., ~50% reduction in killing after 24 h) is observed in $bax^{-/-}$ and $bak^{-/-}$ MEFs following DNA damage, microtubule destabilization, growth factor deprivation and endoplasmic reticulum stress [87]. In contrast, MEFs lacking both proteins are refractory to these apoptotic stimuli as well as overexpression of BH3-only proteins [87]. Likewise, MOMP

is not observed when mitochondria from *bax*$^{-/-}$, *bak*$^{-/-}$ MEFs are incubated with recombinant BH3-only proteins. These findings, combined with pronounced phenotype of *bax*$^{-/-}$, *bak*$^{-/-}$ mice, have led to the conclusion that Bax and Bak activation is required for induction of MOMP by BH3-only proteins. However, the mechanism by which BH3-only proteins activate Bax and Bak remains controversial.

There are two competing models for activation of Bax and Bak by BH3-only proteins. Disagreement between these proposals concerns whether BH3-only proteins promote apoptosis by directly engaging Bax and Bak or *solely* by neutralizing anti-apoptotic Bcl-2 proteins. The "direct activation model" was developed from studies of the ability of BH3-only proteins to release cytochrome *c* from large unilamellar vesicles (LUVs - liposomes with lipid content that mimics the mitochondrial outer membrane) reconstituted with Bax or Bak [91-94]. Because Bid and Bim (and in some studies Puma) induce release of cytochrome *c* in this system, these BH3-only proteins were classified as direct activators (Figure 3.5A; [91, 92]). All other BH3-only proteins failed to activate Bax or Bak and induce release of cytochrome *c* from LUVs [91, 92]. Activity of these BH3-only proteins was apparent, however, in LUVs where activation of Bax by Bim or Bid was blocked by the presence of an anti-apoptotic Bcl-2 protein. For instance, Bid induced release of <20% of cytochrome *c* from LUVs reconstituted with Bax and Bcl-x_L, while combined addition of Bid and Bad resulted in >80% release [92]. These findings suggested that Bad, Bik, Bmf, Hrk, and Noxa promote activation of Bax and Bak by displacing Bid and Bim (and perhaps Puma) from inhibitory binding by anti-apoptotic Bcl-2 proteins. As a result, these BH3-only proteins were classified as sensitizers or de-repressors (Figure 3.5A).

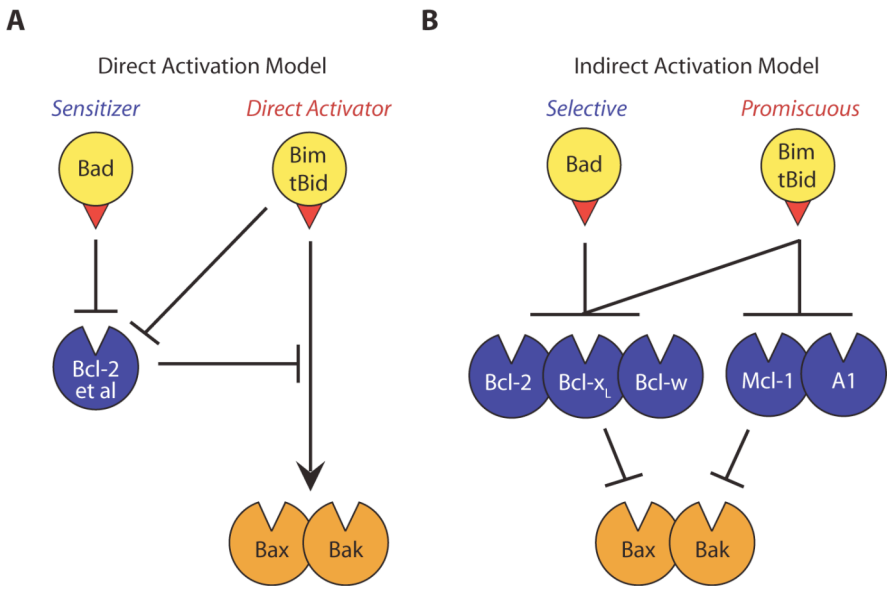

Figure 3.5 - Two models of how BH3-only proteins engage Bax and Bak. (A) In the *direct activation* model, *activator* BH3-only proteins (e.g., Bim and tBid) directly engage Bax and Bak via their BH3-only domain (red triangle). In contrast, *sensitizer* BH3-only proteins (e.g., Bad), which can only bind a subset of anti-apoptotic Bcl-2 proteins, serve only to displace *direct activators* from their pro-survival partners. (B) BH3-only proteins interact solely with anti-apoptotic Bcl-2 proteins in the indirect activation model. Promiscuous binders (e.g., Bim and tBid) readily trigger Bax/Bak activation because they can neutralize all five anti-apoptotic Bcl-2 proteins, whereas selective binders (e.g., Bad) alone are not sufficient to cause Bax/Bak activation. Figure adopted from [82].

The direct activation model implies that the key event in the induction of MOMP is binding of Bax and Bak by direct activator BH3-only proteins. However, the affinity of Bid, Bim and Puma BH3 domain peptides for Bax and Bak is weak (2-10 μM; [84]) relative to their affinity for anti-apoptotic Bcl-2 proteins, which ranges from 2-50 nM depending on the combination of BH3 domain peptide and anti-apoptotic Bcl-2 protein [95]. In addition, immunoprecipitation experiments have failed to detect stable association between Bim and Bax or Bak in thymocytes following treatment with the Ca^{2+} ionophore ionomycin [84], which triggers Bim-dependent apoptosis [96]. Instead, increased association of Bim with anti-apoptotic Bcl-2 proteins is detected in ionomycin-

treated thymocytes. The weak *in vitro* and *in vivo* associations between direct activator BH3-only proteins and the multi-BH-domain proteins Bax and Bak suggested that these interactions are not essential for apoptosis, but that the crucial step leading to MOMP is neutralization of anti-apoptotic Bcl-2 proteins.

This alternative hypothesis is termed the "indirect activation" model (Figure 3.5B). The indirect activation model is supported by studies showing that a Bim variant which is unable to bind Bax or Bak due to alanine substitution of a conserved BH3 domain residue (Gly66) induced apoptosis to an equivalent degree as wild-type Bim [84]. Analogous results were obtained by overexpression of a Bid mutant in which binding to Bax and Bak is impaired by alanine substitution of the corresponding residue (Gly94) in the BH3-only domain of this protein [84]. In addition, the direct activation model suggests that combined deletion of *bim* and *bid* should produce a high rate of neonatal mortality and developmental abnormalities (e.g., interdigital webbing) similar to that observed in $bax^{-/-}$, $bak^{-/-}$ animals. Instead, mice lacking Bim and Bid are born at Mendellian frequency, are developmentally normal, and achieve normal life expectancy [84]. Moreover, MEFs derived from these mice undergo apoptosis in response to DNA damage induced by the UV light or the topoisomerase II inhibitor, etoposide, even if Puma is depleted by RNAi [84].

These findings form the basis for the indirect activation model of Bax and Bak activation by BH3-only proteins. In this model, BH3-only proteins induce apoptosis by engaging multiple anti-apoptotic Bcl-2 proteins rather than directly activating Bax and Bak (Figure 3.5B). Accordingly, the differential ability of BH3-only proteins to activate Bax and Bak derives from the number of anti-apoptotic Bcl-2 proteins neutralized by a

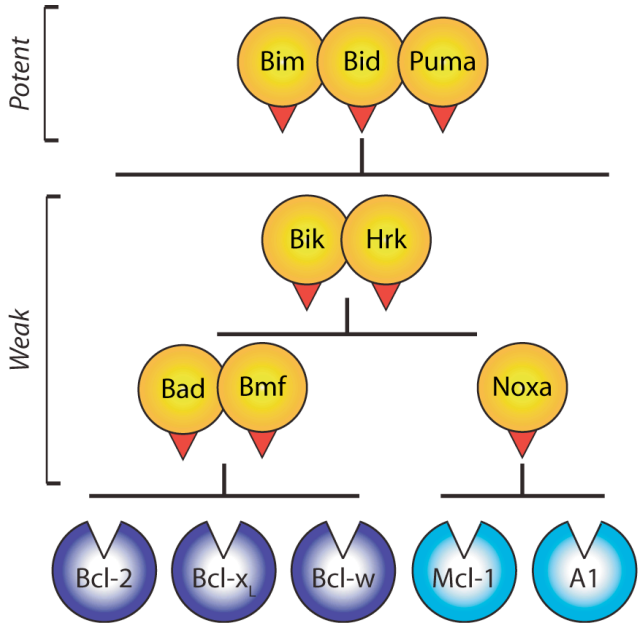

Figure 3.6 - BH3-only proteins can bind promiscuously or selectively to anti-apoptotic Bcl-2 proteins. Bim, Puma and tBid engage all anti-apoptotic Bcl-2 proteins and are therefore potent inducers of Bax/Bak activation. All other BH3-only proteins bind selectively to the indicated subset of anti-apoptotic Bcl-2 proteins and hence are alone unable to trigger activation of Bax or Bak. Figure adopted from [97].

particular BH3-only protein [97]. Consistent with ability of Bim, Bid and Puma to induce MOMP in isolated mitochondria and trigger apoptosis when overexpressed, peptides derived from the BH3 domains of these proteins bind to all five anti-apoptotic Bcl-2 proteins with high affinity (K_d < 50 nM) (Figure 3.6; [95]). By contrast, peptides derived from the BH3 domains of sensitizer BH3-only proteins only associate with a subset of antiapoptotic Bcl-2 proteins. For instance, Bad BH3 peptide binds to Bcl-2, Bcl-x_L and Bcl-w, while a peptide derived from the Noxa BH3 domain preferentially interacts with Mcl-1 and A1 (Figure 3.6; [95]).

Activation of Bax and Bak is prevented in unstressed cells by inhibitory binding of multiple anti-apoptotic Bcl-2 proteins (Figure 3.4). Hence, neither Noxa nor Bad is

alone sufficient to trigger MOMP or apoptosis [54]. However, combined over-expression of these two BH3-only proteins is lethal in wild-type MEFs. Significantly, Noxa and Bad co-expression kills MEFs that lack the purported direct activators Bim and Bid and have reduced levels of Puma [84]. This finding provides additional support for the indirect activation model because, according to the direction activation model, cells lacking direct Bim, Bid and Puma should be unable to activate Bax and Bak. Other sensitizer BH3-only proteins also associate with a subset of anti-apoptotic Bcl-2 proteins; Bmf displays analogous selectivity as Bad, while Bik and Hrk bind tightly (K_d < 50 nM) to Bcl-x_L, Bcl-2 and A1 (Figure 3.6; [95]). Hence, "sensitizer" BH3-only proteins are weak inducers of MOMP and apoptosis because they only engage a subset of anti-apoptotic Bcl-2 proteins.

So which of these models best explains the experimental data? The indirect activation model is consistent with biophysical data indicating that BH3-only proteins bind anti-apoptotic Bcl-2 proteins with greater affinity than Bax and Bak. In addition, this model accounts for the absence of appreciable apoptotic phenotypes in *bim*$^{-/-}$, *bid*$^{-/-}$ mice. Nevertheless, there are two caveats to indirect activation model, that suggest neutralization of anti-apoptotic Bcl-2 proteins may not be sufficient to trigger activation of Bax and Bak.

First, the affinity of BH3-only proteins for Bax and Bak (as well as anti-apoptotic Bcl-2 proteins) has been determined using solution-state binding assays. This *in vitro* system may underestimate the affinity of BH3-only proteins for Bax and Bak by eliminating the hydrophobic context (i.e., the mitochondrial outer membrane) in which these interactions occur *in vivo* [98]. For instance, despite the micromolar affinity of Bim or Bid for Bax in solution-state binding assays [84], namomolar concentrations of either

BH3-only protein are sufficient to permeabilize LUVs reconstituted with Bax [92]. These data indicate that direct activation of Bax and Bak occurs (at least *in vitro*), and suggests that the affinity of direct activator BH3-only proteins for Bax or Bak may be elevated by the presence of a hydrophobic component like the mitochondrial outer membrane. However, this explanation does not address why stable associations with Bax and Bak are not detected by immunoprecipitation of Bim in cells treated with ionomycin, which is a Bim-dependent apoptotic stimulus.

Second, an alternative interpretation of the absence of an apoptotic phenotype in *bim*$^{-/-}$, *bid*$^{-/-}$ mice is that non-Bcl-2 family proteins directly activate Bax and Bak in the absence of Bim and Bid [98]. This explanation is supported by studies demonstrating that p53 can induce MOMP and apoptosis independently of its function as a transcription factor by directly binding to Bax [99]. In addition, the Ca^{2+}-responsive transcription factor Nur77 has been shown to bind Bcl-2 and induce a conformational change in this anti-apoptotic Bcl-2 protein that promotes activation of Bax and Bak [100]. These examples suggest that activation of Bax and Bak by non-Bcl-2 family proteins could contribute to normal development in *bim*$^{-/-}$, *bid*$^{-/-}$ mice. However, activation of Bax and Bak by non-Bcl-2 proteins does not explain why co-expression of Bad and Noxa (two purported sensitizer BH3-only proteins) is sufficient to induce apoptosis in MEFs derived from these animals [84]. In sum, despite these caveats, the indirect activation model is gives a more cohesive fit of the current data and provides a useful framework for understanding how BH3-only proteins trigger activation of Bax and Bak.

Cellular regulation of BH3-only proteins: In the absence of cellular stress, BH3-only proteins are transcriped at low levels or inhibited by post-translational mechanisms

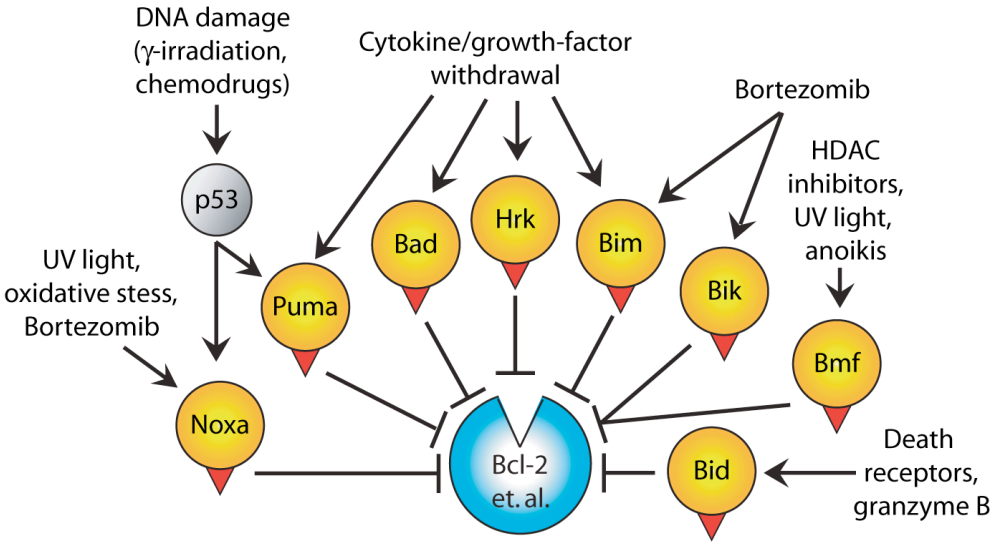

Figure 3.7 - Apoptotic stimuli trigger distinct BH3-only proteins. Specific BH3-only proteins are upregulated in response to a variety of cell stresses. Once upregulated, they promote apoptosis by binding and neutralizing anti-apoptotic Bcl-2 proteins via their BH3 domain (red triangle). See text for details. Figure adopted from [97].

including phosphorylation, sequestrations to cytoskeletal proteins, or expression as an inactive zymogen. Particular BH3-only proteins are either transcriptionaly-induced or activated via a post-translational mechanism in response to distinct forms of cell stress (Figure 3.7; [97]).

Bid: Processing of Bid to its active, truncated form (tBid) is mediated by caspase-8 or -10 following engagement of cell-surface death receptors [101, 102]. Once cleaved, tBid translocates to the mitochondrial outer membrane where it binds to anti-apoptotic Bcl-2 proteins [101, 102]. Thus, Bid cleavage serves as a form of "cross talk" between the extrinsic and intrinsic apoptotic cascades. The contribution of this mechanism to death-receptor induced apoptosis appears to be dependent on cell-type [103]. For instance, lymphocytes from *bid*$^{-/-}$ mice are normally sensitive to Fas-dependent apoptosis,

while fibroblasts and hepatocytes from these animals are resistant to stimulation of Fas and other cell-surface death receptors [103].

Bid can also be activated as a result of cleavage by caspases-2 or -3 independently of cell-surface death receptor ligation [104, 105]. Caspase-3 is an executioner caspase activated downstream of MOMP [1]. Therefore, cleavage of Bid by caspase-3 is thought to amplify apoptotic cascades following loss of mitochondrial outer membrane integrity. By contrast, auto-activation of caspase-2 can occur prior to MOMP that is due induced genotoxic stress [106]. In addition, total Bid *levels* are elevated in response to DNA-damage in a p53-dependent manner [107]. These observations suggested that cleavage of Bid by caspase-2 might contribute apoptosis that is induced by genotoxic stress [107]. However, increased Bid *cleavage* is not observed in lymphocytes or fibroblasts exposed to cisplatin or UV irradiation [107]. Moreover, lymphocytes and fibroblasts from *bid*$^{-/-}$ mice remain sensitive to these DNA damaging agents [103].

The histone deacetylase inhibitor Vorinostat elevates intracellular reactive oxygen species (ROS) levels in a variety of cell-types [108]. In CCRF-CEM T cells, ROS induced by Vorinostat signals caspase-independent Bid cleavage [109]. This observation suggests that Bid may be a substrate for other cellular proteases such as calpains [110]. Unfortunately, the dependence of Vorinostat-induced apoptosis on Bid expression has not been assessed [109].

Noxa and Puma: Although both BH3-only proteins are p53-response genes, they are not regulated redundantly [111]. Puma is induced earlier than Noxa following treatment with cisplatin, etoposide, or γ-irradiation, and is rate limiting for that is apoptosis induced by these agents in lymphocytes, hepatocytes and fibroblasts [112, 113].

In contrast, increased Noxa expression is observed in response to UV light in fibroblasts, while Puma is not induced. In addition, Noxa levels are selectively increased in response to oxidative stress induced by the proteasome inhibitor Bortezomib in multiple myeloma cells lines and patients samples [114]. *Noxa* expression is also induced by agents that stimulate mitochondrial ROS production, such as the chemotherapeutic Trisenox or the herbicide paraquat [115, 116]. These findings indicate that Puma plays an essential role in the p53 death response, whereas Noxa is engaged by a more diverse set of apoptotic stimuli.

Perhaps because Noxa only associates with Bcl-x_L and Mcl-1, developmental abnormalities or perturbations of immune system homeostasis are not detected in mice lacking this BH3-only protein [111]. *Puma*$^{-/-}$ mice also appear developmentally normal [111], but survival of T cells in these animals is enhanced after conclusion of an acute immune response [117]. Puma is induced in activated T cells by the forkhead box transcription factor O3a (FOXO3a) [118]. In the presence of pro-survival cytokines, FOXO3a is subject to inhibitory phosphorylation by the pro-survival kinase Akt [119]. However, the reduction in cytokine levels that accompanies pathogen clearance leads to decreased activation of Akt by the phosphoinositol 3-kinase (PI3K) pathway and induction of *puma* [118].

Bim: The BH3-only protein Bim plays an essential role in immune system homeostasis [120]. Alternative splicing of the *bim* gene produces three isoforms in humans – Bim_{EL} (extra-long), Bim_L (long) and Bim_S (short) – which differ in their capacity to induce apoptosis [104, 121]. Cells are most sensitive to overexpression of Bim_S, because unlike Bim_{EL} and Bim_L, this isoform lacks the binding domain necessary

for association with the dynein light chain LC8 (DLC1), a component of the dynein motor complex on microtubules [122]. UV irradiation or treatment with the microtubule stabilizing chemotherapeutic paclitaxel stimulates release of Bim_{EL} and Bim_L from the dynein motor complex, enabling them to engage anti-apoptotic Bcl-2 proteins [122]. While sequestration by DLC1 regulates Bim activation in endothelial cells, all three Bim isoforms are primarily localized to the mitochondrial outer membrane in T cells where they are bound by Mcl-1 [123, 124]. Binding of Noxa to Mcl-1 disrupts this complex, which results in Bim-dependent apoptosis in response to stimuli that induce *noxa* expression in primary T cells and T cell leukemia lines [115, 125, 126]. While these observations do not address how Bim promotes activation of Bax and Bax once released from Mcl-1, they nevertheless demonstrate that Noxa can functions as a 'sensitizer' by freeing Bim from sequestration by anti-apoptotic Bcl-2 proteins.

In addition to these post-translational mechanisms, *bim* expression is induced in response to intracellular Ca^{2+} flux, endoplasmic reticulum stress (ER) stress and withdrawal of survival factors. The increase in *bim* expression following ER stress is induced by the transcription factors CCAT-enhancer binding protein-α (CEBP-α) or CEBP homologous protein (CHOP) [127]. *Bim* expression is induced by the transcription factor FOXO3a in a manner analogous to *puma* following withdrawal of cytokines or other survival factors [128]. As observed in *puma*$^{-/-}$ mice, T cells from mice lacking *bim* are resistant to cytokine withdrawal *in vitro* and display extended survival after resolution of an immune response [129-131]. In addition, *bim*$^{-/-}$ mice have elevated (3- to 5-fold) numbers of T and B cells as well as macrophages and granulocytes in their

lymphoid tissues and develop a fatal autoimmune disease resembling human systemic lupus erythematosus (SLE) [132].

Bmf: This BH3-only protein shares a conserved amino-terminal dynein light chain-binding motif with Bim [133]. However, Bmf preferentially interacts with the DLC2 subunit of the myosin V motor complex that is associated with the actin cytoskeleton [134]. Release of Bmf from DLC2 is triggered by UV irradiation or anoikis, a form of apoptosis that results from detachment of endothelial cells from their extra-cellular matrix [133]. Release of Bmf from DLC2 in response to UV light is thought to function in conjunction with *noxa* induction to neutralize all five anti-apoptotic Bcl-2 proteins [95, 133]. Bmf is also regulated at the transcriptional level with induction observed in response to the pro-oxidant Trisenox, along with HDAC inhibitors and glucocorticoids [115, 135, 136]. Finally, immune system development and homeostasis appear normal in *bmf*$^{-/-}$ mice, although aged animals develop a B cell-restricted lymphadenopathy [136].

Bad: Bad was identified by screening a λ-phage expression library for binding partners of Bcl-x_L [137]. The pro-apoptotic activity of Bad is inhibited by phosphorylation. Stimulation of growth factor and cytokine-receptors promotes phosphorylation of Bad at Ser136 by Akt [138]. Phosphorylation of Ser136 inactivates Bad by promoting binding to 14-3-3 adaptor proteins [139]. In addition, phosphorylation of Ser136 induces a conformational change in Bad exposing a cryptic phospho-residue (Ser155) within the BH3-only domain [140, 141]. Phosphorylation of Ser155 by protein kinase A (PKA) or p90 ribosomal S6 kinase (RSK) disrupts binding of Bad to Bcl-x_L or Bcl-2 [140, 141]. Ser136 can be dephosphorylated by the Ca^{2+}-dependent protein

phosphatase, calcineurin, which promotes release of Bad from 14-3-3 proteins in response to Ca^{2+} ionophores [142]. These findings suggested that Bad might play a key role in apoptosis that is induced by deprivation of survival factors or intracellular Ca^{2+} flux. However, developmental abnormalities are not observed in *bad*$^{-/-}$ mice, and lymphocytes, MEFs and hepatocytes derived from these animals display normal sensitivity to a broad range of apoptotic stimuli [143].

Bik: Although Bik is expressed in the haematopoietic system, T and B cells from *bik*$^{-/-}$ mice remained sensitive to apoptosis that is induced by cytokine deprivation, glucocorticoids, phorbol esters, Ca^{2+} ionophores, DNA-damaging agents, and antigen-receptor stimulation [144]. As suggested by the sensitivity of *bik* deficient lymphocytes to these apoptotic stimuli, the haematopoietic system appears developmentally normal in *bik*$^{-/-}$ mice. The absence of an apoptotic phenotype may result from the inability of Bik to neutralize Mcl-1 [144]. This proposal is supported by the increased sensitivity of HCT116 colon carcinoma cells to overexpression of Bik if the Mcl-1 levels are reduced by siRNA knockdown or neutralized by overexpression of Noxa [145]. Finally, Bik levels are upregulated in response to proteasome inhibitors in a variety of cell-types [146-148], leading to speculation that this response acts in concert with Noxa induction to neutralize all five anti-apoptotic Bcl-2 proteins [149].

Hrk: This BH3-only protein was identified as a protein that is rapidly induced following deprivation of rat sympathetic neurons of nerve growth factor [150, 151]. Hrk induction appears to be specific for cells of the nervous system because levels of this BH3-only protein are not elevated in fibroblasts of hepatocytes subject to growth-factor withdrawal [152]. Consistent with the preferential induction of Hrk in neural cells,

expression of this BH3-only protein is restricted to the central and peripheral nervous system *in vivo* [152]. Surprisingly, the nervous systems from *hrk*$^{-/-}$ mice are also free of developmental abnormalities, and neurons isolated from these animals remain sensitive to NGF withdrawal [152]. By contrast, neurons from *bim*$^{-/-}$ mice displayed marked survival in the absence of NGF, suggesting that Bim is the BH3-only protein primarily responsible for growth-factor induced apoptosis in neural tissues [152].

T cell apoptosis and immune system homeostasis: The immune system is programmed to mount responses involving both lymphocytes and cells of the innate immune system (macrophages, granulocytes, mast cells and dendritic cells) in response to bacterial and viral pathogens [153]. Innate immune cells non-specifically identify pathogens via Toll-like receptors (TLRs), which recognize pathogen-associated molecular patterns such as bacterial cell wall lipopolysaccharides (LPS) or CpG motifs characteristic of viral DNA [154]. TLR stimulation promotes ingestion of pathogens, which are then processed into small fragments known as antigens [155]. These fragments are displayed on the surface of antigen-presenting cells (APCs) such as macrophages and dendritic cells by loading onto major histocompatability complexes (MHCs) [154, 155]. In addition, TLR stimulation induces upregulation of non-specific alert signals such as the co-stimulatory molecules B7.1 and B7.2 on the surface of APCs [156]. Both the antigen•MHC and co-stimulatory signals are required to activate T cells with surface-antigen receptors specific for the pathogen fragments displayed on APCs [153, 157].

Following antigenic stimulation, T cells rapidly proliferate and differentiate into specific effector classes. $CD4^+$ T cells, or helper T cells, express the cluster-of-differentiation 4 (CD4) glycoprotein on their cell surface and secrete cytokines that

stimulate other T and B cells as well as cells of the innate immune system. Once activated, some $CD4^+$ T cells secrete cytokines such as interleukin-4 and -10 (IL-4 and -10) that support further T cell proliferation and antibody production by B cells [158]. Other activated $CD4^+$ T cells produce cytokines such as interferon-γ (IFN-γ), which act as positive feedback signals for macrophages and other APCs [158]. All activated $CD4^+$ T cells produce IL-2, a cytokine that promotes proliferation of both T and B cells [159, 160]. $CD8^+$ T cells, or cytotoxic T cells, kill infected host cells by secretion of perforin and granzyme [161, 162]. Perforin forms pores in the plasma membrane of target cells, allowing entrance of the serine protease granzyme, which induces apoptosis by cleaving caspase-3 and the BH3-only protein Bid [159, 160].

By promoting antibody production by B cells and killing infected cells, activated $CD4^+$ and $CD8^+$ T cells mediate a coordinated immune response that efficiently removes pathogens [157, 163]. However, activated $CD4^+$ and $CD8^+$ T cells lymphocytes must themselves be elminated at the conclusion of an immune response to limit damage to healthy tissue [157, 163]. Hence, the vast majority of activated T cells generated during an immune response undergo apoptosis following clearance of the pathogen [130]. Defects in this phenomenon, known as T cell contraction, result in immunopathology because many effector mechanisms (e.g., inflammatory cytokines) are not antigen-specific [153]. In addition, failure to delete T cells that are activated by self-antigens (i.e., autoreactive T cells) can be particularly deleterious because self-antigens, which cannot be cleared, provide persistent survival and activation stimuli [164, 165].

An early model of T cell contraction was developed from studies of mice with a lymphoproliferative (*lpr*) disorder [166]. This disorder arises due to a rearrangement in

the gene encoding the Fas death receptor that prevents transcription of full-length Fas mRNA [167, 168]. The Fas death receptor plays an essential role in activation-induced cell death (AICD), a process in which repetitive antigenic stimulation causes apoptosis in T cells due to upregulation of FasL expression [163, 169]. These findings suggested that T cell contraction is mediated by Fas-FasL signaling between activated T cells, which when impaired, results in the pathogenic accumulation of lymphocytes.

Studies of the timing of T cell apoptosis relative to pathogen clearance *after* an acute immune response raised questions concerning the AICD contraction model. Specifically, apoptosis of activated T cells was found to occur after pathogen clearance. AICD is unlikely to be engaged under these conditions because the antigens required to induce FasL expression by TCR re-stimulation have been eliminated [163, 170]. More significantly, normal contraction of activated T cells was observed in $Fas^{lpr/lpr}$ mice following a infection with herpes simplex virus (HSV), which induces an acute immune response [129, 130].

The finding that T cell contraction occurs normally in mice with defective Fas-FasL signaling raised question of how activated T cells are killed *in vivo*. An important clue to this question came from the early studies of cell death that is induced by cytokine-withdrawal, which was found to depend on the intrinsic (mitochondrial) apoptotic pathway [171, 172]. For instance, cytokine or growth-factor withdrawa- induced apoptosis is blocked by overexpression of Bcl-2 or Bcl-x_L [126, 173, 174], which suggests that cytokine withdrawal might trigger induction of BH3-only proteins. Bim appeared to be a likely candidate because levels of this BH3-only protein are elevated following withdrawal of cytokines or growth factors [126, 132, 173, 174]. Consistent

with these observations, activated T cells from *bim*$^{-/-}$ mice are resistant to apoptosis that is induced by IL-2 deprivation [132]. More significantly, contraction of HSV-specific T cells was delayed in *bim*$^{-/-}$ mice, and no additional accumulation of activated T cells was detected in *bim*$^{-/-}$*Fas*$^{lpr/lpr}$ animals [129, 130, 175].

Deletion of the *bim* gene, however, provides less protection against cytokine-withdrawal induced apoptosis than overexpression of Bcl-2 [58, 130], suggesting that other BH3-only proteins may contribute to cytokine-withdrawal induced apoptosis. Puma appeared to be a likely candidate because, like Bim, elevated levels of this BH3-only protein are observed in T and B cells following withdrawal of pro-survival cytokines. In addition, contraction of HSV-specific T cells is delayed in *puma*$^{-/-}$ mice [117]. These findings in *bim*$^{-/-}$ and *puma*$^{-/-}$ mice indicate that contraction of activated T cells following an acute immune response results from induction of BH3-only proteins rather than stimulation of the Fas death receptor.

While contraction of activated T cells after an acute immune response is mediated by induction of BH3-only proteins, the lymphoproliferative autoimmune disease observed in *Fas*$^{lpr/lpr}$ mice suggests that AICD nevertheless plays a role in immune system homeostasis. A distinguishing characteristic of autoimmune responses is that, unlike foreign antigens associated with acute infections, self-antigens cannot be cleared [164, 165]. This difference suggests that persistent stimulation of autoreactive T cells by self-antigens might maintain pro-survival cytokines (e.g., IL-2) at a level sufficient to maintain Akt activation and suppress expression of *bim* and *puma* [129, 176]. Although repetitive stimulation of T cells appears to block cytokine withdrawal induced apoptosis, it also induces FasL [169, 177]. These findings suggest that Fas-FasL signaling serves to

limit expansion of autoreactive T cells that otherwise would be subject to persistent stimulation with self-antigens [177]. Consistent with this model, mice with deficient expression of Fas or FasL appear unable to eliminate autoreactive $CD4^+$ T cells, which results in development of an autoimmune disease resembling SLE [166].

Persistent antigenic stimulation also occurs during chronic viral infections [178], suggesting that Fas signaling might also play a role in reducing activated T cell populations in this context [163]. Corresponding to this prediction, elevated levels activated T cells specific for murine γ-herpes virus, which causes a chronic lung infection [179], were observed following infection of $Fas^{lpr/lpr}$ mice [129]. In sum, Bim-dependent mitochondrial apoptosis is engaged under conditions where pro-survival cytokines become limiting, such as after acute infections. Fas-FasL signaling, on the other hand, is upregulated by persistent antigenic stimulation and eliminates T cells responding to self-antigens or chronic viral infections (Figure 3.8).

Lymphoproliferative autoimmune disease in Fas-deficient mice: As described in the previous section, Fas-FasL signaling is essential for limiting proliferation of autoreactive T cells. This is made apparent by the observation that mice harboring the *lpr* mutation, in which autoreactive T cells accumulate, resulting in lymphadenopathy and splenomegaly [180]. The lymphoproliferative disorder in *lpr* mice is accompanied by production of auto-antibodies against nuclear antigens including DNA, histones, and ribonuclear proteins on some strain backgrounds [166, 180, 181]. Deposition of the resulting immune complexes in the kidneys results in fatal glomerulonephritis [182]. While the *lpr* mutation causes pathogenic accumulation of lymphocytes in a variety of strain backgrounds, severity of the accompanying autoimmune disease is variable. For

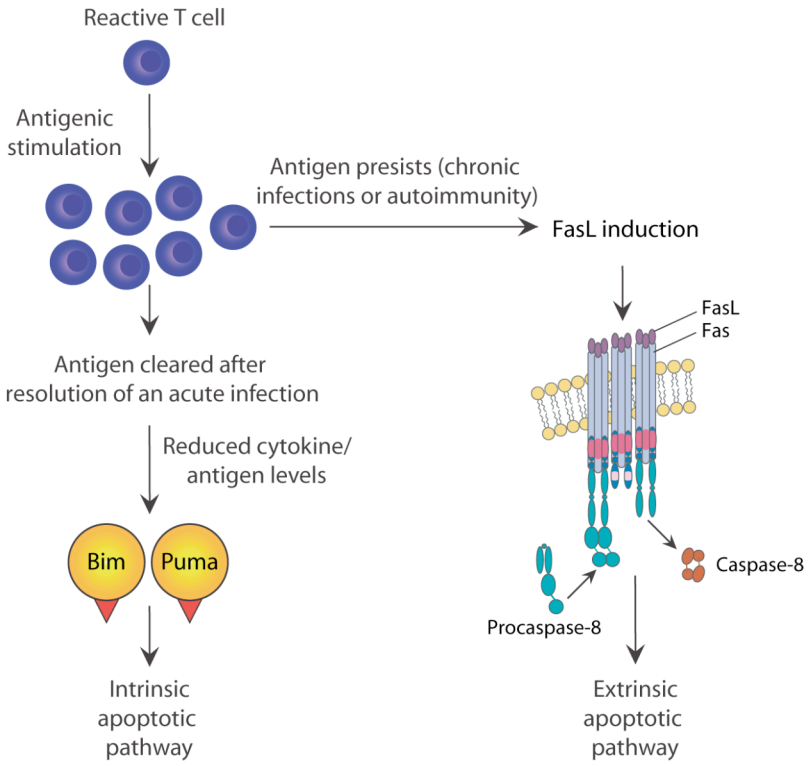

Figure 3.8 - Role of intrinsic and extrinsic apoptotic pathways in immune system homeostasis. During immune responses, T cells become activated and proliferate. If the antigen is rapidly cleared, survival factors from the tissue and from the T cells themselves become limited. As a consequence, expression of the BH3-only proteins Bim and Puma is induced, which then triggers the intrinsic apoptotic pathway. If antigen persists, however, T cells receive successive activation, resulting in increased survival factors and expression of FasL. The resulting Fas-FasL signaling eliminates persistently activated T cells via the extrinsic apoptotic pathway. Figure adopted from [177].

instance, autoimmune disease is accelerated on the MRL background, leading to 50% mortality by 6 months of age [180]. In contrast, disease severity is diminished on the C57BL/6 background, such that no change in lifespan is observed [180]. These differences suggest that genetic abnormalities in the MRL strain promote activation of autoreactive T cells, which cannot be eliminated due to defective AICD in MRL/*MpJ-Fas*^{lpr} (MRL-*lpr*) mice.

The lymphoproliferative disorder in MRL-*lpr* mice results in splenomegaly and lymphadenopathy due to accumulation of $CD4^+$ and $CD8^+$ T cells, as well as a large number of an unusual double-negative T cell subset (DN T cells), which lack both CD4 and CD8 but express the B cell marker B220 [180, 182, 183]. Due to the enormous expansion of DN T cells, this lymphoid subset was thought to be responsible for immunopathology in MRL-*lpr* animals [183]. However, treatment of MRL-*lpr* mice with a depletive anti-CD8 monoclonal antibody blocks the appearance of DN T cells without significantly attenuating autoimmune disease [184]. Depletion of $CD4^+$ T cells, in contrast, reduced autoantibody levels and ameliorated renal disease without decreasing the number of DN T cells in the spleen and lymph nodes [184]. Autoimmune disease in MRL-*lpr* mice, therefore, results from accumulation of activated autoreactive $CD4^+$ T cells, which mediate disease by mechanisms including stimulation of autoantibody production by B cells [185].

T cell activation defects in MRL-lpr mice: In a process referred to as central tolerance, immature T cells with antigen-receptors that bind tightly to self-peptides are deleted in the thymus [186, 187]. Studies of MRL-*lpr* mice that express TCRs which are genetically constrained to recognize only particular antigens have demonstrated that immature T cells are deleted normally in the thymus after injection of the corresponding antigen [188]. This finding indicates that Fas-FasL signaling does not regulate central tolerance, and as such, autoimmune disease in MRL-*lpr* mice results from an inability to restrain mature, autoreactive T cells in the spleen and other peripheral lymphoid organs [185].

As a result of negative selection in the thymus, only those autoreactive T cells expressing antigen-receptors with low affinity for self-peptides escape to the periphery [189]. As described above, peripheral tolerance is maintained by a combination of mechanisms that prevent these autoreactive T cells from mounting an immune response to self-peptides [189, 190]. For instance, repetitively stimulated autoreactive T cells can be deleted by AICD, although this mechanism is not functional in MRL-*lpr* mice [168].

Autoreactive T cells that have escaped negative selection in the thymus and migrated to the periphery are constrained by the requirement for stimulation of both their TCRs and co-receptors (e.g., CD28) to induce an activation response [191]. As described in the discussion to Chapter 2, TCR stimulation triggers a rise in intracellular Ca^{2+} that leads to dephosphorylation of nuclear factor of activated T cells (NFAT), a transcription factor that regulates many processes essential for T cell activation [192]. Ligation of CD28 potentiates T cell activation by initiating mitogen-activated protein (MAP) kinase signaling cascades leading to activation of transcription factors including AP1, CREB and NFκB [192]. Stimulation of the TCR in the absence of CD28 results in defective assembly of transcription factor complexes (e.g., binding of NFAT•AP1 complexes to the IL-2 promoter is necessary for induction of this pro-survival cytokine) and renders T cells hypo-responsive to subsequent TCR stimulation (see Chapter 2 Introduction; [193-196]). Induction of this unresponsive state, known as anergy, is an important mechanism to maintain tolerance to self-antigens and relies on the fact that such self-antigens are not accompanied by pathogen-associated inflammatory triggers such as LPS or viral DNA [190, 193, 194, 197, 198].

The increased severity of *lpr*-related autoimmune disease on the MRL background suggests that this strain might harbor genetic abnormalities that reduce the dependence of T cells on co-stimulation. The role of co-stimulation in MRL-*lpr* autoimmunity was initially addressed by genetic deletion of either CD28 or its cognate co-stimulatory molecules (e.g., B7 receptors) on APCs. Deleting CD28 reduced autoantibody production and glumeronephritis in MRL-*lpr* mice [199]. Renal pathology and serum autoantibody levels were similarly reduced in MRL-*lpr* mice lacking B7.1 and B7.2 [200]. These findings demonstrate that blocking CD28-dependent signaling in MRL-*lpr* mice from birth attenuates disease. However, because these studies use genetic approaches, they cannot address whether co-stimulatory CD28 signaling contributes to the persistent stimulation of autoreactive T cells throughout the course of disease. This distinction is clinically relevant because most SLE patients are diagnosed with active disease, and as such, prophylactic measures that only block the initial activation of autoreactive T cells are unlikely to be ideal clinical strategies [201, 202].

The role of co-stimulation in later stages of disease in MRL-*lpr* mice has been examined using a fusion protein comprised of the extracellular domain of cytotoxic T lymphocyte antigen-4 and the constant region of immunoglobulin G1 (CTLA-4Ig) [203]. Full-length CTLA-4 is a CD28 homolog that is upregulated in activated T cells and binds to B7 molecules with higher avidity than CD28 (See Chapter 3 Discussion; [204, 205]). However, unlike CD28, CTLA-4 dampens T cell activation by transducing negative co-stimulatory signals [204, 205]. CTLA-4Ig does not bind to T cells, but instead prevents transduction of co-stimulatory signals by occupying B7 molecules [206].

Administration of CTLA-4Ig in MRL-*lpr* mice immediately after weaning reduces autoantibody production, kidney disease and mortality to a similar degree as knockout of CD28 or B7.1/2 [207]. However, improved survival was reduced by >40% when treatment was initiated after two months [208], which is prior to clinical manifestations of disease [166]. A similar time-dependence is observed when CTLA-4Ig is administered to NZB/W mice, which develop a lupus-like autoimmune disease due to pathogenic expansion of germinal center B cells (see Chapter 2 Introduction). CTLA-4Ig greatly improves survival (93% after 12-months versus <10% for controls) and prevents development of serum autoantibodies when administered to five-month-old NZB/W mice [209]. In contrast, the reduction of serum autoantibody titers and improvement in survival was reduced by ~50% when treatment is started after eight months, at which points ~40% of NZB/W mice have died [209]. The reduced efficacy of CTLA-4Ig in MRL-*lpr* or NZB/W mice with established disease suggests that, while co-stimulation is necessary for the initial activation of autoreactive lymphocytes, their dependence on CD28/B7 signaling decreases over the disease course.

The reduced contribution of CD28/B7 signaling over the disease course in MRL-*lpr* mice suggests that $CD4^+$ T cells from these animals may be intrinsically (genetically) hyper-responsive to TCR stimulation even in the absence of CD28/B7 signaling. To test the intrinsic responsiveness of MRL $CD4^+$ T cells to TCR stimulation, Craft, *et al* prepared a Fas-intact MRL strain expressing a TCR restricted to binding amino acids 88-104 of pigeon cytochrome *c* (PCC) [210]. The activation response of MRL $CD4^+$ T cells was then compared to $CD4^+$ T cells from two non-autoimmune strains (CBA/CaJ and B10.BR) expressing the same restricted TCR [210]. MRL $CD4^+$ T cells display an

elevated activation response (i.e., more cell divisions and greater IL-2 production) following stimulation with PCC [210]. These differences were exacerbated by stimulation with PCC-derived peptides with reduced affinity for the TCR, which are thought to mimic the low affinity interactions of autoreactive, peripheral T cells with self-peptides [210-212]. Further studies demonstrated that TCR induced Ca^{2+} flux is elevated (two-fold) and prolonged (three-fold) in MRL $CD4^+$ T cells [213]. Intracellular Ca^{2+} flux is essential for T cell activation and the magnitude of this response correlates with the degree to which T cells proliferate and produce cytokines after TCR stimulation [214]. Hence, the enhanced activation phenotype observed in MRL-*lpr* $CD4^+$ T cells may result from exaggerated Ca^{2+} flux following antigenic stimulation, which allows these cells to avoid anergy and respond even when TCR stimulation occurs in the presence of reduced levels of co-stimulatory CD28 signaling [213].

$CD4^+$ T cells derived from MRL, CBA/CaJ, and B10.BR mice all initially proliferate after injection into mice expressing membrane-bound PCC. However, CBA/CaJ- and B10.BR-derived $CD4^+$ T cells fail to respond to subsequent *ex vivo* antigenic stimulation, which is a phenotype characteristic of anergized cells [215]. By contrast, MRL $CD4^+$ T cells proliferate and produce IL-2 in response to this subsequent *ex vivo* stimulation [215]. Collectively, these studies provide direct evidence that MRL $CD4^+$ T cells have an altered activation threshold, which predisposes them to respond productively to stimulation of the TCR with low-affinity self-antigens in the presence of reduced levels of co-stimulatory CD28 signaling.

Phosphatidylinositol-3-kinase (PI3K)-Akt signaling in MRL-lpr mice: The pronounced accumulation of lymphocytes in MRL-*lpr* mice indicates that levels of

inflammatory cytokines and other survival factors are sufficient to prevent growth-factor withdrawal induced apoptosis. A primary intracellular signaling molecule downstream of CD28 as well as cytokine and chemokine receptors is the serine/threonine kinase Akt [216]. Once activated, Akt promotes survival by several mechanisms, which include suppressing expression of the BH3-only proteins *bim* and *puma* by inhibitory phosphorylation of forkhead box O3 (FOXO3) transcription factors [217]. Activation of Akt results results from recruitment of this kinase to the inner face of the plasma membrane via interactions with the lipid second messenger phosphatidylinositol-3,4,5-triphosphate (PtdIns(3,4,5)P_3) [218]. Binding to PtdIns(3,4,5)P_3 promotes Akt activation by inducing a conformation change exposing the phospho-residues Thr308 and Ser473 [217]. Pleckstrin homology-domain kinase1 (PDK1) and mammalian target of rapamycin (mTOR) then phosphorylate Akt at Thr308 and Ser473, respectively [217]. These phosphorylation events stimulate Akt activity by stabilizing the kinase domain [219].

Once activated, Akt dissociates from the plasma membrane and promotes survival and proliferation phosphorylates by phosphosphorylation a variety of substrates in the cytoplasm and nucleus (Figure 3.9; [217]). For example, Akt phosphorylation limits the apoptotic activity of Bad by promoting association of this BH3-only protein by 14-3-3 proteins [140]. Similarly, phosphorylation of forkhead box O (FOXO) proteins by Akt sequesters this transcription factor in the cytosol by promoting binding to 14-3-3 proteins, thereby suppressing expression of the BH3-only proteins Bim and Puma [118, 220]. In addition to regulating BH3-only proteins, Akt blocks apoptosis by inhibitory

phosphorylation of caspase-9 [221], as well as inducing expression of negative regulators of apoptosis including the X-linked inhibitor of apoptosis (XIAP) and Bcl-x_L [222, 223].

PtdIns(3,4,5)P_3 are generated upstream of Akt by phosphorylation of the D3-position of the inositol ring headgroup of plasma membrane lipids by class I phosphoinositide 3-kinases (PI3Ks) [218]. PI3Ks are heterodimers of a 110-kDa catalytic subunit and a smaller, tightly-associated regulatory subunit that controls their activation and subcellular localization [218]. Class I_A PI3Ks (p110α, p110β and p110δ) are recruited to the intracellular tyrosine kinase motifs of antigen, growth factor, and cytokine receptors [224]. The Class I_B isoform PI3Kγ is driven by G-protein-coupled receptors (GPCRs) such as the CXC chemokine receptor (Figure 3.9; [224]).

Genetic deletion of the ubiquitously expressed PI3Kα and β isoforms results in embryonic lethality [225]. PI3Kδ and γ, in contrast, are expressed primarily in cells of the hematopoetic system and mice lacking either isoform are viable and have normal lifespans [224, 225]. However, PI3K$\delta^{-/-}$ and PI3K$\gamma^{-/-}$ mice display altered responses when their immune systems are acutely stressed [224, 225]. For example, T cells from mice lacking PI3Kδ display reduced proliferation and cytokine production in response to antigenic stimulation *in vitro* and blunted T cell-dependent antibody production *in vivo* [226].

PI3Kγ is primarily associated with GPCRs like the CXC chemokine receptor on APCs such as macrophages, monocytes and neutrophils as well as T cells. Chemokines emitted from damaged tissues are often responsible for recruitment of macrophages and neutrophils to sites of inflammation [227]. Consistent with the role of PI3Kγ in transmitting intracellular signals downstream of chemokine receptors, macrophages and

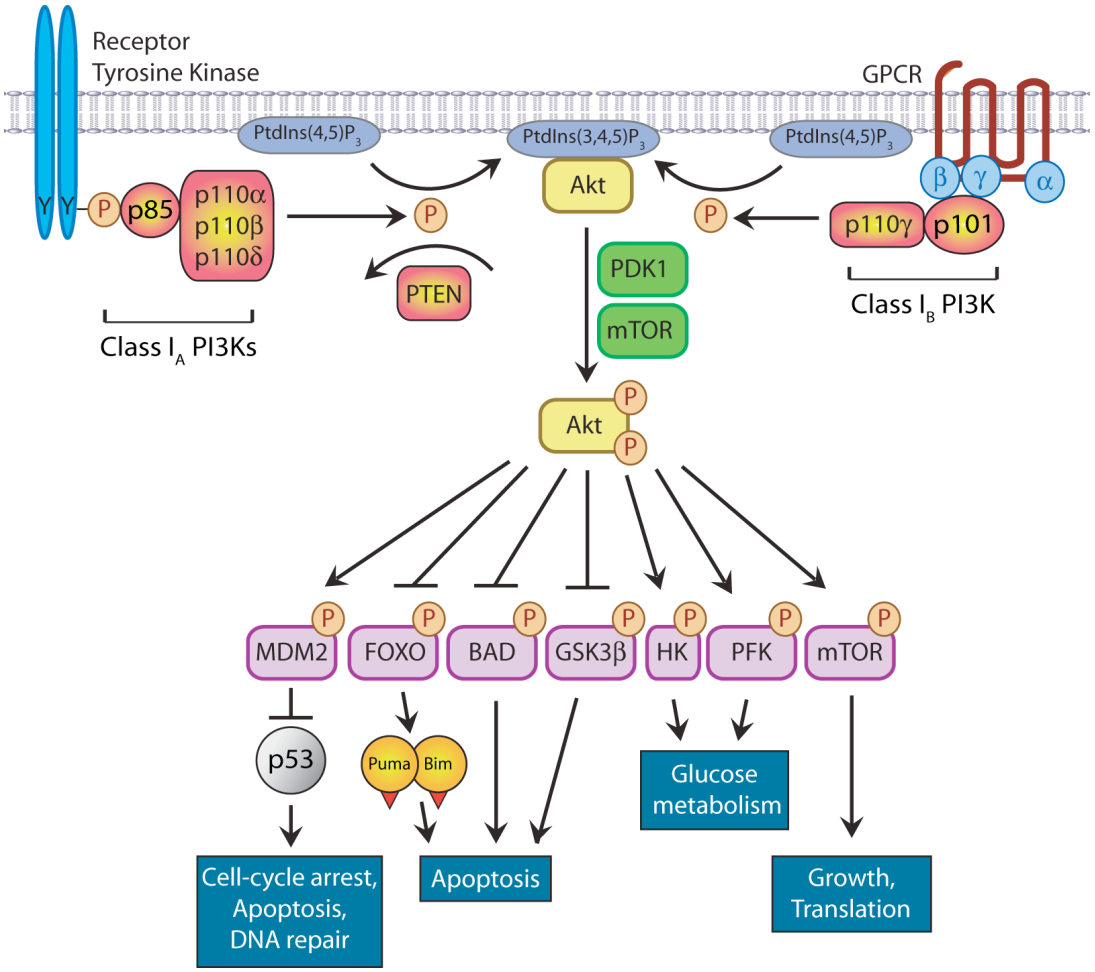

Figure 3.9 - Phosphatidylinositol-3-kinase (PI3K)-Akt signaling. In response to stimulation of cell surface receptors, class I PI3Ks are recruited to the inner face of the plasma membrane, where they generate phosphatidylinositol-3,4,5-triphosphate (PtdIns(3,4,5)P_3) by direct phosphorylation of phosphatidylinositol-4,5-diphosphate (PtdIns(4,5)P_3). Generation of PtdIns(3,4,5)P_3 is opposed by the lipid phosphatase PTEN. Class I_A PI3K isoforms (p110α, p110β and p110δ) associate with receptor tyrosine kinases through interaction their regulatory subunit (p85) with tyrosine-phosphorylated recognition motifs on the cytoplasmic domains of receptors. The only class I_B isoform (p110γ) is recruited to G-protein-coupled receptors (GPCRs) by direct interaction with G-protein βγ subunits. The lipid second messenger PtdIns(3,4,5)P_3 acts as a docking platform for the pleckstrin-homology-domain-containing kinase Akt (also known as PKB). Phosphorylation of membrane-associated Akt by pleckstrin-domain kinase1 (PDK1) and mammalian target of rapamycin (mTOR) activates Akt by stabilizing the catalytic domain. Activated Akt promotes survival and proliferation by phosphorylating a variety of substrates. MDM2, murine double minute2; FOXO, forkhead box, subgroup O; BAD, Bcl-2 agonist of cell death; GSK3β, glycogen-synthase kinase 3β; HK, hexokinase; PFK, phosphofructokinase. Figure adopted from [224, 228].

neutrophils recruitment is impaired in PI3Kγ$^{-/-}$ mice in response to seeding of *Listeria monocytogenes* or *Escherichia coli* into the peritoneal cavity [229, 230]. In addition, PI3Kγ plays a role in T cells activation by regulating formation of stable interactions with APCs [231].Because PI3Kδ and γ serve as an essential link between cell-surface receptors with intracellular signaling in haematopoietic cells, these lipid kinases are attractive targets for drug discovery [224, 228, 232].

PI3K-Akt signaling is reduced cytokine-withdrawal, which leads to induction of the intrinsic (mitochondrial) apoptotic pathway by induced of the BH3-only protens Bim and Puma. Autoreactive T cells are subject to persistent stimulation with self-antigens, which may lead to production of sufficient levels of pro-survival cytokines (e.g., IL-2) to maintain PI3K-Akt signaling. In support of this hypothesis, Carrera, *et al* found a >10-fold increase in phospho-Akt levels in splenic CD4^{+} T cells from four month-old MRL-*lpr* mice relative to age-matched controls from the non-autoimmune C57BL/6 strain [233]. Akt signaling appears to be necessary for disease in this model because reducing phospho-Akt levels with the PI3Kγ inhibitor AS605240 was accompanied by a specific reduction in activated CD4^{+} T cells as well as decreased serum autoantibody titers and renal disease [233]. In addition to the MRL-*lpr* model, elevated PI3K activity is also observed in T cells from mice with chronic graft-versus-host disease [234]. Likewise, elevated phospho-Akt levels are detected in splenic T cells from mice where lymphoproliferative autoimmune disease results from establishing the *Sle1* lupus-susceptibility allele in combination with the *Fas*$^{lpr/lpr}$ mutation on the non-autoimmune prone C57BL/6 background [235]. Collectively, these studies demonstrate that PI3K-Akt

activity is hyperactivated in MRL-*lpr* mice, along with other murine models of autoimmunity, and that modulating this signaling axis can be therapeutic.

Therapeutic effects of Bz-423 in MRL-lpr mice: The immunomodulatory benzodiazepine Bz-423 improves autoimmune glumerulonephritis in the (NZB x NZW)F_1 (NZB/W) murine model of lupus, which results from the pathogenic expansion of germinal center (GC) B cells (See Chapter 2 Introduction). Bz-423 induces apoptosis in GC-derived Burkitt's lymphoma B cell lines *in vitro*, and disease improvement in Bz-423-treated NZB/W mice is accompanied by specific apoptosis of GC B cells [236].

Mechanistic studies in Burkitt's lymphoma B cells demonstrated that a rapid rise in cellular superoxide ($O_2^{\bullet-}$) is the first detectable response induced by Bz-423 [236]. This reactive oxygen species (ROS) response is necessary for Bz-423-induced cell death because antioxidants that scavenge $O_2^{\bullet-}$ block all downstream components of the apoptotic cascade [236]. Cell fractionation experiments revealed that this response results from interaction of Bz-423 with a target in mitochondria [236]. An affinity-based screen identified the oligomycin sensitivity-conferring protein (OSCP) subunit of the mitochondrial F_oF_1-ATPase as a binding partner for Bz-423, and Bz-423 inhibits this enzyme in mitochondrial preparations and whole cells [237]. The OSCP was validated as the target responsible for Bz-423-induced inhibition of the F_oF_1-ATPase and apoptosis using biochemical reconstitution studies and RNAi [237]. Inhibition of the F_oF_1-ATPase in respiring cells both reduces ATP synthesis and induces transition from active to resting (state 3-to-4) mitochondrial respiration [238]. During a mitochondrial respiratory transition, proton motive force within the mitochondria becomes sufficiently high ($\Delta\psi_m$ >150 mV) that reactive intermediates (e.g., Fe-S clusters, flavoproteins and

ubisemiquinones) capable of one-electron reduction of molecular oxygen have extended half-lives [239]. Consistent with this mechanism, Bz-423 induce $O_2^{\bullet-}$ production is only observed in mitochondria under conditions supportive of active (i.e., state 3) respiration [236].

The selectivity of some drugs results from binding to proteins that are expressed in a disease-specific fashion. For example, iminatib mesylate selectively induces apoptosis in chronic myelogenous leukemias by inhibiting BCR-Abl, an oncogenic kinase specific to this cancer [240]. The selective effects of Bz-423 in NZB/W mice could arise from elevated expression of the OSCP in GC B cells. In support of this hypothesis, OSCP expression is greater than four-fold higher in lymphocytes relative to the median expression in all other cell types [241]. However, because the F_oF_1-ATPase is present in all nucleated cells, other factors are likely to also contribute to selectivity [238]. For instance, selective depletion of NZB/W GC B cells may in part result from phenotypic changes that sensitize these cells to Bz-423. Because NZB/W GC B cells are autoreactive, these cells are subject to persistent stimulation with self-antigens. Hence, the selective effects of Bz-423 on the GC B cells compartment of NZB/W mice may result from abnormalities associated with persistent antigenic stimulation. Specific abnormalities in autoreactive lymphocytes expected to predispose these cells to respond to Bz-423 are described in the discussion to this chapter.

The hypothesis that phenotypic changes contributes to specific apoptosis of GC B cells in NZB/W mice treated with Bz-423 suggests that similar selectivity (and therapeutic benefits) might be observed in other diseases where pathogenic cells harbor a similar phenotype. As an initial test of this hypothesis, splenocytes were isolated from

MRL-*lpr* mice and incubated with Bz-423 *ex vivo*. Under culture conditions where lymphotoxicity is observed in Burkitt's lymphoma B cells, Bz-423 caused in concentration- and time-dependent cell death in MRL-*lpr* splenocytes [242]. Analysis of B, T, $CD4^+$ T and $CD8^+$ T subsets revealed no differences in their sensitivity to Bz-423 [242]. These results indicate that the *in vitro* lymphotoxic activity of Bz-423 extends to MRL-*lpr* splenic T cells and does not depend on Fas signaling. In addition, MRL-*lpr* mice were administrated a therapeutic dose of Bz-423 (60 mpk, IP) that is therapeutic in the NZB/W mice [236, 242]) or vehicle control daily. Analysis of the spleen after one week revealed a significant decrease in $CD4^+$ T cells (12%; $p < 0.03$) as well as the atypical DN T cell subset (32%; $p < 0.005$) compared to control animals, while B cell and $CD8^+$ T cell populations were not reduced [242]. The selective reduction of $CD4^+$ and DN T cells *in vivo* suggests that the lymphotoxic activity of Bz-423 *in vivo* is modulated by factors not reproduced in *ex vivo* culture conditions. In addition, these results suggest that NZB/W GC B cells and MRL-*lpr* $CD4^+$ T cells possess a shared drug-responsive phenotype, perhaps related to pathogenic lymphocyte activation, which sensitizes them to Bz-423.

Given that autoreactive $CD4^+$ T cells mediate disease in MRL-*lpr* mice [184, 185], the reduction of this lymphoid subset in short-term dosing experiments suggests that Bz-423 might improve disease in this strain. This hypothesis was examined by treating 8 week-old MRL-*lpr* mice with Bz-423 for 14 weeks, at which point renal disease (glomerulnephritis) is severe [180]. Mice treated with Bz-423 exhibit improved renal function as evidenced by decreased proteinuria and lower levels of serum blood urea nitrogen [242]. The drugs therapeutic effect on kidney function was accompanied

by histopathological evidence showing less glomerulonephritis along with reduced immune complex deposition. Decreased kidney damage was accompanied by lower levels of autoantibodies directed to DNA as well as other nuclear antigens [242]. Importantly, a decrease in total serum immunoglobulines (IgG and IgM) was not observed, indicating that the reduction in autoantibody levels induced by Bz-423 does not result from non-specific suppression of antibody production.

In addition to these histological and serological measurements, splenic lymphocyte populations were assessed at the conclusion of treatment. An overall affect on lymphoproliferation (i.e., spleen weight) or percentage of DN T cells was not observed in Bz-423-treated mice [242]. However, a statistically significant reduction in $CD4^+$ T cells was observed (14%; $p < 0.05$), while the percentage of B cells and $CD8^+$ T cells was unchanged [242]. The reduction of $CD4^+$ T cells in Bz-423-treated MRL-*lpr* mice is consistent with data indicated that this lymphoid subset is responsible for autoantibody production and glomerulonephritis [184]. Cytokine production is a primary effector function of activated $CD4^+$ T cells. Consequently, the number of cytokine-producing splenocytes was assessed in Bz-423-treated MRL-*lpr* mice to determine if the reduction in $CD4^+$ T cells was accompanied by changes in immune effector function. These measures identified reductions in the number of cells producing IL-4 and IL-10 ($p < 0.001$ for both cytokines) [242], which promote B cell maturation and antibody production [158]. These changes were accompanied by increased number of cells secreting IFN-γ, a cytokine that stimulates macrophages and other APCs [158]. This increase is difficult to interpret because the role of IFN-γ in the MRL-*lpr* autoimmune syndrome is complex. For instance, the severity of glomerulonephritis is

reduced in IFN-γ knockout or IFN-γ-receptor deficient mice [243, 244]. However, anti-IFN-γ mAbs fail to modulate disease [245, 246], and administration of IFN-γ reduces anti-DNA autoantibody titers and improves renal disease [247]. In contrast, reduction in the number of cells secreting IL-4 and IL-10 is consistent with disease improvement. Elevated levels of both cytokines are detected in MRL-*lpr* mice [248], and IL-10 levels are reduced in MRL-*lpr* mice treated with the mitochondrial pro-oxidant Trisenox [249]. In addition, blocking IL-4 signaling by genetic deletion of this cytokine or treatment with a soluble IL-4-receptor decoy improves renal disease [243, 250].

The magnitude of the decrease in $CD4^+$ T cells is small (14%) relative to the improvement in autoimmune disease in mice administered Bz-423 for 14 wk [242]. It is possible that these two responses are disproportionate because Bz-423 induces apoptosis selectively in those autoreactive $CD4^+$ T cells responsible for disease. This hypothesis is supported by studies indicating that only 15% of $CD4^+$ T cells from SLE patients are capable of stimulating production anti-DNA autoantibody production by B cells [251, 252]. In addition, unlike the modest overall decrease in $CD4^+$ T cells profound reductions were observed in the number of cells secreting IL-4 and IL-10 [242]. Because cytokine production is a primary effector function of $CD4^+$ T cells, the greater magnitude of the effect on IL-4 and IL-10 producing cells is consistent with the hypothesis that Bz-423 acts selectively within the $CD4^+$ T cell population.

Bioenegetics of T cell activation: Resting T lymphocytes are quiescent cells with low energetic demands [253]. The energetic requirements of T cells increase in response to antigenic stimulation, which triggers rapid proliferation and secretion of effector molecules (e.g., cytokines) [254]. Activated T cells appear to meet this increased

energetic demand primarily by increasing glycolytic ATP production. While oxidative phosphorylation is upregulated following stimulation of naive T cells with mitogens or agonist antibodies against the TCR and CD28, the increase in O_2 consumption is less than two-fold [255]. In contrast, glycolytic ATP production is upregulated to a larger degree as evidenced by approximately four-fold increases in glucose uptake and lactate production [255]. Hence, activated T cells appear to meet their energy demands primarily through increased aerobic glycolysis, which is a metabolic profile characterized by increased glycolytic ATP production despite the presence of sufficient O_2 to support oxidative phosphorylation [253, 254, 256]

The reliance of activated T cells to aerobic glycolysis is surprising because oxidative phosphorylation produces >15-fold more ATP per molecule of glucose than glycolysis. One possible explanation for the reliance of activated T cells on this less efficient mechanism of ATP production is that they have limited capacity to upregulate oxidative phosphorylation. This hypothesis suggests that T cells should be unable to (1) increase O_2 consumption and (2) proliferate and produce cytokines when subject antigenic stimulation under conditions of glucose deprivation. These possibilities have been assessed by stimulation of human peripheral blood $CD4^+$ T cells with agonist antibodies against the TCR and CD28 in media containing reduced levels of glucose. While O_2 consumption is increased less than two-fold by TCR/CD28 stimulation in standard media (11 mM glucose), this change is greater than seven-fold in media where the concentration of glucose is reduced to 0.4 mM [255]. The larger increase in O_2 consumption in low-glucose media indicates that activated $CD4^+$ T cells preferentially produce ATP via aerobic glycolysis rather than fully utilizing oxidative phosphorylation.

However, this finding also suggests that activated human $CD4^+$ T cells may be able to produce sufficient ATP by oxidative phosphorylation to proliferate and produce cytokines when glucose is limiting.

The contribution of glycolytic ATP production to T cell activation responses (e.g., proliferation and cytokine production) has been assessed by antigenic stimulation of naïve T cells in glucose-free media. In these studies, increased oxidative phosphorylation appears to partially compensate for reduced glycolytic ATP production. For example, the fraction of human peripheral blood $CD4^+$ T cells proliferating in response to TCR/CD28 stimulation declined from >50% in 11 mM glucose to <20% in glucose-free media [257]. In contrast, production of the cytokines IL-2, TNF-α, IFN-γ and IL-4 was unaffected by glucose deprivation [257]. However, because cytokine production was assessed in human peripheral blood $CD4^+$ T cells stimulated with the mitogens phorbol 12-myristate 13-acetate (PMA) and ionomycin, a direct comparison with the proliferation and O_2 consumption data is not possible [257].

The effects of glucose-deprivation on T cell activation have also been assessed in murine T cells. Splenic $CD4^+$ T cells from C57BL/6J mice were unable to proliferate or produce IL-2 and IFN-γ in response to TCR/CD28 stimulation in the absence of glucose [258]. However, in media containing 0.5 mM glucose, which is comparable to conditions used in the O_2 consumption study [255], proliferation as well as production of IFN-γ and IL-2 was only reduced by ~25% relative to the response in full glucose [258]. This study, together with the effects of glucose restriction on human peripheral blood $CD4^+$ T cells, demonstrates that glycolytic ATP production is essential for maximum proliferation and cytokine production by activated T cells. However, these findings also suggest that $CD4^+$

T cells can produce sufficient ATP via oxidative phosphorylation to respond to antigenic stimulation, albeit to a reduced degree, when glucose is limiting.

The increases in glycolytic and mitochondrial ATP production in activated T cells are mediated by distinct mechanisms [253]. The PI3K/Akt pathway, which is activated in response to stimulation of CD28, plays an essential role in upregulating glucose metabolism [255]. Akt promotes trafficking of the glucose transporter Glut1 to the plasma membrane activity and stimulates activity of the glycolytic enzymes hexokinase and phosphofructokinase [253, 258]. However, Akt activation is not sufficient to trigger a conversion to aerobic glycolysis. For instance, murine $CD4^+$ T cells expressing a constitutively active Akt transgene do not increase glucose uptake and lactate production in response to TCR stimulation [258]. Instead, additional signals conveyed by CD28 activation are required to induce Glut1 expression to levels that are adequate to support aerobic glycolysis (Figure 3.10; [258]).

Whereas CD28-dependent signals promote glycolytic ATP production, TCR stimulation increases oxidative phosphorylation by modulating intracellular Ca^{2+} levels. TCR engagement promotes recruitment of kinases and adaptor molecules resulting in activation of phospholipase C-γ (PLC-γ). This enzyme mediates a key step in the TCR-induced Ca^{2+} flux by hydrolyzing phosphatidylinositol-3,5-bisphosphate to inositol-1,4,5-trisphosphate ($InsP_3$). Binding of this second messenger to $InsP_3$ receptors on the endoplasmic reticulum (ER) leads to release of Ca^{2+} stored in this organelle. Intracellular Ca^{2+} levels are further elevated following depletion of ER stores by uptake of extracellular Ca^{2+} through plasma-membrane calcium release-activated Ca^{2+} (CRAC) channels [214]. These processes combine to increase in intracellular Ca^{2+} approximately

two-fold (from ~75 to ~150 nM) within seconds of TCR engagement [259]. This early rise in intracellular Ca^{2+} is followed by a decline to basal levels over the period of 1 h [259]. Increased intracellular Ca^{2+} promotes proliferation and cytokine production, in part, by activating transcription factors such as nuclear factor of activated T cells (NFAT) and cAMP response element-binding protein (CREB) [214]).

In addition to promoting Ca^{2+}-dependent gene transcription, TCR-induced Ca^{2+} flux stimulates the tricarboxylic acid (TCA)-cycle due to uptake of intracellular Ca^{2+} into the matrix by transient opening of the mPT pore [260]. Elevated matrix Ca^{2+} stimulates the TCA-cycle enzyme pyruvate dehydrogenase (PDH) by increasing the activity of PDH phosphatase, which dephosphorylates and activates PDH. In addition, increased matrix Ca^{2+} directly activates isocitrate dehydrogenase and oxoglutarate dehydrogenase by lowering the K_m of these enzymes. Stimulation of these Ca^{2+}-dependent TCA-cycle dehydrogenases results in a greater than two-fold increase in NADH levels [259]. Elevated levels of NADH then stimulate the MRC causing proton transport to outpace dissipation of $\Delta\psi_m$ by the passage of protons through F_o during ATP synthesis. While this effect promotes production of ATP by the F_oF_1-ATPase, it also forces the MRC into a reduced state characterized by elevated $\Delta\psi_m$ and increased $O_2^{\bullet-}$ production [254, 259, 261].

Increased mitochondrial $O_2^{\bullet-}$ production appears to play an essential signaling role in T cell activation. This possibility was first suggested by the observation that intracellular H_2O_2 and $O_2^{\bullet-}$ levels are elevated within 10 minutes of TCR stimulation [262, 263]. The contribution of this ROS response to T cell activation was then demonstrated by the ability of antioxidants to limit proliferation and cytokine production

induced TCR stimulation. For instance, reducing H_2O_2 with the glutathione peroxidase mimetic Ebselen or ectopic expression of catalase reduced proliferation of TCR/CD28 stimulated murine $CD4^+$ T cells by >80% [259]. This suggests that, like $InsP_3$ and Ca^{2+}, H_2O_2 is an essential second messenger in the signaling cascade leading to T cell activation (Figure 3.10).

The MRC is not the sole source of H_2O_2 in activated T cells. H_2O_2 can also be produced by a plasma membrane NADPH oxidase following TCR stimulation [263]. T cells from mice in which this enzyme is not functional (*Ncf1*$^{-/-}$ and *Cybb*$^{-/-}$) display a ~40% reduction in H_2O_2 production following TCR stimulation [263]. In contrast, the flavin-modifying compound diphenylene iodonium (DPI), which inhibits both NADPH oxidase and complex I of the MRC, reduced production of H_2O_2 by >75% following TCR stimulation [263]. As suggested by the role of H_2O_2 as second messenger in T cell activation, DPI causes a concentration-dependent decrease (maximum inhibition >80%) in TCR induced proliferation of murine $CD4^+$ T cells [259]. Along with DPI, the complex I inhibitors rotenone, piercidin A, and metformin all induce concentration-dependent reductions in H_2O_2 levels following TCR stimulation [264]. Likewise, knockdown of the chaperone protein NADPH dehydrogenase (ubiquinone) 1α subcomplex, assembly factor 1 (NDUFAF1), which is required for complex I assembly, decreased H_2O_2 levels by >90% following TCR stimulation [264]. The magnitude of this effect suggests that production of H_2O_2 downstream of the plasma membrane NADPH oxidase is signaled by H_2O_2 generated by complex I of the ETC.

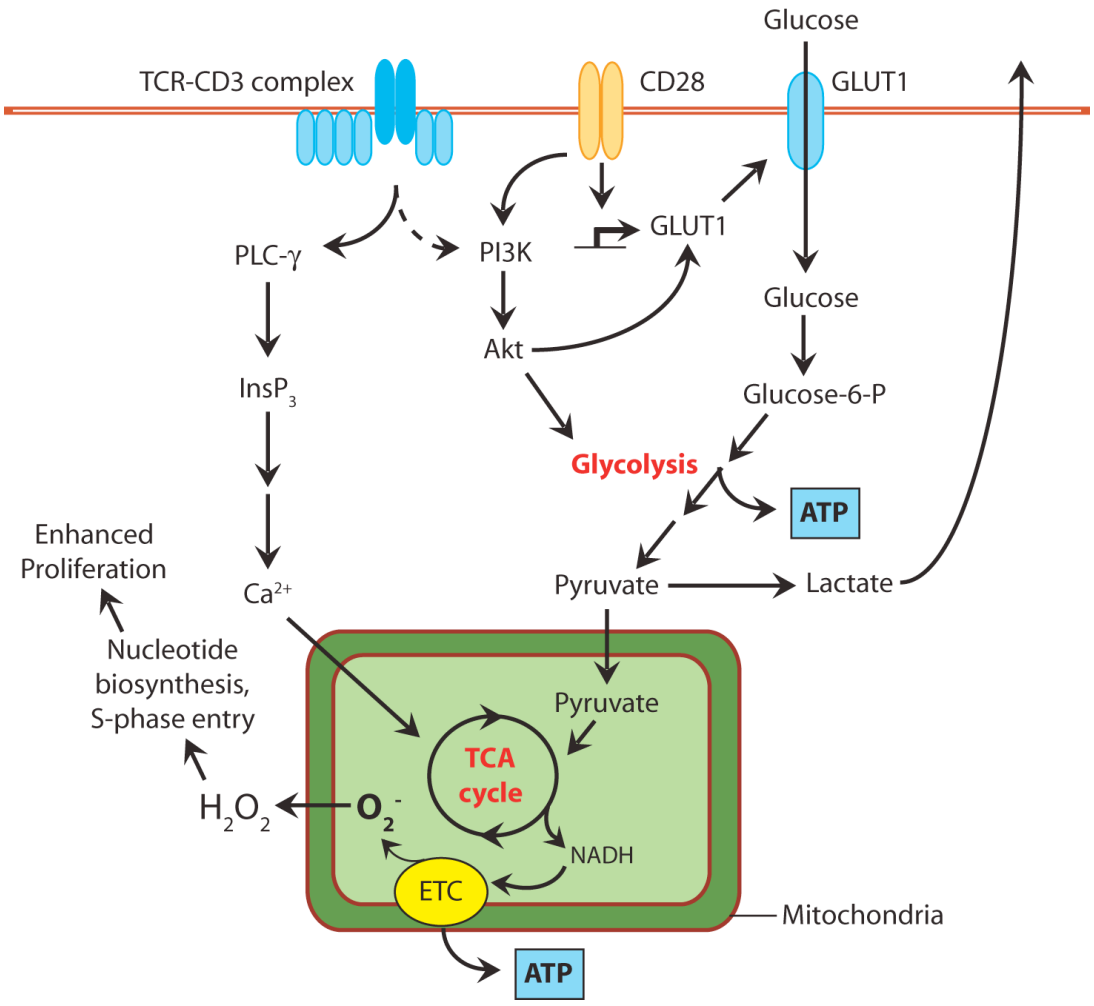

Figure 3.10 - Energy metabolism during T cell activation. Stimulation of the co-receptor CD28 enhances glucose utilization. This results primarily from PI3K-dependent activation of Akt, which promotes localization of the glucose transporter GLUT1 to the plasma membrane and enhances the activity of glycolytic enzymes. However, Akt-independent signals downstream of CD28 are required to induced GLUT1 expression. Stimulation of the T cell-receptor (TCR)-CD3 complex triggers an intracellular Ca^{2+} flux (see text for details). Uptake of elevated intracellular Ca^{2+} into the mitochondrial matrix stimulates Ca^{2+} dependent tricarboxylic acid (TCA)-cycle enzymes, resulting in a doubling of NADH. Increased NADH levels stimulates activity of the electron transport chain (ETC), which both increases production of ATP via oxidative phosphorylation and release of superoxide ($O_2^{\bullet-}$) from complex I into the matrix. Because the mitochondrial inner membrane is impermeable to charged species, $O_2^{\bullet-}$ released into the matrix is converted to H_2O_2 prior to release from the mitochondria. H_2O_2 derived from the ETC serves an essential second messenger that stimulates T cell proliferation in response to TCR/CD28 stimulation. Figure adopted from [254].

Analysis of the "topology" of ROS production by the MRC indicates that complex I selectively releases $O_2^{\bullet-}$ into the matrix (See Chapter 1). Because the mitochondrial inner membrane is impremeable to charged species, $O_2^{\bullet-}$ released into the matrix must dismutate to H_2O_2 in order to escape from mitochondria. Dismutation of $O_2^{\bullet-}$ into H_2O_2 occurs spontaneously (k = 4.5 x 10^5), but is accelerated in the matrix by MnSOD (k = 1.2 x 10^9) [265]. This suggests a model whereby the TCR induced H_2O_2 response is derived from dismutation of $O_2^{\bullet-}$ released into the matrix by complex I.

This proposal is at odds with data demonstrating that the MnSOD mimetic MnTBAP causes an ~50% decrease in IL-2 production by activated murine T cells [266]. If increased H_2O_2 levels are an essential signal for T cell activation, MnTBAP would be expected to promote T cell activation by converting $O_2^{\bullet-}$ generated by the MRC into H_2O_2. However, commercial lots of MnTBAP can possess both SOD and catalase activity resulting in the full reduction $O_2^{\bullet-}$ to water rather than simply dismutation to H_2O_2 [267]. As such, the inhibitory effects of MnTBAP on T cell activation might result from its SOD *and* catalase activity. This explanation is supported by two studies in which MnTBAP was shown to reduce $O_2^{\bullet-}$ *and* H_2O_2 production induced by TCR stimulation [262, 268]. Unfortunately, TCR/CD28 induced proliferation and cytokine production has not been assessed in T cells with elevated levels of MnSOD. However, Marrack, *et al*. has shown that MnSOD overexpression fails to protect T cells from apoptosis induced by staphylococcal enterotoxin B (SEB) [131]. This "superantigen" pathologically activates the fraction of T cells (~20%) that express a TCR bearing variable β chain motif 8 (Vβ8) [269]. In contrast, catalase overexpression caused a three-

fold increase survival of Vβ8$^+$ T cells following stimulation with SEB, which suggests that H_2O_2 is necessary for this response [131].

In sum, although glycolytic ATP production is increased to a greater extent than oxidative phosphorylation in activated T cells, alteration of mitochondria function appears to play a role in this response. Stimulation of the TCR triggers an intracellular Ca^{2+} flux. Uptake of excess intracellular Ca^{2+} into the mitochondrial matrix leads to a doubling of NADH levels by stimulating Ca^{2+}-dependent TCA-cycle enzymes. Increased NADH stimulates mitochondrial ATP production allowing T cells to respond (albeit partially) to antigenic stimulation when glucose is limiting. In addition, increased NADH levels force the MRC into a reduced state favoring production of $O_2^{\bullet-}$. This ROS is then is converted to H_2O_2, which is an essential second messenger in the T cell activation cascade. Hence, Ca^{2+}-dependent changes in mitochondrial bioenergetics occurs during T cell activation even though the majority of cellular ATP is produced via glycolysis.

Statement of Problem: Prior work in Burkitt's lymphoma B cells has established that Bz-423-induced apoptosis is signaled by a rise in intracellular $O_2^{\bullet-}$ within the first hour of treatment. This ROS response results from modulation of the mitochondrial F_oF_1-ATPase. Bz-423 slows the rate of ATP synthesis by the F_oF_1-ATPase, which forces the ETC into a reduced state favoring production of $O_2^{\bullet-}$. Although Bz-423-induced $O_2^{\bullet-}$ is necessary for downstream apoptotic changes (e.g., cytochrome *c* release), the signal transduction pathway linking $O_2^{\bullet-}$ to the apoptotic machinery had not been determined. In addition, although Bz-423 kills MRL-*lpr* T cells, studies of Bz-423-induced apoptosis have been primarily carried out in B cells so it was unknown whether a similar process was engaged in T cells. To address these questions, the apoptotic response initiated by

Bz-423-induced $O_2^{\bullet-}$ was characterized in several $CD4^+$ T cell leukemia lines. These experiments identified factors that dictate if and how a cell responds to perturbation of mitochondrial bioenergetics with Bz-423. Identification of these factors, in turn, provided insight into the basis for the selective effects of Bz-423 on pathogenic lymphocytes (e.g., MRL-*lpr* $CD4^+$ T cells) *in vivo*.

RESULTS

Choice of system: The apoptotic response to Bz-423 was characterized in the Jurkat, MOLT-4, and CCRF-CEM human $CD4^+$ T cell leukemia lines. Transformed T cells were employed rather than primary MRL-*lpr* $CD4^+$ T cells because they can be continuously cultured and are more amenable to genetic manipulation [270]. The Jurkat, MOLT-4 and CCRF-CEM T cells lines were specifically studied because these lines are deficient in phosphatase and tensin homolog (PTEN) [271]. Lack of PTEN renders PI3K activity unopposed in these lines, which results in constitutive activation (i.e., phosphorylation) of Akt [272, 273]. Elevated phospho-Akt levels in these T cell leukemia lines is similar to the Akt activation state in MRL-*lpr* $CD4^+$ T cells (see Chapter 3 Introduction; [233]).

Bz-423 has cytotoxic activity in $CD4^+$ T cell leukemia lines: Akt activation is a pleotropic stimulus that promotes survival and proliferation by blocking apoptosis and stimulating glucose metabolism (see Chapter 3 Introduction). In terms of glucose metabolism, Akt stimulates activity of the glycolytic enzymes hexokinase and phospho-fructokinase and promotes trafficking of the glucose transporter Glut1 to the plasma membrane [253, 258]. Perhaps due to these effects resulting from constitutive Akt activation, comparisons of lactate production and O_2 consumption indicate that Jurkat T cells produce the majority (60-70%) of their ATP by glycolysis [274-276].

The primary dependence of Jurkat T cells on glycolytic ATP production suggests that this cell line may not be susceptive to killing by agents that impair oxidative phosphorylation. In support of this hypothesis, Jurkat T cells remain viable for 24 h when treated with concentrations of oligomycin >100-fold K_i ~10 nM (Figure 3.11A and

[277]). Oligomycin is cytotoxic in Jurkat T cells at >500-fold K_i (Figure 3.11A). However, at these micromolar concentrations, oligomycin also inhibits the vacuolar H^+-ATPase (V-ATPase) [278], which is an ATP-driven H^+ pump responsible for acidification of lysosomes [279]. Specific V-ATPase inhibitors (e.g., bafilomycin A) are cytotoxic [280-282], which suggests inhibition of V-ATPases may contribute to cell death induced by concentrations of oligomycin (>5 μM) in Jurkat T cells (Figure 3.11A). The resistance of Jurkat T cells to cell death induced by concentrations of oligomycin <5 μM does not appear to result from impaired uptake of this F_oF_1-ATPase inhibitor into cells or mitochondria. This is because oligomycin inhibits oxidative phosphorylation (i.e., O_2 consumption) in Jurkat T cells with an IC_{50} ~25 nM (Figure 3.11A), which is near the K_i for inhibition of the F_oF_1-ATPase by oligomycin in mitochondrial preparations [283]. These data indicate that Jurkat T cells are resistant to cell death induced by suppression of oxidative phosphorylation by inhibiting the F_oF_1-ATPase with oligomycin.

An explanation for the ability of Jurkat T cells to survive in the presence of concentrations of oligomycin that inhibit oxidative phosphorylation by >85% could be that this cell type generates sufficient ATP via glycolysis to compensate for a block in mitochondrial ATP production. This hypothesis is supported by studies demonstrating that Jurkat T cells produce ~65% of their ATP via glycolysis, and the remaining ~35% by oxidative phosphorylation [274-276]. Additionally, these studies suggest that inhibition of glycolysis is likely to have a larger effect on ATP levels in Jurkat T cells than suppressing oxidative phosphorylation with oligomycin. Nevertheless, the capacity of the Jurkat T cells used in this study to maintain ATP levels when oxidative phosphorylation is impaired was evaluated by treatment with a concentration of

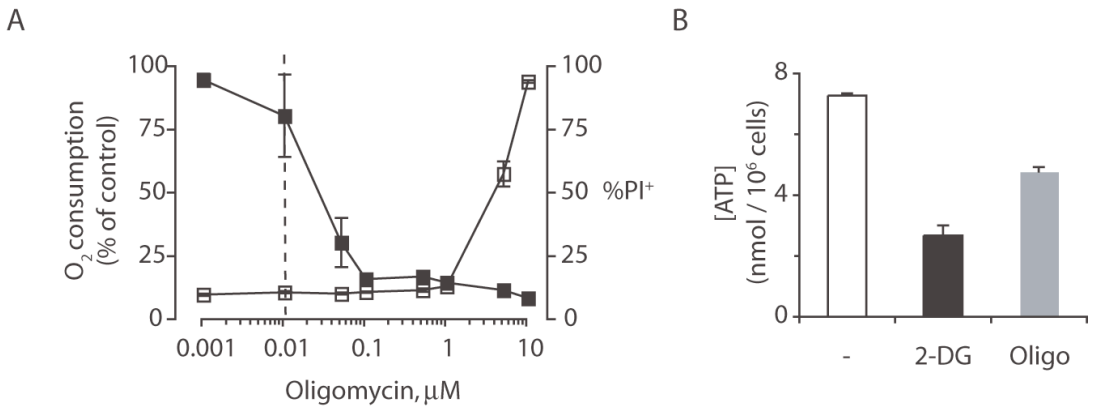

Figure 3.11 - Jurkat T cells are resistant to cell death resulting from inhibition of oxidative phosphorylation with oligomycin. (A) Jurkat T cells were treated with the indicated concentrations of oligomycin and O_2 consumption (■) was measured after 1 h using a BD oxygen biosensor system, while cell death (□) was quantified in terms of PI permeability after 24 h. Dashed line: K_i for inhibition of the F_oF_1-ATPase by oligomycin in mitochondrial preparations [283]. (B) Jurkat T cells were treated with oligomycin (Oligo; 0.5 μM) or 2-deoxyglucose (2-DG; 250 mM) and, at which point cells were lysed with perchloric acid and intracellular ATP levels quantified using a luciferin-luciferase assay. Data is representative of two independent experiments.

oligomycin (0.5 μM) that inhibits O_2 consumption by >85%, but is not cytotoxic (Figure 3.11A). As a control, Jurkat T cells were also treated with 2-deoxyglucose (2-DG), a metabolically inactive glucose analog that reduces glycolytic ATP production by inhibiting hexokinase [284]. In this experiment, oligomycin reduced ATP levels by ~35% in Jurkat T cells after 1 h (Figure 3.11B). In contrast, 2-DG caused a larger reduction in cellular ATP levels (>65%) at the same timepoint (Figure 3.11B). These data suggest that suppressing oxidative phosphorylation with oligomycin is not lethal in Jurkat T cells because they primarily generate ATP via glycolysis. Furthermore, this decreased reliance on oxidative phosphorylation suggests that Jurkat T cells, and other PTEN-deficient T cell leukemia lines, might be desensitized to Bz-423-induced apoptosis, which also results from modulation of the F_oF_1-ATPase [237].

Along with stimulating glucose metabolism, Akt activation promotes survival by suppressing pro-apoptotic signals as well as stabilizing negative regulators of apoptosis (see Chapter 3 Introduction). Hence, constitutive activation of Akt in Jurkat, MOLT-4 and CCRF-CEM T cells is expected suppress apoptosis in these lines. The hypothesis that constitutive Akt activation acts as a barrier to apoptosis in PTEN-deficient T cell lines is supported by the observation that Jurkat, MOLT-4 and CCRF-CEM T cells are killed by the PI3K inhibitor LY294002, which is not cytotoxic in the T cell leukemia line HUT-78, which expresses PTEN [271]. In addition, sub-toxic concentrations of LY294002 sensitize Jurkat T cells to apoptosis induced by the histone deacetylase inhibitor MS-275, the DNA-damaging agent cytosine arabinoside, and 2-methoxyestradiol (2ME), which is thought to stimulate mitochondrial $O_2^{\bullet-}$ production by inhibiting SODs [285-287].

Constitutive activation of Akt stimulates glucose metabolism and suppresses apoptosis, two effects which could desensitize Jurkat T cells and other PTEN-deficient T cell leukemia lines to Bz-423-induced cell death. This possibility was evaluated by comparing lymphotoxic activity of Bz-423 in Jurkat, MOLT-4 and CCRF-CEM T cells to Ramos B cells, a $PTEN^{+/+}$ Burkitt's lymphoma line in which the majority of mechanistic studies of Bz-423-induced apoptosis have been conducted [236, 237, 288-292]. Despite the potentially inhibitory effects of constitutive Akt activation, the T cell leukemia lines were sensitive to Bz-423-induced cell death after 24 h, with EC_{50} values similar to that observed for Ramos B cells under equivalent culture conditions (Table 3.1). (Figure 3.12C). Surprisingly, this concentrations of oligomycin only increased the fraction of cells with elevated intracellular $O_2^{\bullet-}$ levels by 22% (Figure 3.12B).

Cell Line	Cell Type	PTEN Status	Cell Death
Ramos	Burkitt's B Cell Lymphoma	+	6.1 ± 0.2
Jurkat	T Cell Leukemia	-	7.0 ± 0.3
CCRF-CEM	T Cell Leukemia	-	7.8 ± 0.3
MOLT-4	T Cell Leukemia	-	5.9 ± 0.6

Table 3.1 - Lymphotoxic activity of Bz-423 against T cell leukemia lines. Cell death was quantified in terms of PI permeability after 24 h. EC_{50} values (μM) were calculated in triplicate via non-linear regression of the corresponding dose-response curves.

Modulation of the F_oF_1-ATPase by Bz-423 increases $O_2^{\bullet-}$ production without depleting ATP: There are two consequences of inhibition of the F_oF_1-ATPase in cells undergoing active (i.e., state 3) respiration (see Chapter 1). First, the rate of mitochondrial ATP synthesis is reduced [293, 294]. Second, passage of protons through the F_o channel is blocked, which result in their accumulation in the MIS and hyperpolarization of $\Delta\psi_m$ (>150 mV) [293, 294]. Increased proton motive force under these conditions (i.e., state 4 respiration) slows electron transport by the MRC, such that reactive intermediates (e.g., Fe-S clusters, flavoproteins, and ubisemiquinones) capable of single-electron reduction of O_2 are more reduced on average [239]. Transfer of electrons from these reactive intermediates to O_2 is expected to underlie the increase in mitochondrial $O_2^{\bullet-}$ production during state 4 respiration [295]. As described in Chapter 1, an increase in intracellular $O_2^{\bullet-}$ levels can signal apoptosis by a variety of mechanism including activation of the cytosolic redox sensor ASK1, which leads to activation of the downstream MAP kinases such as p38 MAPK and JNK. Therefore, along with effects on mitochondrial ATP synthesis, modulating the F_oF_1-ATPase may induce apoptosis by stimulating production of $O_2^{\bullet-}$ by the MRC.

Jurkat T cells are resistant to cell death induced by concentrations of oligomycin that inhibit mitochondrial respiration by >85% (Figure 3.11A and [277]), presumably because this cell line generates ATP primarily via glycolysis [274-276]. However, Jurkat T cells (and other PTEN-deficient T cell leukemia lines) are sensitive to killing by Bz-423. This contrast between Bz-423 and oligomycin suggests that Bz-423-induced cell death is signaled by an increase in intracellular $O_2^{\bullet-}$ levels, rather than depletion of ATP. In support of this hypothesis, intracellular $O_2^{\bullet-}$ levels are elevated in Ramos B cells treated with Bz-423 for one hour [236]. In addition, scavenging Bz-423-induced $O_2^{\bullet-}$ with the antioxidants MnTBAP or vitamin E blocks killing in Ramos B cells [236, 290, 296].

As an initial test of the hypothesis that the lymphotoxic activity of Bz-423 in Jurkat T cells results from increased mitochondrial $O_2^{\bullet-}$ production rather than depletion of ATP, intracellular $O_2^{\bullet-}$ and ATP *levels* were evaluated in Jurkat T cells treated with Bz-423. $O_2^{\bullet-}$ was measured with dihydroethidium (DHE), a redox-sensitive dye that is specifically oxidized by this ROS (Figure 3.12A; [297]). To measure ATP levels, cells were lysed with perchloric acid and insoluble proteins removed by centrifugation. The resulting supernatants were neutralized and ATP levels were quantified with a luciferin-luciferase assay [298]. Similar to the observations in Ramos B cells, treatment of Jurkat T cells with Bz-423 for 2 h resulted in a concentration-dependent increase in intracellular $O_2^{\bullet-}$ levels with >80% cells displaying elevated DHE staining at 10 μM (Figure 3.12B). In contrast, cellular ATP levels were not reduced by Bz-423 at this timepoint (Figure 3.12C). Oligomycin (0.5 μM) reduced cellular ATP levels by ~40% at this timepoint

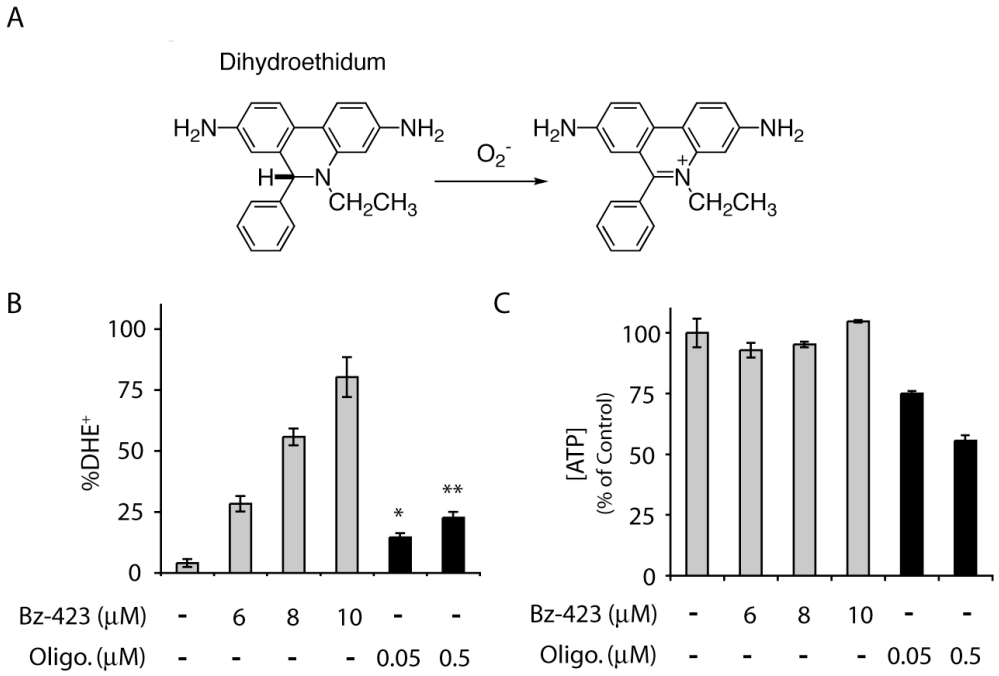

Figure 3.12 - Bz-423 elevates intracellular $O_2^{\bullet-}$ levels without depleting ATP. (A) Oxidation of dihydroethidium (DHE) by $O_2^{\bullet-}$ generates hydroethidum, which intercalates into DNA resulting in increased red fluorescence (λ_{max} 567 nm) [299]. (B and C) Jurkat T cells were incubated with vehicle, indicated concentrations of Bz-423 or oligomycin (Oligo) for 2 h, at which point (B) intracellular $O_2^{\bullet-}$ levels where measured by DHE staining or (C) cells were lysed with perchloric acid and intracellular ATP levels quantified using a luciferin-luciferase assay. *, P <0.05; **, P <0.005. Data is representative of at least four separate experiments.

These data highlight a significant contrast between the cellular consequence of modulting the F_oF_1-ATPase with Bz-423 or oligomycin. Bz-423 increases intracellular $O_2^{\bullet-}$ levels without depleting ATP, while oligomycin significantly reduces ATP but promotes a modest $O_2^{\bullet-}$ response. It is unclear why concentrations of oligomycin that reduce O_2 consumption by >85%, and deplete ATP levels, elevate intracellular $O_2^{\bullet-}$ levels to a lesser extent than Bz-423. However, differences in the binding site and affinity of these two F_oF_1-ATPase inhibitors may contribute to these contrasting effects. Oligomycin binds within F_o, while the recognition site for Bz-423 is the OSCP

[237], which is a component of the peripheral stalk of the F_oF_1-ATPase. In addition, oligomycin is ~10^3 fold higher affinity inhibitor of the F_1F_o-ATPase than Bz-423 (K_i ~10 nM and 10 μM, respectively) [283]. Because oligomycin directly binds to F_o, it may more effectively block passage of protons through this channel than Bz-423. Therefore, oligomycin may trigger regulatory mechanisms (e.g., activation of mitochondrial uncoupling proteins in response to hyperpolarization of $\Delta\psi_m$; [300]), which are not engaged by moderate affinity inhibitors such as Bz-423. In support of this hypothesis, the moderate affinity F_1F_o-ATPase inhibitor 3,3'-diindolylmethane (DIM; K_i ~25 μM) elevates intracellular ROS levels in MCF-7 human mammary carcinoma cells by >70% within 1 h, but only depletes ATP levels by ~10% at this timepoint [301]. In addition, like Bz-423, the pro-apoptotic and growth-inhibitory activities of DIM are blocked by anti-oxidants [301, 302]. Effects of oligomycin, Bz-423 and DIM on the F_oF_1-ATPase are considered in more detail in the discussion to Chapter 3.

A possible explanation for the lack of an effect of Bz-423 on cellular ATP levels in Jurkat T cells is that Bz-423 is unable to inhibit the F_oF_1-ATPase in this cell type. This is explanation is unlikely, however, because the OSCP and other components of the F_oF_1-ATPase are present in Jurkat T cells (Figure 3.13A). In addition, although Jurkat T cells rely heavily on glycolysis, the effects of oligomycin on O_2 consumption and cellular ATP levels suggest that the F_oF_1-ATPase is active. Nevertheless, to exclude this possibility, the effect of Bz-423 on mitochondrial ATP synthesis *rates* was examined in Jurkat T cells. For this assay, Jurkat T cells were permeabilized with digitonin, a detergent that preferentially disrupts the plasma membrane [303, 304].

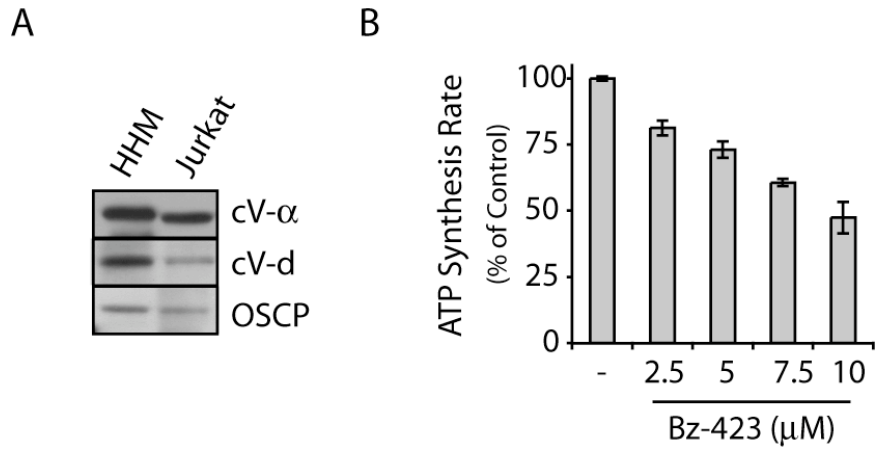

Figure 3.13 - Bz-423 inhibits mitochondrial ATP synthesis in Jurkat T cells. (A) Lysates from human heart mitochondria (HHM) or Jurkat T cells were immunoblotted with antibodies specific for the OSCP, or subunits α (cV-α) or d (cV-d) of the F_oF_1-ATPase. (B) Jurkat T cells were permeabilized with digitonin, ADP and malate/glutamate were added and cells were treated with the indicated concentrations of Bz-423. The rate of ATP synthesis was measured using a luciferase-luciferin reporter assay and ΔRLU was converted to ΔATP using an ATP standard curve. Data are representative of two independent experiments.

Selective permeabilization of the plasma membrane depletes glycolytic enzymes from the cytosol, which forces Jurkat T cells to generate ATP solely by oxidation of exogenous respiratory substrates [298]. In this experiment, ETC activity was stimulate by the addition of malate and glutamate, which promotes production of the complex I substrate NADH by the TCA cycle [298]. Malate and glutamae were employed, rather than the complex II substrate succinate, because complex I supported respiration is thought to better reflect physiological MRC activity [303]. Finally, mitochondrial ATP production in permeabilized Jurkat T cells respiring on malate and glutamate was quantified using a luciferin-luciferase assay [298].

As observed in mitochondrial preparations and Ramos B cells, incubation of permeabilized Jurkat T cells with Bz-423 resulted in a concentration-dependent decrease in the rate of mitochondrial ATP synthesis (Figure 3.13B). These data demonstrates that the lack of an effect of cytotoxic concentrations of Bz-423 on cellular ATP *levels* in Jurkat T cells does not result from an inability to inhibit mitochondrial ATP synthesis. Rather, maintenance of cellular ATP levels in the presence of Bz-423 may arise from the capacity of Jurkat T cells to compensate for a ~50% decrease in F_oF_1-ATPase activity by upregulating other components of the oxidative phosphorylation machinery as well as increasing glycolytic ATP production (see Chapter 3 Discussion).

Bz-423-induced apoptotic changes in T cells: Incubation of Jurkat T cells with Bz-423 for 24 h results in cell shrinkage, cytoplasmic vacuolization, membrane blebbing and chromosomal condensation, which are morphological evidence of apoptosis (Figure 3.14A). These changes are accompanied by biochemical evidence of apoptotic DNA fragmetation (Figure 3.14B). To characterize the apoptotic mechanism in Jurkat T cells, changes in $\Delta\psi_m$, release of apoptogenic proteins from the MIS, caspase activation and the appearance of hypodiploid DNA were measured over time. These endpoints were selected in order to compare the response in T cells with apoptotic indicators already determined in Ramos B cells treated with Bz-423 [236]. $\Delta\psi_m$, monitored using the mitochondria-selective potentiometric probe tetra-methyl rhodamine methylester (TMRM) [305], began to collapse after 3 h, and by 7 h was depolarized in >80% of cells. The time-course of caspase activation, detected by proteolytic cleavage of the pan-caspase-sensitive fluorescent substrate carboxyfluorescein-Val-Ala-Asp-fluoromethyl ketone (FAM-VAD-fmk), lagged behind the collapse of $\Delta\psi_m$ such that >40% of cells

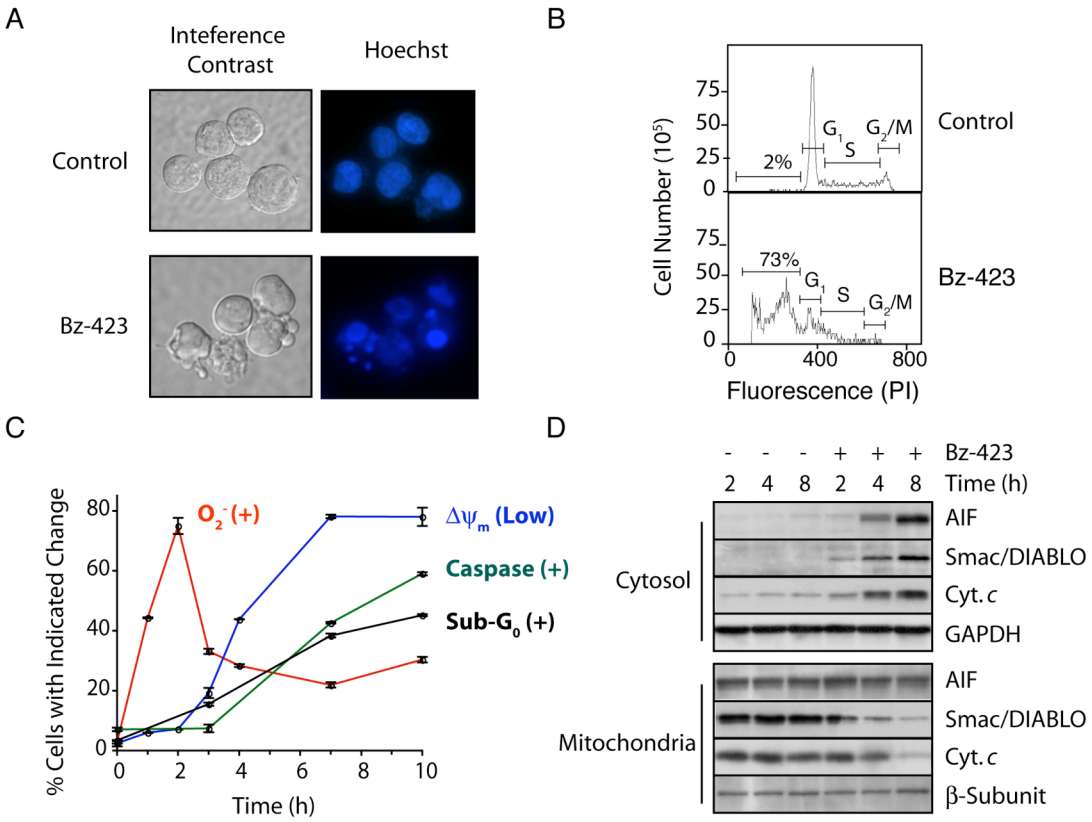

Figure 3.14 - Apoptotic changes induced by Bz-423 in Jurkat T cells. (A) Jurkat T cells were labeled with nuclear stain Hoechst (0.5 μg/mL), treated with vehicle or Bz-423 (10 μM) and analyzed by fluorescence and differential interference contrast micrographs (630x) after 16 h. (B) Jurkat T cells were treated (24 h) with Bz-423 (10 μM) or vehicle and DNA content was assessed by PI staining. (C) Jurkat T cells were treated with Bz-423 (10 μM) and data is presented as percent cells with indicated response relative to time matched vehicle controls. No significant changes in vehicle treated cells were observed during this timeframe. Absence of error bars indicates <1% standard deviation. (D) Jurkat T cells were treated with Bz-423 (10 μM) and separated into mitochondrial and cytosolic fractions at the indicated times, which were then immunoblotted with antibodies for AIF, Smac/DIABLO, cytochrome *c* (Cyt. *c*), GAPDH and β-subunit of the F_oF_1-ATPase. Data for all panels is representative of at least three experiments.

were positive by the caspase assay at 7 h. Finally, apoptotic DNA fragmentation was detected over a time-course similar to caspase activation (Figure 3.14C).

Release of apoptogenic proteins (e.g., cytochrome *c*, Smac/DIABLO, AIF) from the MIS is often the point at which a cell commits to undergo apoptosis [13]. Cytochrome *c* and Smac/DIABLO promote apoptosome formation and inhibit IAPs, respectively [1, 6]. AIF is an endonuclease that is released from the MIS following caspase activation [8]. To determine if Bz-423 induces release of proapoptotic MIS proteins, cytosolic and mitochondrial fractions of Bz-423-treated Jurkat T cells were separated and immunoblotted for cytochrome *c*, Smac/DIABLO and AIF. Cytochrome *c* and Smac/DIABLO were detected in the cytosol by 4 h and were significantly depleted from mitochondrial fractions by 8 h (Figure 3.14D). Although increased AIF levels are evident in the cytosol by 4 h, this protein was not depleted from mitochondrial fractions by 8 h. Singe cell analysis with fluorescently-tagged variants of cytochrome *c*, Smac/DIABLO and AIF has demonstrated that, while cytochrome *c* and Smac/DIABLO undergo rapid, complete release in response to apoptotic stimuli, AIF release is slower and caspase-dependent [12]. Based on this precedent, complete release of AIF may not occur until after 8 h because <50% of Bz-423-treated Jurkat T cells are positive for caspase activation at this time point. These results demonstrate that release of pro-apoptotic MIS proteins occurs in response to Bz-423 and the timing of this response, which begins at 4 h, coincides with collapse of $\Delta\psi_m$ and caspase activation. In sum, analyzing the timing of Bz-423-induced apoptotic changes in Jurkat T cells reveals a set of changes analogous to those observed in Ramos B cells, wherein increased $O_2^{\bullet-}$ production is detected prior to downstream apoptotic events.

Decreased ATP levels accompany Bz-423-induced mitochondrial apoptotic changes: Many apoptotic processes are ATP-dependent. For example, 2'-deoxy-ATP (dATP) is necessary co-factor for assembly of cytochrome *c*, apaf-1 and pro-caspase-9 into the apoptosome, which leads to proteolytic processing of pro-caspase-9 into active caspase-9 [1, 306, 307]. Moreover, apoptosis is often signaled by protein kinases (e.g., p38 mitogen-activated protein kinase (p38 MAPK) or c-Jun amino-terminal kinase (JNK)), which require ATP as the phosphoryl donor for phosphorylation of substrate proteins [308, 309]. Finally, ATP is required for *de novo* synthesis of BH3-only proteins [310]. The need for sufficient energy reserves to fuel these apoptotic processes suggests that severe depletion of ATP may preclude apoptosis. In support of this hypothesis, reduction of ATP levels in Jurkat T cells with oligomycin renders Jurkat T cells unable to undergo apoptosis in response to staurosporine (STS) or tumor necrosis factor-α (TNF-α) [311]. Instead, STS or TNF-α trigger necrosis in Jurkat T cells with reduced ATP levels [311]. Similarly, apoptosis (but not necrosis) is blocked neuronal, cervical carcinoma and multiple myeloma cell-types by depletion of ATP prior to administration of an apoptotic stimulus [312-314].

Despite the requirement for ATP in early stages of apoptosis, cells undergoing this form of cell death eventually lose the capacity to maintain ATP levels. For example, STS causes a >50% reduction in ATP levels in Jurkat T cells within 2 h (Figure 3.15A and [311]). ATP levels are also reduced in Jurkat T cells treated with TNF-α for 4 h [311]. These decreases in ATP levels may result from impairment of MRC function due to release of cytochrome *c* from the MIS [315]. In support of this hypothesis, $\Delta\psi_m$ depolarization and redistribution of cytochrome *c* from the mitochondrial to cytosolic

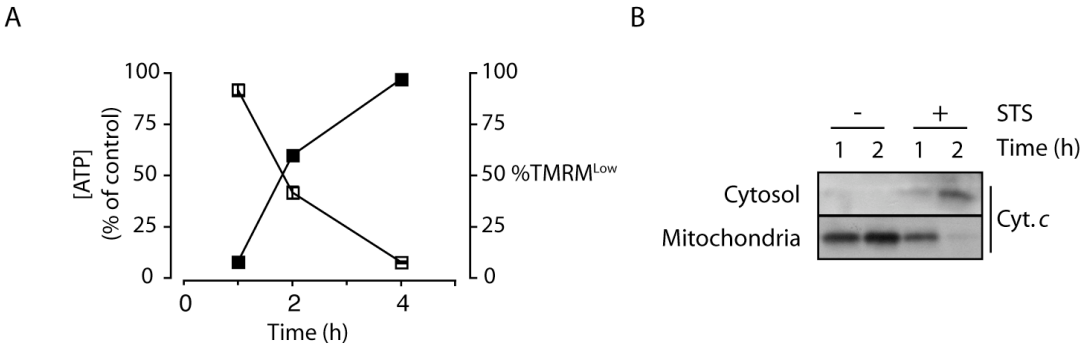

Figure 3.15 - Reduced ATP levels accompany mitochondrial apoptotic changes in Jurkat T cells. (A) Jurkat T cells were treated with staurosporine (0.25 μM) and cellular ATP levels (□) or collapse of $\Delta\psi_m$ ($TMRM^{Low}$; ■) were evaluated at the indicated times. (B) Mitochondrial and cytosolic fractions of Jurkat T cells treated with staurosporine (STS; 0.25 μM) were immunoblotted with an antibody specific for cytochrome *c* (Cyt. *c*).

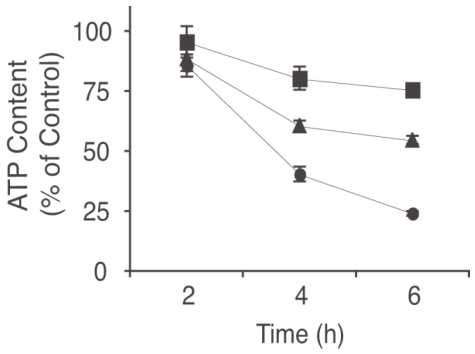

Figure 3.16 - Bz-423 depletes cellular ATP levels after the onset of apoptosis. Jurkat T cells were treated with Bz-423 (6 μM; ■), (8 μM; ▲) and (10 μM; ●) for the indicates times, at which point cells were lysed with perchloric acid and intracellular ATP levels quantified using a luciferin-luciferase assay. Absence of error bars indicates <1% standard deviation. Data is representative of at least two experiments.

fractions is apparent in Jurkat T cells treated with STS for 2 h (Figure 3.15B). These findings demonstrate ATP levels are decrease in Jurkat T cells in a time-frame coincident with mitochondrial apoptotic changes. In addition, because this decrease in ATP levels appears to be a component of the apoptotic cascade, further depletion of ATP after release of cytochrome *c* and collapse of $\Delta\psi_m$ is unlikely to prevent apoptosis. In support of this hypothesis, addition of oligomycin to Jurkat T cells 2 h *after* treatment with STS fails to prevent DNA fragmentation and related apoptotic changes [311].

The reduction in cellular ATP levels accompanying STS induced collapse of $\Delta\psi_m$ and cytochrome *c* release suggests that a similar decrease might accompany Bz-423-induced mitochondrial apoptotic changes. In support of this hypothesis, Bz-423 caused a concentration-dependent reduction in cellular ATP content beginning at 4 h (Figure 3.16), which corresponds to the timing of cytochrome *c* and collapse of $\Delta\psi_m$. The timing of this response, which coincides with collapse of $\Delta\psi_m$ and release of cytochrome *c*, suggests that it results from the onset of apoptosis.

Bz-423-induced T cell apoptosis is $O_2^{\bullet-}$-dependent: Increased $O_2^{\bullet-}$ is detected in Jurkat T cells within 1 h of treatment suggesting that, as in Ramos B cells, it might signal apoptosis. To test this hypothesis, Bz-423-induced $O_2^{\bullet-}$ was scavenged with the antioxidants MnTBAP or vitamin E. MnTBAP is porphyrin-based manganese superoxide dismutase (MnSOD) mimetic that catalyzes dismutation of $O_2^{\bullet-}$ to H_2O_2 (Figure 3.17A; [316]). Vitamin E is collective term for a set of eight lipid-soluble tocopherols and tocotrienols (α-tocopherol was specifically used in this study) that react with a variety of oxidants (Figure 3.17A; [317]). Consistent with prior work in Ramos B cells, scavenging $O_2^{\bullet-}$ blocked Bz-423-induced apoptotic morphological changes (Figure

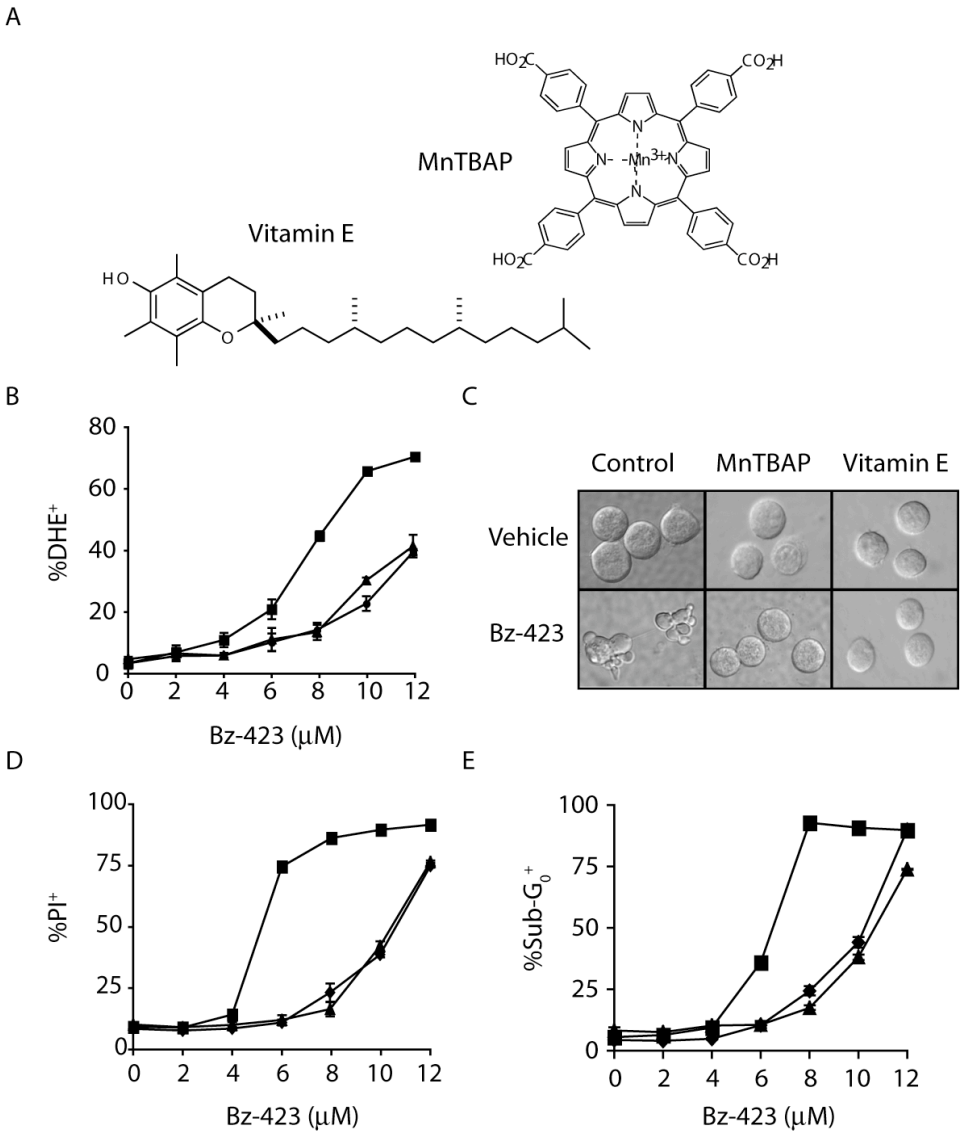

Figure 3.17 - Scavenging $O_2^{\bullet-}$ inhibits Bz-423-induced cell death in Jurkat T cells. (A) Chemical structures of the anti-oxidants MnTBAP and vitamin E (B) Jurkat T cells were pre-treated with vitamin E (100 μM; ▲), MnTBAP (100 μM; ●) or vehicle (■) for 30 min then incubated with Bz-423 for 2 h and intracellular $O_2^{\bullet-}$ was measured with DHE staining. (C) Interference contrast microscopy (630x magnification) of Jurkat T cells pre-treated with vitamin E (100 μM), MnTBAP (100 μM) or vehicle for 30 min and then incubated with Bz-423 (10 μM) for 18 h. (D and E) Jurkat T cells were treated as in A and cell death and DNA fragmentation were measured at 24 h in terms of PI permeability and the presence of Sub-G_0 DNA, respectively. MnTBAP and vitamin E were used at concentrations shown to inhibit Bz-423-induced cell death in Ramos B cells [236]. Absence of error bars indicates <1% standard deviation. Figure is representative of at least four independent experiments.

Cell Line	Anti-oxidant	$O_2^{\bullet-}$	$\Delta\psi_m$	Apoptosis	Cell Death
MOLT-4	-	7.2 ± 0.7	10.2 ± 0.6	6.5 ± 0.5	7.1 ± 0.2
MOLT-4	MnTBAP	12 ± 1.2	>15	9.5 ± 0.8	10.4 ± 0.4
MOLT-4	Vitamin E	>15	>15	11 ± 0.6	11.1 ± 1.1
CCRF-CEM	-	7.9 ± 0.6	7.5 ± 1.4	6.2 ± 0.4	7.1 ± 0.7
CCRF-CEM	MnTBAP	>15	10.2 ± 0.2	10.5 ± 0.6	10.2 ± 0.2
CCRF-CEM	Vitamin E	>15	10.5 ± 0.5	10.1 ± 0.2	10.6 ± 0.5

Table 3.2 - Effect of the anti-oxidants MnTBAP and vitamin E on EC_{50} (μM) values for Bz-423-induced endpoints in T cell leukemia lines. Dose response curves were generated for each cell line pretreated with vitamin E (100 μM) or MnTBAP (100 μM) for 30 min then incubated with Bz-423 for indicated times. Intracellular $O_2^{\bullet-}$ was measured at 2 h with DHE staining. $\Delta\psi_m$ was measured at 8 h with TMRM staining. Apoptosis was measured in terms of accumulation of Sub-G_0 DNA at 24 h. Cell death was quantified by PI permeability after 24 h. EC_{50} values were calculated in triplicate via non-linear regression of the corresponding dose-response curves.

3.17C), and doubled the EC_{50} for cell death and accumulation of apoptotic (Sub-G_0) DNA in Jurkat T cells (Figure 3.17D and 3.17E). Similar shifts in the EC_{50} for Bz-423-induced apoptosis (quantified in terms of accumulation of Sub-G_0 DNA) and overall cell death are observed in MOLT-4 and CCRF-CEM T cells pretreated with MnTBAP or vitamin E (Table 3.2). Because significant differences were not detected in the apoptotic responses between each of the $CD4^+$ T cell leukemia lines to Bz-423, subsequent experiments focused on the Jurkat T cells. This line was selected because it has been widely used for characterizing the apoptotic response to other agents and a variety of clones with deletions of apoptotic and T cell signaling proteins are available [270].

The inhibitory effect of MnTBAP or vitamin E on Bz-423-induced cell death suggests $O_2^{\bullet-}$ is likely to also signal the mitochondrial apoptotic changes. This hypothesis was again tested by pre-incubating Jurkat T cells with MnTBAP or vitamin E,

treating with Bz-423, and analyzing for collapse of $\Delta\psi_m$, reduction in ATP levels at 6 h and release of pro-apoptotic MIS proteins. As predicted by their inhibitory effects on Bz-423-induced cell death, MnTBAP and vitamin E protect against collapse of $\Delta\psi_m$ and maintained ATP levels in Jurkat T cells (Figure 3.18A and 3.18B). Likewise, MnTBAP and vitamin E also prevented Bz-423-induced $\Delta\psi_m$ depolarization in MOLT-4 and CCRF-CEM T cells (Table 3.2). Finally, MnTBAP blocked cytochrome *c*, Smac/DIABLO and AIF release in Jurkat T cells (Figure 3.18C). Taken together, these results demonstrate that Bz-423 induces T cell apoptosis via a mechanism in which all components of the death cascade not only follow, but also depend on the increase in intracellular $O_2^{\bullet-}$ levels observed during the first two hours of treatment.

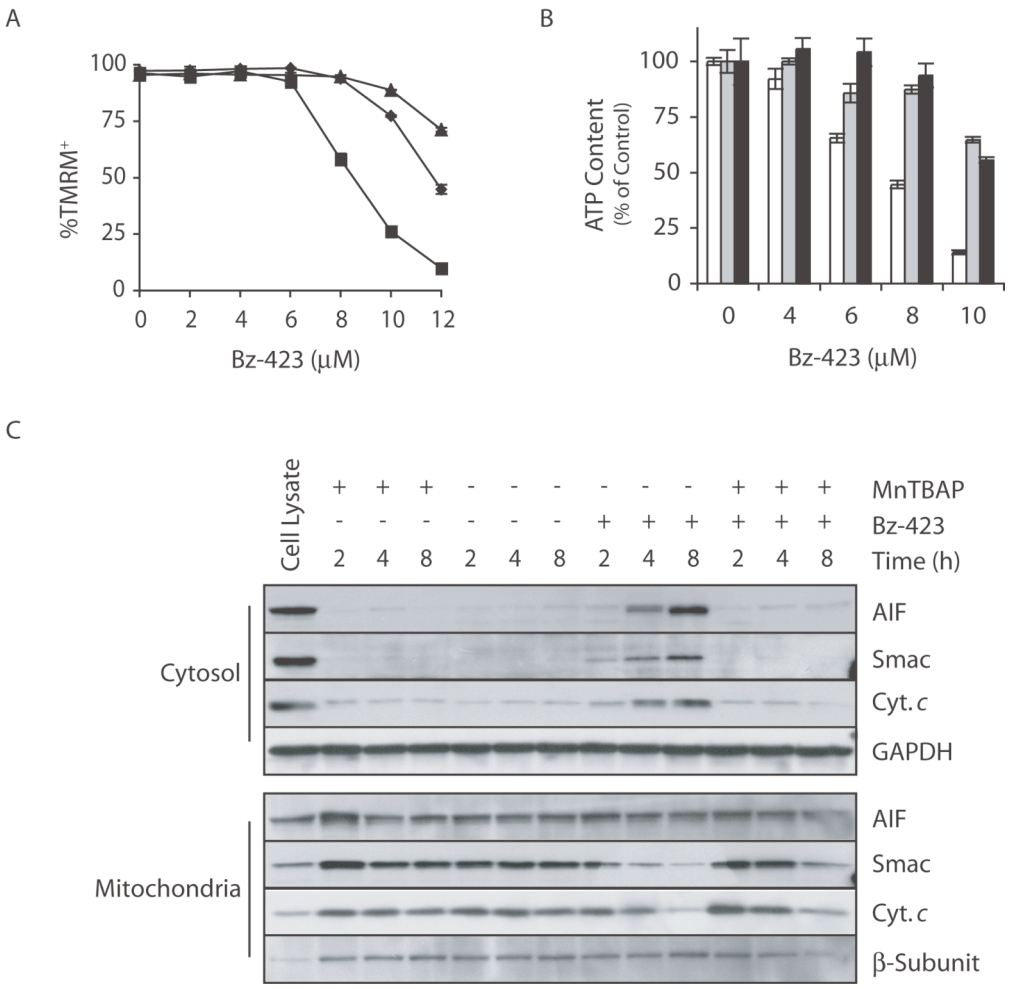

Figure 3.18 - Scavenging $O_2^{\bullet-}$ blocks Bz-423-induced mitochondrial apoptotic changes in Jurkat T cells. (A) Jurkat T cells were pre-treated with vitamin E (100 μM; ▲), MnTBAP (100 μM; ●) or vehicle (■) for 30 min then incubated with Bz-423 for 8 h and intracellular $\Delta\psi_m$ was measured with TMRM staining. (B) Jurkat T cells were pre-treated with vitamin E (100 μM; grey bars), MnTBAP (100 μM; black bars) or vehicle (white bars), at which point cells were lysed with perchloric acid and intracellular ATP levels quantified using a luciferin-luciferase assay. (C) Jurkat T cells were pre-treated with MnTBAP (100 μM) and then incubated with Bz-423 (10 μM) and separated into mitochondrial and cytosolic fractions at the indicated times. These fractions were then immunoblotted with specific antibodies as indicated. MnTBAP and vitamin E were used at concentrations shown to inhibit Bz-423-induced cell death in Jurkat T cells (Figure 3.17). Absence of error bars indicates <1% standard deviation. Data is representative of at least two independent experiments.

Bz-423-induced T cell apoptosis is independent of FasL signaling: The extrinsic apoptotic pathway is initiated by binding of cell surface death receptors by their cognate ligands (see Chapter 3 Introduction; [318]). Death receptor ligation leads to recruitment procaspases-8 and/or -10. Subsequent activation of caspase-8 or -10 initiates a proteolytic cascade that culminates in cell death (Figure 3.1). This pathway has been studied extensively in T cells using the activation-induced cell death (AICD) tissue culture model [163]. In AICD, *in vitro* stimulation of T cells through their antigen receptor or with chemical mitogens induces expression of Fas ligand (FasL), which is both secreted and displayed on the cell surface [169]. Subsequent binding of FasL to its cognate death receptor (Fas) signals extracellular apoptosis [169].

While the Fas death receptor is present on the surface of quiescent T cells, FasL levels are below the limits of detection prior to stimulation, but are highly induced during AICD [163]. This increase appears to depend on the ROS ($O_2^{\bullet-}$ and H_2O_2) burst that accompanies T cell activation [319-321]. Similarly, FasL-dependent apoptosis is observed in response to the pro-oxidant menadione, which generates $O_2^{\bullet-}$ as a result of redox cycling in the MRC [322]. It is tempting to speculate, therefore, that Bz-423-induced $O_2^{\bullet-}$ might signal T cell apoptosis by stimulating FasL expression. However, this hypothesis is not consistent with the observation that T cells isolated from MRL-*lpr* mice, which have defective Fas expression, are killed by Bz-423 [242]. In addition, cell membrane FasL levels are not elevated on Jurkat T cells treated with Bz-423 for 4 h, at which point mitochondrial apoptotic changes are observed (Figure 3.19A). In addition, pre-incubation of Jurkat T cells with a Fas antagonist antibody did not protect against Bz-423-induced cell death, but

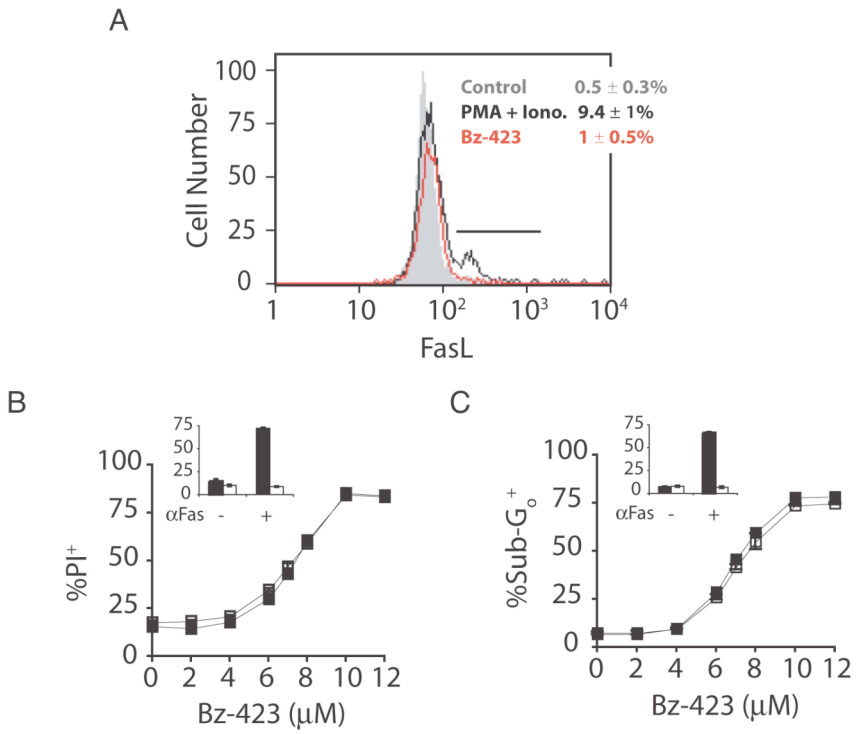

Figure 3.19 - Bz-423-induced apoptosis is independent of Fas signaling. (A) Jurkat T cells were incubated with vehicle (shaded histogram), PMA and ionomycin (both 0.25 μM; black histogram) and Bz-423 (10 μM; red histogram) and cell surface FasL levels were measured by staining with a anti-Fas antibody. (B and C) Jurkat T cells were pre-treated with the Fas antigonist antibody ZB4 (1 μg/mL; □) or vehicle (■) for 30 min and then treated (24 h) with the indicated concentrations of Bz-423 and cell death and apoptosis were measured in terms of PI permeability and accumulation of Sub-G_0 DNA, respectively. *Insets*, Jurkat T cells treated pre-treated with ZB4 (1 μg/mL; white bars) or vehicle (blacks bars) were incubated with the Fas agonist antibody CH11 (0.25 μg/mL) and cell death and apoptosis were measured in terms of PI permeability and accumulation of Sub-G_0 DNA, respectively. ZB4 and CH11 were used at concentrations previously shown to inhibit or induce Fas-dependent apoptosis, respectively [323]. Absence of error bars indicates <1% standard deviation. All data is from a single experiment.

did block apoptosis induced by a Fas agonist antibody (Figure 3.19B and 3.19C). These results, combined with the prior studies using MRL-*lpr* splenocytes, demonstrate that Bz-423-induced apoptosis in T cells is independent of Fas-FasL signaling.

Role of caspase activation in Bz-423-induced cell death: Caspase activation is a key downstream apoptotic event that orchestrates DNA fragmentation and morphological changes characteristic apoptosis [324]. Small molecule caspase inhibitors or genetic deletion of molecules required for caspase activation (e.g., apoptotic protease activating factor-1 (apaf-1)) prevents these changes, and in some cases, maintains cell viability [4, 324-326]. Although caspase inhibition prevents accumulation of apoptotic DNA in Ramos B cells treated with Bz-423, cell death is still observed [236, 292]. This observation suggests that Bz-423-induced mitochondrial apoptotic changes (e.g., cytochrome c release) are sufficient to cause cell death even in the absence of caspase activation.

To determine whether Bz-423-induced cell death is independent of caspases in T cells, caspase activation was blocked in Jurkat T cells with the pan-caspase inhibitor *N*-benzyloxycarbonyl-Val-Ala-Asp(OMe)-fluoromethyl ketone (zVAD-fmk) prior to incubation with Bz-423. In contrast to observations in Ramos B cells, pan-caspase inhibition blocked Bz-423-induced cell death in Jurkat T cells (Figure 3.20B - 3.20D). To determine if the dependence of Bz-423-induced cell death on caspase activation is a unique characteristic of Jurkat T cells, MOLT-4 and CCRF-CEM T cells were pre-incubated with zVAD-fmk, treated with Bz-423, and analyzed for changes in DNA fragmentation and overall viability. Like Jurkat T cells, blocking caspase activation inhibited apoptosis (i.e., DNA fragmentation) and cell death in MOLT-4 and CCRF-CEM T cells after 24 h (Table 3.3). These findings demonstrate that caspase activity is required for the lymphotoxic activity of Bz-423 in the T cell leukemia lines observed at 24 h and highlights a key mechanistic difference with the response in Ramos B cells.

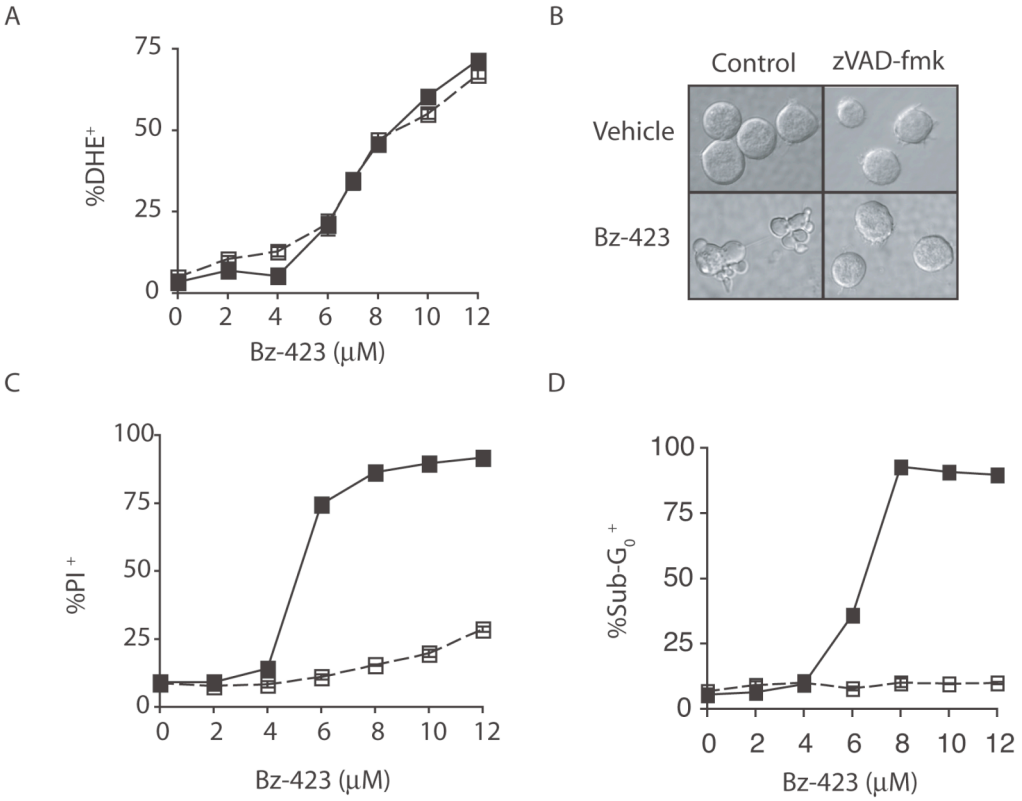

Figure 3.20 - The short-term effects of Bz-423 on viability in Jurkat T cells are caspase-dependent. (A) Jurkat T cells were treated with zVAD-fmk (50 μM; □) or vehicle (■) for 30 min then incubated with Bz-423 for 2 h and intracellular $O_2^{\bullet -}$ was measured with DHE staining. (B) Interference contrast microscopy (630x magnification) of Jurkat T cells treated with zVAD-fmk (50 μM) or vehicle for 30 min and then incubated with Bz-423 (10 μM) for 24 h. (C and D) Jurkat T cells were treated as in A and cell death and DNA fragmentation were measured at 24 h in terms of PI permeability and the presence of Sub-G_0 DNA, respectively. zVAD-fmk was used at a concentration shown to inhibit Bz-423-induced DNA fragmentation in Ramos B cells [236]. Absence of error bars indicates <1% standard deviation. Figure is representative of at least four independent experiments.

Cell Line	zVAD-fmk	$O_2^{\bullet-}$	$\Delta\psi_m$	Apoptosis	Cell Death
MOLT-4	-	7.2 ± 0.7	10.2 ± 0.6	6.5 ± 0.5	6.1 ± 0.2
MOLT-4	+	8.0 ± 0.5	11.2 ± 0.7	>15	12.4 ± 0.5
CCRF-CEM	-	7.9 ± 0.6	7.5 ± 1.4	6.2 ± 0.4	7.1 ± 0.7
CCRF-CEM	+	8.2 ± 0.4	6.9 ± 0.5	>15	11.2 ± 0.6

Table 3.3 - Effect of the caspase inhibitor zVAD-fmk on EC_{50} (μM) values for Bz-423-induced endpoints in T cell leukemia lines. Dose response curves were generated for each cell line pretreated zVAD-fmk (50 μM) or vehicle for 30 min then incubated with Bz-423 for indicated times. Intracellular $O_2^{\bullet-}$ was measured with DHE staining after 2 h. $\Delta\psi_m$ was measured with TMRM staining after 8 h. Cell death was quantified by PI permeability at 24 h. Apoptosis was measured in terms of the presence of Sub-G_0 DNA at 24 h. EC_{50} values were calculated in triplicate via non-linear regression of the corresponding dose-response curves.

The dependence of Bz-423-induced cell death on caspase activation in T cell leukemia lines suggests that release of cytochrome *c* and Smac/DIABLO and/or collapse of $\Delta\psi_m$ might also be caspase-dependent. Support for this hypothesis comes from studies in which zVAD-fmk has been shown to block cytochrome *c* release induced by a variety of apoptotic stimuli [327-329]. The apparent dependence of cytochrome *c* release on caspase activity in other models has suggested the presence of a proteolytic amplification loop - fractional cytochrome *c* release activates caspases, which then leads to "large-scale" release of pro-apoptotic MIS proteins [4]. One mechanism by which caspase acivation may promote loss of mitochondrial outer membrane integrity is through cleavage of the Bid, which leads to activation this BH3-only protein [330]. In its truncated, activate form (tBid), this BH3-only protein promotes activation of the multi-BH-domain pro-apoptotic proteins Bax and Bak, which can lead to permeabilization of the mitochondrial outer membrane (see Chapter 3 Introduction).

Other evidence, however, raises doubts about this two-step mechanism of cytochrome *c* release. Most significantly, fractional release of cytochrome *c* has yet to be detected experimentally [331, 332]. In addition, the failure to detect release of cytochrome *c* in cells exposed to apoptotic stimuli in the presence of zVAD-fmk may be an artifact of sustained proteasome activity under these conditions [333]. To circumvent this issue, Green, *et al* prepared fluorescently-tagged variants of cytochrome *c*, Smac/DIABLO and AIF, which enables release events to be temporally monitored in individual cells [12, 334]. These studies demonstrated that a variety of apoptotic stimuli induce complete, caspase-independent release of cytochrome *c* and Smac/DIABLO from all mitochondria in an individual cell in <5 min [12, 334]. In contrast, AIF release is slower and depends on caspase activation [12]. These data suggest that release of cytochrome c and Smac/DIABLO is a rapid, complete process that is *solely* dependent on factors that regulate integrity of the mitochondrial outer membrane (e.g., Bcl-2 family proteins).

To determine if caspase activation is required for Bz-423-induced release of pro-apoptotic MIS proteins, Jurkat T cells were pre-incubated with zVAD-fmk, treated with Bz-423, and then separated into mitochondrial and cytosolic fractions. Immunoblots of these fractions revealed that Bz-423-induced release of Smac/DIABLO and cytochrome *c* does not depend on caspase activity (Figure 3.21C). In accordance with studies indicating that AIF release is caspase-dependent [11, 12], reduced levels of this MIS protein were detected in the cytosolic fraction of cells treated Bz-423 in the presence of zVAD-fmk (Figure 3.21C). These observations demonstrate that Bz-423-induced release of Smac/DIABLO and cytochrome *c* is caspase-independent. However, they raise

questions concerning how zVAD-fmk pre-treated Jurkat T cells remain viable (at least for 24 h) despite release of cytochrome *c* from the mitochondria.

One possibility is that Bz-423-induced release of cytochrome *c* is not sufficient to collapse $\Delta\psi_m$ and impair oxidative phosphorylation in Jurkat T cells. Because depolarization of $\Delta\psi_m$ often coincides with cytochrome *c* release, it has been assumed to be a consequence of impaired ETC function due to loss of th electron shuttle between from complex III and IV [315]. There is accumulating evidence, however, that release of cytochrome *c* (and other pro-apoptotic MIS proteins) and collapse of $\Delta\psi_m$ occur via distinct processes. For example, inhibition of caspase activity with zVAD-fmk maintains $\Delta\psi_m$ and ATP levels in HeLa cervical carciomal cells for up to 24 h following release of cytochrome *c* caused by either cytotoxic drugs (e.g., STS, etoposide or actinomycin D (Act D)) or perforin/granzyme [11, 335, 336]. The dependence $\Delta\psi_m$ depolarization on caspase activity in these studies suggests that (1) concentrations of cytochrome *c* in the MIS are sufficient to sustain oxidative phosphorylation even after release and (2) that components of the MRC may be caspase substrates. The latter prediction has been verified by identification of a caspase-3 cleavage site in the 75-kDa subunit of complex I [337]. Mutation of this site to a non-cleavable sequence preserves $\Delta\psi_m$, maintains ATP levels and delays death in HeLa cells treated with STS or Act D [337].

The role caspases in disabling the MRC after cytochrome *c* release suggests that zVAD-fmk may inhibit Bz-423-induced cell death by preventing collapse of $\Delta\psi_m$. To evaluate this hypothesis, changes in $\Delta\psi_m$ were monitored in Jurkat T cells pre-incubated with zVAD-fmk and then treated with Bz-423. Similar to the release of cytochrome *c*

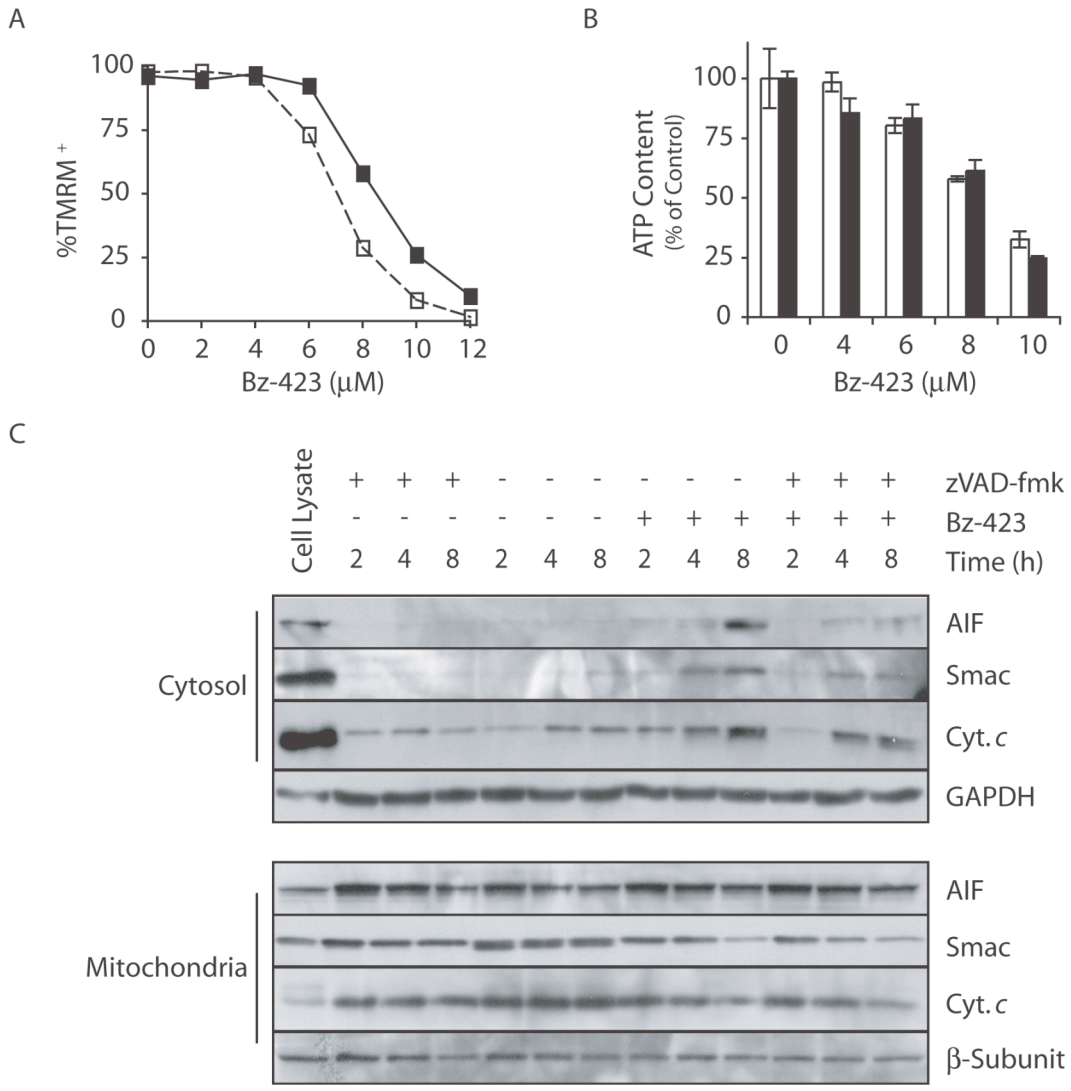

Figure 3.21 - Bz-423-induced mitochondrial apoptotic endpoints are not caspase-dependent. (A) Jurkat T cells were treated with zVAD-fmk (50 μM; □) or vehicle (■) for 30 min then incubated with Bz-423 for 8 h and intracellular $\Delta\psi_m$ was measured with TMRM staining. (B) Jurkat T cells were pre-treated with zVAD-fmk (50 μM; black bars) or vehicle (white bars), at which point cells were lysed with perchloric acid and intracellular ATP levels quantified using a luciferin-luciferase assay. (C) Jurkat T cells were pre-treated with zVAD-fmk (50 μM) and then incubated with Bz-423 (10 μM) and separated into mitochondrial and cytosolic fractions at the indicated times. These fractions were then immunoblotted with antibodies for AIF, Smac, cytochrome *c* (Cyt. *c*), GAPDH and β-subunit. zVAD-fmk was used at a concentration shown to inhibit Bz-423-induced cell death in Jurkat T cells (See Figure 3.20). Absence of error bars indicates <1% standard deviation. This figure is representative of at least two independent experiments.

and Smac/DIABLO, blocking caspase activation with zVAD-fmk failed to prevent Bz-423-induced $\Delta\psi_m$ collapse in Jurkat T cells (Figure 3.21A) or MOLT-4 and CCRF-CEM T cells (Table 3.3). One possible interpretation of these data is that, unlike HeLa cells, cytochrome *c* release may be sufficient to collapse $\Delta\psi_m$ in T cell leukemia lines.

The failure of zVAD-fmk to block Bz-423-induced collapse of $\Delta\psi_m$ in Jurkat, MOLT-4 and CCRF-CEM T cells together with evidence that caspase activity is required for Bz-423-induced cell death argues that Jurkat (and other $CD4^+$ T cells leukemia lines) produce sufficient ATP via glycolysis to maintain viability when oxidative phosphorylation is impaired due to collapse of $\Delta\psi_m$. This hypothesis is supported by studies comparing O_2 consumption and lactate production in Jurkat T cells, which indicates that this cell-type generate between 60-70% of their ATP via glycolysis [274-276]. To determine whether glycolytic ATP production is sufficient to compensate for the mitochondrial apoptotic changes induced by Bz-423, Jurkat T cells were pre-incubated with zVAD-fmk and ATP levels were measured after treatment with Bz-423 for 6 h. In this experiment, cellular ATP content was reduced to a similar degree (~70%) in Jurkat T cells treated with Bz-423 in the presence or absence of zVAD-fmk (Figure 3.21C). These data indicate that glycolytic ATP production does not compensate for the complete disruption of oxidative phosphorylation resulting from release of cytochrome c and collapse of $\Delta\psi_m$. However, the ability of zVAD-fmk to maintain viability suggests that Jurkat T cells are able to survive (at least for 24 h) despite reduction of cellular ATP concentrations to ~30% of their normal levels.

The failure of zVAD-fmk to prevent the Bz-423-induced collapse of $\Delta\psi_m$ and ATP depletion suggests that the short-term inhibition of cell death by zVAD-fmk may

not translate into survival and proliferation at time-points beyond 24 h. The ability of caspase inhibition to promote long-term proliferation and survival has been investigated in HeLa cells treated with etoposide, Act D and STS [325]. As observed for Bz-423 in Jurkat T cells, zVAD-fmk blocked cell death induced by all three cytotoxic drugs for up to 3 d despite the release of cytochrome *c* after 12 h [325]. However, this short-term maintenance of viability did not translate into clonegenic survival (i.e., colony formation when plated on soft-agar) after two weeks [325]. In fact, no colonies were observed when etoposide, Act D or STS were removed after 12 h and HeLa cells were maintained in the presence of zVAD-fmk [325]. This study suggests that in the absence of caspase activation, release of pro-apoptotic MIS proteins can nevertheless kill cells by a mechanism termed caspase-independent cell death (CICD).

To identify regulators of CICD, Green, *et al* treated Jurkat T cells that had been transfected with a retroviral cDNA library with STS in the presence or absence of zVAD-fmk [325]. This approach identified glyceraldehyde-3-phosphate dehydrogenase (GAPDH) as a potential inhibitor of CICD, but not caspase-dependent cell death. While GAPDH is best known for its role in glycolysis, this protein also contributes to nuclear envelope assembly, transcriptional co-activation and DNA repair [338-340]. Studies with GAPDH deletion constructs indicate that GAPDH inhibits CICD by both increasing glycolytic ATP production and inducing expression of the autophagy gene Atg12 [325]. These findings suggest a mechanism whereby the increase in glucose metabolism stimulated by GAPDH maintains ATP levels while damaged mitochondria are removed by autophagy [341].

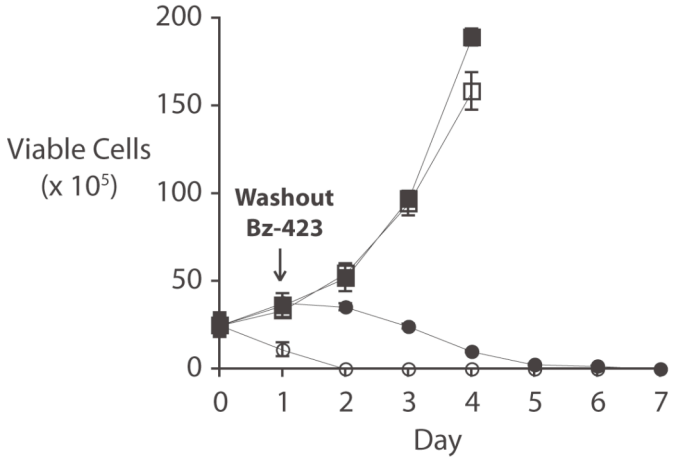

Figure 3.22 - Caspase inhibition delays, but does not block Bz-423-induced cell death. Jurkat T cells were treated with zVAD-fmk (50 μM; ●,■) or vehicle (○,□) for 30 min then incubated with Bz-423 (10 μM; ●,○) or vehicle (■,□) for 24 h, at which point both agents were removed. Cells were then maintained in media containing zVAD-fmk (50 μM) and the number of viable cells was determined daily by Trypan exclusion. zVAD-fmk was used at a concentration shown to inhibit Bz-423-induced cell death in Jurkat T cells (see Figure 3.20). Absence of error bars indicates <1% standard deviation. Figure is from a single experiment.

GAPDH levels increase under conditions where glucose metabolism is upregulated. For instance, GAPDH levels are elevated four-fold during the increase in glycolytic ATP production that accompanices antigen receptor stimulatio of T cells [342]. This increase in GAPDH levels appears sufficient to impair CICD because TCR stimulation of murine $CD4^+$ T cells causes a five-fold improvement in long-term survival when treated with Act D and zVAD-fmk, but provides no protection to Act D alone [342]. These findings suggest that Jurkat T cells may express sufficient GAPDH to preclude CICD induced by combined exposure to Bz-423 and zVAD-fmk. To examine this possibility, Jurkat T cells were treated with a concentration of Bz-423 (10 μM) sufficient to promote release of cytochrome *c* and Smac/DIABLO as well as collapse $\Delta\psi_m$ in the presence of zVAD-fmk (Figure 3.22). After 24 h, Bz-423 was removed and

Jurkat T cells were maintained in the presence of zVAD-fmk. Despite continued inhibition of caspase activity with zVAD-fmk, Jurkat T cells exposed to Bz-423 gradually died over the course of five days (Figure 3.22). This result suggests that unstimulated Jurkat T cells lack sufficient levels of GAPDH to suppress CICD. Altogether, studies of the Bz-423-induced death cascade in the presence of zVAD-fmk demonstrates that caspase activity is required for rapid killing of Jurkat T cells by Bz-423, but caspase-independent release of cytochrome *c* and Smac/DIABLO commits a cell to the death program.

Extra-mitochondrial factors are required for Bz-423-induced release of MIS proteins: Although zVAD-fmk blocks rapid killing by Bz-423, Jurkat T cells nevertheless die over the course of several days, which suggests the possiblity that release of cytochrome *c* and Smac/DIABLO is the point at which they commit to the death program. In contrast, scavenging Bz-423-induced $O_2^{\bullet-}$ blocks all downstream components of the apoptotic cascade and maintains viability at 24 h. A key mechanistic question, therefore, is whether mitochondrial $O_2^{\bullet-}$ is sufficient to trigger release of MIS proteins, or whether factors outside this organelle are also required. This question is significant because if Bz-423-induced $O_2^{\bullet-}$ is sufficient to trigger release of cytochrome *c* and Smac/DIABLO, then selectivity will soley be determined by factors controlling this ROS response. Conversely, if signal transduction pathways outside the mitochondria play a role, levels and activation state of these mediators will also dictate if and how a cell responds to Bz-423.

As described in the introduction to Chapter 3, apoptogenic proteins are liberated from the MIS by opening of the mitochondrial permeability transition (mPT) pore or

mitochondrial outer membrane permeabilization (MOMP). The mPT pore is a multi-protein complex that spans the inner and outer mitochondrial membranes [13]. Proposed components of this complex include voltage-dependent anion channels (VDACs), adenine nucleotide translocator (ANT), cyclophillin D (CypD), hexokinase (HK), creatine kinase (CK) and the peripheral benzodiazepine receptor (PBR) (Figure 3.2). Sustained opening of the mPT permits deregulated influx of cytosolic ions and small molecules (<1.5 kDa) into the matrix resulting in osmotic swelling, disruption of $\Delta\psi_m$ and rupture of the outer membrane [13]. This process can occur independent of cytosolic factors and has been implicated in apoptosis induced by oxidative stress associated with ischemia/reperfusion as well as the ETC inhibitors rotenone and the arsene oxid (As_2O_3) Trisenox [13, 32, 343]. Oxidative stress induced mPT opening may involve oxidation of cysteine residues on the matrix face of the ANT [344-346]. Opening of the mPT pore in response to the Bz-423-induced mitochondrial $O_2^{\bullet-}$ production is mechanistically consistent with the caspase-independent release of MIS proteins.

Pro-apoptotic proteins can also be released from the MIS by selective mitochondrial outer membrane permeabilization (MOMP), which is regulated by the Bcl-2 protein family. A subset of Bcl-2 proteins, termed BH3-only proteins, are transcriptionally induced or post-translationally activated in response to cell stress [58]. Anti-apoptotic Bcl-2 proteins such as Bcl-2, Bcl-x_L and Mcl-1 promote survival by blocking activity of the BH3-only proteins. The multi-BH-domain proapoptotic Bcl-2 proteins Bax and Bak integrate inputs from BH3-only proteins and anti-apoptotic Bcl-2 proteins and undergo a conformational change (termed activation) when signals from BH3-only proteins predominate. Following activation, Bax and Bak homo-oligomerize

and form pores in the mitochondrial outer membrane enabling release of apoptogenic proteins from the MIS. Apoptosis induced by 2-methoxyestradiol (2ME) or tumor necrosis factor-α (TNF-α), two agents that simulate $O_2^{\bullet-}$ production, involves activation of Bax and Bak [286, 347]. Although Bz-423-induced $O_2^{\bullet-}$ originates in the mitochondria, apoptosis may likewise depend on activation of Bax and Bak.

Unlike rotenone and ATO, Bz-423 does not directly inhibit the MRC [32, 348], but instead triggers a mitochondrial respiratory transition by modulating the F_oF_1-ATPase. As a result, reactive intermediates (e.g., ubisemiquinones) accumulate at reactive sites on the matrix and MIS faces of complex III resulting in release of $O_2^{\bullet-}$ into both compartments [293, 349]. $O_2^{\bullet-}$ can also be formed on the matrix side of complex I by transfer of electrons from partially-reduced flavin mononucleotides to molecular oxygen [350]. These findings suggest that Bz-423 may promote release of $O_2^{\bullet-}$ into both the matrix and the MIS.

The TCA-cycle enzyme aconitase contains an active site Fe-S cluster that is rapidly oxidized by $O_2^{\bullet-}$ (k = 3.5 x 10^6 $m^{-1}s^{-1}$; [351]). This reaction forms the basis of a sensitive assay for elevated levels of $O_2^{\bullet-}$ in the mitochondrial matrix (Figure 3.23A; [352, 353]). Aconitase catalyzes the stereo-specific isomerization of citrate to iso-citrate, which is rate-limiting relative to the subsequent step in the TCA-cycle, oxidation of isocitrate to α-ketoglutarate by isocitrate dehydrogenase (Figure 3.23A; [352]). Aconitase activity in mitochondrial extracts from Jurkat T cells was assayed by measuring NAD^+ reduced as a byproduct of isocitrate oxidation [353]. Dependence of the observed NADH production on aconitase activity was validated with the competitive aconitase inhibitor fluorocitrate (FC) (Figure 3.23B; [354]).

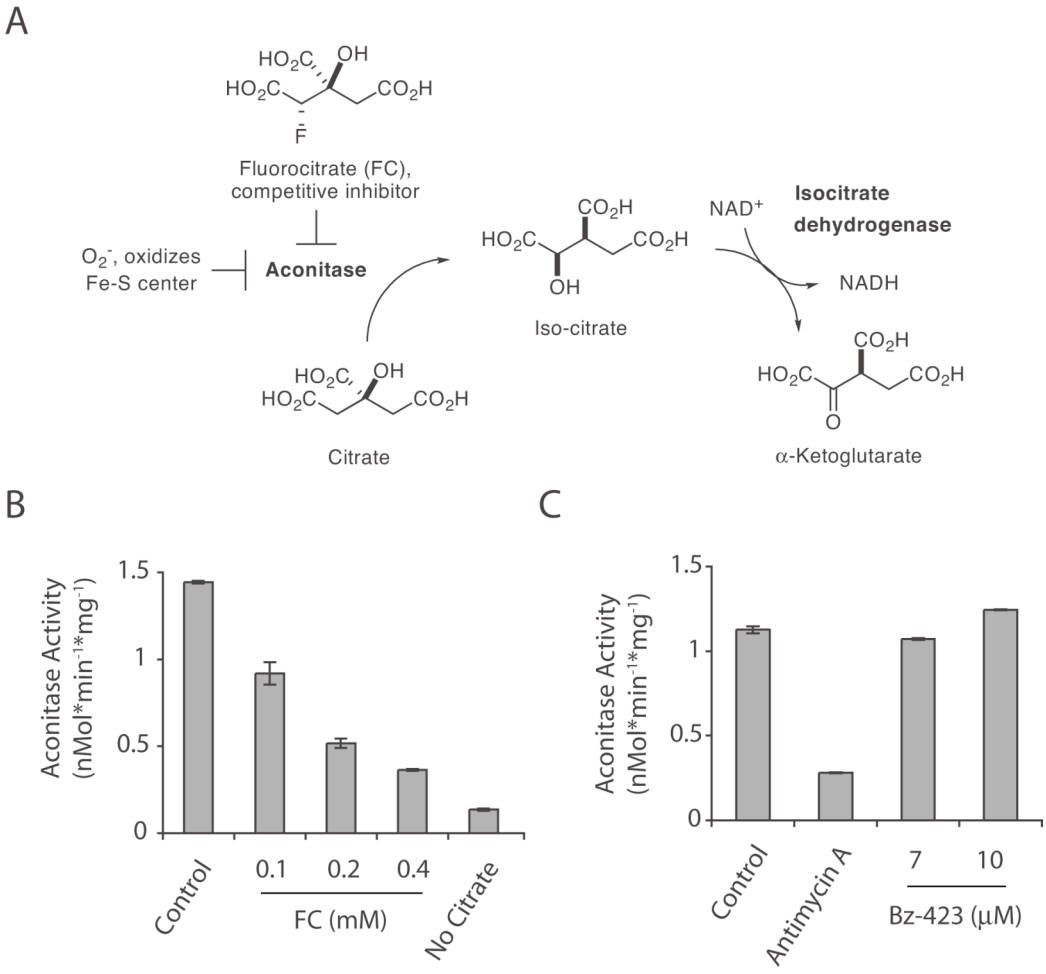

Figure 3.23 - Bz-423-induced $O_2^{\bullet-}$ does not inactivate aconitase. (A) Aconitase is a $O_2^{\bullet-}$-sensitive TCA-cycle enzyme that converts citrate to isocitrate. This reaction is rate limiting relative oxidation of iso-citrate to α-ketoglutarate by isocitrate dehydrogenase, which can be monitored in terms of reduction of NAD^+. (B) Mitochondria isolated from Jurkat T cells were incubated in aconitase reaction buffer (see Materials and Methods) and aconitase activity monitored in terms of NAD^+ reduction by isocitrate dehydrogenase. Specificity was demonstrated by inclusion of the indicated concentrations of FC or exclusion of citrate from the reaction buffer. (C) Jurkat T cells were incubated with the indicated concentrations of Bz-423 or Antimycin A (0.5 μM) for 2 h and aconitase activity was assayed in mitochondrial fractions in terms of NAD^+ reduction by iso-citrate dehydrogenase. FC was used at concentrations shown to inhibit aconitase in other systems [354]. Antimycin A was used at a concentration shown to induce $O_2^{\bullet-}$-dependent inactivation of aconitase by inhibiting complex III of the MRC [355]. Panels B and C are representative of two independent experiments.

To determine whether Bz-423 promotes release of $O_2^{\bullet-}$ into the mitochondrial matrix, Jurkat T cells were treated with Bz-423 for 2 h, at which point the increase in intracellular $O_2^{\bullet-}$ levels is maximal. After 2 h, mitochondrial fractions were isolated and resuspended in aconitase reactions buffer. Surprisingly, aconitase activity was *not* reduced in the mitochondrial fraction of Jurkat T cells incubated with Bz-423 for 2 h (Figure 3.23C). In contrast, reduced aconitase activity was observed in cells treated with antimycin A, a fungicidal antibiotic that promotes release of $O_2^{\bullet-}$ into the matrix by blocking ubiquinone reduction by complex III [30]. The absence of a reduction in aconitase activity indicates that matrix $O_2^{\bullet-}$ levels are not elevated in response to Bz-423, which suggests that production of this ROS likely occurs at the quinol-oxidizing site on the MIS face of complex III. A hypothesis for the absence of $O_2^{\bullet-}$ release into the mitochondrial matrix in the response to Bz-423 is presented in the discussion to this chapter.

The mitochondrial pro-oxidants rotenone and ATO cause release of cytochrome *c* from isolated mitochondrial by triggering sustained mPT pore opening [348, 353, 356]. In addition, both ATO and rotenone have been shown to cause a decrease in aconitase activity, which indicates that they increase matrix $O_2^{\bullet-}$ levels [31, 353]. Elevation of matrix $O_2^{\bullet-}$ levels may lead to mPT pore by oxidizing matrix-exposed cysteine residues on the ANT, a component of the mPT pore that spans the inner mitochondrial membrane [357]. This hypothesis is suggested by studies with liposomes reconstituted with recombinant ANT in which oxidation of these cysteines with H_2O_2, *t*-BHP or thiol-crosslinking reagents to the corresponding disulphides locks the ANT in a high-permeability conformation [35, 37, 345]. Together, these studies suggest a mechanism

whereby release of $O_2^{\bullet-}$ into the matrix in response to rotenone or ATO triggers mPT pore opening by oxidizing ANT cysteines.

Unlike rotenone and ATO, Bz-423 does not elevate matrix $O_2^{\bullet-}$ levels in Jurkat T cells, which suggests that Bz-423 may not cause sustained opening of the mPT pore. The hypothesis that Bz-423 does not trigger mPT pore opening is supported by observationsin rat liver mitochondria treated with Bz-423, in which $O_2^{\bullet-}$ production was not accompanied by large-amplitude swelling [236]. Along with large-amplitude swelling, release of pro-apoptotic MIS proteins from isolated mitochondria is diagnostic of sustained opening of the mPT pore [13]. To test the hypothesis that Bz-423-induced $O_2^{\bullet-}$ is not sufficient to trigger release of pro-apoptotic MIS proteins mitochondria were isolated from Jurkat T cells, labeled with DHE, incubated under conditions supporting active (i.e., state 3) respiration, and treated then with Bz-423. While increased $O_2^{\bullet-}$ was observed after 30 min (Figure 3.24A), release of cytochrome *c*, Smac/DIABLO and AIF was not detected in this cell-free assay (Figure 3.24B). In contrast, incubation of isolated mitochondria with tBid, a BH3-only protein that triggers Bak activation, promoted release of all three MIS proteins [358]. These results, combined with the absence of large-amplitude swelling in rat-liver mitochondria, suggest that Bz-423 does not trigger sustained opening of the mPT pore.

To further examine the role of mPT pore opening in Bz-423-induced apoptosis, Jurkat T cells were pretreated with specific inhibitors of this process, cyclosporine A (CsA) and bonkrekic acid (BA). CsA blocks pore opening by disrupting the association of CypD with ANT (Figure 3.2; [22, 359]). BA inhibits opening of the mPT pore by enforcing a closed confirmation of the ANT (Figure 3.2 [33]). No effect on $O_2^{\bullet-}$

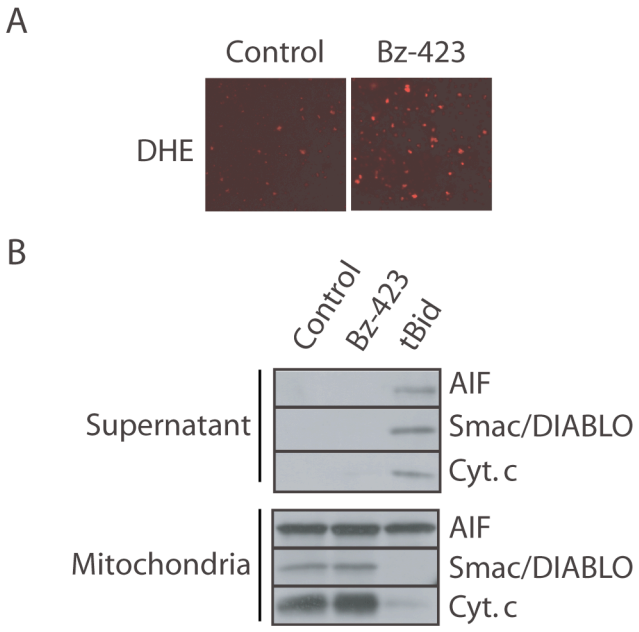

Figure 3.24 - Isolated mitochondria respond to Bz-423, but do not release pro-apoptotic MIS proteins. (A) Images (630x) of mitochondria isolated from Jurkat T cells following incubation (30 min, 37 °C) with Bz-423 (10 μM) or control in buffer containing ADP and malate/glutamate. Mitochondria were stained with DHE (4 μM) to visualize $O_2^{\bullet-}$. (B) Mitochondria isolated from Jurkat T cells were treated with Bz-423 (10 μM), tBid (0.1 μg/mL) or vehicle in buffer containing ADP and malate/glutamate and isolated after 2 h. Release of the pro-apoptotic MIS was determined by immunoblotting isolated mitochondrial fractions and supernatants for AIF, Smac/DIABLO and cytochrome *c* (Cyt. *c*). tBid was used at a concentration shown to induce cytochrome *c* release from mouse liver mitochondria [358]. Data is from a single experiment.

production or any of the downstream apoptotic endpoints was observed with either inhibitor (Table 3.4).Together, these findings demonstrate that although isolated mitochondria respond to Bz-423, extra-mitochondrial factors are necessary to couple $O_2^{\bullet-}$ production to release of proapoptotic MIS proteins and cell death.

Inhibitor	$O_2^{\bullet-}$	$\Delta\psi_m$ collapse	Apoptosis	Cell Death
-	6.3 ± 0.2	8.4 ± 0.8	7.2 ± 0.6	7.1 ± 0.4
Bongkrekic acid	7.4 ± 0.6	9.2 ± 0.3	6.4 ± 0.8	7.5 ± 0.4
cyclosporin A	7.2 ± 0.6	8.0 ± 1.1	7.3 ± 0.4	6.4 ± 0.3

Table 3.4 - Effect of mPT pore inhibitors on EC_{50} (μM) values for Bz-423-induced apoptotic endpoints in T cell leukemia lines. Dose response curves were generated for each cell line pretreated with Bongkrekic acid (50 nM) or cyclosporin A (50 nM) for 30 min then incubated with Bz-423 for indicated times. Intracellular $O_2^{\bullet-}$ was measured at 2 h with DHE staining. $\Delta\psi_m$ was measured at 8 h with TMRM staining. Apoptosis was measured in terms of accumulation of Sub-G_0 DNA at 24 h. Cell death was quantified at 24 h in terms of PI permeability. Bongkrekic acid (50 nM) or cyclosporin A (50 nM) were used at concentrations shown to inhibit mPT pore opening in other systems [343]. EC_{50} values were calculated in triplicate via non-linear regression of the corresponding dose-response curves.

Bz-423 does not cause peroxidation of mitochondrial phospholipids: The data presented above suggest that release of MIS proteins in response to Bz-423 occurs by MOMP rather than opening of the mPT pore [13]. While the Bcl-2 protein family regulates mitochondrial outer membrane integrity, mobilization of cytochrome *c* following MOMP may involve an oxidative amplification loop [5]. Specifically, ~15% of the cytochrome *c* pool is bound to cardiolipin (CL) and can oxidize this mitochondrial-specific phospholipid in response after treatment with H_2O_2 [360, 361].

The role of CL peroxidation in cytochrome *c* release has been primary studied in mouseembryonic fibroblasts (MEFs) [360, 362, 363]. These studies suggest the CL oxidation may be a general characteristic of mitochondrial apoptosis, rather than a specific response to oxidative stress. For instance, CL peroxidation is observed prior to release of pro-apoptotic MIS proteins and caspase activation in MEFs treated with the

RNA polymerase inhibitor Act D, which is not redox active [360]. This timing suggests that oxidation of CL by cytochrome *c* may be required for release of pro-apoptotic MIS proteins from the MIS. In support of this model, oxidation of CL as well as release of Smac/DIABLO from the MIS is not observed in cytochrome $c^{-/-}$ MEFs, although Bax translocation and activation is still detected [360]. Conversely, actinomycin D treatment fails to induce CL oxidation in MEFs deficient in the multi-BH-domain pro-apoptotic Bcl-2 proteins Bax and Bak [362]. Together, these data suggest that oxidation of CL by cytochrome *c* is an essential step in release of MIS proteins following activation of Bax and Bak.

After release into the MIS, $O_2^{\bullet-}$ is rapidly converted into H_2O_2 by Cu,Zn-SOD ($k = 10^8$ $m^{-1}s^{-1}$) [364, 365], suggesting that Bz-423 may trigger CL peroxidation by elevating H_2O_2 levels. To test this hypothesis, Jurkat T cells were incubated with C_{11}-BODIPY$^{581/591}$, a hydrophobic dye containing conjugated diene that is oxidized ($k = 6.0 \times 10^3$ $M^{-1}s^{-1}$) by lipid peroxides (Figure 3.25A; [366]). Diene oxidation increases green fluorescence (λ_{max} 520 nM) of the BODIPY dye (Figure 3.25A; [367]). In preliminary experiments, localization of C_{11}-BODIPY$^{581/591}$ to the mitochondria was demonstrated by co-labeling Jurkat T cells with the mitochondrial specific probe MitoTracker Green (Figure 3.25B). Elevated green fluorescence was observed in >95% of Jurkat T cells treated with *t*-BHP for 1 h, while ~20% increase was detected in response to H_2O_2. By contrast, Bz-423 triggered a <3% increase in C_{11}-BODIPY$^{581/591}$ green fluorescence at this timepoint (Figure 3.25C and 3.25D). After 4 h, at which point release of MIS proteins is observed, no further increase in green fluorescence was detected in response to Bz-423

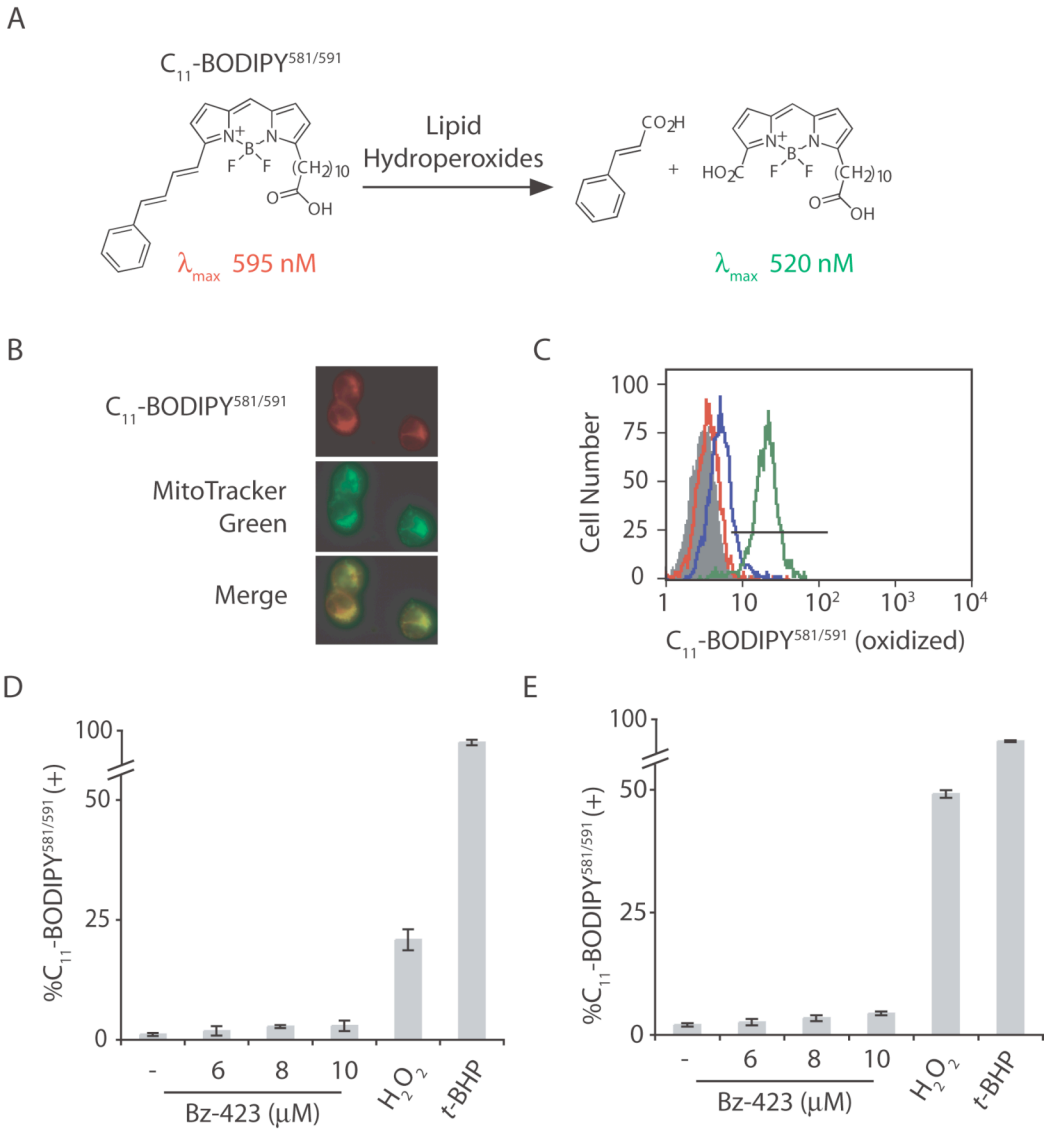

Figure 3.25 - Bz-423 does not cause oxidation of mitochondrial phospholipids. (A) Oxidation of the conjugated diene moiety by lipid hydroperoxides increases green fluorescence of C_{11}-BODIPY$^{581/591}$. (B) Images (630x) of Jurkat T cells co-labeled (30 min) with C_{11}-BODIPY$^{581/591}$ (50 nM) and MitoTracker Green (50 nM). (C) Jurkat T cells were labeled with C_{11}-BODIPY$^{581/591}$ (50 nM) for 30 min and C_{11}-BODIPY$^{581/591}$ green fluorescence was measured after 1 h following treatment with *t*-BHP (100 μM; green histogram), H_2O_2 (100 μM; blue histogram), Bz-423 (10 μM; red histogram) or vehicle (shaded histogram) for 1 h. (D) Jurkat T cells were treated with the indicated concentrations of Bz-423, *t*-BHP (100 μM) or H_2O_2 (100 μM) for 2 h and lipid peroxidation measured in terms of the increase in C_{11}-BODIPY$^{581/591}$ green fluorescence. (E) Jurkat T cells were treated as in D, but increased C_{11}-BODIPY$^{581/591}$ green fluorescence was measured after 4 h. Panel B is from a single experiment. Panels C – E are representative of two independent experiments.

(Figure 3.25E). These observations demonstrate that unlike *t*-BHP and H_2O_2, Bz-423 does not cause peroxidation of mitochondrial phospholipids.

While CL oxidation appears to be necessary for release of MIS proteins in MEFs treated with actinomycin D, the generality of this mechanism in unclear. For instance, the MRC complex I inhibitor rotenone does not induce CL peroxidation despite stimulating mitochondrial $O_2^{\bullet-}$ production [362]. In addition, although cytochrome *c* binds tightly to CL (K_d ~ 2 nM; [368]), only a small fraction of cytochrome *c* (~15%) interacts with CL because cytochrome *c* is localized to the MIS while CL is primarily present on the inside face of the mitochondrial inner membrane [369]. Instead, the majority of cytochrome c is either soluble in MIS or loosely associated with the inner membrane via electrostatic interactions.

Some reports suggest that cytochrome *c* can be retained in the MIS by electrostatic interactions following MOMP [363, 370], these studies have employed low-ionic-strength buffers, which are not physiological, and *promote* electrostatic interactions between cytochrome *c* and the inner mitochondrial membrane [5]. Finally, single-cell imaging has revealed no difference in the kinetics of cytochrome *c* release relative to other pro-apoptotic MIS proteins (e.g., Smac/DIABLO and Omi/Htra2) in HeLa cells treated with actinomycin D [12], which suggests that additional biochemical events are unnecessary to mobilize cytochrome c after MOMP. The absence of detectable lipid peroxidation in response to Bz-423 corresponds to studies, which suggest that CL oxidation is not required for efficient release of cytochrome *c* after MOMP.

Bz-423 does not induce phosphorylation of $p56^{Lck}$: Although elevated intracellular $O_2^{\bullet-}$ levels is the first response detected following treatment with Bz-423, escape of this

ROS from mitochondria is difficult to comprehend because it is charged, and therefore cannot diffuse through lipid bilayers [371]. Nevertheless, the ability of the SOD mimetic MnTBAP to block Bz-423-induced cell death suggests that $O_2^{\bullet-}$, rather than H_2O_2, is the ROS that initiates the extra-mitochondrial signaling. In addition, the absence of a reduction in aconitase activity suggests that Bz-423 causes preferential release of $O_2^{\bullet-}$ into the MIS. While the inner mitochondrial membrane is impermeable to charge species, $O_2^{\bullet-}$ can be transported out of the MIS by channels (e.g., VDAC) located in the outer mitochondrial membrane (see Chapter 1; [295, 372]).

As described in Chapter 1, due to differences in their chemical properties $O_2^{\bullet-}$ and H_2O_2 modulate distinct cellular pathways. Therefore, it may be possible to gain insight into the signal leaving the mitochondria in response to Bz-423 by examining responses characteristic of either ROS. For example, protein tyrosine phosphatases (PTPs) are inactivated by H_2O_2 *in vitro* by oxidation of a catalytic site cysteine residue to the corresponding sulfenic acid [373-375]. PTP inactivation is observed following stimulation of a variety of cell surface receptors and plays an essential role in propagation of the resulting intracellular kinase cascades (e.g., phosphorylation of extra-cellular regulated kinase-1/2 (Erk1/2)) [376-378]. Regulation of PTP by ROS has been studied extensively in the context of endothelial cells stimulated with growth-factors [308, 309]. Levels of both $O_2^{\bullet-}$ and H_2O_2 are elevated in MEFs and other endothelial cells following growth factor stimulation [379-383]. However, several lines of evidence suggest that H_2O_2 is the relevant ROS. First, $O_2^{\bullet-}$ reacts with cysteine thiols at rate ($k < 10^3$) that is slow relative to dismutation to H_2O_2, which can occur spontaneously ($k \sim 4.5 \times 10^5$) or be catalyzed by SODs ($k \sim 10^9$) [384, 385]. Second, the Cu,Zn-SOD inhibitor ATN-224 or

reducing expression of this enzyme by siRNA increase $O_2^{\bullet-}$ levels, decreases H_2O_2 levels, and reduce phosphorylation of Erk1/2 in response to growth factor stimulation [379]. Together, these data demonstrate that Cu,Zn-SOD plays an essential role in growth-factor signaling by converting $O_2^{\bullet-}$ to H_2O_2, which mediates oxidative inactivation of PTPs.

Elevated H_2O_2 levels are also observed in primary and leukemia T cells within 10 minutes of antigenic stimulation (See Chapter 3 Introduction). Evidence that this ROS response is essential for T cell activation comes from studies in which antioxidants reduce proliferation following stimulation of the TCR [259, 386]. In addition, anti-oxidant pre-treatment reduces phosphorylation of signaling molecules downstream of the T cell receptor [262, 386, 387]. One example is lymphocyte-specific kinase ($p56^{Lck}$) [388], a non-receptor tyrosine kinase that plays an essential role in proximal TCR signaling [389]. Following antigenic stimulation, $p56^{Lck}$ phosphorylates intracellular domains of the TCR complex, which promotes recruitment of effector proteins including PI3Ks and phospholipase C [390].

In addition to TCR stimulation, $p56^{Lck}$ phosphorylation can be induced by treatment of Jurkat T cells with H_2O_2 (Figure 3.26A; [388]). $p56^{Lck}$ phosphorylation, then, serves as a biomarker/sensor for elevated levels of cytosolic H_2O_2. To evaluate $p56^{Lck}$ phosphorylation status in the presence of Bz-423, lysates were prepared from Jurkat T cells treated with Bz-423 for 1 or 2 h, at which point the $O_2^{\bullet-}$ response is maximal. While no changes were observed in response to Bz-423, H_2O_2 induced phosphorylation of $p56^{Lck}$ is indicated by a shift in mobility towards increased molecular weight on SDS-PAGE and immunoreactivity with a phospho-specific $p56^{Lck}$ antibody

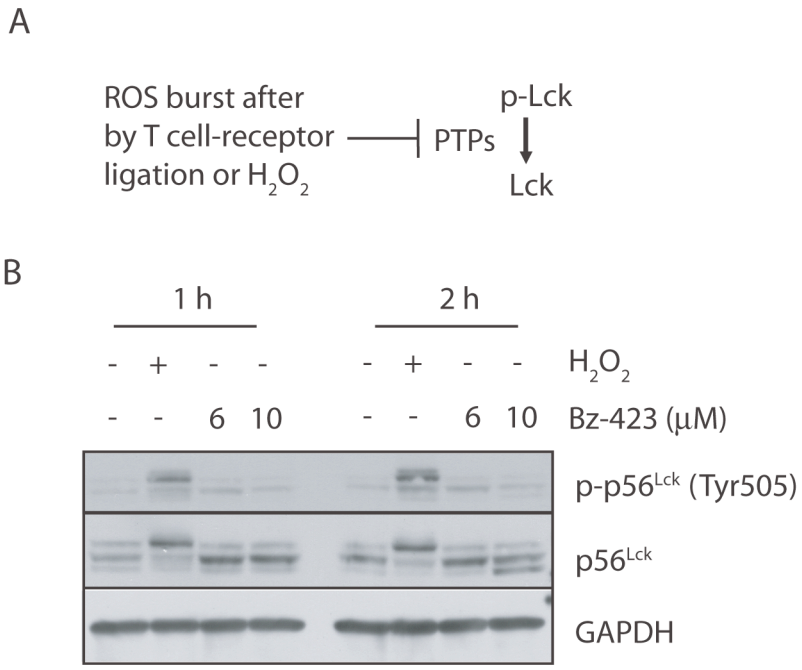

Figure 3.26 - Bz-423 does not induce phosphorylation of p56^{Lck}. (A) In T cells, phosphorylation of intracellular signaling molecules such as p56^{Lck} is pro-longed by inhibition of PTPs by H_2O_2 produced after engagement of the TCR (see text for details). (B) Lysates prepared from Jurkat T cells were treated with the indicated concentrations of Bz-423 or H_2O_2 (100 μM) for 1 or 2 h were immunoblotted with antibodies specific for total p56^{Lck}, p-p56^{Lck} or GAPDH. Panel B is from a single experiment.

(Figure 3.26B). These observations, combined with inhibitory effect of MnTBAP, suggest that cytosolic H_2O_2 levels are not increased in response to Bz-423.

Bz-423-induced cell death involves the Bcl-2 protein family: The absence of evidence for mPT pore opening suggests that release of pro-apoptotic MIS proteins in response to Bz-423 occurs by MOMP, which is regulated by the Bcl-2 protein family [38, 391]. Anti-apoptotic Bcl-2 proteins suppress MOMP by preventing homo-oligomerization of Bax and Bak, and in so doing, confer resistance to a variety of death stimuli [48]. To evaluate the role of Bcl-2 proteins in the death mechanism, the apoptotic

response to Bz-423 was evaluated in a Jurkat T cell clone over-expressing Bcl-2 (Figure 3.27A). The EC_{50} for Bz-423-induced accumulation of apoptotic DNA and overall cell death were increased >2-fold in the Bcl-2 clone (Figure 3.27B & 3.27C).

To determine the point at which Bcl-2 overexpression interferes with the Bz-423 apoptotic response, $O_2^{\bullet-}$ production, $\Delta\psi_m$ collapse and release of MIS proteins were evaluated in the Bcl-2 clone. Although some reports suggest that Bcl-2 has anti-oxidant properties [392, 393], Bz-423-induced $O_2^{\bullet-}$ production was indistinguishable between the Bcl-2 clone and vector control cells (Figure 3.27D). This data indicate that over-expression of Bcl-2 does not suppress Bz-423-induced apoptosis by blocking the increase in intracellular $O_2^{\bullet-}$ levels. In contrast to the effect on cell death, only a 12% shift in the EC_{50} for $\Delta\psi_m$ depolarization was observed in cells overexpressing Bcl-2 (7.0 ± 0.2 to 8.0 ± 0.2 μM; Figure 3.27E). However, over-expression of Bcl-2 prevented release of cytochrome *c*, Smac/DIABLO and AIF from the MIS (Figure 3.27F). These results are consistent with release of MIS proteins in response to Bz-423 occurring via MOMP and further suggests that this process may involve multi-BH-domain pro-apoptotic family members Bax and Bak. However, Bz-423-induced collapse of $\Delta\psi_m$ is observed in cells overexpressing Bcl-2. This finding suggests that MOMP and dissipation of $\Delta\psi_m$ are separable elements of Bz-423-induced apoptosis, with the latter being independent of the Bcl-2 protein family.

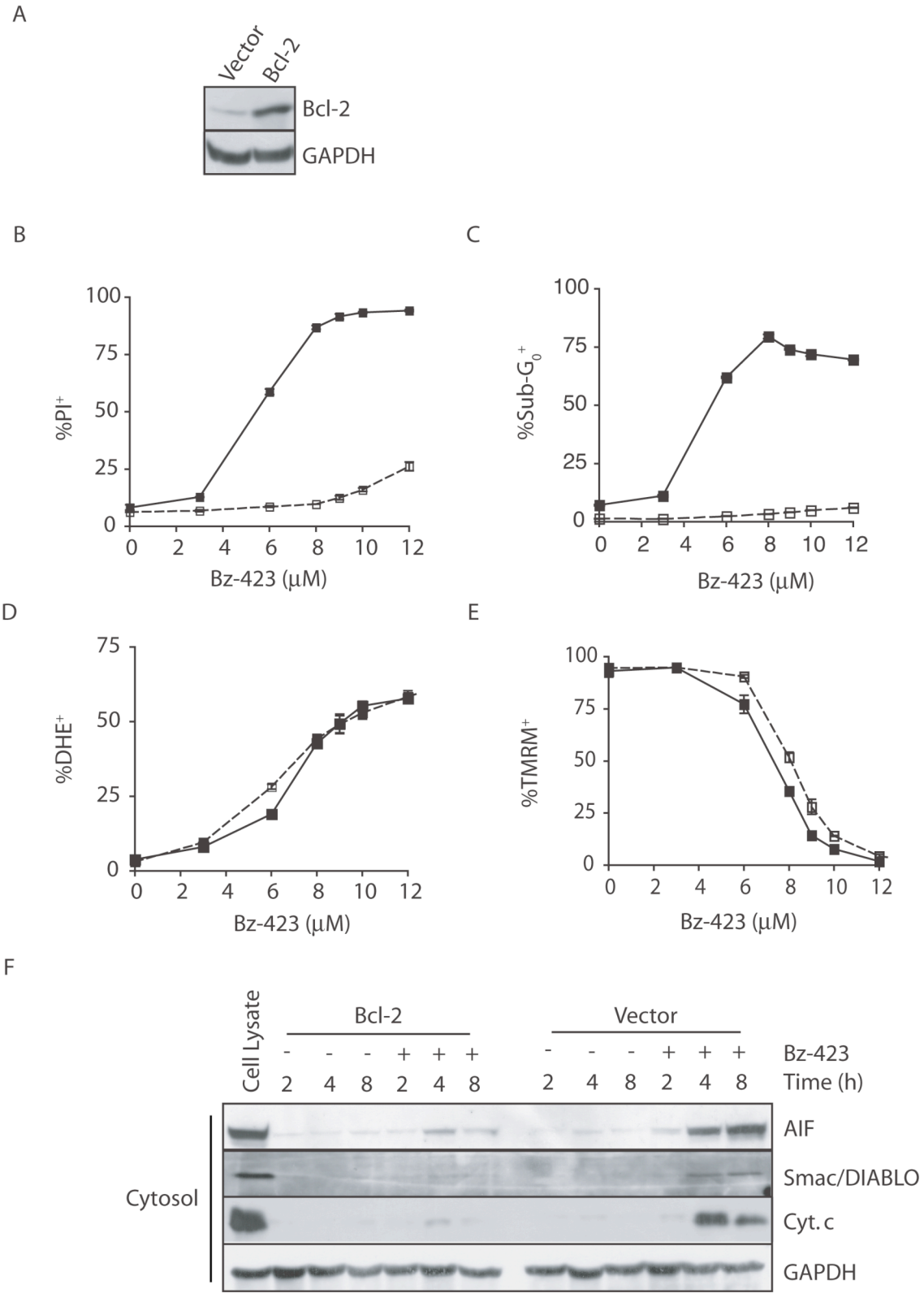
A
Vector
Bcl-2
Bcl-2
GAPDH
B
%PI+
Bz-423 (μM)
C
%Sub-G0+
Bz-423 (μM)
D
%DHE+
Bz-423 (μM)
E
%TMRM+
Bz-423 (μM)
F
Cell Lysate
Bcl-2
Vector
Bz-423
Time (h)
Cytosol
AIF
Smac/DIABLO
Cyt. c
GAPDH

Figure 3.27 - Effect of Bcl-2 overexpression on Bz-423-induced apoptosis. (A) Lysates from single Jurkat T cell clones stably transfected with a plasmid encoding Bcl-2 or empty vector were immunoblotted with antibodies specific for Bcl-2 or GAPDH. (B and C) Jurkat T cell clones stably transfected with Bcl-2 (□) or an empty vector (■) were treated with the indicated concentrations of Bz-423 for 24 h at which point cell death and apoptosis were assessed in terms of PI permeability and accumulation of Sub-G_0 DNA, respectively. (D and E) Jurkat T cell clones stably transfected with Bcl-2 (□) or an empty vector (■) were treated with the indicated concentrations of Bz-423 and $O_2^{\bullet-}$ production was determined by DHE staining at 2 h, while $\Delta\psi_m$ was measured by TMRM staining at 8 h. (F) Cytosolic fractions prepared from Jurkat T cell clones stably transfected with Bcl-2 or empty vector following treatment (indicated times) with Bz-423 (10 μM) were immunoblotted with antibodies specific for AIF, Smac/DIABLO, cytochrome *c* (Cyt. *c*), and GAPDH. Figure is representative of at least two separate experiments.

Collapse of $\Delta\psi_m$ often results from damage of MRC complexes by caspases activated following release of cytochrome *c* and Smac/DIABLO from the MIS [337]. Hence, it is surprising that Bz-423-induced $\Delta\psi_m$ depolarization occurs under conditions where the outer membrane remains intact. To determine if this independence is specific to Bz-423 or a general property of Jurkat T cells undergoing apoptosis, we evaluated how the Bcl-2 clone responded to staurosporine(STS), a non-specific kinase inhibitor that induces apoptosis through mitochondrial-dependent signals (Figure 3.28A; [394]). In contrast to the results with Bz-423, Bcl-2 over-expression blocked $\Delta\psi_m$ depolarization, release of pro-apoptotic MIS proteins, DNA fragmentation and cell death triggered by STS (Figure 3.28B - 3.28E). This data, together with the finding that overexpression of Bcl-2 does not block $O_2^{\bullet-}$ production, suggest that the ability of Bz-423 to dissipate $\Delta\psi_m$ independent of MOMP is unique to this compound rather than a general property of the apoptotic response in Jurkat T cells.

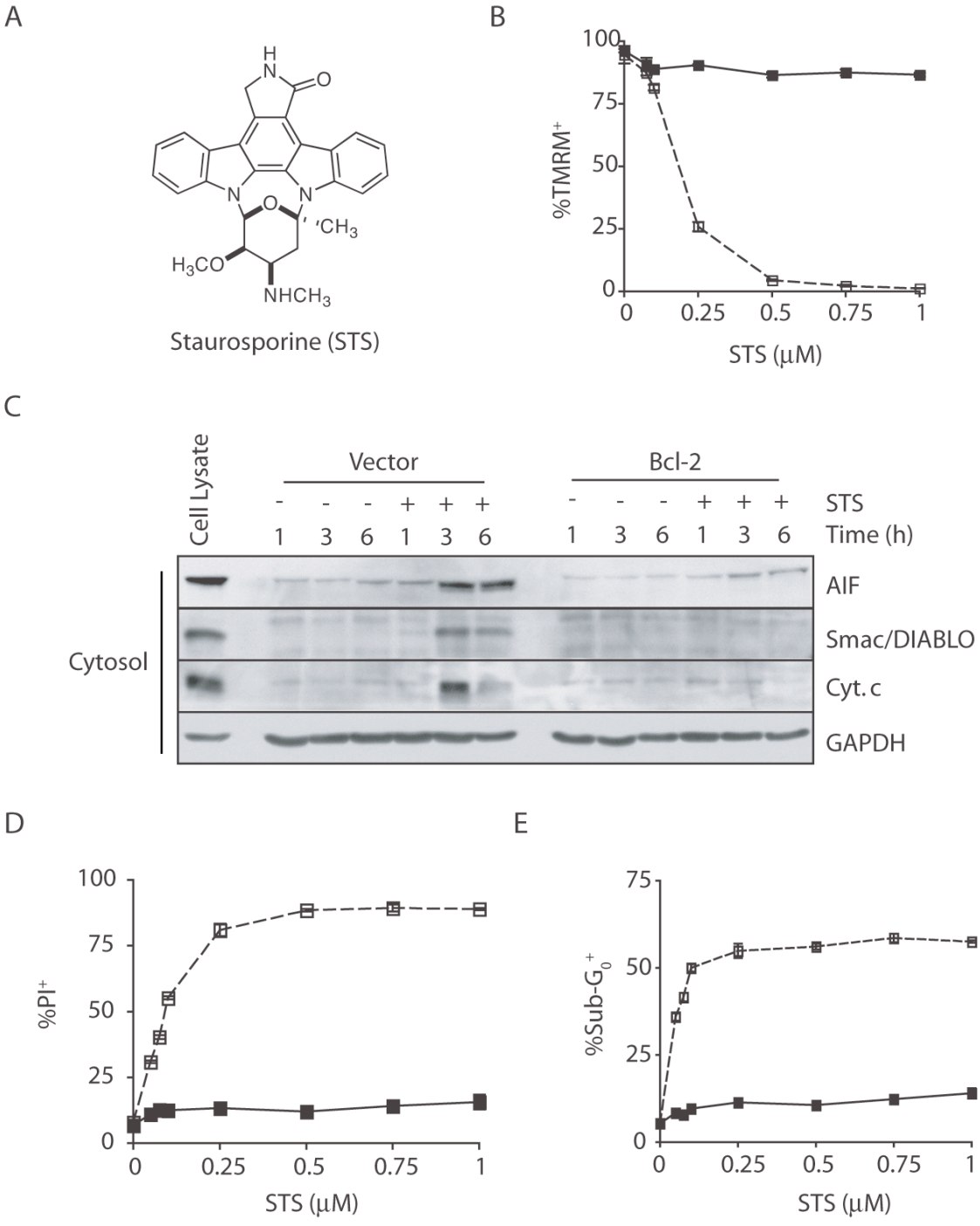
A
Staurosporine (STS)
B
%TMRM+
STS (μM)
C
Cell Lysate
Vector
Bcl-2
STS
Time (h)
Cytosol
AIF
Smac/DIABLO
Cyt. c
GAPDH
D
%PI+
STS (μM)
E
%Sub-G0+
STS (μM)

Figure 3.28 - Effect of Bcl-2 over-expression on staurosporine (STS) induced apoptosis. (A) The pro-apoptotic pan-kinase inhibitor STS. (B) Jurkat T cell clones stably transfected with Bcl-2 (■) or an empty vector (□) were treated (6 h) with the indicated concentrations of STS and $\Delta\psi_m$ was measured by TMRM staining. (C) Cytosolic fractions prepared from Jurkat T cell clones stably transfected with Bcl-2 or empty vector following treatment (indicated times) with STS (0.5 μM) were immunoblotted with antibodies specific for AIF, Smac/DIABLO, cytochrome *c* (Cyt. *c*), and GAPDH. (D and E) Jurkat T cell clones stably transfected with Bcl-2 (■) or an empty vector (□) were treated (24 h) with the indicated concentrations of Bz-423 and cell death and apoptosis were assessed in terms of PI permeability and accumulation of Sub-G_0 DNA, respectively. Panel C is from a single experiment. Panels B, D and E are representative of at least three independent experiments.

To determine if $\Delta\psi_m$ depolarization is sufficient to cause cell death in the absence of MOMP, the Bcl-2 clone was treated with a concentration of Bz-423 (10 μM) sufficient to collapse $\Delta\psi_m$. After 24 h, Bz-423 was removed and proliferation assessed over the next 7 d by vital dye exclusion. Whereas Bz-423-induced release of MIS proteins eventually results in cell death even when caspase activity is blocked, the Bcl-2 clones survive and after a 2 d lag, proliferate normally (Figure 3.29A). This lag may correspond to the time needed to regenerate systems that produce and maintain $\Delta\psi_m$, which is fully recovered in the Bcl-2 clones 48 h after washout of Bz-423 (Figure 3.29B). These findings reinforce that MOMP, rather than dissipation of $\Delta\psi_m$, is the point at which Jurkat T cells irreversibly commit to cell death in response to Bz-423.

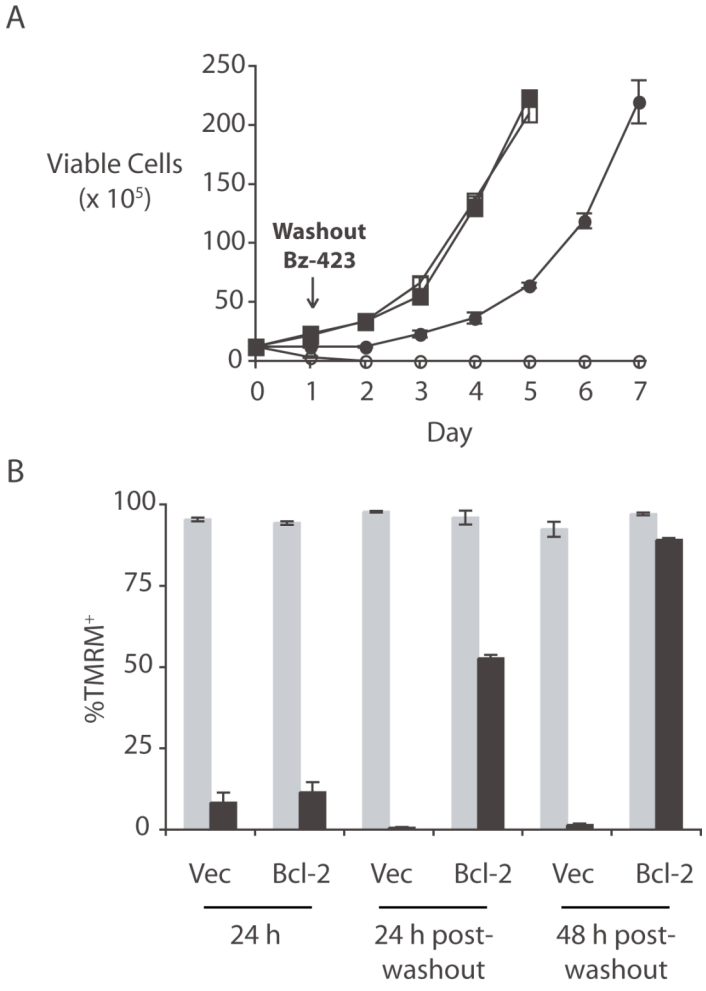

Figure 3.29 - Despite collapse of $\Delta\psi_m$, Bcl-2 over-expression blocks Bz-423-induced cell death. (A) Jurkat T cells stably transfected with Bcl-2 (●,■) or an empty vector (○,□) for 30 min were incubated with Bz-423 (10 μM; ●,○) or vehicle (■,□) for 24 h, at which point Bz-423 agents was removed and the number of viable cells determined daily by Trypan exclusion. (B) Jurkat T cells stably transfected with Bcl-2 or an empty vector were treated with Bz-423 (10 μM; black bars) or vehicle (grey bars) for 24 h, at which point Bz-423 was removed. $\Delta\psi_m$ was determined at indicated times by TMRM staining. Absence of error bars indicates <1% standard deviation. Figure is from a single experiment.

The multi-BH-domain pro-apoptotic Bcl-2 protein Bak is preferentially activated in response to Bz-423: As described in the introduction to Chapter 3, the mitochondrial outer membrane resident protein Bak undergoes a conformational changes in response to apoptotic stimuli that promotes homo-oligomerization and formation of proteolipid channels [53]. Activation of Bax is also associated with homo-oligomerization and the formation of proteolipid channels in the mitochondrial outer membrane. However, since Bax is cytosolic, it must translocate to the mitochondria in order to induce MOMP [395]. To test the hypothesis that Bax is engaged in response to Bz-423, cytosolic and mitochondrial fractions of Jurkat T cells treated with Bz-423 were immunoblotted to define the sub-cellular distribution of this protein. Bz-423 causes redistribution of Bax from the cytosol to the mitochondria after 8 h, which is significantly delayed relative to MOMP (4 h) based on the appearance of cytochrome *c* in the cytosol (Figure 3.30A). This delay indicates that although Bz-423 engages Bax in the Jurkat T cells, it is unlikely to mediate MOMP.

Bak activation does not involve sub-cellular redistribution, but involves a conformational change that exposes a cryptic amino-terminal epitope [391]. To determine if Bak is activated in response to Bz-423, an antibody specific for this epitope was used to monitor its activation, while an antibody that recognizes an analogous region of Bax was used to confirm the Bax translocation results. For these experiments Jurkat T cells were fixed to glass slides with paraformaldehye, permeabilized with the detergent saponin and binding of Bax or Bak amino-terminal specific antibodies was visualized with a biotin-conjugated secondary antibody followed by strepavidin-fluorescein conjugate. Using this immunofluorescence approach, Bak activation is apparent within

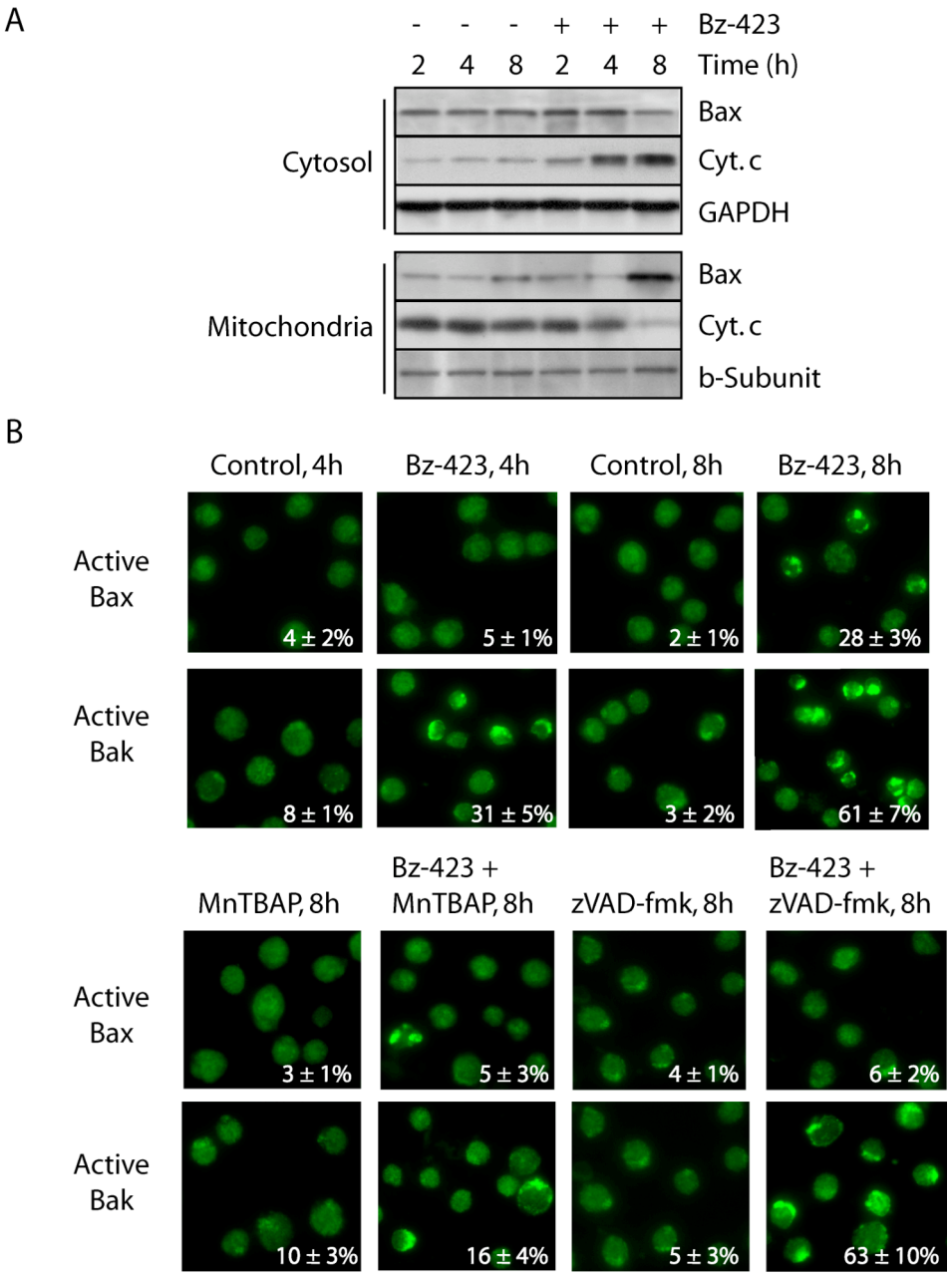

Figure 3.30 - Bak is preferentially activated in response to Bz-423. (A) Mitochondrial and cytosolic fractions of Jurkat T cells treated with Bz-423 (10 μM) or vehicle were immunoblotted with antibodies specific for Bax and cytochrome c (Cyt. *c*), GAPDH and the β-subunit of the F_oF_1-ATPase. (B) Jurkat T cells were pre-incubated with MnTBAP (100 μM) or zVAD-fmk (50 μM) for 30 min prior to treatment with Bz-423 (10 μM) or vehicle for the indicates times. Bax or Bak activation was detected by immunofluorescence microscopy with antibodies specific for an amino-terminal epitope of either protein exposed during activation. Data is representative of at least two independent experiments.

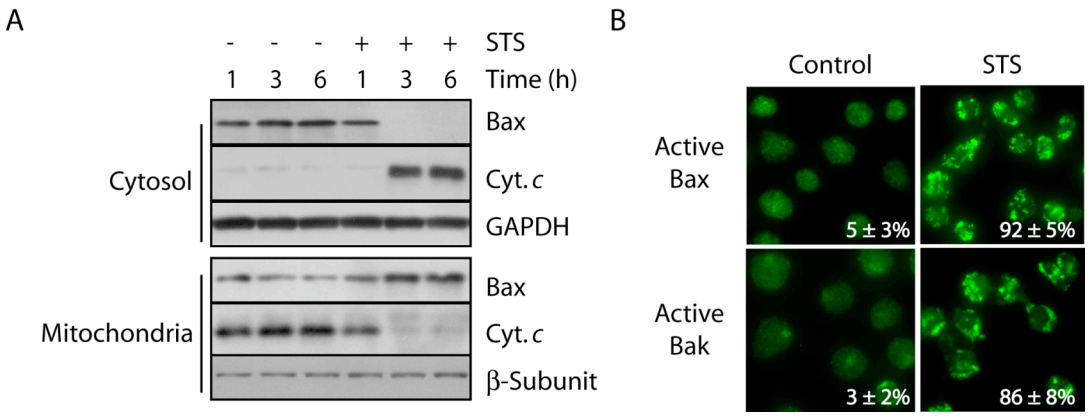

Figure 3.31 - Both Bax and Bak are activated in Jurkat T cells treated with STS. (A) Mitochondrial and cytosolic fractions of Jurkat T cells treated with STS (0.5 μM) or vehicle were immunoblotted with antibodies specific for Bax and cytochrome c (Cyt. *c*), GAPDH and the β-subunit of the F_oF_1-ATPase. (B) Jurkat T cells were treated with STS (0.5 μM) or vehicle for 3 h. Bax or Bak activation was detected by immunofluorescence microscopy with antibodies specific for an amino-terminal epitope of either protein exposed during activation. Figure is representative of at least four separate experiments.

4 h (31 ± 5% of cells positive versus 8 ± 1% in vehicle-treated cells) and the majority of cells (63 ± 10%) were positive by 8 h (Figure 3.30B). Activated Bax, on the other hand, was not detected at 4 h while 28 ± 3% of cells were positive for activated Bax by 8 h (Figure 3.30B). In contrast, treatment of Jurkat T cells with STS for 3 h promoted simultaneous redistribution of Bax to the mitochondria and appearance of cytochrome *c* in the cytosol (Figure 3.31A), and equivalent activation of Bax and Bak (Figure 3.31B). Consequently, preferential activation of Bak appears to be a property of the response to Bz-423 rather than a general characteristic of apoptosis in Jurkat T cells.

Scavenging $O_2^{\bullet-}$ blocks all components of the Bz-423 death response in Jurkat T cells. This inhibitory effect suggests that Bz-423-induced activation of Bax and Bak was

also likely to be $O_2^{\bullet-}$-dependent. In support of this hypothesis, pre-treating T cells with MnTBAP blocked activation of both Bax and Bak (Figure 3.30B). In contrast to $O_2^{\bullet-}$ production, caspase activation is required for Bz-423-induced apoptosis, but not release of cytochrome *c*, Smac/DIABLO and AIF from the MIS. The independence of Bz-423-induced apoptotic mitochondrial changes on caspase activity suggests that activation of Bax and Bak may likewise be caspase-independent. In support of this hypothesis, Bak activation (61 ± 7% of cells positive) was unaffected by zVAD-fmk pretreatment, which suggests that Bak mediates the caspase-independent release of pro-apoptotic MIS proteins in response to Bz-423. Bax activation, in contrast, was not observed (6 ± 2% of cells positive) in cells pretreated with zVAD-fmk (Figure 3.30B). Collectively, these data reveal that Bax and Bak respond differentially to Bz-423-induced $O_2^{\bullet-}$ such that Bak is activated earlier and to a larger extent (greater than two-fold), and occurs within a time frame consistent with it triggering MOMP. Activation of Bax, by contrast, occurs after MOMP and is caspase-dependent.

Bak is required for Bz-423-induced cell death, while Bax is not: Bak is activated to a greater extent than Bax in response to Bz-423. In addition, Bak activation is coincident with MOMP, while Bax translocation and activation is only observed afterwards. Because MOMP is the point at which Jurkat T cells commit to die in response to Bz-423, Bak is predicted to be necessary for Bz-423-induced apoptosis, while Bax is likely dispensable. To evaluate this hypothesis, Jurkat T cells were transiently transfected with siRNAs targeting Bax and Bak. This approach produced cells in which with a control siRNA sequence (Figure 3.32A). Reducing levels of Bak resulted in a

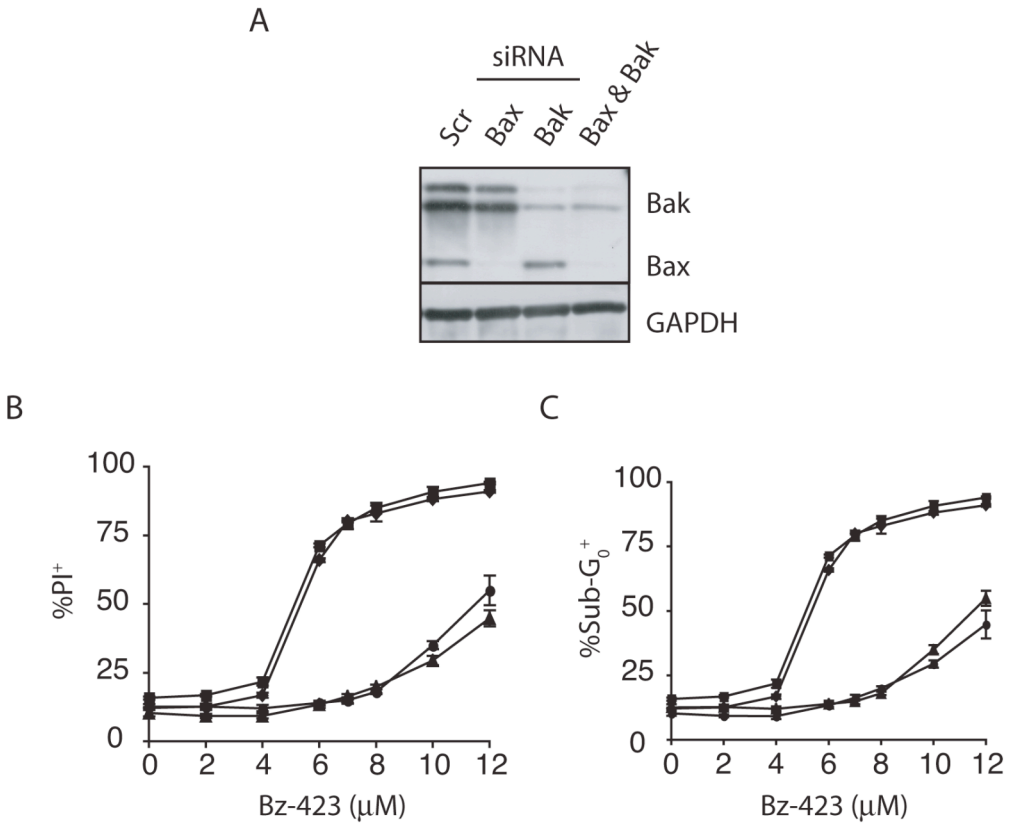

Figure 3.32 - Bak is required for Bz-423-induced cell death in Jurkat T cells while Bax is not. (A) Lysates from Jurkat T cells transiently transfected with siRNAs targeting Bax or Bak or a control siRNA sequence were immunoblotted with antibodies specific for Bax, Bak or GAPDH. (B and C) Jurkat T cells transiently transfected with siRNAs targeting Bax (◆), Bak (▲), both proteins (●) or a control siRNA sequence (■) were treated (24 h) with the indicated concentrations of Bz-423 and cell death and apoptosis were assessed in terms of PI permeability and accumulation of Sub-G_0 DNA, respectively. Absence of error bars indicates standard error is <1%. Figure is representative of at least three independent experiments.

greater than two-fold increase in the EC_{50} for Bz-423-induced DNA fragmentation and cell death, while Bax knockdown did not protect against either response. In addition, knocking down Bax along with Bak provided no additional protection (Figure 3.32B & 3.32C). The dependence of Bz-423-induced cell death on Bak is consistent with the hypothesis that Bak is solely responsible for MOMP.

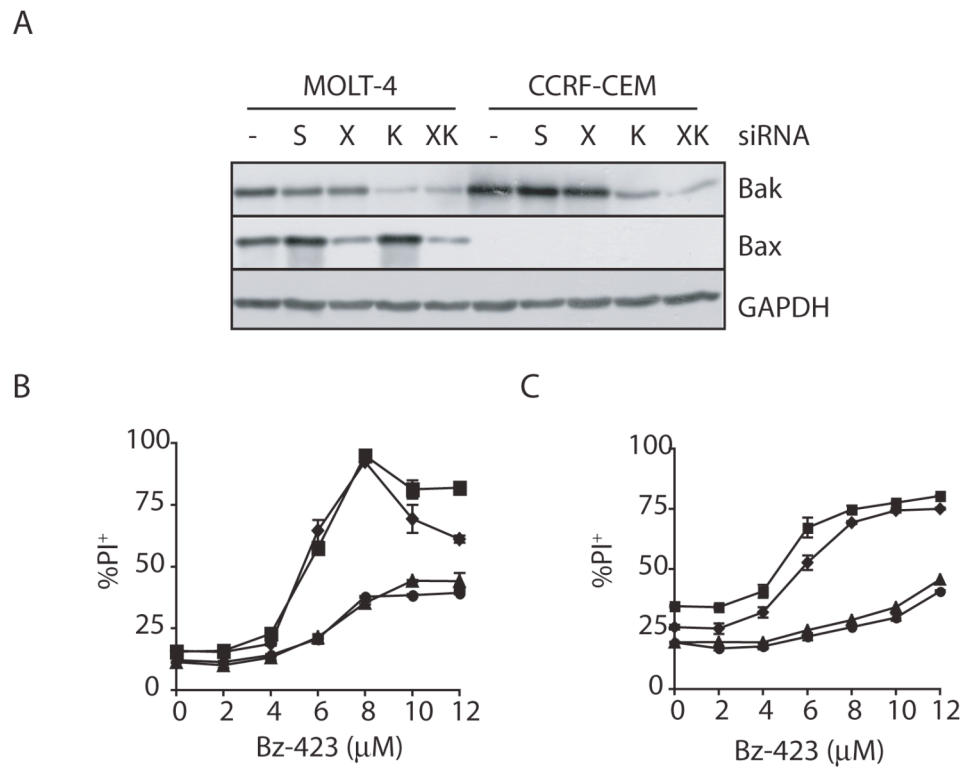

Figure 3.33 - Bak is required for Bz-423-induced cell death in MOLT-4 and CCRF-CEM T cells, while Bax is not. (A) Lysates from MOLT-4 or CCRF-CEM T cells transiently transfected with siRNAs targeting Bax (X), Bak (K), both proteins (XK) or a control siRNA sequence (S) were immunoblotted with antibodies specific for Bax, Bak or GAPDH. (B) MOLT-4 and (C) CCRF-CEM T cells transiently transfected with siRNAs targeting Bax (◆), Bak (▲), both proteins (●) or a control siRNA sequence (■) were treated (24 h) with the indicated concentrations of Bz-423 and cell death was assessed in terms of PI permeability. Absence of an error bar indicates <1% standard error. Figure is from a single experiment.

Bax and Bak function redundantly during development and in a variety of models of apoptosis including MEFs exposed to Bz-423 [87, 396]. This contrast raised questions regarding whether this principle role Bak plays in Bz-423-induced apoptosis in Jurkat T cells extends to other $CD4^+$ T cell leukemia lines. To answer this question, Bax and Bak levels were reduced in the MOLT-4 and CCRF-CEM T cell leukemia lines (Figure

3.33A). Similar to the results in the Jurkat T cells, reducing Bax expression did not block Bz-423-induced cell death in MOLT-4 T cells, while the EC_{50} was increased greater than two-fold by Bak knockdown (Figure 3.33B). Again, no additional protection was provided by knocking down Bax along with Bak in MOLT-4 T cells (Figure 3.33B). Reduction of Bak levels resulted in a greater than two-fold increase in the EC_{50} for Bz-423-induced cell death in CCRF-CEM T cells (Figure 3.33C). Bax appears to be entirely dispensable in this cell line because basal levels of this protein were below the limits of detection by immunoblotting (Figure 3.33A). These data demonstrate that dependence on Bak is not unique to the Bz-423 death response in Jurkat T cells, but is also observed in other PTEN-deficient T cell leukemia lines.

To determine at what point reducing Bak levels interferes with the Bz-423 apoptotic cascade, $O_2^{\bullet-}$ production, $\Delta\psi_m$ collapse, and release of cytochrome *c*, Smac/DIABLO and AIF was assessed in Jurkat T cells transiently transfected with siRNAs targeting this protein. The $O_2^{\bullet-}$ response in Jurkat T cells with reduced Bak levels was equivalent to control cells, and only a 13% increase in the EC_{50} for $\Delta\psi_m$ collapse (8.1 ± 0.5 and 9.1 ± 0.2 μM, respectively) was observed (Figure 3.34A and 3.34B). In contrast, reducing Bak levels prevented release of apoptogenic MIS proteins in response to Bz-423 (Figure 3.34C). These data demonstrate that Bak is required for Bz-423-induced MOMP and support a model where Bax is only activated *after* release of cytochrome *c* and Smac/DIABLO from the MIS.

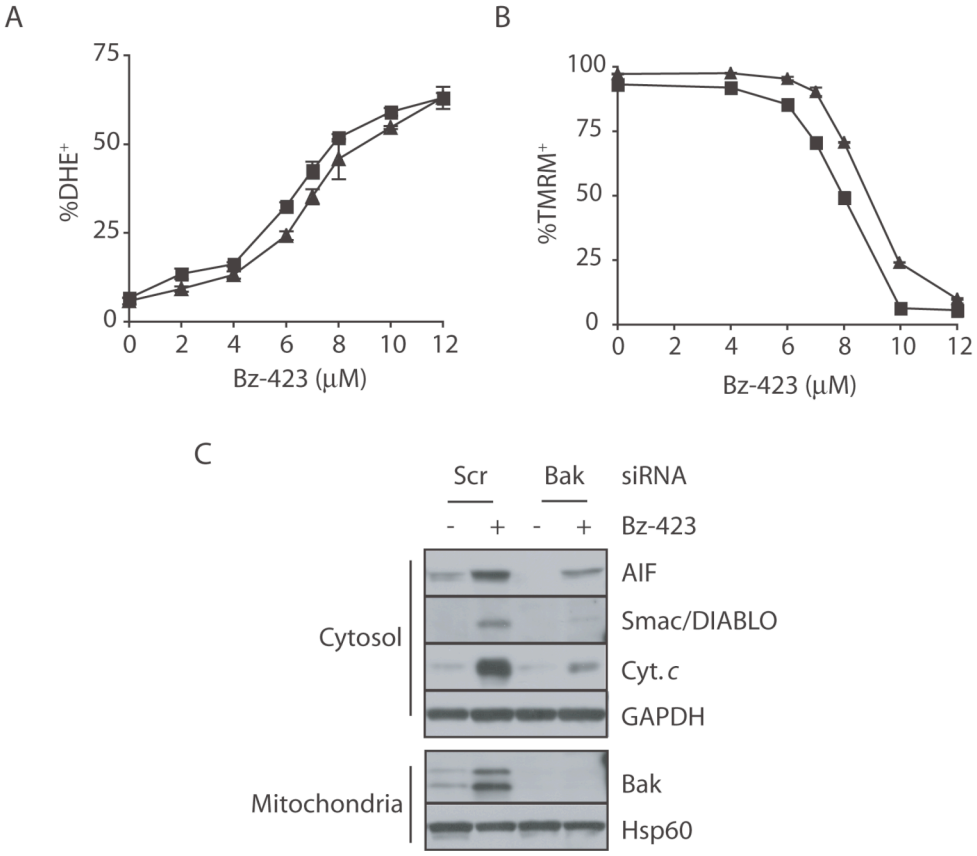

Figure 3.34 - Bak knockdown blocks Bz-423-induced release of pro-apoptotic MIS proteins in Jurkat T cells. (A and B) Jurkat T cells transiently transfected with siRNAs targeting Bak (▲) or a control siRNA sequence (■) were treated with the indicated concentrations of Bz-423 and $O_2^{\bullet-}$ production was measured with DHE staining at 2 h, while $\Delta\psi_m$ was measured with TMRM staining at 8 h. (C) Mitochondrial and cytosolic fractions from Jurkat T cells transiently transfected with siRNAs targeting Bak or a control siRNA sequence were treated with Bz-423 (10 μM, 8 h) were immunoblotted with antibodies specific for AIF, Smac/DIABLO, cytochrome *c* (Cyt. *c*), GAPDH, Bak and Hsp60. Panels A and B are representative of three independent experiments, while panel C is from a single experiment. Absence of an error bar indicates <1% standard error.

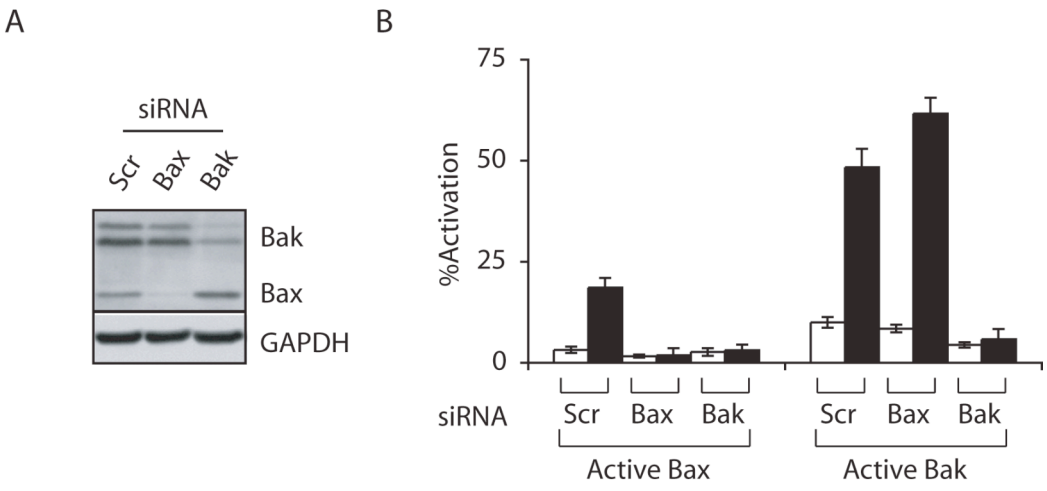

Figure 3.35 - Bak knockdown blocks Bz-423-induced Bax activation in Jurkat T cells. (A) Lysates from Jurkat T cells transiently transfected with siRNAs targeting Bax or Bak or a control siRNA sequence were immunoblotted with antibodies specific for Bax, Bak or GAPDH. (B) Jurkat T cells transiently transfected with siRNAs targeting Bax, Bak or a control siRNA sequence were treated (8 h) with Bz-423 (10 μM, black bars) or vehicle (white bars) and Bax or Bak activation was detected by immunofluorescence microscopy using antibodies specific for amino-terminal epitopes of Bax or Bak exposed during activation.

Finally, the ability of the caspase inhibitor zVAD-fmk to block Bax activation suggests that this response occurs downstream of Bak-dependent MOMP. As such, Bax activation was also expected to be suppressed by reduction of Bak levels. To evaluated this hypothesis, Bz-423-induced Bax and Bak activation were examined Jurkat T cells transiently transfected with siRNAs targeting either protein or a control sequence (Figure 3.35A). Consistent with hierarchical activation of Bax and Bak, Bz-423-induced Bax activation was not observed in Jurkat T cells transfected with siRNAs targeting Bak (Figure 3.35B). In contrast, Bax knockdown *increased* the fraction of cells positive for Bak activation relative to control (Figure 3.35B). Collectively, analysis of the Bz-423 response in T cells with reduced levels of Bax and Bak identifies a hierarchical

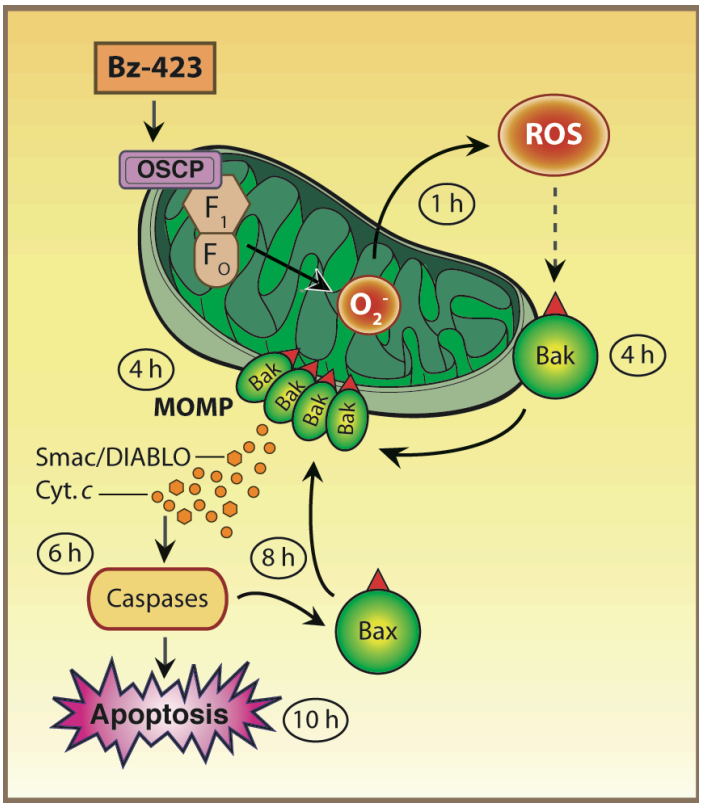

Figure 3.36 - Bz-423 induces hierarchical activation of Bax and Bak in Jurkat T cells. See text for details.

mechanism in which Bak activation links Bz-423-induced $O_2^{\bullet-}$ production to MOMP and cell death, while Bax is engaged downstream of release of cytochrome *c* and Smac/DIABLO from the MIS (Figure 3.36).

Bz-423 promotes changes in the levels of Bcl-2 proteins that are consistent with preferential Bak activation: In unstressed cells, Bak activation is opposed by direct binding of the anti-apoptotic Bcl-2 proteins Bcl-x_L, A1 and Mcl-1 [54]. As described in the introduction to Chapter 3, BH3-only proteins are pro-apoptotic members of the Bcl-2

family that promote Bak activation by neutralizing anti-apoptotic Bcl-2 proteins. BH3-only proteins are either expressed at low levels or restrained by post-translational mechanisms in unstressed cells, but are transcriptionally induced or post-translationally activated in response to stress signals (see Chapter 3 Introduction and Figure 3.7). Among these proteins, Noxa is specifically linked to Bak activation because binding of this BH3-only protein to Mcl-1 displaces Bak and targets Mcl-1 for proteasomal degradation [54]. In addition, Noxa expression is induced by oxidative stress [114-116]. As such, Bz-423-induced $O_2^{\bullet-}$ is hypothesized to signal Bak activation through changes in Noxa and Mcl-1 levels.

As an initial test of this hypothesis, levels of Noxa and Bak were measured by immunoblotting lysates from Bz-423-treated Jurkat T cells. Mcl-1 levels were reduced by 40% at 4 h, and continued to decrease to <10% of levels in vehicle treated cells at 8 h (Figure 3.36). The timing of the Mcl-1 decrease (4 h) is consistent with its mechanistic involvement in MOMP and Bak activation, which are also first observed at 4 h. The decrease in Mcl-1 levels was preceded by a three-fold increase in Noxa at 2 h, which was sustained for up to 8 h (Figure 3.36). These observations support a model in which the rise in Noxa levels promotes Bak activation by triggering proteasomal degradation of Mcl-1.

As a result of inhibitory binding of Bak by both Mcl-1 and Bcl-x_L, neutralizing Mcl-1 by Noxa overexpression is not sufficient to activate Bak in MEFs [54]. In contrast, overexpression of Noxa in Bcl-x_L-deficient MEFs or in conjunction with a BH3-only protein that neutralizes Bcl-x_L (e.g., Bad) is lethal in wild-type MEFs [54]. Similar studies have not been reported in hematopoetic cells. The dependence of Bak activation

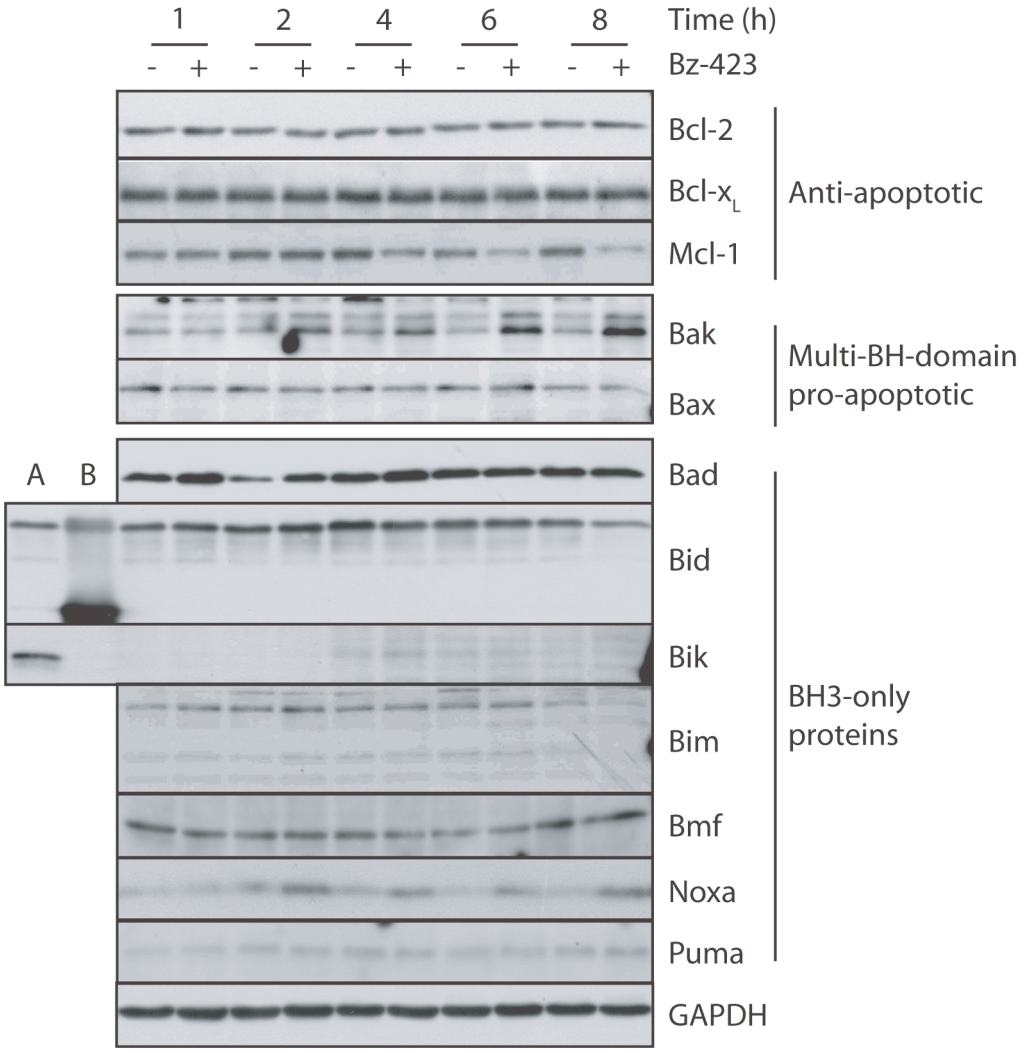

Figure 3.36 - Changes in the levels of Bcl-2 proteins induced by Bz-423. Lysates from Jurkat T cells treated with Bz-423 (10 μM) or vehicle for indicated times were immunoblotted with antibodies specific for Bcl-2, Bcl-x_L, Mcl-1, Bak, Bax, Bid, Bik, Bim, Bmf, Noxa, Puma and GAPDH. Lane A, Lysates from Ramos B cells; Lane B, recombinant human tBid. This figure is representative of at least two independent experiments.

on neutralization of both Mcl-1 and Bcl-x_L suggests that the response to Bz-423 is likely to involve changes in Bcl-2 family proteins in addition to the observed effects on Noxa and Mcl-1.

The hypothesis that Bz-423 causes changes in Bcl-2 proteins in addition to the observed effects on Noxa and Mcl-1 is supported by literature indicating that BH3-only proteins and anti-apoptotic Bcl-2 proteins are regulated by oxidative stress. For instance, the decrease in *bcl2* and *bclxl* transcripts following TCR stimulation appears to be redox-regulated because this change is blocked by pre-treatment with the antioxidant vitamin E [131]. It is not clear whether $O_2^{\bullet-}$ or H_2O_2 signal this decrease in *bcl2* and *bclx* mRNA because both ROS are elevated following TCR stimulation and scavenged by vitamin E [262, 317]. Regardless, if *bcl2* or *bclx* transcripts are destabilized by Bz-423-induced $O_2^{\bullet-}$, these effects are not reflected at the protein level (Figure 3.36). Finally, neither of the anti-apoptotic Bcl-2 proteins A1 and Bcl-w are anticipated block Bak activation because levels of these anti-apoptotic Bcl-2 proteins were below the limits of detection by immunoblotting in Jurkat T cells (Figure 3.36).

Expression of the BH3-only protein Bim, which can neutralize both Mcl-1 and Bcl-x_L, is induced by oxidative stress accompanying T cell activation as well as H_2O_2 and Trisenox [397-399]. Similarly, $O_2^{\bullet-}$ production induced by the histone deacetylase Vorinostat leads to proteolytic processing of the BH3-only protein Bid to its active, truncated form (tBid) [109]. However, neither increased Bim levels, nor Bid cleavage were observed in Jurkat T cells treated with Bz-423 (Figure 3.36). Levels of the BH3-only protein Bad are elevated in response to Bz-423 in MEFs [396]. This response appears to be cell-type specific, however, because an increase in Bad levels was not detected in Jurkat T cells treated with Bz-423 for up to 8 h (Figure 3.36). Additionally, levels of the BH3-only proteins Bmf and Puma were stable in response to Bz-423 for up

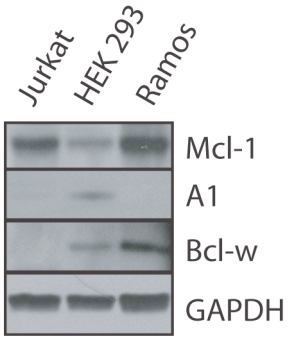

Figure 3.37 - Expression of the anti-apoptotic Bcl-2 proteins A1 and Bcl-w is not detected in Jurkat T cells. Lysates from Jurkat T cells (Jurkat), human embryonic kidney 293 (HEK 293) and Ramos B cells (Ramos) were immunoblotted with antibodies specific for Mcl-1, A1, Bcl-w and GAPDH. Figure is representative of a single experiment.

to 8 h, while expression of the BH3-only protein Bik was not detected in Jurkat T cells (Figure 3.36). Based on these results, Noxa appears to be the only BH3-only protein induced Bz-423-treated Jurkat T cells. However, several BH3-only proteins are regulated post-translationally (e.g., Bad is sequestered by 14-3-3 proteins [400], while Bmf is bound dynein motor complexes [122, 134]) and, therefore, may be activated in response to Bz-423 despite the lack of changes in their levels.

Expression of Bax and Bak in typically not elevated in response to apoptotic stimuli [38]. Instead, *activation* of these multi-BH-domain proteins is regulated post-translationally by the relative levels of BH3-only proteins and anti-apoptotic Bcl-2 proteins [38]. However, there are several examples where Bak levels are increased during apoptosis. For instance, Bak expression induced by stimulation of HL-60 B cells with interferon-γ as well as in HeLa cervical carcinoma cells treated with cyclooxygenase inhibitor Celecoxib [401, 402]. In the latter case, Bak induction is mediated by the

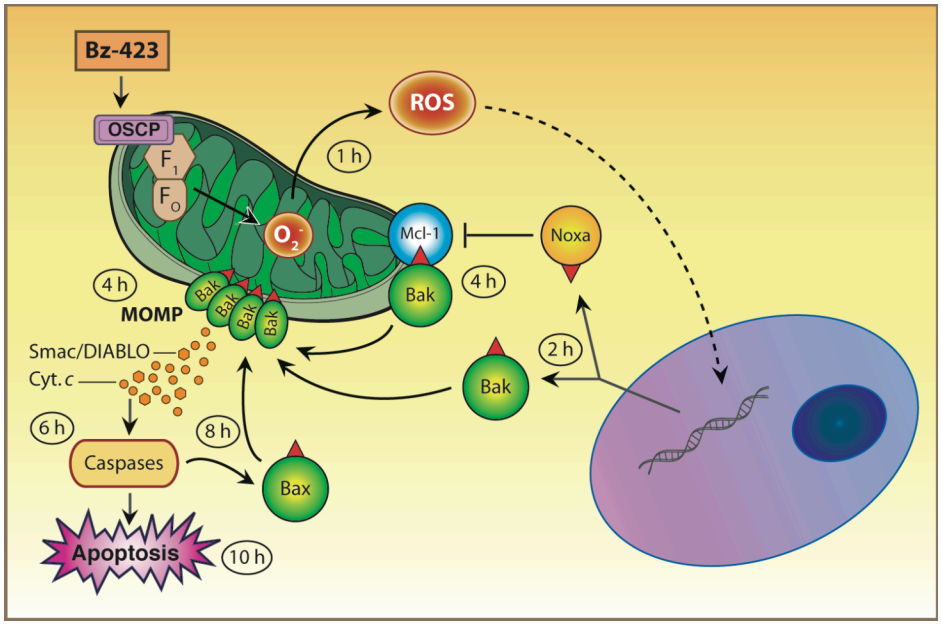

Figure 3.38 - Bz-423 induces changes in Bcl-2 proteins consistent with preferential Bak activation. Levels of the BH3-only protein Noxa along with Bak are elevated in Jurkat T cells treated with Bz-423. Noxa neutralizes the anti-apoptotic Bcl-2 protein Mcl-1, which in conjuction with increased Bak *levels*, is expected to promote *activation* of Bak.

growth arrest and DNA damage (GADD) inducible transcription factor GADD153 [401]. In addition, Bak mRNA and proteins levels are elevated following exposure of SH-SY5Y neuroblastoma cells to H_2O_2, which is thought to result from increased binding of the transcription factors NFκB and NFAT to the *bak1* promoter region [403]. The induction of *bak1* expression by H_2O_2, along with pivotal role this protein plays in Bz-423-induced apoptosis, suggests that Bak levels might be elevated in response to Bz-423. In support of this hypothesis, Bak levels were induced two-fold within 2 h of Bz-423 treatment and steadily increased till present at levels greater than six-fold above control by 8 h (Figure 3.36). In contrast, no change in Bax levels was observed following treatment with Bz-423 treatment (Figure 3.36). Collectively, these data suggest that Bz-423-induced Bak

activation results from neutralization of Mcl-1 by Noxa in conjunction with an increase in Bak *levels* that overwhelms the inhibitory capacity of Bcl-x_L (Figure 3.38).

Noxa contributes to, but is not required for, Bz-423-induced T cell apoptosis: To assess the role of Noxa in Bz-423-induced apoptosis, Jurkat T cells were transiently tranfected with siRNAs targeting this BH3-only protein or a control sequence which reduced Noxa by >95% (Figure 3.39A). Jurkat T cells with reduced Noxa levels are sensitive to Bz-423, albeit with a 25% shift in the EC_{50} for cell death (7.4 ± 0.2 to 9.8 ± 0.4 μM) (Figure 3.39B). Cell death was accompanied accumulation of hypodiploid DNA, again at elevated concentrations of Bz-423 relative to control cells, demonstrating that cell death does not occur via necrosis in the absence of Noxa (Figure 3.39C). Bak activation was attenuated in cells where Noxa expression was reduced (26 ± 2% cells positive) relative to those transfected with a control siRNA sequence (48 ± 5% positive; Figure 3.39D). This partial inhibition of Bak activation was sufficient to block, or at least delay, the downstream activation of Bax at 8 h (Figure 3.39D). These data demonstrate that Noxa contributes to, but is not solely responsible for, Bz-423-induced Bak activation.

Low concentrations of cycloheximide attenuate Bz-423-induced cell death: The ability of Bz-423 to trigger apoptosis in cells with reduced levels of Noxa suggests that the observed increase in Bak *levels* is required for the death response. To determine whether *de novo* protein synthesis is required for death response, Jurkat T cells were incubated with varying concentrations of the protein synthesis inhibitor cycloheximide (CHX) prior to treatment with Bz-423 (Figure 3.40B; [404]). Consistent with inhibition of protein synthesis, CHX promoted a concentration-dependent decrease in the levels of the labile proteins c-Myc and cyclin D3 ($t_{1/2}$ ~30 min; [405, 406]), with reduced levels of

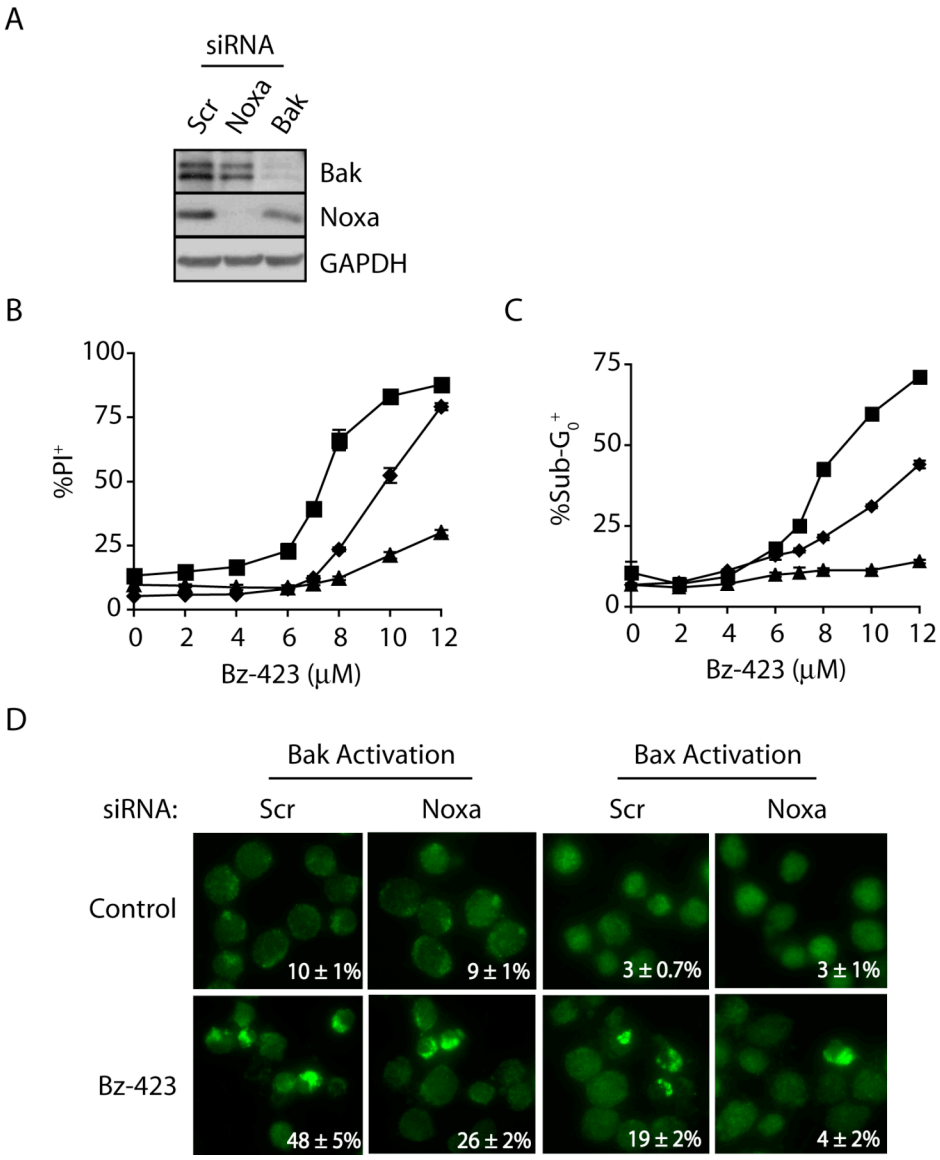

Figure 3.39 - Noxa contributes to Bz-423-induced apoptosis in Jurkat T cells. (A) Lysates from Jurkat T cells transiently transfected with siRNAs targeting Noxa, Bak or a control siRNA sequence (Scr) were immunoblotted with antibodies specific for Noxa, Bak or GAPDH (B and C) Jurkat T cells transiently transfected with siRNAs targeting Noxa (◆), Bak (▲) or a control siRNA sequence (■) were treated (24 h) with the indicated concentrations of Bz-423. Cell death and apoptosis were assessed in terms of PI permeability and accumulation of Sub-G_0 DNA respectively. (D) Jurkat T cells transiently transfected with siRNAs targeting Noxa or a control siRNA sequence (Scr) were treated (8 h) with Bz-423 (10 μM,) or vehicle and Bax or Bak activation was detected by immunofluorescence microscopy using antibodies specific for amino-terminal epitopes of Bax or Bak exposed during activation. Panels A-C are representative of two independent experiments, while panel D is from a single experiment. Absence of error bars indicates that standard error is <1%.

both proteins apparent at 0.1 μg/mL CHX (Figure 3.40B). Concentrations of CHX above 0.5 μg/mL reduced Myc and cyclin D3 levels by >90% (Figure 3.40B). However, these concentrations of CHX were cytotoxic in Jurkat T cells, obscuring the potential to determine if inhibiting protein synthesis blocks Bz-423-induced apoptosis (Figure 3.40C).

While [CHX] >0.5 μg/mL are toxic in Jurkat T cells, concentrations on CHX below <0.5 μg/mL where tolerated and modestly inhibited Bz-423 induce killing. For example, at 0.1 μg/mLCHX increased the EC_{50} for Bz-423-induced cell death by 28% (6.8 ± 0.3 μM to 9.4 ± 0.5 μM) (Figure 3.40C). This protection could result from inhibition of *de novo* synthesis of Bak and Noxa. However, studies in in rat embryonic hippocampal cells have demonstrated that low concentrations of CHX have cytoprotective effects related to the induction of anti-oxidant and pro-survival molecules [407]. For instance, concentrations of CHX <0.5 μg/mL protect rat embryonic hippocampal cells from oxidative insults by inducing expression Bcl-2 and MnSOD [407, 408]. Induction of MnSOD and Bcl-2 would be expected to protect Jurkat T cells from killing by Bz-423 by scavenging $O_2^{\bullet-}$ or inhibiting activation of Bak, respectively. To determine low concentrations of CHX attenuate Bz-423-induced apoptosis by blocking induction of Noxa and Bak, lysates were prepared Jurkat T cells pre-incubated with [CHX] <0.5 μg/mL prior to treatment with Bz-423. In this experiment, [CHX] <0.5 μg/mL failed to block the Bz-423-induced increases in Noxa and Bak levels, although c-Myc and cyclin D3 levels were reduced (Figure 3.40D). These results demonstrate that attenuation of Bz-423-induced cell death by [CHX] <0.5 μg/mL does not result from inhibition of *de novo* synthesis of Noxa Bak.

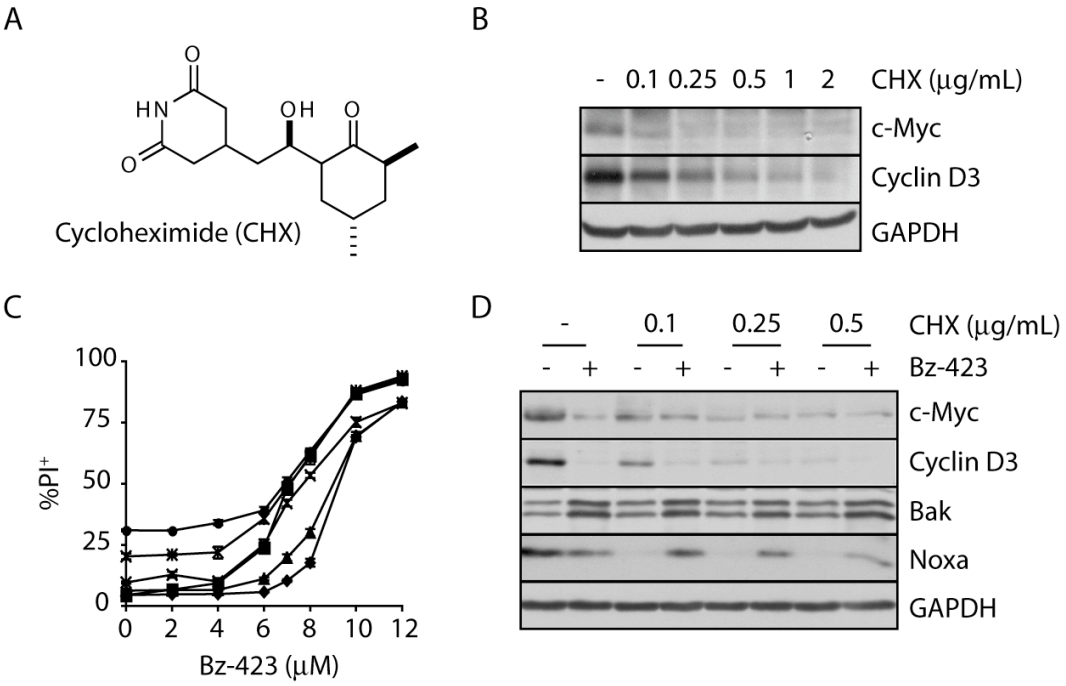

Figure 3.40 - Effect of the protein synthesis inhibitor cycloheximide on Bz-423-induced apoptosis in Jurkat T cells. (A) Chemical structure of the protein synthesis inhibitor cycloheximide. (B) Lysates from Jurkat T cells treated (6 h) with the indicated concentrations of cycloheximide (CHX) were immunoblotted with antibodies specific for c-Myc, cyclin D3 and GAPDH. (C) Jurkat T cells were pretreated (3 h) with CHX (0.1 μg/mL; ◆), (0.25 μg/mL; ▲), (0.5 μg/mL; ×), (1 μg/mL; ∗), (2 μg/mL; ●) or vehicle (■) and then incubated with Bz-423 for 24 h and cell death and apoptosis was assessed in terms PI permeability. (D) Lysates from Jurkat T cells that were pre-treated (2 h) with the indicated concentrations of CHX and then incubated (6 h) with Bz-423 (10 μM) or vehicle were immunoblotted with antibodies specific for c-Myc, cyclin D3, Bak, Noxa and GAPDH. Absence of error bars indicates that standard error is <1%. Panels A-C are representative of two independent experiments, while panel D is from a single experiment.

Bz-423 induces dephosphorylation of Akt: Along with neutralization by Noxa, Mcl-1 is subject to several additional regulatory mechanisms [409]. Of particular interest, phosphorylation of Mcl-1 by glycogen synthase kinase-3β (GSK-3β) targets this anti-apoptotic Bcl-2 protein to the ubiquitin-proteasome pathway [410]. GSK-3β activity, in turn, is subject to inhibitory phosphorylation by serine/threonine kinase

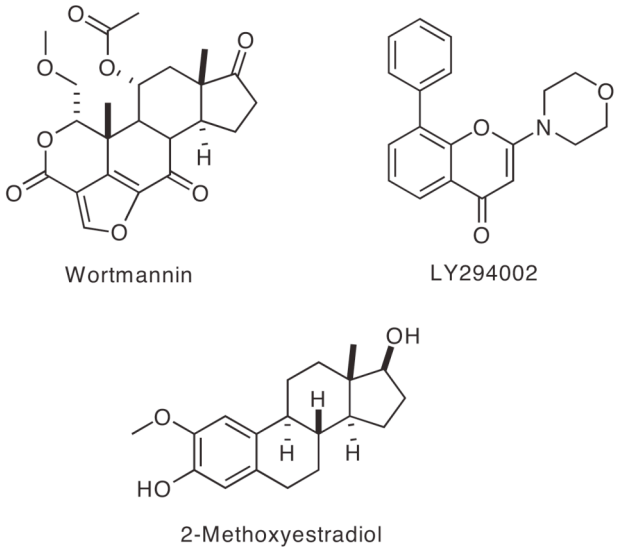

Figure 3.41 - Inhibitors of Akt activation. Wortmannin and LY294002 prevent recruitment of Akt to the plasma membrane by directly inhibiting PI3Ks [228]. 2-methoxyestradiol (2ME) elevates intracellular $O_2^{\bullet-}$ levels by inhibiting SODs, which results in $O_2^{\bullet-}$-dependent inactivation of Akt [286].

protein kinase B (PKB, also known as Akt) [273]. Activation of Akt depends on recruitment of this kinase to the plasma membrane via interaction between its amino-terminal Pleckstrin homology (PH) domain and 3,4,5-phosphoinositides (PtdIns(3,4,5)P_3). Binding of the PH domain to plasma-membrane PtdIns(3,4,5)P_3 induces in a conformational change in Akt enabling phosphorylation of Thr308 by Pleckstrin homology-domain kinase1 (PDK1) at Thr308 and by a rapamycin-insensitive mTOR•Rictor complex at Ser473. Phosphorylation of both residues stabilizes the kinase domain of Akt leading to fully activity. Once active, Akt promotes survival and proliferation by modulating a variety of pathways in addition to stabilizing Mcl-1 downstream of GSK-3β (see Chapter 3 Introduction).

PtdIns(3,4,5)P_3 are generated upstream of Akt by phosphorylation of the D3-

position of inositol ring headgroup of plasma membrane lipids by class I phosphoinositide 3-kinases (PI3Ks) [218]. The class I PI3Ks δ and γ are expressed primarily in leukocytes and are activated in response to cytokine, chemokine and antigen-receptor stimulation (Figure 3.9; [224]). PI3K activity is unopposed in Jurkat, MOLT-4 and CCRF-CEM T cells due to deficent expression of the lipid phosphatase PTEN, which results in elevated basal PtdIns(3,4,5)P_3 levels and constitutive activation of Akt [411]. The dependence of these T cell leukemia lines on Akt activity for survival is evidenced by their sensitivity to the PI3K inhibitors wortmannin and LY294002, which do not kill T cell leukemia lines that express PTEN (Figure 3.41; [271]).

Akt inactivation (i.e., dephosphorylation) is also observed in response to $O_2^{\bullet-}$ induced by 2-methoxyestradiol (2ME), which is thought to inhibit SODs (Figure 3.41; [286]). Treatment of Jurkat T cells with 2ME results in a decrease in Akt phosphorylation, which coincides with Mcl-1 destabilization and cytochrome *c* release [286]. These findings suggest that Akt may also be inactivated by Bz-423-induced $O_2^{\bullet-}$, which could account for Mcl-1 degradation independent of Noxa. This hypothesis is supported by the observation that Akt phosphorylation at Ser473 was decreased by 50% in Jurkat T cells treated with Bz-423 for 4 h, and was further reduced to <10% of control after 8 h (Figure 3.42A).

GSK-3β is an Akt substrate that, once activated, promotes apoptosis by destabilizing Mcl-1 [410]. Regulation of GSK-3β by Akt is unusual because phosphorylation of an amino-terminal residue (Ser9) by Akt generates a "pseudo-substrate" that self-inhibits GSK-3β by occupying the catalytic site [412]. The decrease in Akt phosphorylation induced by Bz-423 suggests that Akt activity might be reduced,

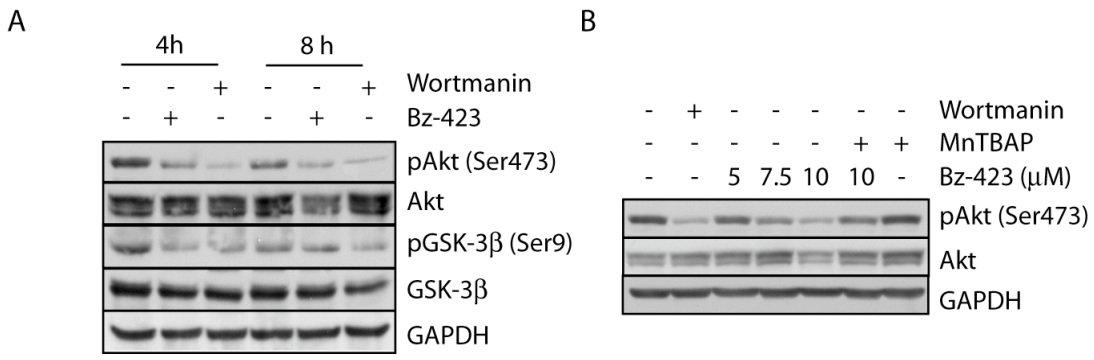

Figure 3.42 - Bz-423 causes $O_2^{\bullet-}$-dependent inactivation of Akt. (A) Lysates from Jurkat T cells treated with Bz-423 (10 μM), wortmannin (50 nM) or vehicle for the indicated times were immunoblotted with antibodies specific for Akt, phospho-Akt, GSK-3β, phospho-GSK-3β or GAPDH. (B) Lysates from Jurkat T cells pre-treated with MnTBAP (100 μM) or vehicle for 30 min and then incubated (6 h) with the indicated concentrations of Bz-423 or wortmannin (50 nM) were immunoblotted with antibodies specific for Akt, phospho-Akt or GAPDH. Wortmannin was used at a concentration shown to cause Akt dephosphorylation in Jurkat T cells [271]. All panels are from single experiments.

which could lead to an increase in GSK-3β activity and destabilization of Mcl-1. To evaluate this hypothesis, levels of GSK-3β phosphorylation at Ser9 were measured in lysates from Jurkat T cells treated with Bz-423. In these lysates, the decrease in Akt phosphorylation was accompanied by reduced phosphorylation of GSK-3β at Ser9 (Figure 3.42A). The decrease phosphorylation GSK-3β at Ser9 indicates that Bz-423 reduces Akt activity and suggests that destabilization of Mcl-1 may result increased activity of GSK-3β.

Scavenging $O_2^{\bullet-}$ with MnTBAP blocks the decrease in Akt phosphorylation and apoptosis induced by 2ME [286]. MnTBAP likewise inhibits all components of the Bz-423 apoptotic response. These inhibitory effects of MnTBAP suggest that Bz-423-

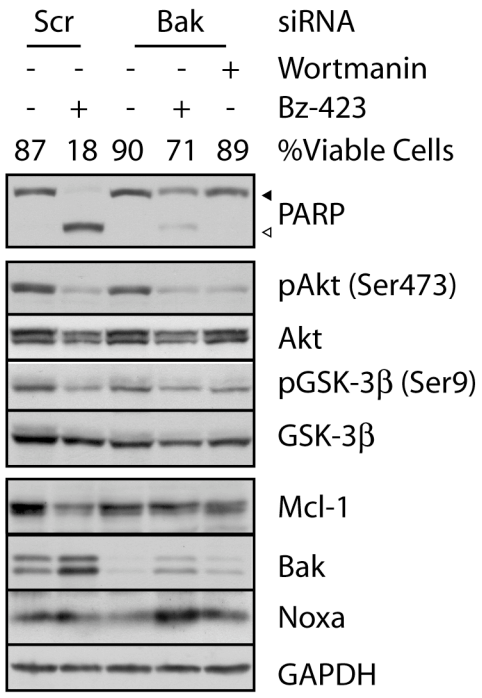

Figure 3.43 - Bz-423-induced Akt dephosphorylation is independent of Bak. Jurkat T cells were transiently transfected with siRNAs targeting Bak or a control siRNA sequence (Scr) and then treated with Bz-423 (10 μM), wortmannin (50 nM) or vehicle 6 h. Lysates were prepared from these cells and immunoblotted with antibodies specific for PARP (◀, full length PARP; ◁, cleaved PARP), Akt, phospho-Akt, GSK-3β, phospho-GSK-3β, Mcl-1, Bak, Noxa or GAPDH. Data is from a single experiment.

induced Akt dephosphorylation might also be $O_2^{\bullet-}$-dependent. To evaluate this hypothesis Jurkat T cells were pre-incubated with MnTBAP and then treated with Bz-423. In this experiment, Bz-423-induced Akt dephosphorylation displayed a concentration-dependence (IC_{50} ~7 μM) that is similar to cell death and was prevented by scavenging $O_2^{\bullet-}$ with MnTBAP (Figure 3.42B). In sum, in an effect similar to that observed for 2ME, Bz-423 induces $O_2^{\bullet-}$-dependent dephosphorylation of Akt in Jurkat T cells.

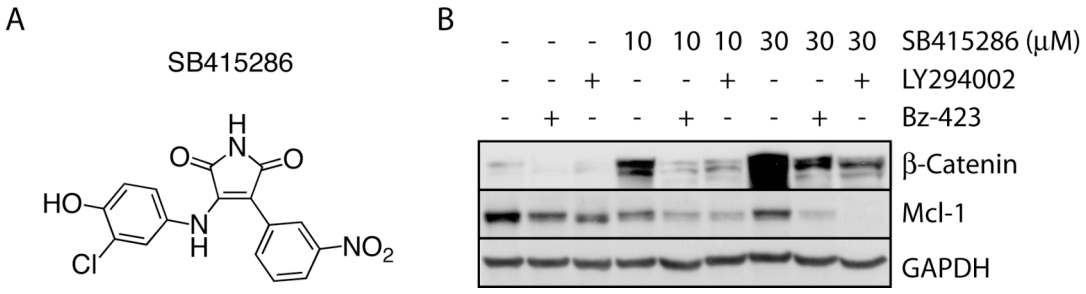

Figure 3.44 - Bz-423-induced Akt dephosphorylation is independent of Bak. (A) The GSK-3β inhibitor SB415286. (B) Jurkat T cells pre-treated with the indicated concentrations of SB415286 or vehicle for 30 min and then incubated with Bz-423 (10 μM) or LY294002 (20 μM) for 6 h. Lysates were prepared from these cells and immunoblotted with antibodies specific for β-catenin, Mcl-1, or GAPDH. SB415286 was used at concentrations sufficient inhibit GSK-3β in other systems [413]. Panel B is from a single experiment.

Effects of Bz-423 on Akt, Mcl-1 and Noxa in cells with reduced levels of Bak: Bz-423-induced Akt dephosphorylation is first detected at 4 h (Figure 3.42), which corresponds to the timing of MOMP and collapse of $\Delta\psi_m$. This timing suggests that the reduction in Akt phosphorylation could be a downstream consequence of the mitochondrial apoptotic changes induced by Bz-423, rather than an upstream signal for Bak activation. To address this possibility, the effect of Bz-423 on Akt phosphorylation was assessed in Jurkat T cells with reduced Bak levels. As described above, transient transfection with siRNAs targeting Bak blocked Bz-423-induced apoptosis as indicated by maintenance of viability and reduced cleavage of the caspase-3 substrate poly (ADP-ribose) polymerase (PARP) (Figure 3.43; [414]). Despite this block in apoptosis, Bz-423-induced Akt desphosphorylation as well as the downstream phosphorylation of GSK-3β at Ser9 were observed in cells with reduced levels of Bak (Figure 3.43).

The observation that Bz-423 decreases Akt and GSK-3β phosphorylation in cells with reduced expression of Bak suggests that the downstream effect on Mcl-1 levels will also be observed in the absence of Bak. Inconsistent with this hypothesis, reduction of Bak expression by siRNA blocked the Bz-423-induced decrease in Mcl-1 levels (Figure 3.43). This data is inconsistent with a mechanism in which Mcl-1 destabilization results from an increase in GSK-3β activity because these effects should not be blocked by reduction of Bak levels. In addition, pre-incubation of Jurkat T cells with the GSK-3β inhibitor SB415286 failed to block the reduction in Mcl-1 levels induced by Bz-423 (Figure 3.44B). Inhibition of GSK-3β by SB415286 was demonstrated in this experiment by the accumulation of β-catenin, a transcription factor that is targeted for ubiquitin-dependent proteasomal degradation after phosphorylation by GSK-3β (Figure 3.44B; [413]).

The inhibitory effect of reducing Bak expression on the Bz-423-induced decrease in Mcl-1 levels, suggest data that this effect is not mediated by GSK-3β. The inhibitory effect of Bak on Bz-423-induced Mcl-1 destablization instead suggests that this response may result from caspase activation after MOMP. For instance, caspase-dependent degradation of Mcl-1 is observed in Jurkat T cells undergoing apoptosis following treatment with the histone deactylase inhibitor LBD589 [135].

In contrast to the effects on Mcl-1, an increase in levels of the BH3-only protein Noxa was observed following Bz-423 treatment in Jurkat T cells with reduced expression of Bak (Figure 3.43). This finding is consistent with a model where Noxa induction serves as an upstream signal for activation Bak. Collecively, analysis of the effects of Bz-423 on Akt phosphorylation as well as Mcl-1 and Noxa levels in cells with reduced

expression of Bak demonstrates that (1) the decrease in phospho-Akt levels is independent of the mitochondrial apoptotic changes, but (2) Mcl-1 destabilization is not mediated via an increase in GSK-3β due to inactivation of Akt.

Bz-423-induced cell death is independent of Akt dephosphrylation: The GSK-3β inhibitor SB415286 does not block Bz-423-induced Mcl-1 destabilization, which suggests that decreased inhibitory phosphorylation of GSK-3β by Akt is not responsible for the reduction in Mcl-1 levels triggered by Bz-423. However, Akt promotes survival by a variety of signals in addition to inhibitory phosphorylation of GSK-3β (see Chapter 3 Introduction). The diversity anti-apoptoic signals downstream of Akt suggests that the Bz-423-induced inactivation of this kinase might promote Bak activation by a mechanism(s) other than Mcl-1 degradation.

2ME induced apoptosis is blocked by expression of an Akt construct bearing an amino-terminal myristoylation sequence (MyrAkt) (Figure 3.45A; [415]). Enzymatic attachment of a hydrophobic myristic acid moiety to amino-terminal Myr sequence targets the MyrAkt transgene to lipid membranes independent of PtdIns(3,4,5)P_3 levels, which leads to constitutive activation of Akt. The inhibitory effect of MyrAkt expression on 2ME-induced apoptosis along with the myriad of anti-apoptoic signals downstream of Akt suggests that Bz-423-induced cell death might also be blocked by constitutive activation of Akt.

To determine whether Akt dephosphorylatin (i.e., inactivation) is required for Bz-423-induced cell death, Jurkat T cells were transiently transfected with a construct in which a MyrAkt transgene is followed by an internal ribosome entry site (IRES) that directs translation of green fluorescent protein (GFP) (Figure 3.45A). Translation

typically begins at the 5' end of an mRNA molecule because recognition of the 5'-7-methylguanosine cap by a series of eukaryotic initiation factors (eIF proteins) is prerequisite for ribosome binding [416]. However, IRES enable initiation of translation in the middle of an mRNA by directly recruiting the 40S ribosomal subunit [417]. As a result, translation of MyrAkt and GFP occurs independently, with the former resulting from a 5'-cap-dependent initiation and the latter directed by the IRES (Figure 3.45A). Consequently, cells with elevated green fluorescence due to expression of GFP will also express the MyrAkt transgene. This allows for the specific assessment of the viability of cells expressing MyrAkt due to their elevated green fluorescence by PI staining of a mixed population (Figure 3.45B).

Transient transfection of Jurkat T cells with either the MyrAkt-IRES-GFP or a vector control plasmid only expressing GFP resulted in 15% and 20% increases in green fluorescence over mock transfected cells, respectively (Figure 3.45B). In vehicle treated MyrAkt or vector control samples >75% of GFP^+ cells are viable based on PI staining. However, no difference in Bz-423-induced cell death was observed in the GFP^+ populations of Jurkat T cells transfected with MyrAkt or the control plasmid (Figure 3.45C). These data suggest that Akt dephosphorylation is not a critical signal for Bz-423-induced cell death.

Reduced Akt phosphorylation can also result from mechanisms unrelated to PI3K activity. For instance, H_2O_2, UV radiation or the mitochondrial pro-oxidant fenretinide increases levels of the lipid second messenger ceramide by inducing sphingomyelin hydrolysis [418-421]. Elevated ceramide levels then stimulate cellular protein

A

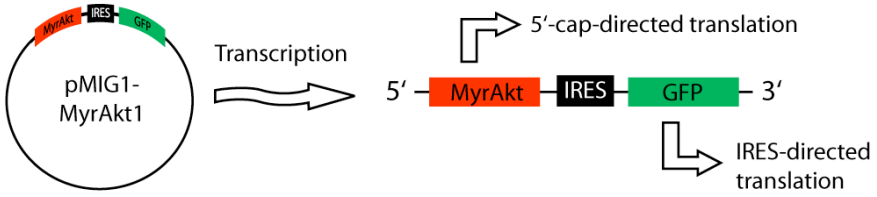
MyrAkt
IRES
GFP
pMIG1-
MyrAkt1
Transcription
5′-cap-directed translation
5′
MyrAkt
IRES
GFP
3′
IRES-directed
translation

B

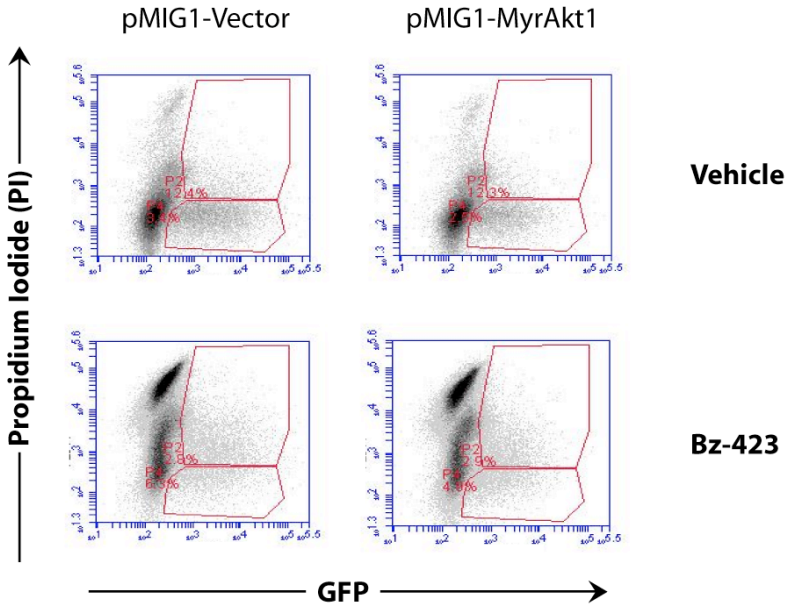
pMIG1-Vector
pMIG1-MyrAkt1
Vehicle
Bz-423
Propidium Iodide (PI)
GFP

C

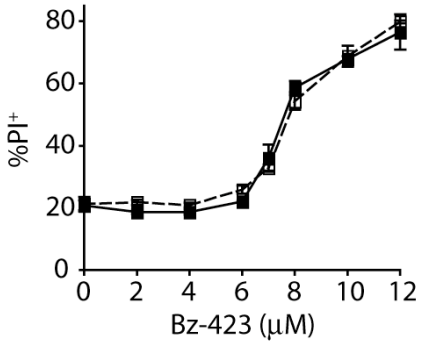
80
60
40
20
0
%PI+
0
2
4
6
8
10
12
Bz-423 (μM)

D

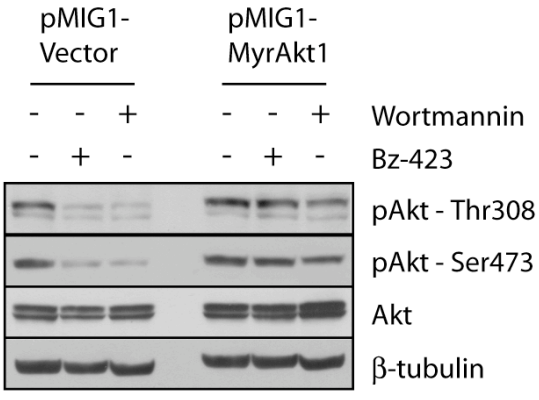
pMIG1-
Vector
pMIG1-
MyrAkt1
- - + - - + Wortmannin
- + - - + - Bz-423
pAkt - Thr308
pAkt - Ser473
Akt
β-tubulin

Figure 3.45 - Constitutive Akt activation fails to block Bz-423-induced apoptosis. (A) pMIG plasmid expressing MyrAkt along with GFP driven by an internal ribosome entry sequence (IRES). (B) Simultaneous PI and GFP staining of Jurkat T cells transiently transfect with pMIG-MyrAkt-GFP or pMIG-Vector following treatment with Bz-423 (10 μM) or vehicle for 24 h. (C) Jurkat T cells were transient transfected with pMIG-MyrAkt-GFP (■) or pMIG-Vector (□) and treated with the indicated concentrations of Bz-423 for 24 h. Cell death was assessed in the GFP^+ population in terms of PI permeability. (D) Jurkat T cells were transient transfected with pMIG-MyrAkt-GFP or pMIG-Vector and then incubated with Bz-423 (10 μM), wortmannin (50 nM) or vehicle for 6 h. Lysates prepared from these cells were immunoblotted with antibodies specific for Akt, phospho-Akt (Ser473), phospho-Akt (Thr308) or GAPDH. Absence of error bars indicates that standard error is <1%. Panel B and C are representative of two separate experiments. Panel D is from a single experiment.

phosphatase 2A (PP2A)-like activity resulting in dephosphorylation of a variety proteins including Akt [420, 422, 423].

To determine whether Bz-423-induced Akt dephosphorylation results from a mechanism other than decreased PI3K activity, Jurkat T cells transiently transfected with MyrAkt or the vector control plasmid where treated with Bz-423 (10 μM, 6 h). Consistent with the findings for 2ME, dephosphorylation of Akt residues Thr308 and Ser473 by Bz-423 was prevented in cells transfected with MyrAkt (Figure 3.45D). This protection suggests that Bz-423-induced Akt dephosphorylation is a consequence of impaired PI3K activity, although unlike 2ME, maintenance of Akt phosphorylation does not inhibit cell death [286].

Summary of results: Inhibition of the F_oF_1-ATPase in respiring cells has two direct consequences: decreased ATP synthesis and increased mitochondrial $O_2^{\bullet-}$ production [238]. The latter effect arises because protons pumped into the MIS by the ETC are unable to return to the matrix via the F_o channel when the F_oF_1-ATPase is inhibited. Excess accumulation of protons in the MIS (i.e., $\Delta\psi_m$ hyperpolarization)

impedes electron transport placing the MRC in a reduced state that favors generation of $O_2^{\bullet-}$ by one-electron reduction of molecular oxygen [293, 350]. The Latter effect appears to be predominant in the case of Bz-423 because elevated intracellular $O_2^{\bullet-}$ levels are detected in Jurkat T cells treated with Bz-423 for 1 h, while ATP levels are maintained until the onset of apoptosis at 4 h. The observation that Bz-423-induced $O_2^{\bullet-}$ production precedes the fall in ATP levels, along with the inhibitory effect of antioxidants on cell death, demonstrates that Bz-423 signals apoptosis by elevating $O_2^{\bullet-}$ rather than depleting ATP.

Studies in isolated mitochondria and reconstituted liposomes indicate that pro-oxidants can promote release of apoptogenic proteins from the MIS by oxidizing matrix-exposed cysteine residues on the ANT [20, 32, 34, 35]. Oxidation of these residues then triggers a conformational change in the ANT which results in sustained opening of the mPT pore [13, 37]. However, unlike pro-oxidants rotenone and ATO [32, 343], Bz-423 does not promote release of $O_2^{\bullet-}$ into the mitochondrial matrix, nor stimulate release of MIS proteins from isolated mitochondria. As a result, extra-mitochondrial factors appear necessary to couple the Bz-423-induced $O_2^{\bullet-}$ response to release of cytochrome *c* and other apoptogenic proteins from the MIS. Pro-apoptotic MIS proteins can also be liberated by permeabilization of the mitochondrial outer membrane as a result of activation of the pro-apoptotic Bcl-2 proteins Bax and Bak [13, 332]. While these proteins play redundant, overlapping roles in response to a variety of apoptotic stimuli [87, 391], they are hierarchically activated in response to the Bz-423. Bak is activated earlier and to a greater extent than Bax, and is required for Bz-423-induced MOMP and

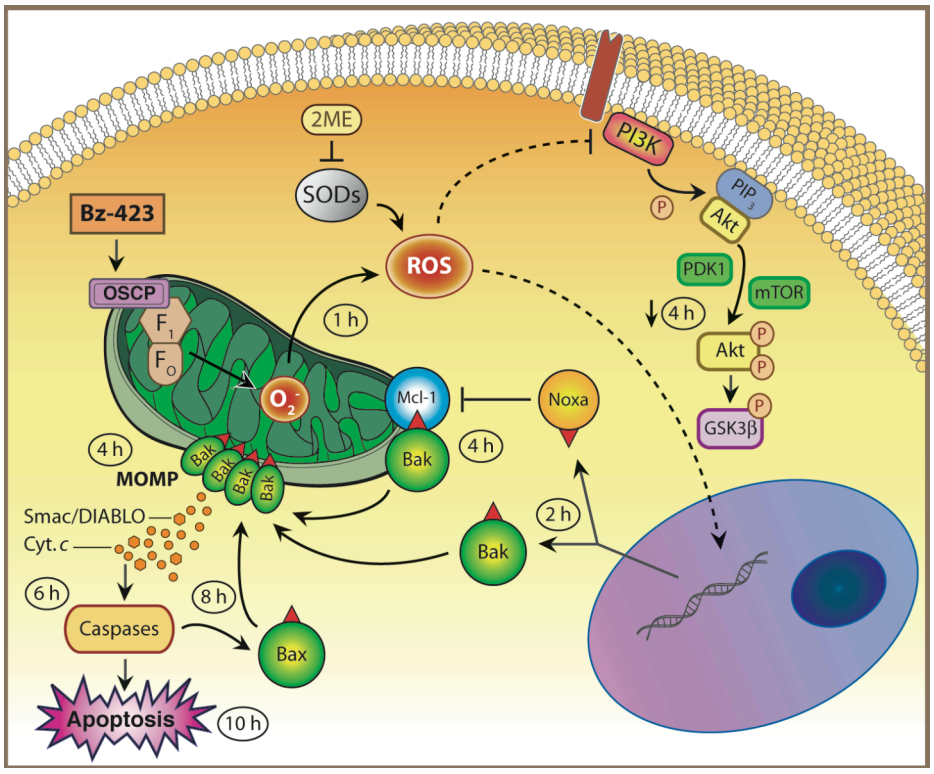

Figure 3.46 - Pro-apoptotic signaling induced by Bz-423 in Jurkat T cells. Levels of the BH3-only protein, Noxa, and Bak are rapidly elevated following treatment with Bz-423. These changes lead to preferential activation of Bak, MOMP and apoptosis. Bz-423 also reduces phosphorylation of the pro-survival kinase Akt at 4 h. A similar decrease in Akt phosphorylation is observed in Jurkat T cells treated with 2ME, which generates $O_2^{\bullet-}$ by inhibiting SODs [286]. Decreased Akt phosphorylation is required for 2ME-induced apoptosis, whereas inactivation of Akt is not required for Bz-423-induced apoptosis. This contrast between Bz-423 and 2ME may result from differences in the kinetics of $O_2^{\bullet-}$ production. See text for further detail.

apoptosis. In contrast, Bax is engaged downstream of Bak activation and is dispensable for killing by Bz-423 (Figure 3.46).

Bak activation is opposed by direct binding of the anti-apoptotic Bcl-2 proteins Bcl-x_L and Mcl-1 [38, 54, 84]. These inhibitory signals are overcome in response to Bz-423 in part by an increase in levels of Noxa, a pro-apoptotic BH3-only protein that specifically neutralizes Mcl-1 [424]. Bak *levels* are similarly elevated during this

timeframe suggesting a mechanism in which Noxa and Bak combine to overwhelm the inhibitory capacity of Mcl-1 and Bcl-x_L. In addition, Bz-423 causes $O_2^{\bullet-}$-dependent inactivation (i.e., dephosphorylation) of Akt, which can destabilize Mcl-1 independent of Noxa. Akt is activated following recruitment of this pro-survival kinase to the plasma membrane through interactions with PtdIns(3,4,5)P_3. Production of this lipid second messenger is, in turn, mediated by PI3Ks downstream of cell-surface receptors. Bz-423-induced $O_2^{\bullet-}$ appears to interfere with PI3K activity because Akt dephosphorylation is blocked by expression of a myristoylated Akt construct that is constitutively targeted to the plasma membrane. However, unlike the apoptotic response of Jurkat T cells to $O_2^{\bullet-}$ induced by the SOD inhibitor 2ME, MyrAkt expression fails to protect Jurkat T cells from killing by Bz-423.

This difference between Bz-423 and 2ME may derive from the kinetics of $O_2^{\bullet-}$ production induced by each pro-oxidant. While Bz-423-induced $O_2^{\bullet-}$ production peaks at 2 h, levels of this ROS are not elevated in response to 2ME until after 6 h [286]. Corresponding to this early increase in $O_2^{\bullet-}$, Noxa and Bak levels are elevated in Bz-423-treated Jurkat T cells by 2 h followed by mitochondrial apoptotic changes at 4 h. In contrast, 2ME induced Akt dephosphorylation along with cytochrome *c* release and caspase activation is first observed at 12 h [286]. It is tempting to speculate, therefore, that the Bz-423 cell death is insensitive to MyrAkt expression because the early rise in $O_2^{\bullet-}$ triggers apoptotic responses (e.g., elevated Noxa and Bak levels) that are independent of the effects on Akt activation. Collectively, these studies demonstrate that $O_2^{\bullet-}$-dependent activation of Bak links the effects of Bz-423 on the F_oF_1-ATPase to loss of mitochondrial outer membrane integrity and apoptosis in T cells (Figure 3.46).

Discussion

The mitochondrial F_oF_1-ATPase is expressed in all nucleated cells and is required for oxidative phosphorylation [238]. Toxicity associated with many drugs that inhibit oxidative phosphorylation has discouraged exploration of this enzyme as a drug target (e.g., the LD_{33} of oligomycin is <0.5 mg/kg in rats [425]). Oligomycin toxicity is thought to result from depletion of ATP, which can trigger necrotic cell death [311, 313, 425, 426]. However, in addition to reducing ATP synthesis, inhibiting the F_oF_1-ATPase in respiring cells forces the MRC into a reduced state that promotes production of $O_2^{\bullet-}$ [237, 238, 293]. As described in Chapter 1, $O_2^{\bullet-}$ and other ROS are increasingly recognized as important signaling molecules. Hence, F_oF_1-ATPase inhibitors that promote mitochondrial $O_2^{\bullet-}$ production without significantly depleting ATP may have regulatory and/or therapeutic properties [283, 301]. For instance, the anti-proliferative and pro-apoptotic activities of the 1,4-benzodiazepine F_oF_1-ATPase inhibitor Bz-423 result from increased mitochondrial $O_2^{\bullet-}$ production rather than depletion of ATP ([236, 237, 289, 290, 292] and this work). Bz-423 is well tolerated in rodents (>100 mg/kg) and ameliorates disease in murine models of lupus, arthritis and psoriasis by selectively depleting pathogenic lymphoid subsets or inhibiting proliferation of psoriatic skin cells, respectively [236, 290, 427]. The therapeutic properties of Bz-423 raise questions regarding why this F_oF_1-ATPase inhibitor does not deplete ATP, how the increase in mitochondrial $O_2^{\bullet-}$ signals apoptosis and, most significantly, what predisposes pathogenic cells (e.g., autoimmune lymphocytes) to its mechanism of action.

The experiments described in this chapter were performed to investigate the apoptotic response of $CD4^+$ T cell leukemia lines to Bz-423 in order to identify factors

that regulate if and how T cells to Bz-423. Some oxidizing agents induce release of cytochrome *c* and other pro-apoptotic MIS proteins from isolated mitochondrial by causing sustained opening of the mPT pore [29, 32, 343, 356]. In contrast, the loss of mitochondrial outer membrane integrity observed in response to Bz-423-induced $O_2^{\bullet-}$ depends on signaling outside the mitochondria that leads to activation of the pro-apoptotic Bcl-2 protein Bak. In unstressed cells, Bak is restrained by direct inhibitory binding of the anti-apoptotic Bcl-2 proteins Bcl-x_L and Mcl-1 [38, 54, 84]. Following treatment with Bz-423, Bak is freed from these inhibitory interactions, in part, by an increase in the levels of Noxa, a BH3-only protein that specifically neutralizes Mcl-1 [424]. Bak *levels* also rise in response to Bz-423 suggesting that increases in both proteins combine to circumvent the inhibitory capacity of Mcl-1 and Bcl-x_L. Integrating knowledge of this apoptotic cascade with unique characteristics of autoimmune lymphocytes provides insight into the selective effects of Bz-423 *in vivo*.

Effect of Bz-423 on steady-state ATP levels: Bz-423 does not reduce steady-state ATP *levels* in normally respiring (non-permeabilized) Jurkat T cells prior to the onset of apoptosis at ~4 h. In contrast, modulation of the F_oF_1-ATPase with Bz-423 elevates intracellular $O_2^{\bullet-}$ levels in Jurkat T cells within 1 h of treatment. Scavenging Bz-423-induced $O_2^{\bullet-}$ with MnTBAP or vitamin E blocks all downstream components of the apoptotic cascade. Together, these data support a model in which Bz-423-induced apoptosis is a consequence of increased mitochondrial $O_2^{\bullet-}$ production rather than depletion of ATP.

The ability to promote mitochondrial $O_2^{\bullet-}$ production without depleting ATP is critical is a critical component of the mechanism of action of Bz-423 because apoptosis is

an ATP-dependent process [313, 314]. Unlike Bz-423, F_oF_1-ATPase inhibitors that cause large decreases in cellular ATP levels (e.g., oligomycin) that can kill cells via necrosis [311, 428]. The lack of a reduction in steady-state ATP concentrations is not due to the failure of Bz-423 to inhibit the F_oF_1-ATPase in Jurkat T cells. Instead, Bz-423 causes a concentration-dependent decrease in the *rate* of mitochondrial ATP synthesis in Jurkat T cells with an IC_{50} similar to the K_i (~10 μM) for inhibition of the F_oF_1-ATPase mitochondrial preparations. In contrast to the lack of an effect on ATP levels, concentrations of Bz-423 approaching K_i induce a large increase in intracellular $O_2^{\bullet-}$ levels that signals apoptosis. These observations suggest that Bz-423 inhibits F_oF_1-ATPase activity to a degree that promotes mitochondrial $O_2^{\bullet-}$ production without depleting cellular ATP levels.

Bz-423 is a mixed inhibitor of ATP synthesis by the F_oF_1-ATPase that binds to both free enzyme and an enzyme•substrate complex with moderate affinity (i.e., K_i ~7 and ~10 μM, respectively) [283]. By binding to free enzyme, Bz-423 is a competitive inhibitor of ADP binding. However, competitive inhibition of the F_oF_1-ATPase by Bz-423 is suppressed in the presence of physiological (high micromolar to low millimolar), concentrations of ADP >> K_i [429]. In addition, Bz-423 acts as an uncompetitive inhibitor that blocks catalytic activity of the F_oF_1-ATPase after ADP is bound. Because substrate must be bound in order for an uncompetitive inhibitor to affect catalysis, increased [substrate] potentiates uncompetitive inhibition by enhancing formation of enzyme•substrate complex. Therefore, competitive inhibition of the F_oF_1-ATPase by Bz-423 will be suppressed at physiological concentrations of ADP, while the uncompetitive component of the mechanism will be enhanced.

As described in Chapter 1, there are two primary consequences of inhibiting the F_oF_1-ATPase in respiring cells: a reduction in the rate of mitochondrial ATP synthesis and a transition from active to resting respiration (state 3 to 4). The latter effect results from the inability of protons to pass through the F_o channel when the F_oF_1-ATPase is inhibited, which causes their accumulation in the MIS and hyperpolarization of $\Delta\psi_m$ (>150 mV) [293, 294]. Increased proton motive force under these conditions (i.e., state 4 respiration) slows electron transport by the MRC. This extends the half-lives of reactive intermediates (e.g., Fe-S clusters, flavoproteins and ubisemiquinones) capable of single-electron reduction of O_2, which results in increased production of $O_2^{\bullet-}$ [239]. The pro-apoptotic activity of Bz-423 is, therefore, a consequence of the fact that moderate inhibition of the F_oF_1-ATPase appears sufficient to induce a mitochondrial respiratory transition, and as a result, promote production of $O_2^{\bullet-}$. This is apparent in the ability of [Bz-423] approaching K_i to hyperpolarize $\Delta\psi_m$ and elevate intracellular $O_2^{\bullet-}$ levels ([237] and Figure 3.12B).

Unlike Bz-423, the polyketide F_oF_1-ATPase inhibitor oligomycin depletes ATP and induces necrosis in cells that rely primarily on oxidative phosphorylation [311, 313, 425, 426]. Although oligomycin is also a mixed inhibitor of ATP synthesis by the F_oF_1-ATPase, it binds free enzyme and an enzyme•substrate complex with much higher affinity (i.e., K_i ~10 nM and ~12 nM, respectively) than Bz-423 [283]. Because oligomycin binds tightly to the free enzyme, physiological concentrations of ADP will compete less effectively (i.e., $K_i << K_m$). In addition, physiological [ADP] will potentiate uncompetitive inhibition of the F_oF_1-ATPase by oligomycin resulting in high-affinity inhibition of both free and substrate-bound enzyme. Like Bz-423, oligomycin induces a

mitochondrial respiratory transition and stimulates mitochondrial $O_2^{\bullet-}$ production [237, 430]. However, these effects are outweighed by a large decrease in F_oF_1-ATPase activity and the resulting depletion of cellular ATP.

The effect of oligomycin on cellular ATP levels highlights the importance of uncompetitive inhibition to the mechanism of action of Bz-423. A competitive inhibitor of the F_oF_1-ATPase must be high affinity in order to bind in the presence of physiological concentrations of ADP. However, a high affinity competitive inhibitor is expected to also potently block F_oF_1-ATPase activity resulting in depletion of ATP and necrotic cell death. High affinity binding is not required for activity of an uncompetitive inhibitor because it does not compete with substrate. Therefore, although Bz-423 has moderate affinity for F_oF_1-ATPase (K_i ~10 μM), binding is possible in the presence of physiological concentrations of ADP because it is an uncompetitive inhibitor [283]. Since moderate inhibition of F_oF_1-ATPase activity appears sufficient to trigger a mitochondrial respiratory transition, Bz-423 is able to stimulate production of $O_2^{\bullet-}$ by the MRC without inhibiting mitochondrial ATP production to a degree that reduces cellular ATP levels.

The unique characteristics (i.e., moderate affinity, uncompetitive inhibition) of Bz-423 may derive from binding to the oligomycin sensitivity-conferring protein (OSCP) [237, 283]. The OSCP is a component of the peripheral stalk that links the integral membrane F_o component of the mitochondrial F_oF_1-ATPase with the soluble catalytic F_1 domain [431]. Cryoelectron microscopy images of the F_oF_1-ATPase show the majority of the OSCP (amino acids 1-120) atop F_1 with the carboxy-terminal amino acids (120-213)

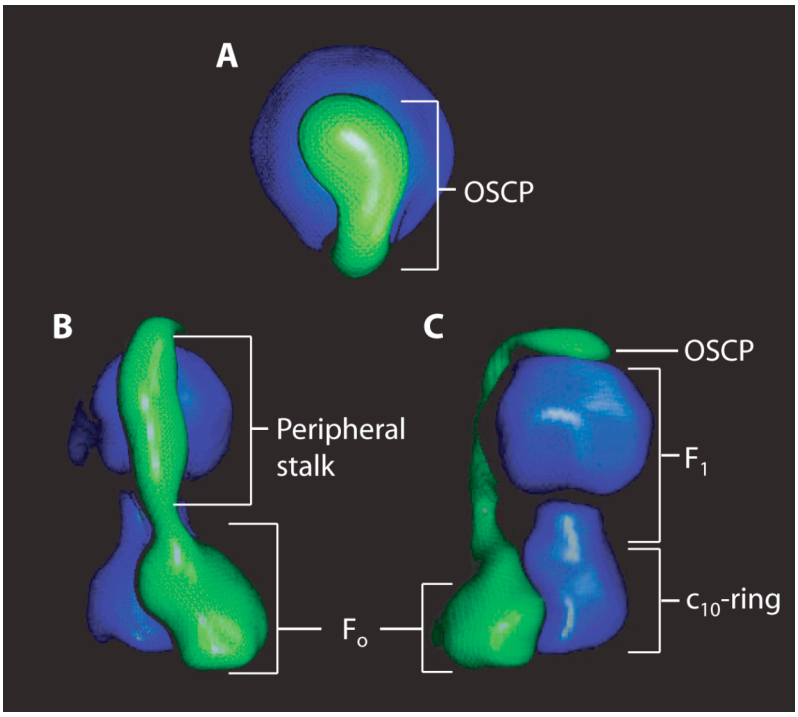

Figure 3.47 - Cryo-electron microscopy images of the F_oF_1-ATPase and peripheral stalk. Blue regions of all images correspond to the F_1-c_{10}-ring subcomplex, while green regions represent the peripheral stalk and membrane-associated F_o domains. (A) Top view of the F_oF_1-ATPase. The OSCP is the terminal subunit of the peripheral stalk and forms a cap over the central axis of F_1. The OSCP is the recognition site for Bz-423 [237]. (B) Side view of the peripheral stalk and membrane-associated F_o subunits. (C) Side view of the F_oF_1-ATPase showing location of peripheral stalk and membrane-associated F_o domain in relation to F_1-c_{10} ring. Oligomycin binds at the interface of c_{10} ring and membrane-associated F_o domain [432]. Cryo-electron microscopy images adapted from [433].

interacting with the peripheral stalk (Figure 3.47). These structural data indicate that the OSCP is solvent-exposed. As such, small molecules are expected to be able to rapidly associate with and dissociate from the OSCP. This prediction is supported by the observation that Bz-423 rapidly dissociates (apparent rate constant >0.3 s^{-1}) from the F_oF_1-ATPase [283]. In contrast, dissociation of oligomycin from the ATPase is >10-fold slower than Bz-423 (apparent rate constant >0.03 s^{-1}), which is consistent with a tight-

binding, slow-dissociating inhibitor [283]. The binding site for oligomycin is within F_o [434]. Hence, the slow off-rate of oligomycin may derive from the constraints associated with dissociation from this membrane-embedded proton channel.

Concentrations of Bz-423 approaching K_i reduced the rate of mitochondrial ATP synthesis by ~50% in permeabilized Jurkat T cells. Although this degreee of inhibition is moderate, it is nevertheless surprising that concentrations of Bz-423 approaching K_i do not deplete cellular ATP levels. The lack of an effect of Bz-423 on cellular ATP levels indicates that Jurkat T cells possess mechanisms to "buffer" a moderate decrease in F_oF_1-ATPase activity.

Inhibition of cytosolic enzymes typically causes a corresponding decrease in flux through the pathway controlled by that enzyme. For instance, reducing activity of the glycolytic enzyme 6-phosphofructo-1-kinase with the small-molecule inhibitor 3-(3-pyridinyl)-1-(4-pyridinyl)-2-propen-1-one (3PO) in Jurkat T cells leads to corresponding decreases in production of the glycolytic endproduct lactate [435]. This contrasts with MRC components, which are present in biochemical excess [436]. Due to this excess capacity, inhibition of ETC complexes or the F_oF_1-ATPase must exceed a critical threshold before an overall reduction in respiration (i.e., O_2 consumption) and ATP levels is observed [436].

This "mitochondrial threshold effect" is thought to limit the deleterious effects of mutations in mitochondrial DNA (mtDNA), which encodes critical subunits of MRC complexes I, III and IV as well as the F_oF_1-ATPase [437]. mtDNA accumulates mutations at a rate >10-fold higher than nuclear DNA presumably due to absence protective proteins (e.g., histones) and exposure to ROS generated by the ETC [438].

Inactivating mutations in mtDNA that impair oxidative phosphorylation and/or stimulate production of $O_2^{\bullet-}$ by the MRC are associated with a wide variety of degenerative diseases [439]. The mitochondrial threshold effect was first observed in studies where cells lacking mtDNA (i.e., ρ^0 cells) were reconstituted with a combination of wild-type and mutant mtDNA [440]. This approach revealed that mutant mtDNA had to be present in excess (>90% in some cases) over wild-type mtDNA before a reduction in mitochondrial respiration (i.e., O_2 consumption) was observed [441-443]. This observation indicates that a subset of wild-type ETC complexes or F_oF_1-ATPase subunits is sufficient to support normal mitochondrial function until their levels fall below a critical threshold.

The presence of excess oxidative phosphorylation capacity also limits the effects of small-molecule inhibitors on mitochondrial respiration. Just as wild-type subunits can maintain mitochondrial function in the presence mtDNA encoding for an inactive mutant, uninhibited MRC complexes or copies of the F_oF_1-ATPase can support oxidative phosphorylation in the presence of an inhibitor. Thus, inhibitors of MRC complexes or the F_oF_1-ATPase must overcome the mitochondrial threshold effect in order to disrupt oxidative phosphorylation. For example, F_oF_1-ATPase activity in rat heart mitochondria must be inhibited by ~80% before a decrease in respiration can be detected [444]. Hence, moderate inhibition of the F_oF_1-ATPase by Bz-423 may not exceed the threshold needed to impair mitochondrial ATP synthesis in Jurkat T cells.

In addition, the extent to which inhibition of the F_oF_1-ATPase overcomes mitochondrial threshold effects and impairs oxidative phosphorylation can be offset by increased glycolytic ATP production. For instance, increases in glucose uptake and/or

production of the glycolytic end-product lactate are often observed cells treated with inhibitors of the MRC or the F_oF_1-ATPase [274, 445-447]. Lactate production is increased by ~30% in Jurkat T cells following inhibition of oxidative phosphorylation by the complex III inhibitor antimycin A [274]. This effect is not unique to Jurkat T cells; lactate production is elevated in PC-3 colon carcinoma cells (26%) or rat hepatocytes (greater than two-fold) treated with oligomycin [445, 446]. Similarly, lactate production is increased three-fold in MEFs treated with the complex I inhibitor metformin [447].

A cellular energy sensor that upregulates glucose metabolism following impairment of oxidative phosphorylation is AMP-activated protein kinase (AMPK) [448]. AMPK is activated by an increase in cellular AMP/ATP ratio such as that caused by treatment of MEFs or hepatocytes with the complex I inhibitor metformin or exposure of Jurkat T cells to oligomycin [447, 449, 450]. Once activated, AMPK induces a cellular response characterized by up-regulation of catabolic pathways that generate ATP and down-regulation of ATP-consuming processes [451]. For example, AMPK activation induces expression of the glucose transporter Glut1 and activates the glycolytic enzyme phosphofructokinase [452, 453]. The essential role of AMPK in up-regulating glucose metabolism following inactivation of oxidative phosphorylation is demonstrated by the inability of *ampk*$^{-/-}$ MEFs to increase lactate production following treatment with metformin [447].

In sum, in the presence of physiological concentrations of ADP, Bz-423 is an uncompetitive inhibitor of the F_oF_1-ATPase with a K_i ~10 μM. At concentrations approaching K_i, Bz-423 inhibits mitochondrial ATP synthesis in permeabilized Jurkat T

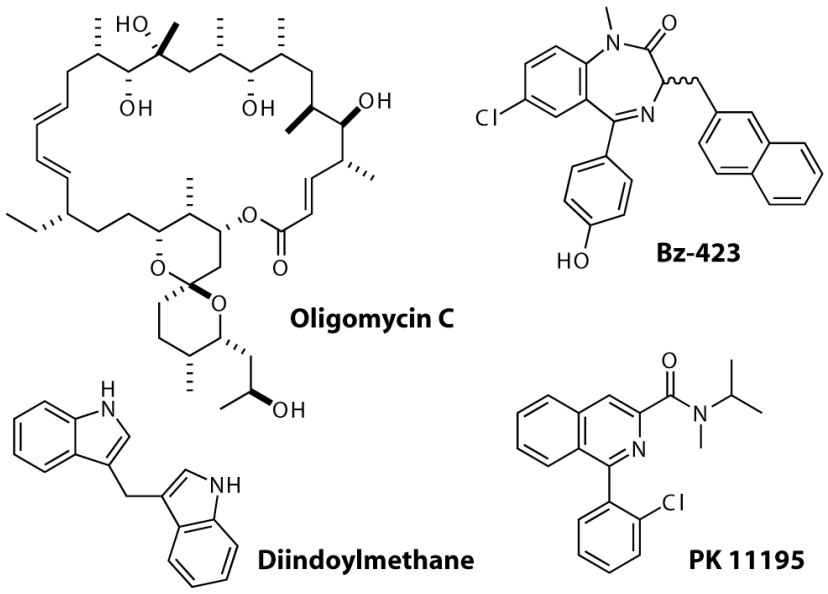

Figure 3.48 - Chemical structures of the F_oF_1-ATPase inhibitors oligomycin, PK 11195, diindoylmethane and Bz-423.

cells by ~50%. However, the same concentrations of Bz-423 increase intracellular $O_2^{\bullet-}$ levels, but do not deplete ATP in normally respiring Jurkat T cells. These data indicate that inhibition of F_oF_1-ATPase activity by Bz-423 may not be sufficient to overcome the mitochondrial threshold effect and impair oxidative phosphorylation. In addition, the small degree to which Bz-423 may reduce mitochondrial ATP production is likely offset by up-regulation of glucose metabolism, perhaps due to activation of AMPK. These buffering effects are essential for the mechanism of activation of Bz-423 because they maintain ATP at level sufficient for apoptosis to occur in response to the $O_2^{\bullet-}$ signal.

There are F_oF_1-ATPase inhibitors with properties similar to Bz-423. For instance, micromolar concentrations of the PBR ligand PK11195 inhibit the F_oF_1-ATPase in an OSCP-dependent manner (Figure 3.48; [296]). Like Bz-423, PK11195 stimulates $O_2^{\bullet-}$

production in Ramos B and Jurkat T cells and scavenging this ROS with MnTBAP blocks apoptosis in both cell-types [296]. These observations suggest that the cytotoxic and anti-proliferative activity observed with micromolar concentrations of this PBR result may result from modulation of the F_oF_1-ATPase.

The tryptophan dimer diindolylmethane (DIM) is an anti-tumor agent isolated from *Brassica* vegetables, which has been shown to inhibit the F_oF_1-ATPase and promote mitochondrial ROS production (Figure 3.48; [301]). Analogous to Bz-423, DIM induced ROS production precedes depletion of ATP and the effects of this F_oF_1-ATPase inhibitor of viability and proliferation are blocked by antioxidants [301, 302]. The anti-tumor properties of DIM in animal models of cancer [454, 455], along with efficacy of Bz-423 in murine models of lupus, arthritis and psoriasis [236, 292, 427], suggests that the F_oF_1-ATPase can be targeting therapeutically by inhibitors that induce ROS production without severely depleting ATP.

Bz-423-induced $O_2^{\bullet-}$ production: Electrons enter the MRC at complexes I or II and exit at complex IV, which catalyzes the four-electron reduction of molecular O_2 to water (see Chapter 1; [239, 350, 456]). This process is tightly regulated to prevent single-electron reduction of molecular oxygen by redox-active ETC intermediates (e.g., Fe-S clusters, flavoproteins and ubisemiquinones) [239, 457]. To minimize this side reaction, reactive ETC intermediates are sequestered within large, hydrophobic protein complexes in the mitochondrial inner membrane [350]. Nevertheless, between 0.5-3% of O_2 consumed during active respiration (i.e., state 3, see Chapter 1) is converted to $O_2^{\bullet-}$ [458-460]. Accumulation of $O_2^{\bullet-}$ is prevented by superoxide dismutases (SODs), which rapidly convert $O_2^{\bullet-}$ into H_2O_2 ($k \sim 10^8$ $M^{-1}s^{-1}$) [384]. In the matrix, this reaction is

accomplished by an SOD containing a manganese co-factor, while another isoform (Cu,Zn-SOD) is present in the cytosol and MIS [265]. H_2O_2, in turn, is reduced to water by catalase or glutathione peroxidase [457, 461]. Together these systems maintain $O_2^{\bullet-}$ and H_2O_2 produced as byproducts of oxidative phosphorylation at $\sim 10^{-11}$ and $\sim 10^{-7}$ M, respectively [371, 462, 463].

Production of $O_2^{\bullet-}$ is enhanced under conditions where F_oF_1-ATPase activity is reduced (e.g., by treatment with xenobiotic inhibitors or low ADP levels) relative to proton pumping by the MRC [293, 464]. Decreased F_oF_1-ATPase activity prevents passage of protons through the F_o channel, which result in their accumulation in the MIS and hyperpolarization of $\Delta\psi_m$ (>150 mV) [293, 294]. Increased proton motive force under these conditions (i.e., state 4 respiration; see Chapter 1) slows electron transport by the MRC. As such, electrons reside longer at redox active sites, which extends the half-lives of reactive intermediates (e.g., Fe-S clusters, flavoproteins and ubisemiquinones) capable of single-electron reduction of O_2 [239].

Although single-electron reduction of molecular oxygen can in principle occur throughout the MRC, studies with isolated mitochondria suggest that complexes I and III are the primary sources of $O_2^{\bullet-}$ [465-467]. Complex I (NADH ubiquinone oxidoreductase) transfers electrons from NADH to a prosthetic flavin-mononucleotide and then a series of Fe-S clusters before reducing ubiquinone (Q) to ubiquinol (QH_2) (Figure 3.49; [468]). $O_2^{\bullet-}$ production by complex I has been studied using the rodenticide rotenone, which inhibits the passage of electrons from the terminal Fe-S cluster (N2) to ubiquinone (Figure 3.49; [469]). This block leaves proximal complex I intermediates in a reduced state and the N1 and N2 Fe-S centers [470, 471], flavin mononucleotide co-

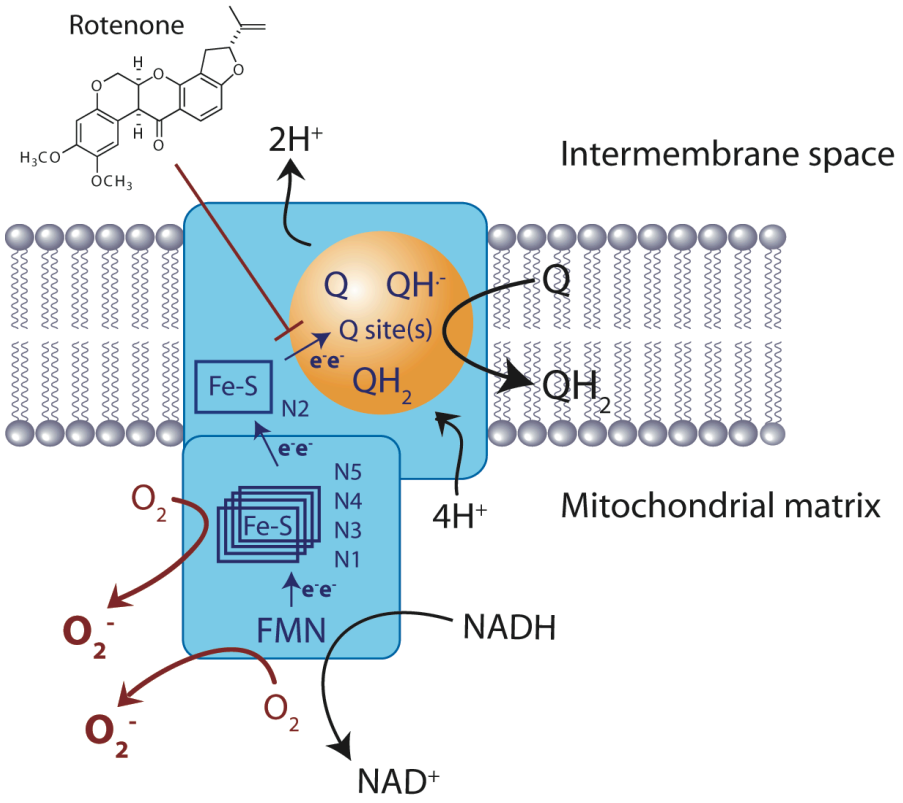

Figure 3.49 - Production of $O_2^{\bullet-}$ by complex I. NADH transfers two electrons (e^-) to a prosthetic flavin-mononucleotide (FMN). These electrons are then passed through a series of iron-sulfur (Fe-S) clusters (N1-N5) before reducing ubiquinone (Q) to ubiquinol (QH_2). The complex I inhibitor rotenone blocks electron transfer from the terminal Fe-S cluster (N2) to the Q binding site(s). This block leaves distal intermediates in a reduced state that can react with O2 to form $O_2^{\bullet-}$, which is then released into the mitochondrial matrix. See text for additional detail. Figure adopted from [457].

factors [472] as well as enzyme-bound NADH [473] have all been implicated in $O_2^{\bullet-}$ production. However, the ability of the flavin-modifying compound diphenyleneiodonium (DPI) to inhibit rotenone induced $O_2^{\bullet-}$ production argues that the flavin-mononucleotide co-factors are the site of incomplete reduction of molecular oxygen [472]. Regardless of which reactive intermediates are implicated, a number of studies have demonstrated that $O_2^{\bullet-}$ produced by complex I is released solely into the mitochondrial matrix [30, 31, 348, 467, 469, 472, 474, 475].

Due to the need to maintain $\Delta\psi_m$, the mitochondrial inner membrane lacks non-specific ion channels (porins), which makes it impermeable to charged species. Those charged species that cross the mitochondrial inner membrane do so via specific channels such as the adenosine nucleotide translocator (ANT), which mediates ATP/ADP exchange [238, 357]. As a result, $O_2^{\bullet-}$ released from the ETC into the matrix is trapped in this compartment as demonstrated by the failure to detected increase release of $O_2^{\bullet-}$ from isolated mitochondria in response to rotenone [462, 476]. Instead, the increase in matrix $O_2^{\bullet-}$ induced by this complex I inhibitor is detected as enhanced release of the lipid-soluble $O_2^{\bullet-}$ dismutation product H_2O_2 from mitochondria [30, 31].

Complex III (ubiquinone-cytochrome *c* oxidase) shuttles electrons from QH_2 to cytochrome *c* via a series redox intermediates including hemes, Fe-S clusters and ubisemiquinones ($QH^{\bullet-}$) [477]. Among these intermediates, production of $O_2^{\bullet-}$ by complex III occurs via autooxidiation of ubisemiquinone (Reaction 3.1; [457, 466, 478, 479]).

(3.1) $$QH^{\bullet-} + O_2 \rightarrow Q + H^+ + O_2^{\bullet-}$$

$QH^{\bullet-}$ are formed at both the Q_O and Q_I reaction sites on complex III, which are adjacent the MIS and matrix, respectively (Figure 3.50; [480, 481]). Oxidation of QH_2 at Q_O occurs over two steps: the first electron transfer (the QH_2 to $QH^{\bullet-}$ redox transition) is to a Fe-S cluster. This redox center is the first in a series of intermediates ultimately resulting in reduction of soluble (mobile) cytochrome *c*. The second electron (the $QH^{\bullet-}$ to Q redox transition) is transferred to the Q_I reaction site via cytochromes b_L and b_H (Figure 3.50).

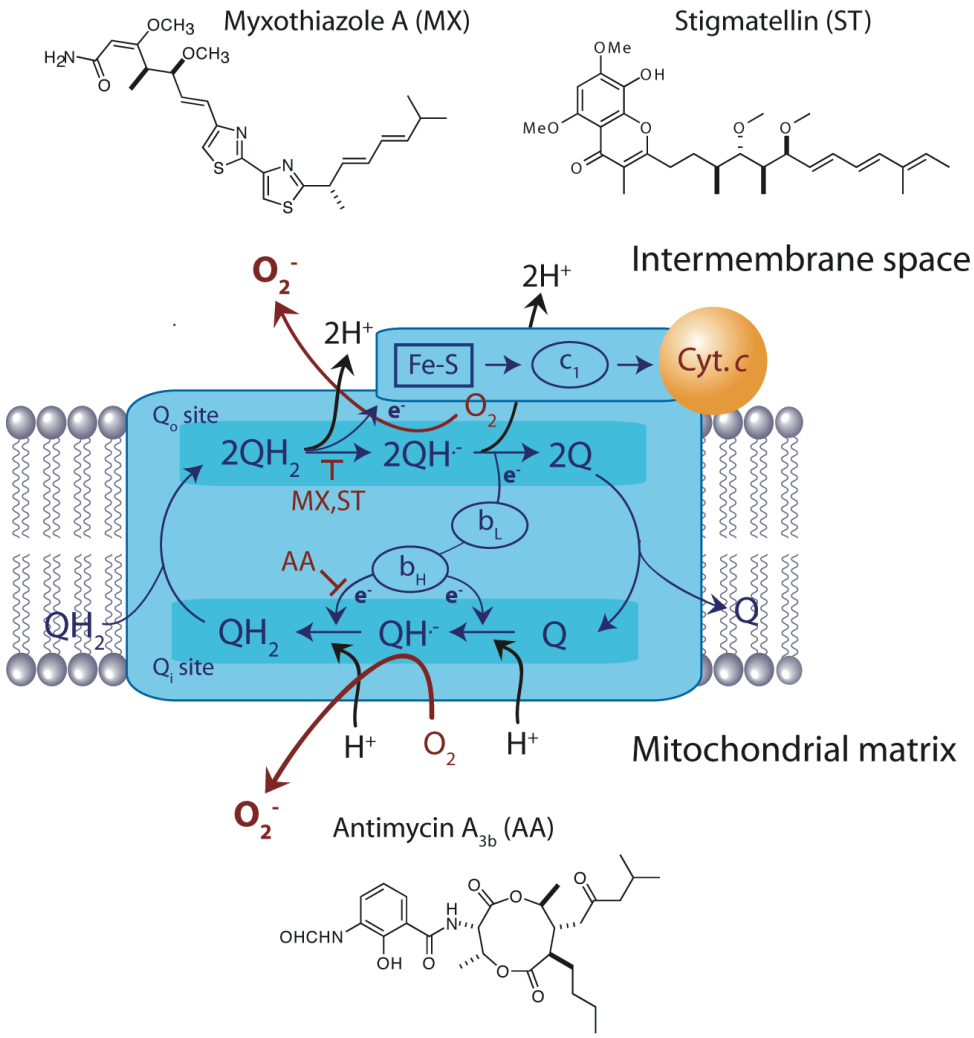

Figure 3.50 - Sites of $O_2^{\bullet-}$ production within the Q-cycle of electron transfer reactions in complex III. Complex III oxidizes ubiquinone (QH_2) to ubiseminquinone ($QH^{\bullet-}$) at the Q_o reaction site adjacent the intermembrane space. This electron (e^-) is transferred to cytochrome c (Cyt. *c*) via a Fe-S cluster and heme (c_1) intermediates. The e^- generated from the subsequent oxidation of $QH^{\bullet-}$ to ubiquinone (Q) is transferred to the Q_i site via two heme intermediates (b_L and b_H). Two-step transfer of electrons from b_H to Q regenerates QH_2 at Q_i with the accompanying H^+ transfers accounting for proton pumping by complex III. Antimycin A blocks the second e^- transfer at Q_i, which leads to accumulation of $QH^{\bullet-}$ at this reaction center as well as the Q_o reaction center adjacent the MIS. $QH^{\bullet-}$ autooxidation then leads to production of $O_2^{\bullet-}$ into both the mitochondrial matrix and intermembrane space. The Q_i site inhibitors myxothiazole A and stigmatellin block initial reduction of QH_2, and thereby inhibit antimycin A induced $O_2^{\bullet-}$ production. See text for additional detail. Figure adopted from [457].

This electron transfer sequence leads to regeneration of QH_2 by the two-step reduction of ubiquinone at the matrix Q_I site (Figure 3.50).

While $O_2^{\bullet-}$ is trapped in the matrix, it escapes from the MIS at a rate of ~0.04 nmol/min/mg protein in normally respiring mitochondria [372]. Consistent with release of $O_2^{\bullet-}$ into both the matrix and MIS, this value is increased >8-fold in the presence of antimycin A [372]. Transport of $O_2^{\bullet-}$ out of the MIS is likely mediated by ion channels (porins) in the mitochondrial outer membrane (e.g., voltage-dependent anion channel (VDAC), translocase of the outer membrane (TOM) and the peptide-sensitive channel (PSC)) that allow non-specific equilibration of solutes <5 kDa with the cytosol (see Chapter 1; [482]). A specific role for the VDAC in this process has been demonstrated by inhibition of this porin with 4,4'-diisothiocyanon-2,2-disulfonic acid stilbene (DIDS), which reduced release of $O_2^{\bullet-}$ from isolated mitochondria by >50% [372].

Transport of $O_2^{\bullet-}$ into the cytosol by VDAC is thought to represent an important mechanism for removal of this ROS from the MIS in addition to dismutation of into H_2O_2 Cu,Zn-SOD. VDAC is selective for transports anions due to the presence of positively charged residues in the core of this channel [483]. Therefore, positively charged amino acids in VDAC may function analogously to positively charged copper atoms which attract $O_2^{\bullet-}$ to the catalytic site of Cu,Zn-SOD [484]. In addition, in regions where the inner and outer mitochondrial membranes are parallel, the average width of the MIS is ~22 nM [485]. This distance is less than estimates of the mean displacement of $O_2^{\bullet-}$ in the matrix, which is >400 nM even taking into account dismutation by MnSOD [486]. If this estimate is applied to the MIS, $O_2^{\bullet-}$ released into this compartment from complex III

is predicated to survive long enough to reach VDAC and other mitochondrial outer membrane porins.

Unlike rotenone and antimycin A [30, 353], Bz-423 does not inactivate the $O_2^{\bullet-}$-sensitive TCA-cycle enzyme aconitase. This finding indicates that Bz-423 does not cause release of $O_2^{\bullet-}$ into the mitochondrial matrix, which precludes a role for complex I in this response. This conclusion is consistent with the inhibitory effect of the SOD mimetic MnTBAP on Bz-423-induced apoptosis. $O_2^{\bullet-}$ release into the matrix would have must be converted to H_2O_2 to escape mitochondria and induce apoptotic signaling outside this organelle. In this case, MnTBAP would be expected to potentiate rather than inhibit Bz-423-induced apoptosis by enhancing formation of H_2O_2.

Release of $O_2^{\bullet-}$ from isolated mitochondria is increased more than four-fold during state 4 respiration induced by treatment with oligomycin [295], which indicates that $O_2^{\bullet-}$ is released into the MIS during state 4 respiration. This observation suggests that complex III is the source of $O_2^{\bullet-}$ during state 4 because this complex can release $O_2^{\bullet-}$ into the MIS. The lack of an effect of Bz-423 on aconitase activity further suggests that $O_2^{\bullet-}$ is preferentially released into the MIS from complex III under state 4 conditions. This contrasts with inhibition of complex III by antimycin A, which promotes production of $O_2^{\bullet-}$ on both sides of the mitochondrial inner membrane due to accumulation of $QH^{\bullet-}$ at Q_O and Q_I (Figure 3.50; [30, 466]). Although the basis for selective release of $O_2^{\bullet-}$ into the MIS by Bz-423 is not clear, an important difference between inhibition of complex III with antimycin A is that $\Delta\psi_m$ is hyperpolarized during state 4 respiration [237]. Therefore, elevated $\Delta\psi_m$ may promote preferential release of $O_2^{\bullet-}$ into the MIS from complex III by suppressing formation and/or autooxidation of $QH^{\bullet-}$ at the Q_I reaction site.

Kinetic modeling of the influence of $\Delta\psi_m$ on complex III activity supports the hypothesis that $O_2^{\bullet-}$ is preferentially released into the MIS when $\Delta\psi_m$ is hyperpolarized [487]. According to this model, production of $O_2^{\bullet-}$ by complex III increases when $\Delta\psi_m$ exceeds 150 mV because the rate of electron transfer between hemes b_L and b_H is reduced [487]. This redox-reaction is thought to be suppressed because it involves transfer of electrons against $\Delta\psi_m$ from the Q_O site on the positive face complex III to the Q_I site near the matrix, which is negatively charged [487]. Due to the reduced passage of electrons from b_L and b_H, $QH^{\bullet-}$ intermediates accumulate at the Q_O reaction site. Conversely, formation of $QH^{\bullet-}$ is suppressed at Q_I because electrons are not available at b_H [487]. Although the topology was not explicitly addressed in this study, $O_2^{\bullet-}$ is predicted to be primarily released into the MIS because $QH^{\bullet-}$ accumulate at Q_O, while formation of this reactive intermediate is suppressed at Q_I [487]. Hence, the Bz-423-induced $O_2^{\bullet-}$ production is predicted to be a consequence of $QH^{\bullet-}$ autooxidation at the Q_O site of complex III. Once released into the MIS, this ROS can be transported into the cytosol by porins (e.g., VDAC) in the mitochondrial outer membrane. This mechanism is consistent with the inhibitory effect of MnTBAP on Bz-423-induced apoptosis because $O_2^{\bullet-}$ itself is predicted to be signal that escapes the mitochondria.

Comparison to other pro-oxidants: Intracellular ROS levels are commonly elevated in cells undergoing apoptosis [488]. However, this increase in cellular ROS levels often coincides with mitochondrial apoptotic changes such as cytochrome *c* release and collapse of $\Delta\psi_m$ and is observed during apoptosis induced by agents that are not redox active [315, 332, 336]. These findings suggest that increased ROS levels in apoptotic cells are a downstream consequence of mitochondrial dysfunction rather than a

specific pro-apoptotic signal [315]. A model in which ROS levels are elevated in apoptotic cells due to mitochondrial apoptotic changes is supported by the identification of a caspase-3 cleavage site in the 75-kDa subunit of MRC complex I [337]. Moreover, mutation of this site to a non-cleavable sequence preserves $\Delta\psi_m$ and reduces $O_2^{\bullet-}$ production in HeLa cells treated with STS or Act D [337].

Although the increase in ROS levels in apoptotic cells appears to often be a consequence of mitochondrial dysfunction, a variety of pro-apoptotic agents induce ROS early in their death cascade as a means of initiating specific downstream effector mechanisms. For example, the inflammatory cytokine tumor necrosis factor-α (TNF-α) signals apoptosis by stimulating production of $O_2^{\bullet-}$ from plasma membrane NADPH oxidases [489]. ROS production also plays a proximal role in apoptosis induced by small-molecules such as the histone deacetylase (HDAC) inhibitors Vorinostat (Figure 3.51; [109, 490]). HDAC inhibition promotes ROS production by suppressing expression of the thioredoxin (Trx), a 12-kDa protein that contributes to cellular redox balance by reducing disulphide linkages (see Chapter 1; [491]). Similarly, the proteasome inhibitor Bortezomib induces ROS production in Jurkat T cells and primary mantle-cell lymphomas prior to the onset of apoptosis (Figure 3.51; [114, 492]). Although the molecular basis for the ROS response accompanying proteasome inhibition is unclear, anti-oxidants inhibit apoptotic signaling (e.g., induction of the proapoptotic Bcl-2 protein Noxa) along with cell death induced by Bortezomib [114, 492]. FDA approval of Vorinostat and Bortezomib for treatment of cutaneous T cell lymphoma and multiple myeloma [493, 494], respectively, demonstrates that small-molecules with pro-oxidant properties can be clinically useful.

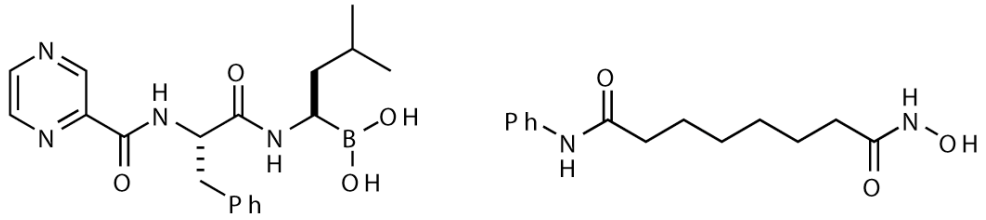

Figure 3.51 - Chemical structure of Bortezomib and Vorinostat.

In addition to Bz-423, a variety of agents signal redox-regulated apoptosis by perturbing mitochondrial function. For instance, the estrogen metabolite 2-methoxyoestradiol (2ME) induces apoptosis in primary leukemia cells and transformed B and T cell lines by promoting a gradual accumulation of $O_2^{\bullet-}$ (Figure 3.52; [495, 496]). 2ME induced $O_2^{\bullet-}$ production is often attributed to inhibition of SOD activity [348, 495, 496], however, some reports have suggested other mechanisms including suppression of hypoxia-inducible factor-1α (HIF-1α) expression and microtubule destabilization [497-500]. Consistent with inhibition of SOD activity, 2ME enhances the response of small molecules that induce mitochondrial $O_2^{\bullet-}$ production [348]. The selectivity of 2ME for neoplastic cells is thought to arise from their increased reliance on antioxidant enzymes such as SOD to detoxify elevated basal ROS levels [348, 501, 502]. Initial clinical studies of 2ME were halted due to poor bioavailability [503, 504], however, Phase II trials using an improved formulation are ongoing [505].

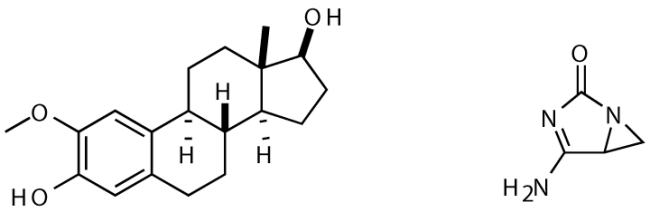

2-Methoxyestradiol **Imexon**

Figure 3.52 - Chemical structure of 2-Methoxyestradiol and Imexon.

Gradual accumulation of $O_2^{\bullet-}$ is also observed during apoptosis induced by the Imexon, a cyanoaziridine that forms covalent adducts with sulphydryls (Figure 3.52; [506, 507]). As a result, Imexon induced $O_2^{\bullet-}$ production may result from depletion of cellular GSH pools [506, 507]).. Mitochondrial ultra-structural changes (i.e., swelling) consistent with opening of the mPT pore are observed after Imexon treatment in RPMI-8226 multiple myeloma cells [506]. This data suggests that Imexon, like other thiol cross-linking agents, may also trigger mPT pore opening by directly reacting with ANT cysteine residues [506]. Imexon has anti-tumor activity in animal models of cancer [508, 509], and was well tolerated in a Phase I clinical trial [510]. Together, the therapeutic properties of 2ME and Imexon demonstrate that modulating cellular redox buffering capacitymay be a therapeutically useful strategy to selectively kill cancer cells.

While rotenone and antimycin A are unsuitably toxic for clinical use, some MRC inhibitors have therapeutic properties [475, 511]. For instance, the arsine oxide (As_2O_3) Trisenox is currently marketed for treatment of acute promyelocytic leukemia [512]. This drug inhibits mitochondrial respiration (i.e., O_2 consumption) and induces $O_2^{\bullet-}$ production in a variety of cell-types [348, 513]. Trisenox induced $O_2^{\bullet-}$ production

requires MRC activity because this response is not observed in cells where oxidative phosphorylation is impaired by depletion of mitochondrial DNA [348]. On a biochemical level, Trisenox conjugates vicinal cysteine residues due to the strong affinity of thiols for the soft As(III) ion [513, 514]. The resulting dithioarsenite linkages modulate the activity proteins that depend on the cross-linked cysteine residues [514, 515]. Trisenox, like other thiol cross-linking agents, induces large-amplitude swelling and cytochrome *c* release in isolated mitochondria [343]. Both responses are diagnostic of mPT pore opening, which suggests that Trisenox may cross-link ANT cysteine residues. However, Trisenox induced mPT pore opening and apoptosis are inhibited by anti-oxidants that scavenge $O_2^{\bullet-}$ [343, 348], which suggests that these responses are mediated by an ROS intermediate rather than direct conjugation of ANT cysteines.

As described in the preceding section, the F_oF_1-ATPase inhibitor DIM, like Bz-423, stimulates mitochondrial ROS production without depleting cellular ATP levels (Figure 3.48; [301, 516]). Consistent with an ROS-dependent mechanism, the growth-inhibitory and pro-apoptotic activities of DIM are both inhibited by anti-oxidants [301, 302]. In addition, therapeutic activity of DIM has been demonstrated by successful treatment (i.e., reduced tumor volume) of mammary cancer in female Sprague-Dawley rats exposed to the chemical mutagen 7,12-dimethylbenz(a)anthracene [454, 455],

Collectively, these results demonstrate that increased intracellular ROS levels can act as an upstream signal leading to apoptosis. Although some inhibitors of the MRC are toxic (e.g., oligomycin, rotenone and antimycin A), the SOD inhibitor 2ME and the F_oF_1-ATPase inhibitors DIM and Bz-423 have have demonstrated efficacy in pre-clinical models of cancer and autoimmune disease. Together, these studies suggest that small-

molecule mitochondrial pro-oxidants can have therapeutic properties. In addition, the recent FDA approval of the proteasome-inhibitor Bortezomib and HDAC-inhibitor Vorinostat, both of which induce ROS-dependent apoptosis, further supports the assertion that small molecule pro-oxidants can be clinically useful.

Preferential Bak activation: Release of cytochrome *c* and other pro-apoptotic proteins from the MIS is often (as in the case for Bz-423) the point at which cells commit to apoptosis. The pro-apoptotic Bcl-2 proteins Bax and Bak promote release of cytochrome *c* from the MIS by permeabilizing the mitochondrial outer membrane. In response to apoptotic stimuli Bax and Bak undergo a conformational change (termed activation) that results in formation of homo-oligomeric pores [517]. Reconstitution of activated Bax or Bak with liposomes indicates that the multimeric forms of either protein are sufficient to permeabilize lipid bilayers [518]. The ability of either Bax or Bak to each individually permeabilize liposomes suggests that they function redundantly, which should allow for apoptosis to proceed if either protein is deleted.

The capacity of Bax and Bak to function redundantly during apoptosis has been tested by determining the sensitivity of MEFs derived from *bax*$^{-/-}$, *bak*$^{-/-}$ or double-knockout mice to a range of apoptotic stimuli [87, 89, 396]. In contrast with the redundant activity of Bax and Bak in liposome permeabilization assays, MEFs derived from *bax*$^{-/-}$ or *bak*$^{-/-}$ mice display equivalent, partial protection (~50%) to apoptosis induced by DNA damage, microtubule destabilization, growth factor deprivation and endoplasmic reticulum stress [87]. Consistent with the response to other apoptotic stimuli, partial protection from Bz-423-induced cytochrome *c* release and apoptosis is observed in *bax*$^{-/-}$ or *bak*$^{-/-}$ MEFs [396]. The inability of Bax and Bak to fully compensate

for one another is not unique to MEFs. Partial protection from dexamethasone or cytokine-deprivation induced apoptosis is observed in thymocytes from *bax*$^{-/-}$ or *bak*$^{-/-}$ mice [89]. Likewise, *in vivo* hepatocyte apoptosis was reduced by ~35% in *bax*$^{-/-}$ or *bak*$^{-/-}$ mice following administration of a Fas agonist antibody [87]. While apoptosis induced by ligation of the Fas death receptor is independent of the mitochondria in lymphocytes, this response depends on activation of Bax and Bak by tBid in hepatocytes [103].

One explanation for the protection of *bax*$^{-/-}$ or *bak*$^{-/-}$ MEFs from apoptotic stimuli is that liposomes are a poor model of the mitochondrial outer membrane, which contains a variety of proteins (e.g., components of the mPT pore or the mitochondrial fission/fussion machinery) that interact with Bax and Bak [53, 519]. These interactions could limit Bax or Bak activation such that both proteins are necessary to efficiently permeabilize the mitochondrial outer membrane. This hypothesis is not supported by studies using isolated mitochondria as a model system [358, 518]. For instance, Bak activation and quantitative release of cytochrome *c* is observed when mitochondria isolated from the liver of *bax*$^{-/-}$ mice are stimulated with the active, truncated form of the BH3-only protein Bid (tBid) [358]. Likewise, the combined addition Bax and tBid can permeabilize mitochondria isolated from the liver of *bak*$^{-/-}$ mice [518]. The ability of Bax or Bak to permeabilize isolated mitochondria suggests that many cell-types may lack sufficient levels of Bax and Bak for either protein to individually permeabilize the mitochondrial outer membrane. However, *bax*$^{-/-}$ MEFs are as sensitive as wild-type MEFs to apoptosis induced by the combined over-expression of Bad and Noxa, which activates Bak by neutralizing Bcl-x_L and Mcl-1, respectively [97]. This experiment suggests that solitary activation of Bak is sufficient to induce MOMP in a cellular

context. As such, the resistance of Bax- or Bak-deficient cells to apoptotic stimuli may result from inefficient activation of the remaining protein.

The sensitivity of *bax*$^{-/-}$ MEFs to combined over-expression of Bad and Noxa demonstrates that Bak is sufficient to induce MOMP. However, expression of full-length BH3-only proteins is not a viable therapeutic approach and small-molecule BH3-domain mimetics have not been validated clinically [520, 521]. An important question, therefore, is whether apoptotic stimuli that do not directly engage Bcl-2 proteins can activate Bak to the same extent as combined over-expression of Bad and Noxa. This question is particularly relevant for induction of apoptosis in cancer cells or autoimmune lymphocytes, which often harbor signals (e.g., elevated PI3K-Akt activity or Bcl-2 overexpression; [224, 228, 521]) that suppress mitochondrial translocation and activation of Bax (see Chapter 3 Introduction). Therefore, robust activation of Bak could be used to induce MOMP in cells where translocation and/or activation Bax is impaired.

In contrast to the results in MEFs, Bax and Bak function non-redundantly during Bz-423-induced apoptosis in Jurkat T cells. Bak is activated earlier (i.e., during a timeframe coincident with MOMP) and to greater extent than Bax in Jurkat T cells treated with Bz-423. In addition, reducing expression of Bak blocks Bz-423-induced MOMP. In contrast, activation of Bax is only detected after MOMP and is blocked by the pan-caspase inhibitor zVAD-fmk or knockdown of Bak by siRNA. Together, these observations indicate that Bak mediates Bz-423-induced MOMP, while Bax is activated as part of a caspase-dependent amplification loop after release of cytochrome *c* and Smac/DIABLO. Given that release of cytochrome *c* and other apoptogenic proteins from the MIS is the point at which Jurkat T cells commit to die in response to Bz-423, it is not

surprising that Bak is necessary for Bz-423-induced apoptosis, while Bax is dispensable. These findings demonstrate that Bak is both necessary *and* sufficient to permeabilize the mitochondrial outer membrane in Jurkat T cells treated with Bz-423.

The preferential activation of Bak in Jurkat T cells treated with Bz-423 suggests the presence of regulatory mechanisms that specifically suppress activation of Bax in this cell-type. Recent advances in the understanding in the understanding how Bax and Bak are regulated supports this hypothesis. Differential regulation of Bax and Bak is apparent in their sub-cellular distribution; Bak is constitutively localized to the mitochondrial outer membrane [53], while Bax resides in the cytosol and redistributes to the mitochondria in response to apoptotic stimuli [395]. The signal(s) responsible for Bax translocation appear to be distinct from the Bcl-2 family because anti-apoptotic Bcl-2 proteins only bind Bax at the mitochondrial outer membrane [38, 84].

In contrast, phosphorylation appears to play a role in regulating the sub-cellular distribution of Bax (see Chapter 3 Introduction). For instance, translocation of Bax to the mitochondria is opposed by the pro-survival kinase Akt. This was first demonstrated by Rathmell, *et al* who found that activation of Bak due to cytokine deprivation in the FL5.12 hematopoietic precursor cell line was suppressed by expression of a constitutively active Akt transgene [62]. Subsequently, constitutive activation of Akt has also been shown to impede Bax translocation in neutrophils and T cells [63, 64]. In primary human neutrophils this results from phosphorylation of Bax by Akt at Ser184 [64]. In the 2B4 and D11S murine T cell lines, however, Akt-dependent sequestration of Bax in the cytosol requires amino-terminal amino acids 13-29 [63]. Regardless of the precise domain requirements, the finding that Akt activation blocks Bax translocation suggests

that this response may be suppressed in Jurkat T cells, where deficiency of the lipid phophatase PTEN leads to elevated basal levels of Akt activity [411].

If constitutive activation of Akt suppresses Bax translocation in Jurkat T cells, inactivation of PI3K-Akt signaling should promote this response. In support of this hypothesis, Bax translocation is first observed in Bz-423-treated Jurkat T cells at 8 h, while levels of phosphorylated (i.e. active) Akt levels are reduced by 4 h. In contrast to Bz-423, Bax translocation coincides with MOMP in Jurkat T cells treated with STS. The apoptogenic activity of STS results from inhibition of cytosolic kinases including c-Src, protein kinase C, IκB kinase as well as Akt [394]. The K_i for inhibition of Akt is ~20 nM [522], which is well below the concentration of STS (0.5 μM) used in this study. As a result, the nearly quantitative (i.e., >90%) translocation and activation of Bax in response to STS is expected to result from direct inhibition of Akt, which frees this proapoptotic Bcl-2 protein to redistribute to the mitochondria.

Even after Bax *translocates* to the mitochondrial outer membrane in response to Bz-423, Bax *activation* opposed by anti-apoptotic Bcl-2 proteins. As described in the introduction to Chapter 3, regulation of Bax and Bak also differs with regards to binding of anti-apoptotic Bcl-2 proteins (Figure 3.4). Bak is subject to inhibitory binding by Mcl-1, A1 and Bcl-x_L [54, 83]. By contrast, after redistribution to the mitochondrial outer membrane, Bax activation is inhibited by association with Mcl-1, Bcl-2, Bcl-x_L and Bcl-w [84]. These differences suggest that the barrier for activation of Bak is lower because (1) it is not obligated to translocate to the mitochondrial outer membrane and (2) it is bound by fewer anti-apoptotic Bcl-2 proteins. Of note, levels of A1 and Bcl-w were below the limits of detection by immunoblot in Jurkat T cells (Figure 3.37). Hence,

activation of Bak in Jurkat T cells is expected to only require neutralization of Mcl-1 and Bcl-x_L.

Levels of the BH3-only protein Noxa are elevated in Jurkat T cells treated with Bz-423. An increase in Noxa levels is consistent with preferential activation of Bak because this BH3-only protein specifically binds to Mcl-1, which frees Bak from this inhibitory interaction (see Chapter 3 Introduction). In addition to playing a role in the apoptotic response of Jurkat T cells to Bz-423, an increase in Noxa levels contributes to apoptosis induced by other oxidizing agents. For example, levels of this BH3-only protein are elevated in multiple myeloma cell lines following treatment with Trisenox or oxidative stress associated with the inhibition of the proteasome [114, 115]. In both cases, Bak is displaced from Mcl-1 following binding of Noxa, although the relative contribution of Bax and Bak to cell death was not examined [114, 115]. In addition, expression of Noxa is induced in SK-N-SH neuroblastoma cells by the herbicide paraquat, which generates $O_2^{\bullet -}$ by redox cycling reactions in the MRC [116]. Hence, the increase in Noxa levels following treatment with Bz-423 is consistent with the apoptotic cascades induced by other oxidizing agents as well as preferential activation of Bak.

Noxa was first identified as a p53 response gene [111]. However, p53-dependent induction of Noxa is unlikely to contribute to the increased levels of Noxa following treatment with Bz-423 because Jurkat T cells lack this transcription factor [523]. Given that Noxa is induced in response to apoptotic stimuli (e.g., oxidative stress, proteasome inhibition and hypoxia) besides DNA damage, it is not surprising that *noxa* expression can be induced by other transcription factors including c-Myc, E2F-1 and hypoxia inducible transcription factor-1α (HIF-1α) [524-526].

The cytotoxic activity of the proteasome inhibitor Bortezomib in melanomas results from over-accumulation of c-Myc, which then induces expression of Noxa [524]. A similar mechanism is not anticipated to underlie the increase in Noxa levels triggered by Bz-423 in Jurkat T cells. This is because Bz-423 has been shown to block growth in Ramos B cells by stimulating proteasomal degradation of c-Myc (see Chapter 2; [289]). In addition, c-Myc levels are reduced in Jurkat T cells treated with by pro-apoptotic concentrations of Bz-423 (Figure 3.40).

After release from retinoblastoma protein (pRb), E2F transcription factors stimulate expression of genes that mediate G_1-S phase cell cycle progression [527], but have also been shown to induce BH3-only proteins including Puma, Noxa and Bim [526]. In Ramos B cells, Bz-423-induced growth arrest is associated with a reduction in pRb phosphorylation [289]. In its hypophosphorylated form, pRb binds to E2F proteins and suppresses their ability to activate transcription [528]. As a result, Bz-423 treatment is expected to result in decreased E2F transcriptional activity, which suggests that induction of *noxa* by E2F proteins are unlikely to be responsible for the increase in levels of this protein in response to Bz-423.

HIF-1α is the principle regulator of the cellular response to hypoxia, which involves upregulation of genes involved in glucose metabolism, cytoskeletal reorganization, iron homeostasis, angiogenesis and apoptosis (e.g. Noxa) [529]. While HIF-1α is expressed constitutively, it is rapidly degraded by the ubiquitin-proteasome system (UPS) at physiological O_2 tension [530]. Targeting of HIF-1α to the UPS involves hydroxylation of proline residues by prolyl hydroxylases, which use O_2 and non-heme Fe^{2+} as co-factors [531]. Although prolyl hydroxylase activity is reduced during

hypoxia due to diminished availability of O_2 [532], inactivation by mitochondrial-derived ROS also appears to play a role [529]. This was first suggested by the observation that HIF-1α stabilization is reduced when HeLa cells which have an inactive MRC due to depletion of mitochondrial DNA are exposed to hypoxic conditions [533]. $O_2^{\bullet-}$ fhas been specifically implicated in prolyl hydroxylase inactivation due to the ability of MnTBAP to block hypoxia induced HIF-1α stabilization in wild-type HeLa cells [533]. Finally, stabilization of HIF-1α has also been observed under physiological O_2 tension in response to the $O_2^{\bullet-}$ burst induced following stimulation of rat alveolar epithelial cells with TNF-α [534]. Hence, Bz-423-induced $O_2^{\bullet-}$ might likewise promote inactive prolyl hydroxylase activity leading to stabilization of HIF-1α and induction of *noxa*.

As described in the introduction to Chapter 3, inhibitory binding by Mcl-1 and Bcl-x_L blocks activation of Bak in unstressed cells. Noxa binds tightly to Mcl-1, but does not associate with Bcl-x_L [95]. Hence, Bz-423-induced activation of Bak is anticipated to require an additional signal to neutralize Bcl-x_L. Another BH3-only protein could serve as this signal. For instance, apoptosis induced by UV irradiation of MEFs is a consequence of increased expression of Noxa *and* release of Bmf from the DLC2 subunit of the myosin motor complex [133, 535]. Once released from DLC2, Bmf binds tightly to Bcl-x_L, which leads to activation of Bak when combined with neutralization of Mcl-1 by Noxa. However, levels of the BH3-only proteins Bim and Puma were not elevated in response to Bz-423. Likewise, processing of Bid to its active, truncated from is not observed. Together, these data argue against a contribution by these BH3-only proteins, which bind promiscuously to all five anti-apoptotic Bcl-2 proteins (see Chapter 3 Introduction). In addition, engagement of Bim, Puma and Bid is inconsistent with

preferential activation of Bak because these BH3-only proteins would neutralize Bcl-2 along with Bcl-x_L, which could lead to activation of Bax [95].

A role for Bad and Bmf are similarly difficult to reconcile with preferential activation of Bak because these BH3-only proteins can activate Bax by neutralizing Bcl-2 [95]. More importantly, levels of Bad and Bmf were stable in Jurkat T cells following treatment with Bz-423 for up to 8 h. Engagement of Bik or Hrk is consistent with preferential activation of Bak because both BH3-only proteins bind Bcl-x_L, but not Bcl-2 [95]. However, Bik levels were below the limits of detection by immunoblot in both vehicle and Bz-423-treated Jurkat T cells. Changes in Hrk were not examined because expression of this BH3-only protein is restricted to the nervous system where it contributes to apoptosis induced by withdrawal of neural growth factors [152].

While increased levels of BH3-only proteins (i.e., besides Noxa) is not observed, Bak levels are elevated more than two-fold after exposure to Bz-423 for 2 h and continue to rise till present at a level greater than six-fold above control at 8 h. The increase in Bak levels in Bz-423-treated Jurkat T cells is unusual because Bax and Bak are not typically regulated transcriptionally, with activation of these proteins instead depending on the relative levels of BH3-only proteins and anti-apoptotic Bcl-2 proteins [38, 97]. There are examples, however, where Bak levels are elevated during apoptosis. Bak expression is induced in HL-60 B cells stimulated with interferon-γ as well as in HeLa cervical carcinoma cells treated with cyclooxygenase inhibitor Celecoxib [401, 402]. In the latter case, Bak induction is mediated by the growth arrest and DNA damage (GADD) inducible transcription factor GADD153 [401]. In addition, Bak expression has been shown to be induced by oxidative stress. For example, Bak mRNA and proteins

levels are elevated in SH-SY5Y neuroblastoma cells treated with H_2O_2. Induction of Bak by H_2O_2 is associated with increased binding of the transcription factors NFκB and NFAT to the *bak1* promoter region [403].

Given the essential role that Bak *activation* plays in Bz-423-induced apoptosis in Jurkat T cells, it seems likely that increased Bak *levels* might contribute to this response. This hypothesis is consistent with the indirect activation model, which contends that neutralization of anti-apoptotic Bcl-2 proteins is sufficient to signal activation of Bax and Bak (see Chapter 3 Introduction). Therefore, an increase in Bak levels is predicted to be a potent apoptotic stimulus because unbound Bak and Bax (i.e., after translocation to the mitochondrial outer membrane) do not require an additional stimulus to induce MOMP [84, 98]. Hence, a contribution by BH3-only proteins in addition to Noxa may not be required to for activation of Bak in response to Bz-423. Instead, neutralization of Mcl-1 by Noxa combined with the increase in Bak levels is predicted to saturate Bcl-x_L resulting in accumulation of free (i.e., active) Bak. This mechanism is consistent with preferential activation of Bak in response to Bz-423 because neither Noxa nor Bak has been shown to disrupt association of Bax with Bcl-2 [84, 95]. In addition, an increase in Bak levels alone could be sufficient to overwhelm the inhibitory capacity of Mcl-1 and Bcl-x_L, which may explain why Bz-423-induced apoptosis is only partially blocked (i.e., the EC_{50} for cell death is increased by ~25%) iin Jurkat T cells by reduction of Noxa expression.

Hierarchical activation of Bak and Bax has been described in apoptotic models besides Jurkat T cells treated with Bz-423. For instance, Bax and Bak are hierarchical activated in HeLa cervical carcinoma or A549 non-small cell lung cancer cells treated with pro-oxidant concentrations of the DNA-damaging agent *cis*-

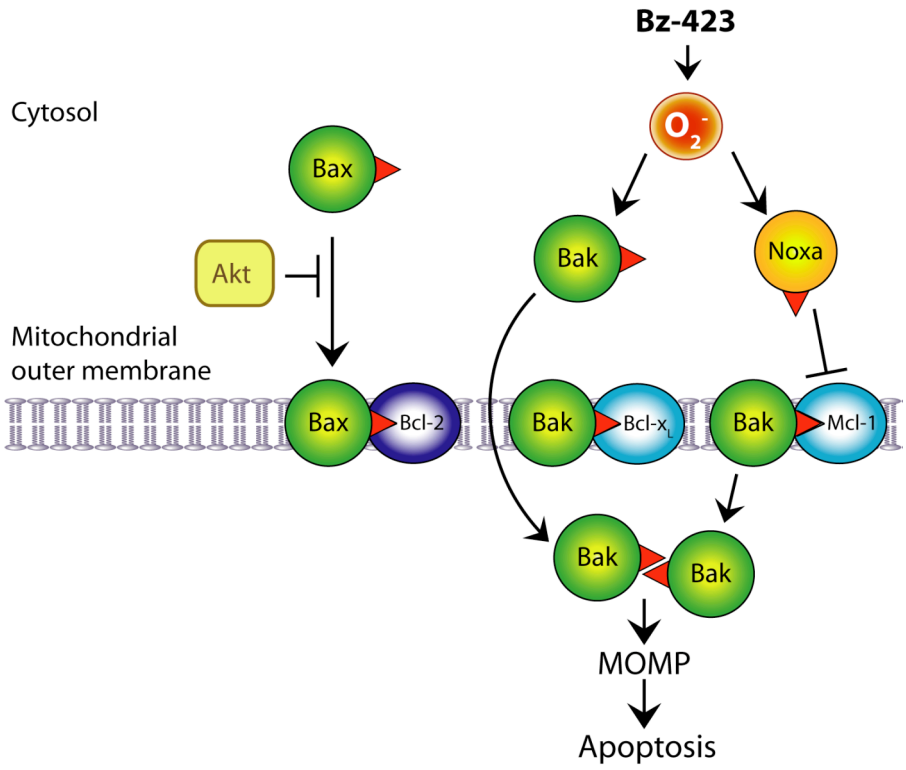

Figure 3.53 - Mechanistic hypothesis for preferential activation of Bak by Bz-423 in CD4$^+$ T cells leukemia lines. Bax activation is suppressed by inhibitory mechanisms that do not affect Bak. The pro-survival kinase Akt, which is constitutively active in CD4$^+$ T cell leukemia lines, suppresses Bax translocation to the mitochondria. In addition, Bax activation is inhibited by Bcl-2, Bcl-x$_L$ and Mcl-1, while activation of Bak is only blocked by Bcl-x$_L$ and Mcl-1. Bz-423 increases levels of Bak and the BH3-only protein Noxa, which speciically neutralizes Mcl-1. The resulting increase in free Bak levels overwhelms the inhibitory capacity of Bcl-x$_L$, leading to Bak activation, MOMP and apoptosis. Bax is not activated by the increases in Noxa and Bak levels because these responses do not reduce Akt activity or disrupt Bax•Bcl-2 interactions. See text for additional detail.

diamminedichloridoplatinum(II) (CDDP) [536, 537]. CDDP is an inorganic platinum complex that cross-links DNA by coordinating basic sites on purine nucleotides [538]. These adducts activate cellular DNA damage machinery, which can cause activation of p53 [539]. Indeed, p53-depedent mechanisms (e.g., induction of Puma) mediate

apoptosis induced by concentrations of CDDP below ~40 μM [540]. However, CDDP induced apoptosis is independent of p53 at concentrations >40 μM and is instead thought to result from increased intracellular $O_2^{\bullet-}$ levels [540]. Depletion of GSH as well as direct oxidation of the platinum ion have been suggested as mechanisms for CDDP induced $O_2^{\bullet-}$ production [541]. Regardless of the mechanism by which CDDP elevates intracellular $O_2^{\bullet-}$ levels, apoptosis induced by 50 μM or 100 μM CDDP is prevented by pre-incubation of A549 cells with the GSH precursor *N*-acetylcysteine (NAC) [542].

The kinetics of Bax and Bak activation have not been examined in HeLa or A549 cells treated with concentrations of CDDP >40 μM [537, 542]. However, in both cases reducing expression of Bak blocks CDDP induced Bax activation [537, 542]. Conversely, activation of Bak in response to CDDP is unaffected by knockdown of Bax [537, 542]. As observed for Bz-423-induced apoptosis in Jurkat T cells, knockdown of Bak blocked CDDP induced cytochrome *c* release in HeLa cells, while reducing Bax expression provided no protection [537]. The role of Bax or Bak in mediating mitochondrial apoptotic changes induced by CDDP was not examined in HeLa cells [542]. However, reducing Bak expression protected A549 cells from cell death induced 100 μM CDDP to a greater extent (55%) than knockdown of Bax (35%) [542].

The herbicide paraquat stimulates mitochondrial $O_2^{\bullet-}$ production by participating in redox cycling reactions in the MRC and induces $O_2^{\bullet-}$-dependent apoptosis in SK-N-SH neuroblastoma cells [116, 475]. As described above, levels of Noxa are elevated in SK-N-SH cells treated with paraquat [116]. Also similar to the effects of Bz-423 in Jurkat T cells, Bax and Bak function non-redundantly in paraquat induced apoptosis in SK-N-SH cells [116]. Reducing Bak levels with siRNA protected SK-N-SH cells against paraquat

induced apoptosis, while Bax knockdown had no effect [116]. Along with these effects in SK-N-SH cells, primary neurons from *bak*$^{-/-}$ mice were resistant to paraquat-induced apoptosis *in vivo* [116].

Two common themes emerge from these studies of the role of Bax and Bak Bz-423, CDDP and paraquat induced apoptosis. First, Bak activation is both necessary *and* sufficient to induce MOMP in several cell-types. Second, preferential activation of Bak appears to be shared response to increased intracellular $O_2^{\bullet-}$ levels, perhaps due to induction of Noxa. As described above, both points are consistent with recent developments in the understanding of the regulation of Bcl-2 proteins, which indicate that the activation barrier for Bak is lower than for Bax [63, 64]. While preferential activation of Bak had been demonstrated by genetic approaches (e.g., combined over-expression Bad and Noxa), these studies demonstrate that similar specificity can be obtained with agents that do not directly engage Bcl-2 proteins. This finding is significant because inducing MOMP (and as a result apoptosis) by specifically activating Bak alone represents a means to circumvent blocks in Bax translocation and/or activation often observed in cancer cells and autoimmune lymphocytes.

Bioenegetics of autoimmune lymphocytes: Characterization of Bz-423-induced apoptosis in $CD4^+$ T cell leukemia lines revealed two critical points of regulation: mitochondrial $O_2^{\bullet-}$ production and activation of the pro-apoptotic Bcl-2 protein Bak. This section of the discussion will focus on factors predisposing autoimmune lymphocytes to produce $O_2^{\bullet-}$ in response to Bz-423.

Bz-423-induced $O_2^{\bullet-}$ production results from modulation of the F_oF_1-ATPase. As described above, inhibition of the F_oF_1-ATPase in respiring cells reduces the rate of

mitochondrial ATP synthesis *and* forces the MRC into a reduced state favoring the production of $O_2^{\bullet-}$ (see Chapter 1). This ROS then activates signaling external to the mitochondria that leads to activation of Bak, and as a result, MOMP and apoptosis. This mechanism of action suggests that increased reliance on oxidative phosphorylation will sensitize cells to Bz-423. This hypothesis is supported by studies in which HepG2 hepatocarcinoma cells were cultured in media in which galactose is substitutued for glucose [543]. While galactose is substrate for glycolysis, its conversion to lactate yields no net ATP, which leads to increased metabolic flux through oxidative phosphorylation [544]. HepG2 cells in galactose/glutamine media were at least four-fold more sensitive to cell death induced by the F_oF_1-ATPase inhibitor oligomyin, the complex I inhibitor rotenone or the complex III inhibitor antimycin A relative to control cells cultured in the presence of glucose [543]. Importantly, rotenone induced apoptosis has been shown to be $O_2^{\bullet-}$-dependent [348], which suggests that increasing dependence on oxidative phosphorylation will sensitize a cell to agents that promote mitochondrial $O_2^{\bullet-}$ production. As such, cells that depend heavily on mitochondrial respiration for ATP production are likely to be sensitized to Bz-423-induced $O_2^{\bullet-}$ production and apoptosis.

Administration of Bz-423 to MRL-*lpr* mice improves autoimmune glumeronephritis and causes specific depletion of splenic $CD4^+$ T cells, which is the lymphoid subset responsible for disease in this murine model of lupus. Differential expression of the OSCP (e.g., levels of this protein are elevated nearly three-fold in lymphocytes relative to other cell-types; [241]) may play a role in the selective effects of Bz-423 in MRL-*lpr* mice. However, because the F_oF_1-ATPase is present in all nucleated cells, other factors are likely to contribute to selectivity. For instance, specific depletion

of MRL-*lpr* $CD4^+$ T cells may result, in part, from phenotypic changes that sensitize this lymphoid subset to Bz-423. In this case, Bz-423 might also display efficacy in other diseases where the pathogenic cells share a similar phenotype. In support of this hypothesis, Bz-423 improves autoimmune glomerulonephritis in the (NZB x NZW)F_1 (NZB/W) murine model of lupus, which results from pathogenic expansion of germinal center (GC) B cells (see Chapter 2 Introduction). Disease improvement in NZB/W mice is accompanied by specific apoptosis of GC B cells. The lineage-specific effects of Bz-423 in MRL-*lpr* and NZB/W mice suggest that autoimmune lymphocytes may harbor a common set of abnormalities that confer sensitivity to Bz-423. As described above, increased reliance on mitochondrial ATP production sensitizes Hep2G cells to drugs that modulate mitochondrial metabolism [543]. Therefore, increased mitochondrial metabolism is expected to likewise predispose cells to produce $O_2^{\bullet-}$ in response to inhibition of the F_oF_1-ATPase, and perhaps, act as a phenotype that predisposes autoimmune lymphocytes to Bz-423.

The hypothesis that autoimmune lymphocytes harbor mitochondrial bioenergetic abnormalities that predispose them to Bz-423 is challenging to evaluate because a means of identifying the pathogenic cell population is not available [201]. Nevertheless, information on disease-related changes in autoimmune lymphocytes can be extracted from examination of the total population (i.e., both pathogenic and non-pathogenic) of peripheral blood lymphocytes from systemic lupus erythematosus (SLE) patients. Analysis mitochondrial and redox characteristic of peripheral blood lymphocytes from SLE patients has been carried out by Perl, *et al.* [294, 545-547]. These experiments have demonstrated that peripheral blood T cells from SLE patients display a ~50% increase in

mitochondrial mass relatove to T cells from healthy volunteers (147 vs. 100 mean fluorescence units, respectively) as measured with MitoTracker Green, a $\Delta\psi_m$-insensitive mitochondrial dye [548]. This increase in mitochondrial mass likely results from the presence of larger numbers of mitochondria per cell in peripheral blood T cells from SLE patients (8.76 ± 1.0) compared to healthy volunteers (3.18 ± 0.28) [548]. Additionally, mitochondria in peripheral blood T cells from SLE patients are more highly energized (i.e., $\Delta\psi_m$ is hyperpolarized) than those of healthy volunteers (130 vs. 100 mean fluorescence units) as measured by the $\Delta\psi_m$-sensitive dye TMRM [548]. Finally, mitochondrial respiration (i.e., O_2 consumption) is elevated by >50% in peripheral blood lymphocytes from SLE patients [549]. Collectively, these findings provide evidence that increased mitochondrial metabolism is a common feature of autoimmune lymphocytes.

The increase in proton motive force that accompanies hyperpolarization of $\Delta\psi_m$ slows electron transport by the MRC by energetically disfavoring translocation of protons across the mitochondrial inner membrane (see Chapter 1) [239]. As a result, the half-life of reactive ETC intermediates (e.g., Fe-S centers, flavoproteins and ubisemiquinones) capable of single-electron reduction of O_2 is extended, which favors production of $O_2^{\bullet-}$. Hence, the increase in $\Delta\psi_m$ in peripheral blood lymphocytes from SLE patients suggests that levels of $O_2^{\bullet-}$ and other ROS might be elevated in these cells. This possibility has been assessed usitg the redox-sensitive dyes DHE, which is specifically oxidized by $O_2^{\bullet-}$, and dichlorofluorescein-diacetate (DCF-DA), which reacts with a variety of ROS including H_2O_2, hydroxyl radical, peroxynitrite and lipid peroxides [366]. This approach identified a 43% increase in $O_2^{\bullet-}$ levels in peripheral blood lymphocytes from SLE patients relative to healthy volunteers (143 vs. 100 mean fluorescence units,

respectively), while levels of DCF-DA reactive ROS were increased by 40% (140 vs. 100 mean fluorescence units, respectively). Hence, basal ROS levels are elevated in peripheral blood lymphocytes from SLE patients, which may be a byproduct of increased mitochondrial metabolism in these cells.

Cellular antioxidant systems maintain $O_2^{\bullet-}$ and other ROS at sub-micromolar levels (see Chapter 1). For example, SODs convert $O_2^{\bullet-}$ to H_2O_2 [265]. H_2O_2 is, in turn, decomposed to water and O_2 by catalase or the glutathione peroxidase/reductase system [550, 551]. Reduction of H_2O_2 by catalase is accomplished by oxidation of a heme cofactor Fe^{2+} [550]. By contrast, reducing equivalents for reduction of H_2O_2 by glutathione peroxidase are obtained by oxidation of glutathione (GSH) to the corresponding disulphide (GSSG) [550]. The elevated levels of $O_2^{\bullet-}$ and DCF-DA reactive ROS in peripheral blood lymphocytes from SLE patients are expected to strain cellular anti-oxidants defense, an effect that may be manifest in reduced GSH stores. In support of this hypothesis, glutathione levels are reduced in peripheral blood lymphocytes from SLE patients relative to the concentrations in peripheral blood lymphocytes from healthy controls (3.6 vs. 5.1 ng GSH / μg protein, respectively) [547]. These data suggest that oxidative stress resulting from the presence of elevated levels of $O_2^{\bullet-}$ and other ROS tax in lupus lympohcytes cellular anti-oxidant systems resulting in depletion of GSH.

Along with peripheral blood lymphocytes from SLE patients, cellular GSH levels have been assessed in splenic T cells from MRL-*lpr* mice using the thiol-reactive fluorescein derivative CMFDA [552]. In this study, glutathione levels were reduced more than five-fold in splenic T cells from four-month-old MRL-*lpr* mice relative to the same lymphoid compartment of age-matched $MRL^{+/+}$ animals (<100 versus >500 mean

fluorescence units, respectively) [249]. Hence, a decrease in cellular glutathione stores appears to be a shared characteristic of human and murine lupus lymphocytes. This commonality suggests that basal ROS levels are likely also elevated in MRL-*lpr* splenic T cells, an effect which again may derive from an increase in oxidative metabolism.

Collectively, these studies in lymphocytes from SLE patients and MRL-*lpr* mice make a strong case that mitochondrial metabolism is elevated in lupus lymphocytes. Because production of $O_2^{\bullet-}$ due to leak of electrons to O_2 is natural consequence of electron transport by the MRC, this increase in oxidative metabolism is expected to contribute to the elevated basal ROS levels and decreased glutathione stores in lupus lymphocytes. The mitochondrial bioenergetic phenotype in lupus lymphocytes is predicted to sensitize these cells to Bz-423. For instance, cells with increased number of mitochondria are predicted to have elevated levels of the OSCP along with other components of the F_oF_1-ATPase. This effect, combined with hyperpolarization of $\Delta\psi_m$, should predisposes lupus T cells to generate $O_2^{\bullet-}$ in response to Bz-423 by increasing the number of available binding partners as well as lowering the threshold of F_oF_1-ATPase inhibition required to trigger a mitochondrial respiratory transition. In addition, the capacity of lupus lymphocytes to detoxify Bz-423-induced $O_2^{\bullet-}$ will be compromised by the decrease in GSH stores. The latter effect has been demonstrated experimentally in MEFs, which are sensitized to Bz-423-induced cell death (42% decrease in EC_{50}) by treatment with L-buthionine sulfoximine (BSO), an inhibitor of the rate-limiting step in GSH synthesis [553].

More generally, the presence of mitochondrial and redox abnormalities in lupus lymphocytes suggests that bioenergetic characteristics of a T cell vary depending on

whether it is responding normally to foreign (typically infections) or abnormally to self-antigens. T cells activated in response to foreign antigens meet their increased energy demands by upregulating glucose metabolism (see Chapter 3 Introduction). This bioenergetic state is termed aerobic glycolysis because glycolytic ATP production is increased despite the presence of sufficient O_2 to support oxidative phosphorylation [253]. In contrast, the mitochondrial bioenergetic phenotype in lupus lymphocytes suggests that T cells responding to self-antigens may generate ATP primarily via oxidative phosphorylation. This hypothesis has important implications for the diagnosis and treatment of autoimmune disorders. For instance, markers of elevated oxidative metabolism (e.g., hyperpolarized $\Delta\psi_m$ or increased mitochondrial mass) could be used to identify the subset of autoreactive T cells mediating disease. More significantly, however, agents that modulate mitochondrial metabolism (e.g., Bz-423) may be able to selectively kill or inactivate autoreactive lymphocytes without affecting T cells responding to foreign antigens. Such phenotypic selectivity would enable treatment of autoimmune disorders (e.g., SLE) without the increased risk of infection resulting from suppression of normal immune function [201]. An essential question, therefore, is why lupus T cells display a mitochondrial bioenergetic phenotype when lymphocytes activated by foreign antigens meet their energetic demands via aerobic glycolysis.

Enhanced proliferation and cytokines are observed following stimulation of the T cell receptor (TCR) and co-stimulatory receptors such as CD28 [193]. Ligation of CD28 is an essential signal for conversion of activated (i.e., TCR-stimulated) T cells to aerobic glycolysis with many of the intracellular consequences of CD28 stimulation mediated by induction of PI3K-Akt signaling (see Chapter 3 Introduction; [253]). In contrast,

oxidative phosphorylation is regulated downstream of the TCR [214, 259]. The presence of distinct signaling networks leading to upregulation of glucose or mitochondrial metabolism suggests that the balance of TCR and CD28 stimulation may dictate how an activated T cell generates ATP.

Stimulation of the TCR and CD28 leads to upregulation of both mitochondrial and glucose metabolism [255, 256, 258]. Glucose uptake and lactate production are increased to a greater extent (approximately six-fold) than mitochondrial respiration (i.e., O_2 consumption is increased nearly two-fold) [255]. The larger increase in glucose metabolism suggests that activated T cells may be unable to generate sufficient ATP via oxidative phosphorylation to meet their energy demands. However, stimulation of human peripheral blood T cells with a TCR agonist antibody in the absence of ligands for CD28 results in a nearly four-fold increase in O_2 consumption, whereas lactate production is not elevated [255]. While T cells stimulated via both the TCR along with CD28 preferentially produce ATP via glycolysis rather than fully utilizing oxidative phosphorylation, additional mitochondrial respiratory capacity is tapped when the TCR is engaged in the absence of CD28. Together these results suggest that the mitochondrial bioenergetic phenotype in lupus lymphocytes may arise due to factors that limit CD28 engagement and/or signaling during stimulation of autoreactive T cells.

T cells are activated *in vivo* by stimulation of the TCR with antigens displayed by MHC complexes on antigen-presenting cells (APCs) such as macrophages, monocytes, mast cells and dendritic cells [153]. The endogenous ligands for CD28 are B7.1 and B7.2, which are upregulated by APCs in response to stimulation of Toll-like receptors (TLRs) by non-specific, pathogen-associated inflammatory triggers such as bacterial cell

wall lipopolysaccharides (LPS) or viral DNA [154]. These non-specific pathogen-associated antigens activated APCs leading to upregulation of the co-stimulatory molecules B7.1 and B7.2 (see Chapter 3 Introduction) [190, 197].

One distinguishing characteristic of self-antigens (e.g., plasma-membrane phospholipids, fragments of DNA or nuclear proteins), therefore, is that they not accompanied by non-specific, pathogen-associated inflammatory triggers [154, 190]. Thus, hile self-antigens are loaded on MHC complexes by APCs, their display is not accompanied by increased levels of B7 molecules [154, 155]. Therefore, the presence of low levels of B7 molecules on APCs displaying self-antigens is one mechanism that may reduce co-stimulatory CD28 signaling during activation of autoimmune lymphocytes.

Presentation of foreign antigens declines after the pathogen they are derived from is cleared [163, 170]. The decrease in pathogen-derived antigens signals termination of an immune response (see Chapter 3 Introduction; [177]). In the absence of antigenic stimulation activated T cells cease to produce pro-survival cytokines such as IL-2. The drop in pro-survival cytokines then leads to induction of the BH3-only proteins Bim and Puma in activated T cells, which initiate a mitochondrial apoptotic cascade by activation of Bax and Bak. In contrast, self-antigens recognized by lupus lymphocytes (e.g., plasma-membrane phospholipids, fragments of DNA or nuclear proteins) are ubiquitous due to their presence on cell membranes or continual release from dying cells [554, 555]. As a result of persistent stimulation with self-antigens, autoreactive T cells produce of sufficient levels of pro-survival cytokines to suppress apoptosis and perpetuate autoimmune responses [177].

In addition to preventing cytokine-withdrawal apoptosis, persistent antigenic stimulation may contribute to the mitochondrial bioenergetic phenotype in lupus lymphocytes by triggering mechanisms that suppress co-stimulatory CD28 signaling. For example, repeated TCR stimulation of naïve, $CD28^{+}$ human peripheral blood T cells (either $CD4^{+}$ or $CD8^{+}$) results in progressive loss of CD28 expression [556]. While <2% of naïve $CD4^{+}$ T cells display low levels of CD28 on their cell-surface (i.e., are $CD28^{null}$), whereas >70% are $CD28^{null}$ after 10 rounds of stimulation with an agonist TCR antibody [557]. This process, termed CD28 extinction, is thought to be responsible for accumulation of $CD28^{null}$ T cells with age [556]. $CD28^{null}$ cells comprise <5% of the $CD4^{+}$ T cell population of adolescents, but are observed at a frequency of up to 70% in individuals older than 50 years [558]. The observation that $CD28^{null}$ T cells are reactive to ubiquitous self-antigens such as DNA fragments and histones also supports a model in which CD28 extinction observed *in vivo* is a consequence of repeated antigenic stimulation [559, 560]. In addition, accumulation of $CD28^{null}$ T cells is accelerated in a variety of autoimmune disorders including rheumatoid arthritis, multiple sclerosis and SLE [561-563].

A decrease in levels of a receptor on the cell-surface can result from transcriptional repression and/or decreased trafficking to the plasma membrane [564]. The contribution of these mechanisms to CD28 extinction has been investigated in $CD4^{+}CD28^{null}$ T cells isolated from rheumatoid arthritis patients or generated by repetitive *ex vivo* stimulation [557, 565]. Both approaches have demonstrated that CD28 extinction results from transcriptional repression [557, 565]. A transcription factor complex composed of nucleolin and heterogeneous ribonucleoprotein-D0 (hnRNP-D0)

regulates CD28 expression in naïve T cells [556]. Surprisingly, nucleolin and hnRNP-D0 remain associated with the CD28 promoter in $CD4^+CD28^{null}$ T cells, but are functionally inactive [557, 565]. These observations suggest that activity of the nucleolin•hnRNP-D0 complex is regulated post-translationally [556].

In addition to CD28 extinction, persistent antigenic stimulation of T cells also suppress co-stimulatory CD28 signaling by upregulating negative regulators such as cytotoxic T lymphocyte antigen-4 (CTLA-4) and programmed death-1 (PD-1). CTLA-4 is a cell-surface receptor that shares the B7 ligand with CD28, but binds with higher avidity [566]. Although PD-1 is structurally related to CD28 and CTLA-4, it binds to PD-1 ligand (PD-1L) rather than B7 [567]. CTLA-4 and PD-1 are both present at low levels on the surface of naive T cells [568, 569]. However, cell surface levels of CTLA-4 are increased six-fold in splenic $CD4^+$ T cells from C57BL/6 mice following *ex vivo* TCR/CD28 stimulation [569]. Similarly, administration of an anti-TCR mAb to C57BL/6 mice results in a 60% increase in cell-surface PD-1 levels in splenic $CD4^+$ T cells after 72 h [568]. CTLA-4 and PD-1 suppress CD28-PI3K-Akt signaling by biochemically distinct mechanisms [570]. Ligation of CTLA-4 stimulates activity of protein phosphatase 2A (PP2A), which dephosphorylates Akt at Thr308 and Ser473 [570]. Phosphorylation of both residues activates Akt by stabilizing the kinase domain and activity [219]. In contrast, stimulation of PD-1 reduces Akt activation by inhibiting generation of $PtdIns(3,4,5)P_3$ by PI3Ks [570]. In sum, upregulation of CTLA-4 and PD-1 along with suppression of CD28 expression may contribute to the mitochondrial bioenergetic phenotype in lupus T cells by dampening co-stimulatory CD28 signaling.

The combined effects of CD28 extinction along with upregulation of CTLA-4 and PD-1 is expected to reduce phospho-Akt levels in autoimmune lymphocytes. However, phospho-Akt levels are elevated nearly five-fold in splenic $CD4^+$ T cells from four-month-old MRL-*lpr* mice relative to the same lymphoid subset in $MRL^{+/+}$ mice or the non-autoimmune C57BL/6 strain [233]. A potential explanation for this apparent inconsistency is the presence of multiple PI3K isoforms that are activated by different classes of cell-surface receptors. In T cells, PI3Kγ is activated by stimulation of the G-protein-couple receptors (GPCRs) that respond to chemokines, which are low-molecular weight cytokines (<10 kDa) that recruit hematopoetic cells to sites of inflammation (Figure 3.54; [224]). In contrast, the increase in PtdIns(3,4,5)P_3 levels following ligation of CD28 is mediated by PI3Kδ, which interacts with tyrosine kinase motifs on the intracellular tail of CD28 (Figure 3.54; [224]).

The contribution PI3Kγ activity to the increase in phospho-Akt levels in MRL-*lpr* mice has been investigated using inhibitors specific to this isofom (Figure 3.54). For instance, administration of the PI3Kγ specific inhibitor AS605240 to MRL-*lpr* mice resulted in a >90% decrease in PI3Kγ activity in bulk splenocytes, while no change in PI3Kδ activity was observed [233]. However, γ-isoform specific inhibition was sufficient reduce phospho-Akt levels by >75% splenic $CD4^+$ T cells [233]. The dependence of phospho-Akt levels on PI3Kγ activity MRL-*lpr* $CD4^+$ T cells suggests that co-stimulatory CD28 signaling may be suppressed in this lymphoid subset. If CD28-PI3Kδ signaling where primarily responsible for generating PtdIns(3,4,P_3 necessary for activation of Akt in MRL-*lpr* $CD4^+$ T cells, inhibition of PI3Kγ would not be expected to reduce phospho-Akt levels.

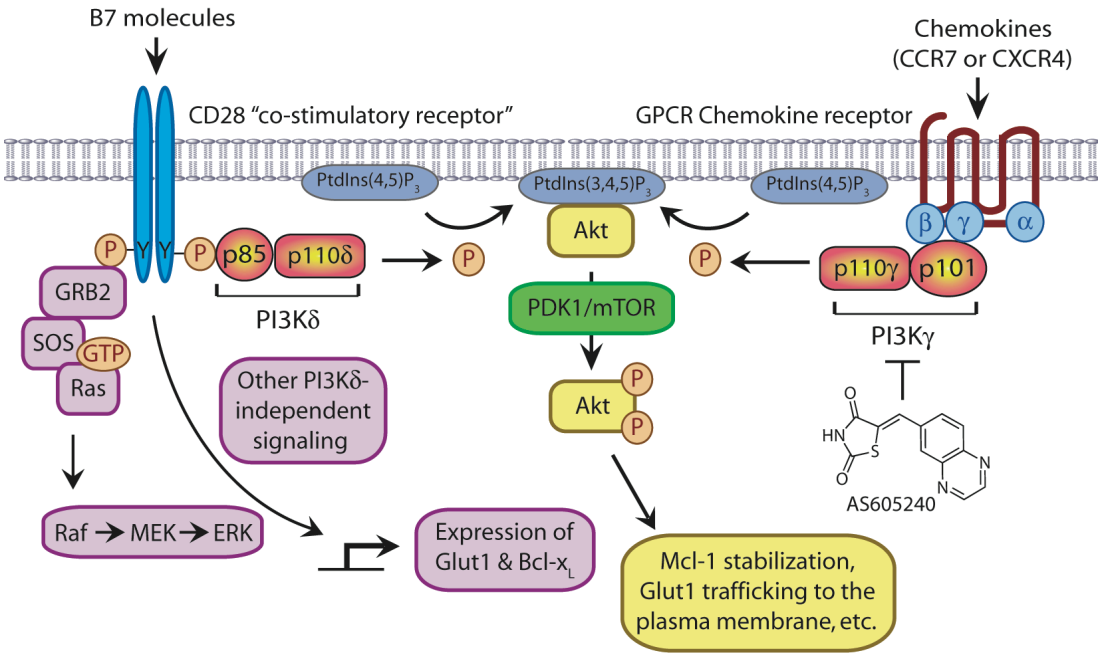

Figure 3.54 - PI3K signaling in T lymphocytes. Studies involving blockade of PI3Kδ or PI3Kγ function, either by gene targeting or pharmacological inhibition (e.g., with the PI3Kγ specific inhibitor AS605240), indicate that these isoforms function downstream of specific cell-surface receptors in T cells. The increase in PtdIns(3,4,5)P_3 levels and resulting activation of Akt following engagement of the co-stimulatory receptor CD28 is highly sensitive to inhibition of PI3Kδ, but not PI3Kγ. By contrast, PI3Kγ primarily mediates GPCR chemokine-receptor signaling, which is essential for recruitment of T cells to sites of inflammation. Stimulation of CD28 also activates PI3Kδ-Akt independent signals by recruiting effector molecules such as GRB2, which leads to activation of Raf → MEK → ERK MAPK cascade (see Chapter 1). As a result, some downstream effects of CD28 stimulation (e.g., Glut1 and Bcl-xL) induction are independent of PI3Kδ-Akt signaling. See text for additional detail. Figure adopted from [224].

In addition to PI3Kδ, ligation of CD28 leads to recruitment of signaling molecules including growth factor receptor bound protein-2 (Grb-2), lymphocyte-specific kinase ($p56^{Lck}$) and IL-2 inducible kinse (Itk). As a result, MAP kinases (e.g., c-Jun amino-terminal kinase (JNK) and transcription factors (e.g., nuclear factor-κB (NFκB)) are activated following CD28 stimulation in an Akt-independent manner (Figure 3.54)

[216, 571]. Not surprisingly then, the upregulation of effector molecules including the anti-apoptotic Bcl-2 protein Bcl-x_L and the glucose transporter Glut1 in response to ligation of CD28 stimulation does not depend on PI3K-Akt signaling (Figure 3.54; [258, 570]).

The presence of PI3K-Akt independent signaling cascades downstream of CD28 has important implications for the bioenergetics or autoreactive T cells because induction Glut1 expression is necessary for upregulation of glycolytic ATP production. Akt plays an essential role in regulating Glut1 activity by stimulating trafficking of this glucose transporter to the plasma membrane [258]. However, expression of constitutively active Akt transgene is not sufficient to induce Glut1 expression and increase glycolytic ATP production when CD28 is not engaged [258]. Hence, the increase in phospho-Akt levels in splenic $CD4^+$ T cells from MRL-*lpr* mice may not correspond to an increase in glucose metabolism in these cells. Rather, the dependence of Akt phosphorylation on PI3Kγ activity suggests that CD28-PI3Kδ signaling may be suppressed in this lymphoid subset, which would be consistent with transcriptional suppression of CD28 due to persistent TCR stimulation.

Proliferation and cytokine production following TCR stimulation of autoreactive T cells is inhibited by a combination of mechanisms collectively termed peripheral tolerance [189]. For instance, repetitive antigenic stimulation of T cells induces expression of FasL, which then triggers extrinisic apoptotic pathway by engaging the Fas death receptor (see Chapter 3 Introduction). This mechanism, termed activation-induced cell death (AICD), can serve to eliminate persistently stimulated autoreactive T cells

[170]. However, this peripheral tolerance mechanim is not engagned in MRL-*lpr* mice due defective expression of the Fas death receptor [167, 168, 188].

Another mechanism by which peripheral tolerance is maintained is suppression co-stimulatory CD28 signaling [192, 194]. Self-antigens are not accompanied by non-specific pathogen-associated inflammatory triggers, and therefore, so do not induce expression of CD28 ligands (i.e., B7 molecules) on APCs [197]. In addition, as described above, B7/CD28 signaling may be suppressed in persistently stimulated T cells due to transcriptional repression of CD28 as well as upregulation of negative regulators such as CTLA-4 and PD-1 [216, 556, 570]. Stimulation of the TCR in the absence of co-stimulatory CD28 signaling can induce anergy, a hyporesponse state in which T cells fail to proliferate or produce cytokines in response to antigenic stimulation (see Chapter 2 Discussion) [193, 194].

Despite peripheral tolerance mechanisms that limit their activation and survival, some autoreactive T cells respond productively (i.e., proliferate and produce cytokines) following stimulation with self-antigens, which can result in autoimmune disease [189]-. The ability of autoreactive T cells to evade peripheral tolerance mechanisms suggests that they contain inherent defects enabling response to TCR stimulation in the absence of co-stimulatory CD28 signaling. The hypothesis that pathogenic autoreactive T cells are hyper-responsive to TCR stimulation has been directly evaluated by Craft, *et al* using the Fas-intact MRL ($MRL^{+/+}$) strain [210, 213, 215]. The lymphoproliferative (*lpr*) allele conveys an AICD defect that results in splenomegaly and lymphoadenopathy in a variety of strains [166, 180]. However, the associated autoimmune disorder is more severe (i.e., increased autoantibody production, glumerulonephritis and early mortality) when

established on the MRL background [180]. This suggests that the MRL strain harbors defects predisposing autoreactive T cells to respond to self-antigens. While the lymphoproliferative disorder in MRL-*lpr* mice is marked by accumulation of a variety of lymphoid subsets, studies with depletive antibodies indicate that $CD4^+$ T cells mediate autoimmune disease [184]. Hence, $CD4^+$ T cells from Fas-intact MRL were used to evaluate whether autoimmune T cells are hyper-responsive to engagement of the TCR in the absence of CD28 [210, 213, 215].

To eliminate differences in TCR affinity, Craft, *et al* prepared a $MRL^{+/+}$ strain expressing a TCR restricted to recognition of amino acids 88-104 of pigeon cytochrome *c* (PCC) [210]. The activation response of MRL $CD4^+$ T cells was then compared to $CD4^+$ T cells from two non-autoimmune strains (CBA/CaJ and B10.BR) expressing the same PCC-restricted TCR [210]. In support of the hypothesis that autoimmune T cells are hyper-responsive to TCR stimulation, MRL $CD4^+$ T cells display an elevated activation response (i.e., more cell divisions and greater IL-2 production) following stimulation with PCC [210]. These differences were exacerbated by stimulation with PCC-derived peptides with reduced affinity for the TCR, which are thought to mimic the low affinity interactions of autoreactive, peripheral T cells with self-peptides [210-212].

Further studies demonstrated that TCR induced Ca^{2+} flux is elevated (two-fold) and prolonged (three-fold) in MRL $CD4^+$ T cells [213]. This exaggerated TCR-induced Ca^{2+} flux may be a consequence of increased phosphorylation of the inositol-1,4,5-triphosphate ($InsP_3$) receptor, which has been shown to promote release of ER Ca^{2+} stores [213, 572]. The increase in $[Ca^{2+}]_i$ following TCR stimulation is necessary for T cell activation and the magnitude of this response correlates with proliferation and cytokine

production [214]. Hence, enhanced proliferation and cytokine production by $MRL^{+/+}$ $CD4^+$ T cells may be a consequence of the exaggerated Ca^{2+} flux following TCR stimulation [213]. Collectively, these studies provide direct evidence that autoreactive T cells are hyper-responsive to stimulation of TCR in the absence of ligands CD28.

Elevated Ca^{2+} flux after TCR stimulation is also observed in peripheral blood T cells from SLE patients [548, 573-576]. For example, peak $[Ca^{2+}]_i$ levels are increased by >50% in peripheral blood T cells from SLE patients compared to healthy controls following TCR stimulation and remain elevated for more than five minutes [573]. This exaggerated Ca^{2+} flux may to result from "rewiring" of proximal TCR signaling. In SLE T cells the ζ-chain of the TCR complex is replaced with the γ chain of the receptor for the antibody constant fragment (FcR) [576]. This substitution results in recruitment of spleen tyrosine kinase (Syk) to the TCR instead of Zap70, and the FcRγ•Syk signaling complex has been shown to transduce an increased Ca^{2+} response relative to TCRζ•Zap70 [575, 577]. In addition to elevated Ca^{2+} flux following TCR stimulation, resting peripheral blood T cells from SLE patients have nearly 40% higher resting $[Ca^{2+}]_i$ levels than peripheral blood T cells from healthy volunteers [548]. This increase in basal $[Ca^{2+}]_i$ in lupus lymphocytes likely results from the exaggerated Ca^{2+} flux after engagement of the TCR combined with persistent antigenic stimulation by self-antigens. In sum, exaggerated Ca^{2+} flux following TCR stimulation and elevated basal $[Ca^{2+}]_i$ are a shared characteristic of human and murine lupus lymphocytes, which may contribute to the ability of these cells to respond to stimulation by self-antigens even when B7/CD28 signaling is suppressed.

As described in Chapter 1, TCR-induced Ca^{2+} flux stimulates the TCA-cycle due to uptake of $[Ca^{2+}]_i$ into the matrix by the Ca^{2+}-uniporter in the mitochondrial inner membrane and transient opening of the mPT pore and [260]. Elevated matrix Ca^{2+} increases the TCA-cycle activity by stimulating Ca^{2+}-dependent dehydrogenases, which elevates NADH levels more than two-fold [259]. This increase in NADH levels then stimulates the ETC causing proton transport to outpace dissipation of $\Delta\psi_m$ by passage of protons through the F_oF_1-ATPase during ATP synthesis (see Figure 1.9). While this increase in $\Delta\psi_m$ stimulates production of ATP by the F_oF_1-ATPase, it also forces the ETC into a reduced state characterized by increased $O_2^{\bullet-}$ production [254, 259, 261]. Hence, the mitochondrial bioenergetic phenotype (e.g., elevated O_2 consumption, $\Delta\psi_m$ and $O_2^{\bullet-}$ levels) observed in lupus lymphocytes could be a result of increased TCA-cycle activity due to abnormalities in Ca^{2+} flux and homeostasis.

To evaluate the hypothesis that TCA-cycle activity is elevated in autoimmune lymphocytes, Wahl, *et al* administered uniformly ^{13}C-labeled glucose to lupus-prone NZB/W and non-autoimmune Balb/c mice [578]. Levels of ^{13}C-labeled lactate and CO_2 were then assessed to determine whether glucose is consumed via glycolysis or the TCA-cycle [579]. This approach identified a >40% increase in production of $^{13}CO_2$ in bulk splenocytes from nine-month old NZB/W mice relative to age-matched Balb/c controls, while incorporation of the ^{13}C label into lactate was unchanged between the two strains [580]. The increase in CO_2 production by NZB/W splenocytes is consitent with a model where elevated in Ca^{2+} flux and increased basal $[Ca^{2+}]_i$ contributes to the mitochondrial bioenergetic phenotype in lupus lymphocytes by stimulating the TCA-cycle.

In sum, glycolytic and mitochondrial ATP production are regulated via distinct mechanisms in activated T cells. Engagement of the TCR stimulates mitochondrial respiration, while glucose metabolism is upregulated by co-stimulatory CD28 signaling. Because the ligands for the TCR and CD28 are both present on APCs displaying foreign antigens, T cells responding to foreign antigens rely primarily on glycolysis to meet their energetic demands. However, mitochondrial respiration is induced in the absence of changes in glucose metabolism when the TCR is stimulated in the absence of ligands for CD28. Interestingly, lupus lymphocytes are characterized by increases in mitochondrial mass, $\Delta\psi_m$ and O_2 consumption as well as elevated basal $O_2^{\bullet-}$ levels and decreased antioxidant stores. This mitochondrial bioenergetic phenotype suggests that co-stimulatory CD28 signaling is suppressed in autoreactive T cells.

In addition to increasing glycolytic ATP production, engagement of CD28 activates signaling cascades, which prevent induction of anergy following stimulation of the TCR. Autoreactive T cells are prevented from responding to stimulation by ubiquitous self-antigens by mechanisms (e.g., CD28 extinction or upregulation of CTLA-4 and PD-1) that suppress co-stimulatory CD28 signaling. In order to mediate autoimmune, disease autoreactive T cells presumably acquire the ability respond to TCR stimulation in the absence of co-stimulatory CD28 signaling. This hypothesis has been demonstrated experimentally in $CD4^+$ T cells from lupus-prone MRL mice, which are hyper-responsive to TCR stimulation in the absence of co-stimulatory CD28 signaling. However, due to suppression of co-stimulatory CD28 signaling, autoreactive T cells responding to persistent TCR stimulation by self-antigens may be unable to upregulate glucose metabolism. The mitochondrial bioenergetic phenotype in lupus lymphocytes is,

therefore, hypothesized to arise because suppression of co-stimulatory CD28 signaling forces autoreactive T cells to generate ATP primarily via oxidative phosphorylation.

Regulation of Bcl-2 proteins in activated T cells: In addition to mitochondrial $O_2^{\bullet-}$ production, Bz-423-induced T cell apoptosis depends on activation of the pro-apoptotic Bcl-2 protein Bak. In unstressed cells, the anti-apoptotic Bcl-2 proteins Mcl-1 and Bcl-x_L inhibit Bak activation [54]. Treatment of Jurkat T cells with Bz-423 leads to an increase in levels of Bak and the BH3-only protein Noxa within 2 h. Both effects are expected to promote accumulation of free, uninhibited Bak. Noxa liberates Bak by binding tightly to Mcl-1 [95]. Increased Bak levels are then expected to saturate the inhibitory capacity of Bcl-x_L (Figure 3.53). Several pieces of evidence support an indirect activation model (see Chapter 3 Introduction), in which neutralization of anti-apoptotic Bcl-2 proteins is sufficient to cause Bak to undergo a conformational change (termed activation) that promotes homo-oligomerization [84]. Bak homo-oligomers then form pores in the mitochondrial outer membrane, which promote release pro-apoptotic proteins (e.g., cytochrome *c*) from the MIS [98]. Based on this apoptotic mechanism, cells with elevated levels of Noxa and Bak and/or reduced levels of Mcl-1 and Bcl-x_L are predicted to be sensitized to Bz-423-induced apoptosis.

Signal transduction pathways downstream of the TCR and/or CD28 regulate Noxa, Bcl-x_L and Mcl-1 [410, 570, 581]. In addition to upregulating glucose metabolism, stimulation of CD28 promotes survival of activated T cells by a variety of mechanisms including post-translational stabilization of Mcl-1 and induction of Bcl-x_L (see Chapter 3 Introduction). Downstream of CD28, stabilization of Mcl-1 is mediated by inhibitory phosphorylaton of GSK-3β by Akt [410]. In its unphosphorylated form, GSK-3β

phosphorylates Mcl-1, which targets this anti-apoptotic Bcl-2 protein to the ubiquitin-proteasome pathway [410]. Unlike post-translational stabilization of Mcl-1, induction of Bcl-x_L expression is independent of the PI3K-Akt signaling. For example, the pan-PI3K inhibitor LY294002 blocks TCR/CD28 induced phosphorylation of Akt, but only reduces Bcl-x_L induction by ~20% [570]. The PI3K-Akt independent induction of Bcl-x_L expression is consistent with the activation of multiple signaling cascade following stimulation of CD28 (Figure 3.54; [216, 571]). Similarly, induction of the glucose transporter Glut1 following stimulation of the TCR and CD28 is not blocked by PI3K inhibitors [258].

As described previously, phospho-Akt levels are elevated nearly five-fold in splenic $CD4^+$ T cells from four-month old MRL-*lpr* mice compared to Fas-intact $MRL^{+/+}$ mice or the non-autoimmune C57BL/6 strain [233]. This increase in phospho-Akt levels suggests that Mcl-1 is likely to be stabilized in MRL-*lpr* $CD4^+$ T cells. However, Bcl-x_L expression may not be elevated in MRL-*lpr* $CD4^+$ T cells because Akt phosphorylation appears to depend on PI3Kγ in this lymphoid subset [233]. PI3Kγ-specific phosphorylation of Akt in this lymphoid subset has been demonstrated by administration of PI3Kγ-selective inhibitor AS605240 to MRL-*lpr* mice [233]. As described previously, PI3Kγ is activated by stimulation chemokine-responsive GPCRs, while CD28 ligation activates PI3Kδ (Figure 3.54) [224]. The dependence of phospho-Akt levels on PI3Kγ activity in MRL-*lpr* $CD4^+$ T cells, therefore, argues that co-stimulatory CD28 signaling is be suppressed in this lymphoid subset. This is because inhibition of PI3Kγ activity would not be predicted to affect phospho-Akt levels in the presence of robust CD28-PI3Kδ signaling. This apparent suppression of co-stimulatory CD28 signaling in MRL-*lpr* $CD4^+$

T cells, therefore, suggests that Bcl-x_L expression may not be elevated in this lymphoid subset.

In contrast to Mcl-1 and Bcl-x_L, expression of Noxa is regulated by signaling downstream of the TCR [581]. TCR stimulation of murine $CD4^+$ or $CD8^+$ T cells leads to induction of Noxa expression (three- or five-fold, respectively) after 24 h [581]. These changes in Noxa levels were maintained for up to 72 h, and no addition increase was afforded by combined stimulation of the TCR and CD28 [581]. Induction of Noxa expression in response to TCR stimulation contrasts with regulation of the BH3-only proteins Bim and Puma in activated T cells, which are induced by the reduction in PI3K-Akt following the drop in pro-survival cytokines after pathogen clearance [117, 129, 175]. This contrast suggests that Noxa induction may serve as mechanism to predispose chronically activated T cells to mitochondrial apoptosis, rather than acting to eliminate acutely activated T cells at the conclusion of an immune response [170]. Furthermore, Noxa expression is likely to be induced in autoreactive T cells because they are subject to persistent TCR stimulation by self-antigens.

Of note, elevated expression of Noxa was not observed in a genome-wide microarray profile of bulk MRL-*lpr* splenocytes [582]. However, Bz-423 depletes a relatively small population (~14%) of $CD4^+$ T cells, which are present overall in low numbers relative to atypical DN T cells in spleens of MRL-*lpr* mice [182, 183]. As such, induction of Noxa expression in a relatively small population of $CD4^+$ T cells may not be detected by assessment of mRNA levels in bulk MRL-*lpr* splenocytes.

In sum, expression of the BH3-only protein Noxa is induced by stimulation of the TCR, while levels of anti-apoptotic Bcl-2 proteins such as Bcl-x_L and Mcl-1 are regulated

downstream of CD28. As described above, negative regulators of co-stimulatory CD28 signaling are upregulated in response to persistent TCR stimulation. These effects are predicted to suppress co-stimulatory CD28 signaling in autoreactive T cells. Consistent with this hypothesis, phospho-Akt levels are elevated in MRL-*lpr* splenic $CD4^+$ T cells, this increase appears to result from stimulation of chemokine-responsive GPCRs rather than CD28 in $CD4^+$ T cells from MRL-*lpr* mice. As such, Noxa levels are predicted to be elevated in persistently TCR stimulated autoreactive T cells, while Bcl-x_L expression may not be induced. This combination of effects should predispose autoreactive lymphocytes (e.g., MRL-*lpr* $CD4^+$ T cells) to Bz-423-induced increases in Noxa and Bak levels.

Summary: The series of experiments described in this chapter identify key signaling events in apoptotic response that is induced by the 1,4-benzodiazepine F_oF_1-ATPase inhibitor, Bz-423, in T cells. Unlike polyketide inhibitors of the F_oF_1-ATPase (e.g., oligomycin), Bz-423 promotes mitochondrial $O_2^{\bullet-}$ production without depleting cellular ATP levels. This lack of an effect on ATP levels (i.e., prior to the commitment to apoptosis) is expected to arise because Bz-423 is a moderate affinity, uncompetitive inhibitor of the F_oF_1-ATPase. As such, Bz-423 does not reduce activity of the F_oF_1-ATPase beyond cellular capacity to buffer a decrease in oxidative phosphorylation by upregulating glycolytic ATP production.

Some oxidizing agents release of apoptogenic MIS proteins (e.g., cytochrome *c*) from isolated mitochondria by triggering sustained opening of the mPT pore. While isolated mitochondria produce $O_2^{\bullet-}$ when treated with Bz-423, this response is not sufficient to cause release of cytochrome *c* in this cell free system. Instead, Bz-423-induced apoptosis depends on extra-mitochondrial factors activated in response to the

increase in mitochondrial $O_2^{\bullet-}$ production. The signal that escapes mitochondria to trigger apoptosis in response to Bz-423 has yet to be defined. However, conversion of Bz-423-induced $O_2^{\bullet-}$ to H_2O_2 with the MnSOD mimetic MnTBAP blocks cell death, which suggests that $O_2^{\bullet-}$ may directly link the initial mitochondrial response to the subsequent apoptotic signaling. This proposal is supported by reports indicating that once present in the MIS, $O_2^{\bullet-}$ is transported out of mitochondria by VDAC and other porins.

Regardless of what signal escapes the mitochondria in response to Bz-423, increased levels of the pro-apoptotic Bcl-2 proteins Noxa and Bak are key elements in the resulting apoptotic cascade. Together these effects lead to activation of Bak, which commits a cell to die in response to Bz-423 by releasing of cytochrome *c* and other apoptogenic proteins from the MIS. Bak bears a high degree of homology to Bax, and these pro-apoptotic Bcl-2 proteins function redundantly in response to many apoptotic stimuli. However, Bak is preferentially activated in response to Bz-423 and is required for apoptosis, while Bax is dispensable. Preferential activation of Bak is expected to result from the presence of mechanisms that selectively inhibit activation of Bax in $CD4^+$ T cell leukemia lines such as constituitive activation of the pro-survival kinase Akt.

Finally, integrating knowledge of this apoptotic mechanism with properties of autoimmune lymphocytes provides insight into the selective effects of Bz-423 on pathogenic lymphocytes (e.g., specific depletion of splenic $CD4^+$ T cells in MRL-*lpr* mice) *in vivo*. Mitochondrial and glycolytic metabolism are regulated by signals downstream of the TCR and CD28 co-stimulatory receptor, respectively. Persistent TCR stimulation, like that experienced by autoreactive lymphocytes, leads to suppression of

co-stimulatory CD28 signaling, which may contribute to the mitochondrial bioeneretic phenotype (i.e., increased mitochondrial numbers, $\Delta\psi_m$, basal $O_2^{\bullet-}$ levels and decreased anti-oxidant stores) in lupus T cells. Together, these mitochondrial bioenergetic abnormalities are expected to predispose autoreactive T cells to produce $O_2^{\bullet-}$ in response to modulation of the F_oF_1-ATPase. In addition, stimulation of the TCR leads to induction of Noxa, while anti-apoptotic Bcl-2 proteins (e.g., Mcl-1 and Bcl-x_L) are upregulated by engagement of CD28. Autoreactive T cells are, therefore, predicted to have elevated levels of Noxa in the absence of similar increases in Mcl-1 and Bcl-x_L. Thus, the selective effects of Bz-423 *in vivo* likely derive from intersection of the apoptotic mechanism described in this chapter with these unique vulnerabilities of autoreactive lymphocytes.

Statement of collaboration: Quantification of intracellular ATP levels and mitochondrial ATP synthesis rates were performed collaboratively with Lara Swenson. Whole cell O_2 consumption experiments were conducted with Lara Swenson. The Jurkat T cell clones ectopically expressing Bcl-2 or the corresponding empty vector were prepared by Li Wang. The pSFFV-Bcl-2 plasmid and corresponding empty vector were a gift from Gabriel Nunez (University of Michigan Comprehensive Cancer Center). Immunoblots for phospho-Akt levels were performed in collaboration with Dan Wahl. The pMIG1-MyrAkt plasmid and corresponding empty vector were a gift from Jeffrey Rathmell (Duke University Medical Center).

Materials and Methods

Reagents: Bz-423 was prepared in DMSO (16 mM), which was diluted to a 10X stock with culture media. SB415286, alpha-tocopherol (Vitamin E), recombinant human tBid, staurosporine (STS), human recombinant iso-citrate dehydrogenase, cycloheximide (CHX), wortmannin, LY294002, oligomycin, antimycin A, *N*-benzoylcarbonyl-Val-Ala-Asp-fluoromethylketone (zVAD-fmk), hydrogen peroxide, *tert*-butyl hydroxperoxide, ionomycin and phorbol 12-myristate 13-acetate (PMA) were purchased from Sigma. Manganese(III) *meso*-tetrakis(4-benzoid acid)porphyrin (MnTBAP) was purchased from Alexis Biochemicals and prepared as a 100 mM stock in 1:1 EtOH:dH_2O (v/v). Dihydroethidium (DHE), tetramethyl rhodamine methyl ester (TMRM), C_{11}-BODIPY$^{581/591}$ were obtained from Invitrogen. Fluoro-citrate was purchased from Pfaltz & Bauer. siRNAs targeting Bax, Bak or Noxa were purchased from Dharmacon as siGENOME SMARTpool reagents. All other reagents were purchased from Sigma-Aldrich.

Cell lines and culture: Ramos B cells were purchased from the American Type Culture Collection. Jurkat T cells were obtained from V. Castle (Univ. of Michigan). MOLT-4 and CCRF-CEM T cells were obtained from the National Cancer Institute. All lines were maintained in RPMI 1640 containing 10% heat-inactivated fetal bovine serum (FBS: Mediatech), penicillin (100 U/mL), streptomycin (100 μg/mL) and L-glutamine (290 μg/mL) (Gibco). Cells were propagated in a humidified incubator (37 °C, 5% CO_2). Experiments were performed in media (5 x 10^5 cells/mL) containing 2% FBS. Cells were incubated with inhibitors at 37 °C for 30 min prior to addition of the compounds being tested.

Mitochondrial ATP synthesis assay: Cells (5 x 10^6) were isolated by centrifugation and washed once with ice-cold PBS. Cell pellets were resuspended in PBS (200 μL) with digitonin (50 μg/mL) at 0 °C for 2 min and then with ice-cold PBS (5 mL) and isolated by centrifugation. Permeabilized cells were resuspended in 300 μL of ATP synthesis buffer; 150 mM KCl, 25 mM Tris-HCl, 2 mM EDTA, 10 mM KH_2PO_4, 0.1 mM $MgCl_2$, 11 mM AMP, 5 mM malate and 5 mM glutamate, pH 7.4. A portion of this cell suspension (15 μL) was combined with ATP-free water (85 μL) in single wells of a white 96-well plate containing 50x drug or DMSO vehicle control (0.5% DMSO final). Promega ENLIGHTEN rLuciferin/Luciferase reagent (100 μL) was then added to each well. Reactions were initiated by addition of ADP (1 mM) and emission at 560 nM was monitored by continuously sampling every 10 s for 10 min using a Molecular Devices Lmax microplate luminometer. Synthetic rates were evaluated over a time frame from 2-4 min in which the increase in luminescence was linear and relative luminescence units were converted to ATP concentrations using a standard curve (10^{-3} - 10^{-8} M ATP).

Detection of cellular ATP content: Cells (5 x 10^5) were isolated by centrifugation and washed once with ice-cold PBS. Cell pellets were resuspended in lysis buffer (50 μL) containing 1% trichloroacetic acid (TCA) along with 2 mM EDTA at room temperature for 1 min. Lysis was by neutralization of samples with 25 mM Tris-acetate (1 mL), pH 7.75. ATP content was determined by combining neutralized sample (5 μL) with 95 μL of ATP-free water (Promega) in one well of a white 96-well plate followed by addition of ENLIGHTEN rLuciferin/Luciferase reagent (100 μL; Promega). ATP content was determined by measuring fluorescence emission at 560 nM using a

Molecular Devices Lmax luminometer. Relative luminescence units were converted to ATP concentrations using a standard curve (10^{-3} to 10^{-8} M ATP).

Oxygen consumption measurements: Oxygen consumption was determined using the BD Oxygen Biosensor System (BD Biosciences,) as described previously [275]. Jurkat T cells were suspended in treatment media (RPMI with 2% FBS) at a density of 5 x 10^6 cells/mL and transferred to a 96-well BD Oxygen Biosensor plate (1 x 10^6 cells/well). After treatment, levels of oxygen consumption were measured using a Molecular Devices Lmax luminometer at 2 min intervals for 1.5 h with an excitiation of 485 nm and emission of 630 nm. For semiquantitative data analysis the slope from a linear portion of curve (typically 0.5 – 1 h) was converted into arbitrary units.

Transient transfections: Jurkat, MOLT-4 or CCRF-CEM T cells (6 x 10^6) were washed once with ice-cold PBS, resuspended in electroporation buffer T (100 μL; Amaxa), combined with desired plasmid (8 μg) or siRNA (4 μg) and electroporated using a 2.0-mm cuvette and a Amaxa Nucleofection apparatus set to program G-16. Samples were then diluted in fresh complete media. Cells were transfected once a day for two days and cells were used to prepare lysates or incubated with Bz-423 three days after the initial transfection.

Detection of intracellular $O_2^{\bullet-}$, $\Delta\psi_m$, and lipid peroxidation: Intracellular $O_2^{\bullet-}$ was measured using DHE. Stocks of DHE (10 mM) were prepared in DMSO prior to each use. To measure intracellular $O_2^{\bullet-}$ levels cell cultures (5 x 10^5 cells/mL) were incubated with DHE (4 μM) for 30 min at 37 °C. The DHE-treated cells were immediately evaluated by flow cytometry. Ethidium fluorescence from the oxidation of DHE was detected in the FL2 channel of a FACSCalibur flow cytometer (Becton Dickinson).

Measurement of the mitochondrial electrochemical gradient ($\Delta\psi_m$) was conducted by labeling cells TMRM (50 nM) for 1 h at 37 °C. Samples were immediately analyzed using the FL2 channel of a BD FACSCalibur flow cytometer. Carbonyl cyanide 4-(trifluoromethoxy) phyenylhydrazone (FCCP; 30 μM) was used as a positive control for disruption of $\Delta\psi_m$. For measurement of lipid peroxides, cells were labeled with for 30 min with C_{11}-BODIPY$^{581/591}$ (50 nM) and increased green fluorescence arising from dye oxidation were quantified in the FL1 channel of a FACSCalibur flow cytometer (Becton Dickenson). Data for all three dyes was analyzed using the CellQuest software (Becton Dickinson).

Detection of cell death and cellular DNA content: Cell viability was assessed by staining with propidium iodide (PI, 1 μg/mL) at room temperature (~25 °C) for 5 min. PI fluorescence was measured in the FL3 channel using a FACSCalibur. Measurement of hypodiploid DNA content was conducted after incubating cells in labeling solution (50 μg/mL of PI in PBS containing 0.2% Triton and 10 μg/mL RNAse A) at 4 ˚C for 12 h. PI fluorescence was measured in the FL2 channel on a linear scale. Data were analyzed excluding aggregates using the CellQuest software (Becton Dickinson).

Detection of cell-surface FasL levels: Cell surface FasL levels were evaluated by labeling cells (0.5×10^6) with a primary biotin-conjugated FasL antibody (Becton Dickenson; catalog #556374) for 20 min at 4 ˚C. Cells were washed twice with ice-cold PBS containing 2% FBS and then resuspended in the same buffer along with a Steptavidin-FITC conjugate (Becton Dickenson; catalog #554061) for 20 min at 4 ˚C. Cells were again washed twice with ice-cold PBS containing 2% FBS, resuspended in the same buffer and FITC fluorescence measured of the FL1 channel of a FACSCalibur flow

cytometer (Becton Dickinson). Data were analyzed excluding aggregates using the CellQuest software (Becton Dickinson).

Preparation of whole cell extracts: Cells (6 x 10^6) were isolated by centrifugation. Cell pellets were washed once with ice-cold PBS (5 mL) before lysis in *w*hole *c*ell *e*xtract (WCE) buffer (500 μL; 25 mM Hepes pH 7.7, 150 mM NaCl, 2.5 mM $MgCl_2$, 0.2 mM EDTA, 0.1% Triton X-100, 20 mM β-glycerophophate, 0.5 mM DTT) with protease inhibitors (1 mM PMSF and complete protease inhibitor cocktail pellet (Roche)) and phosphatase inhibitors (3.3 mM NaF and 0.1 mM sodium orthovanadate). Following incubation on ice for 30 min, the lysed cells were centrifuged (12,000*g,* 30 min at 4 °C). Total protein content in the supernatant was quantified by the Bradford protein assay [583].

Mitochondrial isolation: Cells (7 x 10^6) were harvested and washed once with ice cold PBS. Cells were resuspend in ice cold buffer A (200 μL; 20 mM Hepes-KOH, pH 7.5, 10 mM KCL, 10 mM β-glycerophosphate, 5 mM NaF, 1.5 mM $MgCl_2$, 1 mM sodium EDTA, 1 mM sodium EGTA, 1 mM DTT, 1 mM sodium orthovanadate, 250 mM sucrose, complete cocktail protein inhibitors and 0.1 mM PMSF). The cell suspension was incubated on ice for 20 min and then disrupted by 10 strokes through a 28.5 G needle. The homogenate was spun at 1,000 x g for 10 min at 4 °C to pellet nuclei. The mitochondrial fraction was harvested by centrifugation at 10,000 x *g* for 30 min at 4 °C. The purity of fractions was assessed by immunoblotting with antibodies specific for either β-tubulin (cytoplasmic fraction) or Hsp60 (mitochondrial fraction).

Detection of MIS protein release from and microscopy of isolated mitochondria: Isolated mitochondria were diluted (0.25 mg/mL) in buffer C (200 mM sucrose, 10 mM

Tris, pH 7.4, 1 mM KH_2PO_4, 10 μM EGTA, 5 mM malate, 5 mM glutamate, 11 mM ADP, 2 mM $MgCl_2$) containing DHE (5 μM). Mitochondria were incubated for 30 minutes (37 °C), and an aliquot was examined by microscopy using a Leica DM-LB microscope. Light from a mercury lamp (100 W) was passed through a FITC/rhodamine prism (Chroma). Images (630X) were captured using a SPOT RS slider digital camera (Diagnostic Instruments Inc.) interfaced to a Macintosh PC. After 2 h, mitochondria were isolated by centrifugation by centrifugation at 10,000 x *g* for 15 min at 4 °C. Supernatants were collected and mitochondria lysed using WCE buffer (30 μL).

Sub-cellular fractionation: Cells (7×10^6) were harvested and washed once with ice cold PBS. Cells were suspended in 100 μL *c*ell *l*ysis *a*nd *m*itochondrial *i*solation (CLAMI) buffer (150 mM KCl and 150 μg/mL digitonin in PBS) and incubated on ice for 5 min. Permeabilized cells (mitochondrial fraction) were separated from supernatants (cytosolic fraction) by centrifugation at 1,000 x g for 7 min at at 4 °C. Supernatants were decanted and lysates prepared from the cell pellets (mitochondrial fraction) by resuspending in WCE lysis buffer (60 μL).

Aconitase activity assay: Aconitase activity was determined spectrometrically in mitochondria-enriched fractions by monitoring the formation of NADPH at 340 nm in assay buffer containing 50 mM Tris-HCl, 60 mM sodium citrate, 1 mM $MnCl_2$, 0.2 mM $NADP^+$ and 4 units of $NADP^+$ isocitrate dehydrogenase, pH 7.5 [584]. Mitochondria-enriched fractions were prepared by sub-cellular fractionation of cells (40×10^6) and mitochondrial extract (100 μg) was diluted to 150 μL in 50 mM pH 7.5 Tris-HCl and loaded into one well of a 96-well plate. Reactions were initiated by the addition of assay buffer (150 μL) and the absorbance change at 340 nm was measure for 30 min at 37 °C

using a Molecular Devices Versamax tunable microplate reader. The competitive aconitase inhibitor fluorocitrate was used to validate the specificity of this assay [354]. Aconitase activity was evaluated over a timeframe in which the increase in absorbance at 340 nm was linear and an extinction coefficient of 6.22 $mM^{-1}cm^{-1}$ was used for NADH to calculate nmol citrate isomerized/min.

Immunoblot analysis: Cell lysates were denatured by boiling with one-fifth volume of 5x SDS sample buffer (250 mM Tris Cl pH 6.8, glycerol (40% v/v), SDS (8% w/v), 2-mercaptoethanol (8% v/v), Bromophenol Blue (0.2% w/v)). Proteins were subjected to electrophoresis by SDS-PAGE and transferred on to a PVDF membrane (Bio-Rad), and incubated with primary antibodies from the proteins of interest in phosphate buffered saline containing 5% nonfat dry milk, 0.1% Tween 20. The antibodies for AIF (catalog # sc-13116) and Bik (catalog # sc30552) were purchased from Santa Cruz Biotechnologies. Antibodies for Lck (catalog #2752), phospho-Lck (Tyr505; catalog #2751), Akt (catalog #4691), phospho-Akt (Thr308; catalog #2965), phospho-Akt (Ser473; catalog #4060) and GSK-3β (catalog #9332), phospho-GSK-3β (Ser9; catalog #9336), PARP (catalog #9542), and Bid (catalog #2006) were purchased from Cell Signaling Technology. Antibodies for Myc (catalog #551101), β-Catenin (catalog #610514), cyclin D3 (catalog #554195), Bim (catalog #559685), Bad (catalog #610392), Bcl-x_L (catalog #556361), Hsp60 (catalog #610392) and cytochrome *c* (catalog #556433) were purchased from Becton Dickenson. The antibody to Mcl-1 (catalog #600-401-394) was purchased from Rockland Immunochemicals. The antibody to the β-subunit of the F_oF_1-ATPase (catalog #A21351) was purchased from Invitrogen. The antibodies to GAPDH (catalog #MAB374), Bax (catalog #06-499) and Bak (catalog

#06-536) were purchased from Millipore. The antibody to Smac (catalog #ALX-210-788-C100) was purchased from Alexis Biochemicals. The antibody to Bcl-2 (catalog #M0887) was purchased from DakoCytomanin. The antibody to Bmf (catalog #ab9655) was purchased from Abcam. The antibody to Puma (catalog #PC686) was purchased from Calbiochem. The antibody to Noxa (catalog #IMG-349A) was purchased from Imgenex. Membranes were then incubated with horseradish peroxidase conjugated secondary antibodies and immune complexes visualized with Enhanced Chemiluminescence Reagent (GE Healthcare).

Statistical analysis: P-values were calculated using a two tailed Student T-test. Data are presented as mean ± standard deviation.

BIBLIOGRAPHY

1. Riedl, S.J., and Salvesen, G.S. (2007). The apoptosome: signalling platform of cell death. Nat Rev Mol Cell Biol *8*, 405-413.

2. Falschlehner, C., Emmerich, C.H., Gerlach, B., and Walczak, H. (2007). TRAIL signalling: decisions between life and death. Int J Biochem Cell Biol *39*, 1462-1475.

3. Ashkenazi, A., and Herbst, R.S. (2008). To kill a tumor cell: the potential of proapoptotic receptor agonists. J Clin Invest *118*, 1979-1990.

4. Garrido, C., Galluzzi, L., Brunet, M., Puig, P.E., Didelot, C., and Kroemer, G. (2006). Mechanisms of cytochrome c release from mitochondria. Cell Death Differ *13*, 1423-1433.

5. Ow, Y.L., Green, D.R., Hao, Z., and Mak, T.W. (2008). Cytochrome c: functions beyond respiration. Nat Rev Mol Cell Biol *9*, 532-542.

6. Bratton, S.B., Walker, G., Srinivasula, S.M., Sun, X.M., Butterworth, M., Alnemri, E.S., and Cohen, G.M. (2001). Recruitment, activation and retention of caspases-9 and -3 by Apaf-1 apoptosome and associated XIAP complexes. Embo J *20*, 998-1009.

7. Vaux, D.L., and Silke, J. (2003). Mammalian mitochondrial IAP binding proteins. Biochem Biophys Res Commun *304*, 499-504.

8. Susin, S.A., Lorenzo, H.K., Zamzami, N., Marzo, I., Snow, B.E., Brothers, G.M., Mangion, J., Jacotot, E., Costantini, P., Loeffler, M., Larochette, N., Goodlett, D.R., Aebersold, R., Siderovski, D.P., Penninger, J.M., and Kroemer, G. (1999). Molecular characterization of mitochondrial apoptosis-inducing factor. Nature *397*, 441-446.

9. Li, L.Y., Luo, X., and Wang, X. (2001). Endonuclease G is an apoptotic DNase when released from mitochondria. Nature *412*, 95-99.

10. Widlak, P., Li, L.Y., Wang, X., and Garrard, W.T. (2001). Action of recombinant human apoptotic endonuclease G on naked DNA and chromatin substrates: cooperation with exonuclease and DNase I. J Biol Chem *276*, 48404-48409.

11. Arnoult, D., Gaume, B., Karbowski, M., Sharpe, J.C., Cecconi, F., and Youle, R.J. (2003). Mitochondrial release of AIF and EndoG requires caspase activation downstream of Bax/Bak-mediated permeabilization. Embo J *22*, 4385-4399.

12. Munoz-Pinedo, C., Guio-Carrion, A., Goldstein, J.C., Fitzgerald, P., Newmeyer, D.D., and Green, D.R. (2006). Different mitochondrial intermembrane space proteins are released during apoptosis in a manner that is coordinately initiated but can vary in duration. Proc Natl Acad Sci U S A *103*, 11573-11578.

13. Green, D.R., and Kroemer, G. (2004). The pathophysiology of mitochondrial cell death. Science *305*, 626-629.

14. He, L., and Lemasters, J.J. (2002). Regulated and unregulated mitochondrial permeability transition pores: a new paradigm of pore structure and function? FEBS Lett *512*, 1-7.

15. Gunter, T.E., Yule, D.I., Gunter, K.K., Eliseev, R.A., and Salter, J.D. (2004). Calcium and mitochondria. FEBS Lett *567*, 96-102.

16. Gilabert, J.A., Bakowski, D., and Parekh, A.B. (2001). Energized mitochondria increase the dynamic range over which inositol 1,4,5-trisphosphate activates store-operated calcium influx. Embo J *20*, 2672-2679.

17. Quintana, A., Schwarz, E.C., Schwindling, C., Lipp, P., Kaestner, L., and Hoth, M. (2006). Sustained activity of calcium release-activated calcium channels requires translocation of mitochondria to the plasma membrane. J Biol Chem *281*, 40302-40309.

18. Parekh, A.B. (2003). Store-operated Ca2+ entry: dynamic interplay between endoplasmic reticulum, mitochondria and plasma membrane. J Physiol *547*, 333-348.

19. Ichas, F., and Mazat, J.P. (1998). From calcium signaling to cell death: two conformations for the mitochondrial permeability transition pore. Switching from low- to high-conductance state. Biochim Biophys Acta *1366*, 33-50.

20. Leung, A.W., and Halestrap, A.P. (2008). Recent progress in elucidating the molecular mechanism of the mitochondrial permeability transition pore. Biochim Biophys Acta *1777*, 946-952.

21. Clarke, S.J., McStay, G.P., and Halestrap, A.P. (2002). Sanglifehrin A acts as a potent inhibitor of the mitochondrial permeability transition and reperfusion injury of the heart by binding to cyclophilin-D at a different site from cyclosporin A. J Biol Chem *277*, 34793-34799.

22. Griffiths, E.J., and Halestrap, A.P. (1991). Further evidence that cyclosporin A protects mitochondria from calcium overload by inhibiting a matrix peptidyl-

prolyl cis-trans isomerase. Implications for the immunosuppressive and toxic effects of cyclosporin. Biochem J *274 (Pt 2)*, 611-614.

23. Woodfield, K., Ruck, A., Brdiczka, D., and Halestrap, A.P. (1998). Direct demonstration of a specific interaction between cyclophilin-D and the adenine nucleotide translocase confirms their role in the mitochondrial permeability transition. Biochem J *336 (Pt 2)*, 287-290.

24. Baines, C.P., Kaiser, R.A., Purcell, N.H., Blair, N.S., Osinska, H., Hambleton, M.A., Brunskill, E.W., Sayen, M.R., Gottlieb, R.A., Dorn, G.W., Robbins, J., and Molkentin, J.D. (2005). Loss of cyclophilin D reveals a critical role for mitochondrial permeability transition in cell death. Nature *434*, 658-662.

25. Basso, E., Fante, L., Fowlkes, J., Petronilli, V., Forte, M.A., and Bernardi, P. (2005). Properties of the permeability transition pore in mitochondria devoid of Cyclophilin D. J Biol Chem *280*, 18558-18561.

26. Petronilli, V., Costantini, P., Scorrano, L., Colonna, R., Passamonti, S., and Bernardi, P. (1994). The voltage sensor of the mitochondrial permeability transition pore is tuned by the oxidation-reduction state of vicinal thiols. Increase of the gating potential by oxidants and its reversal by reducing agents. J Biol Chem *269*, 16638-16642.

27. Giorgio, M., Migliaccio, E., Orsini, F., Paolucci, D., Moroni, M., Contursi, C., Pelliccia, G., Luzi, L., Minucci, S., Marcaccio, M., Pinton, P., Rizzuto, R., Bernardi, P., Paolucci, F., and Pelicci, P.G. (2005). Electron transfer between cytochrome c and p66Shc generates reactive oxygen species that trigger mitochondrial apoptosis. Cell *122*, 221-233.

28. Halliwell, B., and Gutteridge, J.M. (1990). Role of free radicals and catalytic metal ions in human disease: an overview. Methods Enzymol *186*, 1-85.

29. Waldmeier, P.C., Feldtrauer, J.J., Qian, T., and Lemasters, J.J. (2002). Inhibition of the mitochondrial permeability transition by the nonimmunosuppressive cyclosporin derivative NIM811. Mol Pharmacol *62*, 22-29.

30. Muller, F.L., Liu, Y., and Van Remmen, H. (2004). Complex III releases superoxide to both sides of the inner mitochondrial membrane. J Biol Chem *279*, 49064-49073.

31. St-Pierre, J., Buckingham, J.A., Roebuck, S.J., and Brand, M.D. (2002). Topology of superoxide production from different sites in the mitochondrial electron transport chain. J Biol Chem *277*, 44784-44790.

32. Isenberg, J.S., and Klaunig, J.E. (2000). Role of the mitochondrial membrane permeability transition (MPT) in rotenone-induced apoptosis in liver cells. Toxicol Sci *53*, 340-351.

33. Henderson, P.J., and Lardy, H.A. (1970). Bongkrekic acid. An inhibitor of the adenine nucleotide translocase of mitochondria. J Biol Chem *245*, 1319-1326.

34. Honda, H.M., Korge, P., and Weiss, J.N. (2005). Mitochondria and ischemia/reperfusion injury. Ann N Y Acad Sci *1047*, 248-258.

35. McStay, G.P., Clarke, S.J., and Halestrap, A.P. (2002). Role of critical thiol groups on the matrix surface of the adenine nucleotide translocase in the mechanism of the mitochondrial permeability transition pore. Biochem J *367*, 541-548.

36. Pebay-Peyroula, E., Dahout-Gonzalez, C., Kahn, R., Trezeguet, V., Lauquin, G.J., and Brandolin, G. (2003). Structure of mitochondrial ADP/ATP carrier in complex with carboxyatractyloside. Nature *426*, 39-44.

37. Costantini, P., Belzacq, A.S., Vieira, H.L., Larochette, N., de Pablo, M.A., Zamzami, N., Susin, S.A., Brenner, C., and Kroemer, G. (2000). Oxidation of a critical thiol residue of the adenine nucleotide translocator enforces Bcl-2-independent permeability transition pore opening and apoptosis. Oncogene *19*, 307-314.

38. Youle, R.J., and Strasser, A. (2008). The BCL-2 protein family: opposing activities that mediate cell death. Nat Rev Mol Cell Biol *9*, 47-59.

39. Tsujimoto, Y., Cossman, J., Jaffe, E., and Croce, C.M. (1985). Involvement of the bcl-2 gene in human follicular lymphoma. Science *228*, 1440-1443.

40. Bakhshi, A., Jensen, J.P., Goldman, P., Wright, J.J., McBride, O.W., Epstein, A.L., and Korsmeyer, S.J. (1985). Cloning the chromosomal breakpoint of t(14;18) human lymphomas: clustering around JH on chromosome 14 and near a transcriptional unit on 18. Cell *41*, 899-906.

41. Cleary, M.L., Smith, S.D., and Sklar, J. (1986). Cloning and structural analysis of cDNAs for bcl-2 and a hybrid bcl-2/immunoglobulin transcript resulting from the t(14;18) translocation. Cell *47*, 19-28.

42. Boxer, L.M., and Dang, C.V. (2001). Translocations involving c-myc and c-myc function. Oncogene *20*, 5595-5610.

43. Vaux, D.L., Cory, S., and Adams, J.M. (1988). Bcl-2 gene promotes haemopoietic cell survival and cooperates with c-myc to immortalize pre-B cells. Nature *335*, 440-442.

44. Nunez, G., London, L., Hockenbery, D., Alexander, M., McKearn, J.P., and Korsmeyer, S.J. (1990). Deregulated Bcl-2 gene expression selectively prolongs survival of growth factor-deprived hemopoietic cell lines. J Immunol *144*, 3602-3610.

45. Hockenbery, D., Nunez, G., Milliman, C., Schreiber, R.D., and Korsmeyer, S.J. (1990). Bcl-2 is an inner mitochondrial membrane protein that blocks programmed cell death. Nature *348*, 334-336.

46. Korsmeyer, S.J., McDonnell, T.J., Nunez, G., Hockenbery, D., and Young, R. (1990). Bcl-2: B cell life, death and neoplasia. Curr Top Microbiol Immunol *166*, 203-207.

47. Newmeyer, D.D., Farschon, D.M., and Reed, J.C. (1994). Cell-free apoptosis in Xenopus egg extracts: inhibition by Bcl-2 and requirement for an organelle fraction enriched in mitochondria. Cell *79*, 353-364.

48. Reed, J.C. (2006). Proapoptotic multidomain Bcl-2/Bax-family proteins: mechanisms, physiological roles, and therapeutic opportunities. Cell Death Differ *13*, 1378-1386.

49. Hetz, C., and Glimcher, L. (2008). The daily job of night killers: alternative roles of the BCL-2 family in organelle physiology. Trends Cell Biol *18*, 38-44.

50. Chen, R., Valencia, I., Zhong, F., McColl, K.S., Roderick, H.L., Bootman, M.D., Berridge, M.J., Conway, S.J., Holmes, A.B., Mignery, G.A., Velez, P., and Distelhorst, C.W. (2004). Bcl-2 functionally interacts with inositol 1,4,5-trisphosphate receptors to regulate calcium release from the ER in response to inositol 1,4,5-trisphosphate. J Cell Biol *166*, 193-203.

51. White, C., Li, C., Yang, J., Petrenko, N.B., Madesh, M., Thompson, C.B., and Foskett, J.K. (2005). The endoplasmic reticulum gateway to apoptosis by Bcl-X(L) modulation of the InsP3R. Nat Cell Biol *7*, 1021-1028.

52. Bassik, M.C., Scorrano, L., Oakes, S.A., Pozzan, T., and Korsmeyer, S.J. (2004). Phosphorylation of BCL-2 regulates ER Ca2+ homeostasis and apoptosis. Embo J *23*, 1207-1216.

53. Cheng, E.H., Sheiko, T.V., Fisher, J.K., Craigen, W.J., and Korsmeyer, S.J. (2003). VDAC2 inhibits BAK activation and mitochondrial apoptosis. Science *301*, 513-517.

54. Willis, S.N., Chen, L., Dewson, G., Wei, A., Naik, E., Fletcher, J.I., Adams, J.M., and Huang, D.C. (2005). Proapoptotic Bak is sequestered by Mcl-1 and Bcl-xL, but not Bcl-2, until displaced by BH3-only proteins. Genes Dev *19*, 1294-1305.

55. Hsu, Y.T., and Youle, R.J. (1998). Bax in murine thymus is a soluble monomeric protein that displays differential detergent-induced conformations. J Biol Chem *273*, 10777-10783.

56. Goping, I.S., Gross, A., Lavoie, J.N., Nguyen, M., Jemmerson, R., Roth, K., Korsmeyer, S.J., and Shore, G.C. (1998). Regulated targeting of BAX to mitochondria. J Cell Biol *143*, 207-215.

57. Hsu, S.Y., Kaipia, A., McGee, E., Lomeli, M., and Hsueh, A.J. (1997). Bok is a pro-apoptotic Bcl-2 protein with restricted expression in reproductive tissues and heterodimerizes with selective anti-apoptotic Bcl-2 family members. Proc Natl Acad Sci U S A *94*, 12401-12406.

58. Strasser, A. (2005). The role of BH3-only proteins in the immune system. Nat Rev Immunol *5*, 189-200.

59. Labi, V., Erlacher, M., Kiessling, S., and Villunger, A. (2006). BH3-only proteins in cell death initiation, malignant disease and anticancer therapy. Cell Death Differ *13*, 1325-1338.

60. Griffiths, G.J., Dubrez, L., Morgan, C.P., Jones, N.A., Whitehouse, J., Corfe, B.M., Dive, C., and Hickman, J.A. (1999). Cell damage-induced conformational changes of the pro-apoptotic protein Bak in vivo precede the onset of apoptosis. J Cell Biol *144*, 903-914.

61. Kim, B.J., Ryu, S.W., and Song, B.J. (2006). JNK- and p38 kinase-mediated phosphorylation of Bax leads to its activation and mitochondrial translocation and to apoptosis of human hepatoma HepG2 cells. J Biol Chem *281*, 21256-21265.

62. Rathmell, J.C., Fox, C.J., Plas, D.R., Hammerman, P.S., Cinalli, R.M., and Thompson, C.B. (2003). Akt-directed glucose metabolism can prevent Bax conformation change and promote growth factor-independent survival. Mol Cell Biol *23*, 7315-7328.

63. Parikh, N., Sade, H., Kurian, L., and Sarin, A. (2004). The Bax N terminus is required for negative regulation by the mitogen-activated protein kinase kinase and Akt signaling pathways in T cells. J Immunol *173*, 6220-6227.

64. Gardai, S.J., Hildeman, D.A., Frankel, S.K., Whitlock, B.B., Frasch, S.C., Borregaard, N., Marrack, P., Bratton, D.L., and Henson, P.M. (2004). Phosphorylation of Bax Ser184 by Akt regulates its activity and apoptosis in neutrophils. J Biol Chem *279*, 21085-21095.

65. Lazebnik, Y. (2001). Why do regulators of apoptosis look like bacterial toxins? Curr Biol *11*, R767-768.

66. Epand, R.F., Martinou, J.C., Montessuit, S., Epand, R.M., and Yip, C.M. (2002). Direct evidence for membrane pore formation by the apoptotic protein Bax. Biochem Biophys Res Commun *298*, 744-749.

67. Saito, M., Korsmeyer, S.J., and Schlesinger, P.H. (2000). BAX-dependent transport of cytochrome c reconstituted in pure liposomes. Nat Cell Biol *2*, 553-555.

68. Chen, H., and Chan, D.C. (2005). Emerging functions of mammalian mitochondrial fusion and fission. Hum Mol Genet *14 Spec No. 2*, R283-289.

69. Perfettini, J.L., Roumier, T., and Kroemer, G. (2005). Mitochondrial fusion and fission in the control of apoptosis. Trends Cell Biol *15*, 179-183.

70. Frank, S., Gaume, B., Bergmann-Leitner, E.S., Leitner, W.W., Robert, E.G., Catez, F., Smith, C.L., and Youle, R.J. (2001). The role of dynamin-related protein 1, a mediator of mitochondrial fission, in apoptosis. Dev Cell *1*, 515-525.

71. Karbowski, M., Lee, Y.J., Gaume, B., Jeong, S.Y., Frank, S., Nechushtan, A., Santel, A., Fuller, M., Smith, C.L., and Youle, R.J. (2002). Spatial and temporal association of Bax with mitochondrial fission sites, Drp1, and Mfn2 during apoptosis. J Cell Biol *159*, 931-938.

72. Muchmore, S.W., Sattler, M., Liang, H., Meadows, R.P., Harlan, J.E., Yoon, H.S., Nettesheim, D., Chang, B.S., Thompson, C.B., Wong, S.L., Ng, S.L., and Fesik, S.W. (1996). X-ray and NMR structure of human Bcl-xL, an inhibitor of programmed cell death. Nature *381*, 335-341.

73. Petros, A.M., Medek, A., Nettesheim, D.G., Kim, D.H., Yoon, H.S., Swift, K., Matayoshi, E.D., Oltersdorf, T., and Fesik, S.W. (2001). Solution structure of the antiapoptotic protein bcl-2. Proc Natl Acad Sci U S A *98*, 3012-3017.

74. Day, C.L., Chen, L., Richardson, S.J., Harrison, P.J., Huang, D.C., and Hinds, M.G. (2005). Solution structure of prosurvival Mcl-1 and characterization of its binding by proapoptotic BH3-only ligands. J Biol Chem *280*, 4738-4744.

75. Suzuki, M., Youle, R.J., and Tjandra, N. (2000). Structure of Bax: coregulation of dimer formation and intracellular localization. Cell *103*, 645-654.

76. Moldoveanu, T., Liu, Q., Tocilj, A., Watson, M., Shore, G., and Gehring, K. (2006). The X-ray structure of a BAK homodimer reveals an inhibitory zinc binding site. Mol Cell *24*, 677-688.

77. McDonnell, J.M., Fushman, D., Milliman, C.L., Korsmeyer, S.J., and Cowburn, D. (1999). Solution structure of the proapoptotic molecule BID: a structural basis for apoptotic agonists and antagonists. Cell *96*, 625-634.

78. Aouacheria, A., Brunet, F., and Gouy, M. (2005). Phylogenomics of life-or-death switches in multicellular animals: Bcl-2, BH3-Only, and BNip families of apoptotic regulators. Mol Biol Evol *22*, 2395-2416.

79. Sattler, M., Liang, H., Nettesheim, D., Meadows, R.P., Harlan, J.E., Eberstadt, M., Yoon, H.S., Shuker, S.B., Chang, B.S., Minn, A.J., Thompson, C.B., and Fesik, S.W. (1997). Structure of Bcl-xL-Bak peptide complex: recognition between regulators of apoptosis. Science *275*, 983-986.

80. Petros, A.M., Nettesheim, D.G., Wang, Y., Olejniczak, E.T., Meadows, R.P., Mack, J., Swift, K., Matayoshi, E.D., Zhang, H., Thompson, C.B., and Fesik,

S.W. (2000). Rationale for Bcl-xL/Bad peptide complex formation from structure, mutagenesis, and biophysical studies. Protein Sci *9*, 2528-2534.

81. Liu, X., Dai, S., Zhu, Y., Marrack, P., and Kappler, J.W. (2003). The structure of a Bcl-xL/Bim fragment complex: implications for Bim function. Immunity *19*, 341-352.

82. Adams, J.M., and Cory, S. (2007). Bcl-2-regulated apoptosis: mechanism and therapeutic potential. Curr Opin Immunol *19*, 488-496.

83. Simmons, M.J., Fan, G., Zong, W.X., Degenhardt, K., White, E., and Gelinas, C. (2008). Bfl-1/A1 functions, similar to Mcl-1, as a selective tBid and Bak antagonist. Oncogene *27*, 1421-1428.

84. Willis, S.N., Fletcher, J.I., Kaufmann, T., van Delft, M.F., Chen, L., Czabotar, P.E., Ierino, H., Lee, E.F., Fairlie, W.D., Bouillet, P., Strasser, A., Kluck, R.M., Adams, J.M., and Huang, D.C. (2007). Apoptosis initiated when BH3 ligands engage multiple Bcl-2 homologs, not Bax or Bak. Science *315*, 856-859.

85. Knudson, C.M., Tung, K.S., Tourtellotte, W.G., Brown, G.A., and Korsmeyer, S.J. (1995). Bax-deficient mice with lymphoid hyperplasia and male germ cell death. Science *270*, 96-99.

86. Lindsten, T., Ross, A.J., King, A., Zong, W.X., Rathmell, J.C., Shiels, H.A., Ulrich, E., Waymire, K.G., Mahar, P., Frauwirth, K., Chen, Y., Wei, M., Eng, V.M., Adelman, D.M., Simon, M.C., Ma, A., Golden, J.A., Evan, G., Korsmeyer, S.J., MacGregor, G.R., and Thompson, C.B. (2000). The combined functions of proapoptotic Bcl-2 family members bak and bax are essential for normal development of multiple tissues. Mol Cell *6*, 1389-1399.

87. Wei, M.C., Zong, W.X., Cheng, E.H., Lindsten, T., Panoutsakopoulou, V., Ross, A.J., Roth, K.A., MacGregor, G.R., Thompson, C.B., and Korsmeyer, S.J. (2001). Proapoptotic BAX and BAK: a requisite gateway to mitochondrial dysfunction and death. Science *292*, 727-730.

88. Hahn, P., Lindsten, T., Tolentino, M., Thompson, C.B., Bennett, J., and Dunaief, J.L. (2005). Persistent fetal ocular vasculature in mice deficient in bax and bak. Arch Ophthalmol *123*, 797-802.

89. Rathmell, J.C., Lindsten, T., Zong, W.X., Cinalli, R.M., and Thompson, C.B. (2002). Deficiency in Bak and Bax perturbs thymic selection and lymphoid homeostasis. Nat Immunol *3*, 932-939.

90. Lindsten, T., and Thompson, C.B. (2006). Cell death in the absence of Bax and Bak. Cell Death Differ *13*, 1272-1276.

91. Kim, H., Rafiuddin-Shah, M., Tu, H.C., Jeffers, J.R., Zambetti, G.P., Hsieh, J.J., and Cheng, E.H. (2006). Hierarchical regulation of mitochondrion-dependent apoptosis by BCL-2 subfamilies. Nat Cell Biol *8*, 1348-1358.

92. Kuwana, T., Bouchier-Hayes, L., Chipuk, J.E., Bonzon, C., Sullivan, B.A., Green, D.R., and Newmeyer, D.D. (2005). BH3 domains of BH3-only proteins differentially regulate Bax-mediated mitochondrial membrane permeabilization both directly and indirectly. Mol Cell *17*, 525-535.

93. Kuwana, T., Mackey, M.R., Perkins, G., Ellisman, M.H., Latterich, M., Schneiter, R., Green, D.R., and Newmeyer, D.D. (2002). Bid, Bax, and lipids cooperate to form supramolecular openings in the outer mitochondrial membrane. Cell *111*, 331-342.

94. Terrones, O., Etxebarria, A., Landajuela, A., Landeta, O., Antonsson, B., and Basanez, G. (2008). BIM and tBID are not mechanistically equivalent when assisting BAX to permeabilize bilayer membranes. J Biol Chem *283*, 7790-7803.

95. Chen, L., Willis, S.N., Wei, A., Smith, B.J., Fletcher, J.I., Hinds, M.G., Colman, P.M., Day, C.L., Adams, J.M., and Huang, D.C. (2005). Differential targeting of prosurvival Bcl-2 proteins by their BH3-only ligands allows complementary apoptotic function. Mol Cell *17*, 393-403.

96. Sandalova, E., Wei, C.H., Masucci, M.G., and Levitsky, V. (2004). Regulation of expression of Bcl-2 protein family member Bim by T cell receptor triggering. Proc Natl Acad Sci U S A *101*, 3011-3016.

97. Willis, S.N., and Adams, J.M. (2005). Life in the balance: how BH3-only proteins induce apoptosis. Curr Opin Cell Biol *17*, 617-625.

98. Chipuk, J.E., and Green, D.R. (2008). How do BCL-2 proteins induce mitochondrial outer membrane permeabilization? Trends Cell Biol *18*, 157-164.

99. Chipuk, J.E., Kuwana, T., Bouchier-Hayes, L., Droin, N.M., Newmeyer, D.D., Schuler, M., and Green, D.R. (2004). Direct activation of Bax by p53 mediates mitochondrial membrane permeabilization and apoptosis. Science *303*, 1010-1014.

100. Lin, B., Kolluri, S.K., Lin, F., Liu, W., Han, Y.H., Cao, X., Dawson, M.I., Reed, J.C., and Zhang, X.K. (2004). Conversion of Bcl-2 from protector to killer by interaction with nuclear orphan receptor Nur77/TR3. Cell *116*, 527-540.

101. Li, H., Zhu, H., Xu, C.J., and Yuan, J. (1998). Cleavage of BID by caspase 8 mediates the mitochondrial damage in the Fas pathway of apoptosis. Cell *94*, 491-501.

102. Luo, X., Budihardjo, I., Zou, H., Slaughter, C., and Wang, X. (1998). Bid, a Bcl2 interacting protein, mediates cytochrome c release from mitochondria in response to activation of cell surface death receptors. Cell *94*, 481-490.

103. Yin, X.M., Wang, K., Gross, A., Zhao, Y., Zinkel, S., Klocke, B., Roth, K.A., and Korsmeyer, S.J. (1999). Bid-deficient mice are resistant to Fas-induced hepatocellular apoptosis. Nature *400*, 886-891.

104. Hsu, S.Y., Lin, P., and Hsueh, A.J. (1998). BOD (Bcl-2-related ovarian death gene) is an ovarian BH3 domain-containing proapoptotic Bcl-2 protein capable of dimerization with diverse antiapoptotic Bcl-2 members. Mol Endocrinol *12*, 1432-1440.

105. Wagner, K.W., Engels, I.H., and Deveraux, Q.L. (2004). Caspase-2 can function upstream of bid cleavage in the TRAIL apoptosis pathway. J Biol Chem *279*, 35047-35052.

106. Baptiste-Okoh, N., Barsotti, A.M., and Prives, C. (2008). A role for caspase 2 and PIDD in the process of p53-mediated apoptosis. Proc Natl Acad Sci U S A *105*, 1937-1942.

107. Sax, J.K., Fei, P., Murphy, M.E., Bernhard, E., Korsmeyer, S.J., and El-Deiry, W.S. (2002). BID regulation by p53 contributes to chemosensitivity. Nat Cell Biol *4*, 842-849.

108. Bolden, J.E., Peart, M.J., and Johnstone, R.W. (2006). Anticancer activities of histone deacetylase inhibitors. Nat Rev Drug Discov *5*, 769-784.

109. Ruefli, A.A., Ausserlechner, M.J., Bernhard, D., Sutton, V.R., Tainton, K.M., Kofler, R., Smyth, M.J., and Johnstone, R.W. (2001). The histone deacetylase inhibitor and chemotherapeutic agent suberoylanilide hydroxamic acid (SAHA) induces a cell-death pathway characterized by cleavage of Bid and production of reactive oxygen species. Proc Natl Acad Sci U S A *98*, 10833-10838.

110. Mandic, A., Viktorsson, K., Strandberg, L., Heiden, T., Hansson, J., Linder, S., and Shoshan, M.C. (2002). Calpain-mediated Bid cleavage and calpain-independent Bak modulation: two separate pathways in cisplatin-induced apoptosis. Mol Cell Biol *22*, 3003-3013.

111. Villunger, A., Michalak, E.M., Coultas, L., Mullauer, F., Bock, G., Ausserlechner, M.J., Adams, J.M., and Strasser, A. (2003). p53- and drug-induced apoptotic responses mediated by BH3-only proteins puma and noxa. Science *302*, 1036-1038.

112. Jeffers, J.R., Parganas, E., Lee, Y., Yang, C., Wang, J., Brennan, J., MacLean, K.H., Han, J., Chittenden, T., Ihle, J.N., McKinnon, P.J., Cleveland, J.L., and Zambetti, G.P. (2003). Puma is an essential mediator of p53-dependent and -independent apoptotic pathways. Cancer Cell *4*, 321-328.

113. Erlacher, M., Michalak, E.M., Kelly, P.N., Labi, V., Niederegger, H., Coultas, L., Adams, J.M., Strasser, A., and Villunger, A. (2005). BH3-only proteins Puma and Bim are rate-limiting for gamma-radiation- and glucocorticoid-induced apoptosis of lymphoid cells in vivo. Blood *106*, 4131-4138.

114. Perez-Galan, P., Roue, G., Villamor, N., Montserrat, E., Campo, E., and Colomer, D. (2006). The proteasome inhibitor bortezomib induces apoptosis in mantle-cell lymphoma through generation of ROS and Noxa activation independent of p53 status. Blood *107*, 257-264.

115. Morales, A.A., Gutman, D., Lee, K.P., and Boise, L.H. (2008). BH3-only proteins Noxa, Bmf, and Bim are necessary for arsenic trioxide-induced cell death in myeloma. Blood *111*, 5152-5162.

116. Fei, Q., McCormack, A.L., Di Monte, D.A., and Ethell, D.W. (2008). Paraquat neurotoxicity is mediated by a Bak-dependent mechanism. J Biol Chem *283*, 3357-3364.

117. Fischer, S.F., Belz, G.T., and Strasser, A. (2008). BH3-only protein Puma contributes to death of antigen-specific T cells during shutdown of an immune response to acute viral infection. Proc Natl Acad Sci U S A *105*, 3035-3040.

118. You, H., Pellegrini, M., Tsuchihara, K., Yamamoto, K., Hacker, G., Erlacher, M., Villunger, A., and Mak, T.W. (2006). FOXO3a-dependent regulation of Puma in response to cytokine/growth factor withdrawal. J Exp Med *203*, 1657-1663.

119. Huang, H., and Tindall, D.J. (2007). Dynamic FoxO transcription factors. J Cell Sci *120*, 2479-2487.

120. Hughes, P., Bouillet, P., and Strasser, A. (2006). Role of Bim and other Bcl-2 family members in autoimmune and degenerative diseases. Curr Dir Autoimmun *9*, 74-94.

121. O'Connor, L., Strasser, A., O'Reilly, L.A., Hausmann, G., Adams, J.M., Cory, S., and Huang, D.C. (1998). Bim: a novel member of the Bcl-2 family that promotes apoptosis. Embo J *17*, 384-395.

122. Puthalakath, H., Huang, D.C., O'Reilly, L.A., King, S.M., and Strasser, A. (1999). The proapoptotic activity of the Bcl-2 family member Bim is regulated by interaction with the dynein motor complex. Mol Cell *3*, 287-296.

123. Zhu, Y., Swanson, B.J., Wang, M., Hildeman, D.A., Schaefer, B.C., Liu, X., Suzuki, H., Mihara, K., Kappler, J., and Marrack, P. (2004). Constitutive association of the proapoptotic protein Bim with Bcl-2-related proteins on mitochondria in T cells. Proc Natl Acad Sci U S A *101*, 7681-7686.

124. Harada, H., Quearry, B., Ruiz-Vela, A., and Korsmeyer, S.J. (2004). Survival factor-induced extracellular signal-regulated kinase phosphorylates BIM,

inhibiting its association with BAX and proapoptotic activity. Proc Natl Acad Sci U S A *101*, 15313-15317.

125. Han, J., Goldstein, L.A., Hou, W., and Rabinowich, H. (2007). Functional linkage between NOXA and Bim in mitochondrial apoptotic events. J Biol Chem *282*, 16223-16231.

126. Huntington, N.D., Puthalakath, H., Gunn, P., Naik, E., Michalak, E.M., Smyth, M.J., Tabarias, H., Degli-Esposti, M.A., Dewson, G., Willis, S.N., Motoyama, N., Huang, D.C., Nutt, S.L., Tarlinton, D.M., and Strasser, A. (2007). Interleukin 15-mediated survival of natural killer cells is determined by interactions among Bim, Noxa and Mcl-1. Nat Immunol *8*, 856-863.

127. Puthalakath, H., O'Reilly, L.A., Gunn, P., Lee, L., Kelly, P.N., Huntington, N.D., Hughes, P.D., Michalak, E.M., McKimm-Breschkin, J., Motoyama, N., Gotoh, T., Akira, S., Bouillet, P., and Strasser, A. (2007). ER stress triggers apoptosis by activating BH3-only protein Bim. Cell *129*, 1337-1349.

128. Dijkers, P.F., Medema, R.H., Lammers, J.W., Koenderman, L., and Coffer, P.J. (2000). Expression of the pro-apoptotic Bcl-2 family member Bim is regulated by the forkhead transcription factor FKHR-L1. Curr Biol *10*, 1201-1204.

129. Hughes, P.D., Belz, G.T., Fortner, K.A., Budd, R.C., Strasser, A., and Bouillet, P. (2008). Apoptosis regulators Fas and Bim cooperate in shutdown of chronic immune responses and prevention of autoimmunity. Immunity *28*, 197-205.

130. Pellegrini, M., Belz, G., Bouillet, P., and Strasser, A. (2003). Shutdown of an acute T cell immune response to viral infection is mediated by the proapoptotic Bcl-2 homology 3-only protein Bim. Proc Natl Acad Sci U S A *100*, 14175-14180.

131. Hildeman, D.A., Mitchell, T., Aronow, B., Wojciechowski, S., Kappler, J., and Marrack, P. (2003). Control of Bcl-2 expression by reactive oxygen species. Proc Natl Acad Sci U S A *100*, 15035-15040.

132. Bouillet, P., Metcalf, D., Huang, D.C., Tarlinton, D.M., Kay, T.W., Kontgen, F., Adams, J.M., and Strasser, A. (1999). Proapoptotic Bcl-2 relative Bim required for certain apoptotic responses, leukocyte homeostasis, and to preclude autoimmunity. Science *286*, 1735-1738.

133. Puthalakath, H., Villunger, A., O'Reilly, L.A., Beaumont, J.G., Coultas, L., Cheney, R.E., Huang, D.C., and Strasser, A. (2001). Bmf: a proapoptotic BH3-only protein regulated by interaction with the myosin V actin motor complex, activated by anoikis. Science *293*, 1829-1832.

134. Day, C.L., Puthalakath, H., Skea, G., Strasser, A., Barsukov, I., Lian, L.Y., Huang, D.C., and Hinds, M.G. (2004). Localization of dynein light chains 1 and 2 and their pro-apoptotic ligands. Biochem J *377*, 597-605.

135. Inoue, S., Riley, J., Gant, T.W., Dyer, M.J., and Cohen, G.M. (2007). Apoptosis induced by histone deacetylase inhibitors in leukemic cells is mediated by Bim and Noxa. Leukemia *21*, 1773-1782.

136. Labi, V., Erlacher, M., Kiessling, S., Manzl, C., Frenzel, A., O'Reilly, L., Strasser, A., and Villunger, A. (2008). Loss of the BH3-only protein Bmf impairs B cell homeostasis and accelerates gamma irradiation-induced thymic lymphoma development. J Exp Med *205*, 641-655.

137. Yang, E., Zha, J., Jockel, J., Boise, L.H., Thompson, C.B., and Korsmeyer, S.J. (1995). Bad, a heterodimeric partner for Bcl-XL and Bcl-2, displaces Bax and promotes cell death. Cell *80*, 285-291.

138. del Peso, L., Gonzalez-Garcia, M., Page, C., Herrera, R., and Nunez, G. (1997). Interleukin-3-induced phosphorylation of BAD through the protein kinase Akt. Science *278*, 687-689.

139. Datta, S.R., Dudek, H., Tao, X., Masters, S., Fu, H., Gotoh, Y., and Greenberg, M.E. (1997). Akt phosphorylation of BAD couples survival signals to the cell-intrinsic death machinery. Cell *91*, 231-241.

140. Datta, S.R., Katsov, A., Hu, L., Petros, A., Fesik, S.W., Yaffe, M.B., and Greenberg, M.E. (2000). 14-3-3 proteins and survival kinases cooperate to inactivate BAD by BH3 domain phosphorylation. Mol Cell *6*, 41-51.

141. Tan, Y., Demeter, M.R., Ruan, H., and Comb, M.J. (2000). BAD Ser-155 phosphorylation regulates BAD/Bcl-XL interaction and cell survival. J Biol Chem *275*, 25865-25869.

142. Shou, Y., Li, L., Prabhakaran, K., Borowitz, J.L., and Isom, G.E. (2004). Calcineurin-mediated Bad translocation regulates cyanide-induced neuronal apoptosis. Biochem J *379*, 805-813.

143. Ranger, A.M., Zha, J., Harada, H., Datta, S.R., Danial, N.N., Gilmore, A.P., Kutok, J.L., Le Beau, M.M., Greenberg, M.E., and Korsmeyer, S.J. (2003). Bad-deficient mice develop diffuse large B cell lymphoma. Proc Natl Acad Sci U S A *100*, 9324-9329.

144. Coultas, L., Bouillet, P., Stanley, E.G., Brodnicki, T.C., Adams, J.M., and Strasser, A. (2004). Proapoptotic BH3-only Bcl-2 family member Bik/Blk/Nbk is expressed in hemopoietic and endothelial cells but is redundant for their programmed death. Mol Cell Biol *24*, 1570-1581.

145. Gillissen, B., Essmann, F., Hemmati, P.G., Richter, A., Richter, A., Oztop, I., Chinnadurai, G., Dorken, B., and Daniel, P.T. (2007). Mcl-1 determines the Bax dependency of Nbk/Bik-induced apoptosis. J Cell Biol *179*, 701-715.

146. Zhu, H., Guo, W., Zhang, L., Wu, S., Teraishi, F., Davis, J.J., Dong, F., and Fang, B. (2005). Proteasome inhibitors-mediated TRAIL resensitization and Bik accumulation. Cancer Biol Ther *4*, 781-786.

147. Nikrad, M., Johnson, T., Puthalalath, H., Coultas, L., Adams, J., and Kraft, A.S. (2005). The proteasome inhibitor bortezomib sensitizes cells to killing by death receptor ligand TRAIL via BH3-only proteins Bik and Bim. Mol Cancer Ther *4*, 443-449.

148. Li, C., Li, R., Grandis, J.R., and Johnson, D.E. (2008). Bortezomib induces apoptosis via Bim and Bik up-regulation and synergizes with cisplatin in the killing of head and neck squamous cell carcinoma cells. Mol Cancer Ther *7*, 1647-1655.

149. Fennell, D.A., Chacko, A., and Mutti, L. (2008). BCL-2 family regulation by the 20S proteasome inhibitor bortezomib. Oncogene *27*, 1189-1197.

150. Imaizumi, K., Tsuda, M., Imai, Y., Wanaka, A., Takagi, T., and Tohyama, M. (1997). Molecular cloning of a novel polypeptide, DP5, induced during programmed neuronal death. J Biol Chem *272*, 18842-18848.

151. Inohara, N., Ding, L., Chen, S., and Nunez, G. (1997). harakiri, a novel regulator of cell death, encodes a protein that activates apoptosis and interacts selectively with survival-promoting proteins Bcl-2 and Bcl-X(L). Embo J *16*, 1686-1694.

152. Coultas, L., Terzano, S., Thomas, T., Voss, A., Reid, K., Stanley, E.G., Scott, C.L., Bouillet, P., Bartlett, P., Ham, J., Adams, J.M., and Strasser, A. (2007). Hrk/DP5 contributes to the apoptosis of select neuronal populations but is dispensable for haematopoietic cell apoptosis. J Cell Sci *120*, 2044-2052.

153. Zinkernagel, R.M., and Hengartner, H. (2001). Regulation of the immune response by antigen. Science *293*, 251-253.

154. Janeway, C.A., Jr., and Medzhitov, R. (2002). Innate immune recognition. Annu Rev Immunol *20*, 197-216.

155. Pasare, C., and Medzhitov, R. (2005). Toll-like receptors: linking innate and adaptive immunity. Adv Exp Med Biol *560*, 11-18.

156. Sharpe, A.H., and Freeman, G.J. (2002). The B7-CD28 superfamily. Nat Rev Immunol *2*, 116-126.

157. Sprent, J., and Tough, D.F. (2001). T cell death and memory. Science *293*, 245-248.

158. Handwerger, B.S., Rus, V., da Silva, L., and Via, C.S. (1994). The role of cytokines in the immunopathogenesis of lupus. Springer Semin Immunopathol *16*, 153-180.

159. Smith, K.A. (1988). Interleukin-2: inception, impact, and implications. Science *240*, 1169-1176.

160. Waldmann, T.A. (2006). The biology of interleukin-2 and interleukin-15: implications for cancer therapy and vaccine design. Nat Rev Immunol *6*, 595-601.

161. Berke, G. (1995). The CTL's kiss of death. Cell *81*, 9-12.

162. Podack, E.R. (1995). Execution and suicide: cytotoxic lymphocytes enforce Draconian laws through separate molecular pathways. Curr Opin Immunol *7*, 11-16.

163. Strasser, A., and Pellegrini, M. (2004). T-lymphocyte death during shutdown of an immune response. Trends Immunol *25*, 610-615.

164. Ledingham, K.W., McKenna, P., and Singhal, R.P. (2003). Applications for nuclear phenomena generated by ultra-intense lasers. Science *300*, 1107-1111.

165. Singh, N.J., and Schwartz, R.H. (2003). The strength of persistent antigenic stimulation modulates adaptive tolerance in peripheral CD4+ T cells. J Exp Med *198*, 1107-1117.

166. Santiago-Raber, M.L., Laporte, C., Reininger, L., and Izui, S. (2004). Genetic basis of murine lupus. Autoimmun Rev *3*, 33-39.

167. Adachi, M., Watanabe-Fukunaga, R., and Nagata, S. (1993). Aberrant transcription caused by the insertion of an early transposable element in an intron of the Fas antigen gene of lpr mice. Proc Natl Acad Sci U S A *90*, 1756-1760.

168. Watanabe-Fukunaga, R., Brannan, C.I., Copeland, N.G., Jenkins, N.A., and Nagata, S. (1992). Lymphoproliferation disorder in mice explained by defects in Fas antigen that mediates apoptosis. Nature *356*, 314-317.

169. Green, D.R., Droin, N., and Pinkoski, M. (2003). Activation-induced cell death in T cells. Immunol Rev *193*, 70-81.

170. Strasser, A., Puthalakath, H., O'Reilly, L.A., and Bouillet, P. (2008). What do we know about the mechanisms of elimination of autoreactive T and B cells and what challenges remain. Immunol Cell Biol *86*, 57-66.

171. Akbar, A.N., Borthwick, N.J., Wickremasinghe, R.G., Panayoitidis, P., Pilling, D., Bofill, M., Krajewski, S., Reed, J.C., and Salmon, M. (1996). Interleukin-2 receptor common gamma-chain signaling cytokines regulate activated T cell apoptosis in response to growth factor withdrawal: selective induction of anti-apoptotic (bcl-2, bcl-xL) but not pro-apoptotic (bax, bcl-xS) gene expression. Eur J Immunol *26*, 294-299.

172. Vella, A.T., Dow, S., Potter, T.A., Kappler, J., and Marrack, P. (1998). Cytokine-induced survival of activated T cells in vitro and in vivo. Proc Natl Acad Sci U S A *95*, 3810-3815.

173. Biswas, S.C., Shi, Y., Sproul, A., and Greene, L.A. (2007). Pro-apoptotic Bim induction in response to nerve growth factor deprivation requires simultaneous activation of three different death signaling pathways. J Biol Chem *282*, 29368-29374.

174. Gomez-Vicente, V., Doonan, F., Donovan, M., and Cotter, T.G. (2006). Induction of BIM(EL) following growth factor withdrawal is a key event in caspase-dependent apoptosis of 661W photoreceptor cells. Eur J Neurosci *24*, 981-990.

175. Hildeman, D.A., Zhu, Y., Mitchell, T.C., Bouillet, P., Strasser, A., Kappler, J., and Marrack, P. (2002). Activated T cell death in vivo mediated by proapoptotic bcl-2 family member bim. Immunity *16*, 759-767.

176. Weant, A.E., Michalek, R.D., Khan, I.U., Holbrook, B.C., Willingham, M.C., and Grayson, J.M. (2008). Apoptosis regulators Bim and Fas function concurrently to control autoimmunity and CD8+ T cell contraction. Immunity *28*, 218-230.

177. Green, D.R. (2008). Fas Bim boom! Immunity *28*, 141-143.

178. Dong, H., and Chen, X. (2006). Immunoregulatory role of B7-H1 in chronicity of inflammatory responses. Cell Mol Immunol *3*, 179-187.

179. Stevenson, P.G., and Efstathiou, S. (2005). Immune mechanisms in murine gammaherpesvirus-68 infection. Viral Immunol *18*, 445-456.

180. Theofilopoulos, A.N., and Dixon, F.J. (1985). Murine models of systemic lupus erythematosus. Adv Immunol *37*, 269-390.

181. Andrews, B.S., Eisenberg, R.A., Theofilopoulos, A.N., Izui, S., Wilson, C.B., McConahey, P.J., Murphy, E.D., Roths, J.B., and Dixon, F.J. (1978). Spontaneous murine lupus-like syndromes. Clinical and immunopathological manifestations in several strains. J Exp Med *148*, 1198-1215.

182. Cohen, P.L., and Eisenberg, R.A. (1991). Lpr and gld: single gene models of systemic autoimmunity and lymphoproliferative disease. Annu Rev Immunol *9*, 243-269.

183. Morse, H.C., 3rd, Davidson, W.F., Yetter, R.A., Murphy, E.D., Roths, J.B., and Coffman, R.L. (1982). Abnormalities induced by the mutant gene Ipr: expansion of a unique lymphocyte subset. J Immunol *129*, 2612-2615.

184. Merino, R., Fossati, L., Iwamoto, M., Takahashi, S., Lemoine, R., Ibnou-Zekri, N., Pugliatti, L., Merino, J., and Izui, S. (1995). Effect of long-term anti-CD4 or

anti-CD8 treatment on the development of lpr CD4- CD8- double negative T cells and of the autoimmune syndrome in MRL-lpr/lpr mice. J Autoimmun *8*, 33-45.

185. Singer, G.G., Carrera, A.C., Marshak-Rothstein, A., Martinez, C., and Abbas, A.K. (1994). Apoptosis, Fas and systemic autoimmunity: the MRL-lpr/lpr model. Curr Opin Immunol *6*, 913-920.

186. Kappler, J.W., Roehm, N., and Marrack, P. (1987). T cell tolerance by clonal elimination in the thymus. Cell *49*, 273-280.

187. Murphy, K.M., Heimberger, A.B., and Loh, D.Y. (1990). Induction by antigen of intrathymic apoptosis of CD4+CD8+TCRlo thymocytes in vivo. Science *250*, 1720-1723.

188. Singer, G.G., and Abbas, A.K. (1994). The fas antigen is involved in peripheral but not thymic deletion of T lymphocytes in T cell receptor transgenic mice. Immunity *1*, 365-371.

189. Sercarz, E., and Raja-Gabaglia, C. (2007). Etiology of autoimmune disease: how T cells escape self-tolerance. Methods Mol Biol *380*, 271-283.

190. Parish, I.A., and Heath, W.R. (2008). Too dangerous to ignore: self-tolerance and the control of ignorant autoreactive T cells. Immunol Cell Biol *86*, 146-152.

191. Baxter, A.G., and Hodgkin, P.D. (2002). Activation rules: the two-signal theories of immune activation. Nat Rev Immunol *2*, 439-446.

192. Serfling, E., Klein-Hessling, S., Palmetshofer, A., Bopp, T., Stassen, M., and Schmitt, E. (2006). NFAT transcription factors in control of peripheral T cell tolerance. Eur J Immunol *36*, 2837-2843.

193. Choi, S., and Schwartz, R.H. (2007). Molecular mechanisms for adaptive tolerance and other T cell anergy models. Semin Immunol *19*, 140-152.

194. Powell, J.D. (2006). The induction and maintenance of T cell anergy. Clin Immunol *120*, 239-246.

195. Gimmi, C.D., Freeman, G.J., Gribben, J.G., Gray, G., and Nadler, L.M. (1993). Human T-cell clonal anergy is induced by antigen presentation in the absence of B7 costimulation. Proc Natl Acad Sci U S A *90*, 6586-6590.

196. Linsley, P.S., Brady, W., Grosmaire, L., Aruffo, A., Damle, N.K., and Ledbetter, J.A. (1991). Binding of the B cell activation antigen B7 to CD28 costimulates T cell proliferation and interleukin 2 mRNA accumulation. J Exp Med *173*, 721-730.

197. Matzinger, P. (2002). The danger model: a renewed sense of self. Science *296*, 301-305.

198. Anderson, C.C., and Chan, W.F. (2004). Mechanisms and models of peripheral CD4 T cell self-tolerance. Front Biosci *9*, 2947-2963.

199. Tada, Y., Nagasawa, K., Ho, A., Morito, F., Koarada, S., Ushiyama, O., Suzuki, N., Ohta, A., and Mak, T.W. (1999). Role of the costimulatory molecule CD28 in the development of lupus in MRL/lpr mice. J Immunol *163*, 3153-3159.

200. Kinoshita, K., Tesch, G., Schwarting, A., Maron, R., Sharpe, A.H., and Kelley, V.R. (2000). Costimulation by B7-1 and B7-2 is required for autoimmune disease in MRL-Faslpr mice. J Immunol *164*, 6046-6056.

201. Merrill, J.T., Erkan, D., and Buyon, J.P. (2004). Challenges in bringing the bench to bedside in drug development for SLE. Nat Rev Drug Discov *3*, 1036-1046.

202. Buhaescu, I., Covic, A., and Deray, G. (2007). Treatment of proliferative lupus nephritis--a critical approach. Semin Arthritis Rheum *36*, 224-237.

203. Moreland, L., Bate, G., and Kirkpatrick, P. (2006). Abatacept. Nat Rev Drug Discov *5*, 185-186.

204. Chikuma, S., and Bluestone, J.A. (2003). CTLA-4 and tolerance: the biochemical point of view. Immunol Res *28*, 241-253.

205. Bluestone, J.A. (1997). Is CTLA-4 a master switch for peripheral T cell tolerance? J Immunol *158*, 1989-1993.

206. Isaacs, J.D. (2007). T cell immunomodulation--the Holy Grail of therapeutic tolerance. Curr Opin Pharmacol *7*, 418-425.

207. Takiguchi, M., Murakami, M., Nakagawa, I., Yamada, A., Chikuma, S., Kawaguchi, Y., Hashimoto, A., and Uede, T. (1999). Blockade of CD28/CTLA4-B7 pathway prevented autoantibody-related diseases but not lung disease in MRL/lpr mice. Lab Invest *79*, 317-326.

208. Takiguchi, M., Murakami, M., Nakagawa, I., Rashid, M.M., Tosa, N., Chikuma, S., Hashimoto, A., and Uede, T. (2000). Involvement of CD28/CTLA4-B7 costimulatory pathway in the development of lymphadenopathy and splenomegaly in MRL/lpr mice. J Vet Med Sci *62*, 29-36.

209. Finck, B.K., Linsley, P.S., and Wofsy, D. (1994). Treatment of murine lupus with CTLA4Ig. Science *265*, 1225-1227.

210. Vratsanos, G.S., Jung, S., Park, Y.M., and Craft, J. (2001). CD4(+) T cells from lupus-prone mice are hyperresponsive to T cell receptor engagement with low and high affinity peptide antigens: a model to explain spontaneous T cell activation in lupus. J Exp Med *193*, 329-337.

211. Lyons, D.S., Lieberman, S.A., Hampl, J., Boniface, J.J., Chien, Y., Berg, L.J., and Davis, M.M. (1996). A TCR binds to antagonist ligands with lower affinities and faster dissociation rates than to agonists. Immunity *5*, 53-61.

212. Alexander, J., Snoke, K., Ruppert, J., Sidney, J., Wall, M., Southwood, S., Oseroff, C., Arrhenius, T., Gaeta, F.C., Colon, S.M., and et al. (1993). Functional consequences of engagement of the T cell receptor by low affinity ligands. J Immunol *150*, 1-7.

213. Zielinski, C.E., Jacob, S.N., Bouzahzah, F., Ehrlich, B.E., and Craft, J. (2005). Naive CD4+ T cells from lupus-prone Fas-intact MRL mice display TCR-mediated hyperproliferation due to intrinsic threshold defects in activation. J Immunol *174*, 5100-5109.

214. Gallo, E.M., Cante-Barrett, K., and Crabtree, G.R. (2006). Lymphocyte calcium signaling from membrane to nucleus. Nat Immunol *7*, 25-32.

215. Bouzahzah, F., Jung, S., and Craft, J. (2003). CD4+ T cells from lupus-prone mice avoid antigen-specific tolerance induction in vivo. J Immunol *170*, 741-748.

216. Parry, R.V., Riley, J.L., and Ward, S.G. (2007). Signalling to suit function: tailoring phosphoinositide 3-kinase during T-cell activation. Trends Immunol *28*, 161-168.

217. Sale, E.M., and Sale, G.J. (2008). Protein kinase B: signalling roles and therapeutic targeting. Cell Mol Life Sci *65*, 113-127.

218. Hawkins, P.T., Anderson, K.E., Davidson, K., and Stephens, L.R. (2006). Signalling through Class I PI3Ks in mammalian cells. Biochem Soc Trans *34*, 647-662.

219. Hanada, M., Feng, J., and Hemmings, B.A. (2004). Structure, regulation and function of PKB/AKT--a major therapeutic target. Biochim Biophys Acta *1697*, 3-16.

220. Rosas, M., Birkenkamp, K.U., Lammers, J.W., Koenderman, L., and Coffer, P.J. (2005). Cytokine mediated suppression of TF-1 apoptosis requires PI3K activation and inhibition of Bim expression. FEBS Lett *579*, 191-198.

221. Cardone, M.H., Roy, N., Stennicke, H.R., Salvesen, G.S., Franke, T.F., Stanbridge, E., Frisch, S., and Reed, J.C. (1998). Regulation of cell death protease caspase-9 by phosphorylation. Science *282*, 1318-1321.

222. Dan, H.C., Sun, M., Kaneko, S., Feldman, R.I., Nicosia, S.V., Wang, H.G., Tsang, B.K., and Cheng, J.Q. (2004). Akt phosphorylation and stabilization of X-linked inhibitor of apoptosis protein (XIAP). J Biol Chem *279*, 5405-5412.

223. Suzuki, H., Matsuda, S., Terauchi, Y., Fujiwara, M., Ohteki, T., Asano, T., Behrens, T.W., Kouro, T., Takatsu, K., Kadowaki, T., and Koyasu, S. (2003). PI3K and Btk differentially regulate B cell antigen receptor-mediated signal transduction. Nat Immunol *4*, 280-286.

224. Rommel, C., Camps, M., and Ji, H. (2007). PI3K delta and PI3K gamma: partners in crime in inflammation in rheumatoid arthritis and beyond? Nat Rev Immunol *7*, 191-201.

225. Vanhaesebroeck, B., Ali, K., Bilancio, A., Geering, B., and Foukas, L.C. (2005). Signalling by PI3K isoforms: insights from gene-targeted mice. Trends Biochem Sci *30*, 194-204.

226. Okkenhaug, K., Bilancio, A., Farjot, G., Priddle, H., Sancho, S., Peskett, E., Pearce, W., Meek, S.E., Salpekar, A., Waterfield, M.D., Smith, A.J., and Vanhaesebroeck, B. (2002). Impaired B and T cell antigen receptor signaling in p110delta PI 3-kinase mutant mice. Science *297*, 1031-1034.

227. Mantovani, A., Bonecchi, R., and Locati, M. (2006). Tuning inflammation and immunity by chemokine sequestration: decoys and more. Nat Rev Immunol *6*, 907-918.

228. Hennessy, B.T., Smith, D.L., Ram, P.T., Lu, Y., and Mills, G.B. (2005). Exploiting the PI3K/AKT pathway for cancer drug discovery. Nat Rev Drug Discov *4*, 988-1004.

229. Hirsch, E., Katanaev, V.L., Garlanda, C., Azzolino, O., Pirola, L., Silengo, L., Sozzani, S., Mantovani, A., Altruda, F., and Wymann, M.P. (2000). Central role for G protein-coupled phosphoinositide 3-kinase gamma in inflammation. Science *287*, 1049-1053.

230. Li, Z., Jiang, H., Xie, W., Zhang, Z., Smrcka, A.V., and Wu, D. (2000). Roles of PLC-beta2 and -beta3 and PI3Kgamma in chemoattractant-mediated signal transduction. Science *287*, 1046-1049.

231. Alcazar, I., Marques, M., Kumar, A., Hirsch, E., Wymann, M., Carrera, A.C., and Barber, D.F. (2007). Phosphoinositide 3-kinase gamma participates in T cell receptor-induced T cell activation. J Exp Med *204*, 2977-2987.

232. Ruckle, T., Schwarz, M.K., and Rommel, C. (2006). PI3Kgamma inhibition: towards an 'aspirin of the 21st century'? Nat Rev Drug Discov *5*, 903-918.

233. Barber, D.F., Bartolome, A., Hernandez, C., Flores, J.M., Redondo, C., Fernandez-Arias, C., Camps, M., Ruckle, T., Schwarz, M.K., Rodriguez, S., Martinez, A.C., Balomenos, D., Rommel, C., and Carrera, A.C. (2005). PI3Kgamma inhibition blocks glomerulonephritis and extends lifespan in a mouse model of systemic lupus. Nat Med *11*, 933-935.

234. Niculescu, F., Nguyen, P., Niculescu, T., Rus, H., Rus, V., and Via, C.S. (2003). Pathogenic T cells in murine lupus exhibit spontaneous signaling activity through phosphatidylinositol 3-kinase and mitogen-activated protein kinase pathways. Arthritis Rheum *48*, 1071-1079.

235. Xie, C., Patel, R., Wu, T., Zhu, J., Henry, T., Bhaskarabhatla, M., Samudrala, R., Tus, K., Gong, Y., Zhou, H., Wakeland, E.K., Zhou, X.J., and Mohan, C. (2007). PI3K/AKT/mTOR hypersignaling in autoimmune lymphoproliferative disease engendered by the epistatic interplay of Sle1b and FASlpr. Int Immunol *19*, 509-522.

236. Blatt, N.B., Bednarski, J.J., Warner, R.E., Leonetti, F., Johnson, K.M., Boitano, A., Yung, R., Richardson, B.C., Johnson, K.J., Ellman, J.A., Opipari, A.W., Jr., and Glick, G.D. (2002). Benzodiazepine-induced superoxide signals B cell apoptosis: mechanistic insight and potential therapeutic utility. J Clin Invest *110*, 1123-1132.

237. Johnson, K.M., Chen, X., Boitano, A., Swenson, L., Opipari, A.W., Jr., and Glick, G.D. (2005). Identification and validation of the mitochondrial F1F0-ATPase as the molecular target of the immunomodulatory benzodiazepine Bz-423. Chem Biol *12*, 485-496.

238. Boyer, P.D. (1997). The ATP synthase--a splendid molecular machine. Annu Rev Biochem *66*, 717-749.

239. Adam-Vizi, V., and Chinopoulos, C. (2006). Bioenergetics and the formation of mitochondrial reactive oxygen species. Trends Pharmacol Sci *27*, 639-645.

240. Capdeville, R., Buchdunger, E., Zimmermann, J., and Matter, A. (2002). Glivec (STI571, imatinib), a rationally developed, targeted anticancer drug. Nat Rev Drug Discov *1*, 493-502.

241. Su, A.I., Cooke, M.P., Ching, K.A., Hakak, Y., Walker, J.R., Wiltshire, T., Orth, A.P., Vega, R.G., Sapinoso, L.M., Moqrich, A., Patapoutian, A., Hampton, G.M., Schultz, P.G., and Hogenesch, J.B. (2002). Large-scale analysis of the human and mouse transcriptomes. Proc Natl Acad Sci U S A *99*, 4465-4470.

242. Bednarski, J.J., Warner, R.E., Rao, T., Leonetti, F., Yung, R., Richardson, B.C., Johnson, K.J., Ellman, J.A., Opipari, A.W., Jr., and Glick, G.D. (2003). Attenuation of autoimmune disease in Fas-deficient mice by treatment with a cytotoxic benzodiazepine. Arthritis Rheum *48*, 757-766.

243. Peng, S.L., Moslehi, J., and Craft, J. (1997). Roles of interferon-gamma and interleukin-4 in murine lupus. J Clin Invest *99*, 1936-1946.

244. Balomenos, D., Rumold, R., and Theofilopoulos, A.N. (1998). Interferon-gamma is required for lupus-like disease and lymphoaccumulation in MRL-lpr mice. J Clin Invest *101*, 364-371.

245. Nicoletti, F., Meroni, P., Di Marco, R., Barcellini, W., Borghi, M.O., Gariglio, M., Mattina, A., Grasso, S., and Landolfo, S. (1992). In vivo treatment with a monoclonal antibody to interferon-gamma neither affects the survival nor the incidence of lupus-nephritis in the MRL/lpr-lpr mouse. Immunopharmacology *24*, 11-16.

246. Horwitz, D.A., and Jacob, C.O. (1994). The cytokine network in the pathogenesis of systemic lupus erythematosus and possible therapeutic implications. Springer Semin Immunopathol *16*, 181-200.

247. Nicoletti, F., Di Marco, R., Zaccone, P., Xiang, M., Magro, G., Grasso, S., Morrone, S., Santoni, A., Shoenfeld, Y., Garotta, G., and Meroni, P. (2000). Dichotomic effects of IFN-gamma on the development of systemic lupus erythematosus-like syndrome in MRL-lpr / lpr mice. Eur J Immunol *30*, 438-447.

248. Tsai, C.Y., Wu, T.H., Huang, S.F., Sun, K.H., Hsieh, S.C., Han, S.H., Yu, H.S., and Yu, C.L. (1995). Abnormal splenic and thymic IL-4 and TNF-alpha expression in MRL-lpr/lpr mice. Scand J Immunol *41*, 157-163.

249. Bobe, P., Bonardelle, D., Benihoud, K., Opolon, P., and Chelbi-Alix, M.K. (2006). Arsenic trioxide: A promising novel therapeutic agent for lymphoproliferative and autoimmune syndromes in MRL/lpr mice. Blood *108*, 3967-3975.

250. Schorlemmer, H.U., Dickneite, G., Kanzy, E.J., and Enssle, K.H. (1995). Modulation of the immunoglobulin dysregulation in GvH- and SLE-like diseases by the murine IL-4 receptor (IL-4-R). Inflamm Res *44 Suppl 2*, S194-196.

251. Adams, S., Leblanc, P., and Datta, S.K. (1991). Junctional region sequences of T-cell receptor beta-chain genes expressed by pathogenic anti-DNA autoantibody-inducing helper T cells from lupus mice: possible selection by cationic autoantigens. Proc Natl Acad Sci U S A *88*, 11271-11275.

252. Rajagopalan, S., Zordan, T., Tsokos, G.C., and Datta, S.K. (1990). Pathogenic anti-DNA autoantibody-inducing T helper cell lines from patients with active lupus nephritis: isolation of CD4-8- T helper cell lines that express the gamma delta T-cell antigen receptor. Proc Natl Acad Sci U S A *87*, 7020-7024.

253. Fox, C.J., Hammerman, P.S., and Thompson, C.B. (2005). Fuel feeds function: energy metabolism and the T-cell response. Nat Rev Immunol *5*, 844-852.

254. Jones, R.G., and Thompson, C.B. (2007). Revving the engine: signal transduction fuels T cell activation. Immunity *27*, 173-178.

255. Frauwirth, K.A., Riley, J.L., Harris, M.H., Parry, R.V., Rathmell, J.C., Plas, D.R., Elstrom, R.L., June, C.H., and Thompson, C.B. (2002). The CD28 signaling pathway regulates glucose metabolism. Immunity *16*, 769-777.

256. Maciver, N.J., Jacobs, S.R., Wieman, H.L., Wofford, J.A., Coloff, J.L., and Rathmell, J.C. (2008). Glucose metabolism in lymphocytes is a regulated process with significant effects on immune cell function and survival. J Leukoc Biol.

257. Tripmacher, R., Gaber, T., Dziurla, R., Haupl, T., Erekul, K., Grutzkau, A., Tschirschmann, M., Scheffold, A., Radbruch, A., Burmester, G.R., and Buttgereit, F. (2008). Human CD4(+) T cells maintain specific functions even under conditions of extremely restricted ATP production. Eur J Immunol *38*, 1631-1642.

258. Jacobs, S.R., Herman, C.E., Maciver, N.J., Wofford, J.A., Wieman, H.L., Hammen, J.J., and Rathmell, J.C. (2008). Glucose uptake is limiting in T cell activation and requires CD28-mediated Akt-dependent and independent pathways. J Immunol *180*, 4476-4486.

259. Jones, R.G., Bui, T., White, C., Madesh, M., Krawczyk, C.M., Lindsten, T., Hawkins, B.J., Kubek, S., Frauwirth, K.A., Wang, Y.L., Conway, S.J., Roderick, H.L., Bootman, M.D., Shen, H., Foskett, J.K., and Thompson, C.B. (2007). The proapoptotic factors Bax and Bak regulate T Cell proliferation through control of endoplasmic reticulum Ca(2+) homeostasis. Immunity *27*, 268-280.

260. Moreau, B., Nelson, C., and Parekh, A.B. (2006). Biphasic regulation of mitochondrial Ca2+ uptake by cytosolic Ca2+ concentration. Curr Biol *16*, 1672-1677.

261. McCormack, J.G., Halestrap, A.P., and Denton, R.M. (1990). Role of calcium ions in regulation of mammalian intramitochondrial metabolism. Physiol Rev *70*, 391-425.

262. Devadas, S., Zaritskaya, L., Rhee, S.G., Oberley, L., and Williams, M.S. (2002). Discrete generation of superoxide and hydrogen peroxide by T cell receptor stimulation: selective regulation of mitogen-activated protein kinase activation and fas ligand expression. J Exp Med *195*, 59-70.

263. Jackson, S.H., Devadas, S., Kwon, J., Pinto, L.A., and Williams, M.S. (2004). T cells express a phagocyte-type NADPH oxidase that is activated after T cell receptor stimulation. Nat Immunol *5*, 818-827.

264. Kaminski, M., Kiessling, M., Suss, D., Krammer, P.H., and Gulow, K. (2007). Novel role for mitochondria: protein kinase Ctheta-dependent oxidative signaling organelles in activation-induced T-cell death. Mol Cell Biol *27*, 3625-3639.

265. Fridovich, I. (1995). Superoxide radical and superoxide dismutases. Annu Rev Biochem *64*, 97-112.

266. Krakauer, T., and Buckley, M. (2008). The potency of anti-oxidants in attenuating superantigen-induced proinflammatory cytokines correlates with inactivation of NF-kappaB. Immunopharmacol Immunotoxicol *30*, 163-179.

267. Day, B.J., Fridovich, I., and Crapo, J.D. (1997). Manganic porphyrins possess catalase activity and protect endothelial cells against hydrogen peroxide-mediated injury. Arch Biochem Biophys *347*, 256-262.

268. Hildeman, D.A., Mitchell, T., Teague, T.K., Henson, P., Day, B.J., Kappler, J., and Marrack, P.C. (1999). Reactive oxygen species regulate activation-induced T cell apoptosis. Immunity *10*, 735-744.

269. Alouf, J.E., and Muller-Alouf, H. (2003). Staphylococcal and streptococcal superantigens: molecular, biological and clinical aspects. Int J Med Microbiol *292*, 429-440.

270. Abraham, R.T., and Weiss, A. (2004). Jurkat T cells and development of the T-cell receptor signalling paradigm. Nat Rev Immunol *4*, 301-308.

271. Uddin, S., Hussain, A., Al-Hussein, K., Platanias, L.C., and Bhatia, K.G. (2004). Inhibition of phosphatidylinositol 3'-kinase induces preferentially killing of PTEN-null T leukemias through AKT pathway. Biochem Biophys Res Commun *320*, 932-938.

272. Tokunaga, E., Oki, E., Egashira, A., Sadanaga, N., Morita, M., Kakeji, Y., and Maehara, Y. (2008). Deregulation of the Akt pathway in human cancer. Curr Cancer Drug Targets *8*, 27-36.

273. Downward, J. (2004). PI 3-kinase, Akt and cell survival. Semin Cell Dev Biol *15*, 177-182.

274. Merlo-Pich, M., Deleonardi, G., Biondi, A., and Lenaz, G. (2004). Methods to detect mitochondrial function. Exp Gerontol *39*, 277-281.

275. Schieke, S.M., Phillips, D., McCoy, J.P., Jr., Aponte, A.M., Shen, R.F., Balaban, R.S., and Finkel, T. (2006). The mammalian target of rapamycin (mTOR) pathway regulates mitochondrial oxygen consumption and oxidative capacity. J Biol Chem *281*, 27643-27652.

276. Brand, K., Leibold, W., Luppa, P., Schoerner, C., and Schulz, A. (1986). Metabolic alterations associated with proliferation of mitogen-activated lymphocytes and of lymphoblastoid cell lines: evaluation of glucose and glutamine metabolism. Immunobiology *173*, 23-34.

277. Salomon, A.R., Voehringer, D.W., Herzenberg, L.A., and Khosla, C. (2000). Understanding and exploiting the mechanistic basis for selectivity of polyketide inhibitors of F(0)F(1)-ATPase. Proc Natl Acad Sci U S A *97*, 14766-14771.

278. Bowman, B.J., and Bowman, E.J. (2002). Mutations in subunit C of the vacuolar ATPase confer resistance to bafilomycin and identify a conserved antibiotic binding site. J Biol Chem *277*, 3965-3972.

279. Forgac, M. (2007). Vacuolar ATPases: rotary proton pumps in physiology and pathophysiology. Nat Rev Mol Cell Biol *8*, 917-929.

280. De Milito, A., Iessi, E., Logozzi, M., Lozupone, F., Spada, M., Marino, M.L., Federici, C., Perdicchio, M., Matarrese, P., Lugini, L., Nilsson, A., and Fais, S. (2007). Proton pump inhibitors induce apoptosis of human B-cell tumors through a caspase-independent mechanism involving reactive oxygen species. Cancer Res *67*, 5408-5417.

281. Hong, J., Yokomakura, A., Nakano, Y., Ishihara, K., Kaneda, M., Onodera, M., Nakahama, K., Morita, I., Niikura, K., Ahn, J.W., Zee, O., and Ohuchi, K. (2006). Inhibition of vacuolar-type (H+)-ATPase by the cytostatic macrolide apicularen A and its role in apicularen A-induced apoptosis in RAW 264.7 cells. FEBS Lett *580*, 2723-2730.

282. Morimura, T., Fujita, K., Akita, M., Nagashima, M., and Satomi, A. (2008). The proton pump inhibitor inhibits cell growth and induces apoptosis in human hepatoblastoma. Pediatr Surg Int *24*, 1087-1094.

283. Johnson, K.M.C., J.; Fierke, C.A.; Opipari A.W.; Glick, G.D. (2006). Mechanistic Basis for Therapeutic Targeting of the Mitochondrial F1Fo-ATPase. ACS Chemical Biology *1*, 304-308.

284. Nakada, H.I., and Wick, A.N. (1956). The effect of 2-deoxyglucose on the metabolism of glucose, fructose, and galactose by rat diaphragm. J Biol Chem *222*, 671-676.

285. Du, L., Smolewski, P., Bedner, E., Traganos, F., and Darzynkiewicz, Z. (2001). Selective protection of mitogenically stimulated human lymphocytes but not leukemic cells from cytosine arabinoside-induced apoptosis by LY294002, a phosphoinositol-3 kinase inhibitor. Int J Oncol *19*, 811-819.

286. Gao, N., Rahmani, M., Dent, P., and Grant, S. (2005). 2-Methoxyestradiol-induced apoptosis in human leukemia cells proceeds through a reactive oxygen species and Akt-dependent process. Oncogene *24*, 3797-3809.

287. Rahmani, M., Yu, C., Reese, E., Ahmed, W., Hirsch, K., Dent, P., and Grant, S. (2003). Inhibition of PI-3 kinase sensitizes human leukemic cells to histone deacetylase inhibitor-mediated apoptosis through p44/42 MAP kinase inactivation and abrogation of p21(CIP1/WAF1) induction rather than AKT inhibition. Oncogene *22*, 6231-6242.

288. Khan, I.H., Mendoza, S., Rhyne, P., Ziman, M., Tuscano, J., Eisinger, D., Kung, H.J., and Luciw, P.A. (2006). Multiplex analysis of intracellular signaling pathways in lymphoid cells by microbead suspension arrays. Mol Cell Proteomics *5*, 758-768.

289. Sundberg, T.B., Ney, G.M., Subramanian, C., Opipari, A.W., Jr., and Glick, G.D. (2006). The immunomodulatory benzodiazepine Bz-423 inhibits B-cell proliferation by targeting c-myc protein for rapid and specific degradation. Cancer Res *66*, 1775-1782.

290. Boitano, A., Ellman, J.A., Glick, G.D., and Opipari, A.W., Jr. (2003). The proapoptotic benzodiazepine Bz-423 affects the growth and survival of malignant B cells. Cancer Res *63*, 6870-6876.

291. Boitano, A., Emal, C.D., Leonetti, F., Blatt, N.B., Dineen, T.A., Ellman, J.A., Roush, W.R., Opipari, A.W., and Glick, G.D. (2003). Structure activity studies of a novel cytotoxic benzodiazepine. Bioorg Med Chem Lett *13*, 3327-3330.

292. Bednarski, J.J., Lyssiotis, C.A., Roush, R., Boitano, A.E., Glick, G.D., and Opipari, A.W., Jr. (2004). A novel benzodiazepine increases the sensitivity of B cells to receptor stimulation with synergistic effects on calcium signaling and apoptosis. J Biol Chem *279*, 29615-29621.

293. Korshunov, S.S., Skulachev, V.P., and Starkov, A.A. (1997). High protonic potential actuates a mechanism of production of reactive oxygen species in mitochondria. FEBS Lett *416*, 15-18.

294. Perl, A., Gergely, P., Jr., Nagy, G., Koncz, A., and Banki, K. (2004). Mitochondrial hyperpolarization: a checkpoint of T-cell life, death and autoimmunity. Trends Immunol *25*, 360-367.

295. Fink, B.D., Reszka, K.J., Herlein, J.A., Mathahs, M.M., and Sivitz, W.I. (2005). Respiratory uncoupling by UCP1 and UCP2 and superoxide generation in endothelial cell mitochondria. Am J Physiol Endocrinol Metab *288*, E71-79.

296. Cleary, J., Johnson, K.M., Opipari, A.W., Jr., and Glick, G.D. (2007). Inhibition of the mitochondrial F1F0-ATPase by ligands of the peripheral benzodiazepine receptor. Bioorg Med Chem Lett *17*, 1667-1670.

297. Fink, B., Laude, K., McCann, L., Doughan, A., Harrison, D.G., and Dikalov, S. (2004). Detection of intracellular superoxide formation in endothelial cells and intact tissues using dihydroethidium and an HPLC-based assay. Am J Physiol Cell Physiol *287*, C895-902.

298. Manfredi, G., Spinazzola, A., Checcarelli, N., and Naini, A. (2001). Assay of mitochondrial ATP synthesis in animal cells. Methods Cell Biol *65*, 133-145.

299. Zhao, H., Joseph, J., Fales, H.M., Sokoloski, E.A., Levine, R.L., Vasquez-Vivar, J., and Kalyanaraman, B. (2005). Detection and characterization of the product of hydroethidine and intracellular superoxide by HPLC and limitations of fluorescence. Proc Natl Acad Sci U S A *102*, 5727-5732.

300. Brand, M.D., Affourtit, C., Esteves, T.C., Green, K., Lambert, A.J., Miwa, S., Pakay, J.L., and Parker, N. (2004). Mitochondrial superoxide: production, biological effects, and activation of uncoupling proteins. Free Radic Biol Med *37*, 755-767.

301. Gong, Y., Sohn, H., Xue, L., Firestone, G.L., and Bjeldanes, L.F. (2006). 3,3'-Diindolylmethane is a novel mitochondrial H(+)-ATP synthase inhibitor that can induce p21(Cip1/Waf1) expression by induction of oxidative stress in human breast cancer cells. Cancer Res *66*, 4880-4887.

302. Nachshon-Kedmi, M., Yannai, S., and Fares, F.A. (2004). Induction of apoptosis in human prostate cancer cell line, PC3, by 3,3'-diindolylmethane through the mitochondrial pathway. Br J Cancer *91*, 1358-1363.

303. Colbeau, A., Nachbaur, J., and Vignais, P.M. (1971). Enzymic characterization and lipid composition of rat liver subcellular membranes. Biochim Biophys Acta *249*, 462-492.

304. Scallen, T.J., and Dietert, S.E. (1969). The quantitative retention of cholesterol in mouse liver prepared for electron microscopy by fixation in a digitonin-containing aldehyde solution. J Cell Biol *40*, 802-813.

305. Rasola, A., and Geuna, M. (2001). A flow cytometry assay simultaneously detects independent apoptotic parameters. Cytometry *45*, 151-157.

306. Jiang, X., and Wang, X. (2000). Cytochrome c promotes caspase-9 activation by inducing nucleotide binding to Apaf-1. J Biol Chem *275*, 31199-31203.

307. Genini, D., Budihardjo, I., Plunkett, W., Wang, X., Carrera, C.J., Cottam, H.B., Carson, D.A., and Leoni, L.M. (2000). Nucleotide requirements for the in vitro activation of the apoptosis protein-activating factor-1-mediated caspase pathway. J Biol Chem *275*, 29-34.

308. Genestra, M. (2007). Oxyl radicals, redox-sensitive signalling cascades and antioxidants. Cell Signal *19*, 1807-1819.

309. Matsuzawa, A., and Ichijo, H. (2005). Stress-responsive protein kinases in redox-regulated apoptosis signaling. Antioxid Redox Signal *7*, 472-481.

310. Webster, K.A., Graham, R.M., Thompson, J.W., Spiga, M.G., Frazier, D.P., Wilson, A., and Bishopric, N.H. (2006). Redox stress and the contributions of BH3-only proteins to infarction. Antioxid Redox Signal *8*, 1667-1676.

311. Leist, M., Single, B., Castoldi, A.F., Kuhnle, S., and Nicotera, P. (1997). Intracellular adenosine triphosphate (ATP) concentration: a switch in the decision between apoptosis and necrosis. J Exp Med *185*, 1481-1486.

312. Watabe, M., and Nakaki, T. (2007). ATP depletion does not account for apoptosis induced by inhibition of mitochondrial electron transport chain in human dopaminergic cells. Neuropharmacology *52*, 536-541.

313. Eguchi, Y., Shimizu, S., and Tsujimoto, Y. (1997). Intracellular ATP levels determine cell death fate by apoptosis or necrosis. Cancer Res *57*, 1835-1840.

314. Saito, Y., Nishio, K., Ogawa, Y., Kimata, J., Kinumi, T., Yoshida, Y., Noguchi, N., and Niki, E. (2006). Turning point in apoptosis/necrosis induced by hydrogen peroxide. Free Radic Res *40*, 619-630.

315. Ricci, J.E., Waterhouse, N., and Green, D.R. (2003). Mitochondrial functions during cell death, a complex (I-V) dilemma. Cell Death Differ *10*, 488-492.

316. Ohse, T., Nagaoka, S., Arakawa, Y., Kawakami, H., and Nakamura, K. (2001). Cell death by reactive oxygen species generated from water-soluble cationic metalloporphyrins as superoxide dismutase mimics. J Inorg Biochem *85*, 201-208.

317. Herrera, E., and Barbas, C. (2001). Vitamin E: action, metabolism and perspectives. J Physiol Biochem *57*, 43-56.

318. Ashkenazi, A., and Dixit, V.M. (1998). Death receptors: signaling and modulation. Science *281*, 1305-1308.

319. Bauer, M.K., Vogt, M., Los, M., Siegel, J., Wesselborg, S., and Schulze-Osthoff, K. (1998). Role of reactive oxygen intermediates in activation-induced CD95 (APO-1/Fas) ligand expression. J Biol Chem *273*, 8048-8055.

320. Sandstrom, P.A., and Buttke, T.M. (1993). Autocrine production of extracellular catalase prevents apoptosis of the human CEM T-cell line in serum-free medium. Proc Natl Acad Sci U S A *90*, 4708-4712.

321. Sandstrom, P.A., Mannie, M.D., and Buttke, T.M. (1994). Inhibition of activation-induced death in T cell hybridomas by thiol antioxidants: oxidative stress as a mediator of apoptosis. J Leukoc Biol *55*, 221-226.

322. Laux, I., and Nel, A. (2001). Evidence that oxidative stress-induced apoptosis by menadione involves Fas-dependent and Fas-independent pathways. Clin Immunol *101*, 335-344.

323. Rodriguez, C.O., Jr., Stellrecht, C.M., and Gandhi, V. (2003). Mechanisms for T-cell selective cytotoxicity of arabinosylguanine. Blood *102*, 1842-1848.

324. Leist, M., and Jaattela, M. (2001). Four deaths and a funeral: from caspases to alternative mechanisms. Nat Rev Mol Cell Biol *2*, 589-598.

325. Colell, A., Ricci, J.E., Tait, S., Milasta, S., Maurer, U., Bouchier-Hayes, L., Fitzgerald, P., Guio-Carrion, A., Waterhouse, N.J., Li, C.W., Mari, B., Barbry, P.,

Newmeyer, D.D., Beere, H.M., and Green, D.R. (2007). GAPDH and autophagy preserve survival after apoptotic cytochrome c release in the absence of caspase activation. Cell *129*, 983-997.

326. Hajra, K.M., and Liu, J.R. (2004). Apoptosome dysfunction in human cancer. Apoptosis *9*, 691-704.

327. Chen, Q., Gong, B., and Almasan, A. (2000). Distinct stages of cytochrome c release from mitochondria: evidence for a feedback amplification loop linking caspase activation to mitochondrial dysfunction in genotoxic stress induced apoptosis. Cell Death Differ *7*, 227-233.

328. Enoksson, M., Robertson, J.D., Gogvadze, V., Bu, P., Kropotov, A., Zhivotovsky, B., and Orrenius, S. (2004). Caspase-2 permeabilizes the outer mitochondrial membrane and disrupts the binding of cytochrome c to anionic phospholipids. J Biol Chem *279*, 49575-49578.

329. Marzo, I., Susin, S.A., Petit, P.X., Ravagnan, L., Brenner, C., Larochette, N., Zamzami, N., and Kroemer, G. (1998). Caspases disrupt mitochondrial membrane barrier function. FEBS Lett *427*, 198-202.

330. Bossy-Wetzel, E., and Green, D.R. (1999). Caspases induce cytochrome c release from mitochondria by activating cytosolic factors. J Biol Chem *274*, 17484-17490.

331. Waterhouse, N.J., Ricci, J.E., and Green, D.R. (2002). And all of a sudden it's over: mitochondrial outer-membrane permeabilization in apoptosis. Biochimie *84*, 113-121.

332. Chipuk, J.E., Bouchier-Hayes, L., and Green, D.R. (2006). Mitochondrial outer membrane permeabilization during apoptosis: the innocent bystander scenario. Cell Death Differ *13*, 1396-1402.

333. Ferraro, E., Pulicati, A., Cencioni, M.T., Cozzolino, M., Navoni, F., di Martino, S., Nardacci, R., Carri, M.T., and Cecconi, F. (2008). Apoptosome-deficient Cells Lose Cytochrome c through Proteasomal Degradation but Survive by Autophagy-dependent Glycolysis. Mol Biol Cell *19*, 3576-3588.

334. Goldstein, J.C., Waterhouse, N.J., Juin, P., Evan, G.I., and Green, D.R. (2000). The coordinate release of cytochrome c during apoptosis is rapid, complete and kinetically invariant. Nat Cell Biol *2*, 156-162.

335. Waterhouse, N.J., Sedelies, K.A., Sutton, V.R., Pinkoski, M.J., Thia, K.Y., Johnstone, R., Bird, P.I., Green, D.R., and Trapani, J.A. (2006). Functional dissociation of DeltaPsim and cytochrome c release defines the contribution of mitochondria upstream of caspase activation during granzyme B-induced apoptosis. Cell Death Differ *13*, 607-618.

336. Waterhouse, N.J., Goldstein, J.C., von Ahsen, O., Schuler, M., Newmeyer, D.D., and Green, D.R. (2001). Cytochrome c maintains mitochondrial transmembrane potential and ATP generation after outer mitochondrial membrane permeabilization during the apoptotic process. J Cell Biol *153*, 319-328.

337. Ricci, J.E., Munoz-Pinedo, C., Fitzgerald, P., Bailly-Maitre, B., Perkins, G.A., Yadava, N., Scheffler, I.E., Ellisman, M.H., and Green, D.R. (2004). Disruption of mitochondrial function during apoptosis is mediated by caspase cleavage of the p75 subunit of complex I of the electron transport chain. Cell *117*, 773-786.

338. Glaser, P.E., Han, X., and Gross, R.W. (2002). Tubulin is the endogenous inhibitor of the glyceraldehyde 3-phosphate dehydrogenase isoform that catalyzes membrane fusion: Implications for the coordinated regulation of glycolysis and membrane fusion. Proc Natl Acad Sci U S A *99*, 14104-14109.

339. Nakagawa, T., Hirano, Y., Inomata, A., Yokota, S., Miyachi, K., Kaneda, M., Umeda, M., Furukawa, K., Omata, S., and Horigome, T. (2003). Participation of a fusogenic protein, glyceraldehyde-3-phosphate dehydrogenase, in nuclear membrane assembly. J Biol Chem *278*, 20395-20404.

340. Zheng, L., Roeder, R.G., and Luo, Y. (2003). S phase activation of the histone H2B promoter by OCA-S, a coactivator complex that contains GAPDH as a key component. Cell *114*, 255-266.

341. Rathmell, J.C., and Kornbluth, S. (2007). Filling a GAP(DH) in caspase-independent cell death. Cell *129*, 861-863.

342. Sabath, D.E., Broome, H.E., and Prystowsky, M.B. (1990). Glyceraldehyde-3-phosphate dehydrogenase mRNA is a major interleukin 2-induced transcript in a cloned T-helper lymphocyte. Gene *91*, 185-191.

343. Zheng, Y., Shi, Y., Tian, C., Jiang, C., Jin, H., Chen, J., Almasan, A., Tang, H., and Chen, Q. (2004). Essential role of the voltage-dependent anion channel (VDAC) in mitochondrial permeability transition pore opening and cytochrome c release induced by arsenic trioxide. Oncogene *23*, 1239-1247.

344. Majima, E., Ikawa, K., Takeda, M., Hashimoto, M., Shinohara, Y., and Terada, H. (1995). Translocation of loops regulates transport activity of mitochondrial ADP/ATP carrier deduced from formation of a specific intermolecular disulfide bridge catalyzed by copper-o-phenanthroline. J Biol Chem *270*, 29548-29554.

345. Majima, E., Koike, H., Hong, Y.M., Shinohara, Y., and Terada, H. (1993). Characterization of cysteine residues of mitochondrial ADP/ATP carrier with the SH-reagents eosin 5-maleimide and N-ethylmaleimide. J Biol Chem *268*, 22181-22187.

346. Valle, V.G., Fagian, M.M., Parentoni, L.S., Meinicke, A.R., and Vercesi, A.E. (1993). The participation of reactive oxygen species and protein thiols in the

mechanism of mitochondrial inner membrane permeabilization by calcium plus prooxidants. Arch Biochem Biophys *307*, 1-7.

347. McKenzie, M.D., Carrington, E.M., Kaufmann, T., Strasser, A., Huang, D.C., Kay, T.W., Allison, J., and Thomas, H.E. (2008). Proapoptotic BH3-only protein Bid is essential for death receptor-induced apoptosis of pancreatic beta-cells. Diabetes *57*, 1284-1292.

348. Pelicano, H., Feng, L., Zhou, Y., Carew, J.S., Hileman, E.O., Plunkett, W., Keating, M.J., and Huang, P. (2003). Inhibition of mitochondrial respiration: a novel strategy to enhance drug-induced apoptosis in human leukemia cells by a reactive oxygen species-mediated mechanism. J Biol Chem *278*, 37832-37839.

349. Camello-Almaraz, C., Gomez-Pinilla, P.J., Pozo, M.J., and Camello, P.J. (2006). Mitochondrial reactive oxygen species and Ca2+ signaling. Am J Physiol Cell Physiol *291*, C1082-1088.

350. Turrens, J.F. (2003). Mitochondrial formation of reactive oxygen species. J Physiol *552*, 335-344.

351. Castro, L., Rodriguez, M., and Radi, R. (1994). Aconitase is readily inactivated by peroxynitrite, but not by its precursor, nitric oxide. J Biol Chem *269*, 29409-29415.

352. Beinert, H., Kennedy, M.C., and Stout, C.D. (1996). Aconitase as Ironminus signSulfur Protein, Enzyme, and Iron-Regulatory Protein. Chem Rev *96*, 2335-2374.

353. Bulteau, A.L., Ikeda-Saito, M., and Szweda, L.I. (2003). Redox-dependent modulation of aconitase activity in intact mitochondria. Biochemistry *42*, 14846-14855.

354. Lauble, H., Kennedy, M.C., Emptage, M.H., Beinert, H., and Stout, C.D. (1996). The reaction of fluorocitrate with aconitase and the crystal structure of the enzyme-inhibitor complex. Proc Natl Acad Sci U S A *93*, 13699-13703.

355. Miwa, S., and Brand, M.D. (2005). The topology of superoxide production by complex III and glycerol 3-phosphate dehydrogenase in Drosophila mitochondria. Biochim Biophys Acta *1709*, 214-219.

356. Bulteau, A.L., Lundberg, K.C., Ikeda-Saito, M., Isaya, G., and Szweda, L.I. (2005). Reversible redox-dependent modulation of mitochondrial aconitase and proteolytic activity during in vivo cardiac ischemia/reperfusion. Proc Natl Acad Sci U S A *102*, 5987-5991.

357. Sharer, J.D. (2005). The adenine nucleotide translocase type 1 (ANT1): a new factor in mitochondrial disease. IUBMB Life *57*, 607-614.

358. Wei, M.C., Lindsten, T., Mootha, V.K., Weiler, S., Gross, A., Ashiya, M., Thompson, C.B., and Korsmeyer, S.J. (2000). tBID, a membrane-targeted death ligand, oligomerizes BAK to release cytochrome c. Genes Dev *14*, 2060-2071.

359. Crompton, M., McGuinness, O., and Nazareth, W. (1992). The involvement of cyclosporin A binding proteins in regulating and uncoupling mitochondrial energy transduction. Biochim Biophys Acta *1101*, 214-217.

360. Kagan, V.E., Tyurin, V.A., Jiang, J., Tyurina, Y.Y., Ritov, V.B., Amoscato, A.A., Osipov, A.N., Belikova, N.A., Kapralov, A.A., Kini, V., Vlasova, II, Zhao, Q., Zou, M., Di, P., Svistunenko, D.A., Kurnikov, I.V., and Borisenko, G.G. (2005). Cytochrome c acts as a cardiolipin oxygenase required for release of proapoptotic factors. Nat Chem Biol *1*, 223-232.

361. Belikova, N.A., Vladimirov, Y.A., Osipov, A.N., Kapralov, A.A., Tyurin, V.A., Potapovich, M.V., Basova, L.V., Peterson, J., Kurnikov, I.V., and Kagan, V.E. (2006). Peroxidase activity and structural transitions of cytochrome c bound to cardiolipin-containing membranes. Biochemistry *45*, 4998-5009.

362. Jiang, J., Huang, Z., Zhao, Q., Feng, W., Belikova, N.A., and Kagan, V.E. (2008). Interplay between bax, reactive oxygen species production, and cardiolipin oxidation during apoptosis. Biochem Biophys Res Commun *368*, 145-150.

363. Huang, Z., Jiang, J., Tyurin, V.A., Zhao, Q., Mnuskin, A., Ren, J., Belikova, N.A., Feng, W., Kurnikov, I.V., and Kagan, V.E. (2008). Cardiolipin deficiency leads to decreased cardiolipin peroxidation and increased resistance of cells to apoptosis. Free Radic Biol Med.

364. Okado-Matsumoto, A., and Fridovich, I. (2001). Subcellular distribution of superoxide dismutases (SOD) in rat liver: Cu,Zn-SOD in mitochondria. J Biol Chem *276*, 38388-38393.

365. Sturtz, L.A., Diekert, K., Jensen, L.T., Lill, R., and Culotta, V.C. (2001). A fraction of yeast Cu,Zn-superoxide dismutase and its metallochaperone, CCS, localize to the intermembrane space of mitochondria. A physiological role for SOD1 in guarding against mitochondrial oxidative damage. J Biol Chem *276*, 38084-38089.

366. Yoshida, Y., Shimakawa, S., Itoh, N., and Niki, E. (2003). Action of DCFH and BODIPY as a probe for radical oxidation in hydrophilic and lipophilic domain. Free Radic Res *37*, 861-872.

367. Drummen, G.P., van Liebergen, L.C., Op den Kamp, J.A., and Post, J.A. (2002). C11-BODIPY(581/591), an oxidation-sensitive fluorescent lipid peroxidation probe: (micro)spectroscopic characterization and validation of methodology. Free Radic Biol Med *33*, 473-490.

368. Gorbenko, G.P. (1999). Structure of cytochrome c complexes with phospholipids as revealed by resonance energy transfer. Biochim Biophys Acta *1420*, 1-13.

369. Cortese, J.D., Voglino, A.L., and Hackenbrock, C.R. (1998). Multiple conformations of physiological membrane-bound cytochrome c. Biochemistry *37*, 6402-6409.

370. Uren, R.T., Dewson, G., Bonzon, C., Lithgow, T., Newmeyer, D.D., and Kluck, R.M. (2005). Mitochondrial release of pro-apoptotic proteins: electrostatic interactions can hold cytochrome c but not Smac/DIABLO to mitochondrial membranes. J Biol Chem *280*, 2266-2274.

371. Nathan, C. (2003). Specificity of a third kind: reactive oxygen and nitrogen intermediates in cell signaling. J Clin Invest *111*, 769-778.

372. Han, D., Antunes, F., Canali, R., Rettori, D., and Cadenas, E. (2003). Voltage-dependent anion channels control the release of the superoxide anion from mitochondria to cytosol. J Biol Chem *278*, 5557-5563.

373. Denu, J.M., and Tanner, K.G. (1998). Specific and reversible inactivation of protein tyrosine phosphatases by hydrogen peroxide: evidence for a sulfenic acid intermediate and implications for redox regulation. Biochemistry *37*, 5633-5642.

374. Meng, T.C., Fukada, T., and Tonks, N.K. (2002). Reversible oxidation and inactivation of protein tyrosine phosphatases in vivo. Mol Cell *9*, 387-399.

375. van Montfort, R.L., Congreve, M., Tisi, D., Carr, R., and Jhoti, H. (2003). Oxidation state of the active-site cysteine in protein tyrosine phosphatase 1B. Nature *423*, 773-777.

376. Rhee, S.G. (2006). Cell signaling. H2O2, a necessary evil for cell signaling. Science *312*, 1882-1883.

377. Sundaresan, M., Yu, Z.X., Ferrans, V.J., Irani, K., and Finkel, T. (1995). Requirement for generation of H2O2 for platelet-derived growth factor signal transduction. Science *270*, 296-299.

378. Tonks, N.K. (2006). Protein tyrosine phosphatases: from genes, to function, to disease. Nat Rev Mol Cell Biol *7*, 833-846.

379. Juarez, J.C., Manuia, M., Burnett, M.E., Betancourt, O., Boivin, B., Shaw, D.E., Tonks, N.K., Mazar, A.P., and Donate, F. (2008). Superoxide dismutase 1 (SOD1) is essential for H2O2-mediated oxidation and inactivation of phosphatases in growth factor signaling. Proc Natl Acad Sci U S A *105*, 7147-7152.

380. Chiarugi, P., and Cirri, P. (2003). Redox regulation of protein tyrosine phosphatases during receptor tyrosine kinase signal transduction. Trends Biochem Sci *28*, 509-514.

381. Chiarugi, P. (2003). Reactive oxygen species as mediators of cell adhesion. Ital J Biochem *52*, 28-32.

382. Tao, Q., Spring, S.C., and Terman, B.I. (2005). Comparison of the signaling mechanisms by which VEGF, H2O2, and phosphatase inhibitors activate endothelial cell ERK1/2 MAP-kinase. Microvasc Res *69*, 36-44.

383. Traore, K., Sharma, R., Thimmulappa, R.K., Watson, W.H., Biswal, S., and Trush, M.A. (2008). Redox-regulation of Erk1/2-directed phosphatase by reactive oxygen species: role in signaling TPA-induced growth arrest in ML-1 cells. J Cell Physiol *216*, 276-285.

384. Forman, H.J., and Fridovich, I. (1973). Superoxide dismutase: a comparison of rate constants. Arch Biochem Biophys *158*, 396-400.

385. Winterbourn, C.C., and Metodiewa, D. (1999). Reactivity of biologically important thiol compounds with superoxide and hydrogen peroxide. Free Radic Biol Med *27*, 322-328.

386. Chaudhri, G., Clark, I.A., Hunt, N.H., Cowden, W.B., and Ceredig, R. (1986). Effect of antioxidants on primary alloantigen-induced T cell activation and proliferation. J Immunol *137*, 2646-2652.

387. Griffiths, H.R. (2005). ROS as signalling molecules in T cells--evidence for abnormal redox signalling in the autoimmune disease, rheumatoid arthritis. Redox Rep *10*, 273-280.

388. Nakamura, K., Hori, T., Sato, N., Sugie, K., Kawakami, T., and Yodoi, J. (1993). Redox regulation of a src family protein tyrosine kinase p56lck in T cells. Oncogene *8*, 3133-3139.

389. Zamoyska, R., Basson, A., Filby, A., Legname, G., Lovatt, M., and Seddon, B. (2003). The influence of the src-family kinases, Lck and Fyn, on T cell differentiation, survival and activation. Immunol Rev *191*, 107-118.

390. Palacios, E.H., and Weiss, A. (2004). Function of the Src-family kinases, Lck and Fyn, in T-cell development and activation. Oncogene *23*, 7990-8000.

391. Danial, N.N., and Korsmeyer, S.J. (2004). Cell death: critical control points. Cell *116*, 205-219.

392. Fang, W., Rivard, J.J., Ganser, J.A., LeBien, T.W., Nath, K.A., Mueller, D.L., and Behrens, T.W. (1995). Bcl-xL rescues WEHI 231 B lymphocytes from oxidant-mediated death following diverse apoptotic stimuli. J Immunol *155*, 66-75.

393. Korsmeyer, S.J., Yin, X.M., Oltvai, Z.N., Veis-Novack, D.J., and Linette, G.P. (1995). Reactive oxygen species and the regulation of cell death by the Bcl-2 gene family. Biochim Biophys Acta *1271*, 63-66.

394. Fabian, M.A., Biggs, W.H., 3rd, Treiber, D.K., Atteridge, C.E., Azimioara, M.D., Benedetti, M.G., Carter, T.A., Ciceri, P., Edeen, P.T., Floyd, M., Ford, J.M., Galvin, M., Gerlach, J.L., Grotzfeld, R.M., Herrgard, S., Insko, D.E., Insko, M.A., Lai, A.G., Lelias, J.M., Mehta, S.A., Milanov, Z.V., Velasco, A.M., Wodicka, L.M., Patel, H.K., Zarrinkar, P.P., and Lockhart, D.J. (2005). A small molecule-kinase interaction map for clinical kinase inhibitors. Nat Biotechnol *23*, 329-336.

395. Hsu, Y.T., Wolter, K.G., and Youle, R.J. (1997). Cytosol-to-membrane redistribution of Bax and Bcl-X(L) during apoptosis. Proc Natl Acad Sci U S A *94*, 3668-3672.

396. Blatt, N.B., Boitano, A.E., Lyssiotis, C.A., Opipari, A.W., Jr., and Glick, G.D. (2008). Bz-423 superoxide signals apoptosis via selective activation of JNK, Bak, and Bax. Free Radic Biol Med.

397. Baysan, A., Yel, L., Gollapudi, S., Su, H., and Gupta, S. (2007). Arsenic trioxide induces apoptosis via the mitochondrial pathway by upregulating the expression of Bax and Bim in human B cells. Int J Oncol *30*, 313-318.

398. Brunet, A., Sweeney, L.B., Sturgill, J.F., Chua, K.F., Greer, P.L., Lin, Y., Tran, H., Ross, S.E., Mostoslavsky, R., Cohen, H.Y., Hu, L.S., Cheng, H.L., Jedrychowski, M.P., Gygi, S.P., Sinclair, D.A., Alt, F.W., and Greenberg, M.E. (2004). Stress-dependent regulation of FOXO transcription factors by the SIRT1 deacetylase. Science *303*, 2011-2015.

399. Sade, H., and Sarin, A. (2004). Reactive oxygen species regulate quiescent T-cell apoptosis via the BH3-only proapoptotic protein BIM. Cell Death Differ *11*, 416-423.

400. Zha, J., Harada, H., Yang, E., Jockel, J., and Korsmeyer, S.J. (1996). Serine phosphorylation of death agonist BAD in response to survival factor results in binding to 14-3-3 not BCL-X(L). Cell *87*, 619-628.

401. Kim, S.H., Hwang, C.I., Juhnn, Y.S., Lee, J.H., Park, W.Y., and Song, Y.S. (2007). GADD153 mediates celecoxib-induced apoptosis in cervical cancer cells. Carcinogenesis *28*, 223-231.

402. Zhou, Y., Weyman, C.M., Liu, H., Almasan, A., and Zhou, A. (2008). IFN-gamma induces apoptosis in HL-60 cells through decreased Bcl-2 and increased Bak expression. J Interferon Cytokine Res *28*, 65-72.

403. Kim, S.Y., Seo, M., Kim, Y., Lee, Y.I., Oh, J.M., Cho, E.A., Kang, J.S., and Juhnn, Y.S. (2008). Stimulatory heterotrimeric GTP-binding protein inhibits

hydrogen peroxide-induced apoptosis by repressing BAK induction in SH-SY5Y human neuroblastoma cells. J Biol Chem *283*, 1350-1361.

404. Pestka, S. (1971). Inhibitors of ribosome functions. Annu Rev Microbiol *25*, 487-562.

405. Malempati, S., Tibbitts, D., Cunningham, M., Akkari, Y., Olson, S., Fan, G., and Sears, R.C. (2006). Aberrant stabilization of c-Myc protein in some lymphoblastic leukemias. Leukemia *20*, 1572-1581.

406. Reisman, D., and Thompson, E.A. (1995). Glucocorticoid regulation of cyclin D3 gene transcription and mRNA stability in lymphoid cells. Mol Endocrinol *9*, 1500-1509.

407. Mattson, M.P., and Furukawa, K. (1997). Anti-apoptotic actions of cycloheximide: blockade of programmed cell death or induction of programmed cell life? Apoptosis *2*, 257-264.

408. Furukawa, K., Estus, S., Fu, W., Mark, R.J., and Mattson, M.P. (1997). Neuroprotective action of cycloheximide involves induction of bcl-2 and antioxidant pathways. J Cell Biol *136*, 1137-1149.

409. Warr, M.R., and Shore, G.C. (2008). Unique biology of mcl-1: therapeutic opportunities in cancer. Curr Mol Med *8*, 138-147.

410. Maurer, U., Charvet, C., Wagman, A.S., Dejardin, E., and Green, D.R. (2006). Glycogen synthase kinase-3 regulates mitochondrial outer membrane permeabilization and apoptosis by destabilization of MCL-1. Mol Cell *21*, 749-760.

411. Astoul, E., Edmunds, C., Cantrell, D.A., and Ward, S.G. (2001). PI 3-K and T-cell activation: limitations of T-leukemic cell lines as signaling models. Trends Immunol *22*, 490-496.

412. Frame, S., Cohen, P., and Biondi, R.M. (2001). A common phosphate binding site explains the unique substrate specificity of GSK3 and its inactivation by phosphorylation. Mol Cell *7*, 1321-1327.

413. Coghlan, M.P., Culbert, A.A., Cross, D.A., Corcoran, S.L., Yates, J.W., Pearce, N.J., Rausch, O.L., Murphy, G.J., Carter, P.S., Roxbee Cox, L., Mills, D., Brown, M.J., Haigh, D., Ward, R.W., Smith, D.G., Murray, K.J., Reith, A.D., and Holder, J.C. (2000). Selective small molecule inhibitors of glycogen synthase kinase-3 modulate glycogen metabolism and gene transcription. Chem Biol *7*, 793-803.

414. Boulares, A.H., Yakovlev, A.G., Ivanova, V., Stoica, B.A., Wang, G., Iyer, S., and Smulson, M. (1999). Role of poly(ADP-ribose) polymerase (PARP) cleavage in apoptosis. Caspase 3-resistant PARP mutant increases rates of apoptosis in transfected cells. J Biol Chem *274*, 22932-22940.

415. Rathmell, J.C., Elstrom, R.L., Cinalli, R.M., and Thompson, C.B. (2003). Activated Akt promotes increased resting T cell size, CD28-independent T cell growth, and development of autoimmunity and lymphoma. Eur J Immunol *33*, 2223-2232.

416. Richter, J.D., and Sonenberg, N. (2005). Regulation of cap-dependent translation by eIF4E inhibitory proteins. Nature *433*, 477-480.

417. Lopez-Lastra, M., Rivas, A., and Barria, M.I. (2005). Protein synthesis in eukaryotes: the growing biological relevance of cap-independent translation initiation. Biol Res *38*, 121-146.

418. Dai, Q., Liu, J., Chen, J., Durrant, D., McIntyre, T.M., and Lee, R.M. (2004). Mitochondrial ceramide increases in UV-irradiated HeLa cells and is mainly derived from hydrolysis of sphingomyelin. Oncogene *23*, 3650-3658.

419. Komatsu, M., Takahashi, T., Abe, T., Takahashi, I., Ida, H., and Takada, G. (2001). Evidence for the association of ultraviolet-C and H(2)O(2)-induced apoptosis with acid sphingomyelinase activation. Biochim Biophys Acta *1533*, 47-54.

420. Martin, D., Salinas, M., Fujita, N., Tsuruo, T., and Cuadrado, A. (2002). Ceramide and reactive oxygen species generated by H2O2 induce caspase-3-independent degradation of Akt/protein kinase B. J Biol Chem *277*, 42943-42952.

421. Morales, M.C., Perez-Yarza, G., Rementeria, N.N., Boyano, M.D., Apraiz, A., Gomez-Munoz, A., Perez-Andres, E., and Asumendi, A. (2007). 4-HPR-mediated leukemia cell cytotoxicity is triggered by ceramide-induced mitochondrial oxidative stress and is regulated downstream by Bcl-2. Free Radic Res *41*, 591-601.

422. Lin, C.F., Chen, C.L., Chiang, C.W., Jan, M.S., Huang, W.C., and Lin, Y.S. (2007). GSK-3beta acts downstream of PP2A and the PI 3-kinase-Akt pathway, and upstream of caspase-2 in ceramide-induced mitochondrial apoptosis. J Cell Sci *120*, 2935-2943.

423. Schubert, K.M., Scheid, M.P., and Duronio, V. (2000). Ceramide inhibits protein kinase B/Akt by promoting dephosphorylation of serine 473. J Biol Chem *275*, 13330-13335.

424. Czabotar, P.E., Lee, E.F., van Delft, M.F., Day, C.L., Smith, B.J., Huang, D.C., Fairlie, W.D., Hinds, M.G., and Colman, P.M. (2007). Structural insights into the degradation of Mcl-1 induced by BH3 domains. Proc Natl Acad Sci U S A *104*, 6217-6222.

425. Kramar, R., Hohenegger, M., Srour, A.N., and Khanakah, G. (1984). Oligomycin toxicity in intact rats. Agents Actions *15*, 660-663.

426. Shchepina, L.A., Pletjushkina, O.Y., Avetisyan, A.V., Bakeeva, L.E., Fetisova, E.K., Izyumov, D.S., Saprunova, V.B., Vyssokikh, M.Y., Chernyak, B.V., and Skulachev, V.P. (2002). Oligomycin, inhibitor of the F0 part of H+-ATP-synthase, suppresses the TNF-induced apoptosis. Oncogene *21*, 8149-8157.

427. Bhagavathula, N., Nerusu, K.C., Hanosh, A., Aslam, M.N., Sundberg, T.B., Opipari, A.W., Jr., Johnson, K., Kang, S., Glick, G.D., and Varani, J. (2008). 7-Chloro-5-(4-hydroxyphenyl)-1-methyl-3-(naphthalen-2-ylmethyl)-4,5-dihydr o-1H-benzo[b][1,4]diazepin-2(3H)-one (Bz-423), a benzodiazepine, suppresses keratinocyte proliferation and has antipsoriatic activity in the human skin-severe, combined immunodeficient mouse transplant model. J Pharmacol Exp Ther *324*, 938-947.

428. Tomiyama, A., Serizawa, S., Tachibana, K., Sakurada, K., Samejima, H., Kuchino, Y., and Kitanaka, C. (2006). Critical role for mitochondrial oxidative phosphorylation in the activation of tumor suppressors Bax and Bak. J Natl Cancer Inst *98*, 1462-1473.

429. Gellerich, F.N., Laterveer, F.D., Zierz, S., and Nicolay, K. (2002). The quantitation of ADP diffusion gradients across the outer membrane of heart mitochondria in the presence of macromolecules. Biochim Biophys Acta *1554*, 48-56.

430. Tirosh, O., Aronis, A., and Melendez, J.A. (2003). Mitochondrial state 3 to 4 respiration transition during Fas-mediated apoptosis controls cellular redox balance and rate of cell death. Biochem Pharmacol *66*, 1331-1334.

431. Devenish, R.J., Prescott, M., Boyle, G.M., and Nagley, P. (2000). The Oligomycin Axis of Mitochondrial ATP Synthase: OSCP and the Proton Channel. J Bioenerg Biomembr *32*, 507-515.

432. Gledhill, J.R., and Walker, J.E. (2005). Inhibition sites in F1-ATPase from bovine heart mitochondria. Biochem J *386*, 591-598.

433. Rubinstein, J.L., Walker, J.E., and Henderson, R. (2003). Structure of the mitochondrial ATP synthase by electron cryomicroscopy. Embo J *22*, 6182-6192.

434. Matsuno-Yagi, A., Yagi, T., and Hatefi, Y. (1985). Studies on the mechanism of oxidative phosphorylation: effects of specific F0 modifiers on ligand-induced conformation changes of F1. Proc Natl Acad Sci U S A *82*, 7550-7554.

435. Clem, B., Telang, S., Clem, A., Yalcin, A., Meier, J., Simmons, A., Rasku, M.A., Arumugam, S., Dean, W.L., Eaton, J., Lane, A., Trent, J.O., and Chesney, J. (2008). Small-molecule inhibition of 6-phosphofructo-2-kinase activity suppresses glycolytic flux and tumor growth. Mol Cancer Ther *7*, 110-120.

436. Rossignol, R., Faustin, B., Rocher, C., Malgat, M., Mazat, J.P., and Letellier, T. (2003). Mitochondrial threshold effects. Biochem J *370*, 751-762.

437. Alberio, S., Mineri, R., Tiranti, V., and Zeviani, M. (2007). Depletion of mtDNA: syndromes and genes. Mitochondrion *7*, 6-12.

438. Haag-Liautard, C., Coffey, N., Houle, D., Lynch, M., Charlesworth, B., and Keightley, P.D. (2008). Direct estimation of the mitochondrial DNA mutation rate in Drosophila melanogaster. PLoS Biol *6*, e204.

439. Schroder, R., Vielhaber, S., Wiedemann, F.R., Kornblum, C., Papassotiropoulos, A., Broich, P., Zierz, S., Elger, C.E., Reichmann, H., Seibel, P., Klockgether, T., and Kunz, W.S. (2000). New insights into the metabolic consequences of large-scale mtDNA deletions: a quantitative analysis of biochemical, morphological, and genetic findings in human skeletal muscle. J Neuropathol Exp Neurol *59*, 353-360.

440. King, M.P., and Attardi, G. (1988). Injection of mitochondria into human cells leads to a rapid replacement of the endogenous mitochondrial DNA. Cell *52*, 811-819.

441. Shoffner, J.M., Lott, M.T., Lezza, A.M., Seibel, P., Ballinger, S.W., and Wallace, D.C. (1990). Myoclonic epilepsy and ragged-red fiber disease (MERRF) is associated with a mitochondrial DNA tRNA(Lys) mutation. Cell *61*, 931-937.

442. Hayashi, J., Ohta, S., Kikuchi, A., Takemitsu, M., Goto, Y., and Nonaka, I. (1991). Introduction of disease-related mitochondrial DNA deletions into HeLa cells lacking mitochondrial DNA results in mitochondrial dysfunction. Proc Natl Acad Sci U S A *88*, 10614-10618.

443. Petruzzella, V., Moraes, C.T., Sano, M.C., Bonilla, E., DiMauro, S., and Schon, E.A. (1994). Extremely high levels of mutant mtDNAs co-localize with cytochrome c oxidase-negative ragged-red fibers in patients harboring a point mutation at nt 3243. Hum Mol Genet *3*, 449-454.

444. Rossignol, R., Malgat, M., Mazat, J.P., and Letellier, T. (1999). Threshold effect and tissue specificity. Implication for mitochondrial cytopathies. J Biol Chem *274*, 33426-33432.

445. Matheson, B.K., Adams, J.L., Zou, J., Patel, R., and Franklin, R.B. (2007). Effect of metabolic inhibitors on ATP and citrate content in PC3 prostate cancer cells. Prostate *67*, 1211-1218.

446. Becker, M., Newman, S., and Ismail-Beigi, F. (1996). Stimulation of GLUT1 glucose transporter expression in response to inhibition of oxidative phosphorylation: role of reduced sulfhydryl groups. Mol Cell Endocrinol *121*, 165-170.

447. Buzzai, M., Jones, R.G., Amaravadi, R.K., Lum, J.J., DeBerardinis, R.J., Zhao, F., Viollet, B., and Thompson, C.B. (2007). Systemic treatment with the

antidiabetic drug metformin selectively impairs p53-deficient tumor cell growth. Cancer Res *67*, 6745-6752.

448. Hardie, D.G. (2004). The AMP-activated protein kinase pathway--new players upstream and downstream. J Cell Sci *117*, 5479-5487.

449. Lopez, J.M., Santidrian, A.F., Campas, C., and Gil, J. (2003). 5-Aminoimidazole-4-carboxamide riboside induces apoptosis in Jurkat cells, but the AMP-activated protein kinase is not involved. Biochem J *370*, 1027-1032.

450. Zhou, G., Myers, R., Li, Y., Chen, Y., Shen, X., Fenyk-Melody, J., Wu, M., Ventre, J., Doebber, T., Fujii, N., Musi, N., Hirshman, M.F., Goodyear, L.J., and Moller, D.E. (2001). Role of AMP-activated protein kinase in mechanism of metformin action. J Clin Invest *108*, 1167-1174.

451. Carling, D. (2004). The AMP-activated protein kinase cascade--a unifying system for energy control. Trends Biochem Sci *29*, 18-24.

452. Jing, M., and Ismail-Beigi, F. (2007). Critical role of 5'-AMP-activated protein kinase in the stimulation of glucose transport in response to inhibition of oxidative phosphorylation. Am J Physiol Cell Physiol *292*, C477-487.

453. Marsin, A.S., Bertrand, L., Rider, M.H., Deprez, J., Beauloye, C., Vincent, M.F., Van den Berghe, G., Carling, D., and Hue, L. (2000). Phosphorylation and activation of heart PFK-2 by AMPK has a role in the stimulation of glycolysis during ischaemia. Curr Biol *10*, 1247-1255.

454. Chen, I., McDougal, A., Wang, F., and Safe, S. (1998). Aryl hydrocarbon receptor-mediated antiestrogenic and antitumorigenic activity of diindolylmethane. Carcinogenesis *19*, 1631-1639.

455. Wattenberg, L.W., and Loub, W.D. (1978). Inhibition of polycyclic aromatic hydrocarbon-induced neoplasia by naturally occurring indoles. Cancer Res *38*, 1410-1413.

456. Lenaz, G. (2001). The mitochondrial production of reactive oxygen species: mechanisms and implications in human pathology. IUBMB Life *52*, 159-164.

457. Adam-Vizi, V. (2005). Production of reactive oxygen species in brain mitochondria: contribution by electron transport chain and non-electron transport chain sources. Antioxid Redox Signal *7*, 1140-1149.

458. Boveris, A. (1977). Mitochondrial production of superoxide radical and hydrogen peroxide. Adv Exp Med Biol *78*, 67-82.

459. Cino, M., and Del Maestro, R.F. (1989). Generation of hydrogen peroxide by brain mitochondria: the effect of reoxygenation following postdecapitative ischemia. Arch Biochem Biophys *269*, 623-638.

460. Kwong, L.K., and Sohal, R.S. (1998). Substrate and site specificity of hydrogen peroxide generation in mouse mitochondria. Arch Biochem Biophys *350*, 118-126.

461. Chance, B., Sies, H., and Boveris, A. (1979). Hydroperoxide metabolism in mammalian organs. Physiol Rev *59*, 527-605.

462. D'Autreaux, B., and Toledano, M.B. (2007). ROS as signalling molecules: mechanisms that generate specificity in ROS homeostasis. Nat Rev Mol Cell Biol *8*, 813-824.

463. Imlay, J.A. (2003). Pathways of oxidative damage. Annu Rev Microbiol *57*, 395-418.

464. Votyakova, T.V., and Reynolds, I.J. (2001). DeltaPsi(m)-Dependent and -independent production of reactive oxygen species by rat brain mitochondria. J Neurochem *79*, 266-277.

465. Boveris, A., Cadenas, E., and Stoppani, A.O. (1976). Role of ubiquinone in the mitochondrial generation of hydrogen peroxide. Biochem J *156*, 435-444.

466. Turrens, J.F., Alexandre, A., and Lehninger, A.L. (1985). Ubisemiquinone is the electron donor for superoxide formation by complex III of heart mitochondria. Arch Biochem Biophys *237*, 408-414.

467. Turrens, J.F., and Boveris, A. (1980). Generation of superoxide anion by the NADH dehydrogenase of bovine heart mitochondria. Biochem J *191*, 421-427.

468. Hirst, J. (2005). Energy transduction by respiratory complex I--an evaluation of current knowledge. Biochem Soc Trans *33*, 525-529.

469. Okun, J.G., Lummen, P., and Brandt, U. (1999). Three classes of inhibitors share a common binding domain in mitochondrial complex I (NADH:ubiquinone oxidoreductase). J Biol Chem *274*, 2625-2630.

470. Genova, M.L., Ventura, B., Giuliano, G., Bovina, C., Formiggini, G., Parenti Castelli, G., and Lenaz, G. (2001). The site of production of superoxide radical in mitochondrial Complex I is not a bound ubisemiquinone but presumably iron-sulfur cluster N2. FEBS Lett *505*, 364-368.

471. Kushnareva, Y., Murphy, A.N., and Andreyev, A. (2002). Complex I-mediated reactive oxygen species generation: modulation by cytochrome c and NAD(P)+ oxidation-reduction state. Biochem J *368*, 545-553.

472. Kudin, A.P., Bimpong-Buta, N.Y., Vielhaber, S., Elger, C.E., and Kunz, W.S. (2004). Characterization of superoxide-producing sites in isolated brain mitochondria. J Biol Chem *279*, 4127-4135.

473. Krishnamoorthy, G., and Hinkle, P.C. (1988). Studies on the electron transfer pathway, topography of iron-sulfur centers, and site of coupling in NADH-Q oxidoreductase. J Biol Chem *263*, 17566-17575.

474. Lambert, A.J., and Brand, M.D. (2004). Inhibitors of the quinone-binding site allow rapid superoxide production from mitochondrial NADH:ubiquinone oxidoreductase (complex I). J Biol Chem *279*, 39414-39420.

475. Bove, J., Prou, D., Perier, C., and Przedborski, S. (2005). Toxin-induced models of Parkinson's disease. NeuroRx *2*, 484-494.

476. Melov, S., Coskun, P., Patel, M., Tuinstra, R., Cottrell, B., Jun, A.S., Zastawny, T.H., Dizdaroglu, M., Goodman, S.I., Huang, T.T., Miziorko, H., Epstein, C.J., and Wallace, D.C. (1999). Mitochondrial disease in superoxide dismutase 2 mutant mice. Proc Natl Acad Sci U S A *96*, 846-851.

477. Crofts, A.R. (2004). The cytochrome bc1 complex: function in the context of structure. Annu Rev Physiol *66*, 689-733.

478. Cape, J.L., Bowman, M.K., and Kramer, D.M. (2007). A semiquinone intermediate generated at the Qo site of the cytochrome bc1 complex: importance for the Q-cycle and superoxide production. Proc Natl Acad Sci U S A *104*, 7887-7892.

479. Forquer, I., Covian, R., Bowman, M.K., Trumpower, B.L., and Kramer, D.M. (2006). Similar transition states mediate the Q-cycle and superoxide production by the cytochrome bc1 complex. J Biol Chem *281*, 38459-38465.

480. Berry, E.A., Guergova-Kuras, M., Huang, L.S., and Crofts, A.R. (2000). Structure and function of cytochrome bc complexes. Annu Rev Biochem *69*, 1005-1075.

481. Trumpower, B.L., and Gennis, R.B. (1994). Energy transduction by cytochrome complexes in mitochondrial and bacterial respiration: the enzymology of coupling electron transfer reactions to transmembrane proton translocation. Annu Rev Biochem *63*, 675-716.

482. Sorgato, M.C., and Moran, O. (1993). Channels in mitochondrial membranes: knowns, unknowns, and prospects for the future. Crit Rev Biochem Mol Biol *28*, 127-171.

483. Colombini, M. (1987). Regulation of the mitochondrial outer membrane channel, VDAC. J Bioenerg Biomembr *19*, 309-320.

484. Dupeyrat, F., Vidaud, C., Lorphelin, A., and Berthomieu, C. (2004). Long distance charge redistribution upon Cu,Zn-superoxide dismutase reduction: significance for dismutase function. J Biol Chem *279*, 48091-48101.

485. Perkins, G.A., Renken, C.W., Song, J.Y., Frey, T.G., Young, S.J., Lamont, S., Martone, M.E., Lindsey, S., and Ellisman, M.H. (1997). Electron tomography of large, multicomponent biological structures. J Struct Biol *120*, 219-227.

486. Antunes, F., Salvador, A., Marinho, H.S., Alves, R., and Pinto, R.E. (1996). Lipid peroxidation in mitochondrial inner membranes. I. An integrative kinetic model. Free Radic Biol Med *21*, 917-943.

487. Demin, O.V., Kholodenko, B.N., and Skulachev, V.P. (1998). A model of O2.- generation in the complex III of the electron transport chain. Mol Cell Biochem *184*, 21-33.

488. Finkel, T. (1999). Signal transduction by reactive oxygen species in non-phagocytic cells. J Leukoc Biol *65*, 337-340.

489. De Keulenaer, G.W., Alexander, R.W., Ushio-Fukai, M., Ishizaka, N., and Griendling, K.K. (1998). Tumour necrosis factor alpha activates a p22phox-based NADH oxidase in vascular smooth muscle. Biochem J *329 (Pt 3)*, 653-657.

490. Rahmani, M., Reese, E., Dai, Y., Bauer, C., Payne, S.G., Dent, P., Spiegel, S., and Grant, S. (2005). Coadministration of histone deacetylase inhibitors and perifosine synergistically induces apoptosis in human leukemia cells through Akt and ERK1/2 inactivation and the generation of ceramide and reactive oxygen species. Cancer Res *65*, 2422-2432.

491. Ungerstedt, J.S., Sowa, Y., Xu, W.S., Shao, Y., Dokmanovic, M., Perez, G., Ngo, L., Holmgren, A., Jiang, X., and Marks, P.A. (2005). Role of thioredoxin in the response of normal and transformed cells to histone deacetylase inhibitors. Proc Natl Acad Sci U S A *102*, 673-678.

492. Yu, C., Rahmani, M., Dent, P., and Grant, S. (2004). The hierarchical relationship between MAPK signaling and ROS generation in human leukemia cells undergoing apoptosis in response to the proteasome inhibitor Bortezomib. Exp Cell Res *295*, 555-566.

493. Marks, P.A., and Breslow, R. (2007). Dimethyl sulfoxide to vorinostat: development of this histone deacetylase inhibitor as an anticancer drug. Nat Biotechnol *25*, 84-90.

494. Paramore, A., and Frantz, S. (2003). Bortezomib. Nat Rev Drug Discov *2*, 611-612.

495. Huang, P., Feng, L., Oldham, E.A., Keating, M.J., and Plunkett, W. (2000). Superoxide dismutase as a target for the selective killing of cancer cells. Nature *407*, 390-395.

496. Zhou, Y., Hileman, E.O., Plunkett, W., Keating, M.J., and Huang, P. (2003). Free radical stress in chronic lymphocytic leukemia cells and its role in cellular sensitivity to ROS-generating anticancer agents. Blood *101*, 4098-4104.

497. Bhati, R., Gokmen-Polar, Y., Sledge, G.W., Jr., Fan, C., Nakshatri, H., Ketelsen, D., Borchers, C.H., Dial, M.J., Patterson, C., and Klauber-DeMore, N. (2007). 2-methoxyestradiol inhibits the anaphase-promoting complex and protein translation in human breast cancer cells. Cancer Res *67*, 702-708.

498. Ho, A., Kim, Y.E., Lee, H., Cyrus, K., Baek, S.H., and Kim, K.B. (2006). SAR studies of 2-methoxyestradiol and development of its analogs as probes of anti-tumor mechanisms. Bioorg Med Chem Lett *16*, 3383-3387.

499. Kachadourian, R., Liochev, S.I., Cabelli, D.E., Patel, M.N., Fridovich, I., and Day, B.J. (2001). 2-methoxyestradiol does not inhibit superoxide dismutase. Arch Biochem Biophys *392*, 349-353.

500. Mooberry, S.L. (2003). New insights into 2-methoxyestradiol, a promising antiangiogenic and antitumor agent. Curr Opin Oncol *15*, 425-430.

501. Hileman, E.O., Liu, J., Albitar, M., Keating, M.J., and Huang, P. (2004). Intrinsic oxidative stress in cancer cells: a biochemical basis for therapeutic selectivity. Cancer Chemother Pharmacol *53*, 209-219.

502. Pelicano, H., Carney, D., and Huang, P. (2004). ROS stress in cancer cells and therapeutic implications. Drug Resist Updat *7*, 97-110.

503. Dahut, W.L., Lakhani, N.J., Gulley, J.L., Arlen, P.M., Kohn, E.C., Kotz, H., McNally, D., Parr, A., Nguyen, D., Yang, S.X., Steinberg, S.M., Venitz, J., Sparreboom, A., and Figg, W.D. (2006). Phase I clinical trial of oral 2-methoxyestradiol, an antiangiogenic and apoptotic agent, in patients with solid tumors. Cancer Biol Ther *5*, 22-27.

504. James, J., Murry, D.J., Treston, A.M., Storniolo, A.M., Sledge, G.W., Sidor, C., and Miller, K.D. (2007). Phase I safety, pharmacokinetic and pharmacodynamic studies of 2-methoxyestradiol alone or in combination with docetaxel in patients with locally recurrent or metastatic breast cancer. Invest New Drugs *25*, 41-48.

505. Rajkumar, S.V., Richardson, P.G., Lacy, M.Q., Dispenzieri, A., Greipp, P.R., Witzig, T.E., Schlossman, R., Sidor, C.F., Anderson, K.C., and Gertz, M.A. (2007). Novel therapy with 2-methoxyestradiol for the treatment of relapsed and plateau phase multiple myeloma. Clin Cancer Res *13*, 6162-6167.

506. Dvorakova, K., Waltmire, C.N., Payne, C.M., Tome, M.E., Briehl, M.M., and Dorr, R.T. (2001). Induction of mitochondrial changes in myeloma cells by imexon. Blood *97*, 3544-3551.

507. Iyengar, B.S., Dorr, R.T., and Remers, W.A. (2004). Chemical basis for the biological activity of imexon and related cyanoaziridines. J Med Chem *47*, 218-223.

508. Hersh, E.M., Gschwind, C.R., Taylor, C.W., Dorr, R.T., Taetle, R., and Salmon, S.E. (1992). Antiproliferative and antitumor activity of the 2-cyanoaziridine compound imexon on tumor cell lines and fresh tumor cells in vitro. J Natl Cancer Inst *84*, 1238-1244.

509. Pourpak, A., Meyers, R.O., Samulitis, B.K., Sherry Chow, H.H., Kepler, C.Y., Raymond, M.A., Hersh, E., and Dorr, R.T. (2006). Preclinical antitumor activity, pharmacokinetics and pharmacodynamics of imexon in mice. Anticancer Drugs *17*, 1179-1184.

510. Dragovich, T., Gordon, M., Mendelson, D., Wong, L., Modiano, M., Chow, H.H., Samulitis, B., O'Day, S., Grenier, K., Hersh, E., and Dorr, R. (2007). Phase I trial of imexon in patients with advanced malignancy. J Clin Oncol *25*, 1779-1784.

511. Lennon, R.E. (1973). Antimycin A, a piscicidal antibiotic. Adv Appl Microbiol *16*, 55-96.

512. Lo-Coco, F., Ammatuna, E., Montesinos, P., and Sanz, M.A. (2008). Acute promyelocytic leukemia: recent advances in diagnosis and management. Semin Oncol *35*, 401-409.

513. Dilda, P.J., and Hogg, P.J. (2007). Arsenical-based cancer drugs. Cancer Treat Rev *33*, 542-564.

514. Hansen, J.M., Zhang, H., and Jones, D.P. (2006). Differential oxidation of thioredoxin-1, thioredoxin-2, and glutathione by metal ions. Free Radic Biol Med *40*, 138-145.

515. Ramirez, P., Eastmond, D.A., Laclette, J.P., and Ostrosky-Wegman, P. (1997). Disruption of microtubule assembly and spindle formation as a mechanism for the induction of aneuploid cells by sodium arsenite and vanadium pentoxide. Mutat Res *386*, 291-298.

516. Riby, J.E., Firestone, G.L., and Bjeldanes, L.F. (2008). 3,3'-diindolylmethane reduces levels of HIF-1alpha and HIF-1 activity in hypoxic cultured human cancer cells. Biochem Pharmacol *75*, 1858-1867.

517. Antignani, A., and Youle, R.J. (2006). How do Bax and Bak lead to permeabilization of the outer mitochondrial membrane? Curr Opin Cell Biol *18*, 685-689.

518. Korsmeyer, S.J., Wei, M.C., Saito, M., Weiler, S., Oh, K.J., and Schlesinger, P.H. (2000). Pro-apoptotic cascade activates BID, which oligomerizes BAK or BAX

into pores that result in the release of cytochrome c. Cell Death Differ *7*, 1166-1173.

519. Karbowski, M., Norris, K.L., Cleland, M.M., Jeong, S.Y., and Youle, R.J. (2006). Role of Bax and Bak in mitochondrial morphogenesis. Nature *443*, 658-662.

520. Mott, J.L., and Gores, G.J. (2007). Piercing the armor of hepatobiliary cancer: Bcl-2 homology domain 3 (BH3) mimetics and cell death. Hepatology *46*, 906-911.

521. Adams, J.M., and Cory, S. (2007). The Bcl-2 apoptotic switch in cancer development and therapy. Oncogene *26*, 1324-1337.

522. Turek-Etienne, T.C., Kober, T.P., Stafford, J.M., and Bryant, R.W. (2003). Development of a fluorescence polarization AKT serine/threonine kinase assay using an immobilized metal ion affinity-based technology. Assay Drug Dev Technol *1*, 545-553.

523. Pise-Masison, C.A., Choi, K.S., Radonovich, M., Dittmer, J., Kim, S.J., and Brady, J.N. (1998). Inhibition of p53 transactivation function by the human T-cell lymphotropic virus type 1 Tax protein. J Virol *72*, 1165-1170.

524. Nikiforov, M.A., Riblett, M., Tang, W.H., Gratchouck, V., Zhuang, D., Fernandez, Y., Verhaegen, M., Varambally, S., Chinnaiyan, A.M., Jakubowiak, A.J., and Soengas, M.S. (2007). Tumor cell-selective regulation of NOXA by c-MYC in response to proteasome inhibition. Proc Natl Acad Sci U S A *104*, 19488-19493.

525. Kim, J.Y., Ahn, H.J., Ryu, J.H., Suk, K., and Park, J.H. (2004). BH3-only protein Noxa is a mediator of hypoxic cell death induced by hypoxia-inducible factor 1alpha. J Exp Med *199*, 113-124.

526. Hershko, T., and Ginsberg, D. (2004). Up-regulation of Bcl-2 homology 3 (BH3)-only proteins by E2F1 mediates apoptosis. J Biol Chem *279*, 8627-8634.

527. Wu, L., Timmers, C., Maiti, B., Saavedra, H.I., Sang, L., Chong, G.T., Nuckolls, F., Giangrande, P., Wright, F.A., Field, S.J., Greenberg, M.E., Orkin, S., Nevins, J.R., Robinson, M.L., and Leone, G. (2001). The E2F1-3 transcription factors are essential for cellular proliferation. Nature *414*, 457-462.

528. Cobrinik, D. (2005). Pocket proteins and cell cycle control. Oncogene *24*, 2796-2809.

529. Guzy, R.D., and Schumacker, P.T. (2006). Oxygen sensing by mitochondria at complex III: the paradox of increased reactive oxygen species during hypoxia. Exp Physiol *91*, 807-819.

530. Salceda, S., and Caro, J. (1997). Hypoxia-inducible factor 1alpha (HIF-1alpha) protein is rapidly degraded by the ubiquitin-proteasome system under normoxic conditions. Its stabilization by hypoxia depends on redox-induced changes. J Biol Chem *272*, 22642-22647.

531. Bruick, R.K., and McKnight, S.L. (2001). A conserved family of prolyl-4-hydroxylases that modify HIF. Science *294*, 1337-1340.

532. Schumacker, P.T. (2005). Hypoxia-inducible factor-1 (HIF-1). Crit Care Med *33*, S423-425.

533. Chandel, N.S., McClintock, D.S., Feliciano, C.E., Wood, T.M., Melendez, J.A., Rodriguez, A.M., and Schumacker, P.T. (2000). Reactive oxygen species generated at mitochondrial complex III stabilize hypoxia-inducible factor-1alpha during hypoxia: a mechanism of O2 sensing. J Biol Chem *275*, 25130-25138.

534. Haddad, J.J., and Land, S.C. (2001). A non-hypoxic, ROS-sensitive pathway mediates TNF-alpha-dependent regulation of HIF-1alpha. FEBS Lett *505*, 269-274.

535. Naik, E., Michalak, E.M., Villunger, A., Adams, J.M., and Strasser, A. (2007). Ultraviolet radiation triggers apoptosis of fibroblasts and skin keratinocytes mainly via the BH3-only protein Noxa. J Cell Biol *176*, 415-424.

536. Tajeddine, N., Louis, M., Vermylen, C., Gala, J.L., Tombal, B., and Gailly, P. (2008). Tumor associated antigen PRAME is a marker of favorable prognosis in childhood acute myeloid leukemia patients and modifies the expression of S100A4, Hsp 27, p21, IL-8 and IGFBP-2 in vitro and in vivo. Leuk Lymphoma, 1-9.

537. Kepp, O., Rajalingam, K., Kimmig, S., and Rudel, T. (2007). Bak and Bax are non-redundant during infection- and DNA damage-induced apoptosis. Embo J *26*, 825-834.

538. Cohen, S.M., and Lippard, S.J. (2001). Cisplatin: from DNA damage to cancer chemotherapy. Prog Nucleic Acid Res Mol Biol *67*, 93-130.

539. Sedletska, Y., Giraud-Panis, M.J., and Malinge, J.M. (2005). Cisplatin is a DNA-damaging antitumour compound triggering multifactorial biochemical responses in cancer cells: importance of apoptotic pathways. Curr Med Chem Anticancer Agents *5*, 251-265.

540. Berndtsson, M., Hagg, M., Panaretakis, T., Havelka, A.M., Shoshan, M.C., and Linder, S. (2007). Acute apoptosis by cisplatin requires induction of reactive oxygen species but is not associated with damage to nuclear DNA. Int J Cancer *120*, 175-180.

541. Havelka, A.M., Berndtsson, M., Olofsson, M.H., Shoshan, M.C., and Linder, S. (2007). Mechanisms of action of DNA-damaging anticancer drugs in treatment of carcinomas: is acute apoptosis an "off-target" effect? Mini Rev Med Chem *7*, 1035-1039.

542. Tajeddine, N., Galluzzi, L., Kepp, O., Hangen, E., Morselli, E., Senovilla, L., Araujo, N., Pinna, G., Larochette, N., Zamzami, N., Modjtahedi, N., Harel-Bellan, A., and Kroemer, G. (2008). Hierarchical involvement of Bak, VDAC1 and Bax in cisplatin-induced cell death. Oncogene *27*, 4221-4232.

543. Marroquin, L.D., Hynes, J., Dykens, J.A., Jamieson, J.D., and Will, Y. (2007). Circumventing the Crabtree effect: replacing media glucose with galactose increases susceptibility of HepG2 cells to mitochondrial toxicants. Toxicol Sci *97*, 539-547.

544. Rossignol, R., Gilkerson, R., Aggeler, R., Yamagata, K., Remington, S.J., and Capaldi, R.A. (2004). Energy substrate modulates mitochondrial structure and oxidative capacity in cancer cells. Cancer Res *64*, 985-993.

545. Nagy, G., Koncz, A., and Perl, A. (2005). T- and B-cell abnormalities in systemic lupus erythematosus. Crit Rev Immunol *25*, 123-140.

546. Gergely, P., Jr., Grossman, C., Niland, B., Puskas, F., Neupane, H., Allam, F., Banki, K., Phillips, P.E., and Perl, A. (2002). Mitochondrial hyperpolarization and ATP depletion in patients with systemic lupus erythematosus. Arthritis Rheum *46*, 175-190.

547. Gergely, P., Jr., Niland, B., Gonchoroff, N., Pullmann, R., Jr., Phillips, P.E., and Perl, A. (2002). Persistent mitochondrial hyperpolarization, increased reactive oxygen intermediate production, and cytoplasmic alkalinization characterize altered IL-10 signaling in patients with systemic lupus erythematosus. J Immunol *169*, 1092-1101.

548. Nagy, G., Barcza, M., Gonchoroff, N., Phillips, P.E., and Perl, A. (2004). Nitric oxide-dependent mitochondrial biogenesis generates Ca2+ signaling profile of lupus T cells. J Immunol *173*, 3676-3683.

549. Kuhnke, A., Burmester, G.R., Krauss, S., and Buttgereit, F. (2003). Bioenergetics of immune cells to assess rheumatic disease activity and efficacy of glucocorticoid treatment. Ann Rheum Dis *62*, 133-139.

550. Zamocky, M., Furtmuller, P.G., and Obinger, C. (2008). Evolution of catalases from bacteria to humans. Antioxid Redox Signal *10*, 1527-1548.

551. Fourquet, S., Huang, M.E., D'Autreaux, B., and Toledano, M.B. (2008). The dual functions of thiol-based peroxidases in H2O2 scavenging and signaling. Antioxid Redox Signal *10*, 1565-1576.

552. Tauskela, J.S., Hewitt, K., Kang, L.P., Comas, T., Gendron, T., Hakim, A., Hogan, M., Durkin, J., and Morley, P. (2000). Evaluation of glutathione-sensitive fluorescent dyes in cortical culture. Glia *30*, 329-341.

553. Bailey, H.H. (1998). L-S,R-buthionine sulfoximine: historical development and clinical issues. Chem Biol Interact *111-112*, 239-254.

554. Shefner, R., Manheimer-Lory, A., Davidson, A., Paul, E., Aranow, C., Katz, J., and Diamond, B. (1990). Idiotypes in systemic lupus erythematosus. Clues for understanding etiology and pathogenicity. Chem Immunol *48*, 82-108.

555. Tan, E.M. (1989). Antinuclear antibodies: diagnostic markers for autoimmune diseases and probes for cell biology. Adv Immunol *44*, 93-151.

556. Vallejo, A.N. (2005). CD28 extinction in human T cells: altered functions and the program of T-cell senescence. Immunol Rev *205*, 158-169.

557. Vallejo, A.N., Brandes, J.C., Weyand, C.M., and Goronzy, J.J. (1999). Modulation of CD28 expression: distinct regulatory pathways during activation and replicative senescence. J Immunol *162*, 6572-6579.

558. Posnett, D.N., Sinha, R., Kabak, S., and Russo, C. (1994). Clonal populations of T cells in normal elderly humans: the T cell equivalent to "benign monoclonal gammapathy". J Exp Med *179*, 609-618.

559. Wedderburn, L.R., Patel, A., Varsani, H., and Woo, P. (2001). The developing human immune system: T-cell receptor repertoire of children and young adults shows a wide discrepancy in the frequency of persistent oligoclonal T-cell expansions. Immunology *102*, 301-309.

560. Khan, N., Shariff, N., Cobbold, M., Bruton, R., Ainsworth, J.A., Sinclair, A.J., Nayak, L., and Moss, P.A. (2002). Cytomegalovirus seropositivity drives the CD8 T cell repertoire toward greater clonality in healthy elderly individuals. J Immunol *169*, 1984-1992.

561. Kimura, H., Kawagoe, Y., Kaneko, N., Fessler, H.E., and Hosoda, S. (1996). Low efficiency of oxygen utilization during exercise in hyperthyroidism. Chest *110*, 1264-1270.

562. Markovic-Plese, S., Cortese, I., Wandinger, K.P., McFarland, H.F., and Martin, R. (2001). CD4+CD28- costimulation-independent T cells in multiple sclerosis. J Clin Invest *108*, 1185-1194.

563. Martens, P.B., Goronzy, J.J., Schaid, D., and Weyand, C.M. (1997). Expansion of unusual CD4+ T cells in severe rheumatoid arthritis. Arthritis Rheum *40*, 1106-1114.

564. Pascual, G., and Glass, C.K. (2006). Nuclear receptors versus inflammation: mechanisms of transrepression. Trends Endocrinol Metab *17*, 321-327.

565. Vallejo, A.N., Bryl, E., Klarskov, K., Naylor, S., Weyand, C.M., and Goronzy, J.J. (2002). Molecular basis for the loss of CD28 expression in senescent T cells. J Biol Chem *277*, 46940-46949.

566. Lee, K.M., Chuang, E., Griffin, M., Khattri, R., Hong, D.K., Zhang, W., Straus, D., Samelson, L.E., Thompson, C.B., and Bluestone, J.A. (1998). Molecular basis of T cell inactivation by CTLA-4. Science *282*, 2263-2266.

567. Nishimura, H., and Honjo, T. (2001). PD-1: an inhibitory immunoreceptor involved in peripheral tolerance. Trends Immunol *22*, 265-268.

568. Agata, Y., Kawasaki, A., Nishimura, H., Ishida, Y., Tsubata, T., Yagita, H., and Honjo, T. (1996). Expression of the PD-1 antigen on the surface of stimulated mouse T and B lymphocytes. Int Immunol *8*, 765-772.

569. Walunas, T.L., Bakker, C.Y., and Bluestone, J.A. (1996). CTLA-4 ligation blocks CD28-dependent T cell activation. J Exp Med *183*, 2541-2550.

570. Parry, R.V., Chemnitz, J.M., Frauwirth, K.A., Lanfranco, A.R., Braunstein, I., Kobayashi, S.V., Linsley, P.S., Thompson, C.B., and Riley, J.L. (2005). CTLA-4 and PD-1 receptors inhibit T-cell activation by distinct mechanisms. Mol Cell Biol *25*, 9543-9553.

571. van Berkel, M.E., and Oosterwegel, M.A. (2006). CD28 and ICOS: similar or separate costimulators of T cells? Immunol Lett *105*, 115-122.

572. Jayaraman, T., Ondrias, K., Ondriasova, E., and Marks, A.R. (1996). Regulation of the inositol 1,4,5-trisphosphate receptor by tyrosine phosphorylation. Science *272*, 1492-1494.

573. Vassilopoulos, D., Kovacs, B., and Tsokos, G.C. (1995). TCR/CD3 complex-mediated signal transduction pathway in T cells and T cell lines from patients with systemic lupus erythematosus. J Immunol *155*, 2269-2281.

574. Nambiar, M.P., Krishnan, S., and Tsokos, G.C. (2004). T-cell signaling abnormalities in human systemic lupus erythematosus. Methods Mol Med *102*, 31-47.

575. Tsokos, G.C. (2008). Calcium signaling in systemic lupus erythematosus lymphocytes and its therapeutic exploitation. Arthritis Rheum *58*, 1216-1219.

576. Nambiar, M.P., Fisher, C.U., Warke, V.G., Krishnan, S., Mitchell, J.P., Delaney, N., and Tsokos, G.C. (2003). Reconstitution of deficient T cell receptor zeta chain restores T cell signaling and augments T cell receptor/CD3-induced interleukin-2

production in patients with systemic lupus erythematosus. Arthritis Rheum *48*, 1948-1955.

577. Feske, S. (2007). Calcium signalling in lymphocyte activation and disease. Nat Rev Immunol *7*, 690-702.

578. Wahl, D.`; Opipari, AW.`; Glick, GD. Oxidative glucose metabolism is upregulated in lupus lymphoyctes. Manuscript in Preparation.

579. Newsholme, E.A., and Board, M. (1991). Application of metabolic-control logic to fuel utilization and its significance in tumor cells. Adv Enzyme Regul *31*, 225-246.

580. Wahl, D.`; Opipari, AW.`; Glick, GD. Oxidative glucose metabolism is upregulated in lupus lymphoyctes. Manuscript in Preparation.

581. Alves, N.L., Derks, I.A., Berk, E., Spijker, R., van Lier, R.A., and Eldering, E. (2006). The Noxa/Mcl-1 axis regulates susceptibility to apoptosis under glucose limitation in dividing T cells. Immunity *24*, 703-716.

582. Liu, J., Karypis, G., Hippen, K.L., Vegoe, A.L., Ruiz, P., Gilkeson, G.S., and Behrens, T.W. (2006). Genomic view of systemic autoimmunity in MRLlpr mice. Genes Immun *7*, 156-168.

583. Bradford, M.M. (1976). A rapid and sensitive method for the quantitation of microgram quantities of protein utilizing the principle of protein-dye binding. Anal Biochem *72*, 248-254.

584. Schulz, T.J., Thierbach, R., Voigt, A., Drewes, G., Mietzner, B., Steinberg, P., Pfeiffer, A.F., and Ristow, M. (2006). Induction of oxidative metabolism by mitochondrial frataxin inhibits cancer growth: Otto Warburg revisited. J Biol Chem *281*, 977-981.